Novel insights into hair structure and the effects of chemical stressors on hair and skin using label-free advanced light microscopy

DUIT, REBECCA,CHRISTINA

Novel insights into hair structure and the effects of chemical stressors on hair and skin using label-free advanced light microscopy

By Rebecca Christina Duit

A thesis submitted for the degree of Doctor of Philosophy

Department of Biosciences

September 2016

Declarations

I declare that the experiments described in this thesis were carried out by myself in the Department of Biosciences, Durham University, under the supervision of Dr Arto Määttä and Dr Timothy Hawkins. This thesis has been composed by myself and is a record of work that has not been submitted previously for a higher degree.

Rebecca Duit

I certify that the work reported in this thesis has been performed by Rebecca Duit, who, during the period of study, has fulfilled the conditions of the Ordinance and Regulations governing the Degree of Doctor of Philosophy.

Dr Arto Määttä

Dr Timothy Hawkins

Abstract

Novel insights into hair structure and the effects of chemical stressors on hair and skin using label-free advanced light microscopy

By Rebecca Duit

There is a need for a better method to image hair as the current methods involve embedding the hair in resin, which may produce artefacts, or using dyes which are limited in their depth of penetration into the hair. The research performed in this thesis endeavours to characterise the cellular structure of human hair with label-free imaging using autofluorescence and fluorescence lifetime imaging. Wavelengths were shown to selectively excite the hair cuticle, cortex and medulla, and subcellular compartments. Development of an optical transverse imaging method enabled discoveries including different fluorescence lifetimes across the cuticle cell layers and suggests the cuticle layers possess differing chemical environments. A new method was developed to distinguish between eumelanin and pheomelanin using 405nm and 633nm wavelengths. The newly developed methods were additionally used in the characterisation of an unidentified hair and skin disorder, which found poorly differentiated cuticle cells and showed differences in the fluorescence lifetimes of the hair compared to control hairs.

The hair care industry needs more efficacious chemical depilatories and information into their action. This was elucidated using the developed methods and a new dynamic imaging method. Potassium thioglycolate was shown to cause drastic expansion of the hair which was amplified by the addition of guanidine carbonate, creating fissures through the cuticle and into the cortex. Other experimental depilatory formulations were tested and were found to have varying effects upon the structure of the hair.

New chemical depilatories require development because existing depilatories can cause irritation in the skin. Potassium thioglycolate and guanidine carbonate were tested on HaCaT cells, isolated cornified envelopes, and HEKn cells in a 3D epidermal model. An investigation into the differentiation, proliferation and acute stress response of the cells showed that the treatments had no significant effect on these markers. However, the chemicals negatively affected HaCaT cell viability and damaged the cornified envelopes. Despite this, the viability and structural integrity of the living cells of the epidermal model were maintained through the protection provided by the stratum corneum.

Acknowledgements

I am thankful for having the opportunity to spend six years studying biology in beautiful Durham. There are many people who merit thanks over the last four years. Firstly, I'd like to thank my supervisors: Dr Arto Maatta, Dr Tim Hawkins and Dr Paul Smith for their valuable guidance and support over the last four years. I'd like to thank Paul's team at P&G, Egham for preparing samples and performing experiments that were not feasible to do in Durham, and to P&G for funding this project. I would like to thank Dr Ian Cummins for his help with the GC/MS analysis, Christine Richardson and Helen Grindley for the TEM sample preparation, and Pamela Ritchie for training me in cell culture. Thank you to Simeon, James and Katherine for being in biology from the beginning to the end and for the fun times in the lab, and to people who've come and gone in ICBL, for their advice and company, including Weiju, Miguel, Sarah, Jacques, Mathilde, Nicola, Vicki, Matty, Rafael, Alice, Yana and Nynke. In addition, I'd like to thank my college mentor, Sushma, and my thesis committee: Akis, Colin and Carrie. I'd like to thank my family: Mum, Dad, John, Thomas, Delphi and Bess for their perpetual support and love. And last but not least, the love of my life I met in my first year as a PhD student and whom I could not have come this far without, Andrew.

Contents

List of tables

List of figures

List of abbreviations

18-MEA: 18-methyleicosanoic acid

ADAM17: A disintegrin and metalloproteinase 17

ADULT: Acro–dermato–ungual–lacrimal–tooth

ANOVA: Analysis of variance

APS: Ammonium persulphate

BMAL1: Brain and muscle Arnt-like protein-1

BMP: Bone morphogenetic protein

BMPR1A: Bone morphogenetic protein receptor type IA

BRB+T: Block rinse buffer plus Tween 20

BSA: Bovine serum albumin

BSTFA: Bistrimethylsilyltrifluoroacetamide

CaTG: Calcium thioglycolate

CDC42: Cell division control protein 42 homolog

CHM: Chemical hair modification

CLEM: Correlative light and electron microscopy

CLSM: Confocal laser scanning microscopy

CMC: Cell membrane complex

CTAB: Cetyltrimethylammonium bromide

DAPI: 4',6-diamidino-2-phenylindole

DI: Deionised

DLX3: Distal-less homeobox 3

DMEM: Dulbecco's modified eagle medium

DMSO: Dimethyl sulfoxide

DNA: Deoxyribonucleic acid

DNase1L2: Deoxyribonuclease 1-like2

DSG4: Desmoglein 4

DTT: Dithiothreitol

ECL: Enhanced chemiluminescence

EDTA: Ethylenediaminetetraacetic acid

ELISA: Enzyme-linked immunosorbent assay

FAD: Flavin adenine dinucleotide

FBS: Fetal bovine serum

FeSEM: Field emission scanning electron microscope

FLIM: Fluorescence lifetime imaging microscopy

FOXC1: Forkhead box C1

FOXE1: Forkhead box E1

G/A: Gentamicin/amphotericin B

GAPDH: Glyceraldehyde 3-phosphate dehydrogenase

GC: Guanidine carbonate

GC/MS: Gas chromatography mass spectrometry

H&E: Haematoxylin and eosin

HEKn: Human epidermal keratinocytes, neonatal

hENT3: Human equilibrative nucleoside transporter 3

HKGS: Human keratinocyte growth factor

HRP: Horseradish peroxidase

HSP: Heat shock protein

IF: Immunofluorescence

IPA: Isopropyl alcohol

JNK: c-Jun N-terminal kinase

KAP: Keratin associated protein

KGF: Keratinocyte growth factor

KIF: Keratin intermediate filament

KTG: Potassium thioglycolate

LEKTI: Lympho-epithelial Kazal-type-related inhibitor

LIPH: Lipase member H

LPAR6: Lysophosphatidic acid receptor 6

M-phase: Mitotic phase

MAPK: Mitogen-activated protein kinase

MEKK1: Mitogen-activated protein kinase kinase kinase 1

MKK4/7: Mitogen-activated protein kinase kinases 4 and 7

MMP: Matrix metalloproteinase

NA: Numerical aperture

NADH: Nicotinamide adenine dinucleotide

OCT: Optimal cutting temperature compound

P&G: Procter and Gamble

PBS: Phosphate buffered saline

PFA: Paraformaldehyde

PLK1: Polo-like kinase 1

PMT: Photomultiplier tube

P/S: Penicillin/streptomycin

RI: Refractive index

RT-PCR: Reverse transcription polymerase chain reaction

S-phase: Synthesis phase

SD: Standard deviation

SDS: Sodium dodecyl sulphate

SEM: Scanning electron microscopy, also, standard error or the mean

SLS: Sodium lauryl sulphate

SMAD1: Mothers against decapentaplegic homolog 1

SPINK5: Serine protease inhibitor Kazal-type 5

TCS: True confocal scanner

TCSPC: Time-correlated single photon counting

TE: Trypsin-EDTA

TEM: Transmission electron microscopy

TEMED: N,N,N',N'-tetramethylethylenediamine

TFIIH: Transcription factor 2 human

TGFβ: Transforming growth factor beta

TIRF: Total internal reflection fluorescence

TN: Trypsin neutraliser

TP63: tumour protein 63

UV: Ultra-violet radiation

WB: Western blotting

Wnt: Wingless-type MMTV integration site family member

Chapter 1

Review of Literature

1.1. Introduction

Hair has long been an object of interest, for people interested in a wide range of fields from fashion, to hair care, to medicine, to forensics, to the use of other similarly structured fibres such as wool (Bost, 1993; Shimomura and Christiano, 2010; Plowman *et al*., 2012; Crawford and Hernandez, 2014; Kim *et al*., 2016). Hair is present all over the human body apart from the palms, soles and lips. It exists in different colours, lengths, thicknesses, cross-sectional shapes and textures (straightness or curliness) (De la Mettrie *et al*., 2007; Randall and Botchkareva, 2009; Buffoli *et al*., 2014). These variable characteristics enable hairs to perform different roles both in humans and other mammals. Hair is important to an individual as it provides protection, from scalp hair protecting against sunburn, to eyebrows and eyelashes protecting the eyes from dirt and sweat (Randall and Botchkareva, 2009; Trueb, 2015). Hair has a role in attractiveness as it is important in both sexual and social communication, as well as being an indicator of health (Randall and Botchkareva, 2009; Trueb, 2015). Society invests time and money in hair care, and disorders of the hair have a psychological impact (Girman *et al*., 1998). During puberty, vellus hairs transition to terminal hairs and signal sexual maturity. Hair also marks seniority, such as with male-pattern baldness or the silver-backed gorilla (Randall and Botchkareva, 2009;). Changes in hair colour can also occur seasonally in mammals for camouflage purposes, such as in the arctic hare, which transitions from brown or grey fur in the summer to white fur in the winter (Stoner *et al*., 2003). Hair has a role in the thermoregulation of mammals, and some species such as the polar bear have larger medullas in their hairs for insulation (Harrison and Davis, 1999). The hair follicle delivers sensory information and contains neuroreceptors such as in whiskers (Buffoli *et al*., 2014). Hair is present on almost all land-mammals and transitions through four stages of hair growth: anagen (growth phase), catagen (transition phase), telogen (resting phase) and exogen (shedding phase) (Higgins *et al*., 2009). In this study human head hair will be the focus and the hair is investigated both for pure scientific research into its structure and for the hair care industry and the effects of chemical depilatory treatments upon the hair.

The hair has been studied extensively in the twentieth and twenty-first centuries. With high resolution confocal microscopy and relatively new techniques such as fluorescence lifetime imaging microscopy, this study is the first to gather high resolution images

of the hair using label-free imaging. These techniques have led to new insights into hair structure and advancement in the understanding of the effect of commercial and novel chemical depilatories on the structure and morphology of human hair.

In this literature review the structure and function of hair, the hair follicle and hair cycle, hair cell differentiation, diseases affecting the hair, and confocal microscopy will be discussed. The structure of hair section explores the components of the cuticle, cortex and medulla in detail to provide a basis for what this study builds upon. The hair follicle cycle and drivers are inspected. An overview is given of factors which affect the differentiation of the hair shaft. The phenotypes expressed in hair by people with various diseases is discussed as it relates to the hair from the patient with an uncharacterised disease which is investigated in this study, and this discussion shows the scope of diagnostic potential with label-free confocal microscopy. Finally, the workings and applications of confocal microscopy and autofluorescence in hair are reviewed.

1.2. Hair structure

The human hair consists of three main compartments: the cuticle, the cortex, and the medulla (fig. 1.1). The cuticle gives the hair its proteinaceous and hydrophobic barrier against chemical, mechanical and thermal challenges (Robbins, 2012). The cortex is made up of spindle-shaped cells filled mostly with keratin intermediate filaments (KIFs), but also contains most of the melanin and makes up the main body of the hair fibre (Langbein and Schweizer, 2005). The medulla is only present in some hairs, and if present it runs through the centre of the hair and it may be thick or thin, continuous or fragmented (Wagner *et al*., 2007).

1.2.1. Keratin intermediate filaments

The formation of KIFs are shown in figure 1.2 and demonstrate that the basic unit of KIFs are monomers which comprise helical domains interrupted three times by nonhelical domains and terminate with the nonhelical nitrogen and carbon termini (Robbins, 2012). These monomers form coiled coil heterodimers with one type I acidic polypeptide dimerising with one type II neutral to basic polypeptide which vary in their amino acid sequences. There are eleven acidic and six basic monomer polypeptides (Langbein *et al*., 2007). Two dimers then coil together in a staggered anti-parallel array to form a

tetramer. These tetramers then assemble end-to-end to form protofilaments, which coil rope-like in bundles of eight to form KIFs (Crewther *et al*., 1983; Rafik *et al*., 2004). Inside the macrofibrils, there is more matrix than KIF (Menkart *et al*., 1966). Electron microscopy has been used to distinguish the darkly stained matrix with osmium tetroxide and the unstained KIFs revealing a heptad structure of intermediate filaments surrounded by matrix (Filshie and Rogers, 1964; Crewther *et al*., 1983). A summary of the type I and type II KIFs found in the cuticle, cortex and medulla of the hair shaft are shown in table 1.1.

Hair compartment	Type I	Type II
Cuticle	K32, K35, K39, K40	K82, K85
Cortex	K31, K33a, K33b, K34, K35, K36, K37, K38, K39	K81, K83, K85, K86
Medulla	K14, K16, K17, K19, K25, K27, K28, K31, K33a, K33b, K34, K36, K37, K38, K39	K5, K6, K7, K75, K80, K81, K83, K85, K86

Table 1.1. KIFs of the hair shaft. Type I and type II KIFs located in the cuticle, cortex and medulla of the fully differentiated hair shaft (Langbein *et al*., 2010).

1.2.2. Keratin associated proteins

Keratin associated proteins (KAPs) are near-spherical proteins which aggregate via disulphide bonds to form ellipsoidal proteins within the matrix of the hair cortex or in the cuticle (Suzuta *et al*., 2012). The KAPs interact with the KIFs through intermolecular forces and do not have a helical structure like the KIFs. In human hair an aggregate of approximately six KAPs form against one KIF (Suzuta and Arai, 2015). There are three main types of KAP in the hair: ultra-high sulphur KAPs, high sulphur KAPs, and high glycine-tyrosine KAPs. The four families of ultra-high sulphur KAPs contain at least 20% serine and 30% cystine, whereas the fourteen high sulphur KAP families contain only 20-30% cystine, and the seven high glycine-tyrosine KAPs comprise 35-60% glycine or tyrosine (Rogers *et al*., 2001; Matsunaga *et al*., 2013). High and ultra-high sulphur KAPs are likely to interact with the KIFs through disulphide bonds, though high glycine-tyrosine KAPs are more likely to interact with other proteins in the hair such as desmoplakin to provide mechanical strength (Matsunaga *et al*., 2013). The high glycine-tyrosine KAP8.1 has also been shown to bind to K85 (Matsunaga *et al*., 2013). In another

study the high-sulphur KAP11-1 has been shown to adhere to cortical and medullary keratins K31, K33 and K34 without the need for disulphide cross-links, though it is likely that disulphide bonds are still required for the stabilisation of the KIF-KAP complexes (Fujimoto *et al*., 2014). The amounts of different KIFs and KAPs vary between individuals, due to factors including genetics, age, or diet (Laatsch *et al*., 2014). A summary of the KAPs located within various hair shaft compartments are summarised in table 1.2.

Ultrastructural location	**KAP type**		
	High sulphur	**Ultra-high sulphur**	**High glycine-tyrosine**
Epicuticle		5, 10	
A-layer	12	4, 5.1, 10.1	
Exocuticle	1.1, 1.2, 1.3, 2.3, 3.2, 11.1, 12.1, 13.1, 13.2, 15.1, 16.6, 23.1, 24.1, 26.1	4.8, 4.12, 5.1, 5.5, 9.2, 9.8, 10.1	6.1, 7.1, 8.1, 19.1, 19.3, 19.4, 19.6, 21.2
Endocuticle	26		
Cortex matrix	1, 2, 3, 11.1, 13.2	4, 9	6, 7, 19.1, 19.2, 20.1

Table 1.2. KAPs of the cuticle and cortex. Location of KAPs within the fully differentiated hair shaft (Jenkins and Powell, 1994; Rogers *et al*., 2001; Shimomura *et al*., 2003; Rogers *et al.*, 2004; Rogers and Langbein, 2006; Bringans *et al*., 2007; Rogers *et al*., 2007; Rogers *et al*., 2008; Koehn *et al*., 2009; Rogers and Koike, 2009; Jones *et al.*, 2010; Fujikawa *et al*., 2012; Fujikawa *et al*., 2013).

1.2.3. The cuticle

The scalp hair cuticle consists of approximately five to ten layers of flattened cells which overlap circumferentially and longitudinally. Each cuticle cell is attached at the proximal end and the free edge is towards the distal end of the hair. The cells are approximately 0.3-0.5µm thick and the external visible length of each cell is approximately 5-10µm. This structure could help anchor the hair into the skin (Kiso *et al.,* 2009), and the overlapping cells may aid with the frictional removal of material, such as dirt, from the hair (Moncrieff, 1954). The cuticle is also the barrier to the cortex of the hair and the

multiple cuticle cell layers provide protection from weathering, especially ultra-violet (UV) damage, chemicals and torsional forces (Tate *et* al., 1993; Gamez-Garcia, 1999; Ruetsch *et al*., 2000; Harper and Kamath, 2007; Richena and Rezende, 2015). In addition, the cuticle aids in the retention of water within the hair, similar to the stratum corneum which provides a barrier in the epidermis (Serita *et al*., 2014).

The cuticle contains β-keratin sheets, rather than α-helical keratins, which bond with KAPs (Shimomura and Ito, 2005; Stanic *et al*., 2015). KAPs 5, 10, 12 and 17.1 are known to be present in the cuticle (Rogers *et al.,* 2006; Jones *et al.*, 2010). The highest expression of keratins in the cuticle are type I keratins K32 and K35, with lower expression of K39 and K40, and the highest expression of type II keratins are K82 and K85, with K82 specific to the cuticle (Langbein *et al*., 1999; Langbein *et al*., 2001).

A cuticle cell is comprised of several sublamellar structures: the outer β-layer at the surface of the hair, the epicuticle, the A-layer, the exocuticle, the endocuticle, and the cell membrane complex which is made up of the inner β-layer, δ-layer, and the outer β-layer once more as a new cell begins (fig. 1.3).

1.2.3.1. The cuticle cell membrane complex

The cell membrane complex (CMC) is present between the cuticle cells, cortical cells, and between the innermost cuticle cells and outermost cortical cells. The constituents of these three CMCs differ, though all are comprised of an inner β-layer, δ-layer, and the outer β-layer and contain non-keratinous proteins and lipids. In this section the cuticle CMC shall be discussed.

It was originally suggested that the epicuticle and the adjoining outer β-layer only covered the surface of the hair (Lindberg *et al*., 1948). To prove this incorrect, the Allworden reaction was performed on isolated cuticle cells which used chlorine water to diffuse into the cuticle cells and attack the thioester bonds to remove the lipids from the cuticle surface, and resulted in bubbles forming on the hair surface, which showed that the CMC is present in each cuticle cell (Allworden, 1916; Leeder and Bradbury, 1968).

The cuticle CMC is not made up of phospholipids as lipid bilayers are in living cells (Leeder *et al*., 1983). This mirrors the changes in the differentiation of the stratum corneum in the epidermis as the lipid bilayers are replaced by covalently attached ceramide lipids on surfaces of cornified envelopes comprising cross-linked proteins by

transglutaminase-1 and transglutaminase-3 (Rice and Green, 1977; Nemes and Steinert, 1999; Thibaut *et al*., 2009; John *et al*., 2012). Robbins showed that the covalently bound lipids of the outer β-layer and the inner β-layer exist as monolayers (Robbins, 2009).

The CMC β-layers are thought to be approximately 3nm thick (Swift, 1999; Kreplak *et al*., 2001b; Ohta *et al*., 2005; Robbins, 2012). The β-layers of the cuticle cells are mainly covalently bound lipids with some free lipids. The outer β-layer of the cuticle cell contains fatty acids, which gives it hydrophobic properties and a low friction surface (Scott and Robbins, 1980). The outer β-layer is sometimes called the fatty layer, or F-layer, because of the presence of 18-methyleicosanoic acid (18-MEA), which is bound through thioester linkages to the epicuticle (Jones and Rivett, 1997). Mammalian 18-MEA is unique to the hair cuticle, although bacteria are also able to synthesise 18-MEA (Jones and Rivett, 1997). Synthesis of 18-MEA requires the precursor amino acid, isoleucine, and a branched-chain 2-oxo acid dehydrogenase, an enzyme which sufferers of maple syrup urine disease do not possess (Jones and Rivett, 1997). Most of the other covalently bound fatty acids are in the inner β-layer (Jones *et al*., 1996; Harper, 1989), and include oleic (C18:1), stearic (C18:0) and palmitic (C16:0) acids (Robbins, 2012). The importance of the hair lipids to the integrity of the cuticle is highlighted by a deficiency in a palmitoyl-acyl transferase, which has been shown in mice to disrupt the hair cuticle and epidermal cornified envelopes, resulting in a poor ability to anchor the hair within the follicle (Liu *et al*., 2015).

By using isolated cuticle cells, all of the 18-MEA was shown to be located in the cuticle (Kalkbrenner *et al.,* 1990). To pinpoint the location of 18-MEA in the cuticle, hair from maple syrup urine disease sufferers, who are deficient in 18-MEA, was studied using transmission electron microscopy (TEM) and lipid analysis. This study showed that a structural defect was only present on the top of the cuticle cells in the outer β-layer, determining the location of 18-MEA to be in the outer β-layer (Jones *et al*., 1996). Of the covalently bound lipids in the outer β-layer, 41% are 18-MEA (Wertz and Downing, 1988). The thickness of 18-MEA in this layer is 2.28nm (Swift, 1999; Robbins, 2012), and it is present as a monolayer with 1nm spacing between molecules and covalently bound with a thioester linkage to an ultra-high sulphur protein, likely to be KAP 5 or 10, in the A-layer (Negri *et al*., 1993; Rogers and Koike, 2009). There is more 18-MEA towards the root of the hair, where there has been less damage to the cuticle and the least

hydrolysation of the fatty acid (Negri *et al.*, 1993). However, the outer β-layer can be removed by alcoholic alkali or chlorine water in acidic conditions to enhance dye uptake, without the loss of the structural integrity of the hair (Leeder and Rippon, 1985).

Through the use of atomic force microscopy, Swift and Smith found that the cuticle is not smooth. They discovered step discontinuities, called “ghosts”, on the surface of the cuticle, which outlined the original location of the overlying cell before its edge had been eroded away. There was also a difference in the longitudinal angular appearance of the surfaces about each ghost. This meant that the distal ends of the cuticle cells had been developed in the hair follicle to be thicker there than where the cells are adjacent to each other. Using the evidence for the ghosts, Swift and Smith could show that when the cuticle cell is eroded away, the fracture occurs between the outer β-layer and the δ-layer, leaving a new cuticle cell surface covered with 18-MEA (Swift and Smith, 2000).

The δ-layer of the CMC is 16nm thick and has been shown to contain desmoglein 4 and plakophilins 1 and 3. This is interesting as plakophilins are part of the intracellular plaque in desmosomes, and desmogleins are desmosomal cadherins, the transmembrane adhesion proteins to desmosomes. This suggests the δ-layer could be a desmosomal remnant (Swift and Smith, 2002; Alibardi *et al*., 2013). These proteins have also been found in the endocuticle along with other organelle remnants and between cortical cells (Alibardi *et al*., 2013).

1.2.3.2. The epicuticle

The epicuticle is one of the main uppermost barriers and it consists of approximately 75% protein and 25% lipid and is approximately 13nm thick (Negri *et al*., 1993; Swift and Smith, 2001). The epicuticle was removed from the hair by hot ethanol treatment and was shown to contain a fatty acid/protein complex consisting of protein (60-70%) with more lysine than cystine (12%), and fatty acids (20-30%) (Holmes, 1961). Of the protein present in the epicuticle, some are identified as KAPs 5 and 10 (Rogers and Koike, 2009).

Swift and Smith also found striations on the undamaged surface of the epicuticle after the removal of the outer β-layer. Where there was damage, the striations terminated at the ghost edge of the cell. These ridges were approximately 9nm in height, and were in parallel array, with a lateral repeat spacing of approximately 350nm. The evidence showed that the striations were formed on the outer surface of each cuticle cell after

contact with the inner root sheath in the hair follicle (Swift and Smith, 2000; Swift and Smith, 2002).

1.2.3.3. The A-layer

The A-layer is approximately 110nm thick and is located between the epicuticle and the exocuticle. It is the most densely cross-linked part of the hair comprised of the disulphide bonds in cystine and isopeptide groups between glutamine and lysine (Steinert and Marekov, 1997). The KAPs 4, 5, 10, 12 are present in the A-layer (Bringans *et al*., 2007; Rogers and Koike, 2009; Jones *et al.*, 2010). The isopeptide cross-links by transglutaminase-3 make the A-layer less susceptible to solubilisation by thioglycolate (Rice *et al*., 1994; Thibaut *et al*., 2009; Laatsch *et al*., 2014), and mirrors the cross-linking of proteins by transglutaminase-1 and transglutaminase-3 in the cornified envelopes of the stratum corneum (Rice and Green, 1977; Nemes and Steinert, 1999; Thibaut *et al*., 2009; John *et al*., 2012). The exocuticle and the A-layer form the stabilisation for the proteinaceous barrier, which is supported by their constituent ultra-high sulphur KAPs, making them more resistant to chemical reagents (Jones, 2001; Alibardi, 2016).

1.2.3.4. The exocuticle

The exocuticle has been shown to comprise approximately 20% cystine, 44% non-polar amino acids, 10% acidic amino acids and 7% basic amino acids, and has a high level of disulphide cross-linking (Bradbury and Ley, 1972; Swift and Bews, 1976; Swift, 1999). The exocuticle is known to contain KAPs 1.1, 1.2, 1.3, 2.3, 3.2, 4.8, 4.12, 5, 5.5, 6.1, 7.1, 8.1, 9.2, 9.8, 10, 11.1, 12.1, 13.1, 16.6, 19.3, 24.1 and 26.1 (Jenkins and Powell, 1994; Rogers *et al.*, 2004; Rogers *et al*., 2008; Koehn *et al*., 2009; Jones *et al.*, 2010; Fujikawa *et al*., 2013), though their bonding to KIFs K32, K35 and K85 are likely to be through disulphide bonds as the exocuticle is almost absent from isopeptide cross-links (Swift and Bews, 1976; Swift, 1999; Rogers *et al*., 2007). Its size varies within the cuticle cell with the varying size of the endocuticle, though on average it is 200nm thick (Swift, 1979; Swift, 1999).

1.2.3.5. The endocuticle

Beneath the exocuticle is the endocuticle, which by contrast has little or no sulphur-containing proteins. The size of the endocuticle varies with the exocuticle and is on average 175nm thick (Swift, 1999). The endocuticle contains a low quantity of cystine of approximately 3%, with few disulphide bonds and little isopeptide cross-linking, and

along with polar amino acid residues this makes the endocuticle susceptible to swelling from hydration (Swift and Bews, 1976). The nucleus and other organelles of the cell are also flattened inside the condensed cytoplasm (Birbeck and Mercer, 1957).

1.2.4. The cortex

The cortex makes up the majority of the mass of the hair and is comprised of spindle-shaped cortical cells which run longitudinally along the hair fibre. Apart from the keratin and melanin present within them, these cells are air-filled pockets also called cortical fusi (Choi *et al*., 2012). Cortical cells are 1-6µm in diameter and approximately 100µm in length. The cortical cells mainly consist of hard α-KIF organised into macrofibrils. The macrofibrils are semi-crystalline and are approximately 100-400nm in diameter, and the KIFs are 7.5nm in diameter (Bhushan, 2010).

The cortex is high in cystine, but not as high as in the cuticle. The cortex is richer in diacidic amino acids, lysine and histidine than the cuticle and there are more unsaturated fatty acids in the cortex than the cuticle (Takahashi and Yoshida, 2014).

Many different KAPs occur in the cortex, mostly KAPs 1, 2, 3, 4, 7, 9, 19.1, 19.2 (Rogers and Langbein, 2006). The KIFs present in the cortex are type I: K31, K33a, K33b, K34, K35, K36, K37, K38, K39 and type II: K81, K83, K85, K86 (Langbein *et al.*, 2010).

The cortex is attached to the cuticle through a process involving phagocytosis which results in interlocking structures between the cortex, CMC and the endocuticle (Piper, 1966). In addition, in the CMC between the cuticle and cortex there are steryl glycoside-like lipids containing N-acetylglucosamine which aid in the adhesion between the cuticle and cortex and provide flexibility to the hair shaft (Takahashi and Yoshida, 2014).

1.2.4.1. Macrofibrils

Cortical cells are made up of bunches of macrofibrils which are spindle-shaped. The macrofibrils themselves consist of KIFs in a matrix, otherwise known as the amorphous region of the hair (Randebrock, 1964).

The KIFs are connected by intercellular desmosomes to provide rigidity to the hair fibre (Bazzi and Christiano, 2007). The KIFs are low in cysteine (approximately 6%), whereas the amorphous matrix of the macrofibrils which contain the KAPs is high in cysteine (approximately 21%) (Bhushan, 2010). The cysteine residues in the end domains of the KIFs can form disulphide bonds with the KAPs in the matrix (Robbins, 2012). The KIFs are

rich in leucine, glutamic acid and amino acids normally found in the α-helical proteins, and lower in cystine, lysine and tyrosine (Leeder and Rippon, 1982). Keratins in the matrix are K32, K35 and K85. Type I keratins of the middle to upper cortex are K31, K33a, K33b, K34, K35, K36, K37, K38. Type II keratins of the cortex are K81, K83, K85, K86 (Langbein *et al*., 1999; Langbein *et al*., 2001). These KIFs have a common central helical rod (Jenkins and Powell, 1994), but differ in their amino and carboxyl domain sequence and size (Langbein and Schweitzer, 2005). The KIFs can form structures which are very anisotropic, giving hair its unique mechanical properties including being highly elastic and swelling with hydration (Fraser *et al*., 1976; Briki *et al*., 1998). Since the matrix contains the highest concentration of disulphide bonds in the cortex it has a high affinity to water and swells when wet (Suzuta and Arai, 2015).

In wool, the packing of the KIFs within the macrofibrils affects the shape of the fibre: KIFs in the paracortex are arranged laterally and are present in straight fibres, in the orthocortex the KIFs within macrofibrils are double-twisted as if around a central pole resulting in curliness, and the mesocortex is a mixture of both also found in wool (Plowman *et al*., 2007). The packing of KIFs within macrofibrils is less clear in human hair, as all KIFs appear double-twisted and the tilt-angles of KIFs within and between macrofibrils vary more than in wool (Harland *et al*., 2014). The alignment of the KIFs appears disordered in the cortex, except for close to the cuticle boundary where they are highly ordered (Stanic *et al*., 2015).

1.2.4.2. Cortical cell membrane complex

Like the cuticle, the cortex also has a CMC between the cells, although there are many differences between the cortical CMC and the cuticle CMC (Robbins, 2009). In the cortical CMC the outer β-layer and the inner β-layer are lipid bilayers, which are not covalently bonded, but are attached to the cortical cell membrane and the δ-layer by polar and ionic bonds, and are likely to be resistant to acids, alkalis, oxidation and reduction (Negri *et al.,* 1996; Robbins, 2009). The cortical CMC is mostly comprised of fatty acids, followed by cholesterol sulphate, and fewer ceramides and cholesterol (Robbins, 2012). The δ-layer of the cortical CMC is also different to the δ-layer of the cuticle CMC as it has five sub-layers consisting of different proteins to that of the cuticle CMC δ-layer (Robbins, 2009). There is a higher disulphide content in the cortical CMC δ-

layer than the cuticle CMC δ-layer (Nakamura *et al*., 1975), even though the cortical CMC also has less cystine than the cuticle CMC (Peters and Bradbury, 1972).

1.2.4.3. Organelle remnants

In the centre of some cortical cells, organelle remnants are present, with the long axis of the organelle parallel to the hair fibre. The specific identity of organelle remnants has raised disagreements. Some researchers believe they are remnants of the nucleus (Kelch *et al.,* 2000; Fischer *et al*., 2011; Szabo *et al*., 2012), while others think they are remnants of other organelles (Harland *et al*., 2011). Despite claims to these organelles being nucleic or otherwise, few papers have offered any evidence.

Nuclear remnants are the result of the breakdown of the chromatin in the nucleus by Deoxyribonuclease 1-like2 (DNase1L2) when the hair keratinocytes undergo terminal differentiation (Fischer *et al*., 2011), leaving the nuclear envelope intact. The number of nuclear remnants in the hair differs between individuals and even in the same individual (Szabo *et al*., 2012). However, no correlation was found between the frequency of nuclear remnants and hair colour, or with age of the individual (Szabo *et al*., 2012), although this may be an artefact created by an attenuation of signal by the melanin in the hair. Nuclear remnants were also found to be present in a range of body hairs (Szabo *et al*., 2012).

Organelle remnants can also be found in the endocuticle, such as nuclear remnants which appear disk-shaped (Kassenbeck, 1981). Other organelle remnants in the cortex may be melanosomes, as some organelle remnants contain melanin granules which would not be expected within nuclear remnants. Melanosomes are transferred to immature cortical cells (Kinebuchi *et al*., 1971) and not all may be completely degraded.

1.2.4.4. Melanin

The only difference in morphology between different coloured hairs is the change in the type or the amount of melanin present. Pheomelanin is predominant in red and blond hair, whereas eumelanin is predominant in brown and black hair, and the ratios and quantities vary to produce a wide range of hair colours (Ito *et al*., 2000; Ito and Wakamutsu, 2003; Ehlers *et al*, 2007). Eumelanin and pheomelanin are both derived from the common precursor dopaquinone which is formed by tyrosinase from tyrosine. Pheomelanin is formed by the addition of cysteine to dopaquinone to form monomers which are further oxidised to produce heterogeneous polymers. Whereas in eumelanin,

production of the dopaquinone cyclises to cyclodopa and redox reactions with dopaquinone produce dopachrome which is converted to 5,6-dihydroxyindole and after oxidation results in the heterogeneous polymer eumelanin (Nezirevic *et al.*, 2007). Melanin forms in granules 0.8-1.0μm x 0.3-0.4μm with the long axis parallel to the hair fibre (Ulrich *et al*., 2004; Choi *et al*., 2012). It is situated between the closely packed keratin filaments in the cortex, and is present in smaller amounts in the cuticle and the medulla (Hallegot *et al*., 2004).

Melanin possesses a broad and continuously decreasing absorption spectrum between the near-UV and near-infrared region (Dimitrow *et al*., 2009). Eumelanin has a photo-protective effect on the proteins in the hair (Hoting and Zimmerman, 1997), as eumelanin is known to absorb UV light, unlike pheomelanin (Thody *et al*., 1991; Brenner and Hearing, 2008).

In addition, lipids have been found to be associated with melanin granules, such as ceramides, and the oxidative metabolites of α-linolenic acid are bound to melanin lipids non-covalently (Takahashi and Yoshida, 2014).

1.2.5. The medulla

Relative to the hair cuticle and cortex, few studies have been carried out on the human hair medulla, and even fewer on scalp hair medulla. The medulla consists of a column of loosely packed spherical cells present in the centre of some hair fibres, has large vacuoles, and is separated from the cortex by a material similar to a CMC (Clement *et al*., 1981).

Previously, it was thought that human hair medulla was either continuous or fragmental (Clement *et al*., 1981), but more recently TEM was used to propose that there are only thick and thin medulla, if a medulla is present, and that they differ morphologically (Wagner *et al*., 2007). The thin medulla has smaller dimensions, a distinct interface with the cortex, and higher contrast than the thick medulla (Wagner *et al*., 2007). The thick medulla has larger cavities, more globular structures, and a gradual organisation of cells towards the border with the cortex (Wagner *et al*., 2007). The medulla may also be divided or duplicated, though this appeared to be more common in beard hair than scalp hair. Thick hairs are more likely to possess a medulla, and the thicker the hair, the wider and more continuous the medulla is likely to be (Das-Chaudhuri and Chopra, 1984;

Banerjee, 1962; Hardy, 1973; Baque *et al*., 2012). Also, the thicker the hair, the faster the rate of growth of the hair (Baque *et al*., 2012).

Scanning electron microscopy (SEM) was used to observe that there are three subunits within the medulla: unorganised cortical cells, globular structures and a smooth covering layer (Wagner *et al*., 2007). Although another study states that the cortical cells in the medulla are vertically orientated (Langbein *et al*., 2010). Wagner *et al*. put forward that the medulla resembles an unshaped cortex (Wagner *et al*., 2007).

The medullary cells are different to the cells in the cuticle and cortex because medullary cells only contain traces of cysteine, instead medullary cells are rich in glutamic acid and citrulline (Clement *et al*., 1981). The low amount of cysteine indicates that the medulla does not have many high-sulphur KAPs. Unlike in the cuticle, involucrin is expressed in the medulla. Involucrin was located in the CMC of the medulla, and more weakly in the CMC of the cortical cells closest to the medulla. In the epidermis, involucrin is a constituent scaffolding protein covalently bonded to the cornified envelope (Steinert and Marekov, 1997; Marekov and Steinert, 1998; Steinert and Marekov, 1999; Sevilla *et al*., 2007). Trichohyalin, KAPs and involucrin mechanically strengthen the medullary cells (Alibardi, 2012). Hardening of the cells of the medulla may also occur through keratinisation (Langbein *et al*., 2010). The medullas of Caucasian hair also have a higher lipid content and lower protein content than the rest of the hair, although this is not true for Afro-American hair (Kreplak *et al*., 2001a), and no data has been collected for Chinese hair.

Wagner *et al*. also used TEM to observe that the medulla contains KIFs (Wagner *et al*., 2007). The medulla is insoluble and hard to isolate. It expresses 12 hair keratins and 12 epithelial keratins (type I keratins: K14, K16, K17, K19, K25, K27, K28, K31, K33a, K33b, K34, K36, K37, K38, K39, type II keratins: K5, K6, K7, K75, K80, K81, K83, K85, K86) (Langbein *et al*., 2010). This study led to the confirmation that cortical cells are present in the beard hair medulla (Langbein *et al*., 2010). The medulla was found to contain cells with an appearance of those in the cortex and expressing cortical keratins, and were named medullary cortex cells (Langbein *et al*., 2010). The only keratin expressed in the medulla which is not also expressed in the cortex of beard hairs was K37. A keratin specific to the cortex but also found in the medullary cortex cells was K38 (Langbein *et al*., 1999). However, K37 was only found in beard hair medullas, not in the medullas of

scalp hairs, though with the supply of dihydrotestosterone the androgen-insensitive scalp hair was able to express K37 (Yoshida *et al*., 2013). Cortical cells were observed intersected into the beard hair medulla, and it may be that the medullary cortex cells stem from these cells (Langbein *et al*., 2010). The cortical keratins K31, K34, K38, K81 and K85 also expressed in the medulla are expressed at the same time in the cortex and medulla of the developing hair shaft (Yoshida *et al*., 2013). These studies suggest that the medullary cortex cells are true cortical cells (Langbein *et al*., 2010).

The medulla does not play a large role in hair strength or chemistry so is of greater importance to forensics than the hair care industry (Menkart *et al*., 1966), as there are significant differences in the structure of the medulla between animal species (Farag *et al*., 2015). Whether the medulla is continuous or fragmental can also be used to distinguish between human ethnic origins (Nataraja and Roy, 2015). The medulla may be useful in future medical diagnostic tests as one study suggests it may reflect the calcium content of the blood from its supply in the hair follicle (Ito *et al*., 2016).

1.3. The hair follicle cycle

The hair follicle (fig. 1.4) produces the hair shaft, which has many functions as described in the introduction. The hair follicle is an important part of skin physiology and architecture. It hosts stem cells (Tiede *et al*., 2007), which can repair wounds (Gharzi *et al*., 2003; Lau *et al*., 2009), and it has an ability to induce angiogenesis (Mecklenburg *et al*., 2000) and nerve growth (Botchkarev *et al*., 2004). The hair follicle is immune privileged, and the collapse of this can lead to diseases such as cicatricial alopecia (Harries *et al*., 2013). The hair follicle cycle (fig. 1.5) demonstrates its regenerative capability and allows for the growth of new hairs, perhaps with different characteristics to the previous hairs. The ability to produce hairs of varying characteristics shows the hair follicle is adaptive and responsive. The hair follicle is able to respond to seasonal changes, age and hormones, (Randall and Botchkareva, 2009; Patel *et al*., 2015; Contreras-Jurado *et al*., 2015).

The hair follicle is a complex dynamic structure which cycles through four stages: growth and hair shaft production (anagen), apoptosis-driven hair follicle regression (catagen), relative quiescence (telogen), and hair shedding (exogen) (Higgins *et al*., 2009). The permanent parts of the follicle containing stem cell populations are the isthmus, bulge

and infundibulum (fig. 1.4). The infundibulum extends from the epidermis to the opening of the sebaceous gland, and the isthmus extends from here to the bulge in the outer root sheath (fig. 1.4), which is also at the insertion point of the arrector pilli muscle. Below the bulge is the lower portion of the hair follicle and is the area which undergoes cycled remodelling (fig. 1.4). The hair bulb contains proliferating keratinocytes, differentiated melanocytes, the matrix and the follicular dermal papilla. The line of Auber extends across the widest part of the bulb and separates the upper region of cells which become differentiated to form the hair shaft and the inner root sheath, and the lower region of undifferentiated mitotically active cells (Auber, 1952). The mesenchymal follicluar papilla encases dermal papilla cells, mesenchymal-derived cells, nerve cells, a capillary and mucopolysaccaride stroma in a basement membrane (Nutbrown and Randall, 1995). The dermal sheath is derived from mesenchymal cells and along with the follicular papilla conducts the differentiation and growth of the underlying epithelial cells. The dermal sheath comprises an outer connective tissue sheath and an inner glassy membrane. The hair shaft extends through the epidermis, the dermis and towards the dermal white adipose tissue. Surrounding the hair shaft is the inner root sheath, which consists of a single layer of cuticle cells, the Huxley's layer and the Henle's layer (fig. 1.4). The cuticle cells of the inner root sheath interlock with those of the cuticle and move upwards together with hair growth and anchor the hair in the follicle (fig. 1.4) (Randall and Botchkareva, 2009). Between the inner root sheath and the dermal sheath is the outer root sheath (fig. 1.4). There is a companion layer between the inner root sheath and the outer root sheath, which is thought to provide the slippage plane between the two sheaths (Poblet *et al*., 2005).

The hair follicle cycle depends upon the epithelial hair follicle stem cells, whose niche is the bulge, and its regulation includes the transcription factor Forkhead box C1 (FOXC1), which if ablated results in stem cell activation, shortened hair cycles, and weakened cellular junctions resulting in hair loss (Lay *et al*., 2016). FOXC1 also activates bone morphogenetic protein (BMP) and nuclear factor of activated T cell c1 signalling to promote quiescence (Wang *et al*., 2016). The bulge is in the outer root sheath and at the insertion point of the arrector pili muscle, and the hair follicle below the bulge is remodelled during cycling (fig. 1.4). Stem cells from the bulge migrate down to the bulb, where they differentiate into cells of the outer root sheath, inner root sheath and hair shaft. These progenitor cells can then migrate to the hair germ, differentiate into matrix

cells and contribute to the anagen stage of building the hair shaft (Panteleyev *et al*., 2001; Tumbar *et al*., 2004). The different populations of cells within the hair follicle operate a complex web of signalling interactions, of which the dermal papilla may be the most heavily involved as it expresses the highest number of ligands and receptors (Rezza *et al*., 2016). The knowledge of human hair cycling is incomplete as most of the data is based on murine follicles which differ to human follicle cycling (Oh et al., 2016).

There are six stages to the anagen phase of hair growth. There is continuous cross-talk between the secondary hair germ and the dermal papilla, so once the secondary hair germ cells activate wingless-type MMTV integration site family member (Wnt) signalling and the threshold is passed in combination with BMP inhibition, the keratinocytes in the lower region of the telogen follicle begin to proliferate vigorously and this marks the start of anagen (Panteleyev *et al*., 2001; Greco *et al*., 2009). Before the onset of anagen the dermal papilla expresses R-spondin1 which activates Wnt signalling in the bulge cells. This signalling has the potential to change the cycle phase as exogenous recombinant R-spondin1 introduced in telogen leads to anagen entry (Li *et al*., 2016). R-spondin2 can also be used to prolong the anagen phase through Wnt signalling (Smith *et al*., 2016). At the commencement of anagen the interfollicular epidermal and adipocyte progenitor cells proliferate, and along with angiogenesis and nerve neogenesis this results in an increased mass of dermal and subcutaneous fat (Donati *et al*., 2014; Driskell *et al*., 2014). This may be caused by the keratinocytes of the outer root sheath producing vascular endothelial growth factor (Yano *et al*., 2001), and is supported by the suppression of angiogenesis resulting in less hair growth (Ahluwalia *et al*., 2000). These adipocyte precursor cells produce platelet derived growth factor which acts on the dermal papilla and is necessary for anagen onset (Festa *et al*., 2011). The anagen follicle contains the matrix which is made up of transit amplifying keratinocytes and surrounds the follicular papilla. The proliferating matrix cells engulf the changing follicular papilla (fig. 1.5 anagen II) and differentiate into the hair shaft and inner root sheath as the bulb grows downwards into the skin (fig. 1.5 anagen III). This produces the upward flow of differentiating epithelial cells. In mid-anagen the melanocytes line the follicular papilla, which has changed shape to become long and narrow, and begin melanogenesis (fig. 1.5 anagen IV). At this stage the follicle has attained its maximum length and the ascending hair shaft and inner root sheath are encased by the outer root sheath (fig. 1.5 anagen IV). Next, the tip of the hair breaks through the inner root sheath.

The proliferative potential of the cells of the matrix determines the length of anagen (Blanpain and Fuchs, 2006). Epidermal growth factor stimulates Survivin and Msx2 which are mediated by the Notch signalling pathway and are related to the proliferation of the dermal papilla (Zhang *et al*., 2016). The upregulation of the epidermal growth factor receptor can in turn supress mitotic regulators and induce catagen (Bichsel *et al*., 2016). The extracellular matrix also has a role in the hair follicle cycle (Larson *et al*., 2012). The extracellular matrix is regulated by matrix metalloproteinases (MMPs) and their inhibitors, and the expression of MMP-2 and MMP-9 are raised in anagen and lowered in catagen and telogen (Hou *et al*., 2016). By late-anagen the hair bulb has encased the follicular papilla and the hair is fully formed (fig. 1.5 anagen VI), stretching from the subcutis to the skin surface (Paus and Cotsarelis, 1999; Muller-Rover *et al*., 2001). The ascension of the new hair to the skin surface may cause exogen, where the original hair is shed from the hair follicle (fig. 1.5 anagen IV). Signalling occurs during anagen between the keratinocytes of the matrix and the fibroblasts of the dermal papilla. The matrix cells express the receptors and signalling components for β-catenin/Lef-1, c-kit, c-met, fibroblast growth factor receptor 2, insulin-like growth factor 1 receptor, and the dermal papilla cells express the corresponding ligands: Wnt5a, stem cell factor, hepatocyte growth factor, fibroblast growth factor 7, insulin-like growth factor-1 (Paus and Cotsarelis, 1999; Botchkarev and Kishimoto, 2003; Randall and Botchkareva, 2009). The circadian clock is involved in the transition from the anagen to catagen phase. Peripheral core clock genes Period1 and brain and muscle Arnt-like protein-1 (BMAL1) have been shown to increase expression and produce signals to terminate anagen, and silencing of these genes prolongs anagen. BMAL1 is connected to cell cycle control (Geyfman *et al*., 2012), which may be how it modulates the hair cycle. The mechanism of Period1 and BMAL1 action is unknown, although c-Myc and p21, hair cycle and cell cycle regulatory genes, are reduced by Period1 knockdown and BMAL1 knockout mice have reduced p21 expression. The authors hypothesised that Period1 and BMAL1 control the hair cycle clock by the regulation of cellular proliferation and apoptosis (Al-Nuaimi *et al*., 2014).

During catagen the fully keratinised club hair regresses towards the skin surface driven by apoptosis (fig. 1.5 catagen). Catagen consists of eight stages (Muller-Rover *et al*., 2001). At the start of catagen, proliferation and differentiation of the keratinocytes of the hair matrix diminishes, as does melanogenesis, and the progenitor cell niches reduce in size (Randall and Botchkareva, 2009). The bulb reduces in size, as does the follicular

papilla, and the matrix and lower outer root sheath keratinocytes undergo apoptosis (fig. 1.5 catagen III & VII). The follicular papilla becomes quiescent and regresses with the lower epithelial regions until it reaches the lower part of the permanent hair follicle to remain in contact with the secondary hair germ and the bulge (Randall and Botchkareva, 2009). The club hair is formed (fig. 1.5 catagen VII) by interdigitation and keratinisation of the pronged rootlets of the trichilemmal keratin layer of the hair club fibre, which attaches to the outer root sheath companion layer to anchor the club hair securely in the follicle. At this point the hair follicle can be up to 70% shorter in length (Randall and Botchkareva, 2009). Apoptosis is the primary driving force of catagen, and most cells within the follicle are susceptible to apoptosis. However, some cells within the follicle are more resistant, such as the fibroblasts of the dermal papilla and the majority of stem cell keratinocytes and melanocytes which are required for the survival of the hair follicle (Seiberg *et al.*, 1995; Lindner *et al*., 1997; Botchkareva *et al*., 2006). The onset of catagen requires Grb2-associated binder1, which is a scaffold protein and acts via mitogen-activated protein kinase (MAPK) signalling, and also allows the establishment of bulge cells and maintains their quiescence at catagen onset (Ozturk *et al*., 2016). The keratinocytes of the hair matrix are affected by the pro-apoptotic p53 expression, especially once the growth factor from the dermal papilla has been withdrawn (Botchkareva *et al*., 2001). The hair matrix and outer root sheath keratinocytes are further affected by the withdrawal of the apoptosis inhibitor Survivin expression with catagen (Botchkareva *et al*., 2007). In addition to the reduction of Survivin expression, the keratinocytes of the outer root sheath also secrete more catagen inducing molecules (Randall and Botchkareva, 2009). One such molecule is the fibroblast growth factor-5 where gene knockout studies produced mice with 50% longer hair than the wild-type (Hebert *et al*., 1994). The outer root sheath contains receptors for neurotrophin, which is involved in the apoptotic pathway, and overexpression of brain-derived neurotrophic factor and neurotrophin-3 in the follicle leads to early catagen onset (Botchkarev *et al*., 2004). Expression of transforming growth factor (TGF)-β1 and TGF-β2 also play a role in catagen onset (Foitzik *et al*., 2000; Tsuji *et al*., 2003).

At the transition of catagen to telogen the fully keratinised hair club fibre is bound by a complex of keratinocytes of the outer root sheath at the base of the bulge (fig. 1.5) (Higgins *et al*., 2009; Hsu *et al*., 2011). At this stage and into telogen the follicular papilla becomes condensed into a sphere close to the base of the secondary hair germ, which

is flattened (fig. 1.5) (Muller-Rover *et al*., 2001). The telogen hair follicle is the smallest in length, there are no melanocytes present and the club hair is not surrounded by an inner root sheath (fig. 1.5). The main function of telogen is to maintain the hair club. Telogen is energy efficient which is important in seasonal mammalian coats as little energy is expired (Geyfman *et al*., 2015), whereas the mosaic approach in human scalp hair is much less energy efficient as 80-90% of the follicles are in the anagen stage simultaneously (Paus and Cotsarelis, 1999). Telogen is also the phase of the follicle cycle in which the hair is the most sensitive and so provides a heightened sensitivity to environmental stimuli, from inflammation to plucking and results in the onset of anagen (Geyfman *et al*., 2015). Circadian clock regulation, innate immunity and cholesterol metabolic processes are the most highly upregulated functions in telogen phase of the hair follicle (Geyfman *et al*., 2011). The circadian clock genes are most highly expressed in the secondary hair germ (Lin *et al*., 2009). There is also high and low expression in the bulge with low expression of TGFβ and high expression of Wnt creating a heterogeneous population which will either contribute to the next anagen phase or wait for a future cycle (Janich *et al*., 2011). Although not proliferative, the progenitor cells of the telogen phase follicle are not inactive, as signalling of BMP4, BMP6 and fibroblast growth factor-18 continues to keep the cells in an undifferentiated state (Woo and Oro, 2011), and quiescence is also ensured epigenetically through methylation of genes (Lien *et al*., 2011). Inhibition of BMP increases methylation whereas the addition of BMP4 reduces histone methylases and increases demethylases (Lee *et al*., 2016). In late telogen the dermal papilla cells begin Wnt signalling and production of fibroblast growth factor-7/10 ligands (Greco *et al*., 2009; Enshell-Seijffers *et al*., 2010), and the Sonic hedgehog pathway is activated to induce anagen (Sato *et al*., 1999). Also in late telogen, some bulge cells migrate to the secondary hair germ to aid its expansion before cell division (Zhang *et al*., 2009). Forkhead box i3 is a recently discovered secondary hair germ marker which when deleted results in poor hair follicle regeneration and the progressive depletion of the secondary hair germ stem cells (Shirokova *et al*., 2016). During telogen the secondary hair germ responds to signals from the dermal papilla. The epithelial progenitor cells located in the secondary hair germ begin proliferation at the end of the telogen phase and mark the start of anagen phase (Panteleyev *et al*., 2001; Rompolas *et al*., 2013).

The shedding phase, exogen, occurs independently of the other cycle phases (Stenn *et al*., 2005; Higgins *et al*., 2009). Exogen was previously thought to be caused by the upwards growth of a new hair fibre, whereas now the club fibre is believed to be attached with the hair follicle (Higgins *et al*., 2009). The pronged rootlets of the trichilemmal keratin layer of the hair club fibre attaches into the outer root sheath companion layer from catagen through to telogen (Higgins *et al*., 2009). Upregulation of proteases and a downregulation of protease inhibitors was found in late exogen, and may play a role in the degradation of the desmosomes connecting the trichilemmal keratin layer to the companion layer (Higgins *et al*., 2011; Bhogal *et al*., 2014). The release of the club hair has also been shown to be modulated by the type 3 isoform of the inositol 1,4,5-trisphosphate/nuclear factor of activated T cell-dependent signalling, possibly by the regulation of keratin 6 in the keratinocytes of the bulge cells which attach to the club hair fibre (Sato-Miyaoka *et al*., 2012). Unlike plucked hairs, exogen club hairs do not retain any of the outer root sheath (fig. 1.5) (Van Neste *et al*., 2007).

1.4. Hair cell differentiation

Hair cell differentiation occurs during anagen to produce a new hair fibre. The matrix is located at the proximal base of fully grown anagen hairs and contains most of the proliferating hair follicle keratinocytes (Oh *et al*., 2016). These cells of the precortical hair matrix terminally differentiate to form the cells of the hair shaft (Langbein and Schweizer, 2005). Several molecules have important roles in the differentiation of keratinocytes to form the hair shaft, including BMP, Wnt and Notch signalling (Lee and Tumbar, 2012). Wnt3 and Wnt10a/b expressed by the matrix and precortical keratinocytes act through signalling cascades to Lef1 (DasGupta and Fuchs, 1999; Reddy *et al*., 2001). The matrix, hair shaft precursors and inner root sheath lineages express many BMP ligands and receptors that stop proliferation of the transit amplifying cells and promote terminal differentiation. In the matrix Bmpr1a/b and Bmpr2 are expressed with Bmp2/4 and Bmp7/8 expressed in the hair shaft precursors and inner root sheath lineages respectively (Rendl *et al*., 2005). A balance of BMP is required in the bulge as ablation of BMP causes keratinocyte proliferation whereas BMP signalling promotes hair follicle differentiation (Kobielak *et al*., 2007). The local and temporal balance of BMP signalling during anagen determines the fate of the hair shaft, inner root sheath and transit amplifying cells (Genander *et al*., 2014). Bulge cells deficient in Notch have been

demonstrated to cause aberrant hair shafts due to defective terminal differentiation (Demehri and Kopan, 2009). In addition, inactive rhomboid proteins 1 and 2 play a role in hair shaft differentiation as mutations in these rhomboid intramembrane serine proteases lead to faulty activation of Notch1 which is associated with downregulation of Lef1 in the matrix, and leads to abnormal hair shaft differentiation (Yang *et al*., 2014).

Hair shaft assembly has been found to be modulated by *miR-22*, a microRNA which represses transcription factors of keratinocyte differentiation and hair shaft formation, and promotes the transition from the anagen to catagen phases (Yuan *et al*., 2015). Laminin γ1, a basement membrane protein, also affects hair shaft differentiation through the regulation of BMP which acts upstream of transcription factors for KIFs and KAPs (Fleger-Weckmann *et al*., 2016). The differentiation of the medulla is affected by *Soat1*, which regulates intercellular cholesterol homeostasis (Lu *et al*., 2011), and is itself a regulatory target for the transcriptional regulator, homeobox C13 (Potter *et al*., 2015).

The isthmus and infundibulum (fig. 1.4) contribute to wound healing through epidermal differentiation and to sebaceous gland formation, but not to hair growth during anagen (Jensen *et* al., 2009; Page *et al*., 2013). However, the deletion of the hair formation and regeneration transcriptional regulator distal-less homeobox 3 (DLX3) only in the isthmus and infundibulum, and not in the bulge or matrix, resulted in deformation of the cuticle. The study suggests hair shaft differentiation begins in the matrix and as the keratinocytes move upwards towards the epidermal surface, the keratinocytes of the isthmus and infundibulum express DLX3 regulated signals to the differentiating hair shaft and influence its formation (Kim *et al*., 2015).

In the approximate lower third of the hair follicle lies the keratinisation zone, where KIFs and KAPs are assembled in a temporal and spatial order. First the KIFs are formed, followed by expression of the high tyrosine-glycine KAPs and then the cysteine-based KAPs (Langbein *et al*., 2001). During terminal differentiation in the keratinisation zone the type I and type II keratin polypeptides compete due to differing expression of keratins in different areas of the cuticle and cortex. This leads to the cuticle containing six keratins and the cortex containing up to thirteen keratins (Langbein *et al*., 2007). The high-sulphur KIFs and KAPs associated with the cuticle and cortex are likely to be oxidised by sulfhydryl oxidase during the differentiation of the cells (Alibardi, 2016). Evidence suggests that the desmosomes, gap- and tight-junctions formed between the

keratinocytes of the hair shaft become part of the CMC during keratinisation (Swift and Smith, 2002; Alibardi *et al*., 2013). In the late stages of keratinisation, water is lost from the hair shaft (Gillespie, 1991).

It has been postulated that some of the keratinocytes in the precortical hair matrix may undergo endoreplication whilst terminally differentiating into the cortex and medulla, in the same manner which epidermal keratinocytes may carry out endoreplication during terminal differentiation (Zanet *et al*., 2010; Gandarillas and Freije, 2014; Edgar *et al*., 2014).

Melanocytes migrate from their stem cell niche in the bulge, differentiate whilst in the outer root sheath, and once fully differentiated the melanocytes are located in the hair matrix where they transfer melanin to the precortex for incorporation into the hair shaft (Tobin *et al*., 1999; Botchkareva *et al*., 2001; Nishimura *et al*., 2002; Osawa *et al*., 2006).

1.5. Hair phenotypes in disease

Some diseases affect the structure and morphology of hair. Some hairs do not have obvious defects when observed using basic light microscopy, but this is where confocal microscopy or fluorescence lifetime imaging microscopy may be of diagnostic value and has not yet been exploited. Observations of the hair could be made utilising label-free autofluorescence to visualise details within the hair structure and fluorescence lifetime imaging to detect differences in the chemical environment of the hair compared to healthy hair.

Focussing on hair which has defects in the hair fibre itself, there are many diseases which affect the structure of the hair shaft. Some diseases cause the hair to become rough, such as maple syrup urine disease which has a mutated branched-chain 2-oxo acid dehydrogenase complex, leading to the absence of 18-MEA on the cuticle cell CMC (Smith and Swift, 2005). Other diseases cause the hair to become coarse, sparse and wiry, such as hypotrichosis 4 otherwise known as Marie Unna hereditary hypotrichosis, which has that phenotype during childhood but leads to progressive hair loss at puberty, and is caused by mutations in the HR gene, the human homolog of the murine gene hairless. (Wen *et al*. 2009). Another disease which causes coarse, sparse, and wiry hair is ankyloblepharon-ectodermal defects-cleft lip/palate syndrome, which has mutations in the transcription factor, tumour protein 63 (TP63) (McGrath *et al*., 2001). A disease

also with mutations in TP63 and causing sparse, thin hair is acro–dermato–ungual–lacrimal–tooth (ADULT) syndrome (Amiel *et al*., 2001).

There are several diseases which cause fine and tightly curled hair. Some of these diseases have mutations in keratin genes, such as autosomal dominant woolly hair which has mutations in the K71 and K74 genes, encoding keratins expressed in the inner root sheath (Shimomura *et al.*, 2010; *Fujimoto et al*., 2012). Hypotrichosis 3 also has mutations in the K74 gene causing woolly hair and alopecia (Wasif *et al*., 2011). Many diseases with a similar phenotype have mutations in desmoplakin, including the disease cardiomyopathy, dilated, with woolly hair and keratoderma (Norgett *et al*., 2000), skin fragility-woolly hair syndrome (Whittock *et al*., 2002), and Carvajal syndrome (Nehme *et al*., 2012). Plakoglobin mutations lead to Naxos disease resulting in curly, woolly hair (McKoy *et al*., 2000), and plakophilin mutations result in short, sparse hair with ectodermal dysplasia skin fragility syndrome (McGrath *et al*., 1997). Hypotrichosis 7 and 8 have mutations in the lipase member H (LIPH) and lysophosphatidic acid receptor 6 (LPAR6) genes respectively, but both present with sparse, fine and tightly curled hair (Kazantseva *et al*., 2006; Pasternack *et al*., 2008; Shimomura *et al*., 2008). Hypotrichosis 7 has also been shown to harbour a missense mutation in keratin 25, which is expressed in the medulla and the inner root sheath, and HaCaT studies showed a deleterious effect upon KIF formation (Zernov *et al*., 2016). Trichodentoosseous syndrome is caused by an autosomal dominant mutation in the DLX3 gene, encoding for a homeodomain transcription factor expressed in the hair matrix and most layers of the hair follicle and leads to kinky hair (Hwang *et al*., 2008). The length and width of hair can change due to disease and cause hypertrichosis. One such disease is histiocytosis-lymphadenopathy plus syndrome, which has autosomal recessive mutations in the SLC29A3 gene encoding human equilibrative nucleoside transporter 3 (hENT3) (Molho *et al*., 2008).

Many diseases cause hair to become brittle, such as ectodermal dysplasia 4, hair/nail type, where there is a mutation in the hair matrix and cuticle keratin gene KRTHB5, a subfamily of K85, causing extreme brittleness and hair loss (Naeem *et al.,* 2006). Photosensitive and nonphotosensitive trichothiodystrophy cause brittle hair but are caused by different mutations. Photosensitive trichothiodystrophy has autosomal recessive mutations in ERCC2, ERCC3, and GTF2H5, which encode subunits of the basal transcription factor 2 human (TFIIH), resulting in sulphur deficiency (Takayama *et al*.,

1996; Weeda *et al*., 1997; Giglia *et al*., 2004), whereas nonphotosensitive trichothiodystrophy has mutations in the MPLKIP gene, encoding M-phase specific polo-like kinase 1 (PLK1) interacting protein which is involved in the control of cell cycle integrity (Nakabayashi *et al*., 2005). Ichthyosis with hypotrichosis, autosomal recessive causes hair to become brittle, curly and sparse and results from mutations in the ST14 gene encoding matriptase, a type II transmembrane serine protease (Basel *et al*., 2007). Brittleness can cause hair to become short as breakages easily occur. Athyroidal hypothyroidism with spiky hair and cleft palate, as noted in the name causes hair to appear spiky from mutations in the forkhead box E1 (FOXE1) gene (Clifton *et al*., 1998). Neonatal inflammatory skin and bowel disease also causes brittle, short hair from mutations in the a disintegrin and metalloproteinase 17 (ADAM17) gene encoding a disintegrase/metalloprotease (Blaydon *et al*., 2011).

Another phenotype of hair in disease is that of twisted and flattened hair, known as pili torti. Menkes is one such disease which is caused by mutations in the ATP7A gene, encoding an ATP-dependent copper transporter (Chelly *et al*., 1993; Mercer *et al*., 1993; Vulpe *et al*., 1993). Pili torti with fine, sparse hair can be a sign of mitochondrial disease where the hair is affected by a defective cellular energy supply (Silengo *et al*., 2003). Rapp-Hodgkin syndrome hair has a similar phenotype but is caused by mutations in the transcription factor TP63 (Kantaputra *et al*., 2003). Other diseases which cause pili torti of the hair include pachyonychia congenita type 2 and Bjornstad syndrome. The former is caused by deletion and missense mutations in the KRT17A gene (Smith *et al*., 2001) which is expressed in the outer root sheath of the hair follicle and the medulla (Langbein *et al*., 2010), and the latter is caused by missense mutations in the BCS1L gene which is expressed in mitochondria (Hinson *et al*., 2007). Pili torti can also be observed in anorexia nervosa where genetic factors and malnutrition in combination with excess carotene, retinyl esters, retinol, and retinoic acid lead to the hair shaft defect (Lurie *et al*., 1996; Strumia *et al*., 2005).

A hair phenotype with a beaded structure is apparent in some hair diseases. One such disease is monilethrix which has autosomal dominant mutations in K81, K83 and K86, keratins which are expressed in the hair cortex and medulla, and this disease also causes hair brittleness (Winter *et al*., 1997; Winter *et al*., 1998; Van Steensel *et al*, 2005; Langbein *et al*., 2010). The autosomal recessive form of monilethrix is characterised by

mutations in desmoglein 4 (DSG4), which cause fewer desmosomes in the hair along with atypical keratinisation, and result in endoplasmic reticulum stress (Kato *et al*., 2015). Netherton syndrome also results in beaded or bamboo hair and is caused by mutations in the serine protease inhibitor Kazal-type 5 (SPINK5) locus, encoding the serine protease inhibitor, lympho-epithelial Kazal-type-related inhibitor (LEKTI) (Chavanas *et al*., 2000). LEKTI deficiency allows unrestricted kallikrein-related peptidase activity and increased proteolysis in the epidermis, and a recent study shows kallikrein-related peptidase 5 inhibition to be a potential target for Netherton syndrome therapy (Furio *et al*., 2015). Beaded hair is also caused by autosomal recessive mutations in DSG4 and LIPH resulting in hypotrichosis 6 (Zlotogorski *et al*., 2006; Kazantseva *et al*., 2006). Another defect to the hair shaft morphology includes that of uncombable hair syndrome, which is a disease resulting from longitudinal grooves in the hair shaft, and gives triangular or kidney bean shaped cross-sections (Calderon *et al*., 2009).

There are diseases that affect the melanin morphology and distribution in hair, such as Chediak-Higashi syndrome and Griscelli syndrome, which result in silver hair with an uneven distribution of large melanin granules. The former syndrome is caused by an autosomal recessive immunodeficiency syndrome (Imran *et al*., 2012), and the latter is caused by an immunodeficiency syndrome with a Rab27a mutation (Sheela *et al*., 2004). Alternating light and dark patterns can be observed in the hair of those with pili annulati, where there is a mutation on chromosome 12q24.32-24.33, and increased lysine and decreased cysteine content in the hair (Giehl *et al*., 2004; Giehl *et al*., 2009). Nutrition also plays a role in melanin production, as demonstrated by the good and poor interspersed nutrition present in kwashiorkor which gives light and dark bands on sparse and brittle hair (Ramirez *et al*., 2011).

Disruption of the cuticle occurs in some disorders. Argininosuccinicaciduria is caused by a metabolic inability to excrete nitrogenous waste as urea and results in cuticle cell disruption as well as cortical cells splaying out (Fichtel *et al*., 2007). Other diseases result in a twisted, grooved, and ruffled cuticle with a distorted hair bulb which is easily plucked, such as loose anagen hair syndrome and Noonan-like syndrome with loose anagen hair. Loose anagen hair syndrome is caused by mutations in the K6HF gene which is required for the development of the inner root sheath (Chapalain *et al*., 2002), and Noonan-like syndrome with loose anagen hair is caused by RASopathy with ectodermal

abnormalities caused by mutations in the SHOC2 gene (Baldassarre *et al*., 2014). Nutritional deficiency can also cause cuticle cell disruption such as in coeliac disease where gluten-free diets are correlated to lower zinc levels in the hair and result in cuticular erosion and decreased hair diameter (Varkonyi *et al*., 1998). People who have deficiencies in iron, l-lysine, l-cysteine, selenium, and zinc also have hair disorders, but it only involves alopecia rather than a shaft defect. In some disorders various amounts of these elements and amino acids have been found in the hair shaft, but they do not appear to affect the hair structure.

An increased amount of sterols in the hair, particularly 7β-hydroxycholesterol, as a result of abnormal cholesterol metabolism has been implicated in cognitive impairment and may be a biomarker for Alzheimer's disease (Son *et al*., 2016).

Finally, pseudofolliculitis barbae appears to be a defect of the hair follicle, as a polymorphism in the KRT75 gene, which is expressed in the companion layer of the outer root sheath, causes ingrown hairs leading to inflamed pustular formations in shaved areas (Winter *et al*., 2004).

These diseases which manifest in hair are summarised in table 1.3 by whether they are hair shaft or follicle defects or caused by nutritional deficiency. There remains potential for further insight and fast diagnosis of these diseases and more through the use of confocal microscopy and fluorescence lifetime imaging microscopy.

Diseases which affect hair structure				
	Name	**Molecular defect if known**	**Hair phenotype**	**Reference**
Hair shaft defects	Hypotrichosis 4 Or Marie Unna hereditary hypotrichosis	Mutation in HR gene, human homolog of murine gene, hairless.	Sparse, coarse and wiry during childhood. Progressive hair loss at puberty.	Wen *et al*. (2009)
	Athyroidal hypothyroidism, with spiky hair and cleft palate	Mutations in FOXE1 gene.	Spiky hair.	Clifton-Bligh *et al*., (1998)
	Netherton syndrome	Mutations in the SPINK5 locus, encoding the serine protease inhibitor LEKTI.	Chorrexis invaginata or "bamboo hair".	Chavanas *et al*., (2000)
	Monilethrix	Autosomal dominant mutations in three loci, KRT86, KRT81, and KRT83, in an epithelial keratin cluster. Autosomal recessive mutation in DSG4.	Beaded structure of hair shaft, brittle.	Winter *et al*., (1997) Winter *et al*., (1998) Van Steensel *et al.*, (2005) Kato *et al*., (2015)
	Hypotrichosis 6	Autosomal recessive mutations in DSG4 and LIPH.	Beaded structure of hair shaft, alopecia.	Zlotogorski *et al*., (2006) Kazantseva *et al*., (2006)
	Ectodermal dysplasia 4, Hair/nail type		Extreme brittleness of the hair, leading to hair loss.	Naeem *et al*., (2006)
	Cardiomyopathy, dilated, with woolly hair and keratoderma	Autosomal recessive mutations in the DSP locus, encoding desmoplakin.	Fine and tightly curled.	Norgett *et al*., (2000).
	Skin fragility-woolly hair syndrome	Autosomal recessive mutations in the DSP locus, encoding desmoplakin.	Fine and tightly curled.	Whittock *et al*., (2002)
	Naxos disease	Mutations in the JUP gene, encoding plakoglobin.	Curly, woolly.	McKoy *et al*., (2000)

	Carvajal syndrome	Autosomal recessive mutation in the DSP (desmoplakin) gene.	Woolly hair.	Nehme *et al*., (2012)
	Hypotrichosis 7	Mutations in the LIPH gene.	Sparse, fine and tightly curled.	Kazantseva *et al*., (2006)
	Trichodentooss-eous syndrome	Autosomal dominant mutations in the DLX3 gene, encoding for a homeodomain transcription factor expressed in the hair matrix and most layers of the hair follicle.	Kinky hair.	Hwang *et al*., (2008)
	Menkes disease	Mutations in the ATP7A gene, encoding a ATP-dependent copper transporter.	Kinky hair.	Chelly *et al*., (1993) Mercer *et al*., (1993) Vulpe *et al*., (1993)
	Photosensitive trichothiodystro-phy	Autosomal recessive mutations in ERCC2, ERCC3, and GTF2H5, encoding subunits of the basal transcription factor 2 (TFIIH). Results in sulphur deficiency.	Brittleness.	Takayama *et al.,* (1996) Weeda *et al*., (1997) Giglia-Mari *et al*., (2004)
	Nonphotosensit-ive trichothiodystro-phy	Mutations in the MPLKIP gene, encoding M-phase specific PLK1 interacting protein involved in the control of cell cycle integrity.	Brittleness.	Nakabayashi *et al*., (2005)
	Hypotrichosis 8	Mutations in the LPAR6 gene.	Sparse, fine and tightly curled.	Pasternack *et al*., (2008) Shimomura *et al*., (2008)
	Inflammatory skin and bowel disease, neonatal	Mutations in the ADAM17 gene encoding a desintegrase/metallo protease.	Broken and short.	Blaydon *et al*., (2011)

	Ichthyosis with hypotrichosis, autosomal recessive	Mutations in the ST14 gene encoding matriptase, a type II transmembrane serine protease.	Sparse, curly, brittle.	Basel-Vanagaite *et al*., (2007)
	Maple syrup urine disease	Mutated BCKD dehydrogenase complex, leading to the absence of 18-MEA on the cuticle cell membrane complex.	Rough texture.	Smith and Swift, (2005)
	Mitochondrial diseases	Defective cellular energy supply.	Pili torti, sparse, fine.	Silengo *et al*., (2003)
	Pachyonychia congenita type 2	Deletion and missense mutations in the KRT17A gene.	Pili torti.	Smith *et al*., (2001)
	Bjornstad syndrome	Missense mutations in the BCS1L gene.	Pili torti.	Hinson *et al*., (2007)
	Uncombable hair syndrome	Autosomal dominant inheritance with complete or incomplete penetrance.	Longitudinal grooves in the hair shaft, triangular or kidney bean cross-section.	Calderon *et al*., (2009)
	Pili annulati	Mutation on chromosome 12q24.32-24.33, and increased lysine and decreased cysteine content in hair.	Alternating light and dark patterns on hair.	Giehl *et al*., (2009) Giehl *et al*., (2004)
	Argininosuccini-caciduria	Metabolic inability to excrete nitrogenous waste as urea.	Trichorrhexis nodosa – cuticle disruption, cortical cells splay out.	Fichtel *et al*., (2007)
	Chediak-Higashi syndrome	Autosomal recessive immunodeficiency syndrome.	Silver hair, uneven distribution of large melanin granules.	Imran *et al*., (2012)
	Griscelli syndrome	Immunodeficiency syndrome with a Rab 27a mutation.	Silver hair, uneven distribution of very large melanin granules.	Sheela *et al*., (2004)
Hair follicle defects	Pseudofolliculitis barbae	Polymorphism in the KRT75 gene.	Ingrown hairs leading to inflamed pustular	Winter *et al*., (2004)

			formations in shaved areas.	
	Autosomal dominant woolly hair	Mutations in the KRT71 and KRT74 genes, encoding keratins expressed in the inner root sheath.	Fine and tightly curled	Fujimoto *et al*., (2012) Shimomura *et al*., (2010)
	Hypotrichosis 3	Mutations in the KRT74 gene.	Woolly hair and alopecia.	Wasif *et al*., (2011)
	Ankyloblephar-on-ectodermal defects-cleft lip/palate syndrome	Mutations in the transcription factor TP63.	Sparse, coarse, wiry.	McGrath *et al*., (2001)
	Rapp-Hodgkin syndrome	Mutations in the transcription factor TP63.	Sparse, dry, coarse, wiry, pili torti.	Kantaputra *et al*., (2003)
	ADULT syndrome	Mutations in the transcription factor TP63.	Sparse, thin.	Amiel *et al*., (2001)
	Ectodermal dysplasia skin fragility syndrome	Mutations in the PKP1 locus encoding plakophilin.	Sparse, short.	McGarth *et al*., (1997)
	Histiocytosis-lymphadenopathy plus syndrome	Autosomal recessive mutations in the SLC29A3 gene encoding the nucleoside transporter hENT3.	Hypertrichosis.	Molho-Pessach *et al*., (2008)
	Loose anagen hair syndrome	Mutations in the K6HF gene, required for the development of the inner root sheath.	Twisted, grooved, ruffled cuticle. Distorted bulb. Easily pluckable.	Chapalain *et al*., (2002)
	Noonan-like syndrome with loose anagen hair	RASopathy with ectodermal abnormalities, caused by mutations in the SHOC2 gene.	Twisted, grooved, ruffled cuticle. Distorted bulb. Easily pluckable.	Baldassarre *et al*., (2014)
Nutrition or trace element deficiency	Coeliac disease	Gluten diets are correlated to lower zinc levels in the hair.	Cuticular erosion and decreased hair diameter.	Varkonyi *et al*., (1998)
	Anorexia nervosa	Genetic factors, and malnutrition in combination with excess carotene, retinyl esters, retinol, and retinoic acid.	Pili torti.	Lurie *et al*., (1996) Strumia *et al*., (2005)

	Kwashiorkor	Good and poor nutrition interspersed gives dark and light bands on hair.	Dark and light bands, sparse, brittle.	Ramirez Prada *et al*., (2011)

Table 1.3. Diseases which affect the structure of human hair.

1.6. Confocal microscopy and hair imaging

Here the workings and applications of laser scanning confocal microscopy and autofluorescence in hair are reviewed. Confocal microscopy gives high resolution and depth of focus to imaging by the use of a pinhole to remove out-of-focus light (Wilson, 2011). This means that clear optical sections can be obtained from samples. However, limitations include the opacity of the sample caused by light-absorbing structures, sample surface reflection, and changes in refractive index within samples. Laser beams are used and allow various wavelengths to be chosen to excite the sample which may itself be stained with a fluorescent dye, harbour and an endogenous fluorophore, or the sample alone may be autofluorescent.

The majority of work carried out on the hair using confocal microscopy has involved the use of fluorescent dyes. Fluorescent dyes may allow specific staining of structures in samples, though they may also alter the nature of the sample itself, or in the case of hair they may be unable to penetrate the sample to the necessary depth. The use of confocal microscopy to image the hair is a relatively unexplored technique. Most work began in the early 1990s.

In 1993 Corcuff *et al*. had early success with using fluorescent stains in the hair. They stained hair in rhodamine B or octadecyl-rhodamine and dried it in an oven at 105°C overnight. They then dry mounted the hair or used glue to attach the hair to the coverslip. Surprisingly they obtained good images of the cuticle. They found the outer cuticle cells of permanently waved hair were lifted by 300nm more than that of untreated hair cuticle cells which were raised by 300nm. This however suggests their sample preparation has also affected the hair as a raised cuticle cell is an indicator of hair damage possibly caused by the 105°C overnight treatment. They found that rhodamine B did not penetrate into the cortex, but the octadecyl-rhodamine staining gave good images of the cortex (Corcuff *et al*. 1993). Other groups also found that rhodamine B gave good images of the cuticle but did not penetrate through to the cortex (Lagarde *et al*., 1994; Hadjur *et al*., 2002). Despite rhodamine B not entering the cortex,

the lack of mounting medium matching the refractive index of the hair would have also contributed to the lack of autofluorescence signal from the cortex. Hadjur *et al*. also found that they could gain high resolution images of the cuticle using reflection confocal microscopy (Hadjur *et al*., 2002).

Hair has often been embedded in resin and sectioned using a microtome which may affect the native structure of the hair and result in little autofluorescence signal. Kelch *et al*., used this technique after staining the hair with octadecanoylaminofluorescein and found that it stains the cortical CMC and organelle remnants within the hair (Kelch *et al*., 2000). Swift *et al*. applied hydrolysed wheat proteins labelled with fluorescein isothiocyanate to the hair and embedded it in resin before sectioning it and imaged using confocal microscopy. They showed that wheat proteins penetrate through to the endocuticle, cortex, organelle remnants, matrix, and the CMC. However, they only gained 15µm penetration into bleached, permanently waved, or relaxer treated hair with less penetration into untreated hairs, which resulted in poor resolution of the untreated hairs (Swift *et al*., 2000). Additionally, with hair care as the focus, Ribeiro *et al*. used γD-crystallin fluorophore labelled hair to strengthen hair chemically damaged by bleaching. The confocal images of the hairs were 3D reconstructed but apart from showing more γD-crystallin in the chemically damaged hair cortex than in untreated hair, confocal microscopy was not used to its fullest potential (Ribeiro *et al*., 2013). Cruz *et al*., also used 3D reconstruction of the confocal images to compare hairs. They used Nile red to compare lipids of the hair across different ethnicities, and then embedded the hair in resin and sectioned it. The 3D reconstruction caused loss of resolution of individual structures, and through confocal microscopy alone was not able to tell which hair contained more lipids (Cruz *et al.*, 2013).

There are two main pathways for diffusion of a fluorescent dye or other molecule into the hair. Small hydrophilic molecules tend to use the transcellular route, which goes across the high and low density cross-linked areas of the cuticle cell, however this route is difficult and only tends to be taken if the densely cross-linked exocuticle and A-layer are damaged (Robbins, 2012). Large hydrophobic or non-polar molecules on the other hand, such as fluorescent dyes, mainly use intercellular diffusion across the low-cystine areas including the endocuticle and CMC (Kelch *et al*., 2000; Formanek *et al*., 2006). Since low-sulphur areas of the cuticle cell such as the endocuticle absorb water,

molecules can enter the hair through this route. Even under non-aqueous conditions, molecules can use the intercellular route because of the high mobility of the protein and lipid molecules of the CMC (Wortmann *et al*., 1997). Once through the cuticle and given sufficient time, molecules can diffuse along the intercellular pathway to the cortical cells and medulla (Kamath *et al*., 1995). Usually a mixture of the transcellular and intercellular pathways is used (Robbins, 2012).

The approaches based on using fluorescent dyes to label structures in the hair have limitations. The penetration of fluorescent dyes into the untreated hair is restricted, and may cause artefacts. Therefore, it is important to develop label-free methods of imaging hair based upon autofluorescence.

1.6.1. Autofluorescence

Autofluorescence is the emission of light from molecules such as those in a fluorophore within a sample when excited by a higher energy and shorter wavelength of light. The hair is an autofluorescent fibre and so can be exploited through confocal microscopy. Some of the molecules or functional groups in the hair which may autofluoresce, and are possible either as free amino acids or incorporated into proteins, are tryptophan, tyrosine, phenylalanine, cystine, lipo-pigments and pheomelanin (Hameka *et al*., 1998; Elleder and Borovansky, 2001; Lakowicz, 2006; Jachowicz and McMullen, 2011).

To date, little advantage has been taken of hair autofluorescence, and the ability to image hair label-free in its native state. Liang *et al*. analysed hair from patients with trichothiodystrophy. Autofluorescence from using 488nm and 543nm excitation shows fractures in the hair, but little other detail. They also 3D rendered the hair and showed the cortex though the identity of structures is unclear, so they could only show the patient's cortex had a rougher surface than that of the control hairs. However, the hair was embedded and cryosectioned (Liang *et al*., 2006). They may have obtained greater cuticle and cortex resolution had the hair been left whole, as there can be a loss of resolution with 3D rendering from separate sections of hair. Kirkbride and Tridico also used autofluorescence with confocal microscopy, but with only 405nm excitation. Despite using the optimum wavelength for exciting hair autofluorescence, they obtained low resolution images of the cuticle and cortex. Unlike the previous study, Kirkbride and Tridico used mountant, however they stated that they did not spend time optimising the images through changing the size of the pinhole, or the mounting media, or through

signal averaging, or by using a higher pixel resolution than 512*512, or by using small z-steps. Their imaging parameters were chosen simply for speed (Kirkbride and Tridico, 2010). This highlights the necessity for optimisation to obtain high quality images.

To obtain images of a high resolution it is necessary to match the refractive index of the hair which is 1.55 (Greenwell *et al*., 1941) with a specific oil and leave the hair whole to take advantage of the great depth of focus of the confocal microscope. Advancements in confocal microscopy resolution and technique have allowed for developing methodology that results in images of a higher quality as shown in this study.

1.7. Aims of the study

There is a need for a better method to image hair as the current methods involve embedding the hair in resin, which may produce artefacts, or using dyes which are limited in their depth of penetration into the hair (Corcuff *et al*., 1993; Lagarde *et al*., 1994; Kelch *et al*., 2000; Swift *et al*., 2000; Hadjur *et al*., 2002; Liang *et al*., 2006; Cruz *et al.*, 2013). Further to this, the mechanisms of action of some existing chemical depilatories on the hair requires analysis, as do the mechanisms of some experimental chemical depilatories. There is a need to develop new chemical depilatories because the existing depilatories have been shown to cause irritation in the skin (Hahn, 1999; Haque and Al-Ghazal, 2004; Kindred *et al*., 2011; Moghimi *et al*., 2013), and an increase in depilatory efficacy is needed by the hair care industry. Therefore, the overall aim of this study was to develop label-free imaging methods for hair, investigate the use of autofluorescence, and to develop optical transverse imaging and dynamic imaging methods.

The further aims of this study were to:

- Use these methods to further knowledge on hair structure and morphology.
- Investigate fluorescence lifetime imaging on the hair to show it reveals structures and chemical environments that cannot be resolved by fluorescence intensity.
- Use the developed imaging techniques to investigate an uncharacterised hair and skin disorder.
- Test commercial and experimental depilatory chemicals on hair for elucidation of their structural and morphological effects.

- Test the most efficacious depilatory chemicals on keratinocytes to investigate their effect upon keratinocyte differentiation, proliferation, apoptosis and acute stress response.

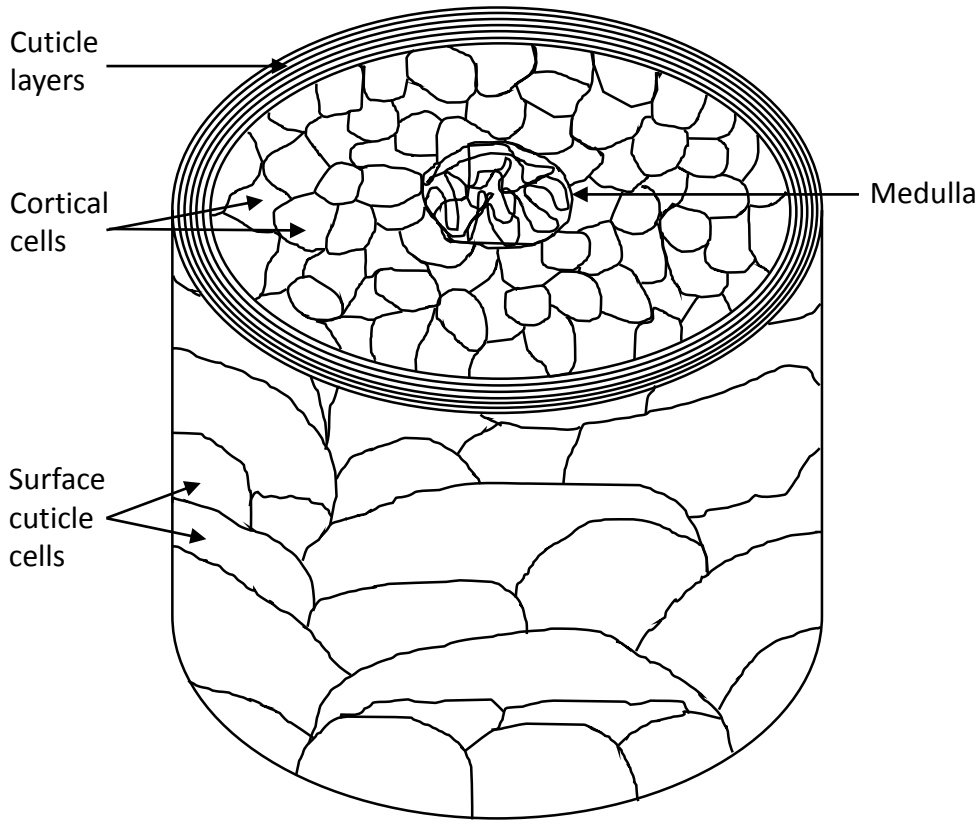

Fig. 1.1. Hair structure schematic. Schematic showing the main compartments of the hair – the cuticle, cortex and medulla. The cortical cells form the cortex.

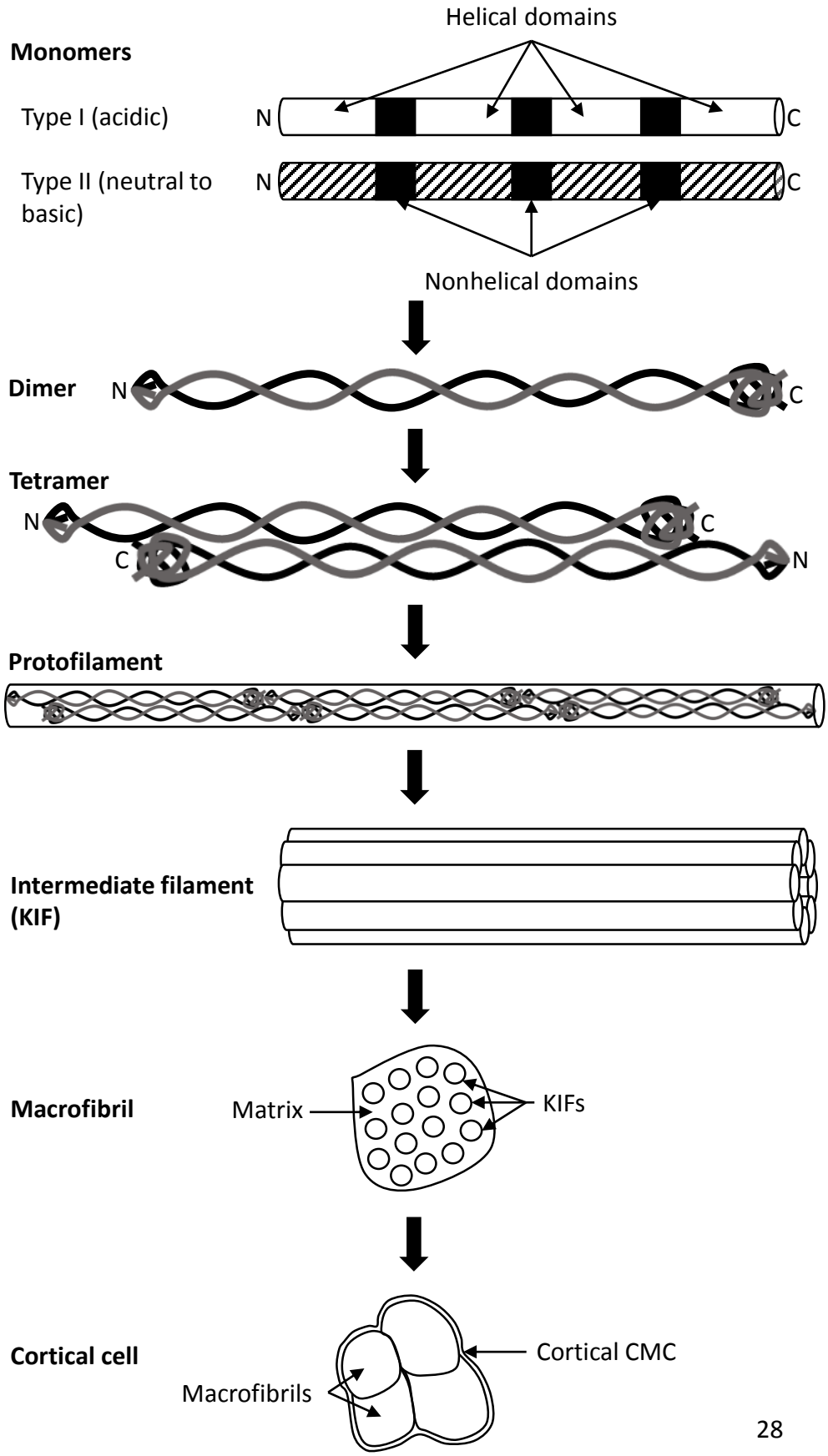
Helical domains
Monomers
Type I (acidic)
N
C
Type II (neutral to basic)
N
C
Nonhelical domains
Dimer
N
C
Tetramer
N
C
C
N
Protofilament
Intermediate filament (KIF)
Macrofibril
Matrix
KIFs
Cortical cell
Cortical CMC
Macrofibrils

Fig. 1.2. The assembly of keratin intermediate filaments in the hair. The monomer polypeptides comprise helical and nonhelical domains. One type I monomer dimerises with one type II monomer to form coiled coil dimers. These then coil around other dimers, head to tail, to form tetramers. Tetramers assemble end-to-end to form protofilaments, which then coil rope-like to form intermediate filaments. The intermediate filaments are embedded within the matrix in the macrofibrils, and bundles of macrofibrils are contained within the CMC bound cortical cell.

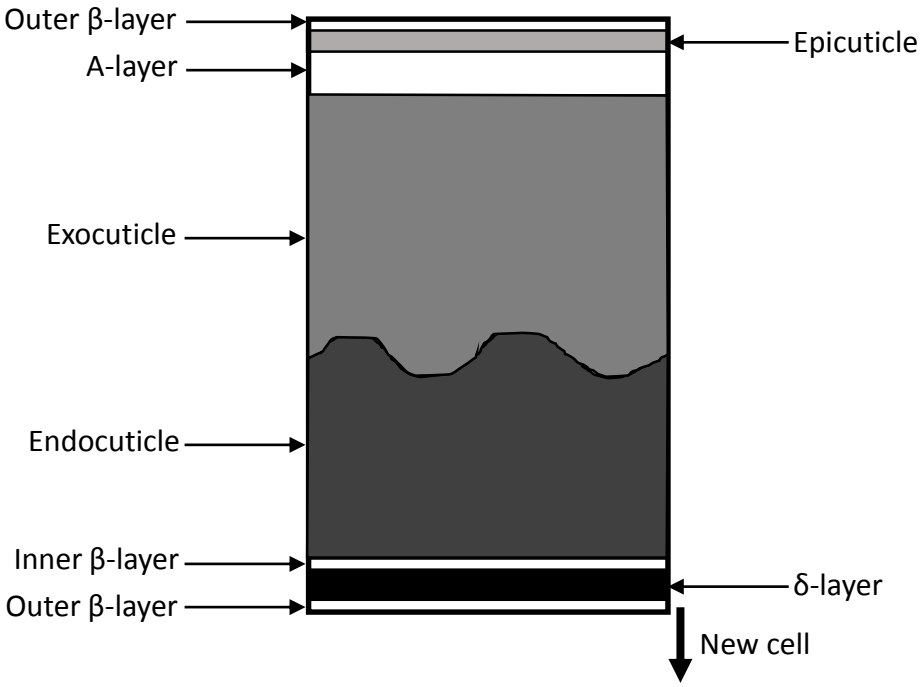

Fig. 1.3. Schematic of a transverse section through a cuticle cell. Schematic showing the sublamellar structure of a cuticle cell at the hair surface. The inner β-layer, δ-layer, and outer β-layer form the cell membrane complex.

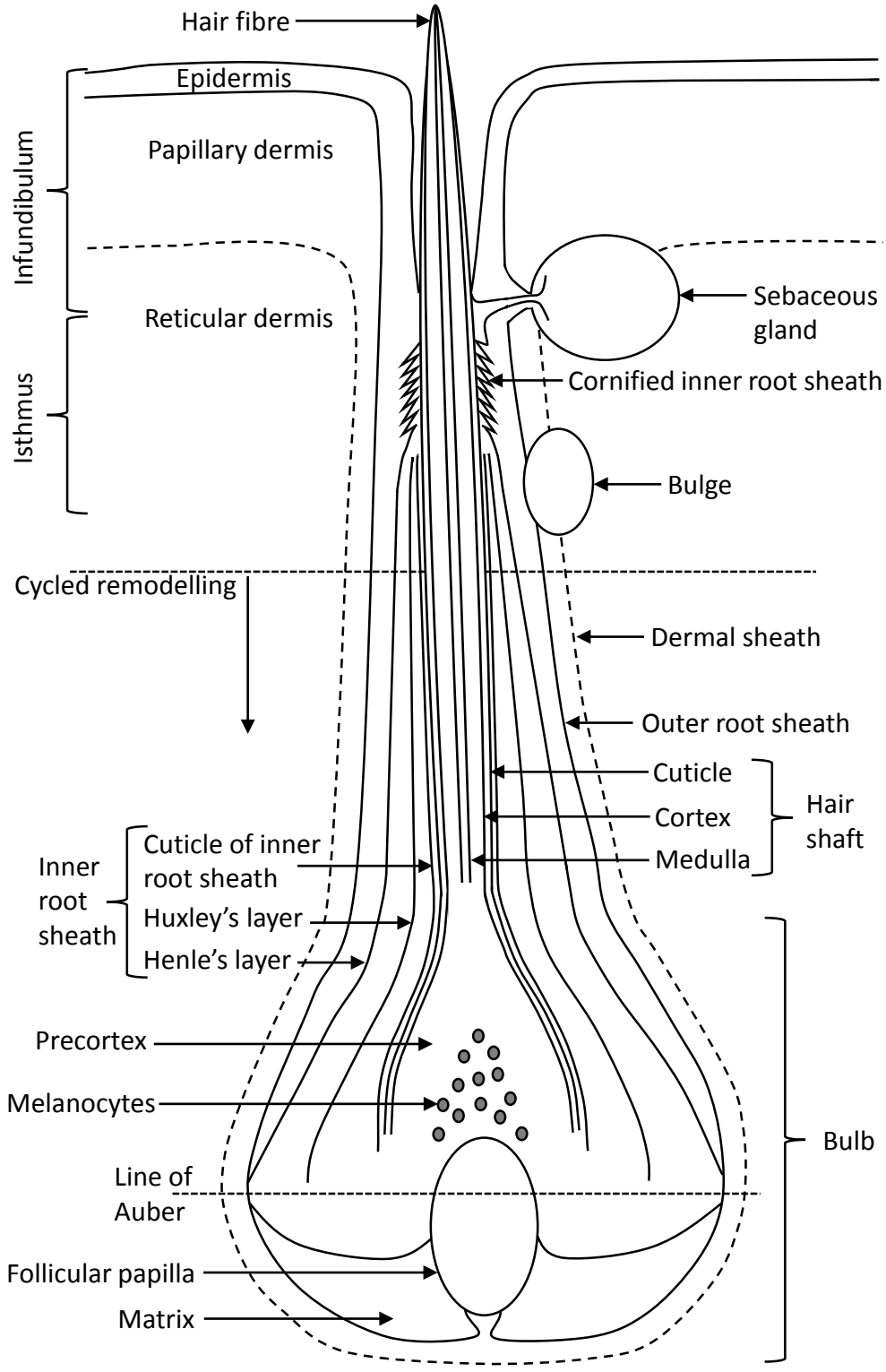

Fig. 1.4. The hair follicle. Schematic of the mature hair follicle in anagen phase.

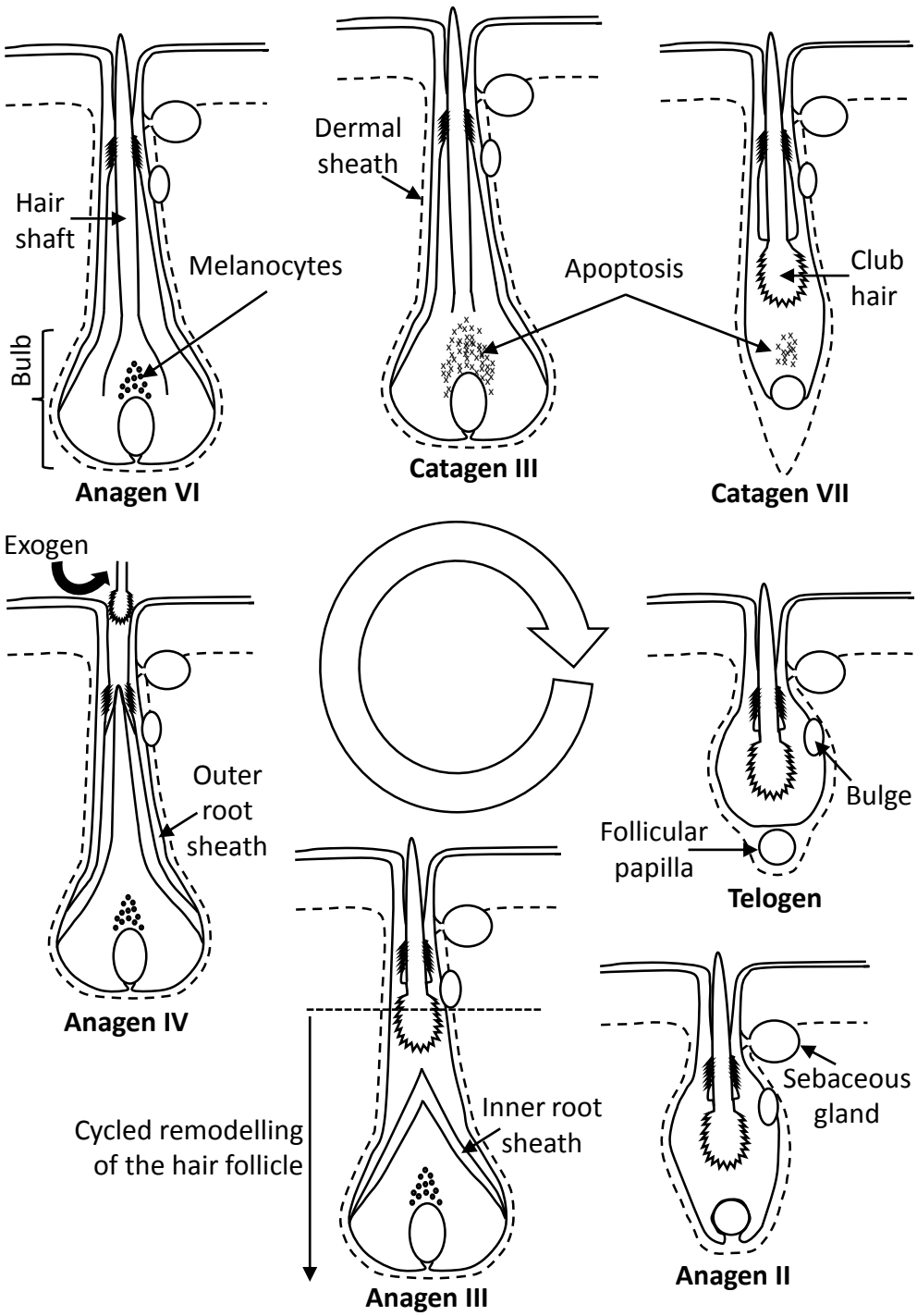

Fig. 1.5. The hair follicle cycle. Schematic of the hair follicle cycle through anagen (growth phase), catagen (regression phase), and telogen (resting phase). The shedding phase, exogen, occurs independently of the other phases (Stenn *et al*., 2005; Higgins *et al*., 2009). During catagen, only some melanocytes but most keratinocytes of the matrix and lower outer root sheath undergo apoptosis. Not all substages of each phase are shown. The selected substages show the main physical changes in the follicle.

Chapter 2

Materials and Methods

2.1. Hair samples and hair treatment methods

2.1.1. Hair

Hair sourced from Kurling International came in the form of swatches, approximately 15cm in length, gathered from a blend of individuals, who had not treated their hair with chemicals other than to wash with shampoo and conditioner. Unless specifically mentioned, all hair samples refer to cut rather than plucked hair.

The Chinese scalp hair was sourced from Kurling International 826515 and 821000-C-20. The European scalp hair (3/0, 5/0, 7/0, 9/0) and Indian scalp hair was also sourced from Kurling International. The plucked scalp and beard hair with and without the cuticle was sourced from Procter and Gamble (P&G) panellists and staff. Skin and hair samples from P&G are covered by the Human Tissue Act Licence (Durham University Project ID BL123). Some hair was also sourced in-house. The hair of the patient with the uncharacterised skin and hair disorder and his unaffected parents' hair was provided by Dr. Thivi Maruthappu, of Queen Mary University of London.

2.2. Hair methodology

2.2.1. Development of hair imaging methods

2.2.1.1. Longitudinal imaging of hair

To image hair longitudinally, a <1cm length was cut from the hair and placed on a glass slide. A drop of Immersol 518F oil (Zeiss) n_e=1.518 was mounted onto the hair and a glass coverslip placed on top. Nail varnish was then used to seal the coverslip to the slide. After drying, the hair sample could be imaged.

2.2.1.2. Development of a method for transverse imaging of hair

The novel transverse optical sectioning of hair offers another perspective of the hair. Once thought up, this method underwent development to achieve the results shown in this thesis. Initially, the widest open end of a 0.1-10µl pipette tip was glued to a 50mmx22mm glass coverslip, and hair cut by scissors was put into the pipette tip (fig. 2.1.A). Immersol 518F oil was then injected into the open end of the pipette tip until the tip was full, ensuring a mounting medium was provided for the hair in contact with the coverslip. This initial method was unsuccessful because the hair was liable to move

inside the pipette tip, barring fluorescence lifetime imaging microscopy (FLIM) as a still sample is required. Also there was poor contact between the cut end of the hair and the coverslip. This was improved by using a diamond-edged blade to cut the hair more cleanly. The final version involved inverting the pipette tip so that the hairs would be guided to stand perpendicular to the coverslip, stay stiller, and more easily be inserted into the wider end of the tip (fig. 2.1.B). A polystyrene block was used to support the inverted pipette tip, secured onto the coverslip with double-sided tape, as glue degraded the polystyrene. A hole was made in the polystyrene around where the hair made contact with the coverslip to allow mounting media to be placed there and to also let light reach the sample, making it easier to find under the microscope eyepiece.

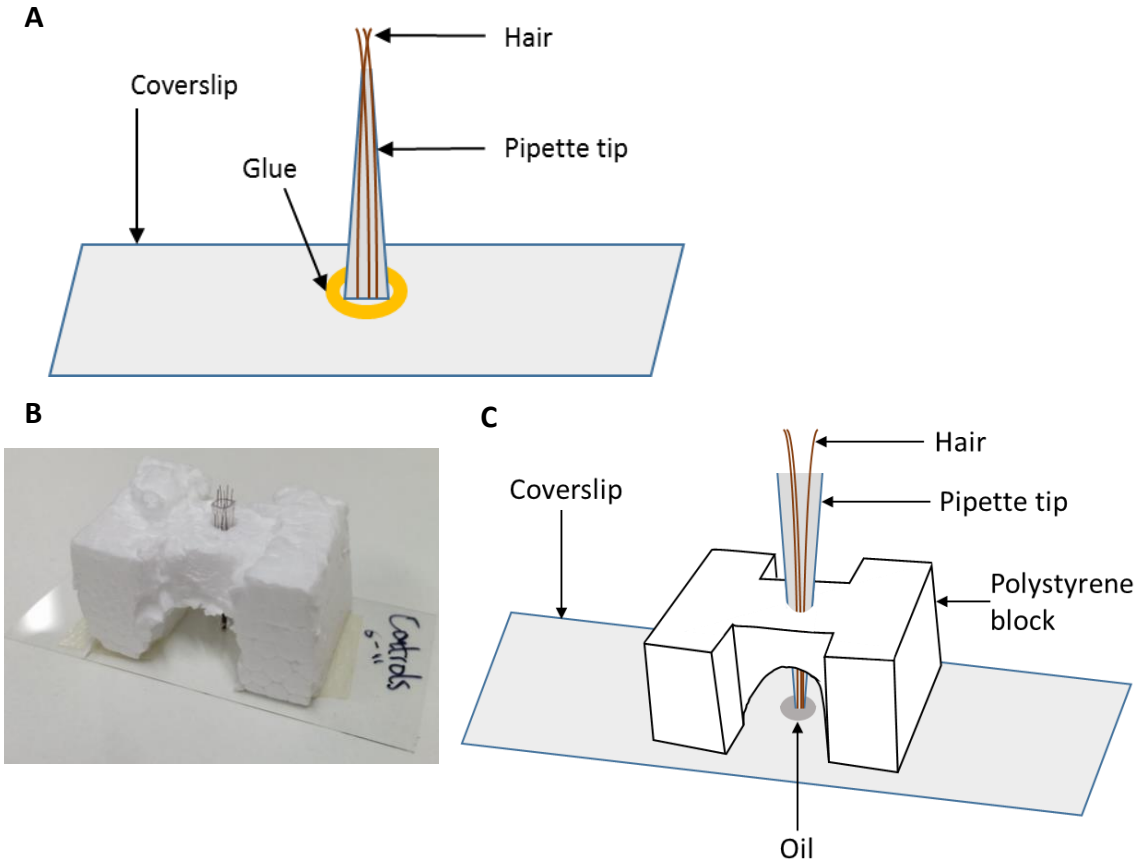

Fig. 2.1. Development of a method for the transverse imaging of hair. A) Schematic of initial design. B) Photograph of final design. C) Schematic of final design.

2.2.1.3. Development of dynamic imaging of hair

In order to image hair during its treatment, a dynamic imaging method needed to be developed. Initially ~2cm length of hair was cut and both ends were secured to a glass bottomed plate with micropore tape leaving the middle of the hair uncovered. Once the treatment was placed on the hair, the hair moved, so was unsuitable for imaging as reference points and regions of interest would be lost. The method was improved by placing a glass coverslip over the hair to keep it in place. The coverslip was secured using glue, which was found to be more effective than nail varnish, and left some free space for the treatment to reach the hair (fig. 2.2.A). Using this method, the hair was stiller, but was still able to move. The final and most successful design involved only having a small length of hair of ~1mm exposed from the tape, and no coverslip, to limit the movement of the hair (fig 2.2.B). A faster scanning speed of 700Hz was used on the Leica SP5 microscope for dynamic imaging, as this was required to capture sufficient data during z-stacks with oversampling in order to capture the whole hair.

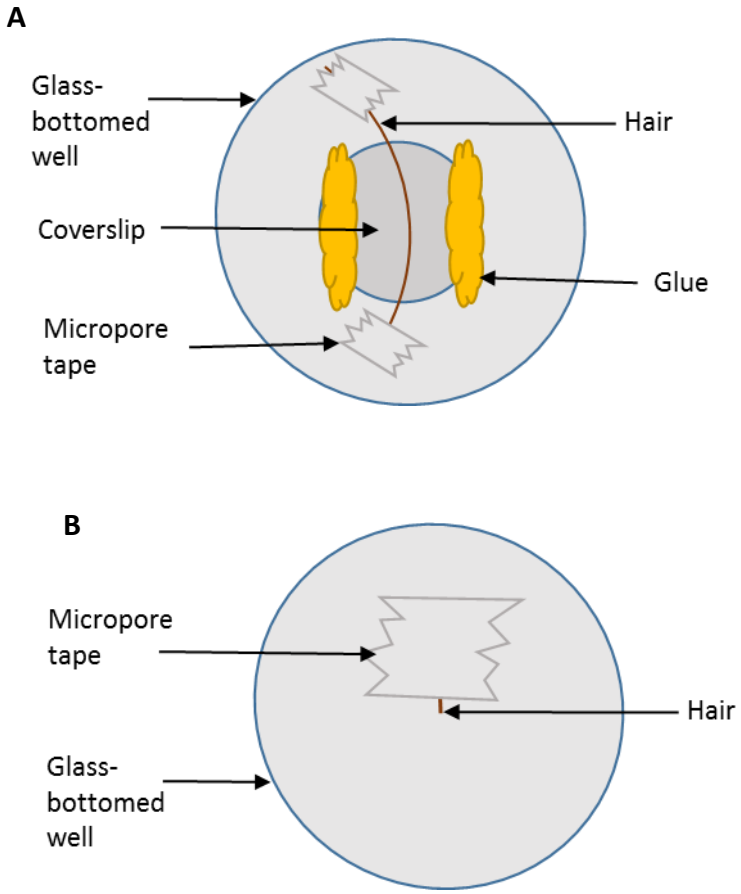

Fig. 2.2. Development of dynamic imaging of hair. A) Initial design. B) Final design.

2.2.1.4. Mounting medium testing

Various mounting media were tested to find which had the refractive index (RI) closest to hair (RI 1.55), in order to give the best imaging resolution. Hair was mounted longitudinally in either distilled water (RI 1.33), glycerol (RI 1.47), Citifluor (Agar Scientific) (RI 1.52), Vectashield (Vector labs) (RI 1.45), Immersol 518F oil (Zeiss) (RI 1.52), DePeX (RI 1.52) or onto double-sided tape. Double-sided tape gave poorer resolution than the alternatives. DePeX did not give a better resolution than the alternatives and also required the inconvenience of samples being mounted and dried in the fume hood. Citifluor gave good resolution if the hair had been kept dry, and Vectashield gave good resolution if the hair had been submerged in water prior to mounting. However, this resolution was comparable to using glycerol as the mounting medium, which was also cheaper to source. Water did not give as clear resolution as glycerol, but has still been vital for use as a medium in the hydration experiments.

Using the transverse optical sectioning method for imaging, later it was found that Immersol 518F oil gave the best resolution of the hair, and the use of FLIM showed that there was also little difference between the effect of Immersol 518F oil, immersion oil type FF (Cargille Laboratories) (RI 1.49), and glycerol on the lifetime of the hair. This also showed that the media was not causing artefacts in the lifetimes seen in the hair.

2.2.1.5. Keeping track of hairs

For some experiments random slices of hair were not suitable to use. For the lipid and protein extraction of hairs, control and sample hairs were paired. To do this, lengths of hair approximately 15cm long were taped at one end across a piece of foil. Foil was used to keep the hairs clean and to stop the potential of plastic from leaching into the hairs. Each hair was numbered, and lengths were cut off as required, keeping note of the allocated hair number.

2.2.1.5.1. Changes along the hair length

For the study into changes down the hair length, a 12cm long hair was cut into 1cm sections, put onto slides for longitudinal imaging and labelled. The hair was left mounted in oil for a day so that the oil had completely penetrated all samples, because some samples may not be imaged for weeks as 1cm of hair takes approximately 2.5 hours to image. On the Leica SP5, the 405nm laser, a tile scan with an oversampling z-stack using

0.45µm steps, the 40x oil objective at 1.7x zoom, and a 700Hz scanning speed with the HyD detector were used for imaging the hair.

2.2.2. Hair treatment chemicals

Hairs were treated with a variety of chemicals, either commercially available or newly developed. Many of those developed by P&G begin with "CHM" which stands for "chemical hair modification". The treatments were produced either as a cream or a liquid or both.

Name	Commercial or novel	Hair treated	Constituents	Application time	Vehicle
CHM1	Commercial (*Sally Hansen Facial Depilatory*)	Kurling International 826515	2.3% CaTG, $Ca(OH)_2$, KOH	4 min	Cream
CHM2	Commercial (*Veet HydroRestor*)	Kurling International 826515	0.45M KTG, 0.47M $Ca(OH)_2$	4 min	Cream and aqueous
CHM3	Novel	Kurling International 826515	0.45M KTG, 0.47M $Ca(OH)_2$, 0.44M GC	4 min	Cream and aqueous
CHM4	Novel	Kurling International 826515	0.44M GC, 0.47M $Ca(OH)_2$	4 min	Aqueous
CHM5	Novel	Kurling International 826515	0.44M GC, 0.47M $Ca(OH)_2$	4 min	Aqueous
CHM22	Novel	Kurling International 821000-C-20	8M LiBr, 25°C	20 min	Aqueous

CHM23	Novel	Kurling International 821000-C-20	8M LiBr, 85°C	20 min	Aqueous
CHM24	Novel	Kurling International 821000-C-20	8M LiBr, 25°C	5 min	Aqueous
CHM25	Novel	Kurling International 821000-C-20	8M LiBr, 25°C	5 day	Aqueous
CaI_2 + SLS	Novel	Kurling International 826515	25% CaI_2 + 2% SLS	10 min CaI_2 + 5 min SLS	Aqueous
SLS	Novel	Kurling International 826515	28% SLS	5 min	Aqueous
CTAB + SLS	Novel	Kurling International 826515	2% CTAB, 0.5% SLS Stepanol	CTAB 5 min, SLS 5 min	Aqueous

Table 1.1. Commercial and novel hair depilatory treatments. CaTG = calcium thioglycolate, KTG = potassium thioglycolate, GC = guanidine carbonate. SLS = sodium lauryl sulphate. CHM = chemical hair modification.

2.2.2.1. CHM1

Sally Hansen Facial Depilatory (Coty), hereafter denoted as "CHM1", was analysed by P&G and stated to contain 3.3% calcium thioglycolate, calcium hydroxide, and potassium hydroxide. These were made up into a cream chassis by P&G and applied to the hair for 4 min. The hair was then washed thrice in distilled water for 2 min each, and left to dry for 24h at room temperature. After drying, the samples were sent to Durham University for imaging.

2.2.2.2. CHM2 and CHM3

Veet HydroRestor (Reckitt Benckiser), hereafter denoted as "CHM2", was analysed by P&G and stated to contain 4.2% or 0.45M potassium thioglycolate (Acros organics, cat# 384702500), and 0.47M calcium hydroxide (Sigma Aldrich, cat# 239232). CHM3 is a

novel depilatory containing 4.2% or 0.45M potassium thioglycolate, 0.44M guanidine carbonate (Aldrich, cat# G11659) and 0.47M calcium hydroxide. These were both made up into cream chassis by P&G, and made up as aqueous solutions in-house for dynamic imaging. Hair was treated for 4 min, and the cream treated hair was then washed thrice in distilled water for 2 min each, and left to dry for 24h at room temperature. After drying, these samples were sent to Durham University for imaging.

2.2.2.3. CHM4 and CHM5

CHM4 is a novel depilatory containing 0.44M guanidine carbonate and 0.47M calcium hydroxide, made up to pH 12.5, and CHM5 was made to pH 11.4. These were prepared as aqueous solutions by both P&G and in-house for dynamic imaging. At P&G, hair was treated for 4 min, and then washed thrice in distilled water for 2 min each, and left to dry for 24h at room temperature. After drying, these samples were sent to Durham University for imaging.

2.2.2.4. CHM22, CHM23, CHM24, CHM25

The LiBr (8M; 69.5g) was slowly added to distilled water (100ml) with slow stirring to avoid significant heat rise on hydration. On completion of the addition, the solution was allowed to cool to ambient temperature. Then the hair fibres were added directly to the solution for the required time and temperature (ensuring the hair is fully immersed in the treatment solution). The hair samples were then removed and briefly immersed in a deionised water bath for 3s to remove excess solution and solid deposition on the fibre surface. After drying, the samples were sent to Durham University for imaging.

2.2.2.5. CaI_2 + SLS

25g CaI_2 (Sigma, cat# 590703) was slowly added to 75ml distilled water with stirring over a 20 min period. The solution was left for 24 hours so it could reduce to 20°C before treating the hair. The pH was tested to ensure it was between pH 7 and 8. Then 2g SLS solution (Sigma, cat# 590703) was added drop-wise into 98ml distilled water and was gently stirred as vigorous stirring may result in foaming. Using clean tweezers, each of the sample fibres was placed into the 25% CaI_2 solution, ensuring complete submersion, and gently stirred once a minute. After 10 min the hair was removed and placed into the 2% SLS solution for 5 min. After drying, the samples were ready for imaging.

2.2.2.6. 28% SLS

Hair was incubated in a solution of 28% active SLS for 5 min in-house. After drying, the samples were ready for imaging.

2.2.2.7. CTAB + SLS

Hair was treated by P&G by incubating with 2% cetyltrimethylammonium bromide (CTAB) at pH 9.41 for 5 min, followed by 0.5% SLS Stepanol for 5 min. After drying, the samples were sent to Durham University for imaging.

2.2.3. Relative humidity

Individual untreated Chinese scalp hairs and CHM3 treated scalp hairs were separated into eppendorfs and left to equilibrate overnight in ambient room humidity, 70% humidity and 100% hydrated conditions at room temperature. Ambient room humidity was approximately 70% and was included in the experiment to test how results would differ to a controlled 70% humidity environment. A set 70% humidity was achieved by using a humidified plant chamber, and for 100% hydration hairs were incubated overnight in distilled water. As they were required for imaging, hairs were immediately mounted in oil to seal the saturated water inside the hair.

2.2.4. Dyes and antibodies used on hair

Chemical	**Concentration / M**	**Excitation wavelength / nm**	**Emission wavelength / nm**	**Supplier**
Octadecyl Rhodamine B chloride (R18)	$1x10^{-6}$ – $2x10^{-4}$	560	590	Invitrogen
Rhodamine B	$1x10^{-6}$ – $2x10^{-4}$	540	625	Sigma Aldrich
Curcumin	$1x10^{-2}$	420	550	Sigma Aldrich
Oil Red O	$1x10^{-2}$	633	643-800	Fisher Scientific
Fluorescein	$1x10^{-1}$	460	515	Edward Gurr Ltd.

Lanthanide EuDAP7A	$3x10^{-2}$	405	450-550 & 650-750	Gift from Professor David Parker, Durham University, Department of Chemistry
Lanthanide EuDGP2	$3x10^{-2}$	405	450-550 & 650-750	Gift from Professor David Parker, Durham University, Department of Chemistry
Lanthanide JW123	$3x10^{-2}$	405	450-550 & 650-750	Gift from Professor David Parker, Durham University, Department of Chemistry
N-(2-aminohexyl)-5-(dimethylamino)naphthalene-1-sulphonamide	$5x10^{-5}$	405	450-600	Gift from Prof. M. Knight, Durham University,

				Department of Biology
Nile red	$1x10^{-3}$ -$1x10^{-6}$	559	629	Sigma Aldrich
DAPI	$1x10^{-9}$	350	470	Sigma Aldrich
Hoechst33258	$2x10^{-4}$	352	461	Invitrogen
C_5 Maleimide	$1x10^{-7}$	622	640	AlexaFluor
H&E	1% eosin	N/A	N/A	RA Lamb
Lamin A/C JOL2 mouse mAb	1:5	N/A	N/A	Gift from Prof. C. Hutchison, Durham University, Department of Biology
Donkey anti-mouse	1:500	594	604-800	AlexaFluor

Table 2.2. The dyes and antibodies used for analysis of the hair.

2.2.5. Lipid extraction

The lipids were extracted from the hair using 3 different methods to selectively remove lipids. The Wertz and Downing method and modified method for stratum corneum lipids method remove soluble lipids, and the CTAB method removes covalently crosslinked lipids from the hair. After each step in each method, the solvents were collected for analysis by GC/MS and some hairs were collected and air-dried for imaging.

2.2.5.1. Wertz and Downing method

The method from Wertz and Downing (1988) was adapted as follows: the hair was rinsed with deionised water, then lipids were extracted using methanol for 2 hours at room temperature, and then in chloroform:methanol at 2:1, 1:1, then 1:2 for 2 hours each, and then 24 hours each at room temperature, and finally the hair lipids were extracted with chloroform for 24 hours.

2.2.5.2. Modified method for stratum corneum lipids

A simpler method adapted from extracting lipids from the stratum corneum in the skin was used, modified from Pappinen *et al*., 2008. This involved extracting the hair lipids in chloroform : methanol at 1:2 for 1 hour at room temperature and then for 1 hour at room temperature in 50mM citric acid : double distilled water : chloroform at 1:1:1.

2.2.5.3. CTAB method

The third method was adapted from Smith *et al*. (2010) as follows: the hair was treated with CTAB 2g/L under alkaline conditions using sodium hydroxide 10g/L at 60°C for 15 min, then rinsed with deionised water at 40°C for 10 min, the hair was then acidified with acetic acid and 25% (v/v) isopropanol at room temperature for 10 min, finally the hair was washed with deionised water for 5 min at room temperature.

2.2.5.4. Gas chromatography mass spectrometry analysis (GC/MS)

Lipid extracts were dried under nitrogen or freeze-dried, then extracted with chloroform:methanol 1:1 and 0.9% KCl. The lower phases were removed into new tubes and dried under nitrogen at 35°C and derivatised with 200µl Tri-Sil TP for 20 min, extracted with 100µl water and 200µl hexane. The phases were separated by centrifugation and the upper hexane layer was analysed by GC/MS. A C17 internal standard was used.

2.2.6. Visualisation of melanin

Following the protocol from Ye *et al*., (2011), synthetic brown/black melanin was suspended in 1mg/ml distilled water. This was used to compare the reflective properties of pure, synthetic melanin against that of the melanin in Chinese scalp hair.

2.2.7. Tensile properties

The tensile properties of the untreated and treated hair were measured by P&G Egham.

2.2.7.1. Measurement of tensile properties

The mechanical tensile (stress/strain) properties of the untreated and treated hair were measured on a Diastron Miniature Tensile Tester with cross-sectional area measurement capabilities (available from Diastron Ltd,UK). Each wheel on the Diaston can contain 100 fibres, with 25 fibres of each treatment required for accurate results, along with 25 untreated as a control. One side of a large weigh boat was marked with ‘root’, and the other side with ‘tip’. A small amount of hair fibres were placed into the

weighing boat in the right orientation. One fibre by the root side was taken and inserted into 2 brass crimps. The hair fibre was placed onto the 'pressure slot', pairing the left side with the root and the right side with the tip. The pressure slot was slid under the equipment. The pump was pressed until pressure reached 110bar. The excess brass crimp and hair fibre was cut off on each side. The fibres were loaded into the wheel, and the Diaston started. The break ratio reduction was calculated, which is a measure of depilatory efficiency and the amount the hair has been chemically weakened compared to untreated control hair, expressed as a percentage change.

2.2.7.2. Measurement of hair swelling

The diametral macro swelling of hair fibres with hydration was measured using a USB optical microscope. This method was designed to provide a rapid indication of the level of uptake of water by individual hair fibres. The hair fibres were treated with the corresponding chemistries for 4min and allowed to thoroughly dry under ambient conditions for 24h prior to swelling with deionised (DI) water. It was found that a USB microscope had sufficient resolution to clearly observe the edges of a fibre at 200x magnification. Three hair fibres of each treatment were fixed ~0.5mm apart to a microscope slide with ~1mm sections exposed from a piece of tape. A cover slip was place on top, allowing for a very small gap to apply water underneath. An image was captured before the water was applied dropwise to the edge of the slide. The water moved under the cover slide by capillary action until the three hair fibres were completely submerged. Subsequent images were then captured after a range of hydration times allowing for the both the rate and total diameter change to be calculated.

2.3. Cell culture

2.3.1. Cells

2.3.1.1. HaCaT cells

HaCaT cells are a spontaneously immortalised keratinocyte cell line derived from adult human skin, which were isolated by Fusenig *et al.*, (1978). For this study they were obtained via Cell Line Services, GmbH, Eppelheim, Germany.

2.3.1.2. Human epidermal keratinocytes, neonatal (HEKn)

HEKn cells are primary human epidermal keratinocytes isolated from neonatal foreskin. They were cryopreserved at the end of primary culture so arrived from the vendor as a frozen aliquot. They were purchased from Invitrogen, cat# C-001-5C, lot# 1653251.

2.3.2. Routine cell culture

2.3.2.1. Passaging

Prior to using cell culture, liquids were warmed to 37°C and all equipment sprayed with 70% ethanol. Cells were brought up from the -150°C freezer and thawed in a 37°C water bath. HaCaT cells were then resuspended in Dulbecco's Modified Eagle Medium (DMEM) (Gibco life technologies, cat# 31966-047) with 10% fetal bovine serum (FBS) and 1% penicillin/streptomycin (P/S). HEKn cells were resuspended, 20µl extracted, and the rest resuspended in 9ml EpiLife (Gibco life technologies, cat# MEPI500CA) with 1% human keratinocyte growth factor (HKGS) (Gibco life technologies, cat# S-001-5) and 0.2% gentamicin/amphotericin B (G/A) (Gibco life technologies, cat# 50-0640). Next, 20µl of the solution was added to 20µl of trypan blue for the cells to be counted on a haemocytometer. This was then used to calculate the volume of cells to be seeded into T75 flask (Greiner bio-one, cat# 658175) at a density of approximately 2500 cells per cm^2. For HaCaT cells the flasks were topped up with 15ml DMEM and for HEKn cells the flasks were topped up with 10ml EpiLife, these were then incubated at 37°C in 5% CO_2. After 48h the media was aspirated and replaced with 20ml DMEM for HaCaT cells or 10ml EpiLife for HEKn cells. The confluency of the cells was checked every day, and once 70-90% confluent the cells were passaged using the following protocol. For HaCaT cells, the media was aspirated from the T75 flasks, washed with 3ml versene (8g NaCl, 0.2g KCl, 1.15g $Na2HPO_4$, 0.2g KH_2PO_4, 0.2g ethylenediaminetetraacetic acid (EDTA)($2Na^{++}$) in 1L distilled water, dispensed into 200ml aliquots and autoclaved) per T75 flask, washed with 3ml versene plus 0.25% v/v trypsin per T75 flask, then trypsinised with 3ml versene plus 0.25% v/v trypsin per T75 flask and incubated at 37°C until the cells had detached from the flask surface. Then 7ml DMEM were added per flask to inhibit the trypsin. For HEKn cells, the media was aspirated from the T75 flasks, washed with 2ml trypsin-EDTA (TE) (Gibco, cat# R-001-100) per T75 flask, then trypsinised with 2ml TE per T75 flask and incubated at 37°C until the cells had detached from the flask surface. Then 5ml trypsin neutraliser (TN) (Gibco, cat# R-002-100) were added per flask to inhibit the

trypsin. This was pipetted into a falcon tube and then each T75 was repeatedly washed (6ml for 4 flasks) and the solution added to the falcon tube. Once the trypsin inhibitor had been added, the falcon tubes were centrifuged at 1000g for 5 min. The supernatant was aspirated and the pellet was resuspended in 10ml DMEM for HaCaT cells or 10ml EpiLife for HEKn cells, then 20µl of the solution was added to 20µl of trypan blue for the cells to be counted on a haemocytometer. This was then used to calculate the volume of cells to be seeded into a new flask, and DMEM or EpiLife added to a final volume of 15ml or 10ml respectively.

2.3.2.1.1. Freezing

Once the cells were confluent, to freeze them down for banking the cells needed to be trypsinised following the passaging protocol, counted, then centrifuged at 1000g for 5 min. The cryovials were prepared by putting them on ice. Next the supernatant was aspirated, and the cells resuspended at a concentration of $1x10^6$ cells/ml in DMEM with 10% FBS, 1% P/S and 10% dimethyl sulfoxide (DMSO) for HaCaT cells or in Synth-a-Freeze medium (Gibco, cat# A13713-01) for HEKn cells. These were left overnight at -80°C and then moved to -150°C.

2.3.2.2. Crystal violet staining of adherent cells

In a modified colony formation assay for cell survival (Feoktistova *et al*., 2016), HaCaT cells were seeded at approximately $8.6x10^4$ cells/well in a 24 well plate, with 1ml DMEM plus 10% FBS and 1% P/S. They were then incubated for 48h at 37°C and 5% CO_2. Next the cells were treated for 4 min with filter sterilised potassium thioglycolate (0.45M, 45mM, 4.5mM) or guanidine carbonate (0.44M, 44mM, 4.4mM). Each chemical and concentration was tested separately, 1ml/well, and repeated three times. There were two control conditions: a phosphate buffered saline (PBS) wash and wells without any interference. After treatment, all wells including controls were given 1ml/well media and incubated overnight. Then the media was aspirated, the cells washed with PBS, and fixed with 10% formalin for 10 min at room temperature before aspirating. Next, 1ml/well of 0.5% (w/v) crystal violet in distilled water was added for 30 min at room temperature. This was then aspirated and the wells were left to air dry. Finally, the wells were washed gently with tap water in a fume hood. The wells were imaged on the Leica M165 FC microscope.

2.3.2.3. Cell viability assay

This cell viability assay or MTT assay (Mosmann, 1983; Denizot and Lang, 1986) uses thiazoyl blue tetrazolium bromide (Sigma, cat# M2128) to measure the metabolic activity of cells. HaCaT cells were seeded at approximately $5.3x10^4$ cells/well in a 24 well plate, with 1ml DMEM plus 10% FBS and 1% P/S. They were then incubated for 48h at 37°C and 5% CO_2. Next the cells were treated for 4 min with filter sterilised potassium thioglycolate (0.45M, 45mM, 4.5mM) or guanidine carbonate (0.44M, 44mM, 4.4mM). Each chemical and concentration was tested separately, 1ml/well, and repeated three times. There were three control conditions: untreated cells, a no-cell control, and a 50µM JNK inhibitor II treatment. Phenol-red free DMEM was prepared with 10% FBS and 1% P/S, and in it was dissolved 1mg/ml thiazoyl blue tetrazolium bromide. This was fully dissolved by incubating at 37°C in the dark for at least 15 min. This was then filter sterilised by passing through a 0.2µm filter using a sterile syringe, and protected from direct light. The media was then removed from the cells, washed with PBS, and 1ml thiazoyl blue tetrazolium bromide MTT reagent solution was added to each well. The wells were incubated for 1h at 37°C in the dark. Next, the solution was removed from the wells and they no longer needed protection from the light. Acidic isopropyl alcohol (IPA), made using 10% HCl in propan-2-ol, was added 500µl/well, and placed on a shaker for 10 min. Subsequently, 100µl of the solution was pipetted into a cuvette, followed by the addition of 900µl IPA to dilute. The no-cell controls were used to blank the spectrophotometer at 570nm to eliminate background absorbance values. The MTT cell viability assay measures colorimetric change due to the conversion of the yellow tetrazolium substrate into an insoluble purple formazan product. This reduction can only be performed by metabolically active and therefore viable cells. The colorimetric change that results is recorded as an absorbance, read at 570nm on a spectrometer, and is directly proportional to the number of living cells in culture.

2.3.2.4. Immunofluorescence

Six-well plates were prepared with three autoclaved 13mm glass coverslips in each well. Using a haemocytometer, HaCaT cells were seeded equally into 6 well plates with DMEM including 10% FBS and 1% P/S. The cells were then incubated at 37°C and 5% CO_2. The cells were checked daily for confluency and the media was changed every 48h. Once the cells were 50-90% confluent they were treated with the depilatory chemicals for 4 min.

Some samples were also treated with 50µM c-Jun N-terminal kinase (JNK) inhibitor II (SP600125) (Calbiochem, cat# 420119), which was protected from light. Cells were then given new media, including 50µM JNK inhibitor II if applicable, and incubated for either 1h or 48h depending upon the protein under investigation. The cells were then fixed with 1ml/well 4% paraformaldehyde (PFA) for 12 min at room temperature. The PFA was removed and 2ml/well PBS was added so the cells could be stored in the fridge for up to a week until staining. Next, 0.5% Triton X-100 (Fisher Scientific, cat# BPE151-100) in PBS was added 1ml/well for 15 min at room temperature. The wells were then washed twice with PBS for 4 min each at room temperature. Following this the cells were incubated with 0.5% fish skin gelatin (Sigma, cat# G7765), 1% Triton X-100, and 1% bovine serum albumen (BSA) with 1ml/well for 30 min at room temperature to block non-specific antigens. The cells were then washed twice in PBS but the second wash was not removed, allowing for the secondary antibody-only controls to be stored in PBS until required, otherwise the controls were treated the same as the test samples. Primary antibodies were prepared in blocking solution. Primary antibodies were pipetted onto labelled parafilm, 50µl for each coverslip, and then the coverslips were placed on top of the droplet cell-side down and incubated for 1h at room temperature or overnight at 4°C in a moist chamber. The coverslips were then washed in 50µl PBS droplets on parafilm four times for 5 min each at room temperature. Secondary antibodies were prepared in blocking solution. Secondary antibodies were pipetted onto labelled parafilm, 50µl for each coverslip, and then the coverslips were placed on top of the droplet and incubated for 1h at room temperature in a moist chamber. The coverslips were then washed five times with PBS, and mounted onto glass slides using ImmunoMount mounting media with 1:1000 4',6-diamidino-2-phenylindole (DAPI). The slides were ready for imaging the following day and could be continuously stored in the dark at 4°C.

2.3.2.5. Protein extraction, electrophoresis and immunoblotting

HaCaT cells cultured in 10cm^2 plates were harvested for total cell protein extraction as follows: the media was removed and the cells washed with PBS. The cells in the plates were then placed on ice. Using cell scrapers, the cells were lysed using 2x Laemmli (Laemmli, 1970) sample buffer (50mM Tris-HCl pH6.8, 20% v/v glycerol, 1mM EDTA, 1% sodium dodecyl sulphate (SDS)) supplemented with protease inhibitor cocktail (Roche,

UK), 1 tablet/10ml sample buffer, 1ml/plate. The samples were then boiled for 5 min. Next, the samples required homogenising through a 25G needle with fifteen repetitions. The samples were then centrifuged at 13g and 4°C for 5 min. Following this the supernatant was moved into a clean Eppendorf and pipetted into 20µl aliquots. The aliquots were frozen at -20°C for up to a month.

Modified Bradford assays (Bradford, 1976) were carried out to determine the total protein concentration in each of the samples (table 2.3).

Reagent	**Standard**						**Sample**
	1	**2**	**3**	**4**	**5**	**6**	
1mg/ml BSA	0	1	2	5	10	15	2 (of sample, not BSA)
0.1M HCl	10	10	10	10	10	10	10
Laemmli sample buffer	2	2	2	2	2	2	0
Distilled water	88	87	86	83	78	73	88
20% Bradford Reagent	900	900	900	900	900	900	900

Table 2.3. Modified Bradford assay standard and sample constituents. Amounts are in microlitres.

After adding the Bradford Reagent, the solutions were then incubated at room temperature for 15 min. The absorbance was read on a spectrophotometer set at a wavelength of 595nm. A standard curve was then plotted using the average absorbance, and compared to the standards and the concentration calculated along with the volume of sample for loading 20µg onto gels.

A protein electrophoresis gel (Tiselius, 1937) was then run using BioRad equipment and stained with coomassie blue (0.1% brilliant blue (BioRad, cat# 161-0400), 10% acetic acid, 50% methanol, 40% water) to check for equal loading as follows: a 10% resolving/running gel was prepared, 6ml/gel (1.5ml 40% acrylamide, 1.5ml 1.5M Tris pH8.8, 60µl 20% SDS, 2.94ml distilled water, 60µl ammonium persulphate (APS), 2.4µl N,N,N',N'-tetramethylethylenediamine (TEMED) (Sigma, cat# T7024)), the APS and TEMED were added last before pouring the gel. A thin layer of ethanol was used to flatten the gel. Once the gel was set, the ethanol was removed and the 4% stacking gel was poured, 3ml/gel (300µl 40% acrylamide, 390µl 1.0M Tris pH6.8, 30µl 20% SDS,

2.28ml distilled water, 30µl APS, 3µl TEMED (APS and TEMED were added immediately before pouring)). A 15-toothed comb was inserted into the gel and left to set. Once set, the comb was removed and the tank buffer (3.03g Tris, 14.42g glycine, 1.0g SDS, in 1L distilled water) was poured into the inner chamber of the BioRad gel tank. Samples were prepared using the volume required for 20µg of sample, adding 2µl 5xSB loading buffer, and topping up to 15µl with distilled water. The samples were then boiled at 95°C for 3-5 min and centrifuged at 12000rpm for 5 min. The samples were then loaded or kept on ice until ready. In each gel 5µl protein standard marker was loaded to the left of the samples. The rest of the tank was filled with tank buffer and run at 120V for approximately 1.5h. The gel was then stained with coomassie blue for about 1h. The gel was then destained (7% acetic acid, 20% ethanol, 73% water) for at least 2h with two changes until the background of the gel was nearly clear. An image of the gel was then taken.

If the samples appeared to be loaded equally another gel was then carried out, but not stained with coomassie. Instead the gel was prepared for transferring by stacking it into the XCell II Blot Module (Invitrogen, cat# EI9051), along with blotting pads and filter paper (amounts and ordering depended upon the number of gels to transfer), a transfer membrane on the anode side of the gel, soaked with transfer buffer (3.03g Tris, 14.4g glycine, 200ml methanol, 800ml water), and a roller was used to remove air bubbles. The chamber was filled with transfer buffer and the outer tank with distilled water to assist with heat transfer. Transfer was run at 250mA for 2h 15min.

After transfer the gel was coomassie stained to check for protein transfer and an image was taken. The membrane was washed thrice on a rocker, 5 min each, in blot rinse buffer (BRB+T) (1.21g Tris, 8.8g NaCl, 0.372g EDTA, 1ml Tween 20 (VWR, cat#437082Q) topped up to 1L with distilled water). The membrane was then stained with Ponceau S for a few minutes, then rinsed with BRB+T, and an image taken to check the protein has transferred equally. The stain was then completely rinsed off the membrane with BRB+T, this was then followed by blocking in 5% milk powder in BRB+T for 1h at room temperature. The membrane was then incubated in primary antibody made up in blocking solution, on a rocker ensuring that the membrane gets equal coverage for 1h at room temperature or overnight at 4°C. The primary antibodies could be reused up to 4 times if stored at -20°C. The membrane was then washed thrice on a rocker, 5 min

each, in BRB+T, before incubating in horseradish peroxidase (HRP) in blocking solution for 1h at room temperature on a rocker. The membrane was then washed thrice on a rocker, 5 min each, in BRB+T. An enhanced chemiluminescence (ECL) Western blotting (WB) analysis system was used for the detection reagents (Amersham, cat# RPN2108). Per membrane, 0.5ml detection reagent 1 was added to 0.5ml detection reagent 2 and mixed. The membrane was put in a plastic envelope and the ECL added for 1 min. The ECL was removed by blotting the corner of the membrane before the membrane was placed in the X-ray film cassette, ensuring there were no air bubbles as the plastic sheet was lowered. In the dark room the X-ray film was cut and placed over the plastic sheet covering the membrane for up to 1 min, depending upon the intensity of the signal. This was then developed and an image was taken for densitometry analysis. This method was then repeated from the wash before the primary antibody incubation for the loading controls.

2.3.2.6. Antibodies utilised

Type	Immunogen	Manufacturer	Class	Dilution
Primary	HSP27	ThermoScientific, cat# MA3-015	Mouse monoclonal	IF: 1:500 WB: 1:1000
Primary	HSP70	ThermoScientific, cat# MA3-028	Mouse monoclonal	IF: 1:200 WB: 1:500
Primary	Keratin 14	Abcam, cat# ab7800	Mouse monoclonal	IF: 1:200 WB: 1:800
Primary	Involucrin	Abcam, cat# 80530	Mouse monoclonal	IF: 1:200 WB: 1:1000
Primary	Ki67	Abcam, cat# ab16667	Rabbit monoclonal	IF: 1:250
Primary	Actin	Abcam, cat# ab11003	Mouse monoclonal	WB: 1:500
Primary	GAPDH	Abcam, cat# ab9485	Rabbit polyclonal	WB: 1:2000
Primary	β-tubulin	Sigma, cat# T8328	Mouse monoclonal	WB: 1:2000

Primary	Periplakin	Santa Cruz Biotechnology, cat# SC-16754	Goat polyclonal	IF: 1:100
Primary	Desmoplakin	Abcam, cat# ab14418	Rabbit polyclonal	IF: 1:400
Secondary	Goat anti-mouse	AlexaFluor	594	IF: 1:800
Secondary	Goat anti-rabbit	AlexaFluor, cat# A11008	488	IF: 1:800
Secondary	Donkey anti-rabbit	AlexaFluor	488	IF: 1:800
Secondary	Donkey anti-goat	AlexaFluor	594	IF: 1:800
HRP	Goat anti-mouse	Dako, cat# P0447	Polyclonal	WB: 1:1000
HRP	Donkey anti-rabbit	Jackson Immunoresearch, cat# 711-035-147	Polyclonal	WB: 1:3000
Other	Phalloidin	AlexaFluor, cat# A12379	488	IF: 1:500
Other	DAPI	Sigma	405	IF: 1:1000

Table 2.4. Antibodies used for HaCaT analysis. IF = immunofluorescence. WB = Western blotting. HRP = horseradish peroxidase.

2.3.3. HEKn cells

2.3.3.1. 3D epidermal model generation

The required number of corning transwell inserts (Corning, cat# CLS3413-48) were transferred into a sterile 24 well tissue culture plate. A collagen coating matrix solution was prepared by diluting coating matrix (Gibco, cat# R011K) 1:100 in dilution medium, and adding 100µl to each insert. The coated inserts were then incubated at room temperature for 30 min. During this time, HEKn cells in 2D cell culture were trypsinised, centrifuged, and the supernatant aspirated. Then the coating matrix solution was aspirated. The cell pellet was resuspended in prepared EpiLife (with 1% HKGS, 0.2% G/A,

10ng/ml keratinocyte growth factor (KGF) (Gibco, cat# PHG0094), 140uM $CaCl_2$, 50µg/ml ascorbic acid (Sigma, cat# A4544) (from frozen sterile filtered aliquots)) to a final concentration of $2.5x10^6$ cells/ml, and distributed at 100µl. Cells were incubated for 1h to allow them to attach to the insert (fig. 2.3.A), then two drops of media were gently added on top of the insert, and 2ml of media were added between the well and the insert. The undersides of the inserts were checked for air bubbles. The seeded inserts were then incubated at 37°C in 5% CO_2 for 48h (fig. 2.3.B). After 48h the cells were taken to the air-liquid interface (fig. 2.3.C). The media was aspirated and newly prepared EpiLife (with 1% HKGS, 0.2% G/A, 10ng/ml KGF, 1.64mM $CaCl_2$, 50µg/ml ascorbic acid) was added 0.5ml to each well, keeping the insert surface dry. This media was changed every 48h for 10 days, after which the cells were either treated or fixed.

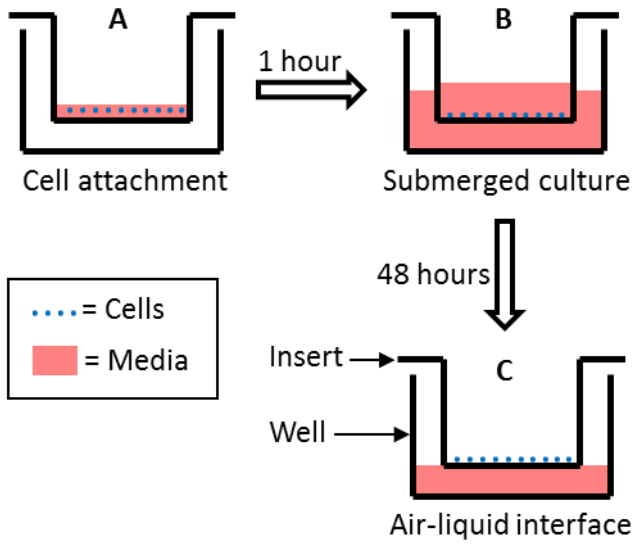

Fig. 2.3. Schematic of part of the 3D epidermal model generation. A) Attachment of the cells on the surface of the insert. B) Incubation of the submerged culture for 48h, C) Removal of the media to give the air-liquid interface.

2.3.3.2. Paraffin embedding

The 3D HEKn epidermal models were fixed by removing the media, cutting the inserts in half with a scalpel (half for paraffin embedding, half for cryofixation (see 2.3.2.4.)), and adding 1ml 4% PFA to the half for paraffin embedding for 1h at room temperature or overnight at 4°C. The inserts were then washed twice with PBS, and dehydrated in ethanol series of 30%, 50%, 70%, 80%, 90%, 95%, and 100% for 10-15 min each at room temperature. They could be left overnight at 4°C in 95% ethanol if necessary. The inserts were then incubated in histoclear (National diagnostics, cat# HS-200) for 10-15 min,

before adding an equal amount of wax from the wax dispenser and placing the inserts in the oven set at 60°C for 30 min. The solution was then poured off and more wax was added and placed in the oven for 1h. Then the inserts were taken out and placed with the straight side in the moulds half filled with molten wax, running parallel with the plastic mould lengthwise so that the cell layers would not separate when sectioning with a microtome and all layers could be seen in one section. The rest of the mould was then filled with wax, the cassette added, and some more wax added on top. These were then placed in the fridge at 4°C overnight or until sectioning. When sectioning, the sections were cut at a thickness of 5µm or 10µm, and left to dry for at least 2h on a hot block, then stored at room temperature prior to staining.

2.3.3.2.1. Immunohistochemistry

First the slides were placed in a rack and deparaffinised in xylene for two washes, 3 min each. The slides were then washed in 1:1 xylene:100% ethanol for 3 min. Next the slides underwent serial ethanol rehydrations for 3 min each in 100% (twice), 95%, 70% and 50%. They were then kept in cold water until ready for antigen retrieval or permeabilisation. Antigen retrieval consisted of placing the slides in a 10mM citric acid + 0.05% Tween 20 pH6.0 bath at 95°C for 20 min. The sections on the slides were then drawn around using an ImmEdge hydrophobic barrier pen (Vector laboratories, cat# H-4000). The cells were then permeabilised in 0.1% Triton X-100 in PBS for 15 min. Next, nonspecific binding was blocked with blocking buffer (2% BSA and 1% fish skin gelatin in PBS). After carefully draining the blocking buffer away the sections were incubated with primary antibody in blocking buffer, 50µl per section, for 1h at room temperature or overnight at 4°C in a moist chamber. The sections were then washed twice with PBS. Following this came incubation with the secondary antibody in 2% BSA in PBS for 1h at room temperature in the dark. The sections were then washed thrice for 5 min each with PBS, before mounting in ImmunoMount mounting media with 1:1000 DAPI. The slides were ready for imaging the following day and could be continuously stored in the dark at 4°C.

2.3.3.2.2. Antibodies utilised

Type	Immunogen	Manufacturer	Class	Dilution
Primary	HSP27	ThermoScientific, cat# MA3-015	Mouse monoclonal	1:500
Primary	HSP70	ThermoScientific, cat# MA3-028	Mouse monoclonal	1:1000
Primary	Ki67	Abcam, cat# ab16667	Rabbit monoclonal	1:100
Primary	Keratin 14	Covance, cat# PRB-155P	Rabbit polyclonal	1:1000
Primary	Involucrin	Abcam, cat# 80530	Mouse monoclonal	1:750
Secondary	Goat anti-mouse	AlexaFluor	488	1:1000
Secondary	Chicken anti-rabbit	AlexaFluor	594	1:1000
Other	Phalloidin	AlexaFluor, cat# A12379	488	1:500
Other	DAPI	Sigma	405	1:1000

Table 2.5. Antibodies used for HEKn epidermal model analysis.

2.3.3.3. Cryo-embedding

The media from the 3D HEKn epidermal models was removed, and the inserts cut in half with a scalpel (half for paraffin embedding (see 2.3.2.3.), half for cryofixation). A layer of optimal cutting temperature compound (OCT) (Scigen, cat# 4583) was placed at the bottom of a plastic mould and put on top of a foiled lined polystyrene box containing liquid nitrogen. The cut semi-circular insert was placed with the straight side in the OCT running parallel with the plastic mould lengthwise so that the cell layers would not separate when microtoming and all layers could be seen in one section. The rest of the mould was then filled with OCT carefully as to not disturb the position of the insert, and lowered into the liquid nitrogen bath. Once frozen, the samples were wrapped in foil at stored at -80°C until cryosectioning. When cryosectioning, the sections were cut to a

thickness of 7µm. They were then dried at room temperature for 1h before storing at -20°C until staining.

2.3.3.3.1. Haematoxylin and eosin staining (H&E)

Slides were placed into a rack and taken through the following procedure for Mayers haematoxylin and eosin staining. For paraffin embedded sections, slides were placed in histoclear for 5 min, 100% ethanol for 2 min, 95% ethanol for 1 min, 70% ethanol for 1 min, distilled water for 1 min, haematoxylin (1g haematoxylin (RA Lamb), 0.2g sodium iodate and 50g aluminium potassium sulphate added to 1L distilled water, stirred overnight then 50g chloral hydrate and 1g citric acid crystals added, boiled for 5 min and ripened at room temperature for 3 months) for 5 min, distilled water for 30s, alkaline alcohol (3% ammonia in 70% ethanol) for 30s, 70% ethanol for 30s, 95% ethanol for 30s, eosin (0.5% eosin (RA Lamb) in 95% ethanol) for 30s, 95% ethanol twice for 10s each, 100% ethanol for 15s then 30s, histoclear twice for 3 min each. For cryo-embedded sections, slides were placed in PBS for 10 min for rehydration, then fixed in 4% PFA at 4°C for 15 min, then washed thrice in PBS for 5 min per wash, then washed in distilled water for 1 min, stained in Mayers Haematoxylin for 5 min, washed in distilled water for 30s, blued the nuclei in alkaline alcohol for 30s, dehydrated in 70% followed by 95% ethanol for 30s each, stained in eosin for 1 min, dehydrated in 95% ethanol twice for 10s each, dehydrated in 100% ethanol for 30s, and washed in histoclear twice for 3 min each. All the slides remained in the histoclear until coverslips were mounted using DePeX (BDH, cat# 361252B) and were then left to dry for at least 1h in a fume hood. The Leica DM500 compound light microscope was used to image H&E HEKn epidermal sections.

2.3.4. Cornified envelope extraction

Cornified envelopes were extracted according to Maatta *et al*., (2001) and Sevilla *et al*., (2007). Rat ear tip tissue samples were cut into smaller pieces using sterile scissors and added to cornified envelope extraction buffer (20mM TrisHCl pH7.5, 5mM EDTA, 10mM dithiothreitol (DTT) and 2% w/v SDS) and boiled for 20 min at 95°C. The pieces of remaining bulk were then removed with tweezers, and the mixture was centrifuged at 1000g for 5 min. The supernatant was then removed and the mixture was resuspended in cornified envelope wash buffer (0.2% w/v SDS). This centrifugation and wash was repeated twice, before the cells were resuspended in PBS with 0.6mg/ml Nile red for imaging.

2.3.5. Treatment of cells with hair modifying chemicals

The commercial potassium thioglycolate and novel guanidine carbonate component were tested on cells with an application time of 4 min. This required staggering of the treatments to ensure each treatment lasted precisely 4 min. 50µM JNK inhibitor II (SP600125) (Calbiochem, cat# 420119) was also tested with treatments and alone along with 1.5mM $CaCl_2$ to investigate the effect of the treatments on differentiation pathways. As JNK inhibitor II is soluble in DMSO, a DMSO control was also used along with the no-treatment control. All experiments were carried out in triplicate.

Chemical	Concentrations (M)	Cells tested
Potassium thioglycolate	0.45	HaCaT, HEKn, cornified envelopes
Potassium thioglycolate	0.2	Cornified envelopes
Potassium thioglycolate	0.045	HaCaT, HEKn
Potassium thioglycolate	0.0045	HaCaT, HEKn
Guanidine carbonate	0.44	HaCaT
Guanidine carbonate	0.2	Cornified envelopes
Guanidine carbonate	0.1	Cornified envelopes
Guanidine carbonate	0.044	HaCaT, HEKn
Guanidine carbonate	0.0044	HaCaT, HEKn

Table 2.6. Concentrations of the treatments, and the cells on which they were tested. KTG = potassium thioglycolate, GC = guanidine carbonate.

2.4. Imaging

2.4.1. Confocal microscopy

2.4.1.1. Leica TCS SP5

The Leica TCS SP5 confocal laser scanning microscope was used as the main system for imaging hair and skin samples. The microscope system has a choice of 9 laser lines for excitation: 405nm, 458nm, 476nm, 488nm, 496nm, 514nm, 543nm, 594nm, and 633nm. Though all of these laser lines were used in this study, 405nm was predominantly used for autofluorescence, and 633nm was also used in reflection mode. In addition, there are two pulse lasers: 470nm and 640nm for use with FLIM using the TCSPC method

(time-correlated single photon counting). FLIM data was acquired (photons counted) until 1000 photons were counted in the brightest image pixel. This microscope is capable of selective spectral detection ranges of 400nm-800nm and spectral scans, and has 5 detectors: PMT1-4 (PMT 2 and 4 are FLIM PMTs) and HyD. In the SP detection system, instead of filters, spectral separation is performed by a prism and adjustable mirror-sliders in front of each detector. It is this arrangement that allows simultaneous data acquisition at five individually tuneable spectral bands. The HyD detector reduces acquisition times and allows the use of lower laser intensities, giving reduced photobleaching, phototoxicity and improved cell viability. Images were acquired with either a 1.4NA 63x or a 1.25NA 40x oil immersion objective, or a 1.2NA 63x water immersion objective. In the majority of cases, images were acquired at a scanning speed of 400Hz with a pixel resolution of 1024x1024, with line averaging.

To image hair autofluorescence with an UV excitation source below 405nm, a second Leica SP5 II system was used which possessed an 80mW coherent 355nm 3rd harmonic NdYAG laser. Images were acquired with the same settings as described above.

2.4.1.2. Zeiss 880 Airyscan

The superior image quality and sensitivity of the Zeiss 880 Airyscan, which arrived towards the end of the project, was used to further image putative melanin granules within the hair. The 405nm laser line was used for autofluorescence and the 633nm laser line was used for reflection, along with the 1.4NA 63x oil immersion objective.

2.4.2. Super-resolution

The system is an Applied Precision OMX BLAZE Super-Resolution microscope supplied by GE Healthcare. The microscope can use two light based modalities to achieve multichannel super-resolution or sub-diffraction imaging below 200nm. The first is 3D-SIM (structured illumination microscopy) which provides an 8-fold improvement in volumetric resolution (xy 100nm by z 250nm) using a wide variety of common fluorophores at high frame rates (16 3D-SIM sections (0.125nm, 2µm) in 1s (240 images)). Secondly the system is also equipped with Deltavision localisation microscopy, allowing lateral resolution of 20-50nm, <100nm axial. In addition to the super-resolution methods mentioned above, this microscope can be used in ultra-high speed conventional widefield mode which can then be subjected to deconvolution to very

quickly generate high quality 3D images. This setting with 405nm excitation and the 1.40NA 63x oil immersion objective was used to image the hair transversely to give a high resolution of the exocuticle and endocuticle.

2.4.3. Total internal reflection fluorescence (TIRF)

The Leica AM TIRF MC was used to selectively image the surface of the hair when stained with R18. The 561nm laser line was used for excitation with the 1.47NA 100x oil immersion objective. TIRF uses the evanescent field generated by total internal reflection to excite fluorophores. Instead of illuminating an entire specimen with excitation light, as in widefield fluorescence microscopy, the evanescent field only penetrates the specimen to a depth of 70–200 nm. The system uses an EMCCD camera providing fast acquisition speed and images with excellent signal to noise.

2.4.4. Transmission electron microscopy (TEM)

Hairs were prepared for imaging on the Hitachi H-7600 TEM by undergoing serial ethanol dehydrations, followed by incubating for 10 min in 1% alcoholic uranyl acetate to stain the phosphate and amino groups. The hydroxyl groups were then stained using lead citrate for 10 min. The hairs were then embedded in hard LR white, and sectioned at 50-70nm onto 50 and 100 mesh grids. Samples were imaged on the TEM using an HV of 100kV.

2.4.5. Field emission scanning electron microscopy (FeSEM)

This Hitachi S-5200 FeSEM has a very high resolution of up to 0.5nm. Hairs were prepared for imaging on the field emission scanning electron microscope in glass vials and placed on a rotator. First they were fixed in 2.5% glutaraldehyde and 0.1M cacodylate buffer for 30 min. Then they were washed twice for 5 minutes each in 0.1M cacodylate buffer, stained with 1% osmium tetroxide for 30 minutes, then washed thrice for 5 minutes each time in 0.1M cacodylate buffer. Hairs were then serially dehydrated for 10 minutes in each of 50%, 70%, 95% and 100% ethanol. Next, the hairs underwent critical point drying, then were cut into 0.5cm lengths, and attached to silicon chips with conductive tape. Finally, hairs were sputter coated with 5nm platinum at a 50° tilt before imaging.

2.4.6. Software

ImageJ was used for the image analysis of Western blots and images from microscopes. LAS AF Lite software was used for the analysis of Leica SP5 confocal images. SymPhoTime 32 software was used for the gathering of data using FLIM on the Leica SP5 as well as for the curve fitting and analysis of data. LAS EZ software was used to gather images on the Leica DM500 microscope. Zen Blue is the analysis component of the software used for image analysis on the Zeiss 880 microscope. The AMT V600 image capture engine was used to capture images on the TEM. With all software, only linear adjustments were made to the brightness (luminosity) and contrast of the images. All raw data with accompanying metadata is available on the instrument computers and on personal hard drives.

Once the data was gathered, most of the numerical data analysis was carried out in Microsoft Excel. Graphs were produced where necessary, and displayed with error bars of ± 2* standard error of the mean (SEM) unless otherwise stated. Error bars of ±2*SEM were chosen as these represent an approximate confidence interval of 95% of the true parametric mean, whereas ±1*SEM only gives a ~68% confidence interval of the true mean (McDonald, 2014). The approximate 95% confidence interval is a more useful metric to view on the graphs. Statistical analysis was performed using Microsoft Excel and Minitab 17. Parametric and non-parametric statistical tests were used where appropriate and after performing an Anderson-Darling normality test. The parametric f-tests, t-tests and paired t-tests were used to analyse data for significant differences. The non-parametric tests used were the Wilcoxon paired test, Mann-Whitney U-test and the Kruskal-Wallis test. For a result to be considered significant enough to reject the null hypothesis the p-value was <0.05.

Chapter 3

Visualisation of hair structures by label-free imaging

3.1. Introduction

In order to study the effects of chemical depilatories on hair, first the structure of the untreated hair must be understood. Chinese scalp hair was used as the standard hair model, as it is very uniform in shape, size and colour compared to other body hairs and other ethnicities (Wei *et al*., 2005).

The overall aim of this chapter was to develop label-free imaging methods for hair, investigate the use of autofluorescence, and to develop optical transverse imaging and dynamic imaging methods. The subsequent aims were to use these methods to further the knowledge on hair structure and morphology, and to investigate an uncharacterised hair and skin disorder.

The first aim to visualise hair structures using label-free imaging is important because label-free imaging allows the native state of the hair to be observed, without dyes or processing prior to imaging which can cause artefacts. To date, the majority of hair imaging was done either using standard light microscopy, which does not allow resolution of the cellular structure of the cortex (Wagner *et al*., 2007); the use of histological dyes and sectioning (Swift *et al*., 2000); lower resolution confocal microscopy (Lagarde *et al*., 1994; Swift *et al*., 2000; Kirkbride and Tridico, 2010); or electron microscopy which requires time-consuming sample preparation (Bradbury and O'Shea, 1969; Clement *et al.*, 1981; Wagner *et al*., 2007), potentially changing the state of the native hair. In addition, hair has previously been imaged with digital volumetric imaging utilising autofluorescence of the hair (Gruber and Kerschman, 2004). Although similarly to electron microscopy the sample must be embedded in a polymeric matrix, potentially altering the hair, and additionally, the resolution of the images was not as high as those gathered with the equipment available for this study. This meant that to image hair quickly, in its native state, and with high resolution, new methods needed to be developed in this study. First, the imaging of hair longitudinally using the various excitation wavelengths of confocal microscopy was optimised to find which wavelengths caused autofluorescence in specific areas of the hair. Next, other avenues were explored, including imaging the hair in real-time during treatment. The aim to develop label-free dynamic imaging methods was needed because these methods allow changes

in the hair to be followed in real-time, whereas all previously published methods only show the static end-point of the hair after treatment. The aim to develop the transverse optical sectioning method was important because the z-axis resolution in confocal microscopy is less than the x-axis and y-axis resolution, so the new method allows for more detailed analysis of structures through the hair than longitudinal imaging would allow. This method has paved the way for new insights to be made into the structure of hair. Mostly, confocal microscopy was used with a 405nm excitation laser because it induced the optimal autofluorescence in the hair. When necessary, findings were then validated using dyes and other microscopy techniques. The aim of label-free imaging was also achieved by using the reflection mode of the confocal microscope to detect reflective structures in the hair, without the need to stain the hair and at a higher resolution than previous research (Kimura *et al*., 1999; Hadjur *et al*., 2002; Rudnicka *et al*., 2008). Collection of image data in reflection mode differs from that used in conventional confocal fluorescence mode in that the range in which the detector operates is moved to overlap the wavelength being emitted only, omitting induced fluorescence wavelengths.

This study accomplishes the aims to further knowledge on hair structure and morphology through the following approaches. First the emission spectra of the hair cuticle and cortex when excited with 9 different wavelengths is explored to show why 405nm was chosen as the primary wavelength for exciting the hair. The chapter then goes through the layers of the hair, concentrating on each in turn and highlighting the novel insights made. Firstly, the cuticle is investigated, centring on the cuticle surface, the exocuticle and the endocuticle, the cuticle in beard hair, and the effect upon the cuticle of plucking the hair. Next the cortex is examined, focussing on organelle remnants and melanin-like particles, followed by the medulla. The results of measuring the cuticle cell length, organelle area and cortical cell area along a year's worth of hair growth are then shown to determine whether there are any annual trends in the cell and organelle sizes. These measurements were also done to investigate the effect upon the results of randomly sampling hair from any region along its length. Subsequently, the final aim is achieved by using the newly developed methods which enabled the investigation of a sample of hair from a patient with an unknown hair and skin disorder, wherein insights were made to help with the characterisation of the disorder.

3.2. Experimental approach

All the shown images are representative examples of at least 5 hairs imaged longitudinally or 6 hairs imaged transversely with each setting, unless stated otherwise.

3.2.1. Spectral scans

Spectral scans were carried out using the Leica TCS SP5 confocal laser scanning microscope. All scans were done using 30% of the power capacity of each of the 9 laser lines. Non-normalised emission spectra were used to show the intensity of autofluorescence caused by each laser, and normalised emission spectra were used to show at which wavelengths on the spectrum the emission from the sample fluoresced. Only spectra from one particular hair is shown, but there was little difference in the patterns of emission from different hairs.

A power of 0.15mW for each laser was chosen to image the hair as this was the power of the weakest laser, which was 543nm, at 100% capacity. All other lasers were adjusted to emit a power of 0.15mW. The images are representative of the hair samples.

3.2.2. Dyed/stained hair

Hair was stained with a variety of dyes, the details of which follow. Hair was soaked in 0.6mg/ml Nile red in ethanol for 5 min, then washed for 10 min in ethanol prior to imaging. For 50µM N-(2-aminohexyl)-5-(dimethylamino)naphthalene-1-sulphonamide stained hair, the dye was made up in DMSO. 200µM Rhodamine B chloride was made up in 90% ethanol, in which the hair was also washed after staining, as was the 10µM R18 stained hair. After hair was stained with 0.01M curcumin in ethanol, it was washed in water before imaging. Hair stained with H&E was done following the standard H&E staining procedure. Hair stained with 0.1M fluorescein in water was water washed before imaging. Finally, Oil Red O in 100% isopropanol was incubated with hair, and then the hair was washed in the same solvent. 10µM AlexaFluor 633 C_5 maleimide in DMSO was incubated with hair overnight in the fridge in the dark (n=11).

3.2.3. Melanin-like particles study

Six different hair colours were studied with all hair from blended hair swatches, except for the ginger and darker ginger/brown hair which was collected from two individuals,

with the samples split evenly for ginger and darker ginger/brown. The hair colours were black (n=3), brown (n=3), blond (n=3), ginger (n=6), darker ginger/brown (n=4), pale yellow/white old-age (n=5). The melanin-like particles were imaged at the upper cortex for the clear resolution of that depth, and densities of the particles were used to account for differences in area between the hairs.

3.2.4. Measurements along a year of hair growth

A hair was chosen for these measurements that possessed a cuticle and organelle remnants. Measurements were taken from the root to the tip direction, although it is unknown exactly where along the donor's hair the 12cm length was taken from, and which specific months of growth this corresponds to. The 12 individual "months" were separated from the hair using a ruler and a razor blade to measure and cut 1cm of hair corresponding to each month of hair growth. In total, there were 17512 cuticle cells measured for their length, 1795 circular organelle remnant areas measured, and 1425 cortical cells and corresponding organelle remnant areas measured using ImageJ. The cuticle cells were measured along the centre of the hair, and the cortical cells and their organelle remnants were measured at the upper cortex where they are clearest.

3.2.5. Uncharacterised hair and skin disorder

Samples were provided from close to the root of the hair. For confocal imaging of the hair longitudinally, 5 hairs were imaged from each donor – the patient and his parents. For confocal imaging of the hair transversely, 6 hairs were imaged from each donor. To assess the presence of lipid on the hair, the hairs were stained in 0.6mg/ml Nile red for 5 min, then washed in 100% ethanol. Three hairs from each of the donors was imaged using TEM.

3.3. Results

3.3.1. Structures in the hair can be resolved utilising label-free autofluorescence

3.3.1.1. Emission spectra validate 405nm as the optimum excitation wavelength

Spectral scans were carried out on the hair to find out which wavelengths caused the greatest autofluorescent response from the hair, and the differences between the cuticle and the cortex. Non-normalised spectra show the intensity of autofluorescence induced by each laser, and normalised spectra allow the shape and position of the smaller emission peaks to be viewed in more detail.

The non-normalised emission spectra show the intensity of autofluorescence after excitation of the cuticle and cortex with a range of lasers at mid-power from 405nm to 633nm. The lasers were used at mid-power for practicality when imaging. All wavelengths caused excitation of the fluorophores in the hair, although 633nm excitation caused a higher intensity of emission in the cuticle (fig. 3.1A) than the cortex (fig. 3.1B). The 405nm excitation caused the largest emission of photons from the hair at a 30% laser power, and excited many of the cellular structures found in the hair (fig. 3.2A), so was chosen as the main excitation wavelength for autofluorescent imaging of hair. The gap in the 405nm emission peak was due to a faulty notch filter in the equipment set up at the time of study.

The normalised emission spectra show the intensity of the fluorescence from the cuticle and cortex from excitation with wavelengths from 405nm to 633nm. The normalised spectra are useful as they show the effect of each laser individually, even if it only caused a small amount of autofluorescence as shown by the non-normalised spectra. The spectra were converted by the LAS AF Lite software by taking the largest intensity value for each wavelength and re-scaling with the largest intensity as 1. The main difference between the cuticle and cortex is that 543nm excitation caused emission of photons at a slightly longer wavelength in the cuticle (fig. 3.1C) than the cortex (fig. 3.1D).

Figure 3.2A shows the autofluorescent cuticle and cortex from excitation with 0.15mW power of 405nm to 633nm wavelengths. This power was chosen because this was the highest power of the weakest laser, 543nm. The range of wavelengths being detected

was equal to the wavelength of the laser plus 10nm, up to 800nm. Wavelengths 405nm to 543nm caused autofluorescence of the whole of the cuticle and cortex, with the overlap between 405nm and 543nm in particular inducing autofluorescence of spindle-shaped outlines within which were streaks. These could be the cortical CMC and organelle remnants respectively, which are examined in more detail below. The 594nm and 633nm excitation mainly excited the free edge of the cuticle cells. The graph of the intensity of the fluorescence (fig. 3.2B) showed the cortex is more autofluorescent than the cuticle although they respond similarly to the different excitation wavelengths. The composite image (fig. 3.2C) showed how the excitation wavelengths can be used to excite different structures at various depths in the hair. The 405nm excitation showed clarity of the cuticle and cortex, whereas 543nm excited the organelle remnants in the deeper cortex, and 633nm excitation was used to only excite the cuticle when the optical section was focussed deeper into the hair, and so 633nm can be used to selectively highlight and investigate cuticle structures.

To image hair autofluorescence with an UV excitation source below 405nm, a 355nm laser was used. However, this wavelength did not appear to excite any different structures in the hair compared with the 405nm laser excitation (data not shown).

3.3.1.2. Dyes validate autofluorescence

Several lipophilic histological dyes were tested to validate the structures resolved with autofluorescence and to see if any more structures could be stained, as the hair contains many lipids (Wertz and Downing, 1988; Masukawa *et al*., 2005a,b), or if label-free imaging can be used equally well to visualise structures both in the cuticle and in the cortex. Figure 3.3A showed the label-free 405nm excited autofluorescent cuticle, and compared to the 0.6mg/ml Nile red stained cuticle (fig. 3.3B), gave full view of the cuticle, whereas Nile red stained the area of the cuticle cells towards the free edge. Nile red is used to stain neutral lipids (e.g. cholesterol, cholesterol esters, triacylglycerols), phospholipids, sphingolipids, and fatty acids (Fowler *et al*., 1987). In the past it has been used as a stain for covalently cross-linked lipids on the surfaces of mature cornified envelopes in the epidermis (Sevilla *et al*., 2007). Figures 3.3D and 3.3E also showed staining more specifically on the free edge of the cuticle cells and punctate staining on the cuticle surface, where hairs have been stained with 200µM rhodamine B chloride stains and 10µM R18 respectively. N-(2-aminohexyl)-5-(dimethylamino)naphthalene-1-

sulphonamide (fig. 3.3C), curcumin (fig. 3.3F), and fluorescein (fig. 3.3H) also stain the cuticle, and H&E stained the free edge of the cuticle cells as seen at an optical slice within the hair (fig. 3.3G). Oil Red O is often used to stain storage lipids in adipocytes, but also stains neutral lipids although not biological membranes (Ramirez-Zacarias *et al*., 1992; Mehlem, *et al*., 2013). Here, Oil Red O was able to show lipids were present in the cortex of a sectioned hair (fig. 3.3I).

Transverse optical sectioning was developed to provide a novel perspective of the hair whilst using confocal microscopy. It allowed the individual cuticle cells to be distinguished, unlike in longitudinal imaging, and the whole of a cross-section of hair to be imaged at once without fluorescence being quenched by melanin granules as it is in longitudinal imaging. In addition to use with longitudinal imaging, transverse imaging allowed a fuller understanding of the structures of the hair. Using transverse optical sectioning to image 0.6mg/ml Nile red stained hair (fig. 3.4), Nile red stained the lipids present in the cuticle, CMC and vesicles (fig 3.4A,B). However, the same could be resolved without any dyes by using autofluorescence excited by the 405nm laser (fig. 3.4C,D).

In conclusion, label-free autofluorescence provides a similar level of visual information as dyes, and dyes cannot penetrate far past the cuticle into the hair. Dyes may also give rise to artefacts, which imaging using only autofluorescence avoids. Therefore, dyes were simply useful to validate the structures resolved using autofluorescence.

3.3.2. The cuticle

After the optimal label-free conditions were established, a detailed study of the structures that can be resolved was carried out. Firstly, cuticle structures were investigated using light microscopy including confocal, TIRF, and super resolution microscopy. SEM was used to confirm structures resolved by light microscopy on the cuticle surface.

3.3.2.1. The exocuticle is autofluorescent after 405nm excitation, but the endocuticle is not

By sectioning the hair transversely, TEM was able to resolve the cuticle cells (fig. 3.5A) and their sublamellar structure (fig. 3.5B), consisting of the darkly stained endocuticle, the lighter stained exocuticle, the lightest stained A-layer, and the CMC between the

cuticle cells. To understand the behaviour of the cuticle cell sublamellar structure under 405nm excitation, super resolution microscopy was used, as it has a 2x greater resolution than standard confocal microscopy. This required adapting the transverse imaging method by replacing the bottom glass coverslip with a glass bottomed well as required by the equipment set-up. Remarkably, super resolution microscopy using 3D structured illumination reconstruction was able to achieve resolution of the exocuticle and endocuticle utilising autofluorescence. The exocuticle was found to be autofluorescent after 405nm excitation, whereas the endocuticle was not (fig. 3.6). This was concluded as both a light band and a dark band together (double headed arrow) gave a width of approximately 500nm, which is the width of a cuticle cell, and the exocuticle is approximately 250nm in width, although the endocuticle can vary more in width (fig. 3.5B). Further to this, the innermost band appears to be dark, and the endocuticle would be innermost and closest to the cortex, whereas the outermost band appears light, and the exocuticle is closest to the air. Imaging of longitudinal sections was possible and gave a slightly higher resolution of the cortex (data not shown), but no new insights were made.

3.3.2.2. The cuticle can be sufficient to halt the penetration of light

Most of the experiments were carried out on scalp hair, through which the confocal microscope lasers were able to penetrate approximately half way, depending upon hair thickness and colour. The image also became blurry deeper into the hair when the returning light was unable to reach the detector without significant refraction or scattering. When experiments were carried out on beard hair, longitudinal imaging of the cortex was not possible (fig. 3.7B), as the extra cuticle cells of the beard hair absorbed the light (fig. 3.7A). Once the cuticle cells were removed, resolution of the cortex was possible (fig. 3.7C). This shows that with enough cuticle cell layers, typically 9 or more such as those found in beard hairs, the penetration of light into the cortex can mostly be blocked. So label-free visualisation of the cortex in intact hair is possible in scalp hair, but not in the thicker beard hair.

3.3.2.3. The cuticle cells beneath the skin surface curl upon plucking

Hair was plucked to investigate whether through label-free imaging it would be possible to see a difference between hair which has been above the skin and exposed to the ambient environment, and hair which has been below the skin interface and protected

by the hair follicle. Interestingly, when hair was plucked, there were thick autofluorescent bands around the outside of the root of the hair (fig. 3.7H). Using FeSEM the area below the skin interface was imaged (fig. 3.7D), and found the area where the cuticle starts, before which there is only cortex (fig. 3.7E,F). On the hair which had been beneath the skin there were the bands across the cuticle (fig. 3.7E), which at higher magnification were seen to be cuticle cells curled up in the direction the hair had been plucked (fig. 3.7G).

3.3.2.4. Cracks on the cuticle surface

TIRF allows the top 200nm of the cuticle to be imaged, which is useful for isolating the top cuticle cell for imaging. As seen in figure 3.8A, the free edges of the cuticle cells are stained with R18. The use of TIRF did not result in any more data than other confocal techniques. To get a higher resolution of the cuticle surface, FeSEM was used (fig. 3.8B), and showed where the exocuticle had been degraded away through everyday wear and tear to leave the endocuticle exposed (fig. 3.8C). Using a magnification of x150k, it was possible to resolve cracks on the surface of the cuticle (fig. 3.8D). This could be useful for industrial hair scientists to measure wear and tear, and possibly investigate the cracks as penetration pathways for chemicals.

3.3.3. The cortex

After examining the cuticle, an investigation was carried out into the next main section of the hair, the cortex. Firstly, a comparison was made between structures resolved using 405nm induced autofluorescence and Nile red stained hair. Nile red was able to penetrate to the outer cortex and stain the CMC of the cortical cells (fig. 3.9A). However, compared to 405nm induced autofluorescence of the same hair (fig. 3.9B), the dye does not add much more information other than highlighting the cortical CMC, as autofluorescence reveals the rest of the hair, including some melanin granules. Based upon the distribution of the melanin granules, the cortical cells can still be distinguished. Using FeSEM, these spindle shaped cortical cells can be seen when the hair is sliced open (fig. 3.9C,D). A TEM image of a transverse section through the cortex shows the CMC (fig. 3.9E) around a cortical cell, and the keratin macrofibrils within.

3.3.3.1. Organelle remnants are present in the cortex

Previous literature had identified structures within cortical cells, some papers of which call them nuclear remnants (Fischer *et al*., 2011; Szabo *et al*., 2012; Kelch *et al*., 2000), and others cytoplasmic remnants (Harland *et al*., 2011). Here, to encompass both possibilities, they are called organelle remnants. Organelle remnants were resolved within cortical cells throughout the cortex of some hairs, with one remnant per cortical cell, as defined by the CMC. These were resolved as more fluorescent areas than the surrounding area, and were more circular in shape in the cuticle, and more streak-like in shape towards the centre of the cortex, as shown in the diagonal optical section in figure 3.10A. Maleimide conjugated to 633nm AlexaFluor stains thiol groups (Taneda *et al*., 1980), which was used for an experiment in chapter 5 to stain the area which thioglycolate had attacked. Coincidently it was found to particularly stain the organelle remnants in the untreated hair (fig. 3.10B). The 405nm induced autofluorescence does not excite the Maleimide stain, and shows the hair as it is naturally (fig. 3.10C). In another hair, 543nm excitation can be used to show the organelle remnants using autofluorescence (fig. 3.10D), but 633nm excitation of the same hair does not excite the organelle remnants (fig. 3.10E).

Transverse TEM sections (fig. 3.11A) showed that organelle remnants are varied in shape (fig. 3.11B). Magnification by x30k of these remnants revealed that they are surrounded by keratin macrofibrils and are located towards the centre of the cortical cells (fig. 3.11C). Some of these remnants are encased by a double membrane, reminiscent of the nucleus or mitochondria or perhaps of the CMC, with lightly and darkly stained areas within (fig. 3.11D). Finally, some remnants also contain melanin granules (fig. 3.11E).

Attempts to stain the DNA with Hoechst33258 or the nuclear envelope with a lamin A/C antibody were unsuccessful in visualising any organelle remnants (data not shown).

3.3.3.2. Two types of melanin-like particles are present at different proportions in various hair colours

The presence of melanin-like particles in previous images led the investigation on to examining these more closely. This was done using different hair colours as they are known to have differing amounts of eumelanin and pheomelanin present in them, and could therefore be compared (Ito and Wakamatsu, 2011). Comparisons were made

using two lasers. Firstly, 405nm induced autofluorescence was used as black voids had been observed with that excitation wavelength in previous images. The second was reflection of the 633nm wavelength, as hair that was examined in the early stages of the study showed reflective particles in the cortex of the hair, and a previous study using optical coherence tomography which uses reflection showed similar images and named the particles as melanin (Choi *et al*., 2012).

Figure 3.12A shows confocal microscopy of longitudinal sections of hair at the upper cortex of various hair colours, displaying 405nm excited autofluorescence and reflection of the 633nm wavelength. Pale yellow/white hair shows no black or dark areas of voids where 405nm laser induced autofluorescence is absent. There are very few reflectant particles of this hair colour reflecting the 633nm wavelength. Dark ginger/brown hair had more black voids absorbing the 405nm, and more 633nm reflectant particles. Ginger hair again had few black voids absorbing the 405nm, and fewer 633nm reflectant particles than the darker ginger hair, but more than the white hair. The blond hair was similar to the dark ginger/brown hair in appearance, although had slightly more 405nm absorbing black voids and 633nm reflectant particles. The brown and black hair both had more numerous black voids absorbing the 405nm wavelength, and more 633nm reflectant particles than the other hair types.

The cuticle is also reflective, though not from the melanin granules, and just beneath it the 633nm reflectant particles can be imaged in the shape of a cortical cell (fig. 3.12B). To test whether the reflectant particles could be melanin, synthetic black/brown melanin was put under the microscope and was also found to reflect the 633nm wavelength (fig. 3.12C), confirming that at least some of the reflectant particles could be black/brown melanin (eumelanin). In addition, these melanin-like particles can be traced back to the plucked hair bulb where they absorb the 405nm wavelength (fig. 3.12D) and reflect 633nm (fig. 3.12E). Interesting autofluorescent swirls and waves in the hair shaft plucked from within the follicle can also be resolved in figure 3.12D, which could be from ongoing cortical keratinisation in the formation of the hair shaft.

It was found that the melanin-like black voids which absorb the 405nm wavelength also reflect the 633nm wavelength. Figure 3.12F shows a blond European hair imaged with the 633nm wavelength and detecting the reflection, with some of the reflectant

particles circled. Figure 3.12G shows the same area with 405nm excited autofluorescence. Black voids where only the 405nm wavelength is absorbed are visible, and the areas where there were 633nm reflectant particles in the previous image are circled, but contain no black voids. In figure 3.12H and zoomed in figure 3.12I these two images are merged. The particles appear to be similar sizes. These results showed that all the particles that absorb the 405nm wavelength reflect the 633nm wavelength, but not all particles that reflect the 633nm wavelength absorb the 405nm wavelength. The optical properties of the particles are summarised in table 3.1. This suggests that there are two types of melanin-like particle present in the hair.

Optical property	**405nm absorbing particle**	**405nm non-absorbing particle**
405nm absorbance	Yes	No
405nm autofluorescence	No	Yes
633nm reflection	Yes	Yes

Table 3.1. Summary of the optical properties of the two particles. NB. Under a 405nm laser the 405nm absorbing particle appears as a black void and the 405nm non-absorbing particle cannot be distinguished from the background fluorescence.

The number of 633nm wavelength reflecting particles and the number of 405nm wavelength absorbing particles were counted for black, brown, blond, ginger, darker ginger/brown, and pale yellow/white old-hair hair (fig. 3.13C). Since there are two types of these melanin-like particles, the number of 405nm non-absorbing particles was calculated by subtracting the number of 405nm absorbing particles from the number of 633nm reflecting particles, as all the melanin-like particles reflect 633nm. These were then plotted as densities in figure 3.13A. There appears to be grouping within the various hair colours. Black and brown hair have similar densities of 405nm absorbing and non-absorbing particles, and ginger and darker ginger/brown hair also have similar densities of particles to each other. Blond hair had a higher density of 405nm non-absorbing particles than the other hair colours, but also had a higher density of 405nm absorbing particles than the ginger, darker ginger/brown, and pale yellow/white old-age hair. The pale yellow/white old-age hair did not contain 405nm absorbing particles, and had the lowest density of 405nm non-absorbing particles.

The following graph, figure 3.13B, shows the proportions of the two different categories of melanin-like particles in the various hair colours. There appears to be a significant difference between the all of the hair colours, except between black and brown hair, blond and the shades of ginger, and between the shades of ginger themselves ($p=1.21x10^{-3}$, Kruskal-Wallis test). Black and brown hair have the lowest proportion of 405nm non-absorbing to absorbing particle density. Blond, ginger and darker ginger/brown hair have a slightly higher proportion of 405nm non-absorbing to absorbing particles, although the ginger hair proportions are significantly different to the blond proportions, as ginger hair has a higher proportion of 405nm non-absorbing to absorbing particles. Finally, the pale yellow/white old-age hair has the highest proportion of 405nm non-absorbing to absorbing particles. This shows the proportions of the two different categories of melanin-like particles are different in various hair colours.

3.3.4. The medulla is reflective and its autofluorescence intensity is variable

Finally, after investigating the cuticle and cortex, the medulla is reached, which runs through the centre of some hairs. Figure 3.14A shows a TEM image of a transverse section through a scalp hair with a medulla, zooming into figure 3.14B to show the medulla more clearly. The medulla is made up of many air spaces with a CMC surrounding the cells (fig. 3.14C), making the medulla appear as quite a disorganised collection of keratin-containing cells. Figure 3.14D shows the boundary between the medulla and the cortex. Using TEM the cells of the medulla appear more darkly stained than those of the cortex, and the medulla and cortex appear to be separated by a CMC. Figure 3.14E shows a SEM image of the medulla in a sliced open hair, with the higher magnification image (fig. 3.14F) showing the disorganised nature of the cells with plenty of air spaces.

Figure 3.14G shows the formation of the medulla within the developing hair, and figure 3.14H shows the fully developed medulla with cells creating a web-like structure amongst the air spaces. In addition to melanin, the medulla is also reflective (fig. 3.14I), and appears differently to the structures resolved utilising autofluorescence and SEM, as the reflective medulla appears as though it is made up of bundles, whereas using autofluorescence and SEM the medulla appears filamentous. Although only some

terminal hairs contain a medulla, beard hairs are thicker than scalp hairs and often possess a medulla, sometimes containing more than one, such as in figure 3.14J.

The autofluorescence intensity of the medulla varies between hairs. Figure 3.14K shows a high intensity autofluorescent medulla, whereas figure 3.14L shows a lower intensity autofluorescent medulla. Both contain empty air spaces and cells, but the cells of one medulla are much more autofluorescent than those of another medulla. The cortex surrounding the medulla can also sometimes appear more autofluorescent.

3.3.5. Measurements along a year of hair growth

Measurements were taken of exposed cuticle cell lengths, organelle remnants found both in the cuticle and cortex, and cortical cells along 12cm of hair. This approximately corresponds to a year of hair growth, with a month equalling approximately 1cm along the hair (Bost, 1993; Wennig, 2000; LeBeau *et al*., 2011). This was done for three purposes, firstly for biological interest to see whether there were any changes along the hair length, secondly to see whether it would matter that the samples taken throughout this study were taken from random lengths of hair, and thirdly to test how the label-free imaging method could be used to get high throughput measurements out of hair.

3.3.5.1. Exposed cuticle cell organisation

The exposed cuticle cell length varied between 0.9µm and 26.6µm, averaging at 7.2µm (fig. 3.15A). Often, after a cuticle cell had a small length, the next cuticle cell would have a large length, perhaps due to the cuticle cell above it being worn away.

The box and whisker plot (fig. 3.15B) shows there is greater variation in the lengths of the largest quartile of cuticle cells in each 1cm segment compared to the smallest quartile of lengths, as the minimum length stays relatively constant. Interestingly there also appears to be a 3-4cm segment repeating pattern to the largest quartile of cuticle cell lengths, as there is a decrease along the hair length from the 1cm segment (19.0µm) to the 2cm segment (17.7µm), then an increase in lengths up until the 5cm segment (26.6µm), then the 6cm segment (21.9µm) is the same as the 3cm segment, which then increases to the 8cm segment (28.2µm). There is then a decrease down to the 9cm segment (18.9µm) which has a similar largest quartile to the 1cm segment, which then increases to the 11cm segment (24.0µm), followed by a slight decrease in length for the 12cm segment (23.6µm).

Figure 3.15C shows the average length of the exposed cuticle cells does not vary much, particularly after the first 6cm segments, though there is an increase between segments 1cm and 2cm to the 3cm segment, and also between the 4cm and 6cm segments compared to the larger average lengths recorded in the 5cm segment. From the 6cm segment onwards there is little difference between the average cuticle cell lengths.

3.3.5.2. Circular organelle remnant area

Circular organelle remnants were measured because in addition to cuticle cells, cortical cells and cortical organelle remnants they are one of the most autofluorescent structures in the hair. It would be biologically interesting to see if there is a correlation to their area and numbers along the hair. Figure 3.16D shows the circular organelle remnants which are found in the cuticle. The circular organelle remnant area varied continuously over 12cm of hair between 11µm^2 and 103µm^2, averaging at 47µm^2 (fig. 3.16A).

The box and whisker plot (fig. 3.16B) shows the upper quartile increases from the 1cm segment (80µm^2) to the 2cm segment (103µm^2), then decreases until the 8cm segment (68µm^2), at which point it increases until the 10cm segment (83µm^2), with a decrease at the 11cm segment (72µm^2), increasing back up to the previous area for the 12cm segment. The lower quartile of circular organelle remnant area shows less of a pattern and do not correlate with the upper quartile trend. The lower quartiles increase from the 1cm segment (13µm^2) to the 2cm segment (22µm^2), decrease slightly to the 3cm segment (19µm^2), then increase until the 5cm segment (32µm^2), then decrease to the 7cm segment (14µm^2), increase to the 8cm segment (28µm^2), then decrease to the 10cm segment (11µm^2), then increase to the 11cm segment (23µm^2) then decrease to the 12cm segment (13µm^2).

Figure 3.16C shows the average area of the circular organelle remnants does vary, as there is an increase in area from the 1cm segment to the 3cm segment, then a decrease in the areas recorded in the 4cm segment, there is then an increase in the 5cm segment. From the 5cm segment onwards the average area decreases until the 10cm segment, then increases slightly for the 11cm and 12cm segments. This appears to show an annual pattern to the circular organelle remnant area. There is a similar pattern seen in the average cuticle cell lengths.

Finally, the number of remnants varied along the 12cm length of the hair (fig. 3.16E). The number of circular organelle remnants is an approximate indicator of the frequency of the remnants per centimetre of hair. Segments 1cm-4cm had between 238 and 277 remnants each, however the number recorded in the 5cm segment decreased to 183, which continued decreasing down to 23 in the 8cm segment. The number then increased up to 101 in the 12cm segment, with the exception of finding 152 in the 10cm segment. There does not appear to be any co-correlation between the number of remnants and remnant size. Therefore, there may be an annual pattern or a correlation with the distance along the hair with the number of circular organelle remnants, perhaps related to wear and erosion of the cuticle cell layers.

3.3.5.3. Cortical organelle remnant area

Figure 3.17D shows the cortical organelle remnants which are streak-like in shape and found within the cortical cells. The cortical organelle remnant area varied continuously over 12cm of hair between 2µm^2 and 59µm^2, averaging at 18µm^2 (fig. 3.17A).

The box and whisker plot (fig. 3.17B) shows the range of areas recorded in each segment increased from the 4cm segment onwards. The lower quartiles show the minimum areas recorded in each segment remained relatively steady from the 1cm-5cm segments, then increased from the 6cm segment onwards. The upper quartiles showed a similar trend to the average areas in figure 3.17C.

Figure 3.17C shows the average area of the cortical organelle remnants does vary. Segments 1cm and 2cm average at 11µm^2 and 10µm^2 respectively, after this there is an increase between every 1cm segment which peaks at the 6cm segment (23µm^2) and has a large average cortical organelle remnant area along with the 7cm segment (24µm^2). From here there is a decrease in the average area compared to the 8cm segment (20µm^2), segments 9cm and 10cm are not different in their average areas, however there is then an increase in area in the 11cm segment (25µm^2), which is similar to the 12cm segment. This appears to show a pattern for the cortical organelle remnants in which the area increases, then decreases and increases again over the course of a year.

3.3.5.4. Cortical cell area

The cortical cell area varied continuously over 12cm of hair between 32µm^2 and 650µm^2, averaging at 285µm^2 (fig. 3.18A).

The box and whisker plot (fig. 3.18B) shows that there is a larger range of areas recorded in segments 1cm-4cm than in segments 5cm-12cm. With the decrease in the range of cell areas comes an increase in the lower quartile of areas.

Figure 3.18C shows the average area of the cortical cells does vary in the first 7cm segments. Up to the 4cm segment, the average cell area increases in each segment from 210μm^2 to 327μm^2. The 5cm segment (301μm^2) is then on a similar level to the 3cm segment (294μm^2), and the 6cm segment (321μm^2) is on a similar level to the 4cm segment (327μm^2). The cell areas measured from the 7cm segment (284μm^2) are smaller than those of the 6cm segment, but from segments 7cm to 12cm there are no changes to the cell areas. This appears to show that the cortical cell size initially increases, then decreases and settles over the course of a year. This may be related to seasonal hair growth (Randall and Botchkareva, 2009).

The linear regression analysis (table 3.2) obtained from figure 3.18D shows there is a positive correlation between cortical organelle remnant area and the corresponding cortical cell area. The earlier segments have larger corresponding cortical cell areas to the cortical organelle remnant areas than the latter segments, which tend to have larger remnant areas, though there is much overlap. The gradient of the linear lines indicates that on average there is a stronger positive correlation between remnant and cell area for segments 1cm-4cm, and a weaker positive correlation for segments 5cm-12cm (table 3.2). The strongest positive correlation was in the 1cm and 2cm segments, and the weakest in the 3cm and 11cm segments (table 3.2). However, the R^2 values for the linear regression lines are low, indicating the diffuse distribution of the data (table 3.2).

Segment (cm)	**Line equation**	**R^2 value**
1	y = 6.7268x + 138.8	0.1926
2	y = 6.7643x + 193.47	0.153
3	y = 2.0731x + 267.58	0.0232
4	y = 4.5215x + 257.94	0.1254
5	y = 3.8182x + 227.98	0.1526
6	y = 4.4622x + 216.29	0.3236

7	y = 3.7296x + 194.54	0.1586
8	y = 4.0337x + 223.14	0.208
9	y = 4.0523x + 200.19	0.1773
10	y = 3.2407x + 218.02	0.1145
11	y = 2.961x + 227.75	0.1497
12	y = 3.4465x + 210.55	0.2425

Table 3.2. Linear regression analysis of the correlation between cortical organelle remnant area and the cortical cell area. Based on the data shown in figure 3.18D.

3.3.6. Uncharacterised hair and skin disorder

Through a collaboration with Queen Mary University of London, samples were obtained from a patient who presented with an uncharacterised hair and skin disorder. Confocal microscopy of the hair longitudinally showed detached material around the outside of the cuticle (fig. 3.19A,B,C). Although 1 in 5 hairs appeared normal (fig. 3.19D), the affected area may simply have been outside of the field of view.

The patient's hair appeared greasy and stuck to other hairs in the sample batch, unlike the unaffected parent's hairs. Transverse optical sections of Nile red stained hair showed a flaky cuticle present on the hairs, raised, but still joined to the rest of the cuticle (fig. 3.20A). Of the hairs imaged, 5/6 of the patient's hairs had strong Nile red staining (fig. 3.20B), and 4/10 of the unaffected parent's hairs showed strong Nile red staining (fig. 3.20C,D). This shows that the patient's hair may contain more lipids than the unaffected parents' hairs, and the lipid is present internally in the hair as well as externally.

To gain a higher resolution of the flaky cuticle, the hairs were imaged transversely using TEM. Figure 3.21A shows a normal hair from the patient which displays the usual cuticle cell sublamellar structures, as do hairs from the patient's unaffected parents (fig. 3.21E,F). Figure 3.21B shows the flaky cuticle or deposit on the outside of the cuticle, with which it appears to be continuous. This deposit appears to be membrane-bound (fig. 3.21C) with a structure similar in appearance to the CMC. Within the cuticle cells of the patient's hair, there also appeared to be poorly defined CMC as well as normal CMC (fig. 3.21D).

3.4. Discussion

3.4.1. Structures in the hair can be resolved utilising label-free autofluorescence

All of the 9 wavelengths, ranging from 405nm to 633nm, caused autofluorescence from excitation of the fluorophores in the hair. There were some wavelengths that caused more autofluorescence than others, such as 633nm primarily exciting the cuticle and not the cortex, which is useful for selective visualisation of this structure. No other studies appear to have imaged the autofluorescent cuticle selectively using 633nm excitation. On the whole, wavelengths 405nm to 543nm caused autofluorescence of the whole of the cuticle and cortex, and 594nm and 633nm excitation mainly excited the free edge of the cuticle cells. The cortex was found to be more autofluorescent than the cuticle, and it was concluded that the optimum excitation wavelength was 405nm. Previous studies have utilised hair autofluorescence (Liang *et al*., 2006; Kirkbride and Tridico, 2010). Liang *et al*. imaged hair from trichothiodystrophy patients finding structural breaks in the hair and a "smoother" cortex which they believed to be due to changes in melanin distribution. However, the resolution of the images was limited and 405nm was not utilised (Liang *et al*., 2006). Kirkbride and Tridico studied human hairs as well as animal hairs and textile fibres. They did use 405nm excitation and also found that it was the optimum excitation wavelength for human hair fibres, however they did not optimise their techniques and little detail can be observed in their images (Kirkbride and Tridico, 2010). The transverse optical sectioning method developed in this project and improvements in imaging systems mean that this project has achieved hair images of a higher quality than previously seen in the literature.

The emission spectra for the cuticle and cortex may be different due to their constituent fluorophores. There may be different fluorophores in the cuticle compared to the cortex, or they may have similar fluorophores, but present in different amounts. Some of these fluorophores may be the oxidised metabolites of tryptophan, namely N-formylkynurenine, kynurenine and 3-hydroxykynurenine, as well as melanin, lipo-pigments, keratin and cystine, which are all excited by UV provided by the 405nm wavelength and emit within the detectable range of 400-800nm (Hameka *et al*., 1998; Elleder and Borovansky, 2001; Lakowicz, 2006; Ehlers *et al*., 2007; Jachowicz and McMullen, 2011).

Dyes were used to validate the structures resolved using autofluorescence. As dyes and sample preparation can cause artefacts in the hair, dyes and non-confocal microscopy techniques were used secondary to label-free imaging and only in order to highlight or clarify structures. Without sectioning, the dyes could not penetrate past the cuticle of the hair, with the exception of Nile red which also stained the outer cortical cells. Interestingly, some of the dyes tested only stained the free edge of the cuticle cells, namely Nile red, rhodamine B chloride, R18, and H&E staining. These dyes all stain lipids, except H&E which may be staining proteinaceous eosinophilic and calcified material in the cuticle (Kizawa *et al*., 2002). These dyes are likely to be staining the free edge of the cuticle cells because of the exposed transverse section through the cell exhibiting many lipids and proteins. The stained puncte are likely to be damaged areas of the cuticle cell surface, exposing the various sublamellar structures within.

3.4.2. The cuticle

Using FeSEM it was possible to resolve areas on cuticle cells where the exocuticle had been worn away, leaving the endocuticle exposed. Using a magnification of x150k, cracks were resolved on the cuticle surface, which have not been reported in previous studies. This would be useful for assessing wear on the samples. These cracks were seen on all hairs, and may be caused by everyday wear and tear of the hair, or they may be artefacts caused by the sample preparation required for FeSEM imaging.

Using the novel method for the transverse imaging of hair along with label-free super-resolution microscopy, which is faster and more convenient than electron microscopy with sufficiently high resolution for most purposes, the exocuticle and the endocuticle within each cuticle cell could be distinguished as the exocuticle was autofluorescent and the endocuticle was not. This could be because of the high level of cystine content (about 20%) and crosslinking in the exocuticle, whereas the endocuticle is almost devoid of cystine and crosslinking (Swift, 1999). Cystine is excited by 405nm light and emits at 700nm (Hameka *et al*., 1998), within the detectable range of the super-resolution microscope, and is the likely cause of the autofluorescence of the exocuticle.

With sufficient cell layers, the cuticle was found to halt the penetration of light into the cortex. This is useful as more cuticle cell layers means the hair is less likely to become photodamaged, which results in photo-yellowing, lipid and protein degradation

(Millington, 2006; Hoting, 1996; Fernandez, 2011). This shows it is important to maintain the cuticle to prevent the loss of cell layers.

When hair was plucked it caused the upper cuticle cell layer on the hair beneath the skin to curl back upon itself. This is caused by the cuticle of the inner root sheath tearing the almost differentiated cuticle layers apart, and the curled up cuticle cell keeping its shape due to the CMC reconstituting (Chapman, 1997). This is a good marker for visualising under the microscope the area of hair which was beneath the skin, but may only be applicable for hairs in anagen, as it is the cuticle cells which are not fully differentiated that are curled back.

3.4.3. The cortex

3.4.3.1. Organelle remnants are present in the cortex

Organelle remnants were mostly found within the cortex of some hairs. They were found to be more fluorescent than the surrounding area, and were more circular in shape in the cuticle, and more streak-like in shape with proximity to the centre of the cortex. The maleimide stain highlighted them within the cortex, and TEM showed some to be encased by a double membrane, and others to contain melanin granules, or have both lightly and darkly stained areas.

The increased fluorescence of the organelle remnants made them easier to identify. They may be more autofluorescent due to more fluorophores being present in the organelle than in the surrounding cornified cells. The organelle remnants may have been circular in the cuticle due to the flattening of the cuticle cells during differentiation. The remnants were likely to be rounder in the outer cortex and streak-like deeper into the cortex due to the increased pressure exerted on the inner-most part of the hair during formation of the hair shaft in the follicle. The streaks are unlikely to be the crystalline α-helical keratin phase in the hair because if the streak is present, there is only one per cell, whereas the α-helical keratins are present throughout the cortical cells.

The specific identity of organelle remnants has raised disagreements. Some researchers believe they are remnants of the nucleus (Swift and Bews, 1976; Swift *et al*., 2000; Kelch *et al*., 2000; Fischer *et al*., 2011; Szabo *et al*., 2012), while others think they are remnants of other organelles (Harland *et al*., 2011). Despite claims to these organelles being

nucleic or otherwise, few papers have offered any evidence. Szabo *et al*. 2012 used a nucleic acid stain, Hoechst33258, to reveal the nuclear remnants in the hair, however our replication of this experiment did not highlight nuclear remnants within the hair. In addition to this, immunofluorescence against lamin A/C JOL2, which may have been present if the nuclear envelope was retained, was not found in any hairs. It may be that no nucleic acids or lamin A/C remained in the hair after cornification. On the other hand, maleimide stained the remnants in transverse sections of hair. Maleimide stains thiol groups, so there may be thiol groups present in the remnants. Thiol groups are present in histones, so it could be that the remnants are nucleic, but thiol groups are also prevalent in some KIFs and KAPs. In figure 3.16D darker dots were resolved in the circular organelle remnants, resembling the DAPI staining of nuclei in other bodily cells. In 1981 Kassenbeck found nuclear disks in the endocuticle reminiscent to the circular organelle remnants in figure 3.16D, although imaging of the remnants in figure 3.16D was done label-free and non-invasively. TEM imaging shows some of these remnants are bound by double membranes, which could be the remaining nuclear envelope. They also have light and dark staining within them, which could be the euchromatin and heterochromatin respectively. However, some remnants contain melanin granules, which would not be expected within nuclear remnants. These remnants may be melanosomes, as melanosomes are transferred to immature cortical cells (Kinebuchi *et al*., 1971) and not all may be completely degraded. Finally, the organelle remnants are not present in all hairs. Nuclear DNA is normally degraded by DNase1L2 during cornification, however expression of this enzyme varies between individuals (Fischer *et al*., 2011). This may account for the absence of remnants in some hairs, though another enzyme or mechanism would also be required to remove the remnants of the nuclear envelope.

In conclusion, the remnants may be both nucleic and from other organelles, particularly melanosomes. It is difficult to distinguish between the two as little work has been done on the area. Currently, it would be safest to name these structures as organelle remnants, which encompasses both possibilities.

3.4.3.2. There are two types of melanin-like particles present at different proportions in various hair colours

Two types of melanin-like particles were found in the cortex of hair – those that absorb 405nm radiation and those that fluoresce under it (non-absorbing particles). In general, the darker the colour of the hair, the higher the number of 405nm absorbing particles were found. Blond and ginger hair colours had more 405nm non-absorbing particles than those that absorb 405nm radiation. Pale yellow/white hair from elderly donors had very little of both types of particle. The amount and proportions of the two types of particle together make up the vast array of hair colours.

The results suggest that the two types of melanin-like particles may be eumelanin and pheomelanin. When various lasers were emitted onto hair, all of the particles reflected the light. The reflection was strongest and clearest when a wavelength of 633nm was emitted (fig. 3.12F). Synthetic black/brown melanin was found to reflect 633nm, just as the eumelanin in the hair was found to be reflective. In future experiments, synthetic pheomelanin would also be useful to test the validity of the observations made on the 405nm non-absorbing particles in the hair. The reflectant particles seen in figure 3.12F may be both eumelanin and pheomelanin granules, as there were more granules resolved here (see circles in figure 3.12F-H) than there were black voids resolved in figure 3.12G. The 405nm absorbing black voids in the 405nm-induced autofluorescence image (fig. 3.12G) are thought to be eumelanin as it is known to absorb UV light, unlike pheomelanin which photodegrades and produces reactive oxygen species (Brenner and Hearing, 2008; Thody *et al*., 1991). Pheomelanin fluoresces immediately under 405nm irradiation, hence is a 405nm non-absorbing particle, but eumelanin only begins to fluoresce after 2 hours of irradiation, hence is a 405nm absorbing particle (Elleder and Borovansky, 2001).

Eumelanin gives hair its black/brown colour and pheomelanin is responsible for the reddish colour. If eumelanin is the 405nm absorbing particle (shown as black voids in 405nm autofluorescence images) and pheomelanin is the 405nm non-absorbing particle (fluorescent with background structures in autofluorescence images), and both reflect 633nm, the amounts seen agree with the hair colours shown in figures 3.12A and 3.13. Virtually no melanin was resolved in the pale yellow/white old-age hair for both autofluorescence and reflection, as the melanocytes in the hair follicles of white hairs

are no longer functional (Tobin, 2009). High levels of pheomelanin were only found in ginger/darker ginger coloured hairs to the exclusion of most eumelanin, and in blond hairs (Ito *et al*., 2000; Ito and Wakamutsu, 2003), shown by the lack of black voids in the autofluorescence images and particles in the reflection images. Black and brown hairs had the most eumelanin and lower amounts of pheomelanin (Ito *et al*., 2000; Ito and Wakamutsu, 2003), shown by the particles in both autofluorescence and reflection images. The location of these particles suggests they are melanin granules, as the particles gathered in spindle shaped cortical cells, which is where melanosomes are transferred during hair growth (Kinebuchi *et al*., 1971).

In future experiments correlative light and electron microscopy (CLEM) could be used to confirm that all reflective particles in confocal microscopy correspond to melanin granules in TEM. In conclusion, it is likely that the particles which absorb the 405nm wavelength are eumelanin, and the particles which do not absorb the 405nm wavelength are pheomelanin. This method of using the 405nm and 633nm wavelengths gives a new way to distinguish between eumelanin and pheomelanin through label-free optical sectioning of the hair.

3.4.4. The medulla is reflective and autofluorescence intensity varies

The medulla is made up of many keratin bundle-filled cells and air spaces with a CMC surrounding those cells. The cells of the medulla were distinguishable from the cortical cells as the medullary cells appeared slightly more darkly stained when imaged with TEM. This suggests the cells of the medulla are slightly denser than cortical cells, or it could be that because the medullary cells have the highest lipid content in the hair (Kreplak *et al*., 2001a), they are being stained by the uranyl acetate in TEM preparation. Using confocal microscopy, the medulla was reflective under 633nm and appeared differently to the structures resolved utilising 405nm autofluorescence and SEM. The reflective medulla looks as if it is made up of bundles of material, whereas the autofluorescent medulla appears filamentous as it also does using SEM imaging. In addition to the medulla, the hair cuticle is also reflective, though not to the same extent as the medulla. This reflectiveness may be caused by lipids, as the cuticle and medulla may both contain higher levels of lipid than the cortex, and the medulla may have the highest lipid content (Kreplak *et al*., 2001a). Alternatively, the dramatic refractive index

difference between the medullary CMC and the air could account for the reflection, and this would agree with the “bundle” shape of the reflectants.

The autofluorescence intensity of the medulla was found to vary between hairs. This may be down to a higher level of lipids in some medullas than others (Kreplak *et al*., 2001a), as some of the lipids may be lipo-pigments. The cortex surrounding the medulla can also appear more autofluorescent. This may be because glycine/tyrosine keratin associated proteins (KAPs) are present at a higher density towards the centre of the hair, which would be around the medulla (Shimomura and Ito, 2005), and tyrosine is autofluorescent.

3.4.5. Measurements along a year of hair growth

3.4.5.1. Exposed cuticle cell length is an indicator of wear

The exposed cuticle cell length was measured along 12cm of a Chinese scalp hair. One previous study has also measured the length of exposed cuticle cells from Chinese scalp hair and found an average length of 7.82µm (Baque *et al*., 2012), only 0.62µm larger than the average of 7.2µm measured here. This small difference may be due to the hair of Baque *et al*. undergoing SEM preparation, the dehydrations of which may have affected the proportions of the hair. Additionally, Baque *et al*. measured along a smaller length across several hairs, so the exposed cuticle cell lengths may have varied more, since they found that regardless of the origin of the hair, the thicker the hair, the faster it grows and the shorter the exposed cuticle cell length.

Measuring along 12cm of hair, it was often found that after a small exposed cuticle cell, the next exposed cuticle cell would be large. This cuticle cell probably appears large because the cell above it has been worn away which causes it to appear small. Therefore, a pattern of small exposed lengths and large exposed length, rather than cuticle cells which are of average length, is an indicator of how worn the hair is.

There was a 3-4 month pattern to the largest quartile of the cuticle cell lengths (fig. 3.15B). This may be because the largest cells are growing in a quarterly fashion. Since the average size of the cuticle cell was unchanging in the latter 6 months, this may have occurred in a period of stable climate and diet, unlike in the first 6 months.

3.4.5.2. Circular organelle remnant number is an indicator of cuticle wear

The area and number of circular organelle remnants were measured along 12cm of a Chinese scalp hair. There appeared to be an annual pattern to the average area of the circular organelle remnants, where the size of the remnant increased, decreased and increased again over the course of a year, although a longer study would be needed in order to confirm this finding.

The number of circular organelle remnants was found to vary along the hair. Along some sections of hair where there were no remnants found, there were very few cuticle cell layers before the cortex. It seems likely that a decrease in remnants would be linked to a decrease in cuticle cells, resulting in a thinner layer of cuticle cells around the hair. The reasoning being that if the remnants are nuclear and situated in the endocuticle, then the likelihood of imaging one decreases if there are fewer cuticle cell layers. This effect may be more pronounced because not every cuticle cell appeared to have a remnant, though they may not have been visible because there are step-size limits in the z-axis imaging of the Leica TCS SP5 confocal microscope, here of 0.5µm. The decrease in remnant numbers may be correlated to the distance down the hair, as the older the hair the higher the chance cell layers of the cuticle have been worn away by daily hair care regimes and weathering (Inoue *et al*., 2000). Although this may generally be true, as there were fewer remnants found at the distal part of the hair than at the proximal, remnant loss may be exacerbated by a particularly harsh hair care regime or illness (Inoue *et al*., 2000; Fichtel *et al*., 2007), resulting in fewer cuticle cells, which may have been experienced by the hair around months 8 and 9 in figure 3.16E. Another reason for the change in remnant numbers could be that there may be seasonal changes to DNase1L2, which degrades nuclear material, if indeed the remnants are nuclear. However, since remnant number and cuticle thickness appeared to be linked, remnant number is a useful indicator of cuticle cell layer thickness, as it is difficult to tell how many cuticle cell layers there are if imaging the hair longitudinally.

3.4.5.3. Biannual pattern in cortical organelle remnant area

The areas of cortical organelle remnants were measured over 12cm of a Chinese scalp hair. The range of areas recorded for each month increased from month 4 onwards. The average areas recorded for each month of cortical organelle remnants increased, decreased and increased again over the course of a year. A longer study would be

needed to show whether this is a true biannual pattern to the size of the remnants. If so, it may be down to seasons, otherwise individual health and nutrition may affect the growth of hair and the size of the remnants. Seasonal hair growth is a known phenomenon in some animals, and has also been reported in humans (Randall and Botchkareva, 2009). The seasonal cycle was an annual pattern with 90% of hairs in anagen in the spring falling to 80% in the autumn in a study on men and similar results were found in women (Randall and Ebling, 1991; Orentreich, 1969). These changes in the hair follicle phase may be due to the change in day length, as follicles can respond to changes in prolactin, melatonin and cortisol secretion (Foitzik *et* al., 2006; Fischer *et al*., 2008; Paus *et al*., 2008).

3.4.5.4. There is a positive correlation between the area of cortical cells and their organelle remnants

The areas of cortical cells were measured along 12cm of Chinese scalp hair. Cortical cell size decreased in range after months 1-4, along with the smallest cell sizes increasing from month 5 onwards. The average area of the cortical cells increased and then decreased again over a year of hair growth. As previously mentioned, these changes may be an annual pattern, but a longer study with more hairs from independent donors would need to be taken to show this, otherwise the changes in cortical cell size may be due to seasonal, nutritional or health factors (Randall and Botchkareva, 2009; Trueb, 2015).

A positive correlation was found between cortical organelle remnant area and the corresponding cortical cell area. The larger cortical cells in the earlier months had smaller organelle remnants compared to those of the latter months. Although nucleus size is said to be proportional to cell size (Wilson, 1925; Cavalier-Smith, 2005), this data suggests there may be some variability depending upon the circumstances in which the hair was growing.

There appeared to be patterns in the organisation of the exposed cuticle length, organelle number and remnant area and cortical cell area. However, the value of this data is limited as measurements were only taken from one hair, despite that hair being chosen as it appeared to be undamaged and possessed organelle remnants. Thus this experiment only provides preliminary data for an insight into the structural changes

along a year of hair growth. To increase the validity of similar data in the future, more hairs could be examined, with fewer measurements taken to restrict the time required to obtain the data. This would provide more confidence in the value of the data with statistically valid proof of any observations on the structure of the hair over a year of growth.

3.4.5.5. Measurements from random sections of hair are valid for experiments

Although there are some differences in the size of hair structures along a year of hair growth, this does not have a significant effect on measurements taken from hairs which have been selected randomly with only a small section of hair analysed. This is because multiple hairs have been selected randomly as both controls and samples, so differences due to the location of the hair are seen in both sets, and therefore not significant in the analysis. In addition, although the study of structures along a year of hair growth provides interesting information regarding the nature of the hair, it is not feasible to carry out imaging of 12cm of hair for all other experiments due to time restraints.

3.4.6. The uncharacterised hair and skin disorder presents a poorly differentiated hair cuticle

The affected hair was greasy and also contained more lipids within it than in control hairs. In addition, it had a flaky cuticle or deposit which was still joined to the rest of the hair cuticle, but did not have the normal sublamellar structures except from being membrane-bound by what appeared to be a CMC. From these observations, it appeared to possibly be made up of poorly differentiated cuticle cells.

The greasy appearance of the hair may be due to sebum from the sebaceous glands in the hair follicles (Nicolaides *et al*., 1968; Stewart *et al*., 1983; Koch *et al*., 1982). The internal lipids found within the affected hair may be caused by the raised levels of sebum penetrating the hair from within the follicle (Masukawa *et al*., 2005a).

The researchers, from Queen Mary University of London, who donated the hair samples for investigation, also carried out a skin biopsy from the affected individual along with genetic analysis. The skin biopsy showed that the keratinocytes were smaller and more compact throughout the epidermis, perhaps poorly differentiated (unpublished information). The genetic analysis showed a mutated gene which is involved in mothers against decapentaplegic homolog 1 (SMAD1) and bone morphogenetic protein receptor

type IA (BMPR1A) signalling. BMPR1A has been shown to be involved in hair follicle differentiation (Yuhki *et al*., 2004; Kwan *et al.*, 2004; Andl *et al*., 2004; Kobielak *et al*., 2007; Genander *et al*., 2014). These results support the observations made through analysis of the hair that there could be a defect in the differentiation of the hair cuticle.

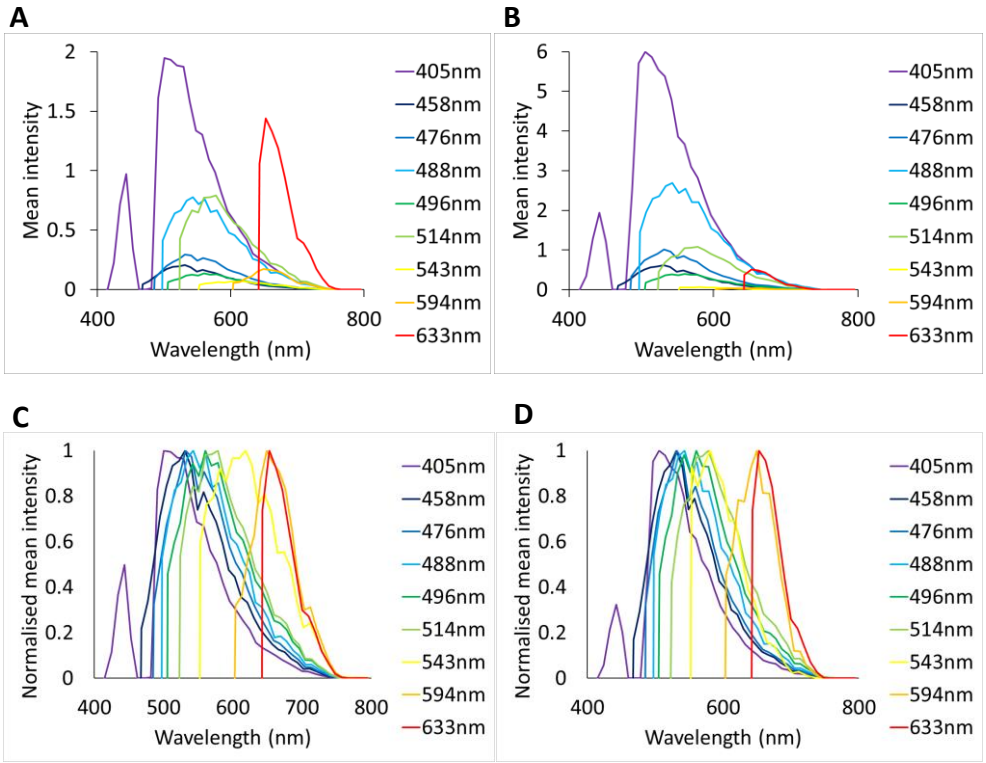

Fig. 3.1. Emission spectra of human hair. A) Emission spectra of the cuticle excited with indicated wavelengths, using 30% of the power capacity of the lasers. B) Emission spectra of the cortex excited with various wavelengths, using 30% of the power capacity of the lasers. C) Normalised emission spectra against the largest intensity value for each wavelength of the cuticle excited with indicated wavelengths. D) Normalised emission spectra against the largest intensity value for each wavelength of the cortex excited with indicated wavelengths. These emission spectra for one hair are representative of the five hairs analysed.

A

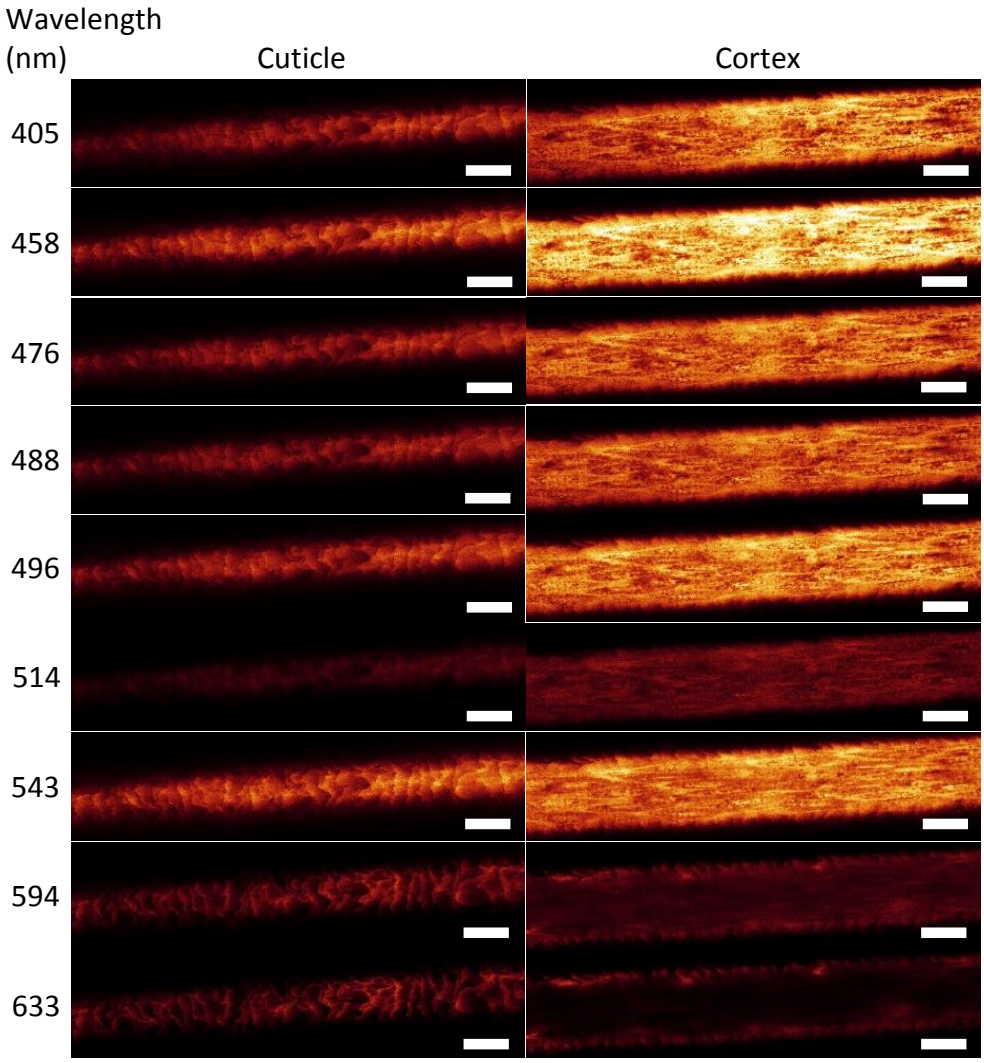
Wavelength (nm)
Cuticle
Cortex
405
458
476
488
496
514
543
594
633

B

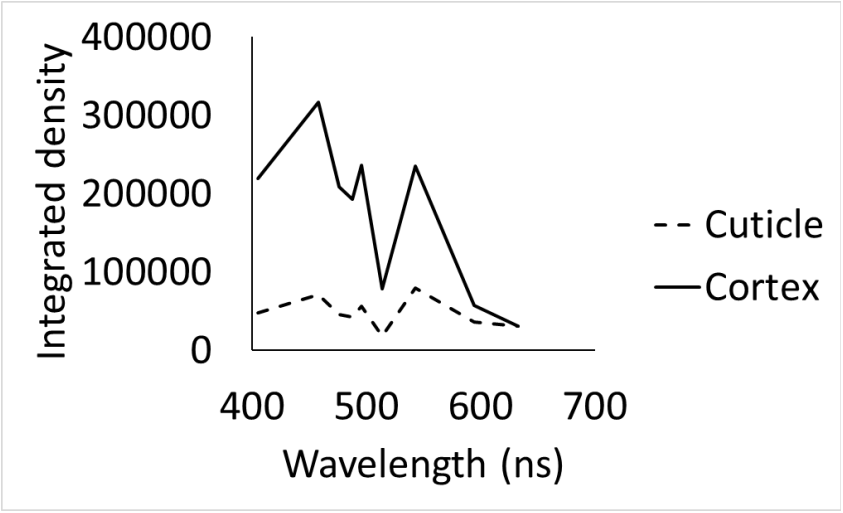
Integrated density
400000
300000
200000
100000
0
400
500
600
700
Wavelength (ns)
Cuticle
Cortex

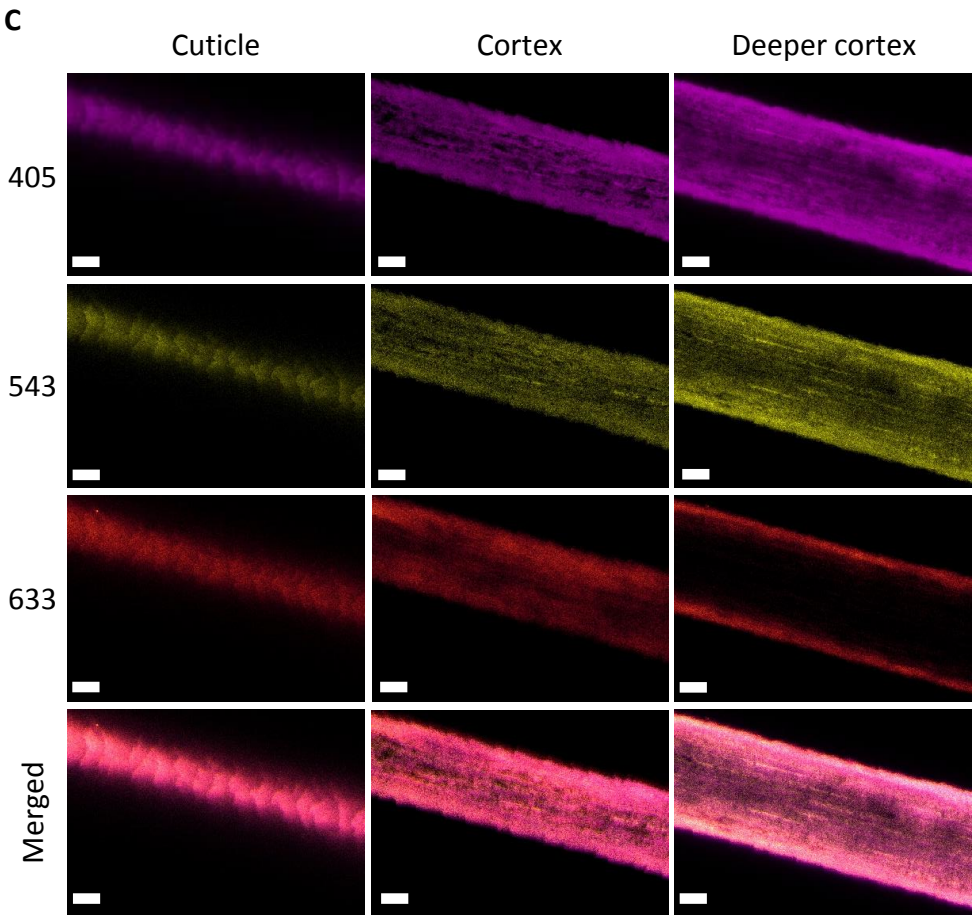

Fig. 3.2. Fluorescence intensity of the cuticle and cortex excited with a range of wavelengths. (A) Confocal microscopy of the autofluorescent cuticle and cortex from excitation with 0.15mW of the listed wavelengths, scale bars = 25µm. B) Intensity of the fluorescence of the cuticle and cortex when excited with various lasers at 0.15mW. (C) Confocal microscopy composite image of 405nm (magenta), 543nm (yellow), and 633nm excitation (orange), at the cuticle, cortex and deeper cortex, scale bars = 10µm. The photomicrographs shown are representative of five hairs imaged.

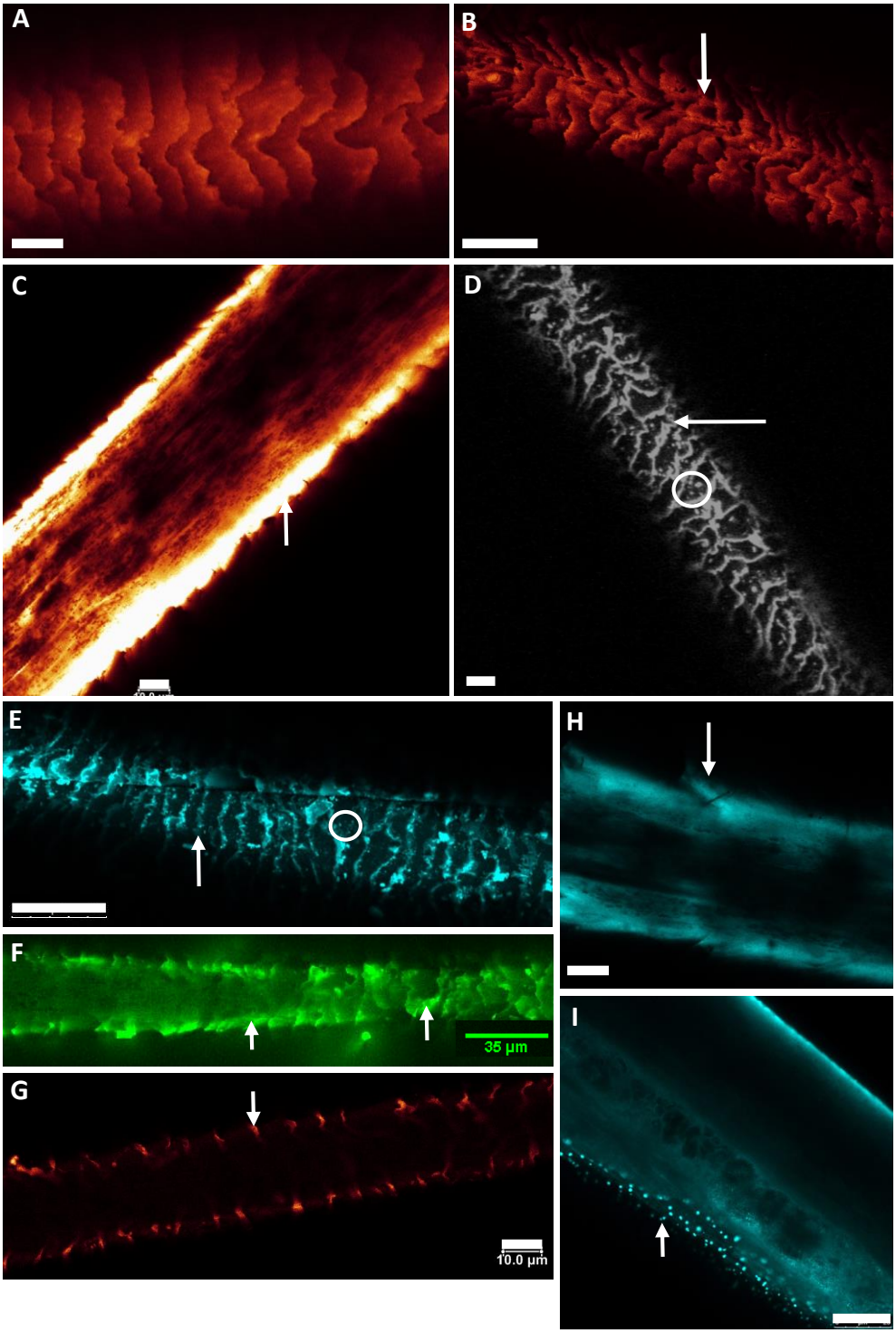
A
B
C
D
E
H
F
35 µm
I
G
10.0 µm

Fig. 3.3. Confocal microscopy of hairs stained with fluorescent dyes. A) 405nm excited autofluorescence, scale bar = 10µm. B) 0.6mg/ml Nile red stained hair at the cuticle (arrow), scale bar = 25µm. C) 50µM N-(2-aminohexyl)-5-(dimethylamino)naphthalene-1-sulphonamide stains the cuticle (arrow), scale bar = 10µm. D) 200µM Rhodamine B chloride stains the cuticle free edge (arrow) and punctate staining (circled), scale bar = 10µm. E) 10µM R18 stained hair showing the free edge of the cuticle (arrow) and punctate staining (circled), scale bar = 25µm. F) Hair stained with 0.01M curcumin, which stains the cuticle (arrows), scale bar = 35µm. G) H&E staining highlights the free edge of the cuticle (arrow), scale bar = 10µm. H) 0.1M Fluorescein stained hair, staining the cuticle (arrow), scale bar = 10µm. I) Oil red o staining of split head hair, showing lipids in the cortex of the hair (arrow), scale bar = 25µm. A representative photomicrograph of 3 imaged hairs is shown for each dye.

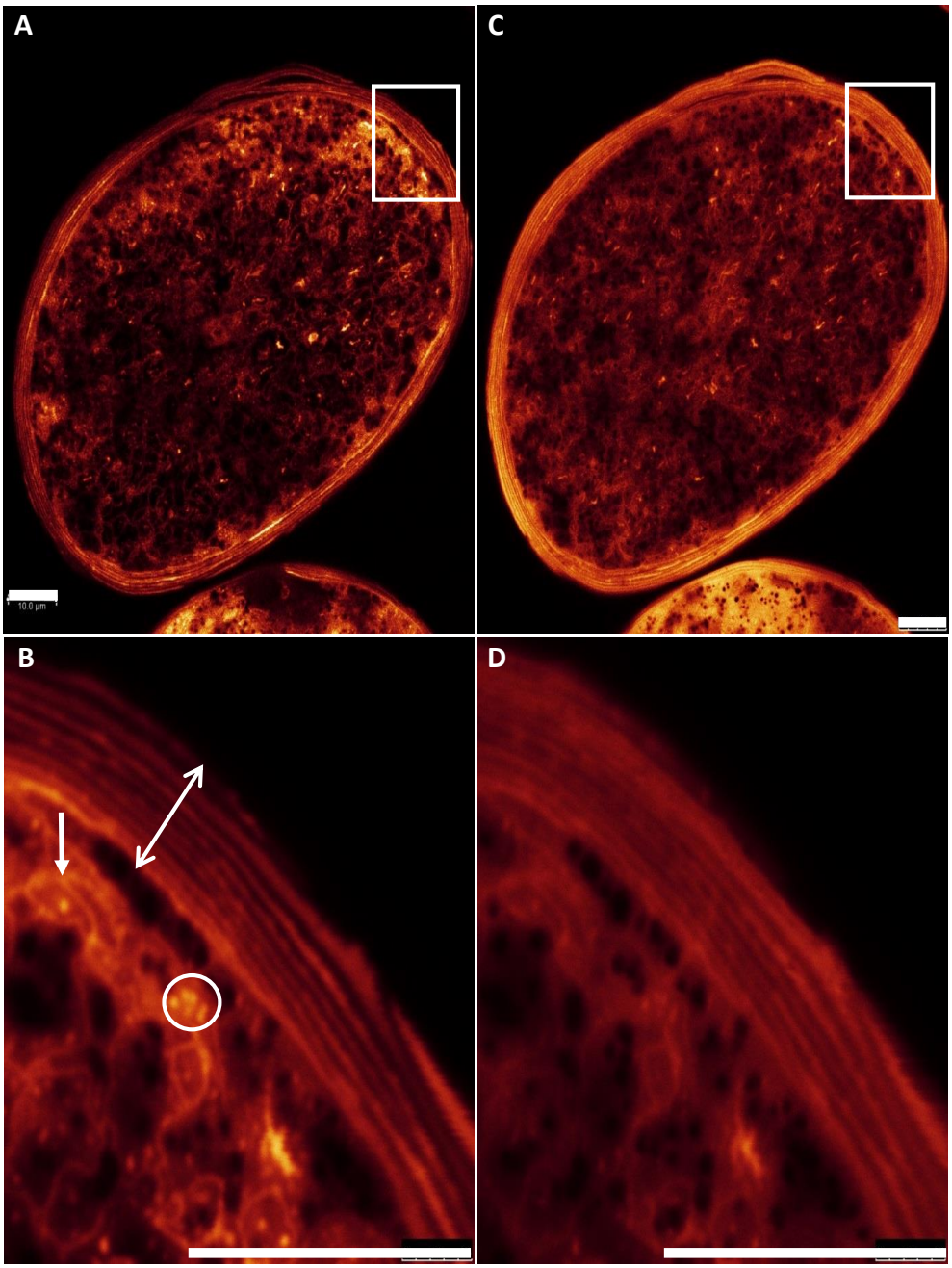

Fig. 3.4. Confocal microscopy of transverse optical sections of hairs stained with 0.6mg/ml Nile red. A) Image showing zoomed-in area of (B) which shows the cuticle layers (double headed arrow), cortical CMC (arrow) and vesicles (circled). (C) Image showing the autofluorescent hair and zoomed-in area of (D). A representative photomicrograph of 6 imaged hairs is shown. Scale bars = 10µm.

A

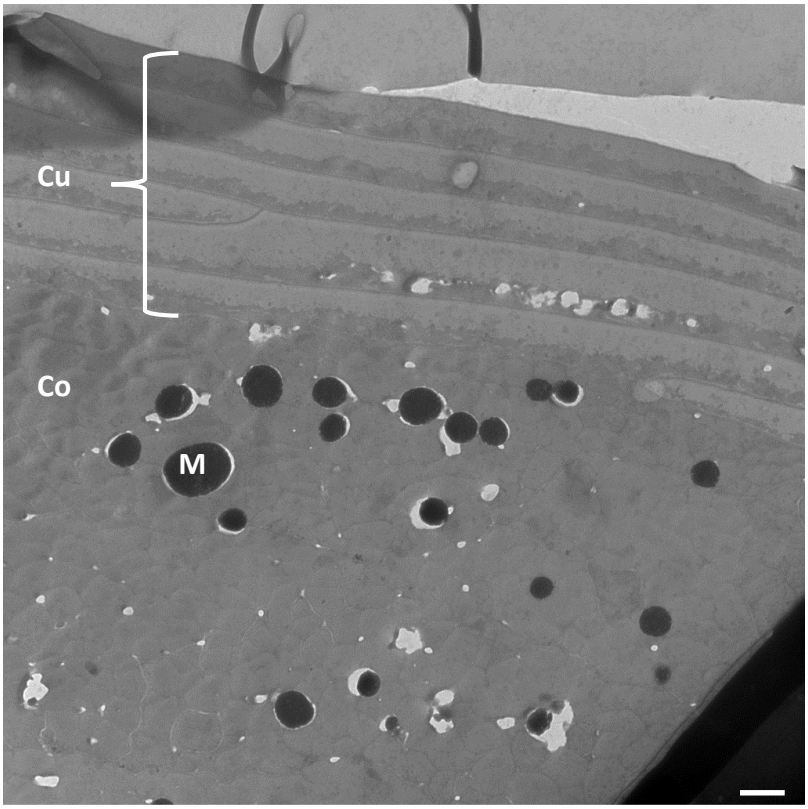

B

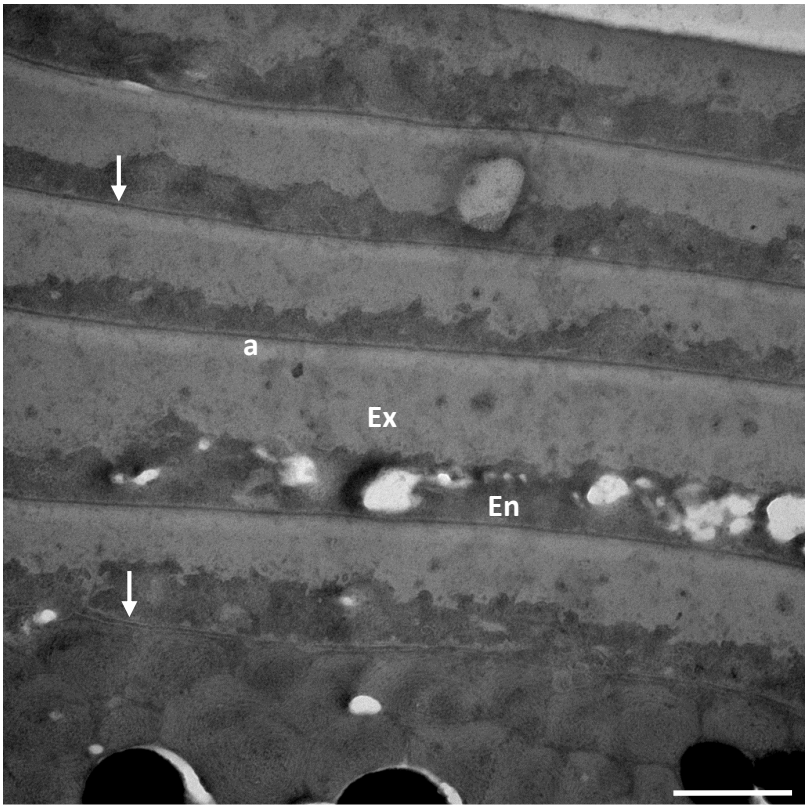

Fig. 3.5. TEM of the cuticle. A) Transverse section of hair at x15k and at (B) x40k. Cu=cuticle, Co=cortex, M=melanin, a=α-layer, Ex=exocuticle, En=endocuticle, arrows=CMC. HV = 100kV. A representative photomicrograph of 12 imaged hairs is shown. Scale bars = 500nm.

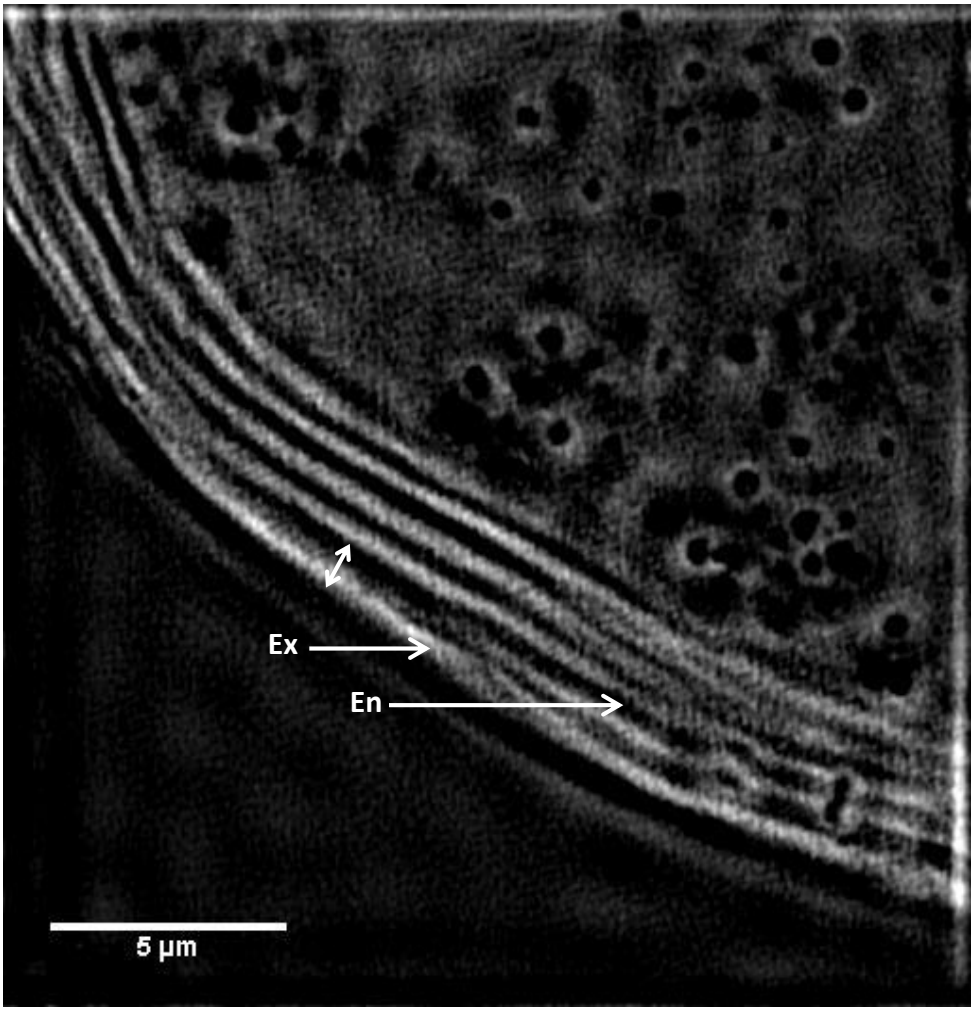

Fig. 3.6. Super resolution microscopy of a transverse optical section of hair. The light exocuticle (Ex), dark endocuticle (En), and an entire cuticle cell (double headed arrow) are indicated. A representative photomicrograph of 5 imaged hairs is shown. Scale bar = 5µm.

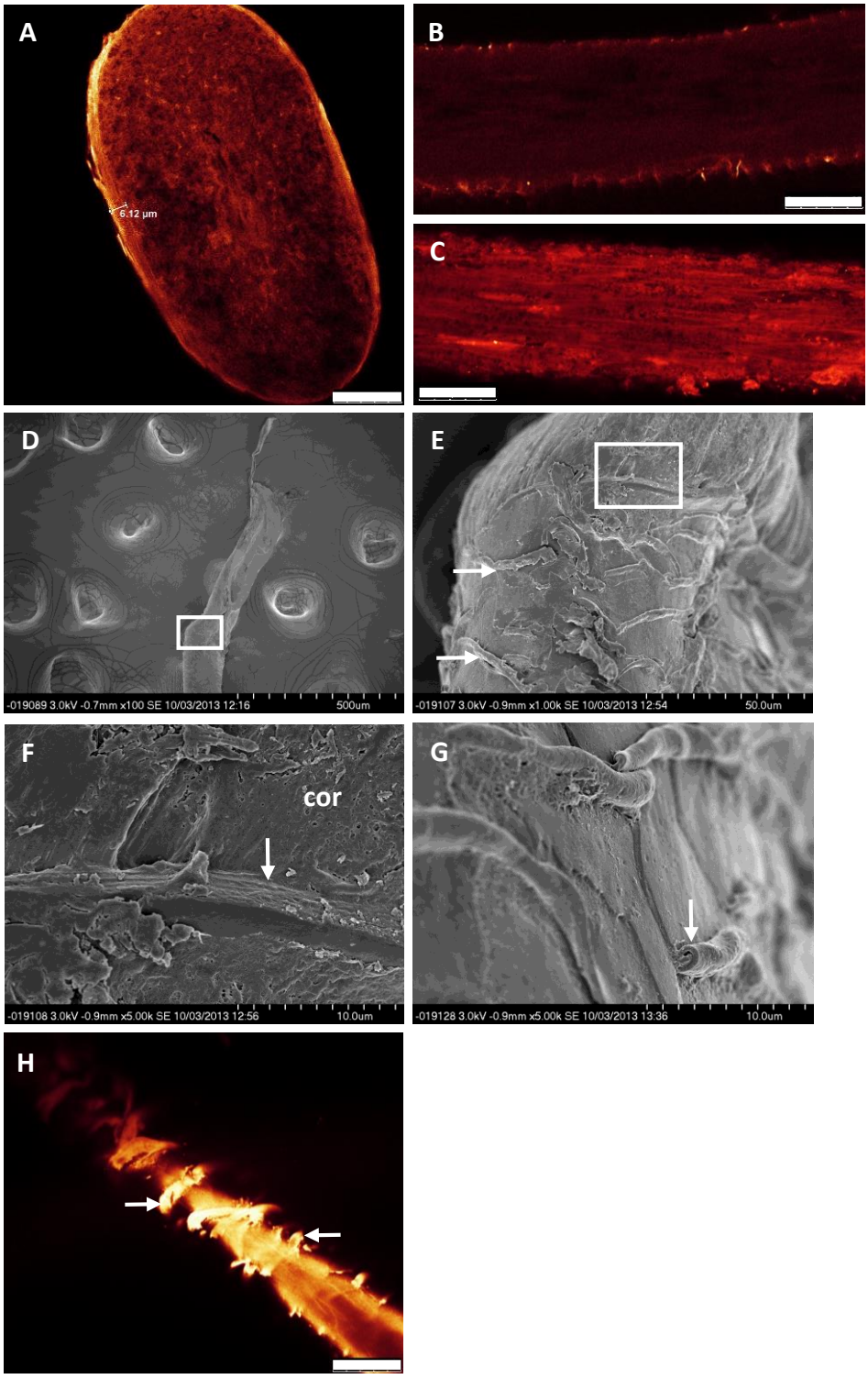
A
6.12 µm
B
C
D
-019089 3.0kV -0.7mm x100 SE 10/03/2013 12:16
500um
E
-019107 3.0kV -0.9mm x1.00k SE 10/03/2013 12:54
50.0um
F
cor
-019108 3.0kV -0.9mm x5.00k SE 10/03/2013 12:56
10.0um
G
-019128 3.0kV -0.9mm x5.00k SE 10/03/2013 13:36
10.0um
H

Fig. 3.7. Thick cuticle limits the use of label-free imaging for plucked beard hair. A) Confocal transverse section through a beard hair, showing the thick cuticle layer, scale bar = 25µm. B) Confocal longitudinal section through a beard hair, showing the cortex is poorly visible, scale bar = 25µm. C) Confocal longitudinal section of cuticle-free beard hair, showing detailed structure of the cortex, scale bar = 25µm. D) SEM of a plucked beard hair, with box showing magnified panel E) where the cuticle begins, and apparent bands across the cuticle (arrows). F) Layers of cuticle (arrow), proximal of which there is only cortex (cor). G) The bands across the cuticle are curled up cuticle cells (arrow). H) Confocal imaging of a plucked beard hair in the subepidermal area, showing thick bands of curled up cuticle cells (arrows), scale bar = 25µm. Representative photomicrographs of 5 imaged hairs for each section are shown.

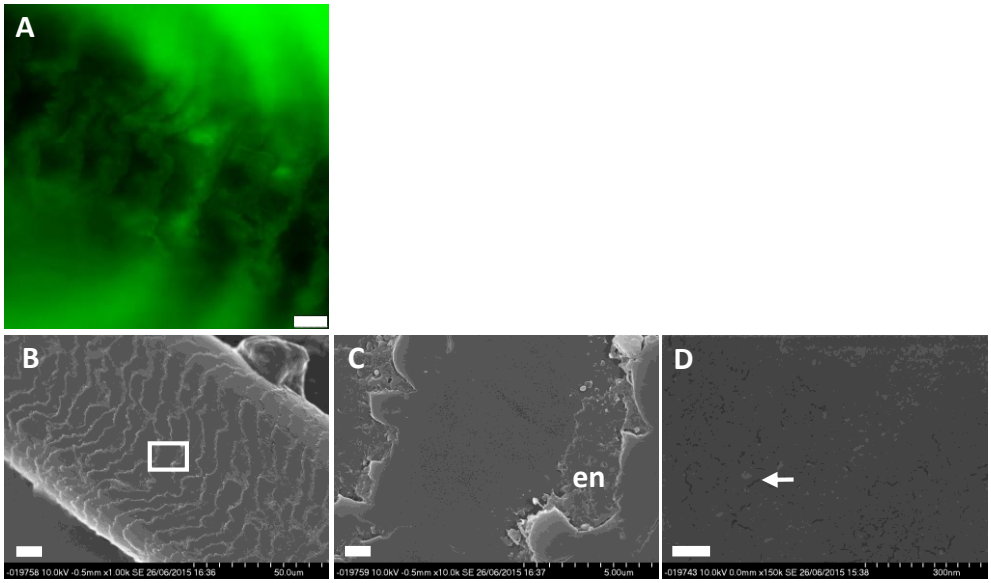

Fig. 3.8. Imaging of the cuticle surface. A) TIRF of 200µM R18 stained hair showing the cuticle, scale bar = 5µm. A representative photomicrograph of 3 imaged hairs is shown. B) SEM of the cuticle of untreated Chinese head hair at x1k, scale bar = 10µm. C) SEM of the cuticle of untreated Chinese head hair at x10k showing remaining endocuticle (en), scale bar = 1µm. D) SEM of the cuticle of untreated Chinese head hair at x150k showing cracks (arrow), scale bar = 100nm. SEM photomicrographs shown are representative of 5 imaged hairs.

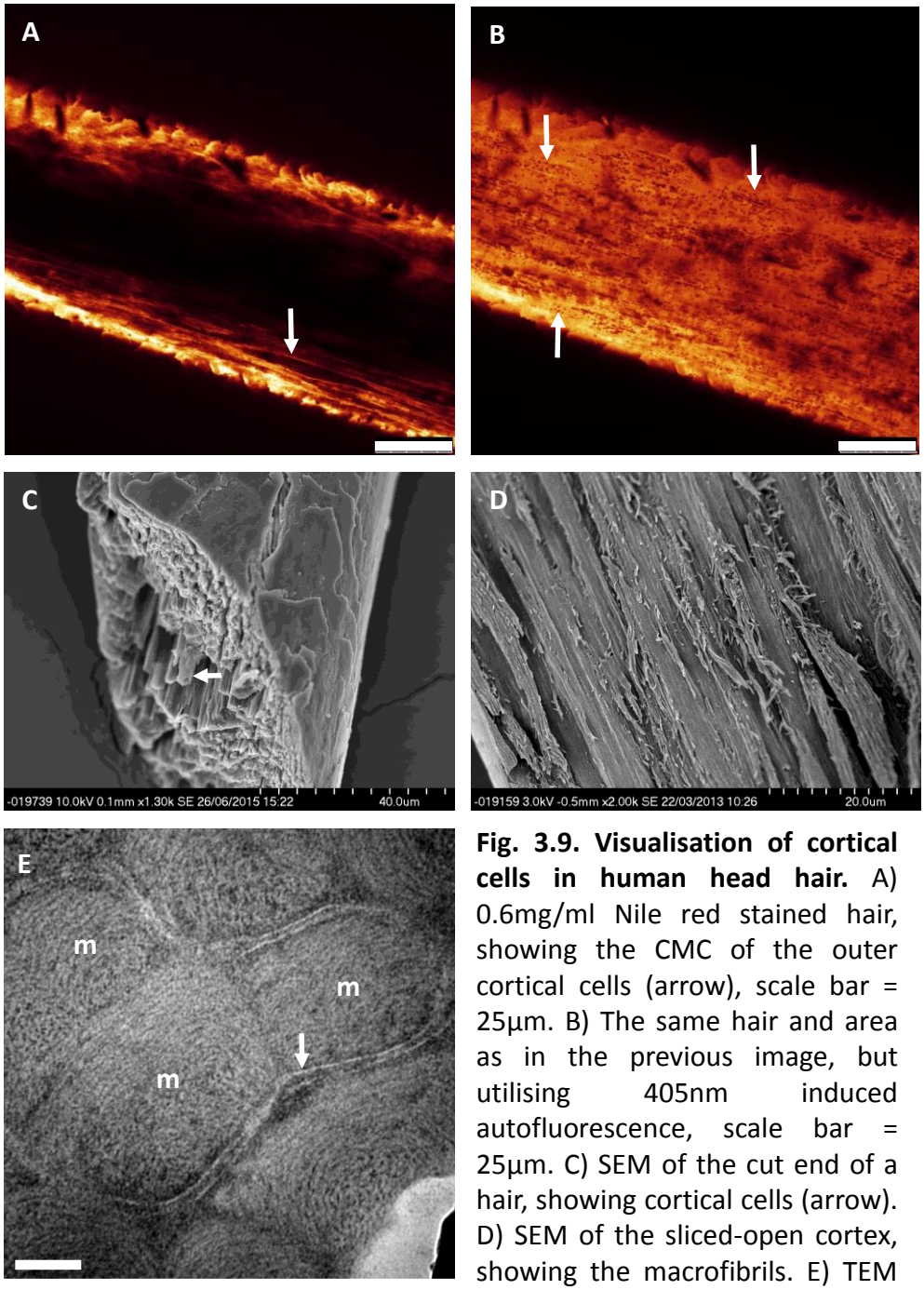

Fig. 3.9. Visualisation of cortical cells in human head hair. A) 0.6mg/ml Nile red stained hair, showing the CMC of the outer cortical cells (arrow), scale bar = 25µm. B) The same hair and area as in the previous image, but utilising 405nm induced autofluorescence, scale bar = 25µm. C) SEM of the cut end of a hair, showing cortical cells (arrow). D) SEM of the sliced-open cortex, showing the macrofibrils. E) TEM of the cortex showing a cortical cell containing macrofibrils (m) surrounded by the CMC (arrow), scale bar = 100nm. Photomicrographs from images A, B, C and D are representative of 5 hairs, and image E is representative of 12 hairs.

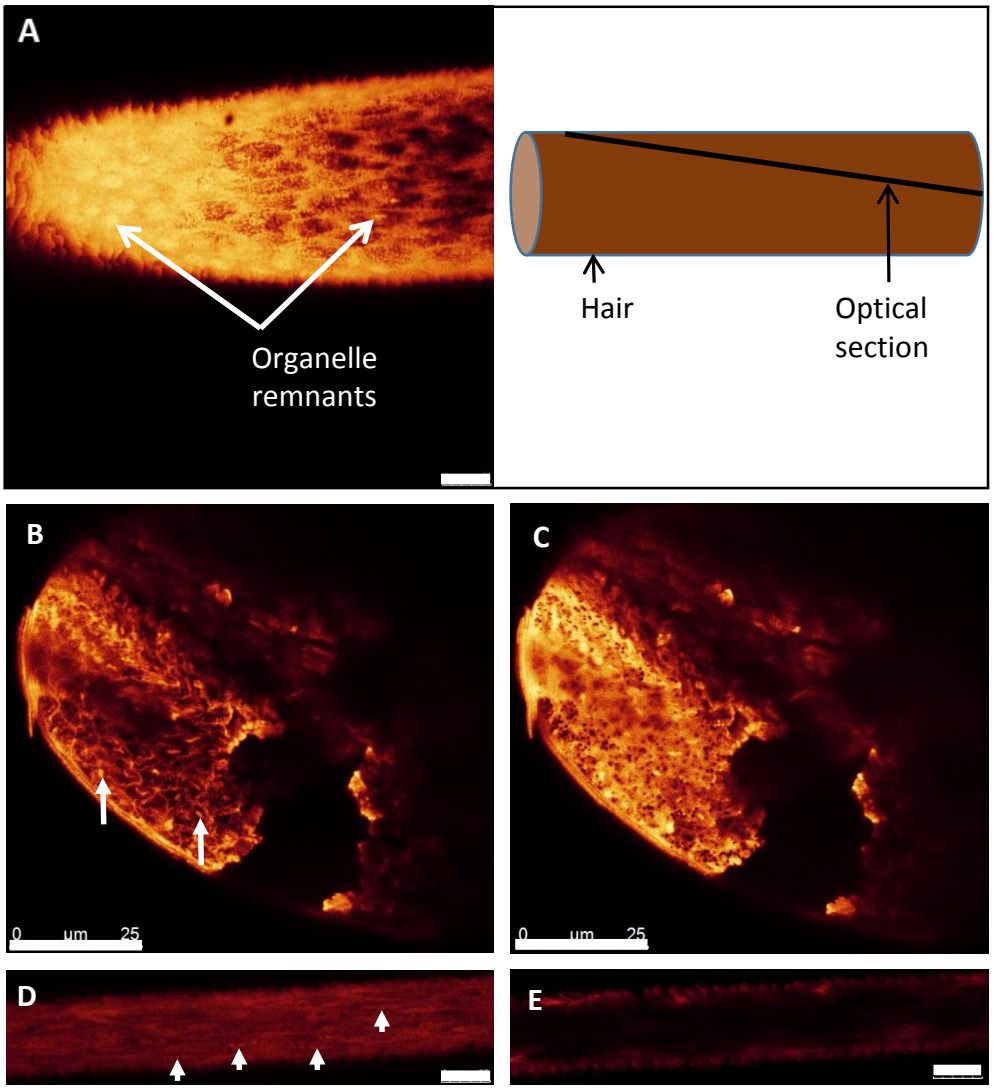

Fig. 3.10. Confocal microscopy of organelle remnants. A) Diagonal optical section through the hair showing how organelle remnants change shape between the cuticle and the cortex and are more autofluorescent than the surrounding area, scale bar = 25µm. The adjoining drawing shows the plane of the optical section taken through the hair. B) Maleimide conjugated to 633nm AlexaFluor stained hair picks up the organelle remnants, scale bar = 25µm. C) The same area as previously, utilising 405nm excited autofluorescence, scale bar = 25µm. D) 543nm excitation showing organelle remnants (arrows), scale bar = 25µm. E) The same area as previously but with 633nm excitation, showing organelle remnants are not usually excited by 633nm, scale bar = 25µm. Images A, D and E are representative photomicrographs of 5 imaged hairs, and images B and C are representative of 6 imaged hairs.

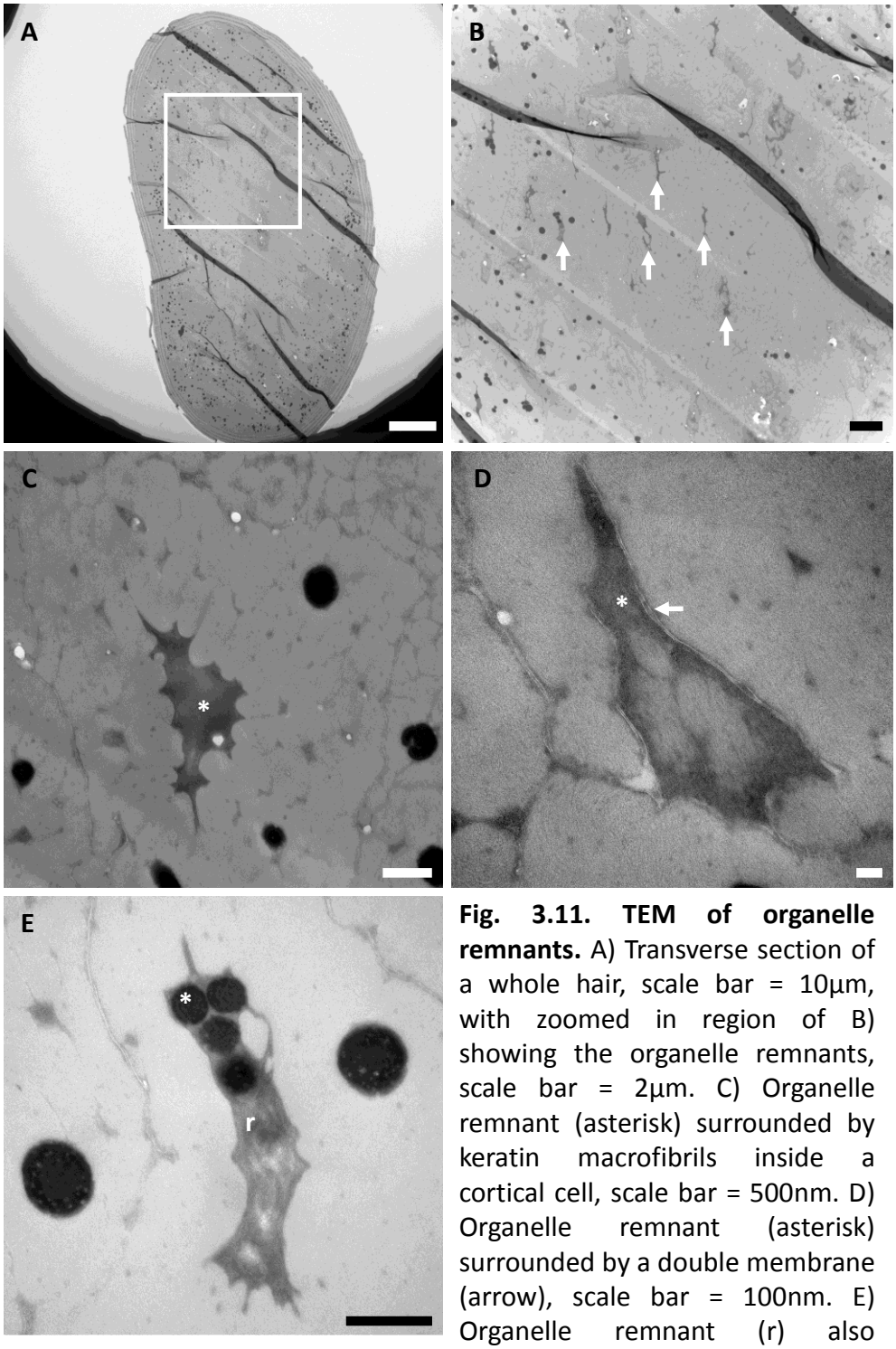

Fig. 3.11. TEM of organelle remnants. A) Transverse section of a whole hair, scale bar = 10µm, with zoomed in region of B) showing the organelle remnants, scale bar = 2µm. C) Organelle remnant (asterisk) surrounded by keratin macrofibrils inside a cortical cell, scale bar = 500nm. D) Organelle remnant (asterisk) surrounded by a double membrane (arrow), scale bar = 100nm. E) Organelle remnant (r) also containing melanin granules (asterisk), scale bar = 500nm. Photomicrographs are representative of 12 imaged hairs.

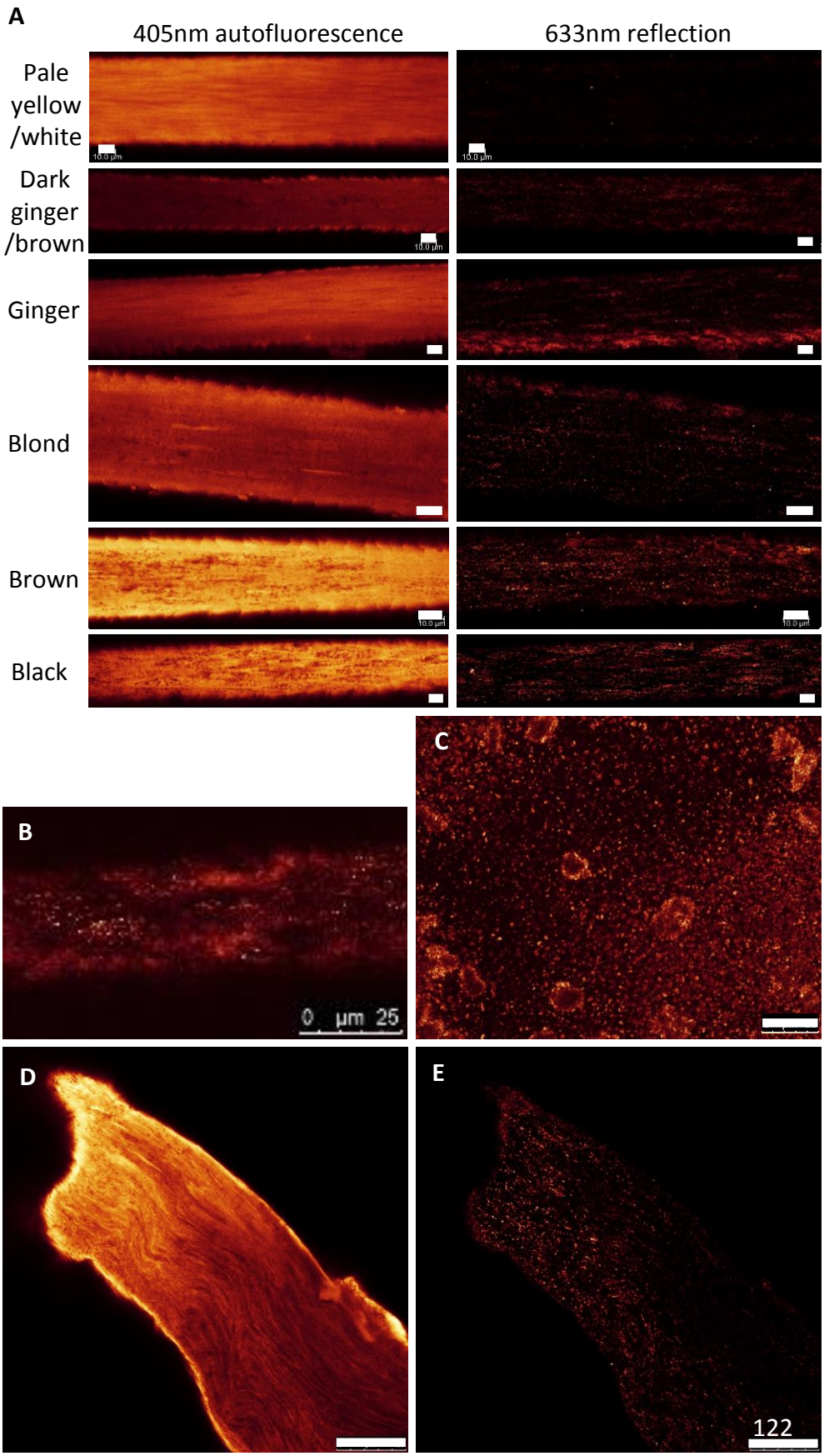
A
405nm autofluorescence
633nm reflection
Pale yellow /white
Dark ginger /brown
Ginger
Blond
Brown
Black
B
0 µm 25
C
D
E
122

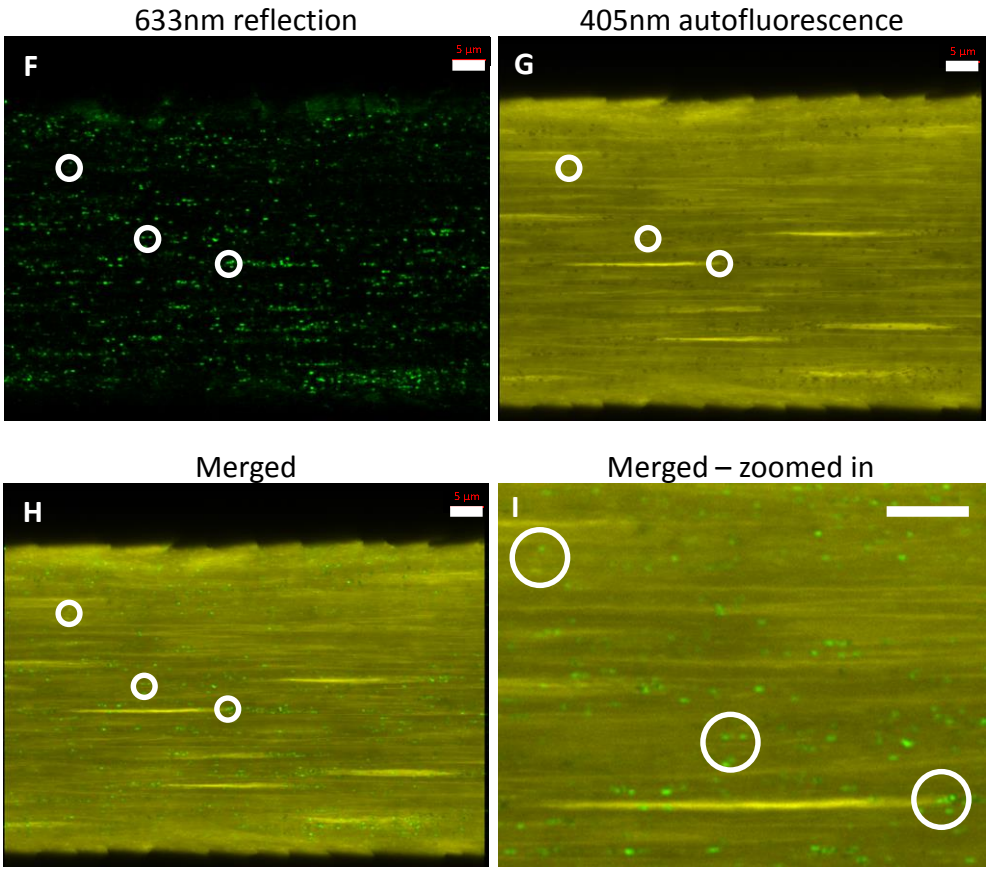

Fig. 3.12. Label-free imaging of melanin-like particles. A) Confocal of the upper cortex level for the best resolution, showing 405nm autofluorescence and 633nm reflection of various hair colours, to show how the melanin-like particle content differs, scale bars = 10µm. Used Eu 5.0 for brown hair and Eu 7.0 for blond hair. The pale yellow/white hair was from elderly Chinese donors. B) 633nm excitation of the cuticle/upper cortex, showing reflective melanin-like particles. C) Synthetic melanin reflects 633nm laser emission, scale bar = 25µm. D) R18 stained beard hair follicle shows melanin present in the follicle with 405nm excitation, and with (E) 633nm reflection, scale bars = 25µm. F) Melanin-like particles in the cortex are reflective in European blond hair and reflect 633nm laser emission, examples of one type of particle are circled, scale bar = 5µm. G) 405nm induced autofluorescence, showing black melanin-like particles, NB the particles circled in (F) are not present here, scale bar = 5µm. H) Merged image, scale bar = 5µm. I) Merged image, zoomed in to show circled areas more clearly, scale bar = 5µm. Representative photomicrographs shown are from black (n=3), brown (n=3), blond (n=3), ginger (n=6), darker ginger/brown (n=4), pale yellow/white old-age (n=5) hairs imaged.

A

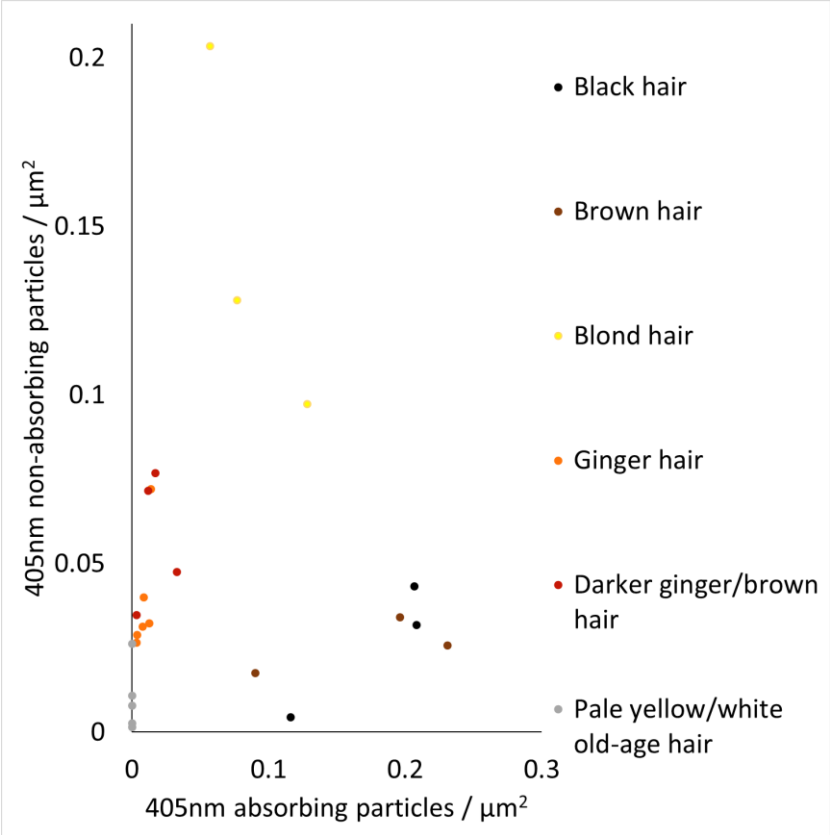
0.2
0.15
0.1
0.05
0
405nm non-absorbing particles / µm²
0
0.1
0.2
0.3
405nm absorbing particles / µm²
Black hair
Brown hair
Blond hair
Ginger hair
Darker ginger/brown hair
Pale yellow/white old-age hair

B

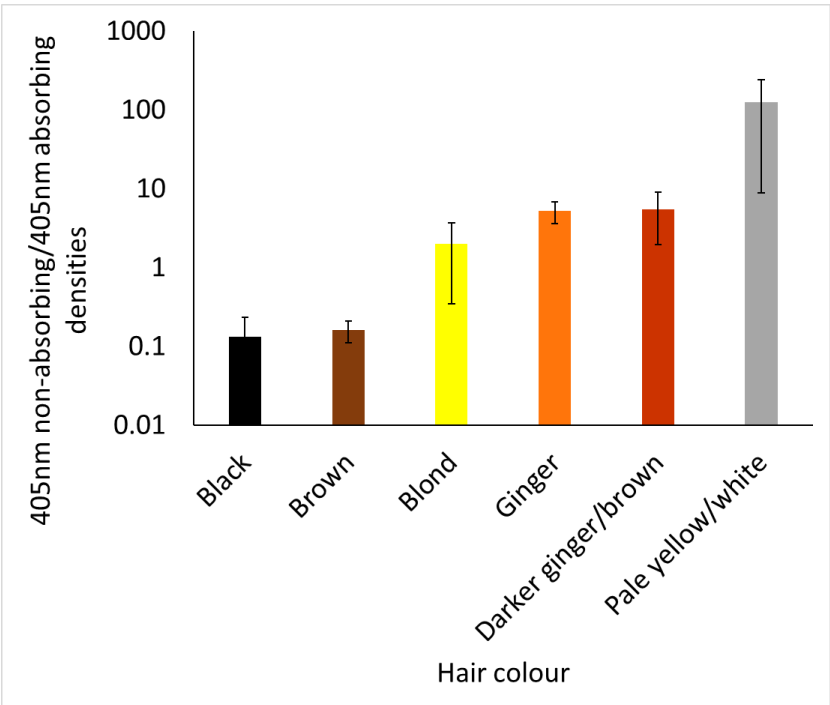
1000
100
10
1
0.1
0.01
405nm non-absorbing/405nm absorbing densities
Black
Brown
Blond
Ginger
Darker ginger/brown
Pale yellow/white
Hair colour

C

Hair colour	No. of particles absorbed 405nm	No. of particles reflected 633nm
Black	1845, 992, 1653	2126, 1199, 1715
Brown	1098, 1121, 334	1220, 1315, 399
Blond	481, 294, 443	1280, 1340, 779
Ginger	47, 49, 129, 100, 173, 104	391, 412, 452, 497, 1078, 592
Darker ginger/brown	186, 63, 198, 350	1025, 694, 1382, 857
Pale yellow/white	1, 1, 1, 1, 1	123, 19, 128, 23, 342

Fig. 3.13. Quantification of the melanin-like particles. A) The densities of the two different categories of melanin-like particles in the indicated hair colours. B) Graph to show the proportion of the two different categories of melanin-like particles in various hair colours, error bars = +/- 2*SEM. C) Table of the number of particles which absorbed 405nm and reflected 633nm for each piece of hair. Black hair (n=3), brown hair (n=3), blond hair (n=3), ginger hair (n=6), darker ginger/brown hair (n=4), pale yellow/white old-age hair (n=5).

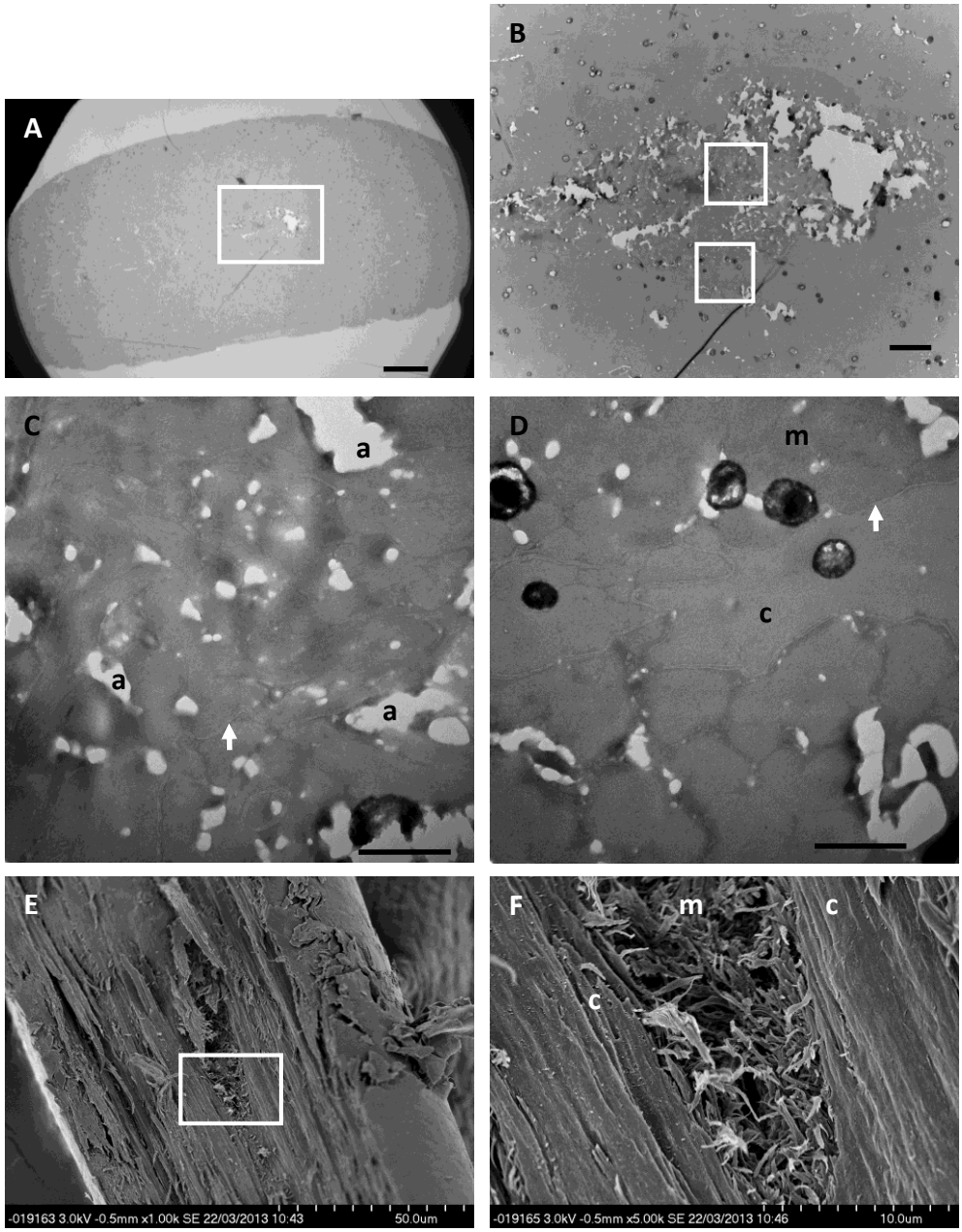
A
B
C
a
a
a
D
m
c
E
F
m
c
c
-019163 3.0kV -0.5mm x1.00k SE 22/03/2013 10:43
50.0um
-019165 3.0kV -0.5mm x5.00k SE 22/03/2013 10:46
10.0um

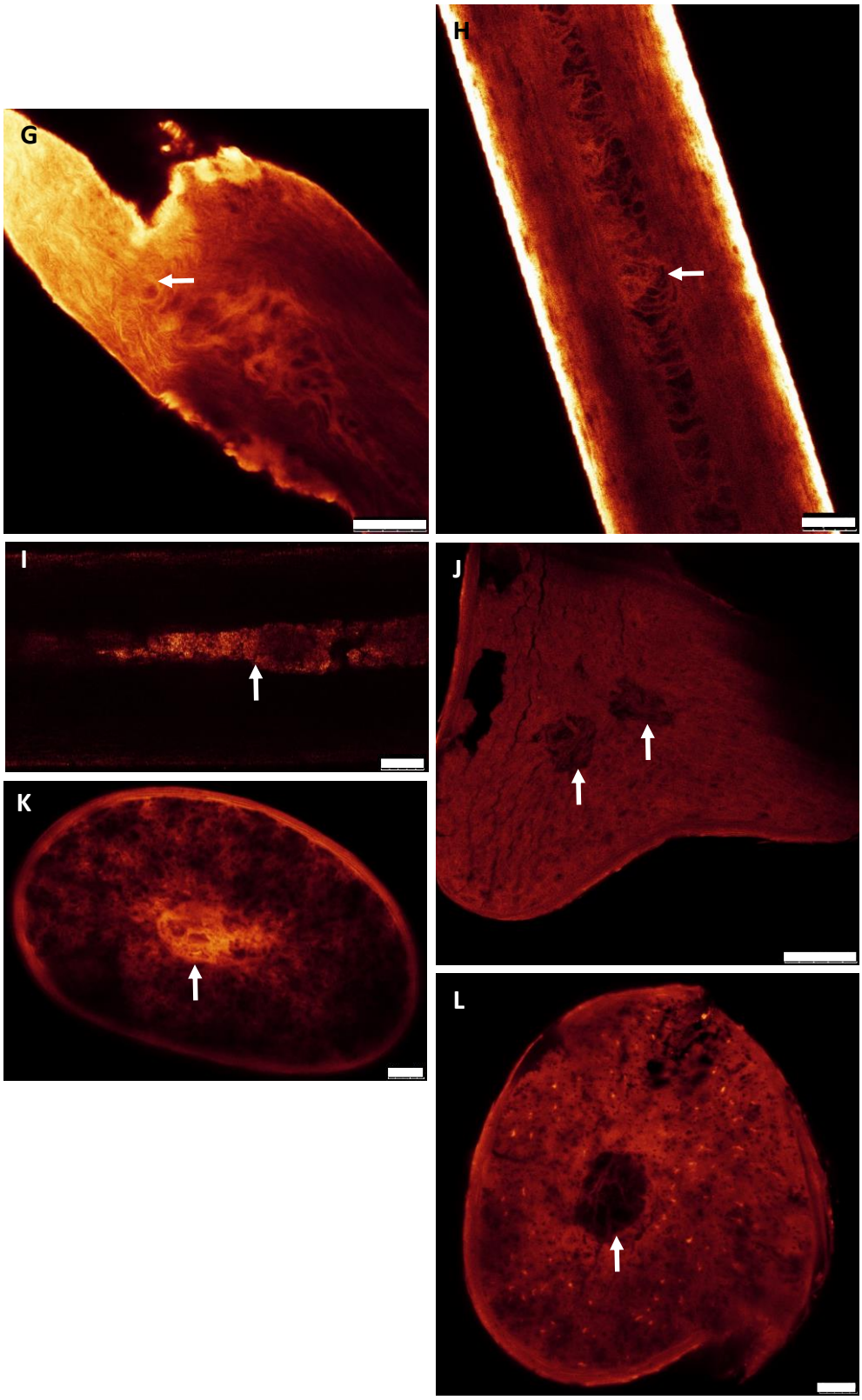
G
H
I
J
K
L

Fig. 3.14. Visualisation of the medulla of human head hair. A) TEM of a transverse section through a hair, with the medulla enlarged in the next image, scale bar = 10µm. B) TEM transverse section through a hair showing the medulla, scale bar = 2µm. C) Enlargement of the upper selected area in the previous image, showing the airspaces (a) and CMC (arrow), scale bar = 500nm. D) Enlargement of the lower selected area, showing the CMC (arrow) between the medulla (m) and cortex (c), scale bar = 500nm. E) SEM of a hair cut in half, exposing the medulla. F) Enlargement of the previous image, showing the medulla (m) in the centre of the cortex (c). G) Confocal of a beard hair follicle stained with R18 showing the beginnings of the medulla (arrow), scale bar = 25µm. H) Confocal of a longitudinal section through the centre of a hair using 405nm excited autofluorescence, showing the medulla (arrow), scale bar = 25µm. I) Confocal using 633nm reflection to show the medulla (arrow), scale bar = 25um. J) Confocal of a transverse optical section through a beard hair which appears to have two medullas (arrows), scale bar = 25µm. K) Confocal transverse sections of hairs with highly autofluorescent medullas (arrow), scale bar = 10µm. L) Confocal transverse section of a hair with a less autofluorescent medulla (arrow), scale bar = 10µm. Representative TEM photomicrographs of 12 TEM imaged hairs, 5 SEM imaged hairs, 5 confocal longitudinal and 6 confocal transverse imaged hairs are shown.

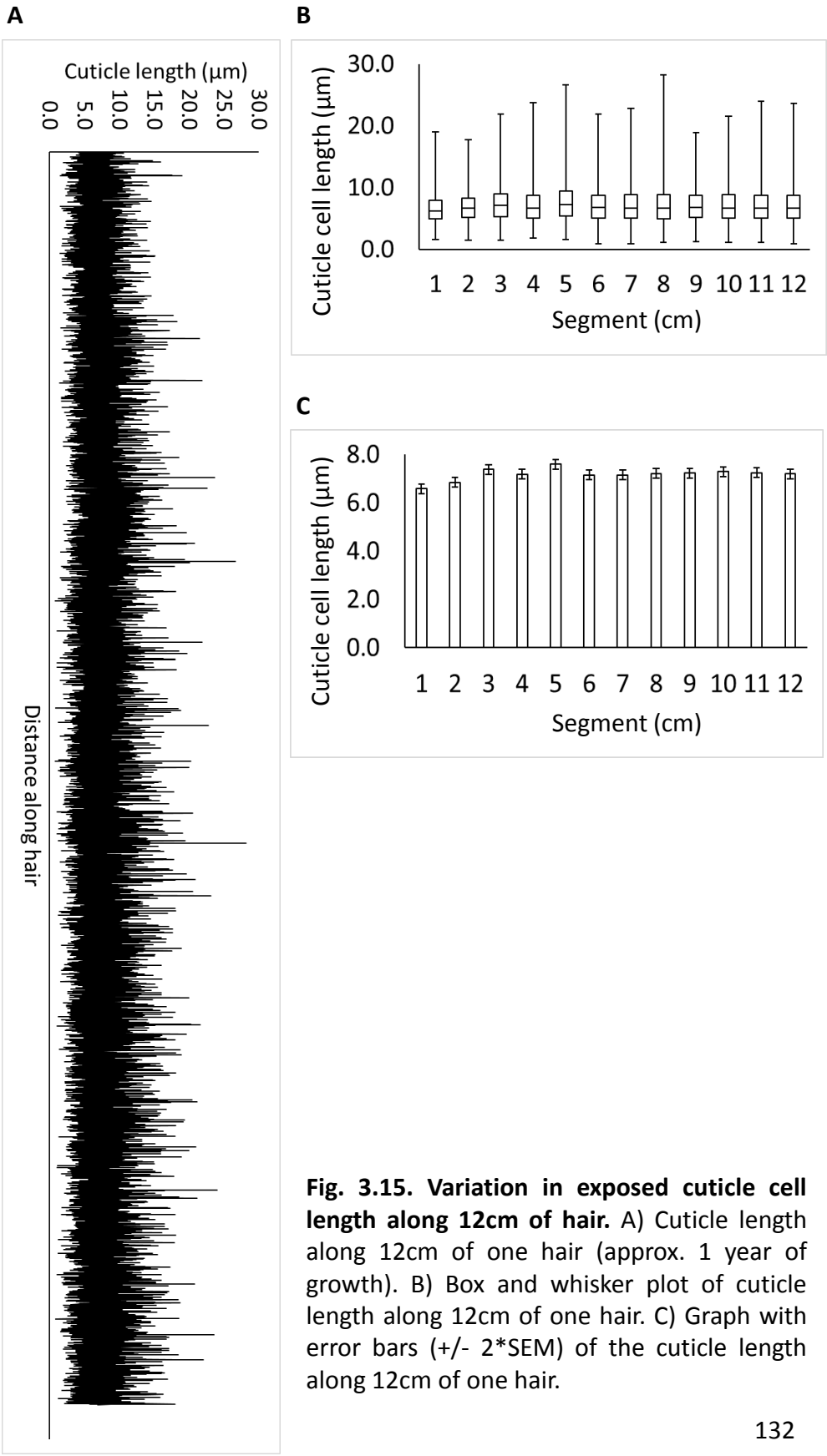

Fig. 3.15. Variation in exposed cuticle cell length along 12cm of hair. A) Cuticle length along 12cm of one hair (approx. 1 year of growth). B) Box and whisker plot of cuticle length along 12cm of one hair. C) Graph with error bars (+/- 2*SEM) of the cuticle length along 12cm of one hair.

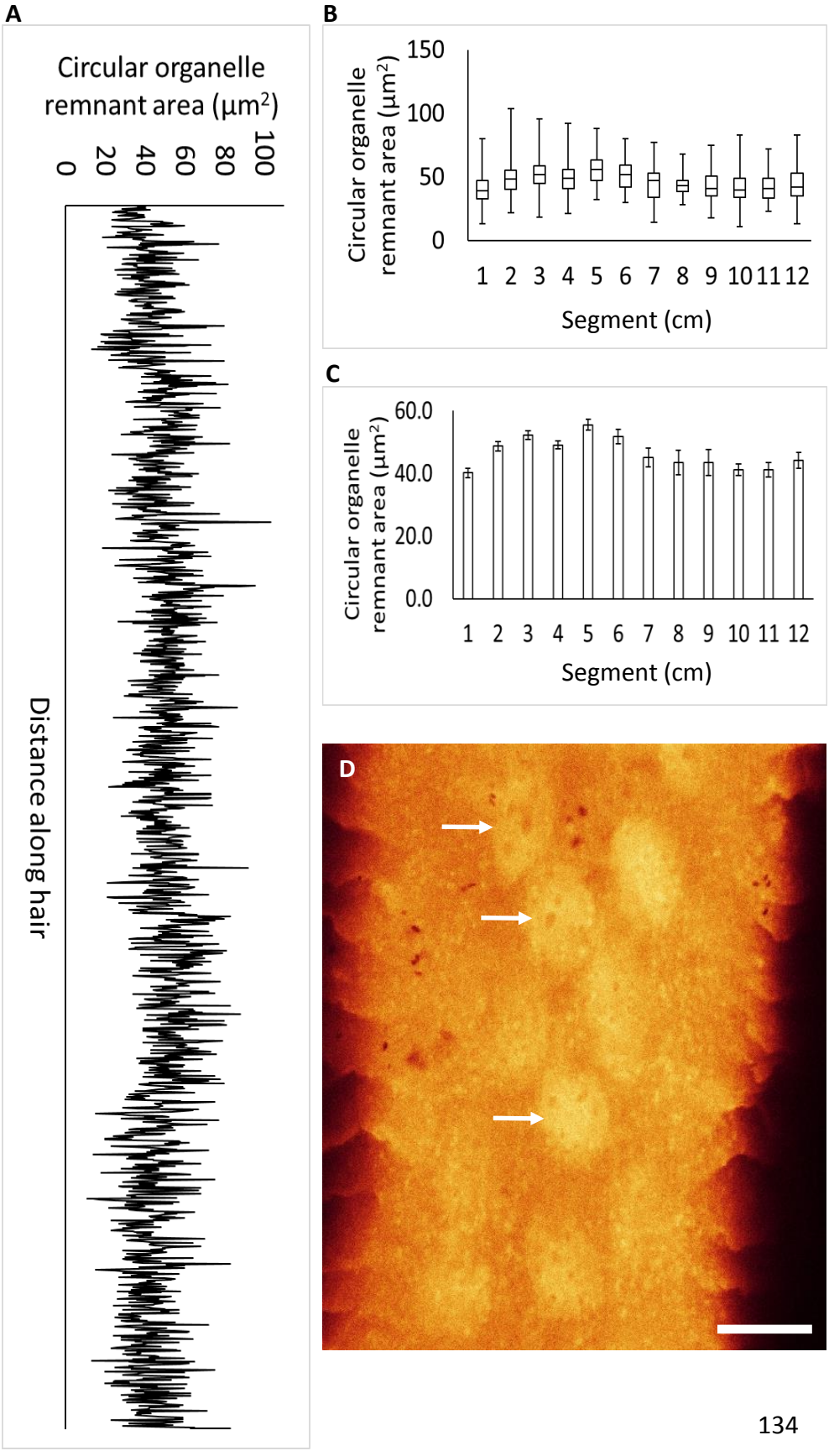
A
Circular organelle remnant area (µm²)
0
20
40
60
80
100
Distance along hair
B
Circular organelle remnant area (µm²)
150
100
50
0
1 2 3 4 5 6 7 8 9 10 11 12
Segment (cm)
C
Circular organelle remnant area (µm²)
60.0
40.0
20.0
0.0
1 2 3 4 5 6 7 8 9 10 11 12
Segment (cm)
D

E

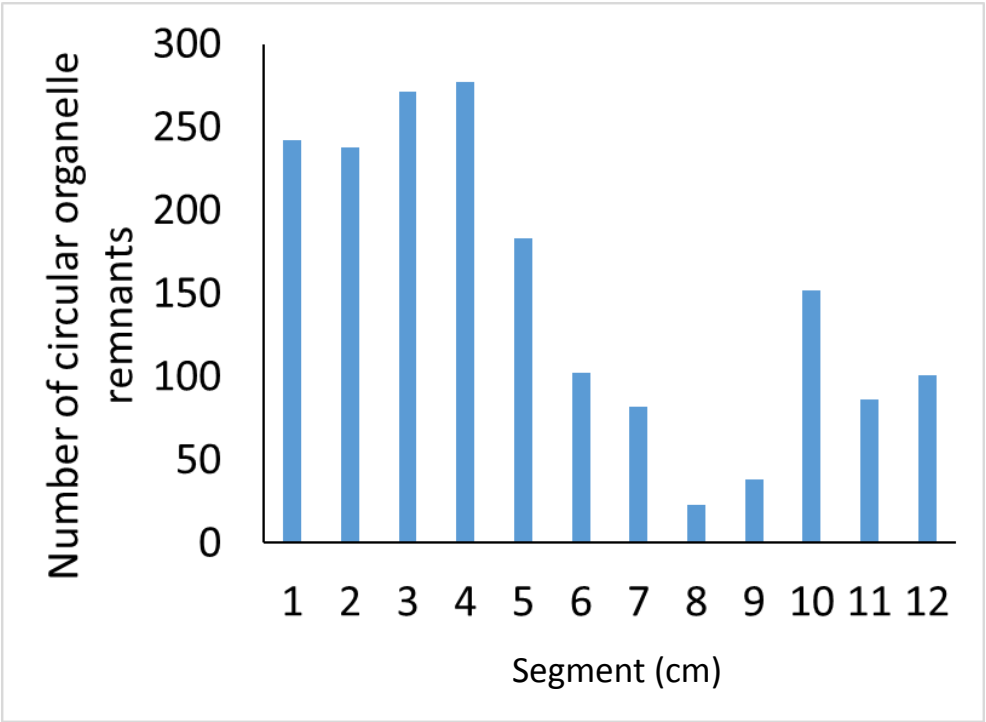

Fig. 3.16. Variation in circular organelle remnant area along 12cm of hair. A) Circular organelle remnant area along 12cm of one hair (approx. 1 year of growth). B) Box and whisker plot of circular nuclear remnant area along 12cm of one hair. C) Graph with error bars (+/- 2*SEM) of the circular nuclear remnant area along 12cm of one hair. D) Confocal image showing circular organelle remnants (arrows), scale bar = 10µm. E) Approximate number of circular organelle remnants recorded in each 1cm segment.

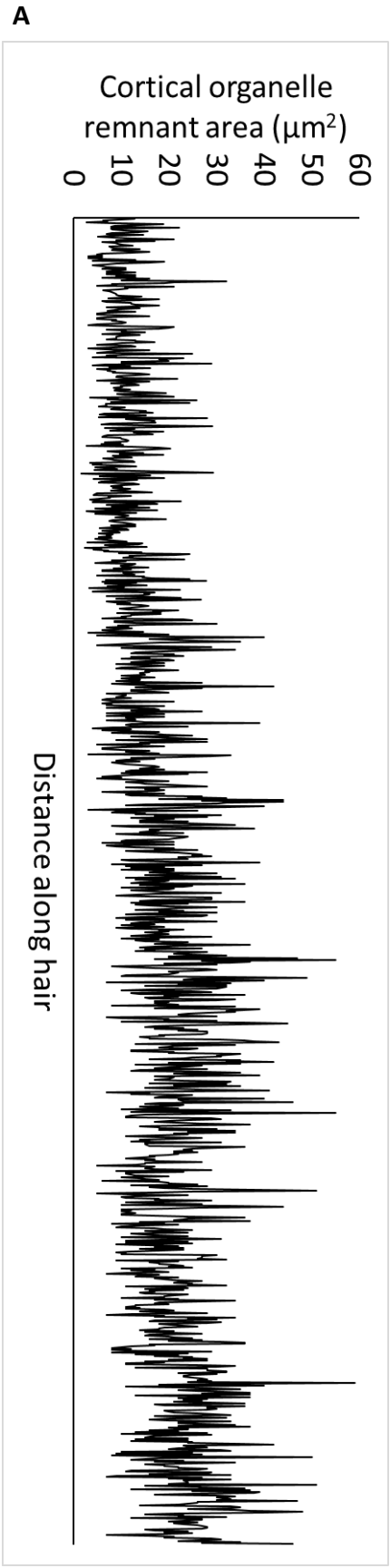
A
Cortical organelle remnant area (µm²)
0
10
20
30
40
50
60
Distance along hair

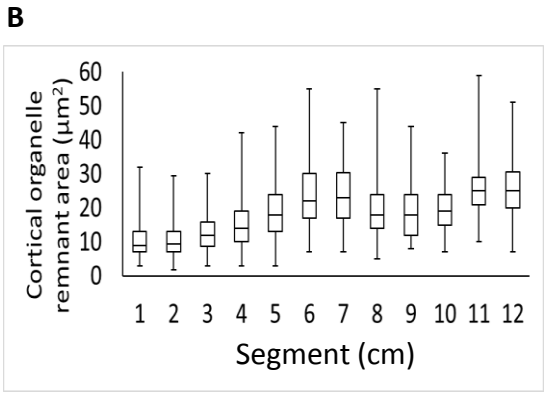
B
Cortical organelle remnant area (µm²)
0
10
20
30
40
50
60
1 2 3 4 5 6 7 8 9 10 11 12
Segment (cm)

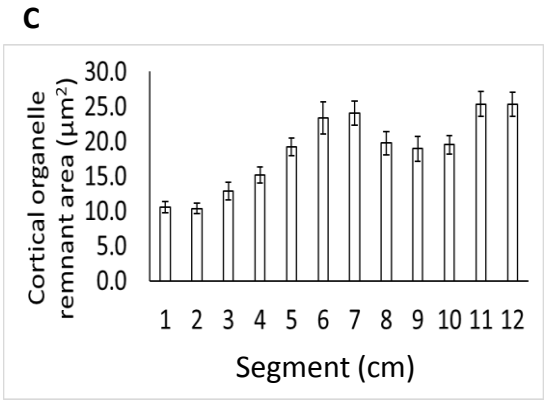
C
Cortical organelle remnant area (µm²)
0.0
5.0
10.0
15.0
20.0
25.0
30.0
1 2 3 4 5 6 7 8 9 10 11 12
Segment (cm)

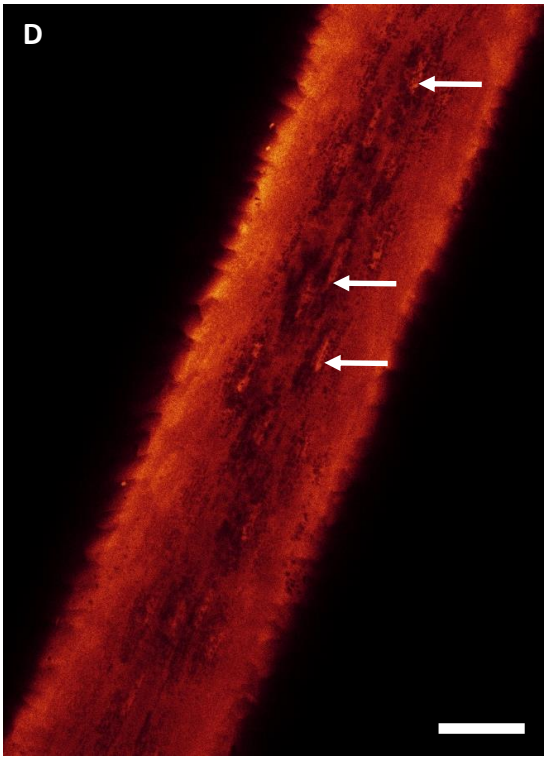
D

Fig. 3.17. Variation in cortical organelle remnant area along 12cm of hair. A) Cortical nuclear remnant area along 12cm of one hair (approx. 1 year of growth). B) Box and whisker plot of cortical nuclear remnant area along 12cm of one hair. C) Graph with error bars (+/- 2*SEM) of the cortical nuclear remnant area along 12cm of one hair. D) Confocal image showing cortical organelle remnants (arrows), scale bar = 25µm.

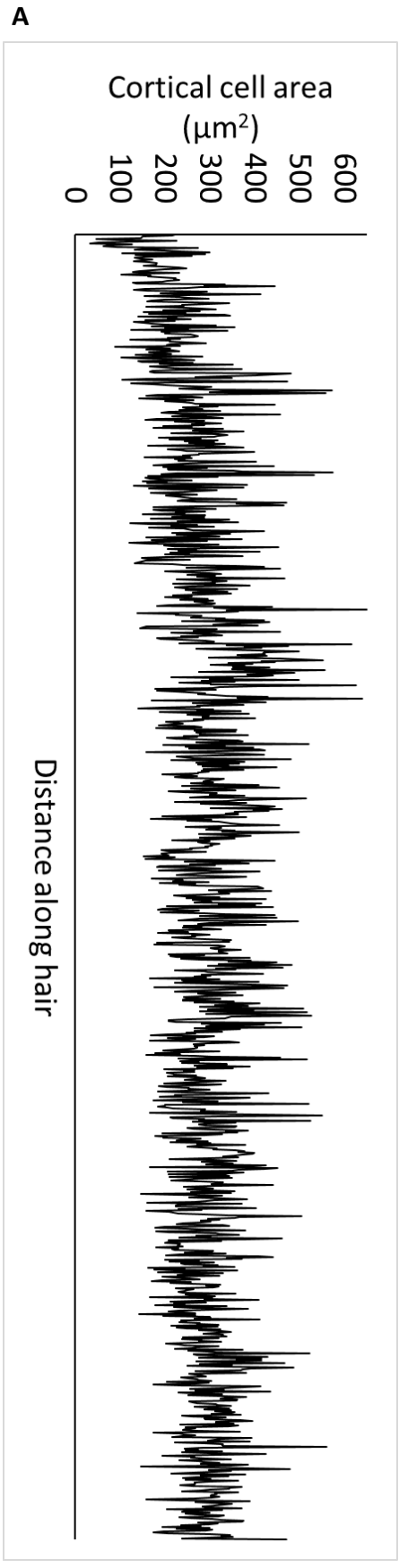
A
Cortical cell area (µm²)
0
100
200
300
400
500
600
Distance along hair
B
Cortical cell area (µm²)
600
500
400
300
200
100
0
1 2 3 4 5 6 7 8 9 10 11 12
Segment (cm)
C
Cortical cell area (µm²)
350.0
300.0
250.0
200.0
150.0
100.0
50.0
0.0
1 2 3 4 5 6 7 8 9 10 11 12
Segment (cm)
D
Segment (cm)
1
2
3
4
5
6
7
8
9
10
11
12
Cortical cell area (µm²)
700
600
500
400
300
200
100
0
0
20
40
60
Cortical organelle remnant area (µm²)

Fig. 3.18. Variation in cortical cell area along 12cm of hair. A) Cortical cell area along 12cm of one hair (approx. 1 year of growth). B) Box and whisker plot of cortical cell area along 12cm of one hair. C) Graph with error bars (+/- 2*SEM) of the cortical cell area along 12cm of one hair. D) Graph of the correlation between cortical organelle remnant area and corresponding cortical cell area.

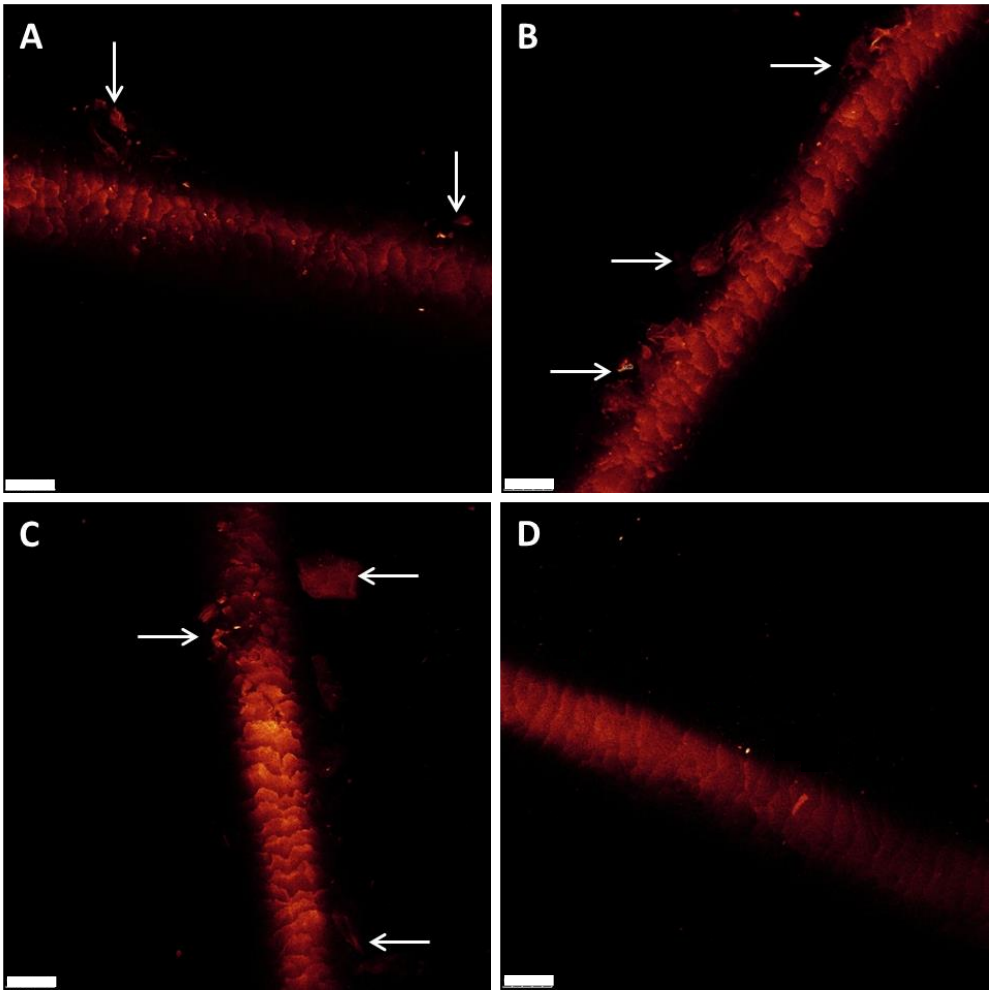

Fig. 3.19. Confocal imaging of the uncharacterised hair and skin disorder. A,B,C) Hairs from a patient with an uncharacterised skin and hair disorder, which show detached material around the outside of the cuticle (arrows). D) Hair from the same patient which appears to be normal. Photomicrographs shown are representative of 5 hairs imaged. Scale bars = 25µm.

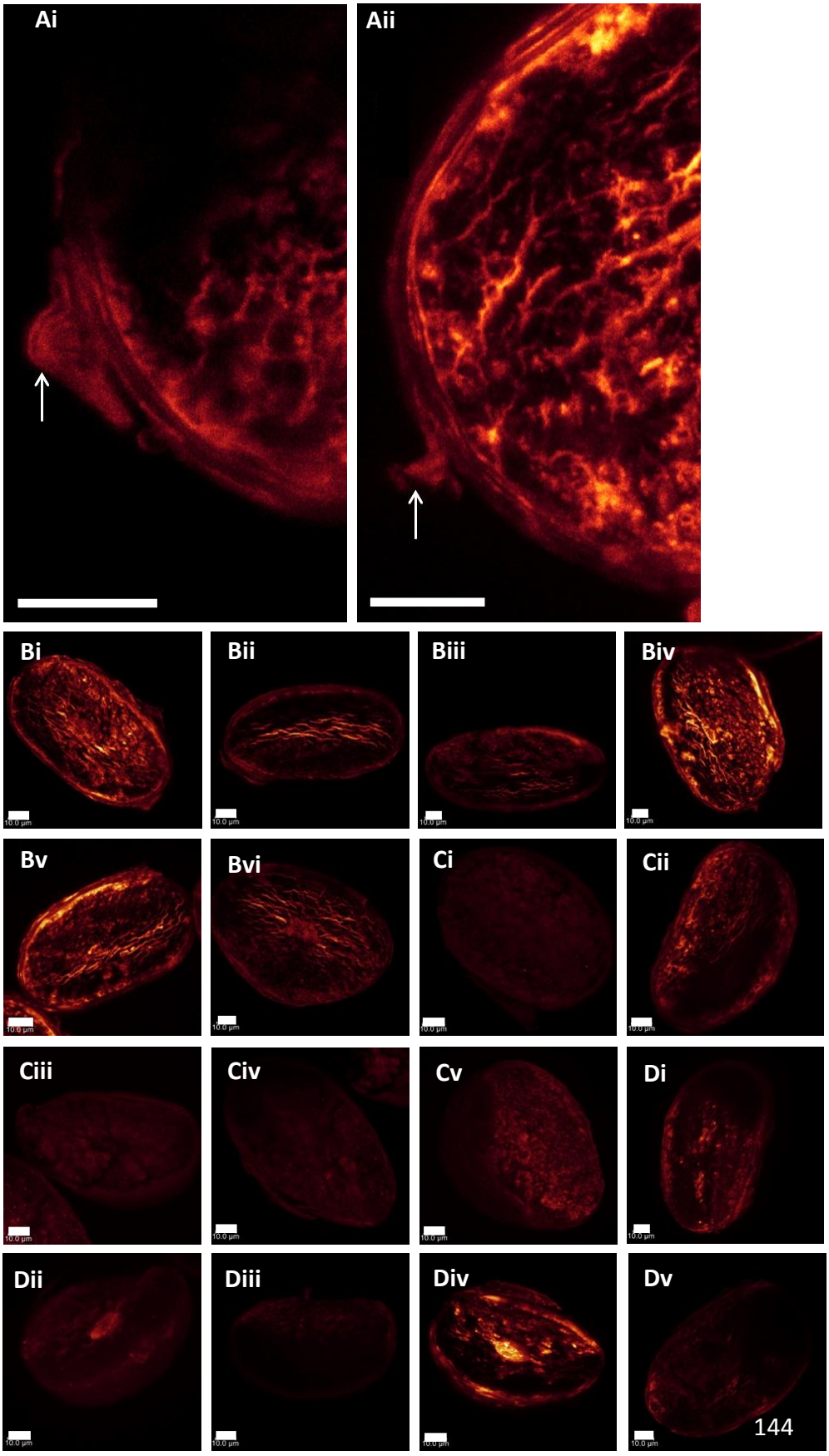
Ai
Aii
Bi
Bii
Biii
Biv
Bv
Bvi
Ci
Cii
Ciii
Civ
Cv
Di
Dii
Diii
Div
Dv

Fig. 3.20. Max projection of transversely optical sectioned hairs stained with 0.6mg/ml Nile red and 543nm laser excitation. A) Hairs from a patient with an uncharacterised skin and hair disorder, showing the flaky cuticle (arrows). B) Hairs from the patient with an uncharacterised skin and hair disorder, showing the patient has more Nile red staining and therefore more lipids present in their hair than their unaffected parents (C and D). Photomicrographs shown are representative of 6 hairs imaged from each of the three donors. Scale bars = 10µm.

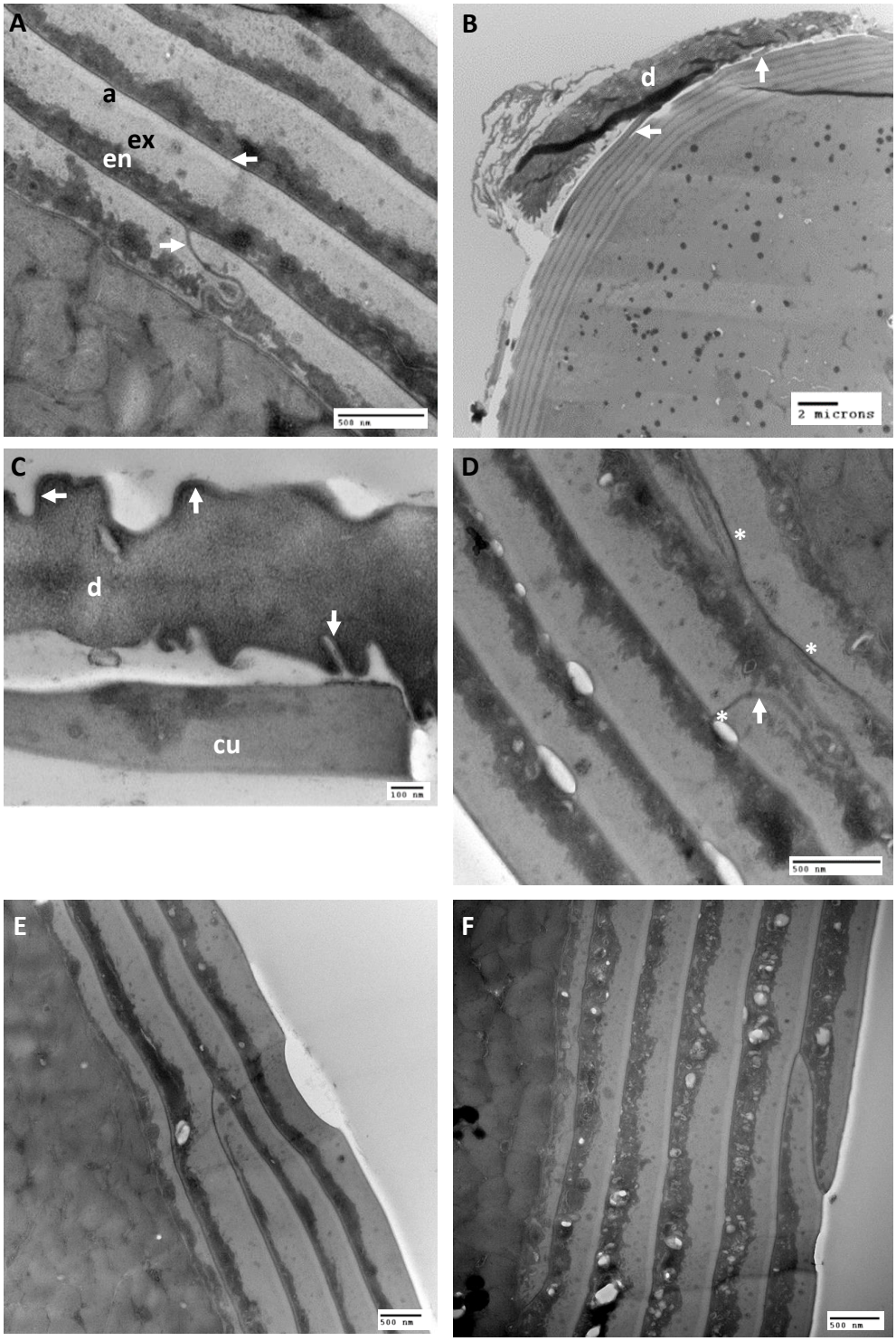
A
a
ex
en
500 nm
B
d
2 microns
C
d
cu
100 nm
D
500 nm
E
500 nm
F
500 nm

Fig. 3.21. TEM of a transverse section of hair from a patient with an uncharacterised skin and hair disorder. A) Normal looking hair showing the A-layer (a), exocuticle (ex), endocuticle (en), and the CMC (arrows), scale bar = 500nm. B) Hair showing a membrane-bound deposit (d) at the outer cuticle layer, perhaps continuous with the cuticle (arrows), scale bar = 2µm. C) Part of the membrane-bound (arrows) deposit (d) outside of the hair cuticle (cu), scale bar = 100nm. D) Hair showing normal CMC (asterisks) and lack of CMC distinction (arrows), scale bar = 500nm. E) Patient's Father's unaffected hair, scale bar = 500nm. F) Patient's Mother's unaffected hair, scale bar = 500nm. Photomicrographs shown are representative of 3 hairs imaged from each donor.

Chapter 4

Analysis of hair structure by fluorescence lifetime imaging

4.1. Introduction

Continuing from the exploration of the autofluorescent hair in the previous chapter, it was noted that label-free imaging of autofluorescence intensity often resulted in structures appearing uniform. However, it could be predicted that the imaged structures are actually encountering different chemical environments, so fluorescence lifetime imaging microscopy was used to further investigate the structures and properties of the untreated hair, again using label-free imaging.

4.1.1. FLIM

Fluorescence lifetime imaging microscopy, or FLIM, measures the exponential decay rate of a fluorophore (Lakowicz *et* al., 1992; Lakowicz, 2006). It is useful in addition to photon intensity measurements as an area of a sample may emit the same number of photons and therefore appear homologous in intensity imaging, whereas FLIM can be used to further distinguish structures and chemical environments because the fluorophore lifetimes may differ.

To image with FLIM, samples are either labelled with fluorophores or imaged using the endogenous fluorophores. FLIM is non-invasive and relatively non-destructive besides possible photobleaching. FLIM works by a pulsed laser emitting photons that are absorbed by fluorophores, which then enter an excited state, S1 (fig. 4.1). The Jablonski diagram (fig. 4.1) shows that there are many pathways in which to return to the ground state, S0. To do this, the fluorophore can: emit a photon (fluorescence); transfer energy to surrounding molecules; or through the conversion of energy into heat. Alternatively, the fluorophore can cross into the reactive triplet state, T1, from where it can transit to S0 via phosphorescence or cross back to the S1 state from where it can again transit to S0 via the pathways described above (Lakowicz, 2006). The fluorescence lifetime is the time constant for this decay in a homogenous population of molecules; the reciprocal sum of the rate constants of all possible return routes to the ground state:

$$\frac{1}{\tau} = \sum k_i$$

Where τ is the fluorescence lifetime, and k_i is the rate of the decay pathway. The fluorescence lifetime is usually measured in the order of nanoseconds. When the fluorescence lifetime is low the rate constants are greater, and vice versa. The rate

constants differ depending upon the type and conformation of the fluorophores, and upon their constituent environment such as the metabolic state, concentration of oxygen and protein binding. Thus, irrespective of fluorophore concentration, differing lifetimes suggest different chemical environments within a sample (Konig and Riemann, 2003; Richards-Kortum *et al*., 2003; Schweitzer *et al*., 2007; Becker, 2012). Such changes in lifetime with chemical environment have been demonstrated in living cell systems, for instance where the lifetime of nicotinamide adenine dinucleotide (NADH) decreases as pH increases (Ogikubo *et al*., 2011). Another example is the differing redox ratio between flavin adenine dinucleotide (FAD) and NADH which changes the fluorescence lifetimes of FAD and NADH and shows lifetime is affected by a change in metabolic state such as increased glycolysis (Skala *et al*., 2007; Provenzano *et al*., 2008a). An increase in the lifetime of FAD in mammary tissue has also been linked with invading metastatic cells (Provenzano *et al*., 2008b).

FLIM has only been utilised by a small number of researchers in the analysis of hair in the past, and not in conjunction with confocal microscopy. Studies have been carried out which have been proposed to distinguish pheomelanin and eumelanin in hair, and can therefore distinguish hair colour, separately using multiphoton microscopy (Ehlers *et al*., 2007) and two-photon excited fluorescence lifetime imaging (Krasieva *et al*., 2012). However, the images produced are of low resolution and the studies fail to take into account that red hair, the sample used for pheomelanin, also contains eumelanin, and vice versa for black hair. Other researchers have also worked on melanin in the skin using multiphoton microscopy FLIM (Sugata *et al*., 2009). Further research using FLIM has been carried out on the epidermis. One study has shown that normal skin can be discriminated from basal cell carcinoma skin by changes in lifetime, perhaps due to the degradation of collagen by tumour-associated matrix metalloproteinases as well as changes in pH (Galletly *et al*., 2008). Another study on the epidermis has shown the location of calcium in the stratum granulosum and the release of calcium from the endoplasmic reticulum following perturbation of the epidermal barrier (Celli *et al*., 2016). FLIM has also been used to test the penetration of commercial products into the epidermis (Leite-Silva *et al*., 2013). FLIM carries a lot of potential for further use and already has applications in clinical research from dermatology such as melanoma characterisation (Konig, 2008) to oncology (Skala *et al*., 2007; Provenzano *et al*. 2008ab).

As FLIM has the potential to distinguish structures in a label-free manner, it was used to further the investigation into the hair structures. The research within this chapter uses the time-correlated single photon counting (TCSPC) method for FLIM (Becker, 2012) implemented on a Leica SP5 confocal laser scanning microscope. This was used to gather images as well as numerical data to analyse the hair samples. The unit of measurement of the fluorescence lifetime was in nanoseconds, and a lower limit and an upper limit of lifetimes for each sample were measured. The lower limit up to the upper limit cover a lifetime frequency curve of approximately 95% of the lifetimes measured, and sometimes an average lifetime of the lower and upper limits was used in analysis. Different studies have used various excitation lasers, here 470nm and 640nm are used as they were the only wavelengths available. The hairs were measured longitudinally and transversely to further distinguish structures within the hair.

4.1.2. Aims of the study

The overall aim of this chapter was to investigate if fluorescence lifetime imaging reveals structures and chemical environments that cannot be resolved by fluorescence intensity. The first aim was to test whether using ambient room humidity to measure lifetime yields consistent results. This needed to be done as a control to ensure that the varying humidity of the laboratory was not affecting the fluorescence lifetime of the hairs. The following aim was to compare autofluorescence and FLIM data in all the layers of fully differentiated hair. This was done to investigate whether there is a significant difference between and within the hair cuticle, cortex and medulla and along the hair length which can be detected using FLIM. The fluorescence lifetimes of the individual cell layers of the cuticle were explored in detail by extracting specific lipids and reducing disulphide bonds to discover how these affect the chemical environment of the hair. The final aim was to use FLIM to investigate an uncharacterised hair and skin disorder to see whether a difference in lifetime could be measured between the affected son's hair and his unaffected parents'. Since FLIM detects changes in chemical environment, there could be a detectable difference in hair affected by a disease compared to healthy hair.

4.2. Experimental approach

FLIM was used to further investigate the structures of the hair, and following a similar procession through the hair as in the previous chapter, investigations were first made into the cuticle, followed by the cortex and medulla. Imaging was carried out by imaging hairs with the 405nm wavelength before and after taking FLIM images with each of the 470nm and 640nm lasers for reference to hair structures and to test for movement of the sample during fluorescence lifetime imaging as this would void the results. When imaging hairs longitudinally the cuticle, cortex and medulla were imaged separately by adjusting the z-axis. For transverse images, the SymPhoTime software was used post-imaging to draw and extract distinct regions of interest to separate the hair compartments for individual analysis. In total, 1540 FLIM images were taken of hairs, with 1-4 images taken of each hair. Images shown in figures are representative of the hairs imaged.

4.2.1. Relative humidity

Nine untreated Chinese scalp hairs were taken and placed in water (n=3), a controlled 70% relative humidity environment (n=3), or left at ambient humidity (n=3) for 18h at room temperature. Once removed from these conditions they were immediately placed in oil and imaged.

4.2.2. FLIM of the cuticle, cortex and medulla

Where the average lifetimes of the cuticle, cortex and medulla are compared, numbers were obtained from untreated transverse optical sections of Chinese scalp hair. Using the SymPhoTime software, regions of interest were drawn to separate the cuticle, cortex and medulla. In total, the lifetimes of thirty-eight hairs were measured using excitation from the 470nm and thirty-six using the 640nm laser. Only some hairs possessed a medulla (n=19).

The average lifetimes of beard hairs are compared, and in total, the lifetimes of four hairs at the mid-section of the hair were measured, three of which had a medulla, using excitation from the 470nm and 640nm laser. The lifetimes of the root, mid-section and distal tip of the hair were measured on two of the four hairs, though only one hair possessed a medulla. The lifetimes were measured for five plucked scalp hairs, where

the root area is defined as being under the skin, the mid-section is above the skin, and the distal tip is the very end of the hair.

FLIM images were taken along the lengths of three hairs to test whether there are changes in lifetime along the hair length. Since FLIM takes much longer than intensity confocal imaging, the imaging could not be taken continuously along the length of the hair. Instead, each hair was cut into six or seven equal lengths of 2cm and a FLIM image with each laser was taken of the cuticle and cortex of the hair for each section.

4.2.3. Multiple cuticle lifetimes

All hairs showed different lifetimes in the cuticle than in the cortex immediately below it. The cuticle was removed on some hairs (n=10) to show the effect was not an artefact. Cuticle lifetimes were analysed from 470nm (n=21) and 640nm (n=23) excited untreated Chinese scalp hairs.

4.2.4. Lipid extraction methods

Three lipid extraction methods were carried out on the hair to understand if hair lipids contribute to the FLIM images observed. To assess general lipid loss Nile red staining was carried out and fluorescence intensity measurements made using ImageJ. Comparisons of Nile red staining should not be made between the lipid extraction methods. This is due to the differing intensities, as for the CTAB method maximum projections of the hairs were used to account for uneven cutting through the hair, and the linear brightness of the images was different between methods so as to account for over-saturation of the colour channel.

4.2.4.1. Modified method for stratum corneum lipids

For each step of the seven stage protocol adapted from Pappinen *et al*., 2008, there were control (n=11) and treated hairs (n=11). Of these, some were used for longitudinal optical sectioning (n=5), and the others for transverse optical sectioning (n=6).

For GC/MS analysis, 3.36mg/ml of Chinese scalp hair was used with repeats in triplicate. Lipid extracts were dried under nitrogen and derivatised with 400µL Tri-Sil TP for 20 min, extracted with 200µL water and 400µL hexane. The phases were separated by centrifugation and the upper hexane layer was analysed by GC/MS using splitless injection. Fatty acid peaks were identified as follows: C14:0 – 8.0 min, C15:0 – 8.3 min,

C16:0 – 8.7 min. Other lipids were identified as follows: squalene – 12.2 min, cholesterol – 14.1 min.

4.2.4.2. Wertz and Downing method lipid extraction

For each step of the seven stage protocol adapted from Wertz and Downing, 1988, there were control (n=11) and treated hairs (n=11). Of these some were used for longitudinal optical sectioning (n=5), and the others for transverse optical sectioning (n=6). The linear brightness for hairs stained with 0.6mg/ml Nile red was darkened to 50-255 for the maximum projection images of the hairs, as the original brightness of the control hairs may have been close to the saturation point of the colour channel.

For GC/MS analysis, 2.6mg/ml of Chinese scalp hair was used with repeats in triplicate. The samples were derivatised with bistrimethylsilyltrifluoroacetamide (BSTFA) and splitless injection was used to acquire sufficient signal. Lipids were identified as follows: fatty acid 16:0 – 8.4 min, squalene – 12.2 min, cholesterol – 14.1 min, C18:C16 ester – 16.5 min, C18:C14 ester – 17.9 min.

4.2.4.3. CTAB method lipid extraction

For each step of the seven stage protocol adapted from Smith *et al*., 2010, there were control (n=11) and treated hairs (n=11). Of these some were used for longitudinal optical sectioning (n=5), and the others for transverse optical sectioning (n=6). The linear brightness for hairs stained with 0.6mg/ml Nile red was darkened to 200-255 for the maximum projection images of the hairs.

For GC/MS analysis, 27.6mg/ml of Chinese scalp hair was used with repeats in triplicate. The lipid extracts were dried under nitrogen or freeze-dried, then extracted with chloroform:methanol 1:1 and 0.9% KCl. The lower phases were removed into new tubes and dried under nitrogen at 35°C and derivatised with Tri-Sil TP (200µL) for 20 min, extracted with 100µL water and 200µL hexane. The phases were separated by centrifugation and the upper hexane layer was analysed by GC-MS. Splitless injections resulted in overloading of the detector for the HAc/IPA sample. Split injections were performed for all samples, with the existing method being altered to start at a lower temperature to spread the derivatives. Peaks were identified as follows: CTAB – 13.6 min, squalene – 23.07 min, cholesterol – 25.8 min, fatty acids – 12-17 min.

In the FLIM images of the transverse optical sections, the 470nm excited control and sample hairs have had their colour spectrum re-scaled with a lower average lifetime of 2ns and an upper average lifetime of 5ns so that they are directly comparable. The 640nm excited control and sample hairs have had their colour spectrum re-scaled to 0.7ns - 3.5ns. The transverse image re-scaling was only carried out for this lipid extraction as it was the only one which had a significant effect upon the lifetimes within the hair. Of the FLIM images, some hairs with low photon counts had the linear brightness increased.

4.2.4.4. Potassium thioglycolate treated hair

In addition to the lipid extraction methods, a treatment was also carried out to disrupt the sulphydryl bonds in the hair to test their effect on the fluorescence lifetimes. For the 45mM potassium thioglycolate treatment, there were control (n=11) and treated hairs (n=11). Of these, some were used for longitudinal optical sectioning (n=5), and the others for transverse optical sectioning (n=6).

In the FLIM images of the transverse optical sections, the 470nm excited control and sample hairs have had their colour spectrum re-scaled with a lower average lifetime of 3ns and an upper average lifetime of 5ns so that they are directly comparable. The 640nm excited control and sample hairs have had their colour spectrum re-scaled to 0.3ns - 3.5ns.

4.2.5. Contribution of melanin to FLIM

Hairs of different colour were imaged using FLIM and categorised as white (n=2), blond (n=7), ginger (n=1) and dark (n=25). Only measurements of the cortex were included in the analysis as this part of the hair contains the majority of the melanin.

4.2.6. Fluorescence lifetime indicators of hair cycle

FLIM was carried out on hairs in anagen (n=3) and in telogen (n=3) of the hair protruding from the bulb but still under the skin. Measurements were taken just underneath the cuticle and into the cortex.

4.2.7. Uncharacterised hair and skin disorder

For analysis of the hair from the patient with the uncharacterised hair and skin disorder, the unaffected mother and father were used for control hair samples. In total there were affected son (n=10), unaffected mother (n=11) and unaffected father (n=11) hairs

analysed using FLIM. Measurements were taken of the cuticle and cortex using the 470nm and 640nm lasers.

4.3. Results

FLIM was carried out on the hair to investigate whether more structures could be identified using label-free imaging by exciting the endogenous fluorophores. Lifetimes are represented in the images as colours, with red as the highest lifetime and blue as the lowest. For each image the distribution of the colours or scale has been adjusted to best cover the range of lifetimes present in that hair and this shows the hair structures in the most detail. The 470nm and 640nm lasers each gave a different distribution of lifetimes when emitted onto the hair, so both have been used in this study.

4.3.1. The cuticle

The compartments of the hair were investigated in a similar order to the previous chapter, so first the cuticle was studied, and it was found to have multiple fluorescence lifetimes.

4.3.1.1. Fluorescence lifetime imaging further distinguishes structures in the hair showing the cuticle possesses multiple lifetimes

FLIM images were taken of longitudinal and transverse optical sections of hair to explore the lifetimes of the hair cuticles. All previous FLIM work had been done on longitudinal hair sections and regarding hair colour (Ehlers *et al*., 2007; Krasieva *et al*., 2012), so the transverse optical sectioning method offered a new perspective on the FLIM of the hair. Figure 4.2 shows FLIM images and the corresponding intensity images for three hairs excited with the pulsed 470nm laser or 405nm continuous wave laser. In each image the lifetimes change across the hair as well as in the cuticle. The top longitudinal image shows the cuticle has a predominant lifetime shown in blue of 1.26ns. There seems to be variation in the outer cuticle lifetime between hairs, as some hairs had much lower outer cuticle lifetimes than others. Most biological endogenous fluorophores have longer fluorescence lifetimes, such as phenylalanine of 7.5ns, tryptophan of 3.03ns, and tyrosine of 2.5ns (de Melo *et al*., 2007; Berezin and Achilefu, 2010). Transverse imaging to investigate the cuticle was found to be more suitable than longitudinal imaging because transverse images offer a clear view of the individual cuticle cells as the optical slice is perpendicular to them and signal for the cortex and medulla is not lost from the depth of penetration into the hair. The middle transverse image shows three lifetimes, a small amount of yellow of 3.62ns on the two or three cells closest to the cortex,

followed by green of 3.25ns and then blue of 2.88ns on the outer couple of cells. The bottom FLIM image shows the cuticle with two lifetimes – red of 3.66ns and yellow of 3.34ns. Previous hair FLIM papers have not used methods which resolve the cuticle lifetimes (Ehlers *et al*., 2007; Krasieva *et al*., 2012).

The top two images in figure 4.3 show the same hairs as in the previous figure but excited with 640nm, and the bottom hair is a different hair but shows an interesting detail. The lifetime distribution in the top longitudinal hair appears similar to when it is excited with 470nm, whereas the transversely imaged hair differs. This middle image excited with 640nm appears to have four different lifetimes – an innermost red coloured lifetime of 2.52ns, followed by a slightly shorter lifetime of 2.31ns coloured yellow, then an even shorter lifetime of 1.99ns coloured green. Some of the outer cuticle cells have an even shorter lifetime of 1.78ns coloured blue. The bottom FLIM image appears to have three lifetimes within the cuticle, red of 2.52ns, green of 2.10ns and blue of 1.92ns, however, part of the cuticle has broken away (arrow) and the outer blue lifetime is lost.

To test whether the multiple outer lifetimes of the hair were part of the cuticle or whether they were an artefact from immersion of the hair in the oil mounting medium, the cuticle was removed from hairs by sandpapering. As figure 4.4 shows, the physical removal of the cuticle resulted in the loss of the rings of outer lifetimes. Therefore, the multiple fluorescence lifetimes are an intrinsic component of the cuticle layer.

4.3.1.2. There are four observable classes of cuticle structures or chemical environments

In the majority of samples studied the cuticle lifetimes decrease with progression outwards from the cortex to the cuticle surface for both 470nm and 640nm excitation. The remaining hairs within the dataset showed either an increase or a single unvarying lifetime across the cuticle layers. This suggests there may be four observable classes of cuticle structures or chemical environments that can be detected using FLIM. Using transverse optical sectioning only, FLIM images were taken of hairs and the cuticle cell layers were separated into distinct regions of interest using the SymPhoTime software. Figure 4.5A shows the decrease in cuticle lifetime over the cuticle cell layers radiating out of the hair from the cuticle-cortex border towards the hair surface for individual hairs excited with 470nm and accounted for 90% of the hairs imaged in this study. Figure 4.5B shows one of these hairs with decreasing lifetimes. This figure zoomed in (fig. 4.5C) showed the cuticle had two lifetimes, the smallest of which was the outer lifetime of

approximately 2ns. Figure 4.5D is a graph of 470nm excitation of the cuticle showing the average cuticle lifetime increasing or unvarying with cuticle cell layer, which accounted for 10% of hairs imaged in this study. Figure 4.5E shows one of these hairs, and zooming into the cuticle (fig. 4.5F) shows the cuticle lifetime is unvarying. For 640nm excitation, figure 4.5G shows a graph of the average lifetimes of the cuticle decreasing with cuticle layer from the cuticle-cortex border to the surface of the hair, which accounted for only 53% of hairs imaged in this study. Figure 4.5H shows a corresponding FLIM image and the enlarged cuticle image (fig. 4.5I) shows a cuticle lifetime which is decreasing towards the outside of the hair. Figure 4.5J is a graph of the other hairs excited by 640nm and shows the average lifetime increasing or unvarying with cuticle cell layer radiating out of the hair, and accounted for 47% of the hairs imaged in this study. Figure 4.5K shows the corresponding FLIM image with an enlarged cuticle image (fig. 4.5L) showing the cuticle lifetimes were relatively constant. As 470nm and 640nm excitation were carried out on the same hairs, it shows that a hair may have increasing or decreasing cuticle lifetimes for either wavelength excitation, leading to the proposal that there are four observable classes of cuticle structures or chemical environments that can be detected using FLIM.

4.3.2. The cortex

After the investigation of the cuticle, the cortex was further explored using FLIM. Figure 4.6A shows 470nm and 640nm excited transverse optical sections of a representative hair, which has a lower green lifetime of 3.30ns for 470nm and of 2.30ns for 640nm excitation in the outer cortex, and incorporates increasing amounts of the longer red lifetime of 3.88ns for 470nm and of 2.73ns for 640nm excitation towards the centre of the hair.

As well as appearing autofluorescent from 405nm excitation, organelle remnants (some circled) distinguish themselves in FLIM images by their fluorescent lifetimes (fig. 4.6B). These lifetimes tend to be approximately the average lifetime of the hair, such as those in figure 4.6B, coloured yellow-green in the reference colour spectrum denoting the average lifetime for that hair, with lifetimes of 3.83ns for 470nm and of 2.04ns for 640nm excitation. Although the hair in figure 4.6B appeared different to the hair in figure 4.6A, the few organelle remnants visible in the autofluorescence image still have average lifetimes, coloured yellow-green in the FLIM images, of 3.30ns for 470nm and

of 2.31ns for 640nm excitation. These are also visible within the cortical cells in figure 4.6C coloured yellow-green with lifetimes of 3.30ns for 470nm and of 2.05ns for 640nm excitation.

Longitudinal optical sections of the hair resolved spindle-shaped cortical cells (fig. 4.6C). In the 470nm image, these were dark spindle shapes (arrows) each containing a bright organelle remnant. When the hair was excited with 640nm however, the cortical cells appeared blue, denoting the lowest lifetime for that hair of 1.68ns.

The majority of the melanin in the hair is found in the cortex, so FLIM measurements only from the cortex of hairs were taken in order to compare the lifetimes of different hair colours. The average fluorescence lifetimes of white, blond, ginger, and dark hair colours excited with 470nm were measured (fig. 4.7A), but no significant differences were found between the different hair colour lifetimes (p=0.318, Kruskal-Wallis test). Additionally, no significant differences were found between the hair colours when excited with 640nm (fig. 4.7B) (p=0.086, Kruskal-Wallis test). However, the white hair had a higher fluorescence lifetime than the other hair colours, though unfortunately blond hairs were not imaged. Since white hairs do not contain melanin, the difference between the white hairs and the coloured hairs supported previous findings that melanin has a role in the overall lifetime of the hair autofluorescence (Ehlers *et al*., 2007; Krasieva *et al*., 2012). The lifetime of the hair may be affected by the chemical composition of the melanin granules or the lipids bound to it.

4.3.3. The medulla lifetime changes with its autofluorescent intensity

Within the centre of the cortex of some hairs lies the medulla. As the autofluorescence of the medulla varies between hairs, so does the fluorescence lifetime. Figure 4.8 shows the range of lifetimes within the medulla. Starting with the most autofluorescent medulla, figure 4.8A shows the colour spectrum of the 470nm excited medulla was mainly light green of 3.36ns with some blue of 3.15ns, showing it had a fairly low lifetime within the range of lifetimes for that hair which increased up to 3.98ns. The same 640nm excited medulla appeared red of 3.15ns and green of 2.60ns, so it had high and mid-range lifetimes for that hair. Figure 4.8B shows a slightly less autofluorescent medulla, and when excited with 640nm this had a similar colour, with an average lifetime of 2.36ns, to the hair in figure 4.8A, though the 470nm medulla had a more mid-range lifetime of 3.46ns. Figure 4.8C shows the least autofluorescent medulla, and had a

different lifetime than the brightly autofluorescent medullas. The medulla of this hair when excited with 470nm was blue of 3.41ns, the lowest lifetime for that hair, and when excited with 640nm the medulla had lower lifetimes – green of 1.99ns and blue of 1.05ns, than the more autofluorescent medullas. Finally, of medullas that had a similar intensity of autofluorescence to the adjoining cortex, figure 4.8D shows that they were almost indistinguishable from the cortex. The differences in autofluorescence do not seem to be related to the volume of air-space in the medulla, as it is the medullary cells which are fluorescing and all the medullas contain air-spaces. These results suggest that the autofluorescence intensity of the medulla may affect the fluorescence lifetime.

4.3.4. Relative humidity as a control for FLIM

The effect of humidity upon the hair was tested. The purpose of this was twofold: firstly, as a control to ensure that the varying humidity of the laboratory was not affecting the hairs, and secondly also as a control for the later experiments in the next chapter into the hydration of hairs. Hairs were tested at ambient room humidity (approximately 80% relative humidity), 70% relative humidity, and 100% humidity in the form of fully hydrated hairs.

With 470nm excitation, the hairs in 70% relative humidity had the highest average lifetimes followed by the hairs in ambient humidity, with the hydrated hairs having the lowest average lifetimes (fig. 4.9A). However, there was no significant difference between the lifetime of the hairs at the different humidities ($p=0.173$, Kruskal-Wallis test). For the same hairs excited with 640nm (fig. 4.9B), although there was a higher average lifetime of the cortices of hairs at ambient humidity compared to those that were fully hydrated, there was no significant difference ($p=0.129$, Kruskal-Wallis test).

These results show that there is little difference in fluorescence lifetime between hairs in ambient humidity, a controlled humidity of 70% and fully hydrated hair when excited with either laser.

4.3.5. Exploration of cuticle constituents contributing to the multiple lifetimes

In order to explore the constituents of the cuticle which may be contributing to the multiple lifetimes, the hair was modified in four experiments. The main structural components of a cuticle cell are the CMC, epicuticle, A-layer, exocuticle and endocuticle and these are made up of different lipids, keratins, and desmosome remnants in the

CMC (Robbins, 2012). Lipid extractions which remove different lipids were required to determine which constituents in the cuticle layer were causing the multiple lifetimes. In addition, a proteinaceous role was assessed by reducing disulphide bridges in the KIFs and matrix.

4.3.5.1. Wertz and Downing lipid extraction method

This method involved incubation of the hair in varying ratios of chloroform : methanol, as well as each solvent alone. Wertz and Downing showed that extractions with chloroform and methanol at room temperature removes soluble lipids from the hair (Wertz and Downing, 1988). Thus this method was chosen to assess whether soluble lipids have a role in the lifetime of the hair cuticle. After the lipid extraction treatment, the hairs were stained with 0.6mg/ml Nile red (fig. 4.10). Nile red is used to stain neutral lipids (e.g. cholesterol, cholesterol esters, triacylglycerols), phospholipids, sphingolipids, and fatty acids (Fowler *et al*., 1987). In the past it has been used as a stain for covalently bound lipids in mature cornified envelopes in the epidermis (Hirao *et al*., 2001). Compared to the controls, the treated hairs took up less stain particularly in the cortex, with fluorescence intensity measurements of 29.0 and 5.2 respectively ($p=4.80x10^{-3}$, Mann-Whitney U-test), showing there had been a loss of lipid.

There were seven steps to this lipid extraction method and after each step the elutant was analysed by GC/MS (fig. 4.11). Deionised water washing was the first step which extracted a little squalene. The second step was incubation in methanol, which extracted the fatty acid 16:0, squalene, cholesterol, C18:C16 ester and C18:C14 ester. Steps 3 to 6 extracted the same lipids as in step two, and consisted of ratios of chloroform : methanol 2:1, 1:1, 1:2 respectively, and then for the sixth step one ratio after the other for 24h incubation each. In the seventh and final step the hair was incubated in chloroform, and cholesterol and C18:C16 ester were extracted from the hair. The relative amounts of the lipids for each step were recorded, however comparisons could not be made between the lipids as they ionise to differing degrees. The largest amount of fatty acid 16:0 was found in step 2 (fig. 4.12A). The most squalene was also found in step 2 and the amounts reduced down to step 5, and then increased slightly in step 6 (fig. 4.12B). The most cholesterol was also found in step 2, with less found in the following chloroform : methanol ratios, except for in the prolonged step 6 treatment (fig. 4.12C). The C18:C16 ester was found in largest amount in steps 3, 4, and

6 elutants, with approximately half as much found in step 2 and a third as much in step 5 (fig. 4.12D). The most C18:C14 ester was from step 2, with much less being found in steps 3 to 6 (fig. 4.12E). This shows that the 2:1 chloroform : methanol combination was the most effective solvent for extracting the above lipids from the hair, and the method likely removed most of those lipids which were present in the hair as little was extracted in the final two steps.

Next the treated hairs and untreated control hairs were imaged using FLIM to see if there was an effect from the removal of those lipids on the fluorescence lifetime. The distribution of lifetimes across the hairs was similar when control hairs were compared to the paired treated hairs (fig. 4.13). The colour mapping showed that when excited with 470nm there were slightly more blue regions of low lifetime, of 3.041ns, on the lipid extracted sample cuticle than the control cuticle, where the lowest lifetime was 3.355ns. This control hair cuticle lifetime is higher than that of the three untreated hairs in figure 4.2, but only higher than one of the hairs by 0.01ns. This shows the variability between the hairs and the importance of paired control and treated hairs. In the 470nm excited lipid extracted sample cortex image, the cuticle appeared more prominent than in the control image. Overall, the lifetime frequency graphs appeared broader, giving a significantly larger range of lifetimes in lipid extracted sample hair cortices excited with 640nm ($p=0.171$, $p=0.635$, normality tests for samples and controls respectively; $p=0.0361$, t-test).

The box and whisker plot gives information about the median, quartiles and range of the data. The box represents the two mid-quartiles of the data with a line between them to represent the median, and the whiskers represent the upper and lower quartiles of the numerical data. The box and whisker plot (fig. 4.14A) of control and lipid extracted sample hairs excited with 470nm shows the lifetimes seem similar, with the median 50% of lifetimes for each part of the hair overlapping for control and lipid extracted sample hairs. This is with the exception of the medulla, which was possessed by only 2 of the lipid extracted sample hairs. The lifetimes of the cuticles of the lipid extracted sample hairs all match the top 75% of the lifetimes of the cuticles of the control hairs. For the same hairs excited with 640nm, the median 50% of cuticle lifetimes do not overlap for the control and lipid extracted sample hairs (fig. 4.14B). On the whole this graph shows that all parts of the hair showed a lower lifetime once treated with the lipid extraction

method, though there is still some overlap of lifetimes between the control and lipid extracted sample hairs, and the only significant difference was between the control and treated hair cuticles excited with 640nm ($p=0.0344$, Mann-Whitney U-test).

The lifetimes of individual cuticle cell layers were taken to examine how they changed from the cuticle-cortex border to the hair surface. For 470nm excited hair, all of the lipid extracted sample cuticle cell layers decreased in lifetime radiating out of the hair from the cortex to the surface, but still remained within the lifetimes covered by the control cuticle cell layers which also decreased in lifetime (fig. 4.14C). For the same hairs excited with 640nm, all the lipid extracted sample cuticle lifetimes increased with cuticle cell layer, although they remained within the lower range of lifetimes covered by all the hairs, whilst only some of the control cuticle cell layers decreased in lifetime (fig. 4.14D). The fact that the control and lipid extracted sample cuticle cells do not follow suit, as not all control cuticles increase in lifetime, means that the cuticle lipids contribute to the FLIM profile of the different cuticle cell layers.

Paired controls with treated samples take into account variation between hairs (fig. 4.15). The graphs show the range of the lifetime for each hair, and the average lifetime is where the lower and upper limit meet. The lower and upper limit encompass approximately 95% of the lifetimes of the hair. The results show that when excited with 470nm (fig. 4.15A) the average cuticle lifetime is always significantly lower than or equal to the average cortex lifetime ($p<0.001$, Wilcoxon paired test). Apart from hair 71, the range of lifetimes of the cuticle increased or remained constant after treatment ($p>0.2$, Wilcoxon paired test). The average cortex lifetime was found to either decrease or stay the same after treatment ($p>0.2$, Wilcoxon paired test), and the cortex lifetime range either stays constant or increases after treatment ($p>0.2$, Wilcoxon paired test). For the same hairs excited with 640nm (fig. 4.15B), again it was found that the average cuticle lifetime was higher than the average cortex lifetime ($p<0.001$, Wilcoxon paired test). With the exception of hair 71, the average cuticle and cortex lifetimes decrease after treatment ($0.1<p<0.2$ and $p>0.2$ respectively, Wilcoxon paired test). The range of the cortex lifetimes was found to increase significantly after treatment ($p<0.001$, Wilcoxon paired test).

In conclusion, treatment of hairs with the Wertz and Downing lipid extraction method resulted in significantly lower cuticle lifetimes than control hairs when hair was excited

with 640nm (p=0.0208, Mann-Whitney U-test), the average cuticle lifetime decreasing by 0.18ns from 2.51ns to 2.33ns after treatment. This shows that soluble lipids contribute to the fluorescence lifetimes of untreated hair. For 470nm excitation the average cuticle lifetimes decreased very slightly by 0.01ns from 3.78ns for control hairs to 3.77ns for sample hairs (p=0.925, Mann-Whitney U-test). The cuticle was also affected by the lifetime range increasing or staying constant after treatment when excited by 470nm (p>0.2, Wilcoxon paired test). Though cortex lifetime ranges changed significantly (p<0.001, Wilcoxon paired test), an effect upon the 640nm excited cuticle range was not observed (p>0.2, Wilcoxon paired test).

4.3.5.2. Modified method for stratum corneum lipids

This method involved incubating the hair in chloroform:methanol 1:2, and then in 50mM citric acid:ddH2O:chloroform. This lipid extraction method was chosen to be a harsher treatment for the hair than the Wertz and Downing method, as the free soluble lipids are removed in the first step leaving the covalently bound lipids behind, some of which are then removed by the second step. First, hairs were stained with 0.6mg/ml Nile red to assess general lipid loss (fig. 4.16). It appeared that the cuticles of the treated sample hairs were less strongly stained than those of the controls, with fluorescence intensity measurements of 2.8 and 5.7 respectively (p=0.0286, Mann-Whitney U-test), and suggests some lipid loss, but demonstrates that the bound lipids were not extracted.

Since there were two steps to this lipid extraction protocol, the elutant from each was separately analysed by GC/MS for certain lipids. In the first step with the chloroform : methanol extraction, squalene, cholesterol and fatty acids C14:0, C15:0 and C16:0 were found (fig. 4.17). In the second step with the citric acid:ddH2O:chloroform extraction, the same fatty acids were found again (fig. 4.17).

Next the treated hairs and untreated control hairs were imaged using FLIM to see if there was an effect from the removal of those lipids on the fluorescence lifetime. The images in figure 4.18 show two longitudinal hairs and two transverse hairs excited with each laser, one control and lipid extracted sample hair of each. The longitudinal hairs were paired, so the sections of the same hair could be compared untreated against treated. Each image also has a corresponding graph of the frequency of lifetimes, with the pink lines denoting the lower and upper lifetime limits. The longitudinal image of the control hair cuticle excited with 470nm shows it has a lower lifetime limit of 3.460ns

and an upper lifetime limit of 4.194ns. Compare this to the treated sample hair cuticle excited with 470nm which has a very similar lower lifetime limit of 3.250ns and an upper limit of 4.194ns. This trend is the same for the other control and sample hairs in this figure. Despite losing some lipids, the lifetimes of the hairs have not been overly affected, and the images along with the graphs show that the distribution of the fluorescence lifetimes in the hair has not been changed by treatment.

A box and whisker plot shows how the average lifetime medians and ranges change after treatment using 470nm excitation (fig. 4.19A). Studying the hair as a whole there is little difference between the control and sample hairs ($p=0.716$, Mann-Whitney U-test), bearing in mind the truncated y-axis may visually exaggerate the variability of the results. If looking at the cuticle in particular, the lifetimes of the treated hairs all fall within the range of lifetimes of the control hairs, suggesting there has been little effect of the treatment on the hair cuticle ($p=0.571$, Mann-Whitney U-test). The lower 75% of lifetimes of the sample cuticles are below the top 50% of control cuticle lifetimes. The cortex measurements between control and sample hairs are very similar ($p=1.0$, Mann-Whitney U-test). Conversely, the medulla measurements had a greater range in the control than in the sample ($p=1.0$, Mann-Whitney U-test). However, variation between hairs may occur as this data was taken from transverse optical sections where the hair compartments could be clearly separated. The same hairs were then excited with 640nm to see whether it would show changes in other fluorophores (fig. 4.19B). Here there appeared to be more difference between the control and lipid extracted sample hairs than when using 470nm excitation. There is a general trend showing the lipid extracted sample lifetimes are lower than the control lifetimes, for the cuticle ($p=0.227$, Mann-Whitney U-test), cortex ($p=0.622$, Mann-Whitney U-test), and medulla ($p=0.773$, Mann-Whitney U-test). In the cuticle, the lower 50% of the sample lifetimes are lower in value than the lowest quartile of control cuticle lifetimes. Again, this is true in the cortex, although the highest quartile of lipid extracted sample lifetimes are larger in value than the lifetimes of the control hairs. This is once again true in the medulla, and the higher 50% of control medulla lifetimes are higher than those of the lipid extracted sample.

The effect of removing the soluble lipids on the individual cuticle cell layers after treatment was measured when hairs were excited with 470nm (fig. 4.19C). There was

much cross-over of lifetimes between the control and lipid extracted sample hairs. For all hairs, both controls and lipid extracted samples, the cuticle lifetime decreased with cuticle cell layer radiating out of the hair, except for one control hair and one lipid extracted sample hair. This lipid extracted sample hair had lifetimes where the outer cuticle cell lifetime was lower than the innermost cuticle cell lifetime, but the cells in the middle of the cuticle had higher lifetimes. The control cuticle simply increased in lifetime in the direction of the cuticle cell layer radiating out of the hair. Figure 4.19D shows the same hairs but with 640nm excitation. As shown by the previous box and whisker plot (fig. 4.19B), the cuticle lifetimes were lower for the lipid extracted sample than the control hairs. Two thirds of the lipid extracted sample and control cuticles increased in lifetime with cuticle cell layer. One control hair cuticle decreased in lifetime and another stayed constant. The lowest two lifetimes were those of the lipid extracted sample hairs, the lowest of which decreased in lifetime with cuticle cell layer, and the other first increased and then decreased in lifetime.

Paired controls with treated samples take into account variation between hairs. The results showed that when excited with 470nm (fig. 4.20A) the average cuticle lifetime was shown to be significantly lower than or equal to cortex lifetime, for both control ($p<0.001$, Wilcoxon paired test) and lipid extracted sample hairs ($p<0.001$, Wilcoxon paired test), as it was in the previous lipid extraction method. The lifetime range of the cuticles significantly increased after treatment in all lipid extracted sample hairs ($p<0.001$, Wilcoxon paired test), and the lifetime range of the cortex significantly increased or stayed constant after treatment ($p<0.001$, Wilcoxon paired test). Figure 4.20B shows the same hairs excited with 640nm. Opposite to what was found when excited with 470nm, with 640nm excitation the average cuticle lifetime was higher than the average cortex lifetime for all hairs, for control ($p<0.001$, Wilcoxon paired test) and treated sample hairs ($p<0.001$, Wilcoxon paired test), as it was in the previous lipid extraction experiment. Comparing the control hairs with the lipid extracted sample hairs, with the exception of hair 14 where the sample cortex lifetime increased, the average cuticle and cortex lifetimes either decreased or stayed the same after treatment ($p>0.2$ for both cuticle and cortex, Wilcoxon paired test).

In conclusion, treatment of hairs with the stratum corneum lipid extraction method resulted in slightly lower cuticle lifetimes than control hairs, particularly when excited

with 640nm (p=0.0566, Mann-Whitney U-test). The average cuticle lifetime decreased by 0.12ns from 2.30ns to 2.18ns after treatment; a slightly smaller decrease than in the Wertz and Downing lipid extraction method where the decrease was by 0.18ns. This may have been because more soluble lipids were extracted in the Wertz and Downing method. The soluble lipids were extracted over four days in the Wertz and Downing method, whereas they were only extracted over two hours in the stratum corneum lipid extraction method. For 470nm excitation the average cuticle lifetime decreased by 0.07ns from 3.81ns for control hairs to 3.74ns for lipid extracted sample hairs (p=0.710, Mann-Whitney U-test), which was a larger decrease than with the Wertz and Downing method. This may have been because in addition to the fatty acid C16:0 extracted in the Wertz and Downing method, fatty acids C14:0 and C15:0 were also extracted in the stratum corneum lipid extraction method. The range of the cuticle lifetimes increased after treatment with 470nm excitation (p<0.001, Wilcoxon paired test), as it did in the Wertz and Downing lipid extraction, so the lipid extraction may have slightly affected the distribution of lifetimes.

4.3.5.3. CTAB lipid extraction method

This method was chosen as the first two methods mainly remove soluble lipids, whereas this method also removes the covalently bound 18-methyleicosanoic acid (18-MEA) from the outer β-layer of the cuticle cell CMC (Smith *et al*., 2010). This method involved incubating hair with CTAB under alkaline conditions in the first step, rinsing the hair with water in the second step, acidifying the hair in acetic acid and isopropanol in the third step, and finally rinsing the hair in water in the fourth step. First the treated hair was stained with 0.6mg/ml Nile red, and figure 4.21 shows maximum projections of the control and treated hair. The treated hairs were less strongly stained than the control hairs, with fluorescence intensity measurements of 10.8 and 69.3 respectively (p=0.0222, Mann-Whitney U-test), suggesting lipids had been lost during treatment.

To confirm the loss of some lipids, GC/MS analysis was carried out on the elutant of each step. Figure 4.22 shows the first two steps contained the treatment chemical CTAB. The third acidifying step contained fatty acids, squalene and cholesterol, and the final step also contained squalene and cholesterol. Although 18-MEA was not found in the elutant, this may have been down to the large relative amounts of CTAB, squalene and cholesterol found, and contaminants and noise make it difficult to identify smaller

peaks, although 18-MEA should account for approximately 40% of total fatty acids (Wertz and Downing, 1989). Therefore, it is possible that the 18-MEA was simply not detected by our GC/MS method or system. Smith *et al*., 2010 has shown that this method is able to remove 18-MEA from wool, and with the significant fluorescence lifetime changes, it is likely 18-MEA has been removed by the replication of the method here. In future experiments, an 18-MEA standard should be used to test whether it is detectable in the GC/MS system and method.

The treated and control hairs were then imaged using FLIM. Figure 4.23 shows some of the images taken and their corresponding lifetime frequency graphs. These images show that the CTAB method gave the most striking changes of all the lipid extraction methods. The longitudinal image of the control cuticle excited at 470nm had a lower lifetime limit of 3.355ns and an upper lifetime limit of 4.089ns. After treatment this same hair had a lower lifetime limit of 2.097ns and an upper lifetime limit of 2.621ns. This decrease in lifetime after treatment holds true for the other lipid extracted samples in figure 4.23. For the longitudinal paired control and lipid extracted sample hairs excited with 470nm there was a significant difference in lifetime post-treatment for the cuticle ($p<0.001$, Wilcoxon paired test) and cortex ($p<0.001$, Wilcoxon paired test). For the same hairs excited with 640nm there was also a significant difference in lifetime post-treatment for the cuticle ($p<0.001$, Wilcoxon paired test) and cortex ($p<0.001$, Wilcoxon paired test). The transverse images have had their colour spectrum changed so that they are comparable to each other. For the transverse hairs, the control hairs appeared yellow with a lifetime of 4.04ns whereas the lipid extracted sample hairs were green, denoting a lower lifetime of 3.36ns. Changes to the hair structure can also be observed. The longitudinal section of the control hair cuticle had clearly defined cuticle cells, whereas the treated hair did not. In the longitudinal section of the control cortex the cuticle along the edge of the hair was easily definable, flecked with blue zones of 3.57ns when excited with 470nm and red/yellow of 2.52ns when excited with 640nm. Following treatment, lifetimes within the cuticle layers became homogenous with lifetimes of 2.36ns with 470nm excitation and 1.78ns with 640nm excitation, and the cuticle was no longer clearly definable by its distinctly different lifetime to the cortex. After treatment the paired longitudinal hairs have also experienced an increase in the mode lifetime frequency, denoted by the y-axis of the graphs, by 3.3 and 2.5 M.counts for the 470nm excited cuticle and cortex respectively, and by 0.9 and 2.5 M.counts for the 640nm

excited cuticle and cortex respectively. This indicated an increase in the autofluorescence of the hair which may have been brought about by chemical changes in the hair from the treatment.

The box and whisker plot of control and lipid extracted sample hairs excited with 470nm (fig. 4.24A) showed that none of the control hair lifetimes overlap with the lipid extracted sample hair lifetimes, with the exception of the medulla which was only possessed by two sample hairs. The lifetimes of the hair were much lower after treatment for both the cuticle and cortex measurements (both $p=8.0x10^{-3}$, Mann-Whitney U-test). For the hair cuticles there was a difference in lifetime between the closest control and lipid extracted sample cuticles of 0.79ns and a difference in median values of 1.34ns. For the hair cortices there was a difference in lifetime between the closest control and sample cortices of 0.26ns and a difference in median values of 0.71ns. Figure 4.24B shows the same hairs excited by 640nm. Again the treated hairs had much lower lifetimes than the control hairs for both the cuticle ($p=7.70x10^{-3}$, Mann-Whitney U-test) and cortex ($p=8.0x10^{-3}$, Mann-Whitney U-test) measurements, and no lifetimes overlap between the groups with the exception of the medulla. For the hair cuticles there was a difference in lifetime between the closest control and lipid extracted sample cuticles of 0.63ns and a difference in median values of 0.94ns. For the hair cortices there was a difference in lifetime between the closest control and sample cortices of 0.11ns and a difference in median values of 0.43ns.

Next the individual cuticle layers radiating out of the hair from the cuticle-cortex border to the hair surface for 470nm excited hair were studied to evaluate their lifetime changes (fig. 4.24C). As expected from figure 4.24A, there was complete separation between the control and lower lifetime lipid extracted sample hairs, even taking into account lifetime increases and decreases with cuticle layer. Of the treated hairs, two of the cuticle cell lifetimes increased with cuticle layer radiating out of the hair, and three of the cuticle lifetimes decreased. In contrast, all of the control hair cuticle lifetimes decreased with cuticle layer radiating out of the hair. Since both groups of hairs originated from the same batch, this meant that the treatment had changed the nature of the cuticle cells more than simply lowering the lifetimes of them all. Figure 4.24D shows the same hairs excited with 640nm. Again there was a large lifetime gap between the control cuticle layers and the lower lifetimes of the lipid extracted sample cuticle

layers. All of the lipid extracted sample lifetimes increased or stay constant with cuticle layer radiating out of the hair. All of the control lifetimes increased or stayed constant too, with the exception of one hair, showing that with 640nm the treatment also had an effect upon the lifetime of the cuticle layers.

To take into account hair-to-hair variation, paired controls and lipid extracted samples were compared. The lifetime ranges and averages of hair excited by 470nm in longitudinal section (fig. 4.25A), show that the treated hairs had lower lifetimes than their paired control hairs for both the cuticle ($p<0.001$, Wilcoxon paired test) and cortex ($p<0.001$, Wilcoxon paired test) measurements, and the only overlap between lifetimes was the cortex of hair 59. Figure 4.25B shows the same hairs excited by 640nm. Here however, there was overlap between the control and lipid extracted sample hairs, although the average lifetimes of the lipid extracted sample hairs were always lower for both the cuticle ($p<0.001$, Wilcoxon paired test) and cortex ($p<0.001$, Wilcoxon paired test) measurements. Interestingly, the lifetime range of the lipid extracted sample hairs was much smaller than their counterpart control hairs for both the cuticle ($p<0.001$, Wilcoxon paired test) and the cortex ($p<0.001$, Wilcoxon paired test) when excited with 640nm.

In conclusion, treatment of hairs with the CTAB lipid extraction method resulted in much lower lipid extracted sample cuticle lifetimes than control hairs when excited with both 470nm ($p=1x10^{-4}$, Mann-Whitney U-test) and 640nm ($p=1x10^{-4}$, Mann-Whitney U-test). With 470nm excitation the cuticle lifetime of all hairs in the experiment decreased by an average of 1.18ns from 3.75ns to 2.57ns after treatment. This was a larger decrease in lifetime than both the stratum corneum lipid extraction method and the Wertz and Downing lipid extraction method. For 640nm excitation the cuticle lifetimes decreased by an average of 0.81ns from 2.54ns for control hairs to 1.73ns for lipid extracted sample hairs. This was also a larger decrease in lifetime than the previous two methods. The cuticle was also affected by the lifetime range ($p<0.001$, Wilcoxon paired test), which decreased after excitation with 640nm, and was more pronounced than it was with the stratum corneum lipid extraction method when excited with 640nm. These greater differences in cuticle lifetime after treatment with the CTAB lipid extraction method compared to the previous lipid extraction methods are likely due to the extraction of 18-MEA from the outer β-layer of the cuticle CMC (Smith *et al*., 2010). It is unlikely that it is

the lipid which is producing the fluorescence, but its presence clearly has an effect on the chemical environment that the fluorophore inhabits, and as such the lifetime changes.

4.3.5.4. Potassium thioglycolate treated hair

In this method hairs were treated with 45mM potassium thioglycolate and 47mM calcium hydroxide. This is a x10 dilution of a commercial depilatory treatment, diluted so that the hair structure remains intact for FLIM imaging. The potassium thioglycolate was used to break disulphide bonds within the hair and was investigated as to how this affected the cuticle lifetime. Reducing the disulphide bonds could change the fluorescence lifetimes because of the change in the chemical environment of the hair with the creation of thiol groups.

FLIM images were taken of the control and treated sample hair and their corresponding lifetime frequency graphs, some of which are shown in figure 4.26. The paired longitudinal control and treated sample hairs did not appear very different from one another, either in the scaling of lifetime colours of the hairs or in the lifetime frequency graphs. The transverse images have had their colour spectrum changed so that they are comparable to each other. Although the images for the 470nm excited transverse section hairs were very similar, the treated sample hair had a slightly yellower lifetime colour mapped cuticle, showing it had a slightly higher cuticle lifetime of 4.14ns than the control hair of 3.98ns. The images of the 640nm excited hair also appeared similar in lifetime colouration, although the treated sample hair had a slightly redder cuticle, showing it had a slightly higher cuticle lifetime of 2.60ns than the control hair of 2.28ns. This shows that both lasers produce an increase in cuticle lifetime after treatment.

A box and whisker plot of control and treated sample hairs excited with 470nm (fig. 4.27A), showed the treated sample hairs all had a higher median lifetime than the control hairs for all parts of the hair. However, there was also overlap between the control and treated sample lifetimes, unlike in the CTAB method. The median 50% of the treated sample hair cuticles had higher lifetimes than all of the control hair cuticle lifetimes ($0.1<p<0.2$, Wilcoxon paired test). There was less of a difference between the hair cortices ($p>0.2$, Wilcoxon paired test), as the median 50% of treated sample hair cortices only had lifetimes higher than the top 50% of the control hair cortex lifetimes. Figure 4.27B shows the same hairs excited with 640nm. There was a more striking

difference between the cuticle and the cortex of the hairs here, as the cuticles had much higher lifetimes than the cortices ($p<0.001$, Wilcoxon paired test). Again, the median 50% of the treated sample hair cuticles had higher lifetimes than all of the control hair cuticle lifetimes. However, the lower quartile of the treated sample hair cuticle lifetimes overlapped with the whole of the control hair cuticle lifetimes. The treated sample hair cortex lifetimes were mostly slightly lower than those of the control hairs ($p>0.2$, Wilcoxon paired test), with the median 50% of sample cortex lifetimes overlapping with the lower 50% of the control cortex lifetimes.

The lifetimes of the individual cuticle cell layers radiating out of the hair from the cortex to the hair surface were measured for 470nm excited hair (4.27C). With the exception of one control and one treated sample hair with much lower lifetimes that were likely to be from the same hair, there is overlap between the two groups. Most of the treated sample hairs had higher lifetimes than the other control hairs. All of the control cuticle cell layers decreased in lifetime, whereas only two of the treated sample hairs decreased in lifetime, showing the cuticle lifetimes have been affected. Figure 4.27D shows the same hairs excited with 640nm excitation. Again, there was much overlap between the two groups, with the exception of one outlier hair where the control half of the hair and the treated sample half of the hair had much lower lifetimes. These outlier hairs may have been treated differently prior to collection for the experiment, such as in their daily hair care regime, which may have affected the chemical environment of the cuticle. The treated sample cuticle cells in the direction radiating out of the hair from the cuticle-cortex border to the hair surface increased in lifetime. The same is true for all but one of the control cuticle cell layers which decreased in lifetime, suggesting a possible effect of the potassium thioglycolate on the lifetimes of the individual cuticle cell layers.

The lifetime ranges and averages of hair excited by 470nm in longitudinal section of paired hairs of controls and treated samples were compared (fig. 4.28A). In all of the hairs, the cuticle of the treated sample hair had a significantly higher lifetime than the cuticle of the same hair but untreated ($p<0.001$, Wilcoxon paired test). The cortices of the treated sample hairs also had higher than or equal to lifetimes than the control hair cortices ($p<0.001$, Wilcoxon paired test). There was no difference in the range of the lifetimes between control and treated sample hairs. Figure 4.28B shows the same hairs excited with 640nm. Again, all of the treated sample hairs had significantly higher

lifetimes than the paired control hairs for both the cuticle ($p<0.001$, Wilcoxon paired test) and cortex ($p<0.001$, Wilcoxon paired test). The lifetime range of the treated sample cuticles (averaged 0.75ns) was smaller than or equal to the lifetime range of the control cuticles (averaged 1.08ns) ($p=0.0525$, paired t-test).

In conclusion, treatment of hairs with 45mM potassium thioglycolate resulted in significantly higher cuticle lifetimes than control hairs for both 470nm ($0.01<p<0.02$, Wilcoxon paired test) and 640nm ($p=0.201$, $p=0.222$, normality tests for control hairs and treated hairs respectively; $p=0.0276$, paired t-test) excitation. In the previous three lipid extraction experiments, the lifetimes decreased on average. With 470nm excitation the average cuticle lifetime of all hairs in the experiment increased on average by 0.19ns from 3.81ns to 4.00ns after treatment. For 640nm excitation the cuticle lifetimes increased on average by 0.16ns from 2.34ns for control hairs to 2.50ns for treated sample hairs. The cuticle was also affected by the lifetime range, which decreased after excitation with 640nm from an average of 1.08ns for the control hair cuticles to 0.75ns for the treated hair cuticles ($p=0.0525$, paired t-test), as it did in the stratum corneum and CTAB lipid extraction methods. These lifetime changes may have occurred due to the reduction of disulphide bonds in the KIFs and matrix in the cuticle cells, resulting in a change to the chemical environment or to fluorophores.

All of the four treatments to the hair changed the lifetime of the cuticle but to differing degrees. Figure 4.29 shows a graph of the average lifetimes for each treatment and each laser excitation. In ascending order for the hair cuticle excited with 470nm (fig. 4.29A), the Wertz and Downing method changed the average lifetime by 0.01ns; the stratum corneum method changed the average lifetime by 0.07ns; the potassium thioglycolate method significantly changed the average lifetime by 0.19ns; and the CTAB method changed the average lifetime by a significant 1.18ns. In ascending order for the hair cuticle excited with 640nm (fig. 4.29B), the stratum corneum method changed the average lifetime by 0.12ns; the potassium thioglycolate method changed the average lifetime significantly by 0.16ns; the Wertz and Downing method significantly changed the average lifetime by 0.18ns; and again the CTAB method changed the average lifetime by a significant 0.81ns. These findings are summarised in figure 4.30. The CTAB method caused the largest lifetime change and decrease with treatment, but the potassium thioglycolate method caused the only increase in lifetime. It could be possible that a loss

of lipid in the cuticle causes a decrease in lifetime, and a protein change in the cuticle causes an increase in lifetime. More specifically, the loss of covalently bound lipids and 18-MEA from the cuticle cell CMC has a greater effect on the fluorescence lifetime than the loss of soluble lipids from the cuticle.

4.3.6. Comparison between the fluorescence lifetimes of the cuticle, cortex and medulla

After looking in detail at the fluorescence lifetimes of the cuticle, cortex and medulla, they were compared against each other. Figure 4.31A shows a box and whisker plot of the total scalp hair, cuticle, cortex and medullary lifetimes after excitation with 470nm. This shows that the median 50% of lifetimes overlapped for each part of the hair, though the cortex had the highest median value. The cuticle had the largest range of lifetimes, though the medulla which had the shortest range of lifetimes had a median 50% of hairs which covered the largest range of all the hair compartments. For the same hairs excited with 640nm, figure 4.31B shows that while the median 50% of lifetimes of the cortex and medulla overlapped, the median 50% of cuticle lifetimes were higher with a median lifetime of 2.36ns. The cuticle again had the longest range of lifetimes.

For the average lifetimes of the same hairs excited with 470nm (fig. 4.31C), the cuticle had the lowest average lifetime and the cortex had the highest, though there is no significant difference between the lifetimes ($p=0.086$, Kruskal-Wallis test). For the same hairs excited with 640nm (fig. 4.31D), the cuticle had a significantly higher average lifetime than the cortex and medulla ($p=7.96 \times 10^{-9}$, Kruskal-Wallis test). There was no significant difference between the lifetimes of the cortex and medulla.

4.3.7. Beard hair lifetimes compared to scalp hair lifetimes

The lifetimes of beard hairs at the cuticle, cortex and medulla were then measured to compare them against those of scalp hair. The average lifetimes of beard hairs excited with 470nm (fig. 4.32A) were not significantly different from one another and averaged 3.41ns, with an average cuticle lifetime of 3.54ns, cortex lifetime of 3.46ns and medulla lifetime of 3.64ns. This was a similar result to the scalp hair comparison which averaged 3.72ns, with an average cuticle lifetime of 3.59ns, cortex lifetime of 3.78ns and medulla lifetime of 3.68ns. The same hairs were excited with 640nm (fig. 4.32B), and although there was no significant difference between the results ($p=0.492$, Kruskal-Wallis test), the cuticle did have the highest average lifetime as it did in the scalp hair samples. The

lifetime with 640nm excitation of the total beard hair averaged at 2.55ns, with an average cuticle lifetime of 2.73ns, cortex lifetime of 2.30ns and medulla lifetime of 2.28ns. This was a similar result to the scalp hair comparison which averaged 1.96ns, with an average cuticle lifetime of 2.35ns, cortex lifetime of 1.91ns and medulla lifetime of 1.97ns. The differences in lifetime between beard hair and scalp hair were not significant, contributed to by the fact that the beard hair lifetimes had a larger range than those of the scalp hairs.

Following this analysis, an investigation was carried out into the lifetimes of the beard hair compartments at the root of the hair below the skin interface, mid-way along the hair above the skin interface and at the distal tip of the hair. This was done to determine whether FLIM could be used as a marker for hair below the skin interface, and could be of interest to the hair care industry when researching mechanical depilatories. Figure 4.32C shows the average lifetimes of these areas excited by 470nm. Although no areas were significantly different (p=0.315, Kruskal-Wallis test), the average lifetimes of the cuticle and cortex in the root of the hair were higher than those of the hair above the skin interface. When the same hairs were excited with 640nm (fig. 4.32D), the same observations were made, with no significant differences but a higher cuticle average lifetime in the hair root (p=0.575, Kruskal-Wallis test).

4.3.8. Limited lifetime changes along the hair length

Following the lifetime measurements of the beard hair above and below the skin interface, the same measurements were carried out on plucked scalp hair for comparison. Figure 4.33A shows these hairs excited with 470nm, which gave the same results as for beard hair though with more variability. There was no significant difference between the areas, and the measurements taken at the root of the hair had a higher average lifetime (p=0.870, Kruskal-Wallis test). When the same hairs were excited with 640nm (fig. 4.33B) again there was no significant difference between the measurements (p=0.412, Kruskal-Wallis test).

Following this initial work, it was of interest to take further FLIM readings along the length of the hair. This was done for two purposes, firstly for biological interest to see whether there were any lifetime changes along the hair length, especially taking into account wear during the growth of long hair, such as from combing and UV damage (Marsh *et al.*, 2015). Secondly to see whether it would matter that the samples taken

throughout this study are taken from random lengths of hair. Figure 4.34 shows the lifetime ranges of 3 hairs excited with 470nm with measurements taken every 2cm of the 12cm or 14cm length. In all hairs at all lengths along the hair the cuticle had a lower average lifetime than the cortex (p=0.000, Mann-Whitney U-test). There was little variation between the 2cm intervals within each hair and little difference between the lifetime ranges.

4.3.9. Hairs in the telogen cycle phase have higher lifetimes than those in anagen

Focussing on the root of the hair including the some of the matrix allowed distinctions to be made between the lifetime of hairs in the anagen and telogen hair cycle phases. Hairs in anagen phase were chosen for their dark clubs and telogen hairs for their white clubs, as melanogenesis halts after anagen and the fully differentiated melanocytes on the hair bulb undergo apoptosis during catagen (Tobin *et al*., 1998). These differences could be exploited by using the fluorescence lifetimes as indicators of the hair cycle. Measurements were made of the hair shaft in the matrix, as it is here that growing anagen hairs may differ from resting telogen hairs, otherwise further along the hair length anagen hairs would appear the same as telogen hairs in the form of fully keratinised hair. Figure 4.35 shows the average lifetimes for these hairs excited with 470nm and 640nm. The average lifetime of the telogen hair cortex was 3.13ns when excited by 470nm, which was significantly higher than that of the anagen hair cortex at 2.82ns (p=0.057, p=0.171, normality tests for telogen and anagen hairs respectively; $p=6.94x10^{-3}$, t-test). When the hairs were excited with 640nm there was no significant difference between the groups, but the telogen hairs still had a higher average lifetime than the anagen hairs of 2.25ns compared to 1.85ns (p=0.190, Mann-Whitney U-test).

4.3.10. The uncharacterised hair and skin disorder

Following the investigation into the uncharacterised hair and skin disorder in the previous chapter, FLIM was also carried out on the hairs to explore whether there was a difference between the fluorescence lifetimes of the hairs of the affected son and his unaffected parent's hairs as controls.

A box and whisker plot of the hairs excited by 470nm (fig. 4.36A) showed that there is no overlap between the cuticle lifetimes of the affected son and his parents. There was also no overlap between the median 50% of the affected son's hairs lifetimes and those of his parents for the cuticle or the cortex. The parental control hairs were more similar

to one another as the lifetime for the cuticle and cortex overlapped and the median 50% of lifetimes for the cortex for each parent is similar. The parental control hairs also had a much larger range in lifetimes than the affected hairs. The same hairs excited with 640nm showed a similar result (fig. 4.36B); the median 50% of lifetimes of the affected hair cuticle and cortex were higher than the median 50% of lifetimes of the control hairs. There was less of a distinction using the 640nm excitation though as the lowest quartile of lifetimes from the affected hair and the highest quartile from the control hairs did overlap.

After examining the range and medians of lifetimes the average lifetimes were investigated for further insight. Figure 4.36C shows the average lifetimes of the hairs excited with 470nm and figure 4.36D shows the same hairs excited with 640nm. For both excitation wavelengths, the average lifetime of the affected son's hair was significantly higher than the average lifetime of the parental control hairs, for 470nm (cuticle: $p=8.36x10^{-6}$ and cortex: $p=3.40x10^{-5}$, Kruskal-Wallis test) and 640nm (cuticle: $p=4.88x10^{-6}$ and cortex: $p=1.40x10^{-5}$, Kruskal-Wallis test). The average lifetime of the affected son's hair when excited with 470nm was 3.47ns for the cuticle and 3.81ns for the cortex, and when excited with 640nm it was 2.45ns for the cuticle and 2.19ns for the cortex. The average lifetime of the unaffected mother's hair when excited with 470nm was 1.21ns for the cuticle and 1.37ns for the cortex, and when excited with 640nm it was 1.03ns for the cuticle and 1.02ns for the cortex. The average lifetime of the unaffected father's hair when excited with 470nm was 1.69ns for the cuticle and 1.74ns, and when excited with 640nm it was 1.44ns for the cuticle and 1.35ns for the cortex. Although the hair from the unaffected father had a significantly higher average lifetime than that of the unaffected mother when excited with 640nm, there was a much greater difference between the parents' and son's hair. This highlights the dissimilarity between the unaffected control lifetimes and the affected hair lifetimes.

The affected son's hair had a higher fluorescence lifetime than his unaffected parents. A higher fluorescence lifetime was also observed in hairs which had fewer disulphide bonds caused by potassium thioglycolate treatment. This suggests the hair of the affected son may contain fewer disulphide bonds than his unaffected parents. The fluorescence lifetime of the affected son's hair was not significantly different to the lifetime of thioglycolate treated hair when excited with 640nm for the cuticle or cortex,

or for the cortex with 470nm excitation. This shows the similarity between the affected son's hair and disulphide reduced hair. However, there was a significant difference for the lifetime of the cuticle with 470nm excitation between the affected hair, the potassium thioglycolate treated hair, and also CTAB treated hair ($p=2.96x10^{-6}$, Kruskal-Wallis test). There was a significant difference in the lifetime of the affected hair and CTAB treated hair both with 470nm (cortex: $p=7.34x10^{-6}$, Kruskal-Wallis test) and 640nm excitation (cuticle: $p=3.06x10^{-7}$, Kruskal-Wallis test; cortex: $p=1.29x10^{-3}$, Kruskal-Wallis test). For the 640nm excited hair these significant differences were also present when compared to hair treated with the stratum corneum lipid extraction method. This suggests the hair of the affected son does not have fewer covalently bound lipids including 18-MEA compared to the unaffected parents. However, there were no significant differences in the fluorescence lifetimes between the affected son's hair and hair treated with the Wertz and Downing lipid extraction method, for either laser at either the cuticle or cortex. This suggests the soluble lipid depleted hair and the affected son's hair may be similar.

The difference in fluorescence lifetimes between the affected son's hair and the unaffected parents' hair may be due to differences in the chemical environment of the hairs. The difference in chemical environment may be due to the affected son's hair containing increased levels of covalently bound lipid, and high lipid levels were observed with Nile red staining in the previous chapter, but low soluble lipid levels. There may also be differences in the disulphide bonding within the KIFs and KAPs of the affected son's hair. A poorly differentiated cuticle may have implications for the lipids and proteins within.

4.4. Discussion

Very little has previously been published on the use of FLIM to image the hair. Two papers have been published on using FLIM to distinguish between hair colours, but the images are of low resolution and do not go into detail regarding structures within the hair and neither study uses confocal microscopy (Ehlers *et al*., 2007; Krasieva *et al*., 2012). Therefore, the results obtained in this project significantly advance the field.

4.4.1. The cuticle has multiple fluorescence lifetimes

The results showed that it was valid to image hairs using FLIM at an uncontrolled ambient room humidity, as there was little difference between the fluorescence lifetimes of hairs at different humidities. This means the water has little effect on the lifetime of hair when it is treated with water-containing depilatories.

Any difference of beard hair compared to scalp hair may be of interest to the hair care industry for research into mechanical depilatories. However, little difference was found between the fluorescence lifetimes of the hairs from the different body sites. A similar average lifetime for the hair compartments between scalp and beard hair was found, but more beard hairs would be required to test whether the beard hair cuticle has a significantly higher lifetime when excited with 640nm as it does in scalp hair.

Previously the hair cuticle had not been explored using FLIM and investigations have led to new insights into its structure and composition. FLIM experiments demonstrated that the cuticle cell layers have multiple fluorescence lifetimes, indicating that they are composed of multiple chemical environments, and a difference between the cuticle cell layers of untreated hair has not been previously reported. Four observable classes of cuticle population were found, those which had increasing or unvarying lifetimes, or decreasing lifetimes with cuticle cell layer radiating out of the hair, for each laser. The decreasing lifetime with excitation from both lasers was the predominant class. Through the use of chemicals to remove soluble and covalently bound lipids and to reduce the disulphide bonds in keratins, the CTAB lipid extraction method and potassium thioglycolate method caused significant changes in cuticle lifetime when excited with both lasers, and the Wertz and Downing lipid extraction method also caused significant changes when the hair was excited with 640nm. This suggests the cuticle lifetime

changes could be due to covalently bound lipids, including 18-MEA, and keratin differences across the cuticle cell layers.

The four possible types of cuticle stem from each laser exciting fluorophores differently, allowing further distinction than if only one laser was used. Interestingly, when the hair was excited with 640nm, the cuticle had the highest lifetime. This result agrees with previous research which found that the cuticle had a lifetime of more than 1ns whereas the cortex had a lifetime of less than 1ns, though longer excitation wavelengths were used along with a different FLIM technique (Ehlers *et al*., 2007), so the comparison is limited. The higher cuticle lifetime indicates that there is a molecule or a functional group in a molecule within the cuticle which is not present within the cortex or medulla that is contributing to this high lifetime. Covalently bound cross-linking within or between molecules may also contribute to the lifetime changes as spatial dynamics and therefore fluorescence are affected (Jachowicz and McMullen, 2011). Alternatively, it may be a molecule which is also present in the cortex or medulla, but is under different conditions and chemical environment in the cuticle and so has a different lifetime. The fatty acid 18-MEA is unique to the cuticle (Jones and Rivett, 1997; Swift, 1999), though amino acids found in the cuticle are also present within the cortex as are the majority of lipids (Bradbury *et al*., 1966; Robbins and Kelly, 1970; Wolfram and Lindemann, 1971; Swift and Bews, 1974; Wertz and Downing, 1988; Masukawa *et al*., 2005b), so it may be the cuticle chemical environment causing a difference in lifetime.

The reducing agent potassium thioglycolate reduced disulphide bridges in the keratin of the hair and caused a significant change in lifetime. The keratins in the cuticle are K32, K35, K39, K40, K82, K85 (Langbein *et al*., 2010), so it is these which may have been affected. Previous research using pure artificial keratin from Sigma found it has a lifetime of 1.4ns, though different excitation wavelengths were used (Ehlers *et al*., 2007).

Keratin is autofluorescent due to its constituent tryptophan and its oxidised metabolites, N-formylkynurenine, kynurenine and 3-hydroxykynurenine, as well as cystine and tyrosine (Jachowicz and McMullen, 2011). Tryptophan fluorescence is strongest when it is located more than 1nm from the quenching effect of a cystine disulphide bond, or from amino acid side chain groups including glutamine, glutamate, aspargine, aspartate, and lysine (Jachowicz and McMullen, 2011). So the use of thioglycolate to reduce the disulphide bonds is likely to have an effect upon the protein interactions in the hair and

lead to a different fluorescence lifetime. Additionally, the removal of lipids including 18-MEA from the cuticle may have affected protein-protein interactions including that of tryptophan and its oxidised metabolites, and also hydrogen bonding (Jachowicz and McMullen, 2011). The change in protein-protein interactions, hydrogen bonding and the loss of lipids alters the space and mobility between the proteins and therefore has the potential to change the fluorescence lifetimes.

In conclusion, the cuticle cell layers may be different due to covalently bound lipids and keratin proteins, and there may be four observable classes of hair cuticle resulting from this. This work may be of interest biologically and to industry as another parameter to measure hair damage.

4.4.2. The cortex contains many areas of differing fluorescence lifetime

As the FLIM investigation moved into the next compartment of the hair, the cortex was found to have several points of interest. Fluorescence lifetime tended to increase with depth into the cortex. Towards the centre of the hair there are more glycine/tyrosine keratin associated proteins (KAPs) (Shimomura and Ito, 2005), whereas the outer cortex has steryl glycoside-like lipids containing N-acetylglucosamine (Takahashi and Yoshida, 2014). The presence of compounds such as these in different depths through the cortex may account for the differing lifetimes.

Cortical cells were found to have low lifetimes when excited with 640nm, and a lack of lifetime when excited with 470nm. The spindle shapes could be distinguished from one another, which suggests the CMC between cortical cells are not contributing to the low lifetime. The low lifetime may be due to the 640nm wavelength exciting the keratins within the cortical cells. When Ehlers *et al*. excited pure artificial keratin with 720-930nm they found a low lifetime of 1.4ns, and here 640nm excitation of the hair in figure 4.6C gave the cortical cells a low lifetime of 1.68ns.

Within the cortical cells the organelle remnants were distinguishable. Interestingly they mostly had the same lifetime of 3.83ns for 470nm and of 2.04ns for 640nm excitation, suggesting the organelle remnants of the same lifetime are of the same chemical environment and may therefore be from the same type of organelle. The uppermost circled remnant in figure 4.6B had a lower lifetime than the other organelles, and may therefore be of a different origin. Variety could be provided by the double membrane of

the nucleus or mitochondria or the lower pH compared to other organelles of the lysosomes and late endosomes. FLIM may provide a method to help distinguish nuclear remnants from melanosome remnants and other organelle remnants.

The cortex is where the majority of melanin granules are found. In this study the white hair had a higher fluorescence lifetime compared to the coloured hairs when excited with 640nm. This may be due to the difference of the eumelanin and pheomelanin granules in the coloured hair. Further clarity would be required by using a larger sample batch of hair colours to see if this difference is statistically valid and whether the difference can be distinguished using excitation from 470nm and 640nm. Although this result may show that distinguishing between the hair colours by using fluorescence lifetimes may only be possible using the longer wavelengths, as past research has only achieved this using excitation wavelengths of 615nm and longer (Ehlers, 2007; Krasieva, 2012).

4.4.3. The autofluorescence of the medulla may be linked to its fluorescence lifetime

At the centre of some hairs a medulla can be found, and in the previous chapter the 405nm induced autofluorescence of the medulla was shown to vary. Using FLIM, it seemed that the more autofluorescent the medulla, the higher its fluorescence lifetime, a phenomenon observed with both 470nm and 640nm. The lifetime change is not simply a result of autofluorescence alone, as other highly autofluorescent structures in the hair do not follow suit. For instance, the highly autofluorescent organelle remnants only have mid-range lifetimes. Therefore, this phenomenon may be due to a higher level of autofluorescent lipids in some hair medullas than others (Kreplak *et al*., 2001a), which may be affecting the chemical environment and therefore the fluorescence lifetime of the fluorophores in the medulla.

4.4.4. Few fluorescence lifetime changes along the length of hair

The average lifetime of hair excited with 470nm above and below the skin interface differed but was not significantly different. The average lifetime of the root of the hair below the skin was higher than the hair measurements taken above the skin. This was true for both scalp and beard hair. More samples would be necessary to further test any significance in this difference. To be able to distinguish hair from above and below the skin interface would be useful in research interested in the follicle and proximal end of hair. Alternatively, as these results suggest, hair protected under the skin does not have

a different chemical environment to hair exposed to the outside environment, and may have implications for the hair care industry as hair above and below the skin interface could be treated similarly.

As indicated by the prior measurements of the lifetimes of hair mid-way along its length and at the distal tip, the more in depth study imaging the hair at 2cm intervals showed there is little difference in lifetime along the length of the hair. This is despite changes in the hair structures observed along the length of the hair in the previous chapter. Changes may have been observed in the structure size, number and area when imaging utilising autofluorescence, but no lifetime changes were seen in the cuticle and cortex overall because concentration of the fluorophore does not affect the lifetime given through FLIM. This result is useful because it means measurements can safely be taken from random sections along the hair length without the lifetime being affected.

4.4.5. Hairs in telogen have a higher fluorescence lifetime than hairs in anagen

Focussing on the hair protruding from the matrix has shown that when excited with 470nm, hairs in telogen have a significantly higher lifetime than hairs in anagen. When imaged with 640nm the difference was not significant but the average lifetime of telogen hairs was still higher. This shows the 470nm and 640nm wavelengths are exciting different fluorophores. The tissue surrounding the club hairs at the end of telogen could possess protease inhibitors which could change the fluorescence lifetimes through changing the hair structure and chemical environment (Higgins *et al*., 2011). The development of the trichilemmal keratin layer during late catagen, which is thought to secure the hair in place, means it would be present during telogen, but not anagen, and could provide another difference observed by FLIM between the telogen and anagen phase hair clubs (Higgins *et al*., 2009). A further difference in fluorescence lifetime could be provided by matrix metalloproteinases MMP-2 and MMP-9 which are raised in anagen (Hou *et al*., 2016). The difference may also be accounted for by the different environment, as anagen hairs have a dark club still attached with plentiful melanosomes and may affect the lifetime, as might ongoing processes such as keratinisation (Tobin *et al.*, 1999; Langbein *et al*., 2001). The difference between the fluorescence lifetime of hairs in anagen and telogen may have medical uses for patients, and it could be possible to determine the hair cycle through the patient's skin using FLIM. Such investigations may be made into patients with hair diseases such as

androgenetic alopecia which has a shortened anagen phase (Hibino and Nishiyama, 2004), and loose anagen hair syndrome (Chapalain *et al*., 2002). It should be noted that in this study the hairs were plucked and fluorescence lifetimes may be different for hair embedded within the skin.

4.4.6. FLIM can be used to indicate a hair disorder

A significant difference in the fluorescence lifetime was found between the hair of the affected son with the uncharacterised hair and skin disorder, and that of his unaffected parents. Intriguingly, the affected son's hair had normal fluorescence lifetimes compared to untreated Chinese scalp hair, whereas the unaffected parents' hairs had unusually low lifetimes. This difference may be an aspect of ethnicity as hair structure and lipid composition may differ (Takahashi *et al*., 2006; Cruz *et al*., 2013), or an indicator of something unusual regarding the parents' hair, although it is seen in both the mother and the father. Interestingly, the affected son's hair showed the normal occurrence of the cuticle having a significantly higher lifetime than the cortex when excited with 640nm. Although the parents' hair did have higher average lifetimes for the cuticle compared to the cortex for 640nm excited hair, it was not a significant difference. Therefore, it is important to use the unaffected parents' hairs as controls. A clinical trial would be necessary to control for age, gender and ethnicity, though on a smaller scale samples from other unaffected family members with untreated hair or unrelated untreated hair of the same ethnicity and colour would additionally be useful to ensure the parents are not showing carrier phenotypes through the fluorescence lifetimes.

Nevertheless, the whole of the hair of the affected son showed a significantly higher lifetime than the hair of his unaffected parents. This may be because his hair contained more lipids, as shown by the Nile red staining in figure 3.20A&B, possibly with more covalently bound lipids and fewer soluble lipids, and the lipid extractions have shown that lipids affect fluorescence lifetime. The cuticle lifetime may be affected by the possible poorly differentiated cuticle of the affected son's hair. The chemical environment in the poorly differentiated cuticle cell may be different to that of the rest of the cuticle cell layers through changes in both the lipid composition and disulphide bonds within the KIFs and KAPs, causing a different lifetime. However, the lifetime of the cortex is also affected, suggesting it too may be different in some way undetected though confocal and TEM imaging, perhaps poorly differentiated too, as the mutated

gene involved in BMPR1A signalling affects hair follicle differentiation (Yuhki *et al*., 2004; Kwan *et al*., 2004; Andl *et al*., 2004; Kobielak *et al.,* 2004; Genander *et al*., 2014).

These results show that hairs could be imaged using FLIM to highlight differences between hairs and possibly diagnose diseases in the future.

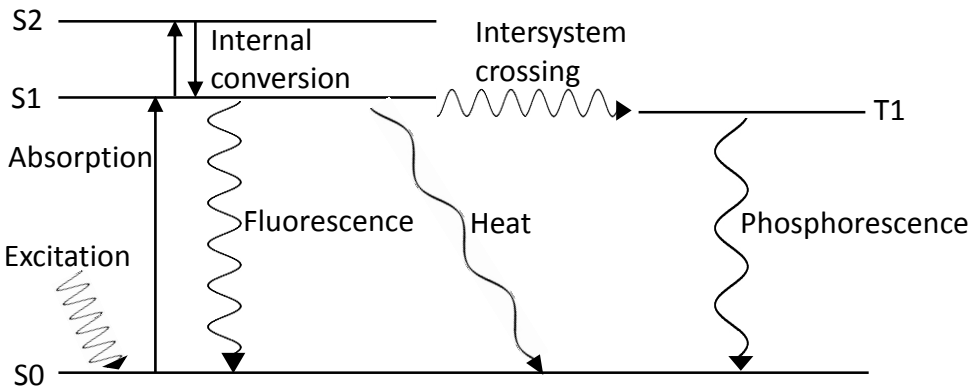

Fig. 4.1. Jablonski diagram. S0 = singlet ground state; S1, 2 = increasing energy electronic states; T1 = triplet state.

405nm Intensity

470nm FLIM

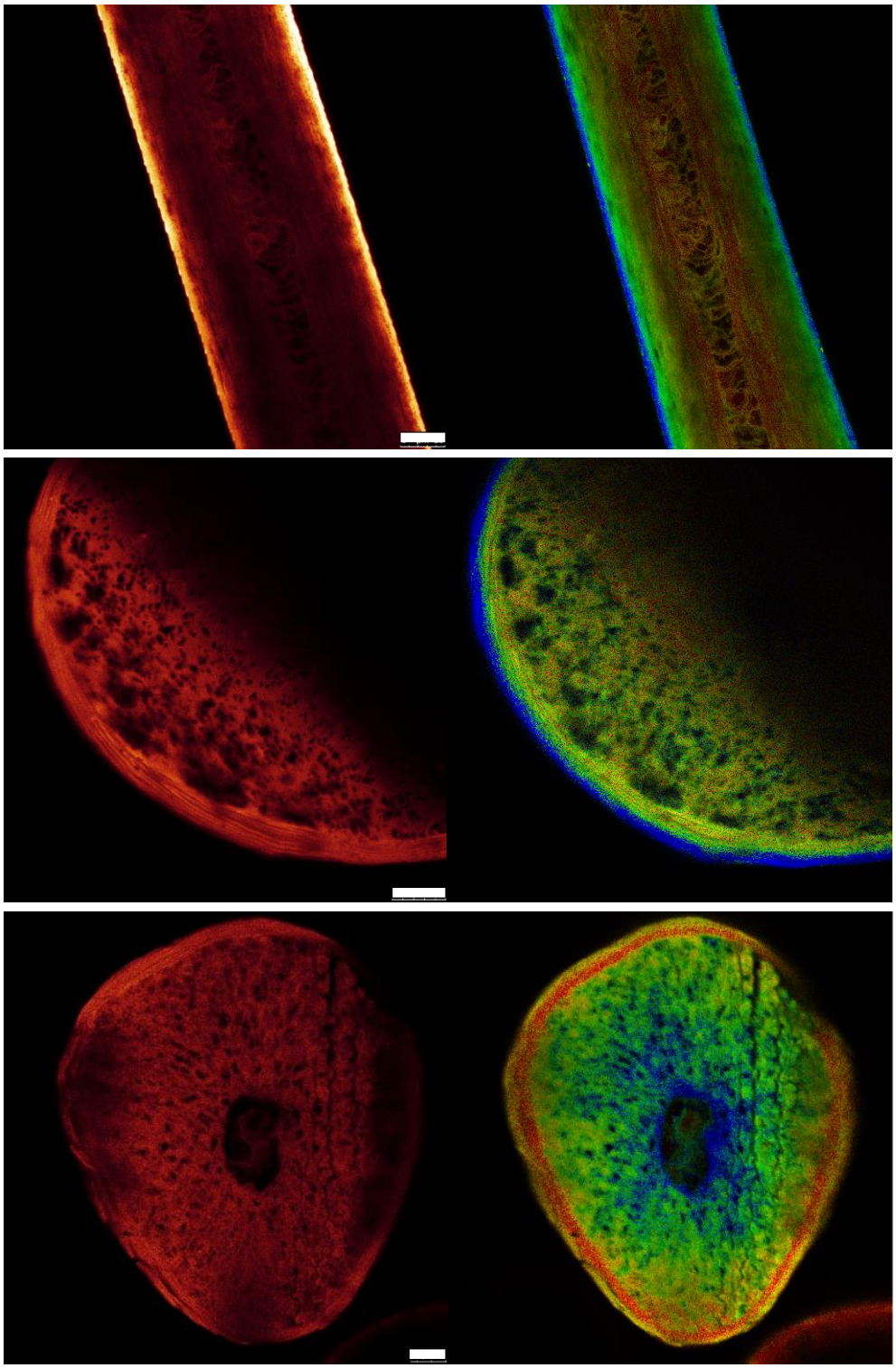

Fig. 4.2. Fluorescence lifetime imaging with 470nm further distinguishes structures in the hair showing the cuticle possesses multiple lifetimes. Fluorescence intensity (405nm) and FLIM images of optical longitudinal and transverse sections of the hair with 470nm excitation, scale bars = 25µm for longitudinal sections and 10µm for transverse sections. Representative photomicrographs for 36 imaged hairs are shown.

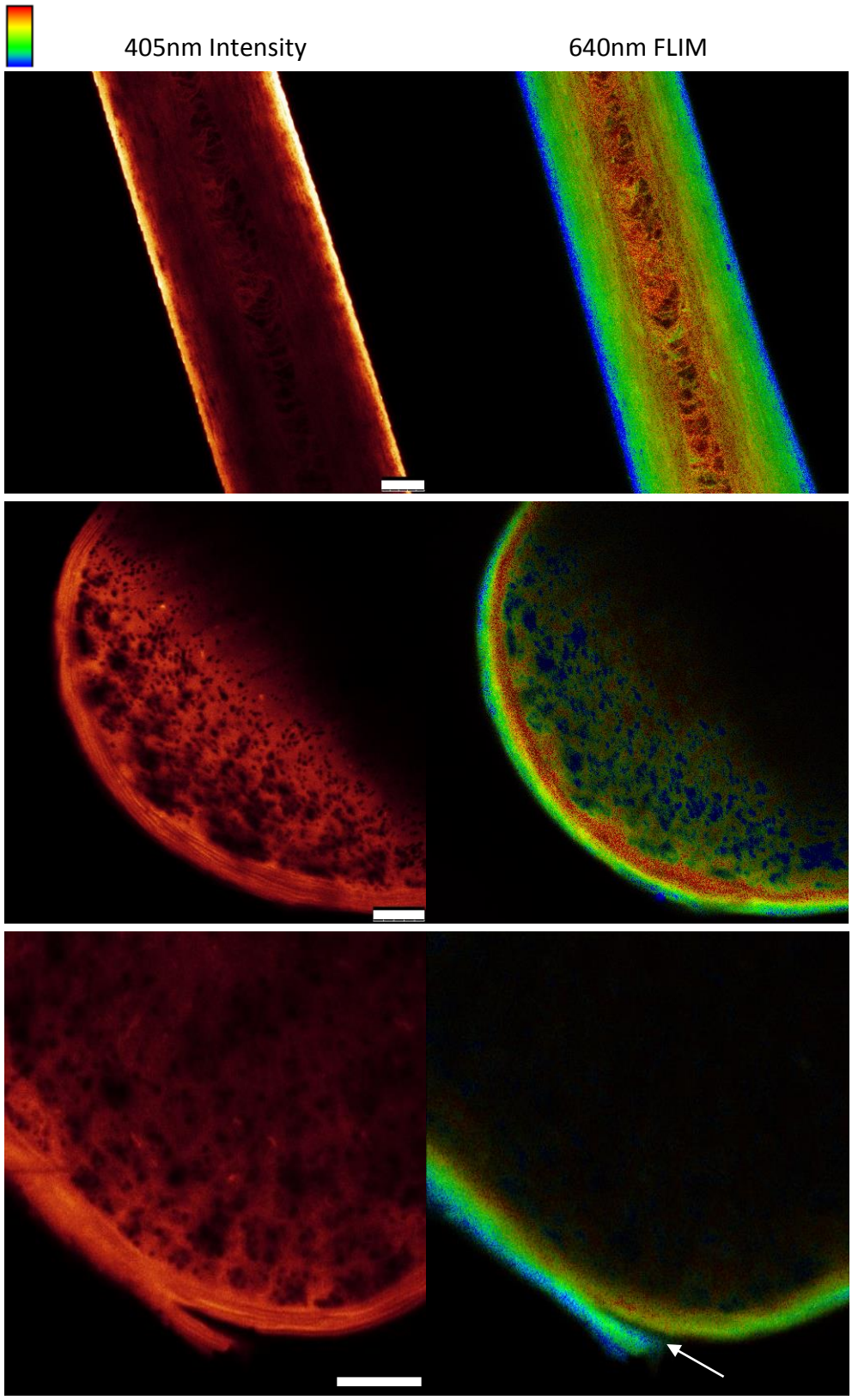
405nm Intensity
640nm FLIM

Fig. 4.3. Fluorescence lifetime imaging with 640nm further distinguishes structures in the hair showing the cuticle possesses multiple lifetimes. Fluorescence intensity (405nm) and FLIM images of optical longitudinal and transverse sections of the hair with 640nm excitation, scale bars = 25µm for longitudinal sections and 10µm for transverse sections. An arrow in the bottom image shows cuticle layers broken off. Representative photomicrographs for 36 imaged hairs are shown.

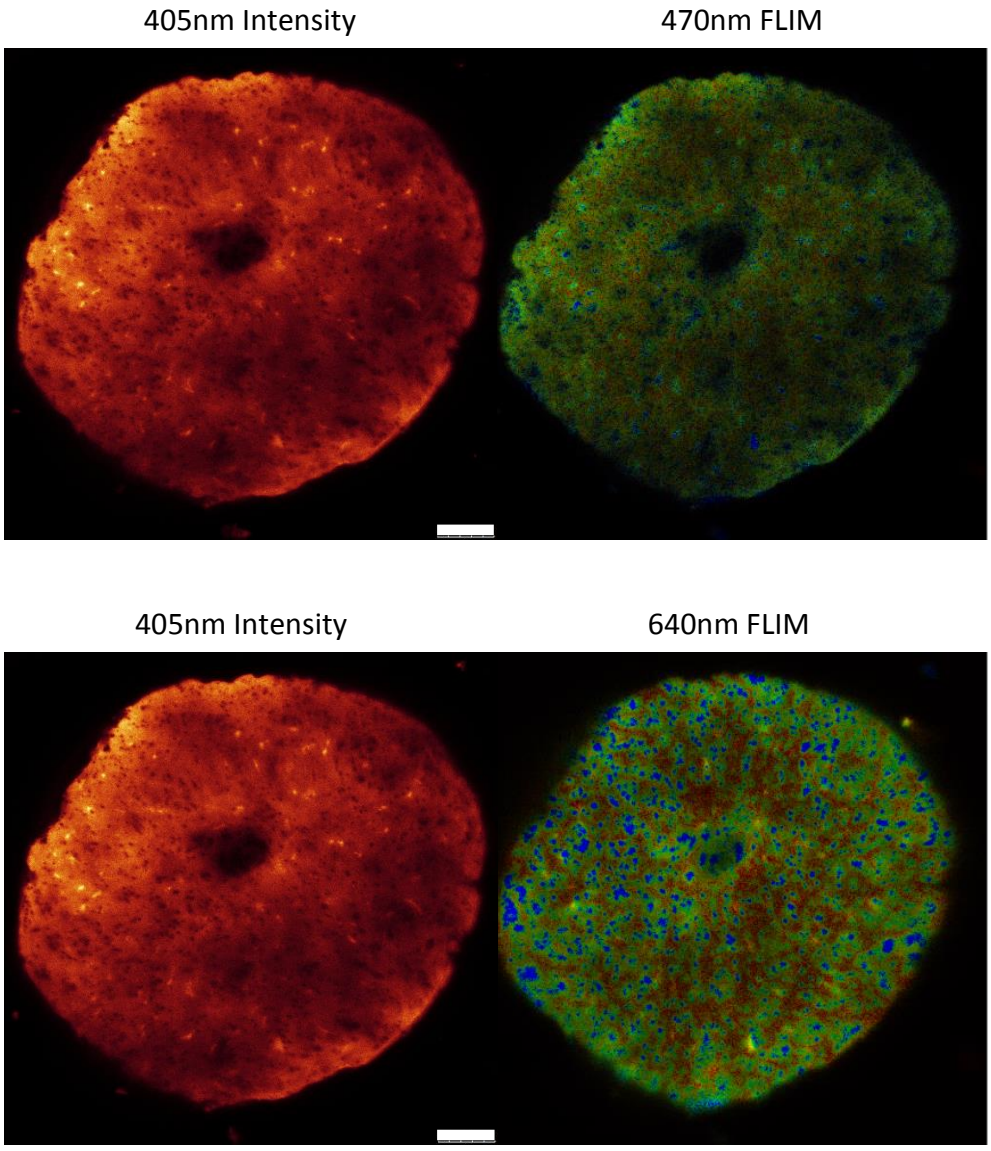

Fig. 4.4. Sandpapering away the cuticle removes the outer lifetimes. Fluorescence intensity (405nm) and FLIM images of optical transverse sections of the hair with 470nm and 640nm excitation, scale bars = 10µm. Representative photomicrographs for 10 imaged hairs are shown.

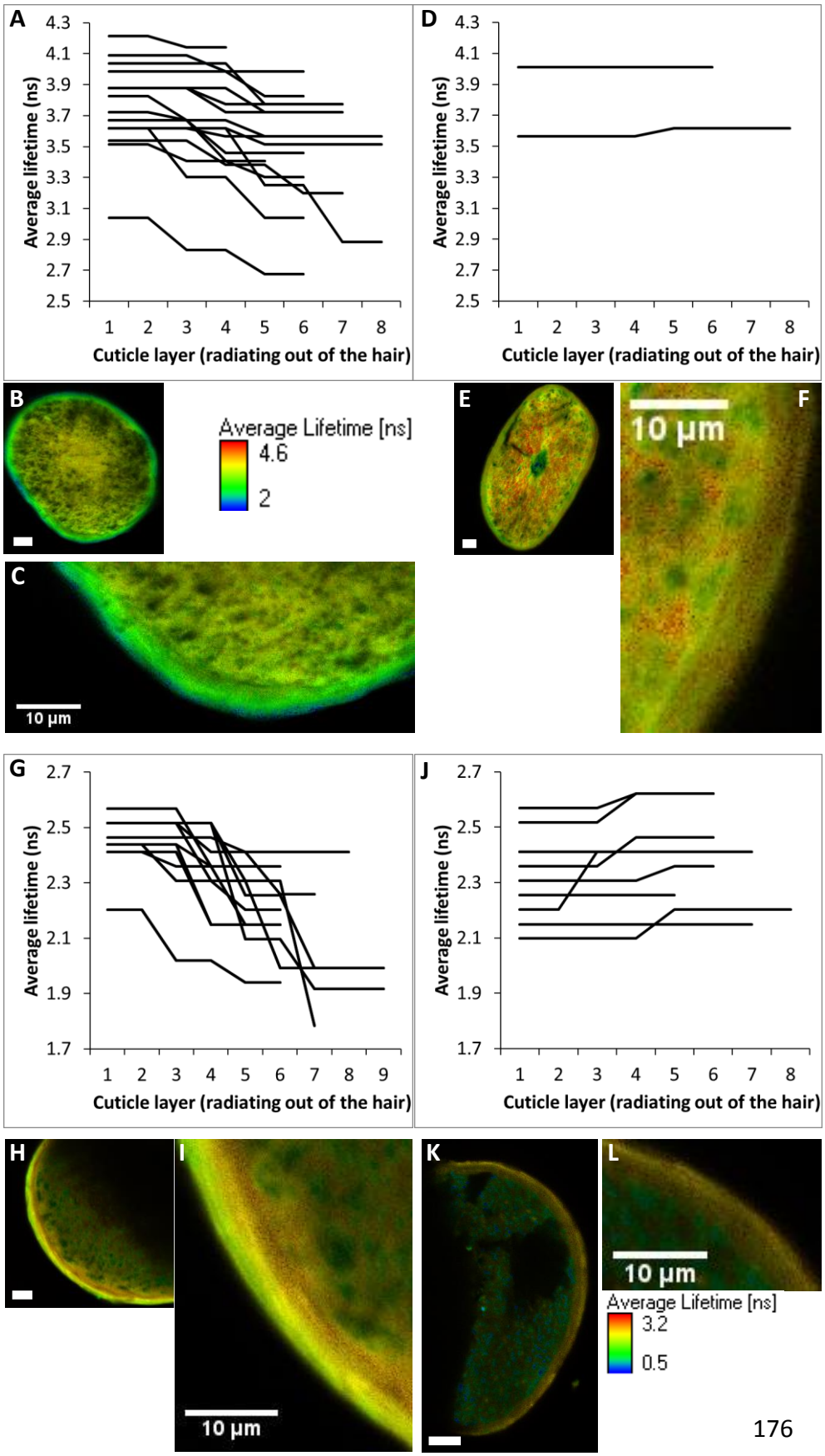
A
Average lifetime (ns)
4.3
4.1
3.9
3.7
3.5
3.3
3.1
2.9
2.7
2.5
1 2 3 4 5 6 7 8
Cuticle layer (radiating out of the hair)
D
Average lifetime (ns)
4.3
4.1
3.9
3.7
3.5
3.3
3.1
2.9
2.7
2.5
1 2 3 4 5 6 7 8
Cuticle layer (radiating out of the hair)
B
Average Lifetime [ns]
4.6
2
E
F
10 µm
C
10 µm
G
Average lifetime (ns)
2.7
2.5
2.3
2.1
1.9
1.7
1 2 3 4 5 6 7 8 9
Cuticle layer (radiating out of the hair)
J
Average lifetime (ns)
2.7
2.5
2.3
2.1
1.9
1.7
1 2 3 4 5 6 7 8
Cuticle layer (radiating out of the hair)
H
I
10 µm
K
L
10 µm
Average Lifetime [ns]
3.2
0.5

Fig. 4.5. There are four observable classes of cuticle populations: decreasing and increasing lifetimes for 470nm and 640nm excitation. A) 470nm excitation of the cuticle showing the average cuticle lifetime decreasing with cuticle layer. B) Corresponding FLIM image with C) enlarged cuticle image. D) 470nm excitation of the cuticle showing the average cuticle lifetime increasing or unvarying with cuticle layer. E) Corresponding FLIM image with F) enlarged cuticle image. G) 640nm excitation of the cuticle showing the average lifetime decreasing with cuticle layer. H) Corresponding FLIM image with I) enlarged cuticle image. J) 640nm excitation of the cuticle showing the average lifetime increasing or unvarying with cuticle layer. K) Corresponding FLIM image with L) enlarged cuticle image. Representative photomicrographs from 470nm (n=21) and 640nm (n=23) excited imaged hairs are shown. Scale bars = 10µm.

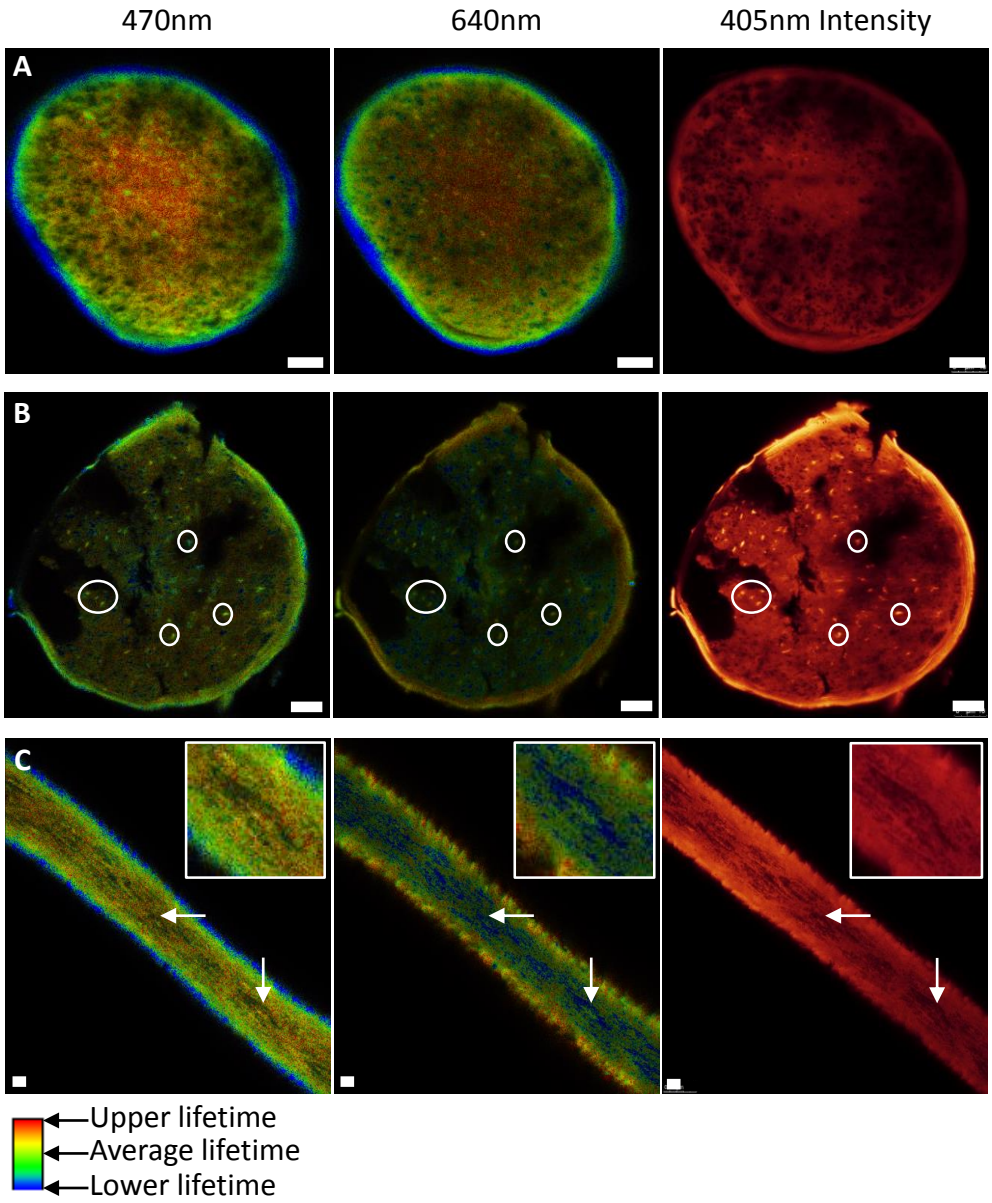

Fig. 4.6. FLIM images of the cortex. A) Transverse optical section of hair showing how lifetimes can vary across the cortex. B) Transverse optical section of hair with organelle remnants (circled). C) Longitudinal optical section showing cortical cells (arrows) and a magnified cortical cell to show the organelle remnant within. Representative photomicrographs for 36 imaged hairs are shown. Scale bars = 10µm.

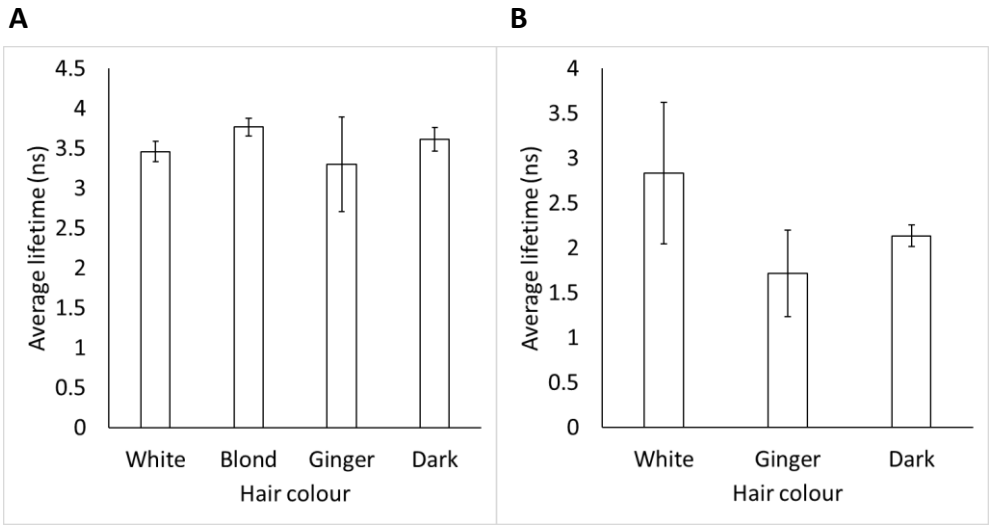

Fig. 4.7. Fluorescence lifetimes of indicated hair colours. A) Average lifetimes of hair excited with 470nm. The number of hairs examined for each colour are white (n=2), blond (n=7), ginger (n=1) and dark (n=25). B) Average lifetimes of hair excited with 640nm. The number of hairs examined for each colour are white (n=1), ginger (n=1) and dark (n=13). Error bars = +/- 2*SEM.

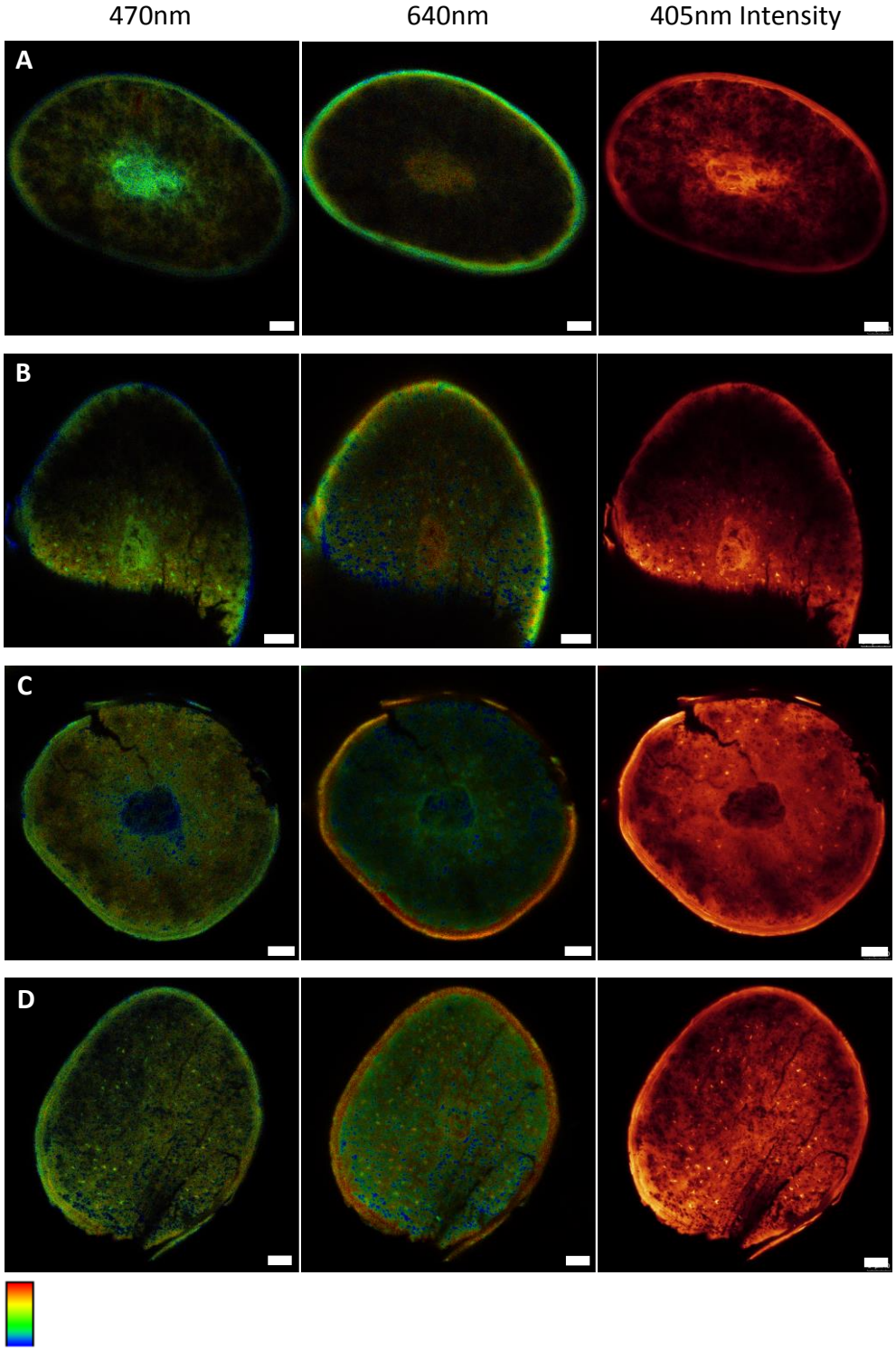

Fig. 4.8. FLIM of transverse optical sections of the medulla. A) Highly autofluorescent medulla. B) Slightly less autofluorescent medulla. C) The least autofluorescent medulla. D) Medulla with similar autofluorescence to the cortex. Representative photomicrographs for 19 imaged hairs are shown. Scale bars = 10µm.

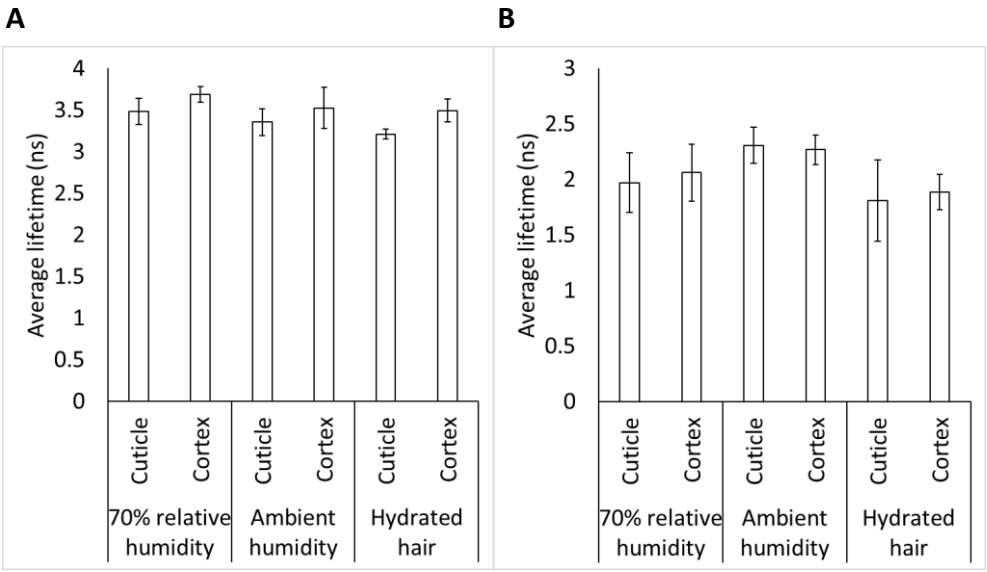

Fig. 4.9. Average lifetimes of untreated Chinese head hair at 70% humidity, ambient humidity and hydrated hair. A) Hairs excited with 470nm. B) Hairs excited with 640nm. Hairs at 70% relative humidity (n=3), ambient humidity (n=3), hydrated (n=3). Error bars = +/- 2*SEM.

Controls

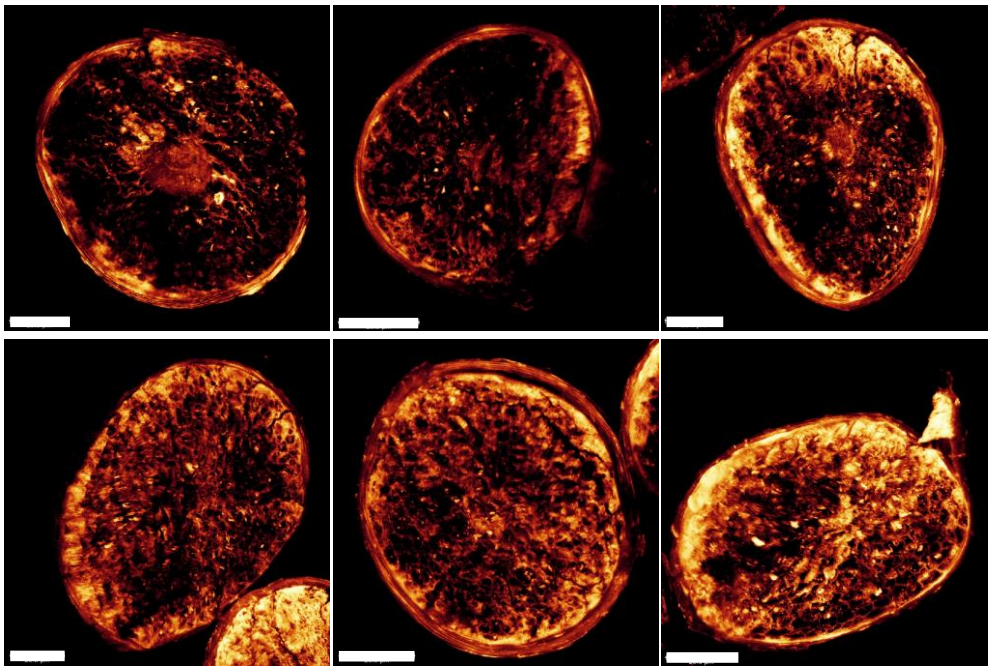

Wertz and Downing lipid extraction method treated samples

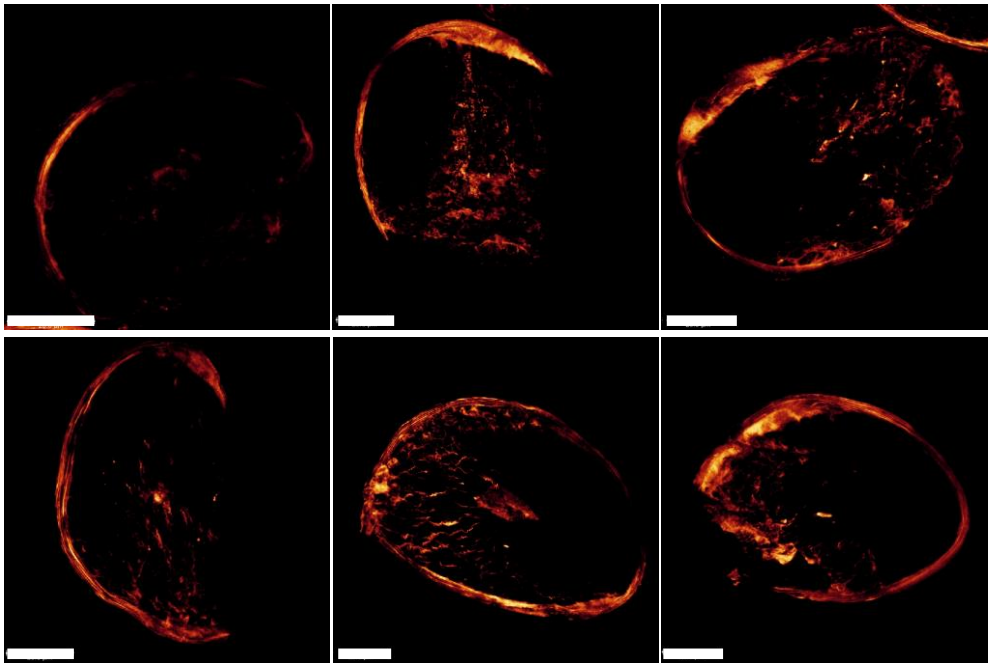

Fig. 4.10. Nile red stained hairs treated with the Wertz and Downing lipid extraction method. Untreated control hairs and sample hairs treated with the Wertz and Downing lipid extraction method. Optically sliced confocal images of 0.6mg/ml Nile red stained control and sample hairs after treatment. Scale bars = 20µm.

Step 1

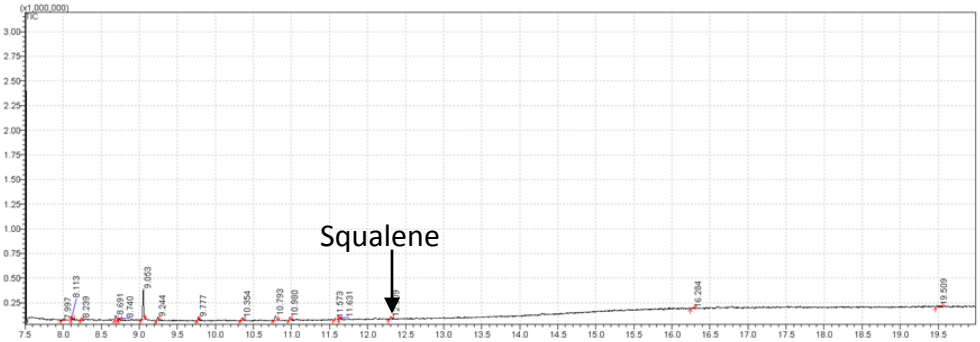

Step 2

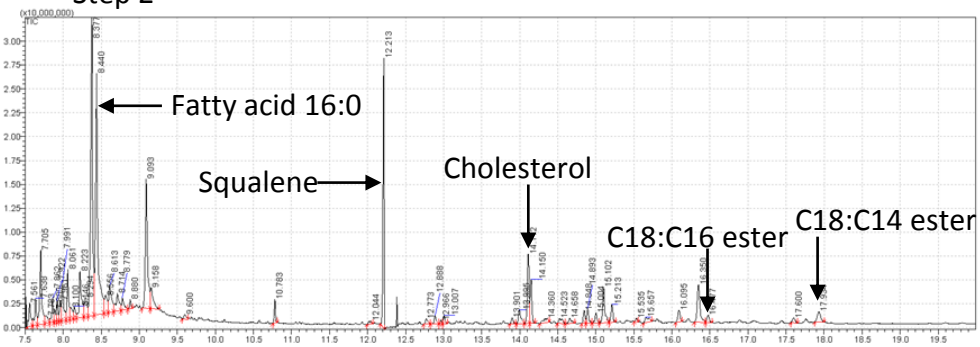

Step 3

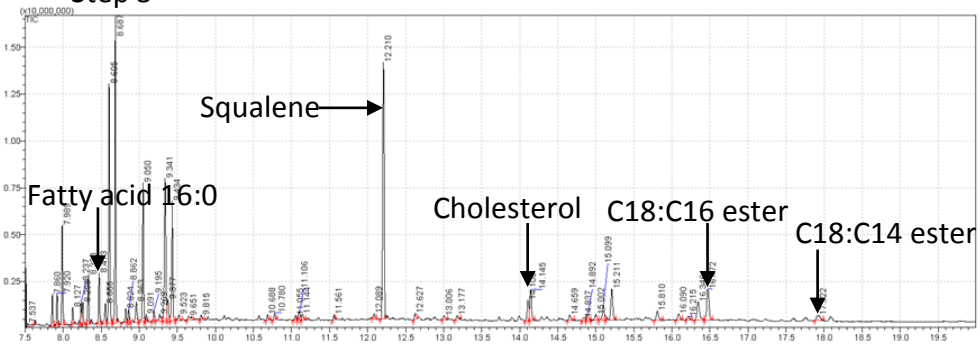

Step 4

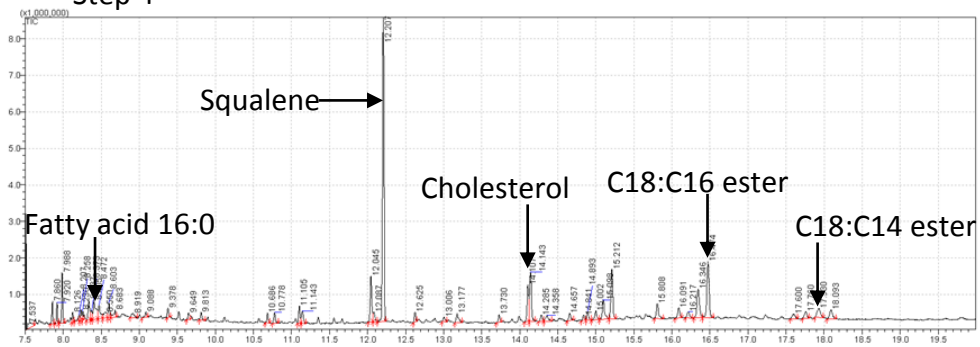

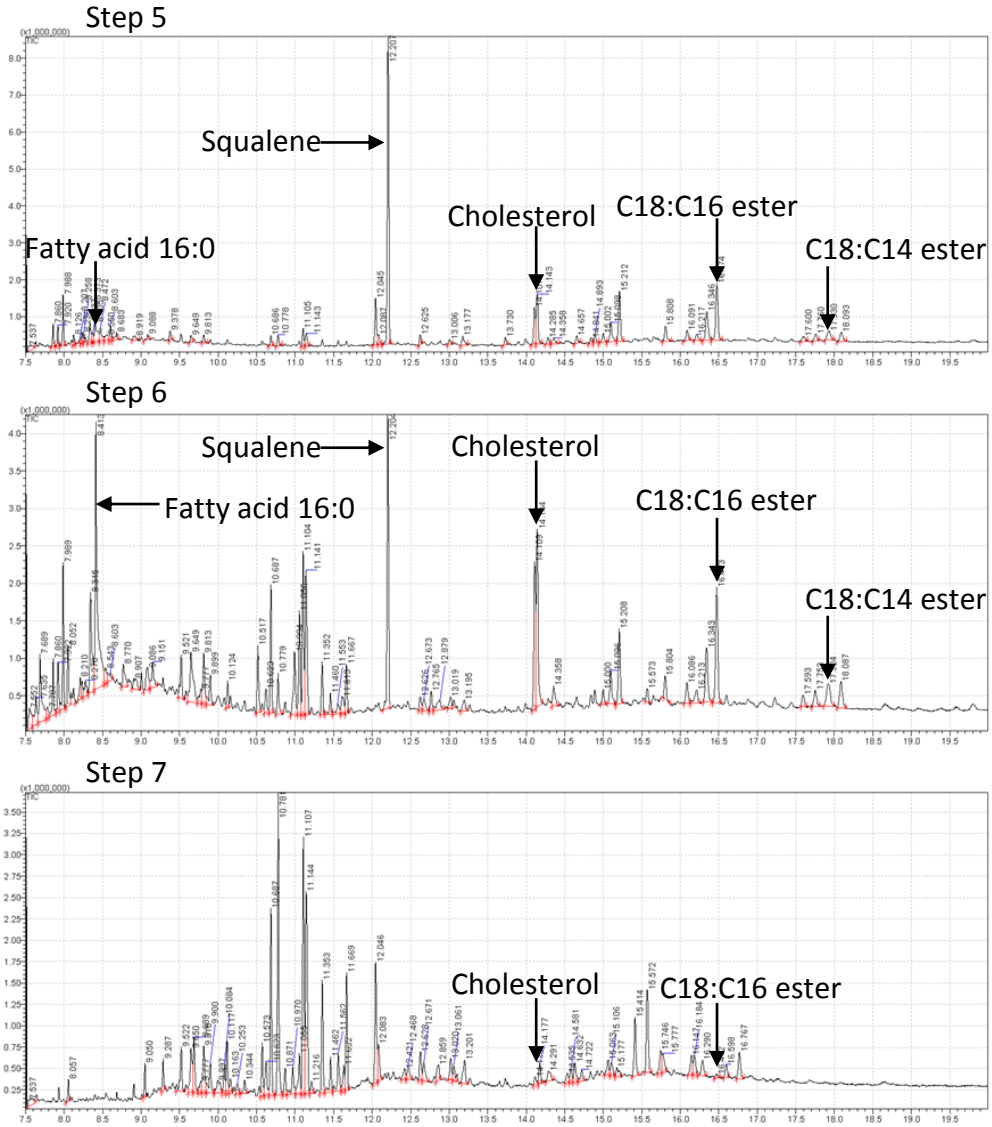

Fig. 4.11. GC/MS chromatograms of the hair elutant from each stage of the Wertz and Downing lipid extraction method. GC/MS chromatograms of each of the seven steps in the protocol showing the main lipids present in the elutant from the treated hair.

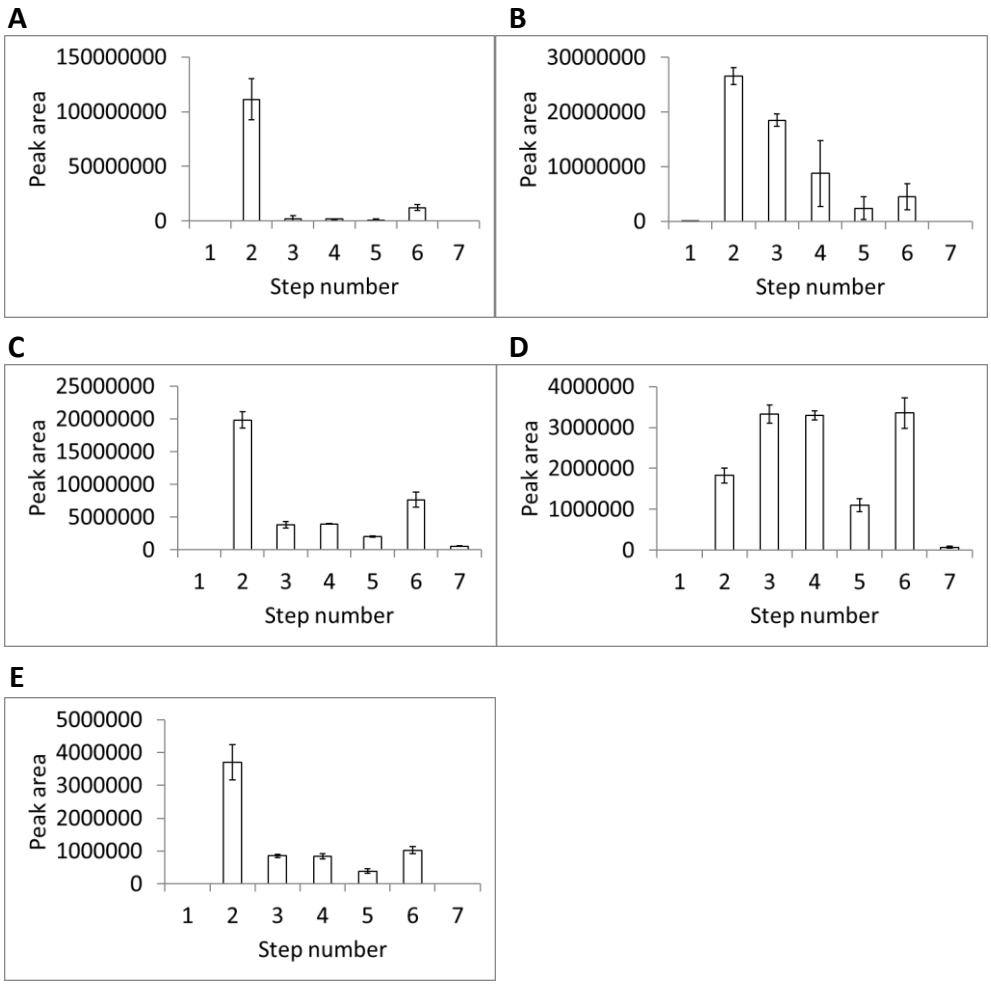

Fig. 4.12. Relative amounts of lipid extracted in each step of the Wertz and Downing lipid extraction method. Relative amounts of lipid extracted from treated hairs per step of the protocol of: A) fatty acid 16:0; B) squalene; C) cholesterol; D) C18:C16 ester; E) C18:C14 ester. N.B. Comparisons cannot be made between the lipids as the different species ionise to differing degrees. Error bars = +/- 2*SEM.

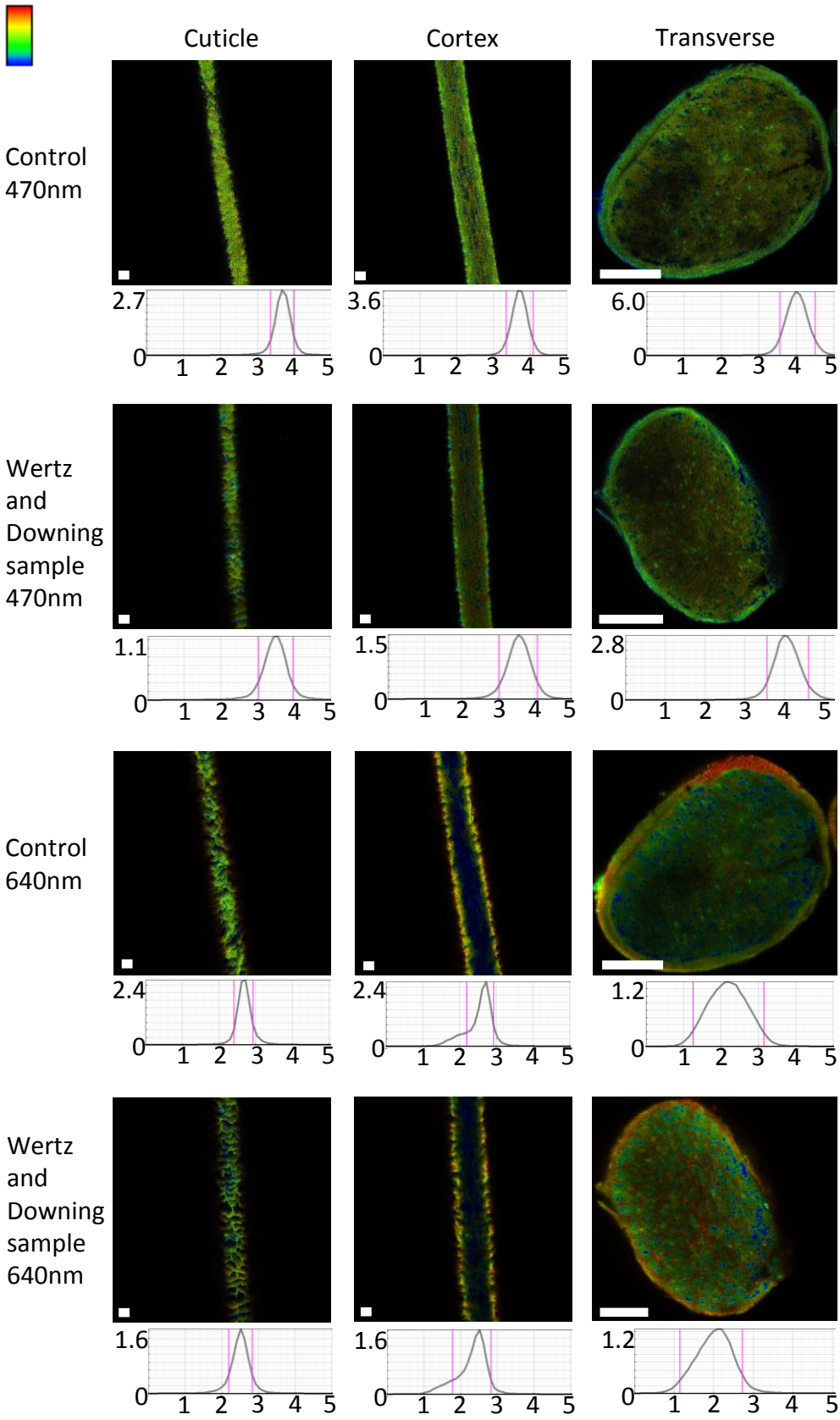
Cuticle
Cortex
Transverse
Control 470nm
2.7
0
3.6
0
6.0
0
Wertz and Downing sample 470nm
1.1
0
1.5
0
2.8
0
Control 640nm
2.4
0
2.4
0
1.2
0
Wertz and Downing sample 640nm
1.6
0
1.6
0
1.2
0
1 2 3 4 5

Fig. 4.13. FLIM of hair treated with the Wertz and Downing lipid extraction method. Untreated control hairs and sample hairs treated with the Wertz and Downing lipid extraction method. Longitudinal images show the same strand of hair which has been halved, with one half as a control and the other undergoing treatment, showing FLIM of the cuticle and cortex, as well as transverse sections of other hairs, for 470nm and 640nm excitation. Each image also shows a graph of the frequency of lifetimes, x-axis = time (ns), y-axis = frequency (M.counts). Representative photomicrographs for 11 control and 11 treated imaged hairs are shown. N.B. The pink markers on the lifetime graphs indicate the upper (red) and lower (blue) lifetime limits. Scale bars = 25µm.

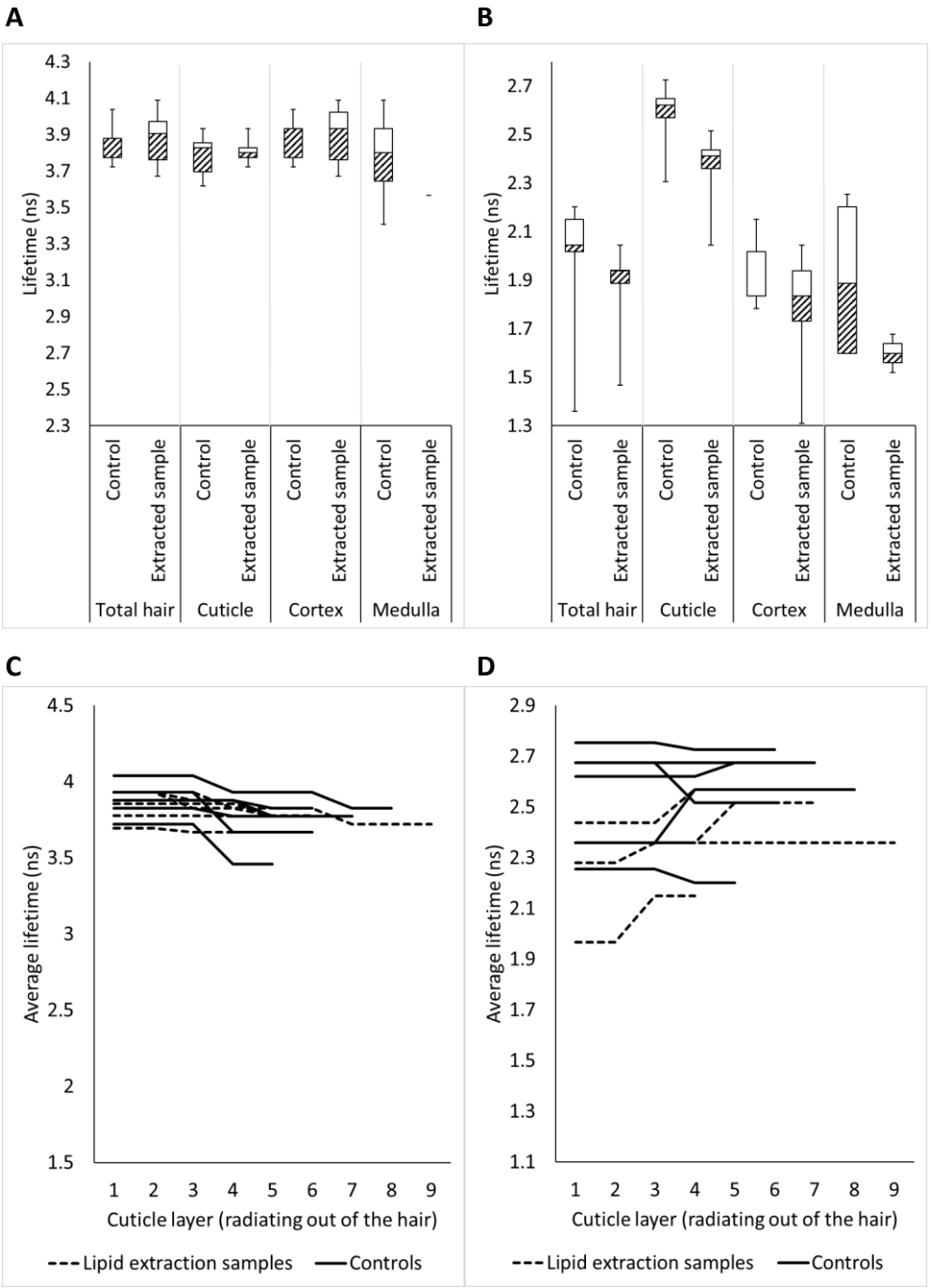

Fig. 4.14. Fluorescence lifetimes of hair treated with the Wertz and Downing lipid extraction method. A) Box and whisker plot showing how the average lifetimes change after treatment using 470nm excitation. B) Box and whisker plot showing how the average lifetimes change after treatment using 640nm excitation. C) 470nm excitation of the cuticle showing how cuticle lifetime changes with cuticle layer after treatment. D) 640nm excitation of the cuticle showing how cuticle lifetime changes with cuticle layer after treatment. Control hairs (n=6), treated hairs (n=6).

A

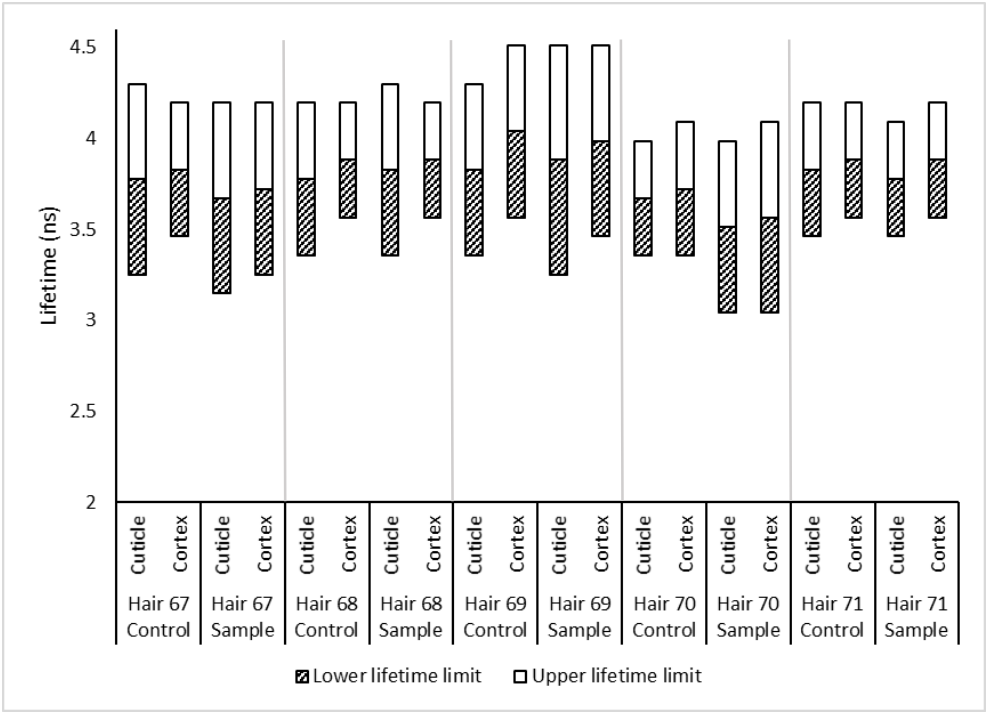

B

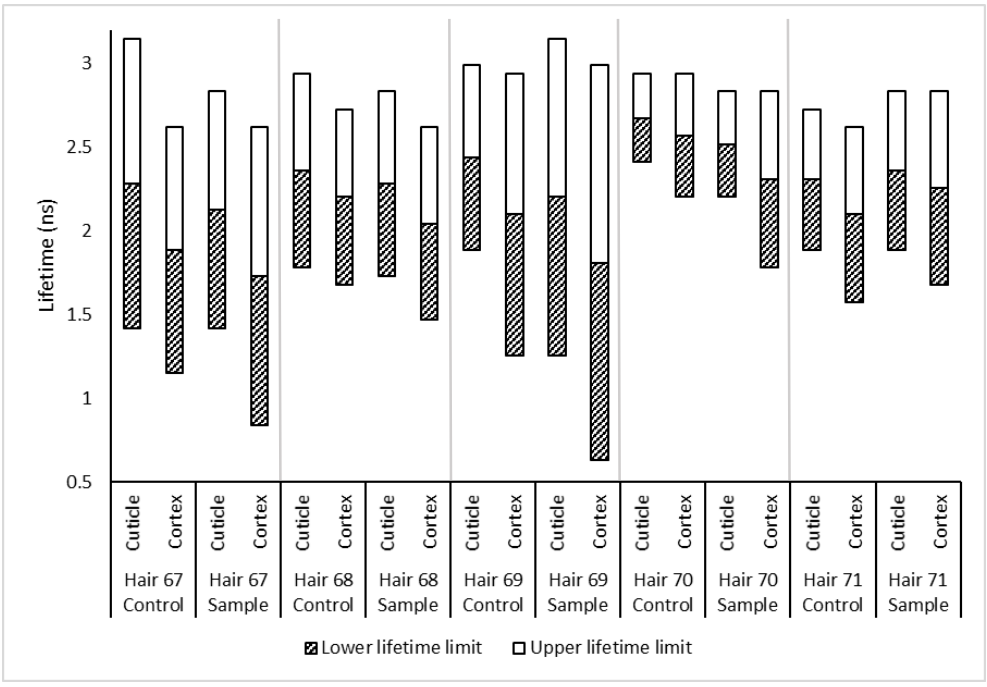

Fig. 4.15. Range of fluorescence lifetimes of paired control hair and sample hair treated with the Wertz and Downing lipid extraction method. A) Lifetimes of hair excited by 470nm, in longitudinal section, of paired controls compared to treated samples. B) Lifetimes of hair excited by 640nm, in longitudinal section, of paired controls compared to samples. Control hairs (n=5), treated hairs (n=5).

Controls

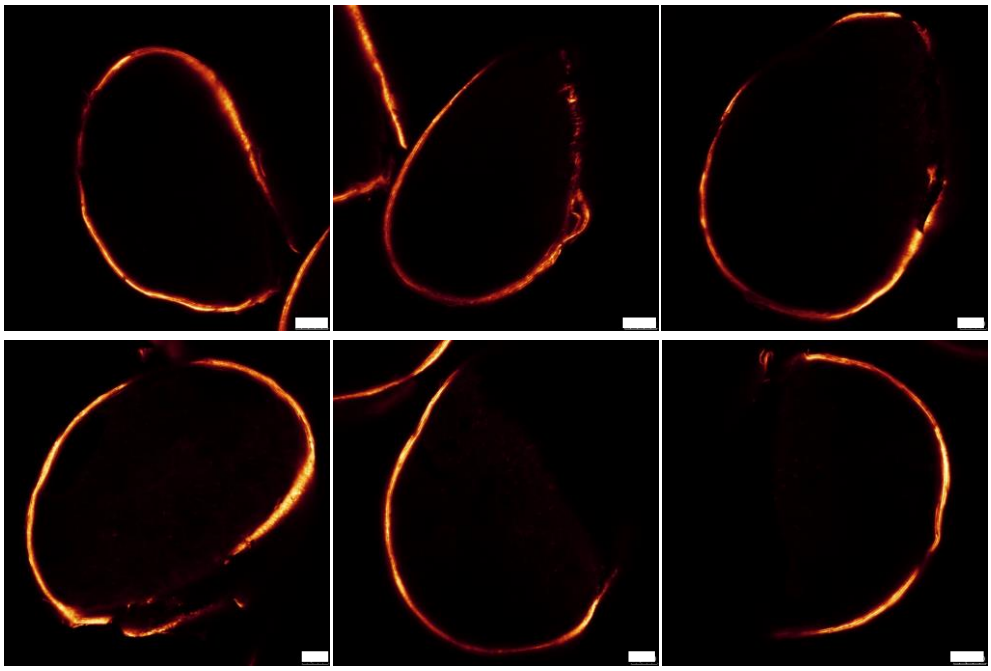

Cornified envelope lipid extraction method treated samples

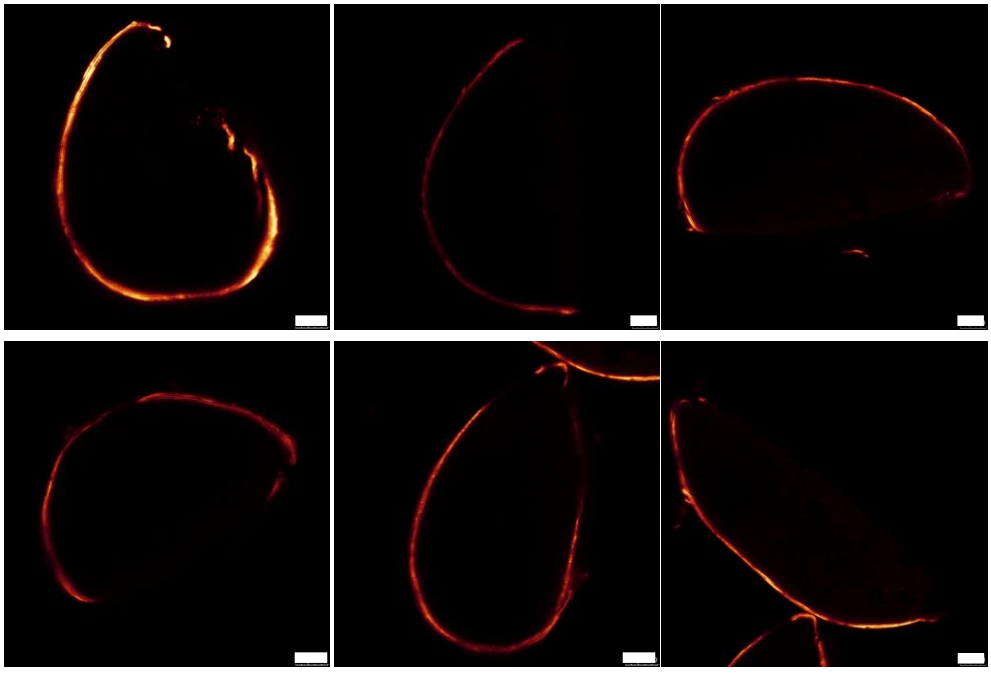

Fig. 4.16. Nile red stained hairs treated with the modified method for stratum corneum lipids. Untreated control hairs and sample hairs treated with the stratum corneum lipid extraction method. Optically sliced confocal images of 0.6mg/ml Nile red stained control and sample hairs after treatment, scale bars = 10µm.

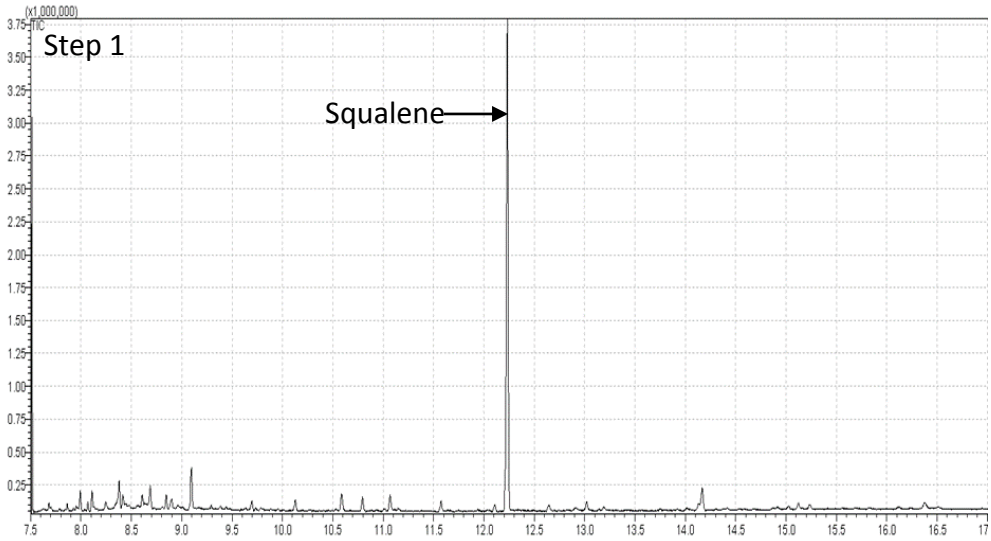
(x1,000,000)
TIC
Step 1
Squalene

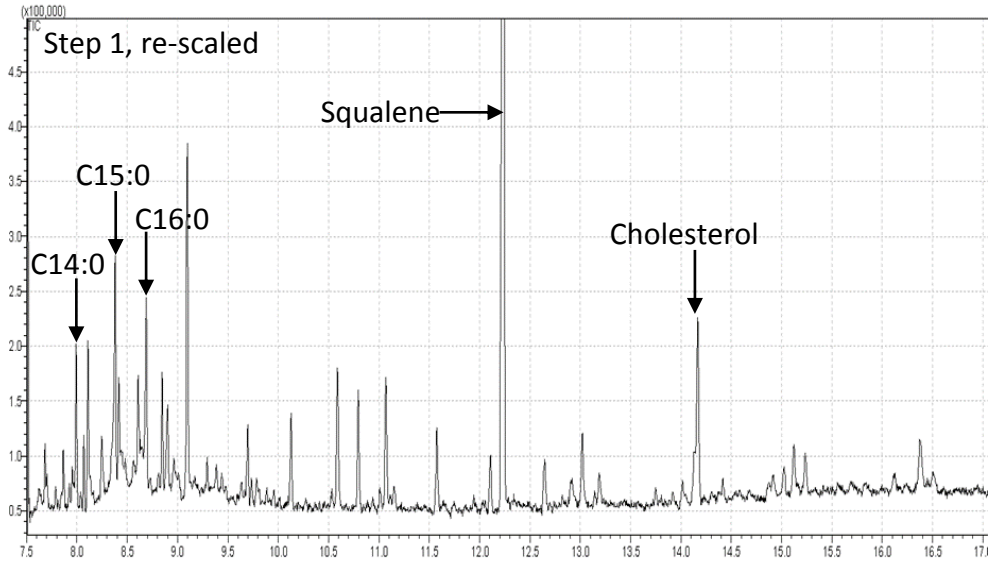
(x100,000)
TIC
Step 1, re-scaled
Squalene
C15:0
C16:0
C14:0
Cholesterol

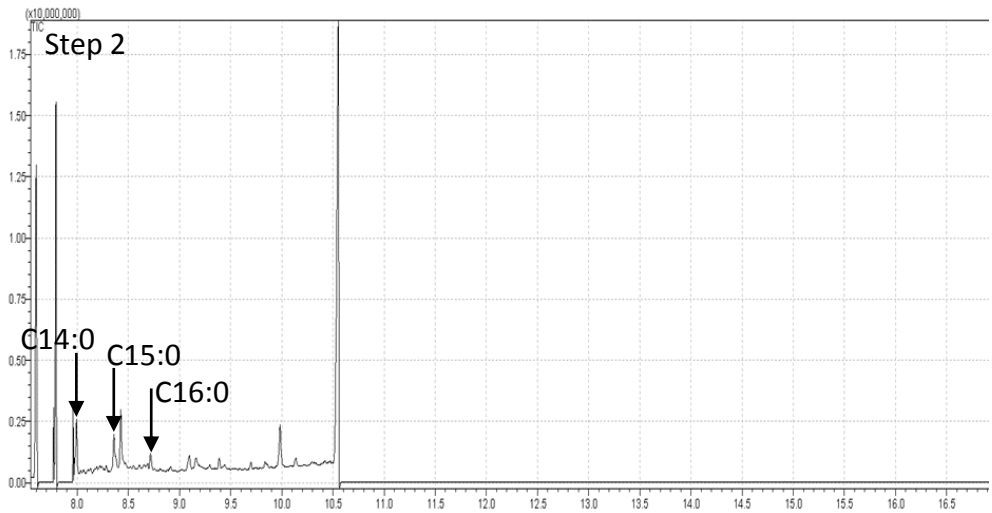
(x10,000,000)
TIC
Step 2
C14:0
C15:0
C16:0

Fig. 4.17. GC/MS chromatograms of the hair elutant from each stage of the modified method for stratum corneum lipids. Untreated control hairs and sample hairs treated with the stratum corneum lipid extraction method. GC/MS chromatograms of the two steps in the protocol showing the main lipids present. The chromatogram of the first step has also been re-scaled to increase the size of peaks other than squalene. N.B. Step two seems to affect the detector, with the way the signal drops off to the baseline.

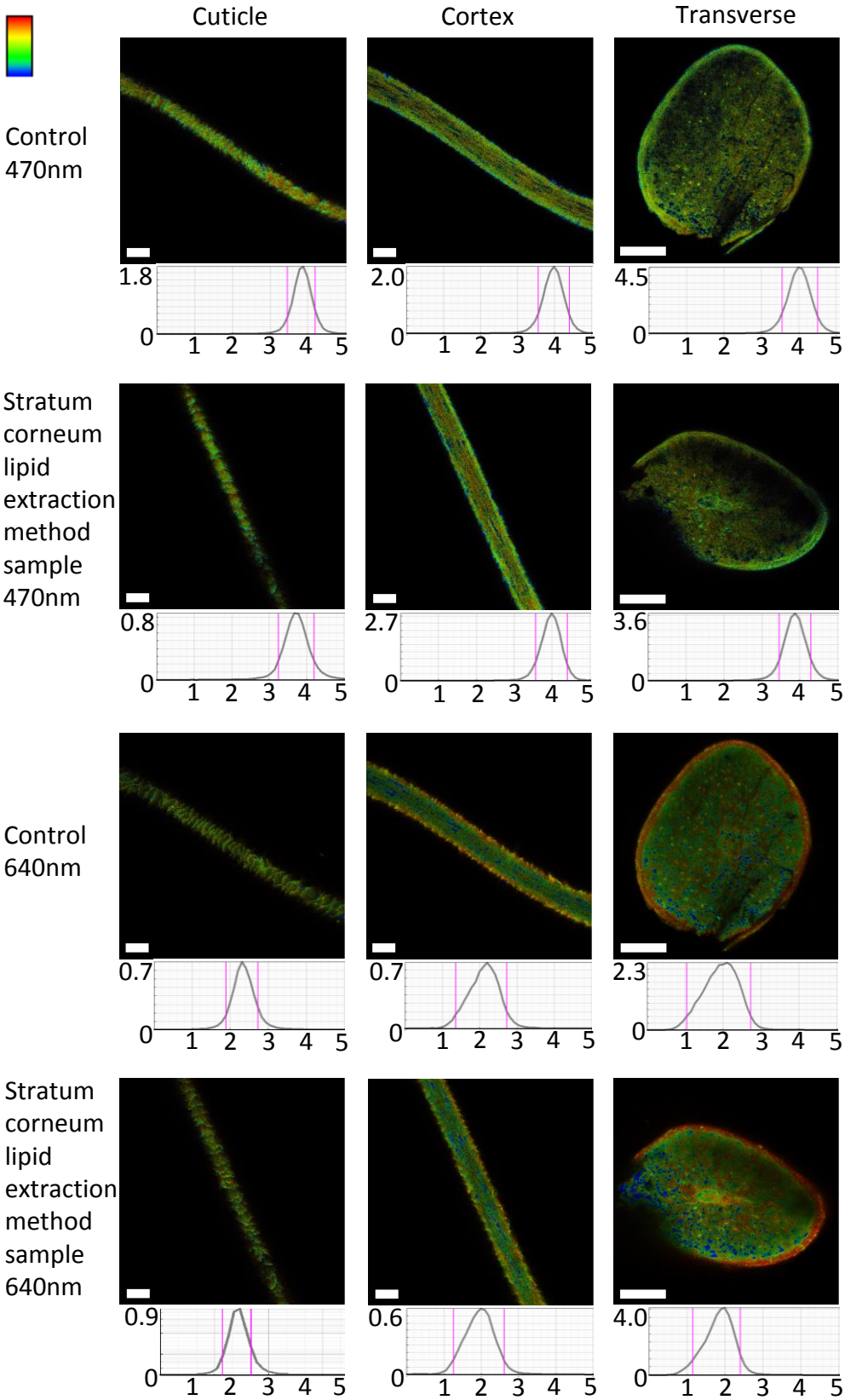
Cuticle
Cortex
Transverse
Control 470nm
1.8
0
2.0
0
4.5
0
1 2 3 4 5
Stratum corneum lipid extraction method sample 470nm
0.8
0
2.7
0
3.6
0
Control 640nm
0.7
0
0.7
0
2.3
0
Stratum corneum lipid extraction method sample 640nm
0.9
0
0.6
0
4.0
0

Fig. 4.18. FLIM of hair treated with the modified method for stratum corneum lipids. Untreated control hairs and sample hairs treated with the stratum corneum lipid extraction method. Longitudinal images show the same strand of hair which has been halved, with one half as a control and the other undergoing treatment, showing FLIM of the cuticle and cortex, as well as transverse sections of other hairs, for 470nm and 640nm excitation. Each image also shows a graph of the frequency of lifetimes, x-axis = time (ns), y-axis = frequency (M.counts). Representative photomicrographs for 11 control and 11 treated imaged hairs are shown. N.B. The pink markers on the lifetime graphs indicate the upper (red) and lower (blue) lifetime limits. Scale bars = 25µm.

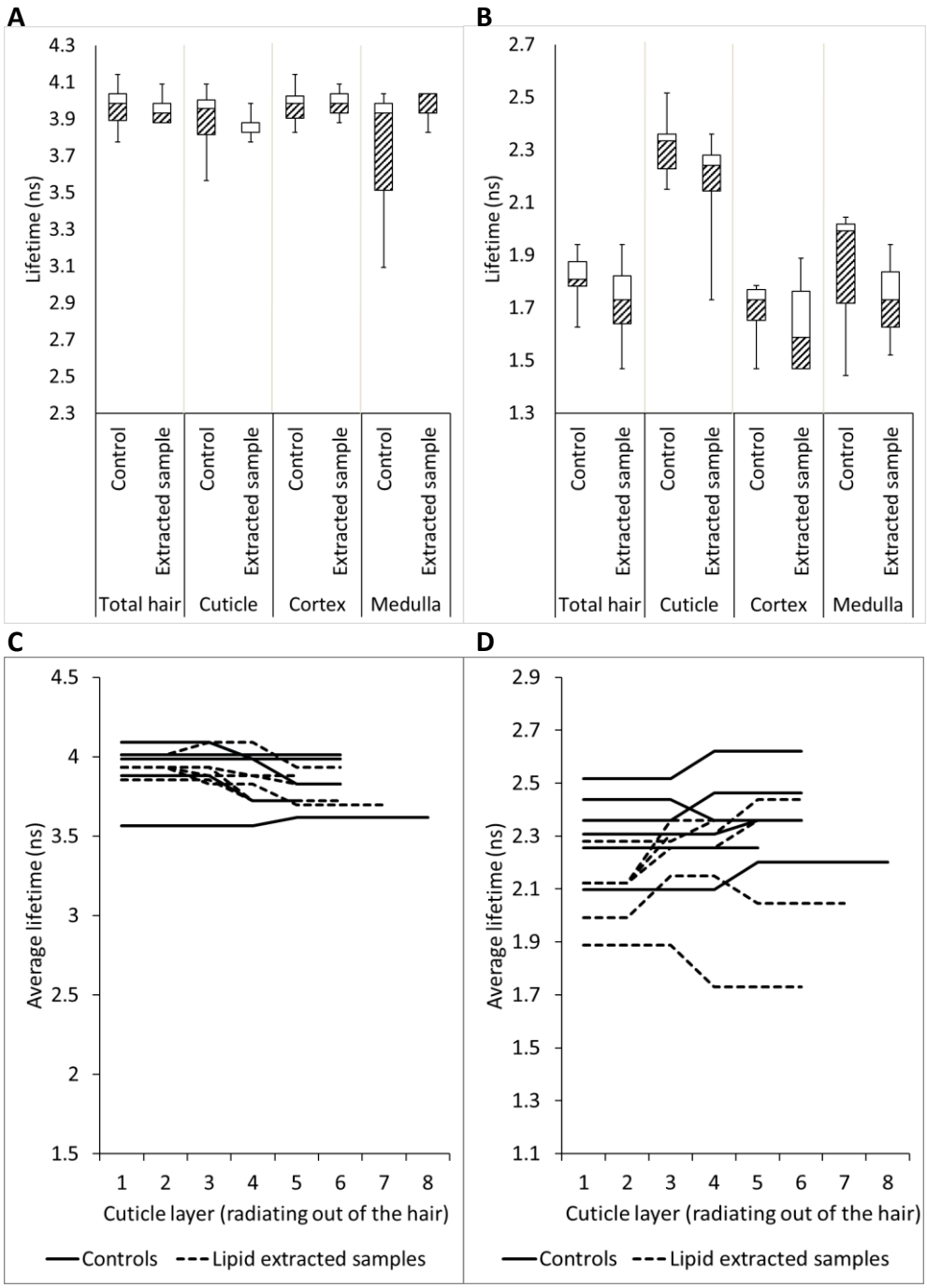

Fig. 4.19. Fluorescence lifetimes of hair treated with the modified method for stratum corneum lipids. A) Box and whisker plot showing how the average lifetimes change after treatment using 470nm excitation. B) Box and whisker plot showing how the average lifetimes change after treatment using 640nm excitation. C) 470nm excitation of the cuticle showing how cuticle lifetime changes with cuticle layer after treatment. D) 640nm excitation of the cuticle showing how cuticle lifetime changes with cuticle layer after treatment. Control hairs (n=6), treated hairs (n=6).

A

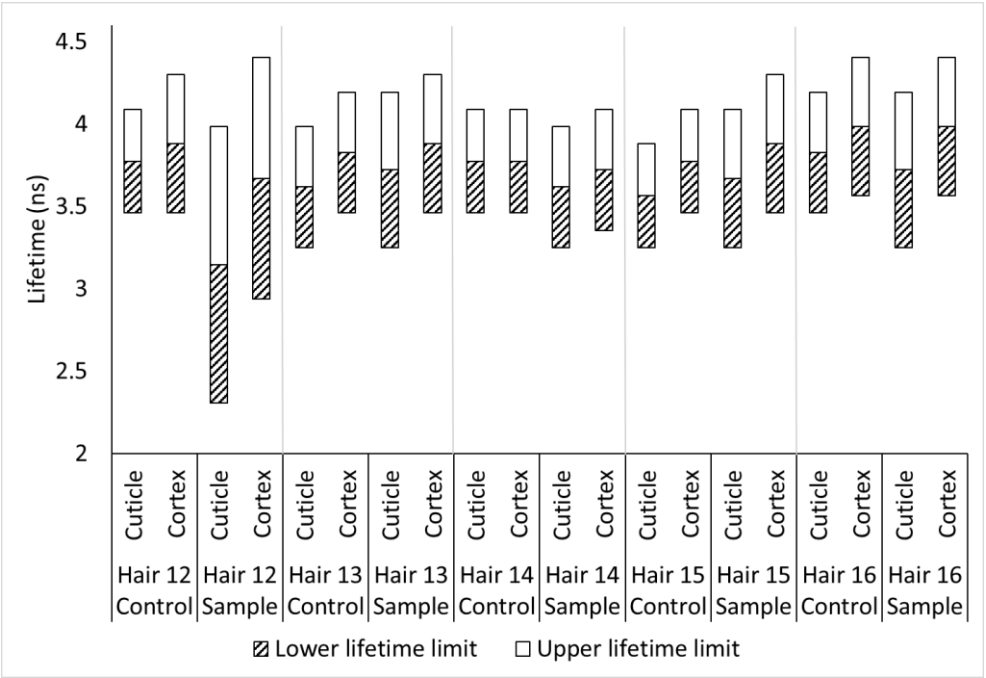

B

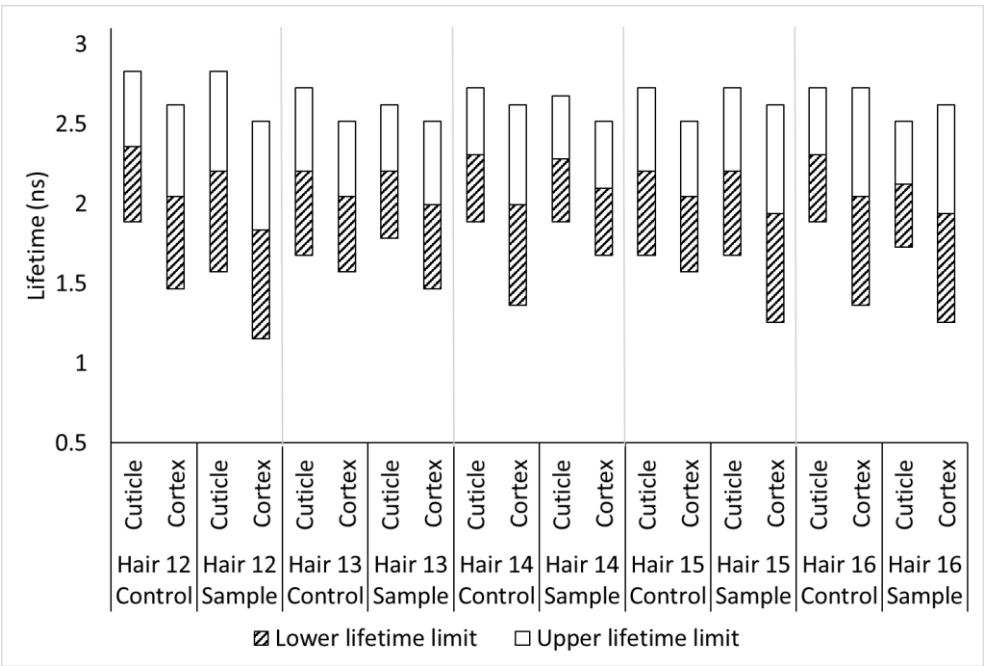

Fig. 4.20. Range of fluorescence lifetimes of paired control hair and sample hair treated with the modified method for stratum corneum lipids. A) Lifetimes of hair excited by 470nm, in longitudinal section, of paired controls compared to treated samples. B) Lifetimes of hair excited by 640nm, in longitudinal section, of paired controls compared to samples. Control hairs (n=5), treated hairs (n=6).

Controls

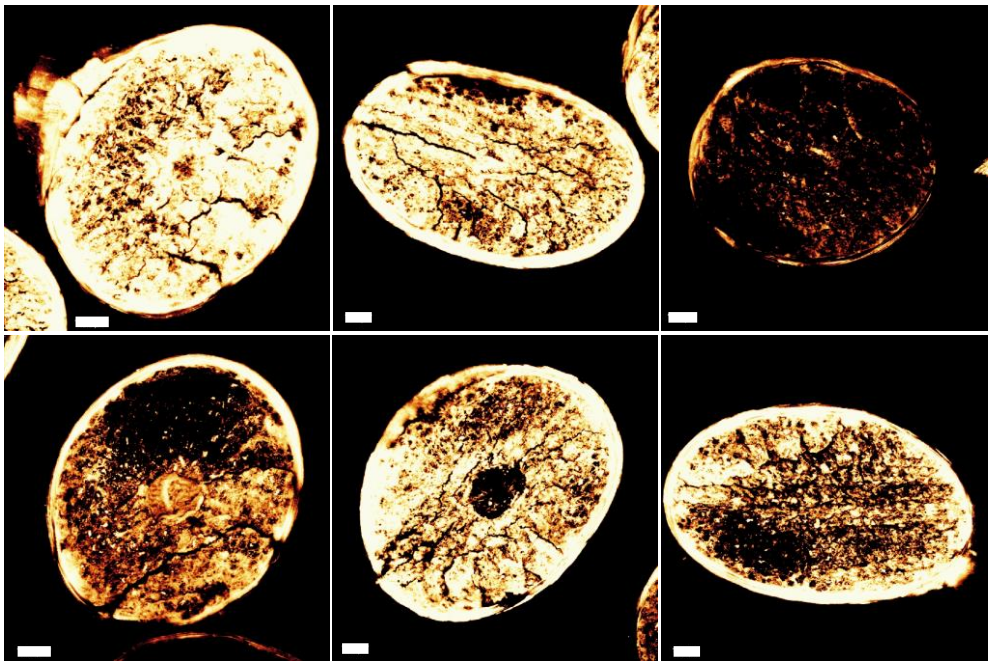

CTAB lipid extracted treated samples

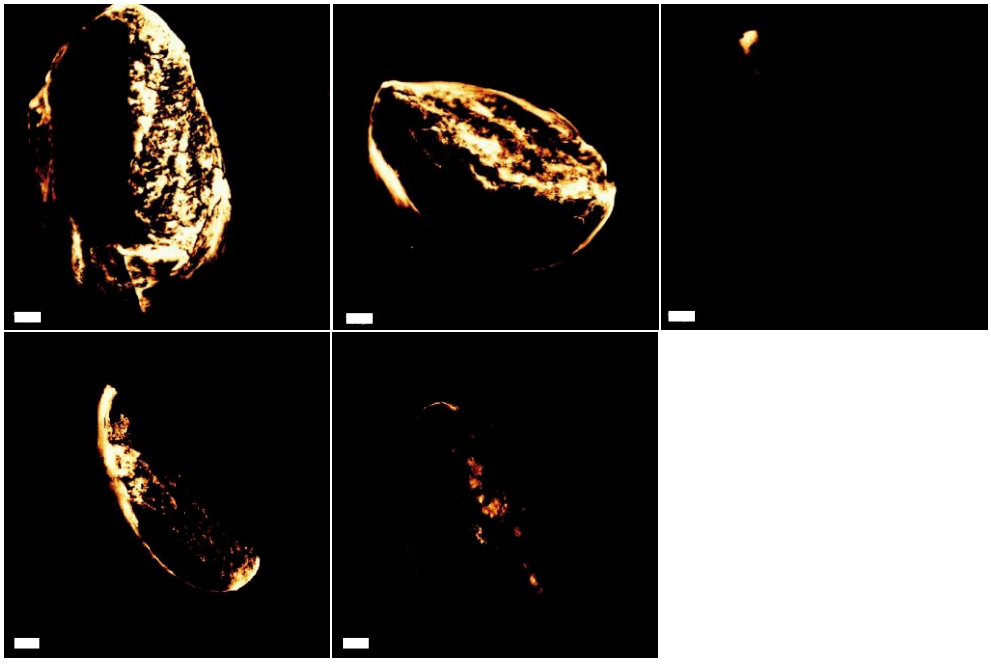

Fig. 4.21. Nile red stained hairs treated with the CTAB lipid extraction method. Untreated control hairs and sample hairs treated with the CTAB lipid extraction method. Optically sliced maximum projection confocal images of 0.6mg/ml Nile red stained control and sample hairs after treatment, scale bars = 10µm.

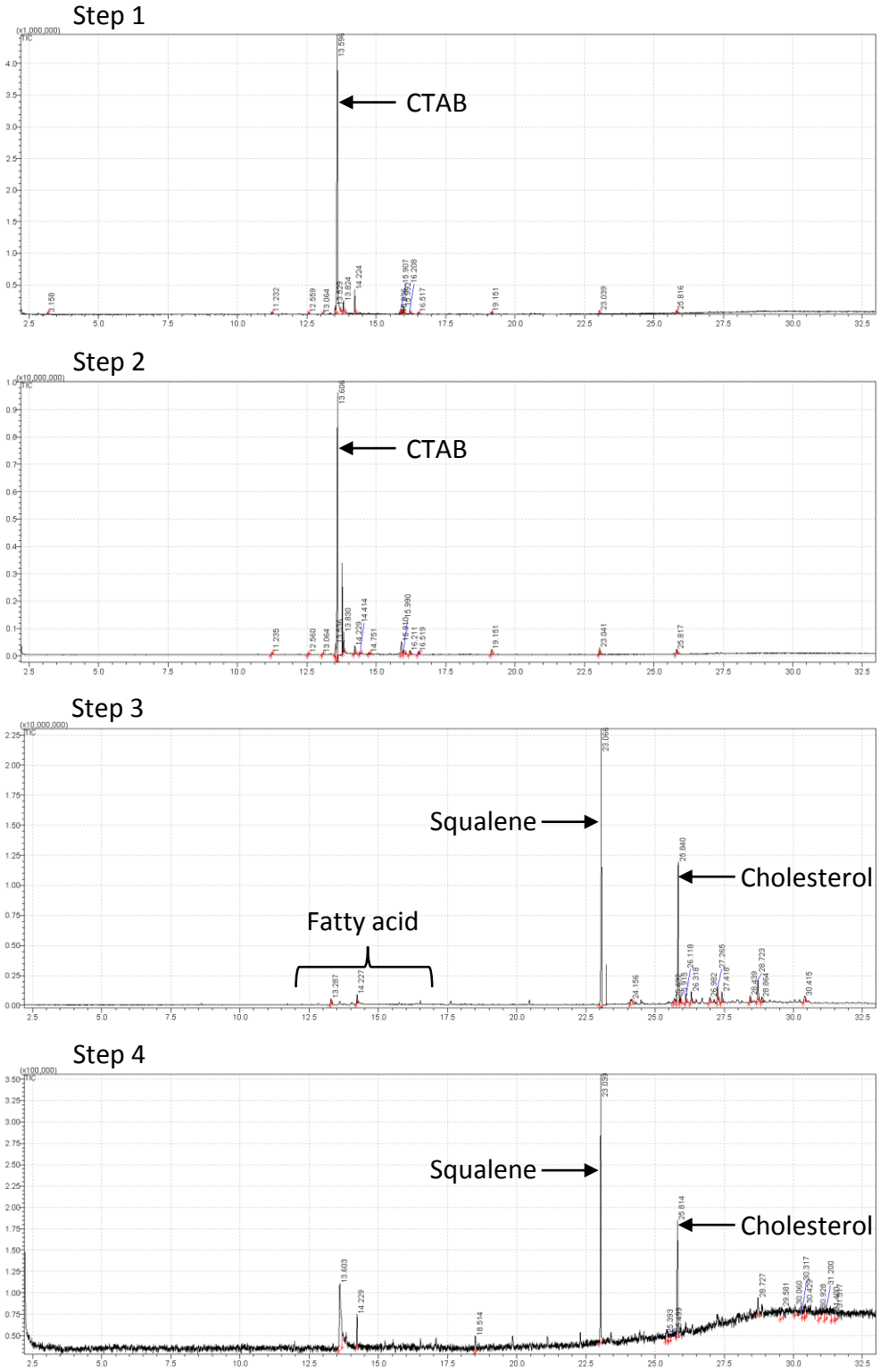

Fig. 4.22. GC/MS chromatograms of the hair elutant from each stage of the CTAB lipid extraction method. GC/MS chromatograms of each of the four steps in the protocol showing the main lipids present.

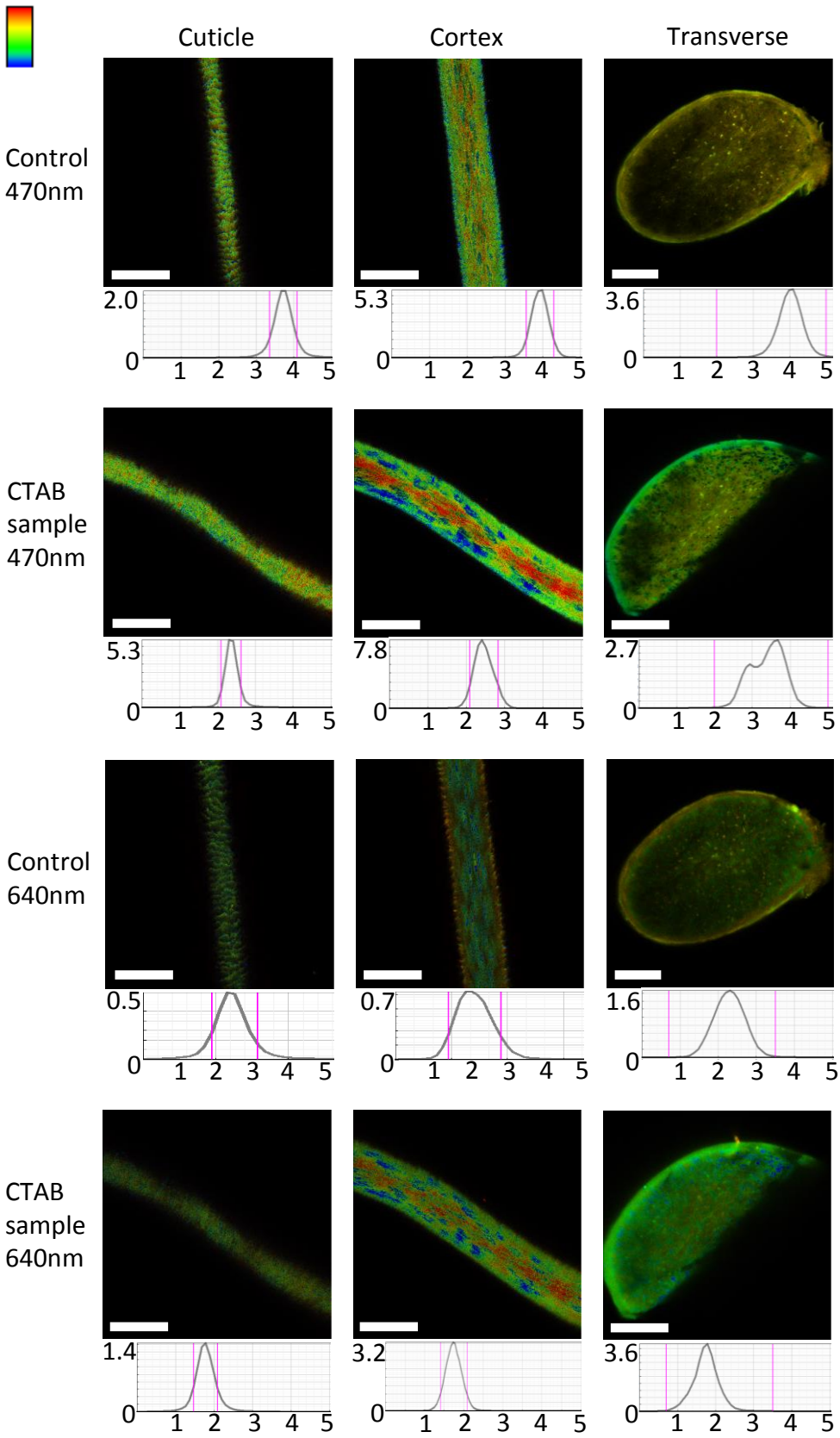
Cuticle
Cortex
Transverse
Control 470nm
CTAB sample 470nm
Control 640nm
CTAB sample 640nm
2.0
5.3
3.6
7.8
2.7
0.5
0.7
1.6
1.4
3.2
0
1 2 3 4 5

Fig. 4.23. FLIM images of hairs treated with the CTAB lipid extraction method. Untreated control hairs and sample hairs treated with the CTAB lipid extraction method. Longitudinal images show the same strand of hair which has been halved, with one half as a control and the other undergoing treatment, showing FLIM of the cuticle and cortex, as well as transverse sections of other hairs which have been coloured to the same scale, for 470nm and 640nm excitation. Each image also shows a graph of the frequency of lifetimes, x-axis = time (ns), y-axis = frequency (M.counts). Representative photomicrographs for 11 control and 11 treated imaged hairs are shown. N.B. The pink markers on the lifetime graphs indicate the upper (red) and lower (blue) lifetime limits. Scale bars = 25µm.

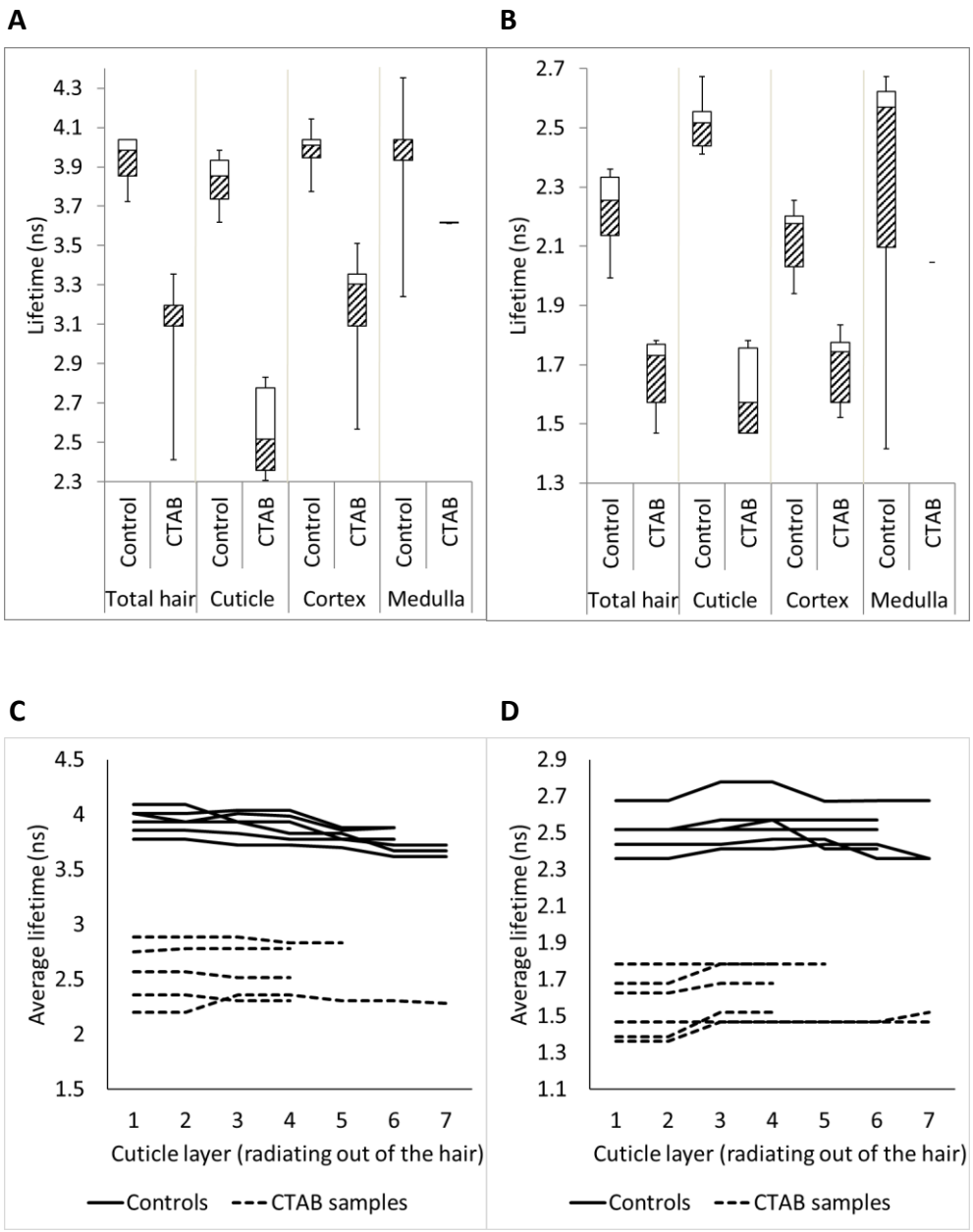

Fig. 4.24. Fluorescence lifetimes of hairs treated with the CTAB lipid extraction method. A) Box and whisker plot showing how the average lifetimes change after treatment, using 470nm excitation. B) Box and whisker plot showing how the average lifetimes change after treatment, using 640nm excitation. C) 470nm excitation of the cuticle showing how cuticle lifetime changes with cuticle layer after treatment. D) 640nm excitation of the cuticle showing how cuticle lifetime changes with cuticle layer after treatment. Control hairs (n=6), treated hairs 470nm (n=5), treated hairs 640nm (n=6).

A

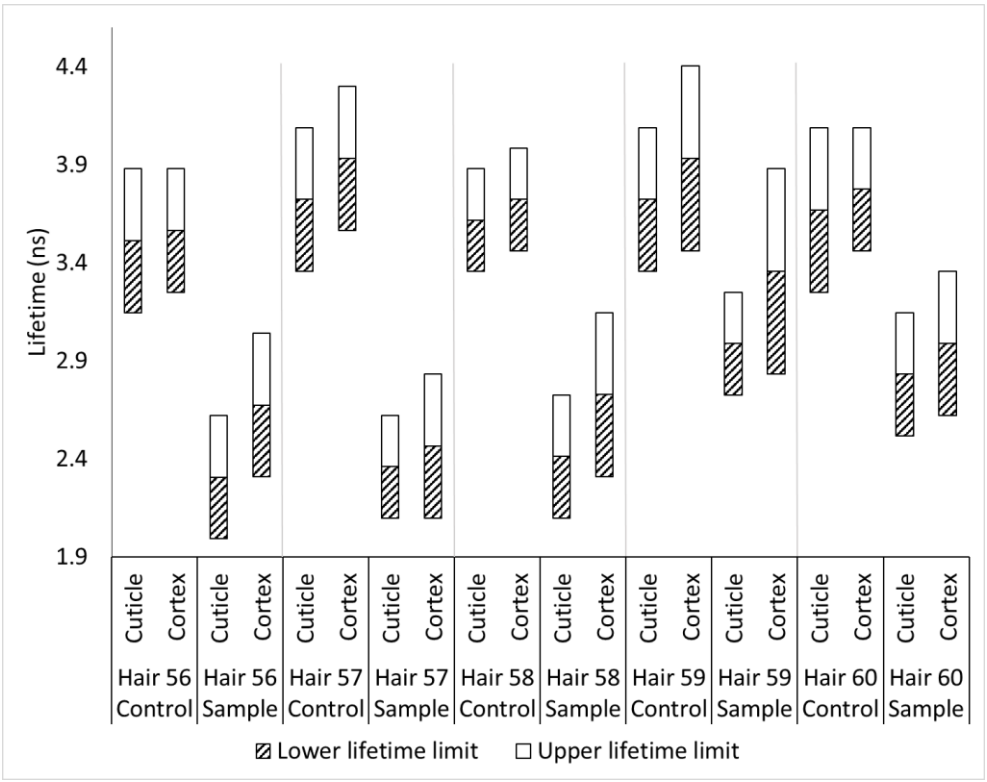
Lifetime (ns)
4.4
3.9
3.4
2.9
2.4
1.9
Cuticle
Cortex
Hair 56 Control
Hair 56 Sample
Hair 57 Control
Hair 57 Sample
Hair 58 Control
Hair 58 Sample
Hair 59 Control
Hair 59 Sample
Hair 60 Control
Hair 60 Sample
Lower lifetime limit
Upper lifetime limit

B

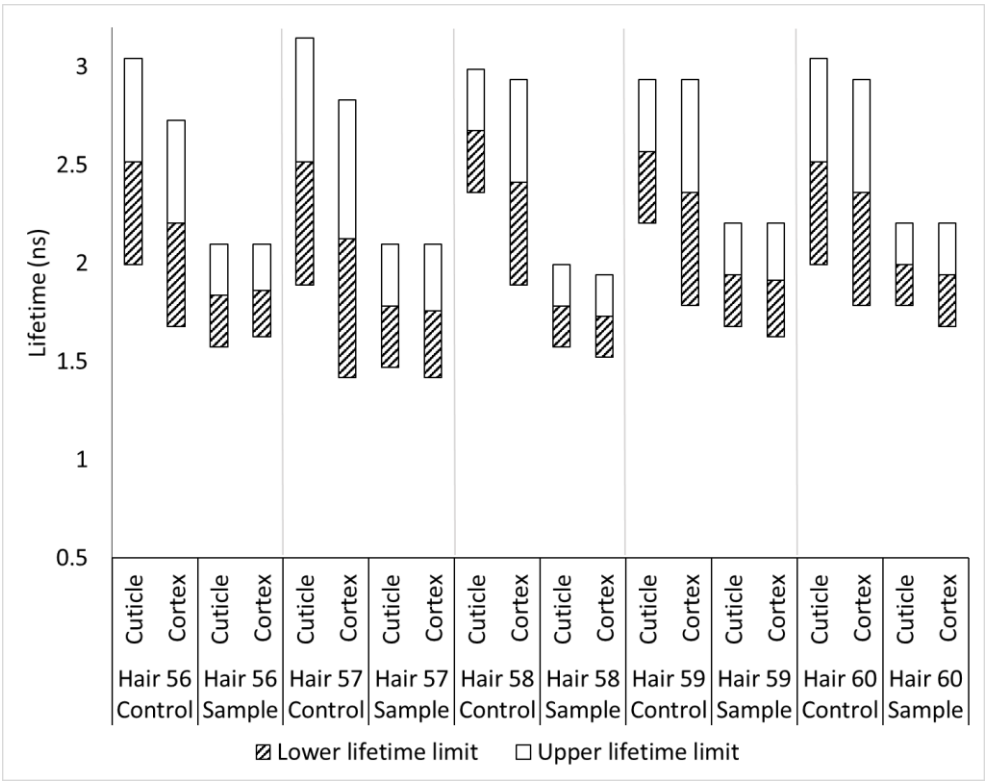
Lifetime (ns)
3
2.5
2
1.5
1
0.5
Cuticle
Cortex
Hair 56 Control
Hair 56 Sample
Hair 57 Control
Hair 57 Sample
Hair 58 Control
Hair 58 Sample
Hair 59 Control
Hair 59 Sample
Hair 60 Control
Hair 60 Sample
Lower lifetime limit
Upper lifetime limit

Fig. 4.25. Range of fluorescence lifetimes of paired control hair and sample hair treated with the CTAB lipid extraction method. Untreated control hairs and sample hairs treated with the CTAB lipid extraction method. A) Lifetimes of hair excited by 470nm, in longitudinal section, of paired controls compared to treated samples. B) Lifetimes of hair excited by 640nm, in longitudinal section, of paired controls compared to samples. Control hairs (n=5), treated hairs (n=5).

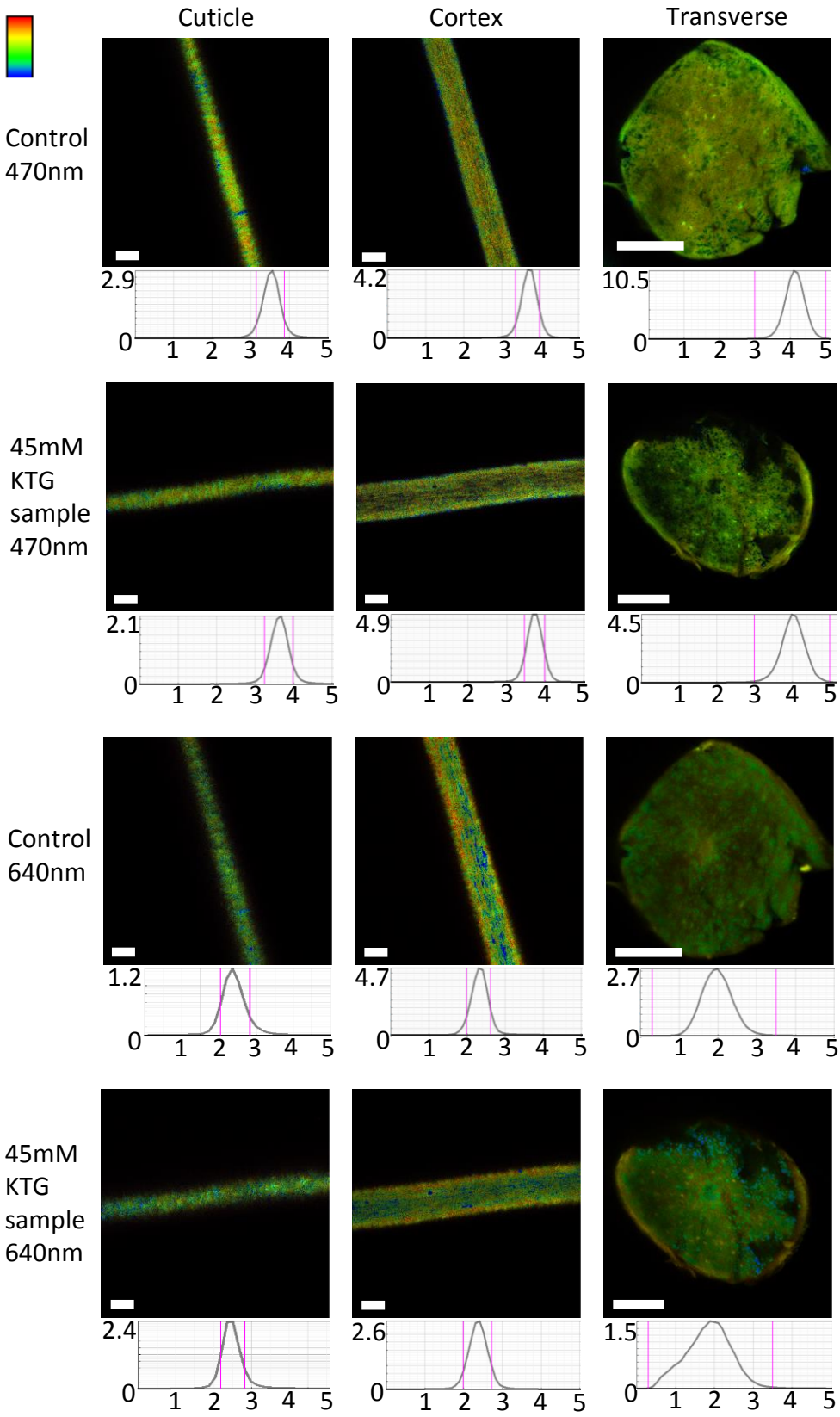
Cuticle
Cortex
Transverse
Control 470nm
45mM KTG sample 470nm
Control 640nm
45mM KTG sample 640nm
2.9
4.2
10.5
2.1
4.9
4.5
1.2
4.7
2.7
2.4
2.6
1.5
0
1 2 3 4 5

Fig. 4.26. FLIM images of hairs treated with 45mM potassium thioglycolate. Untreated control hairs and sample hairs treated with 45mM potassium thioglycolate (KTG). Longitudinal images show the same strand of hair which has been halved, with one half as a control and the other undergoing treatment, showing FLIM of the cuticle and cortex, as well as transverse sections of other hairs which have been coloured to the same scale, for 470nm and 640nm excitation. Each image also shows a graph of the frequency of lifetimes, x-axis = time (ns), y-axis = frequency (M.counts). Representative photomicrographs for 11 control and 11 treated imaged hairs are shown. N.B. The pink markers on the lifetime graphs indicate the upper (red) and lower (blue) lifetime limits. Scale bars = 25µm.

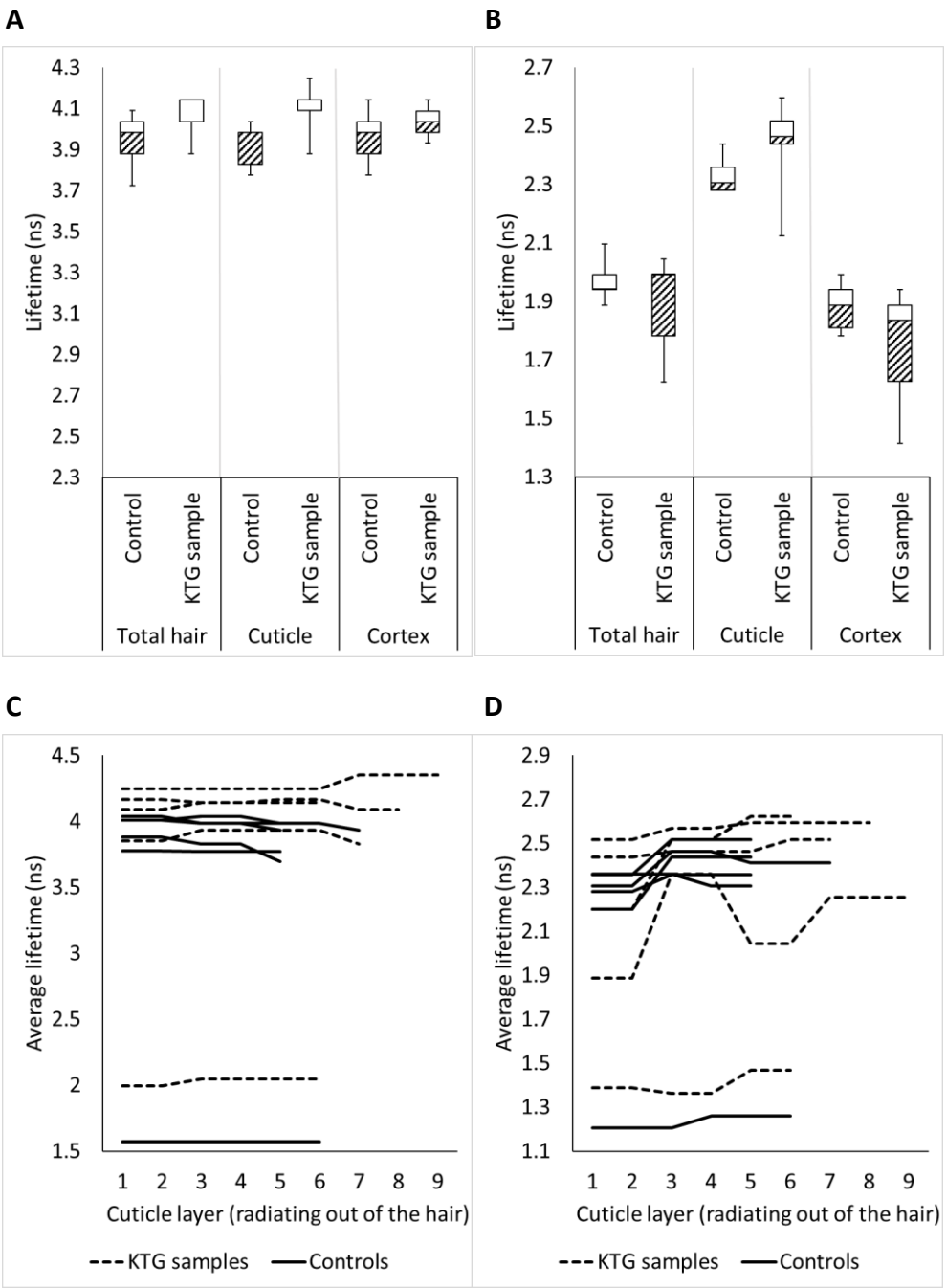

Fig. 4.27. Fluorescence lifetimes of hairs treated with 45mM potassium thioglycolate. A) Box and whisker plot showing how the average lifetimes change after treatment, using 470nm excitation. B) Box and whisker plot showing how the average lifetimes change after treatment, using 640nm excitation. C) 470nm excitation of the cuticle showing how cuticle lifetime changes with cuticle layer after treatment. D) 640nm excitation of the cuticle showing how cuticle lifetime changes with cuticle layer after treatment. Control hairs (n=6), treated hairs (n=6).

A

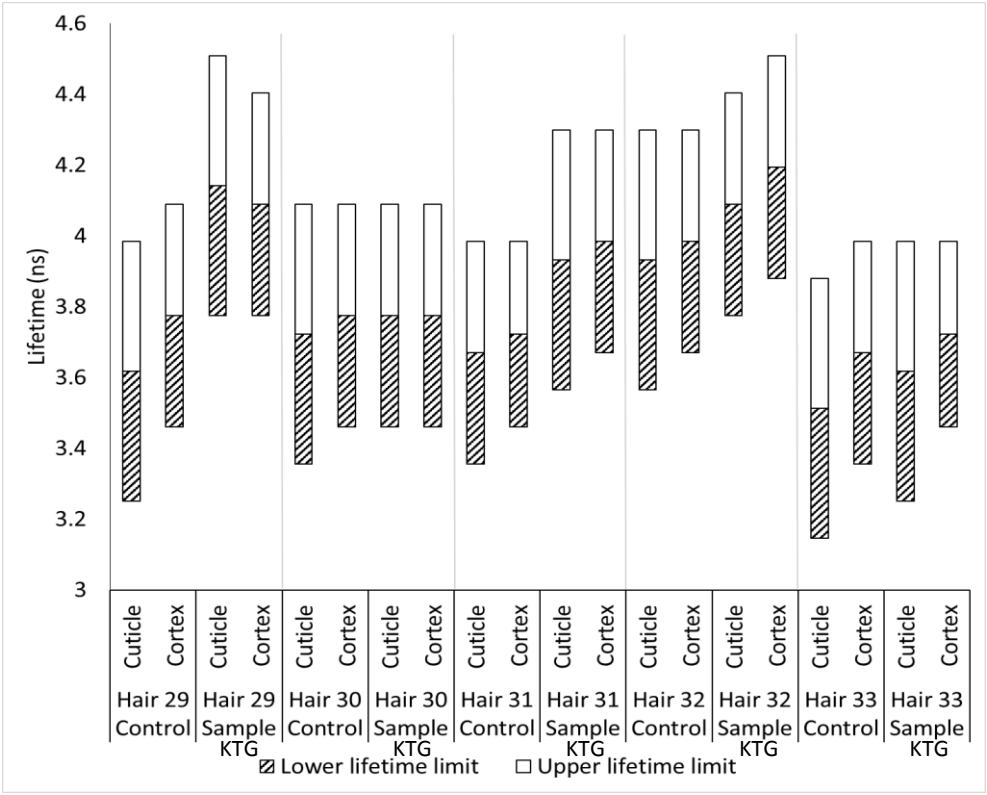
Lifetime (ns)
4.6
4.4
4.2
4
3.8
3.6
3.4
3.2
3
Cuticle
Cortex
Hair 29 Control
Hair 29 Sample KTG
Hair 30 Control
Hair 30 Sample KTG
Hair 31 Control
Hair 31 Sample KTG
Hair 32 Control
Hair 32 Sample KTG
Hair 33 Control
Hair 33 Sample KTG
Lower lifetime limit
Upper lifetime limit

B

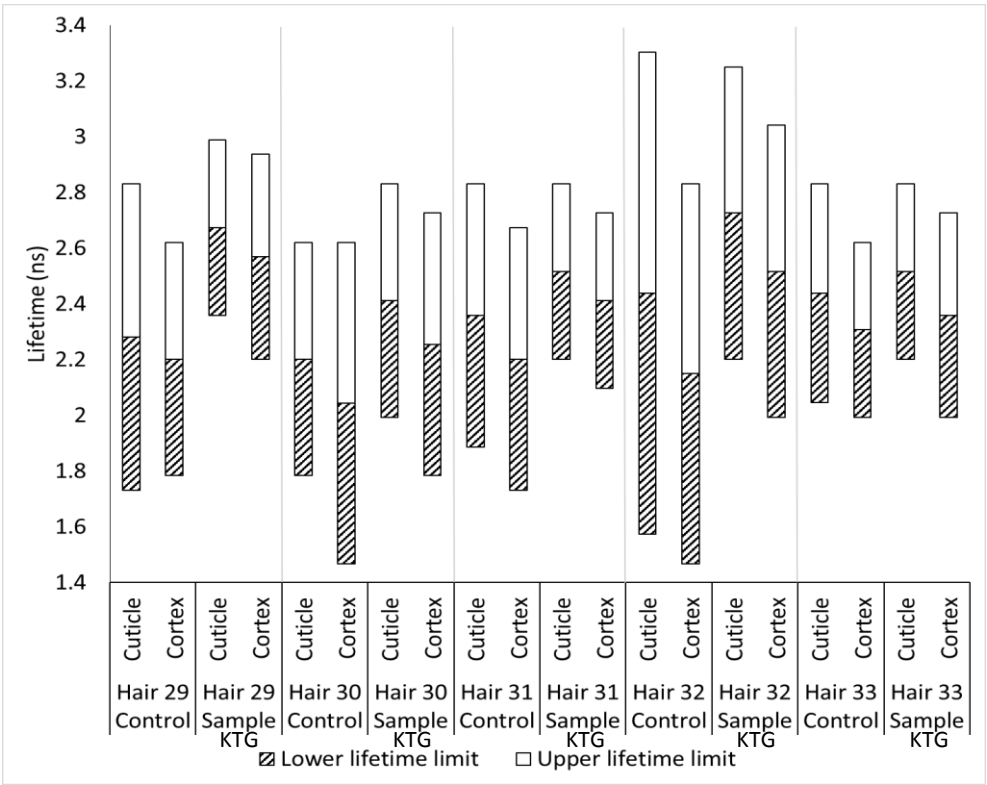
Lifetime (ns)
3.4
3.2
3
2.8
2.6
2.4
2.2
2
1.8
1.6
1.4
Cuticle
Cortex
Hair 29 Control
Hair 29 Sample KTG
Hair 30 Control
Hair 30 Sample KTG
Hair 31 Control
Hair 31 Sample KTG
Hair 32 Control
Hair 32 Sample KTG
Hair 33 Control
Hair 33 Sample KTG
Lower lifetime limit
Upper lifetime limit

Fig. 4.28. Range of fluorescence lifetimes of paired control hair and sample hair treated with 45mM Potassium thioglycolate. Untreated control hairs and sample hairs treated with 45mM potassium thioglycolate (KTG). A) Lifetimes of hair excited by 470nm, in longitudinal section, of paired controls compared to treated samples. B) Lifetimes of hair excited by 640nm, in longitudinal section, of paired controls compared to samples. Control hairs (n=5), treated hairs (n=5).

A

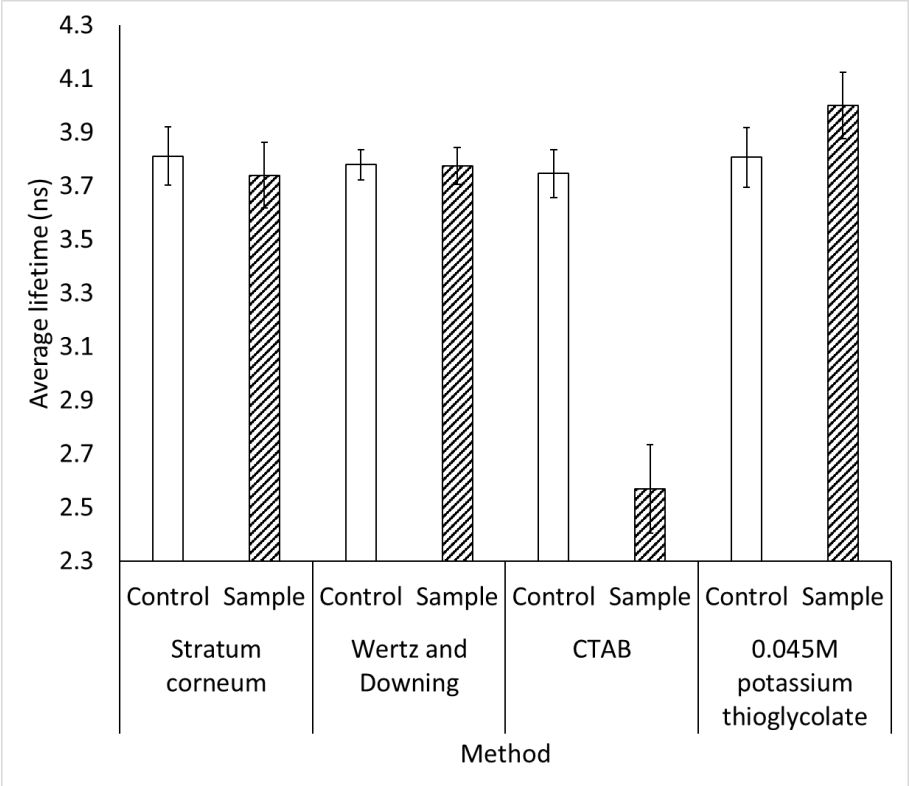
4.3
4.1
3.9
3.7
3.5
3.3
3.1
2.9
2.7
2.5
2.3
Average lifetime (ns)
Control Sample
Stratum corneum
Control Sample
Wertz and Downing
Control Sample
CTAB
Control Sample
0.045M potassium thioglycolate
Method

B

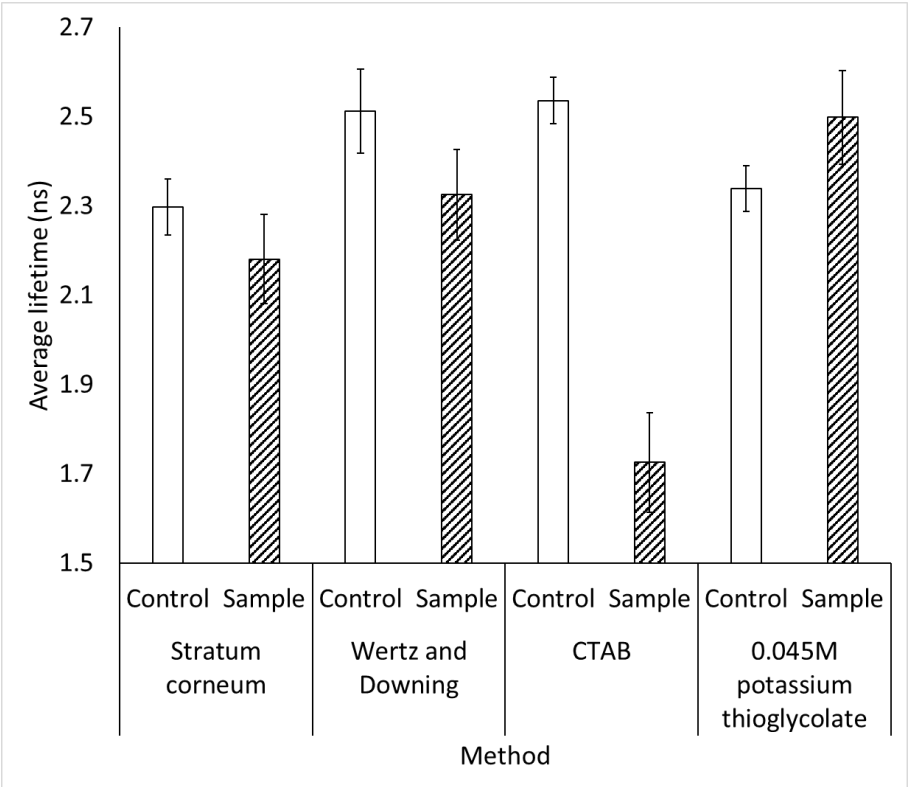
2.7
2.5
2.3
2.1
1.9
1.7
1.5
Average lifetime (ns)
Control Sample
Stratum corneum
Control Sample
Wertz and Downing
Control Sample
CTAB
Control Sample
0.045M potassium thioglycolate
Method

Fig. 4.29. Average lifetimes of the control and treated sample hair cuticles with each method. A) Hair excited with 470nm. B) Hair excited with 640nm. Each method examined 11 treated hairs and 11 control hairs. Error bars = +/- 2*SEM.

A

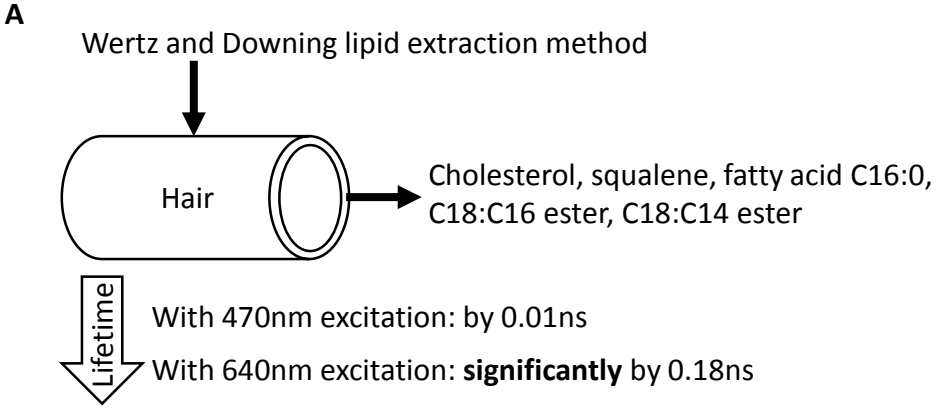
Wertz and Downing lipid extraction method
Hair
Cholesterol, squalene, fatty acid C16:0, C18:C16 ester, C18:C14 ester
Lifetime
With 470nm excitation: by 0.01ns
With 640nm excitation: **significantly** by 0.18ns

B

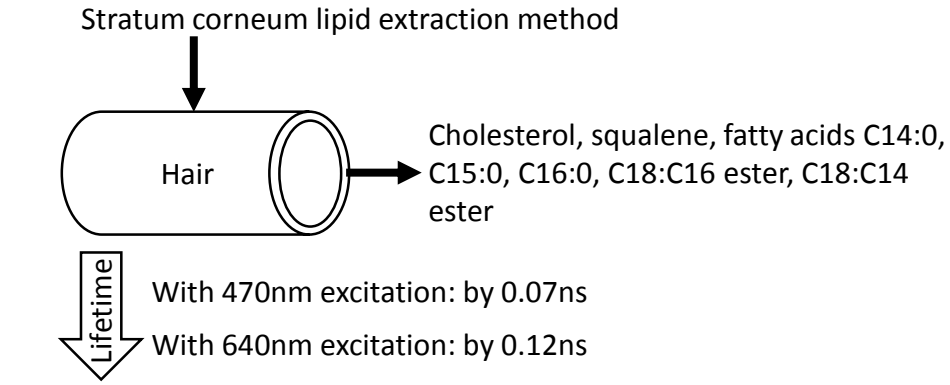
Stratum corneum lipid extraction method
Hair
Cholesterol, squalene, fatty acids C14:0, C15:0, C16:0, C18:C16 ester, C18:C14 ester
Lifetime
With 470nm excitation: by 0.07ns
With 640nm excitation: by 0.12ns

C

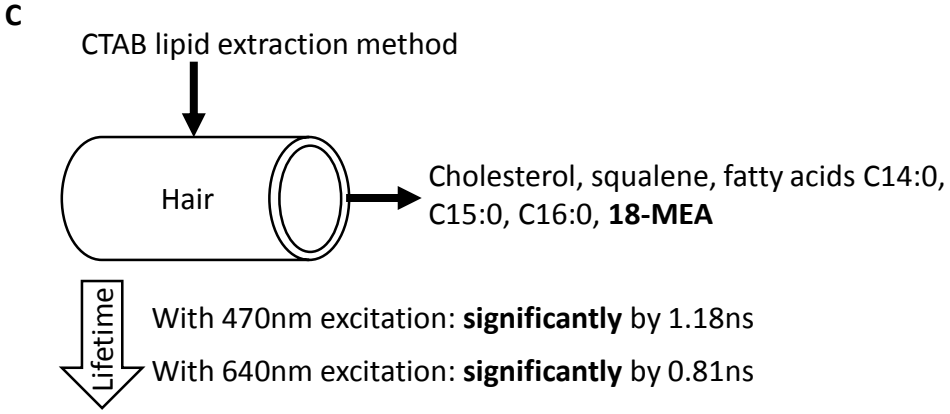
CTAB lipid extraction method
Hair
Cholesterol, squalene, fatty acids C14:0, C15:0, C16:0, **18-MEA**
Lifetime
With 470nm excitation: **significantly** by 1.18ns
With 640nm excitation: **significantly** by 0.81ns

D

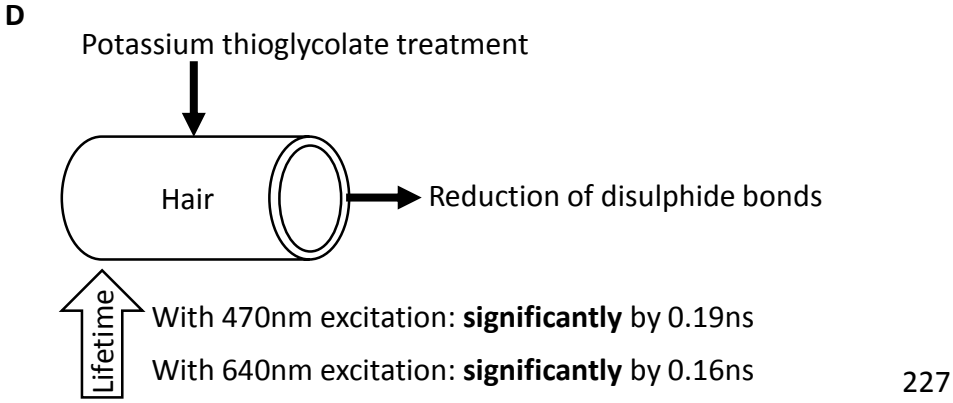
Potassium thioglycolate treatment
Hair
Reduction of disulphide bonds
Lifetime
With 470nm excitation: **significantly** by 0.19ns
With 640nm excitation: **significantly** by 0.16ns

Fig. 4.30. Summary of the treatments to elucidate the multiple cuticle lifetimes with the main extractions and the effect upon lifetime. A) Wertz and Downing lipid extraction method. B) Stratum corneum lipid extraction method. C) CTAB lipid extraction method. D) Potassium thioglycolate treatment method.

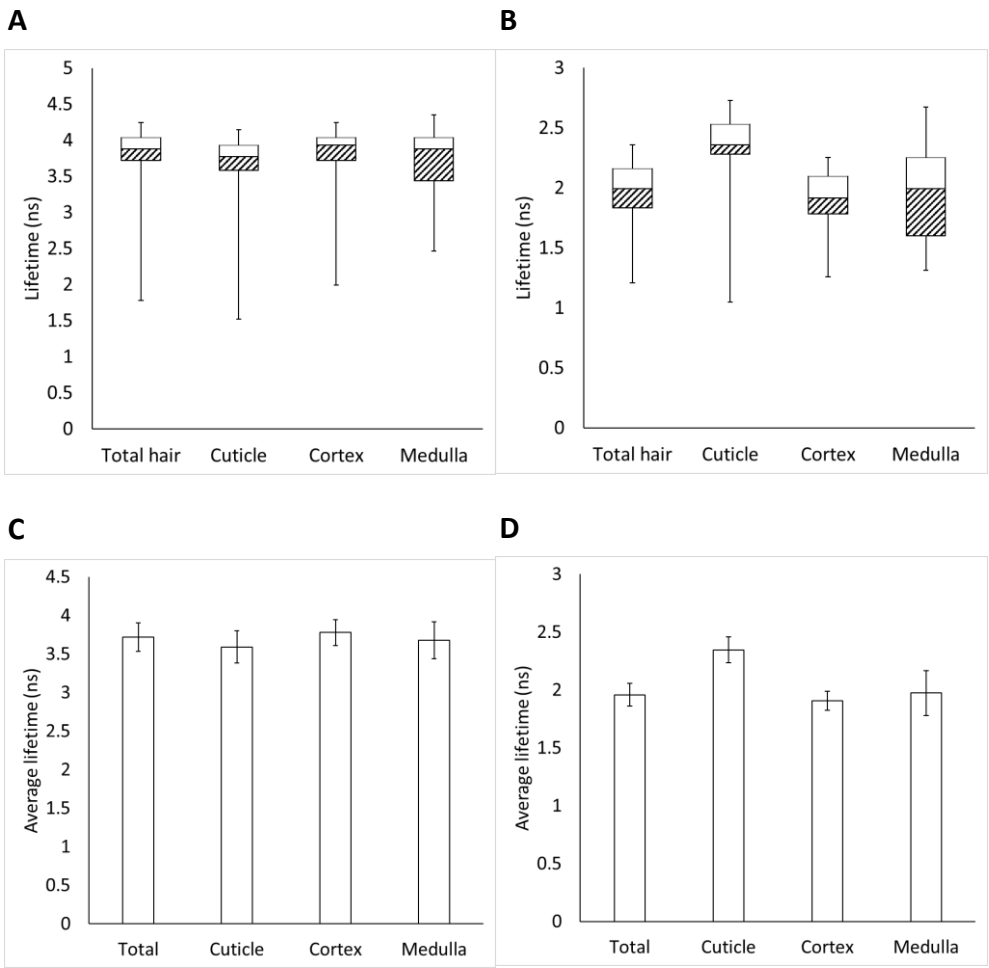

Fig. 4.31. Fluorescence lifetimes of the cuticle, cortex and medulla of untreated Chinese scalp hair. A) Box and whisker plot of hair excited with 470nm (n=38). B) Box and whisker plot of hair excited with 640nm (n=36). C) Average lifetimes of hair excited with 470nm (n=38). D) Average lifetimes of hair excited with 640nm (n=36). Error bars = +/- 2*SEM.

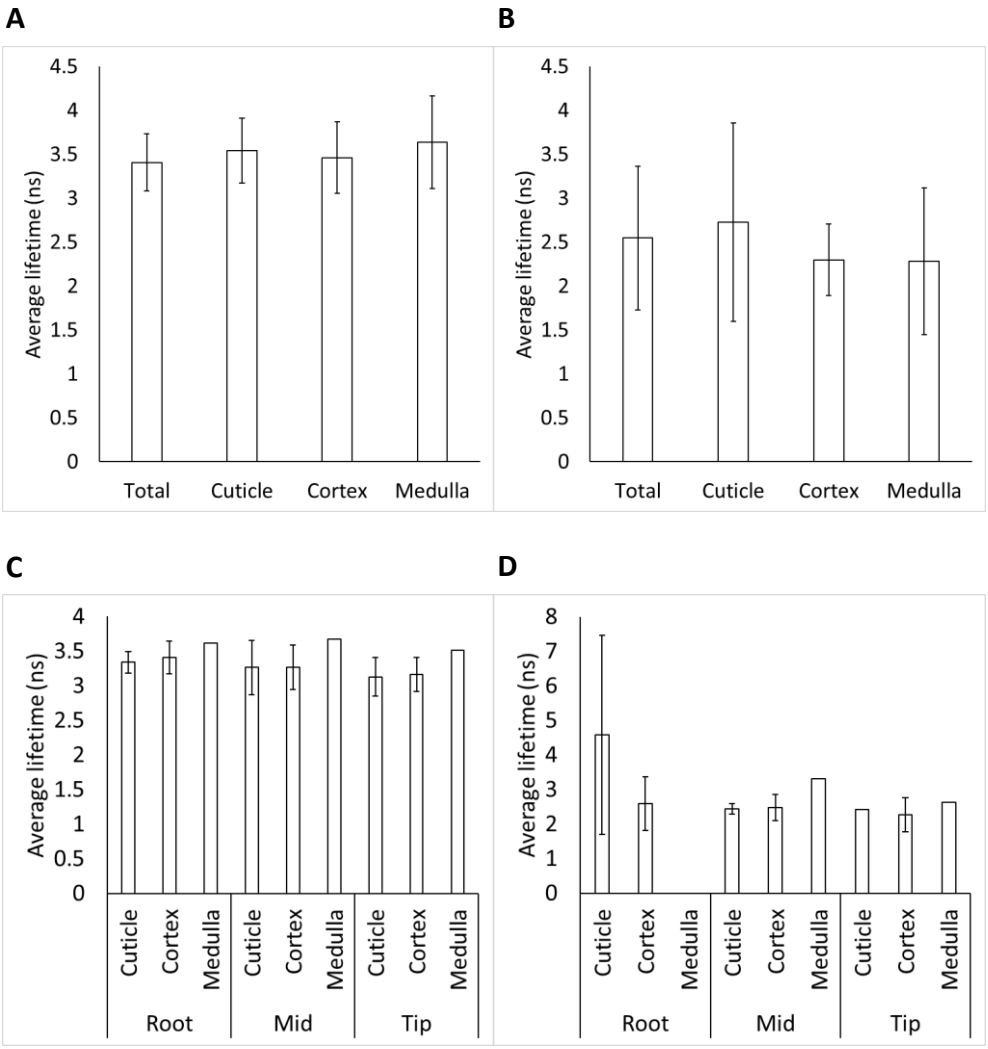

Fig. 4.32. Fluorescence lifetimes of untreated beard hair. A) Average lifetimes of beard hair excited with 470nm (n=4). B) Average lifetimes of beard hair excited with 640nm (n=4). C) Average lifetimes of the root, mid-section and distal tip of 470nm excited beard hair (n=2). D) Average lifetimes of the root, mid-section and distal tip of 640nm excited beard hair (n=2). Error bars = +/- 2*SEM.

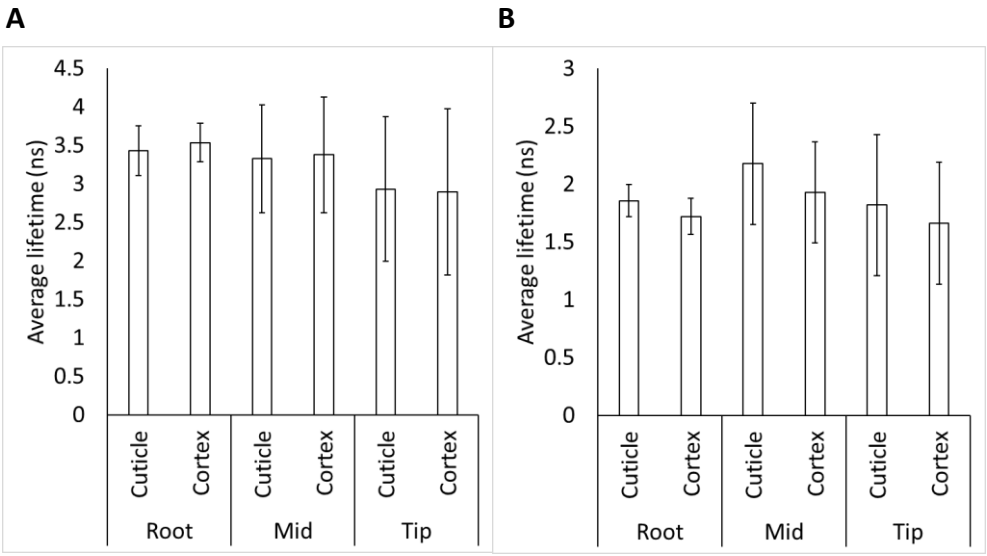

Fig. 4.33. Fluorescence lifetimes of the root, mid-section and distal tip of plucked scalp hair. A) Hair excited with 470nm (n=5). B) Hair excited with 640nm (n=5). Error bars = +/- 2*SEM.

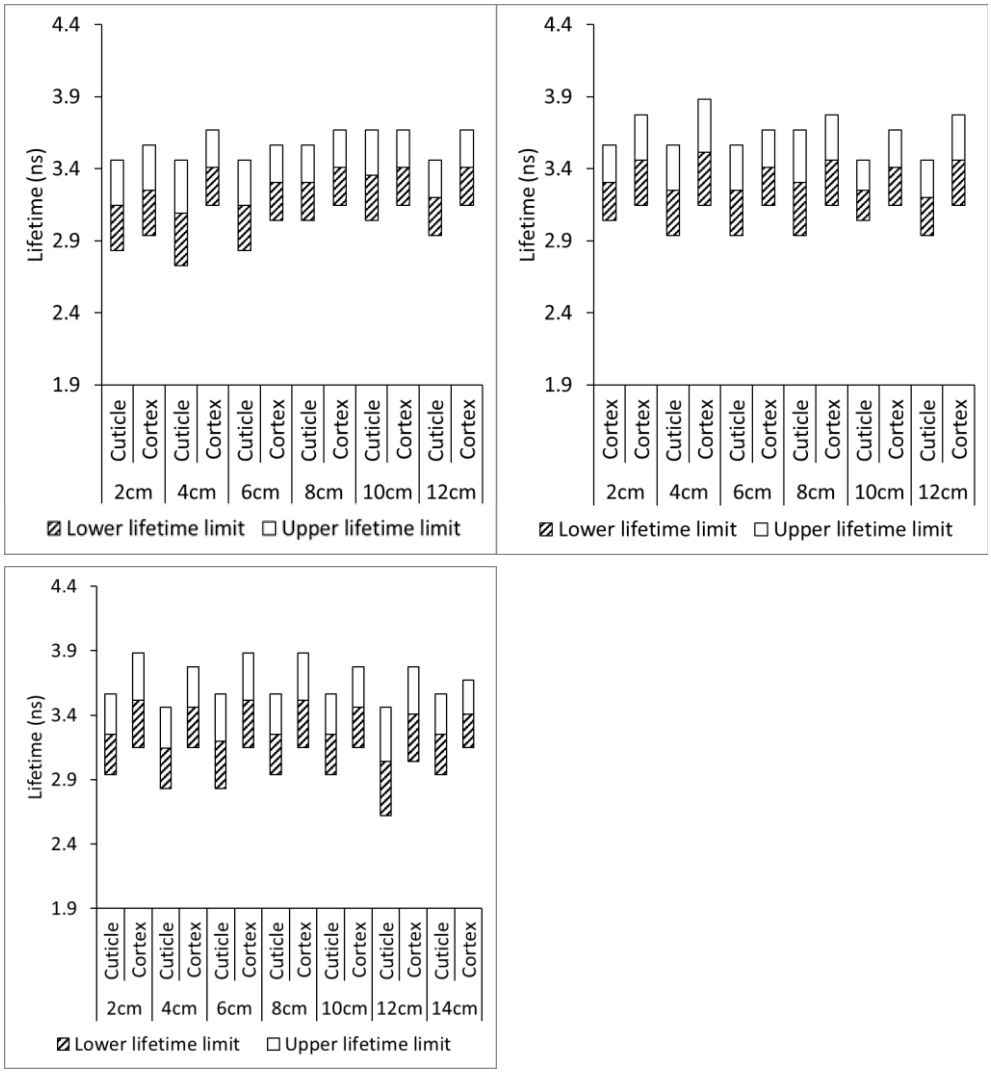

Fig. 4.34. Fluorescence lifetime changes along the hair length of 3 hairs excited with 470nm. The range of lifetimes from the cuticle and cortex of each hair, taken at 2cm intervals.

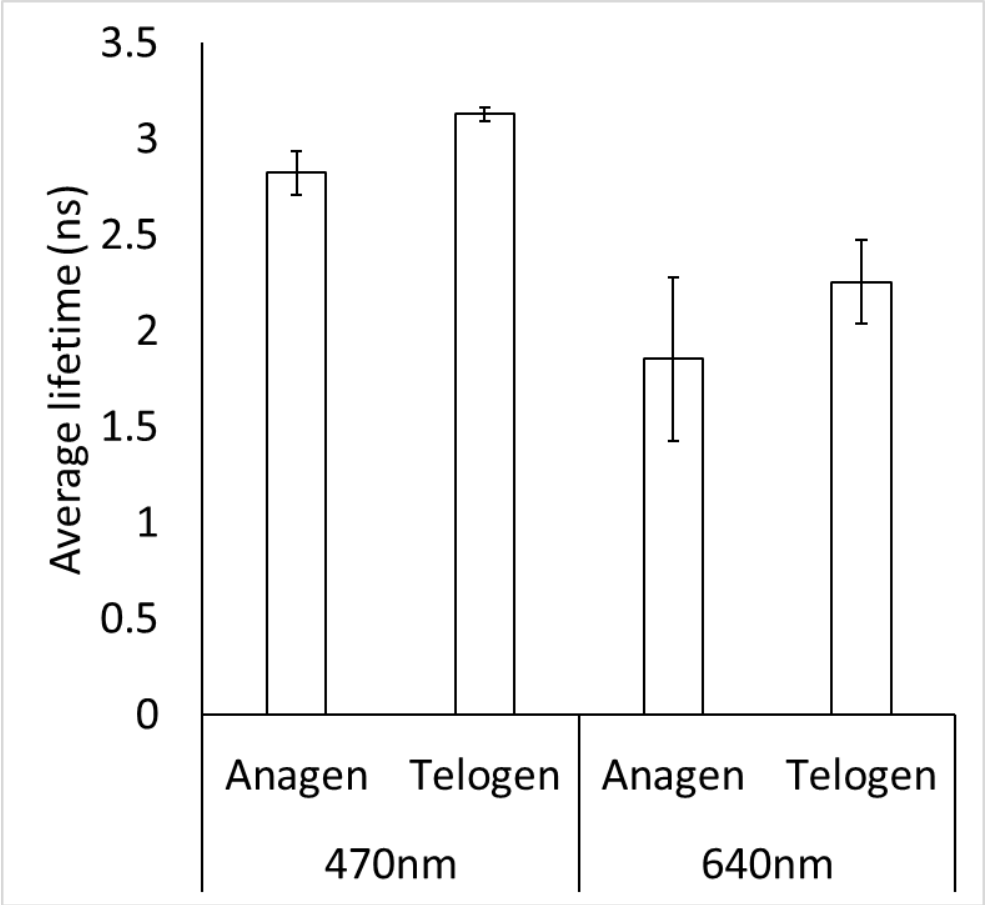

Fig. 4.35. Fluorescence lifetime differences with the hair cycle. Average lifetimes of the hair emerging from the matrix of anagen (n=3) and telogen (n=3) hairs. Error bars = +/- 2*SEM.

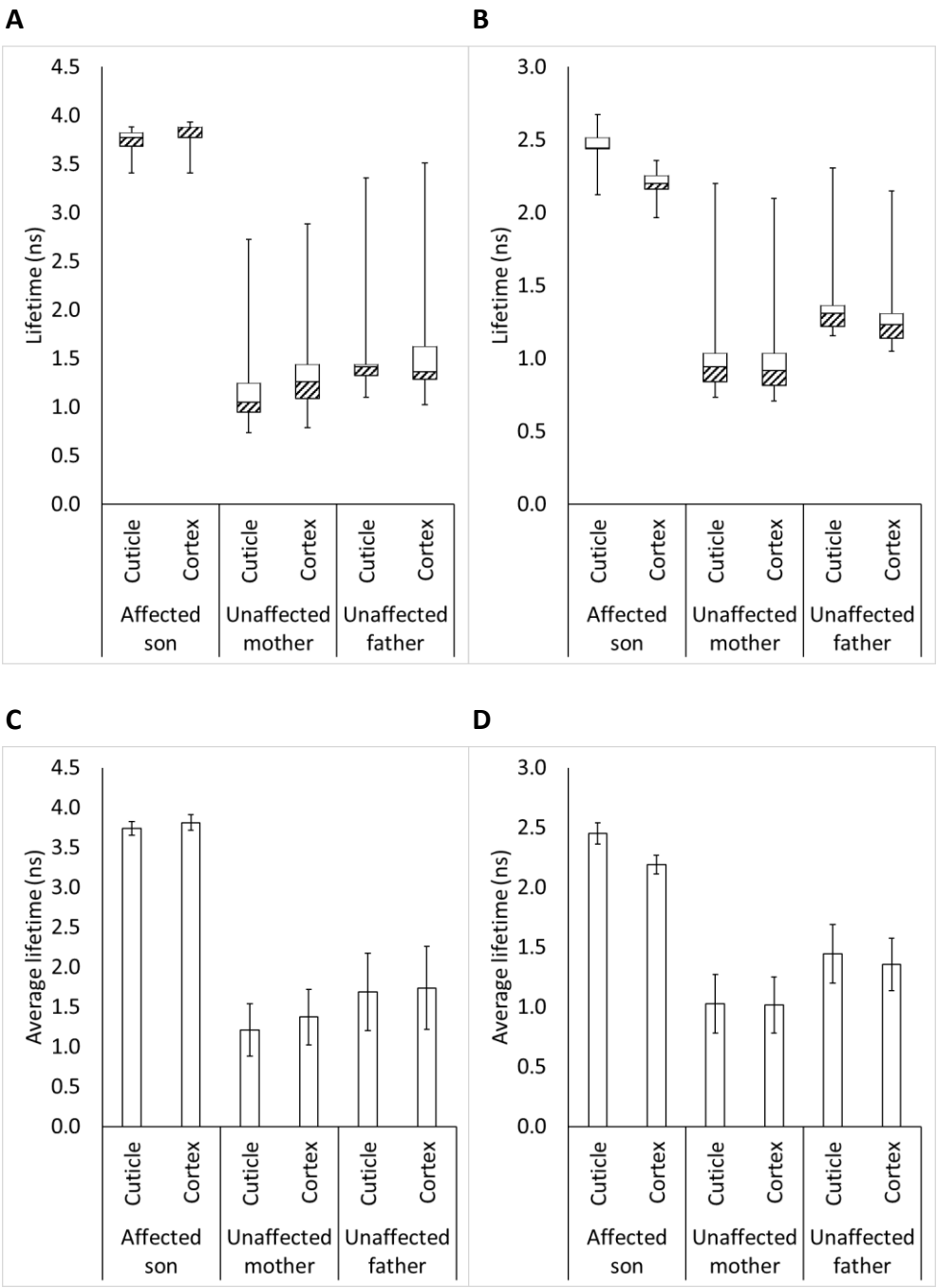

Fig. 4.36. Fluorescence lifetimes of hair from the affected son with the uncharacterised hair and skin disorder, and his unaffected parents as controls. A) Box and whisker plot of 470nm excited hair. B) Box and whisker plot of 640nm excited hair. C) Average lifetimes of 470nm excited hair. D) Average lifetimes of 640nm excited hair. Affected son (n=10), unaffected mother (n=11) and unaffected father (n=11). Error bars = +/- 2*SEM.

Chapter 5

Elucidation of morphological and structural changes in hair caused by chemical hair modification

5.1. Introduction

5.1.1. Chemical depilation

Chemical hair modification refers to the action of chemical depilatory treatments to change the structure and morphology of the hair. Commercial chemical depilatory treatments include Sally Hansen Facial Depilatory (Coty) and Veet HydroRestor (Reckitt Benckiser) which, like the majority of modern chemical depilatories, are based on thioglycolic acid (fig. 5.1A) as calcium thioglycolate and potassium thioglycolate respectively. It is important for the consumer for depilatories to have a short application time, and as such the treatments above are designed to break down the structure of the hair within four minutes.

In this project the investigation into chemical depilatories is for hair removal purposes, though at lower pH and concentrations thioglycolate is also used for permanent hair waving. Hair removal may be required for many purposes, from cosmetics to treatment of hair disorders. With regards to hair disorders, patients troubled by hirsutism often use thioglycolate to temporarily relieve them of their symptoms (Richards *et al*., 1990; Fisher *et al*., 2006), and thioglycolate has been used as a therapy for pseudofolliculitis barbae for a more comfortable alternative to shaving (Bridgeman-Shah, 2004; Ribera *et al*., 2010). Thioglycolate is also used to treat hair tourniquet syndrome, wherein hair has wrapped itself around a digit or other extremity and caused oedema (Quinn, 1971; Alruwaili *et al*., 2015). Interestingly, it has been found that using thioglycolate to remove the hair of diabetic rats increases the absorption of insulin into the skin (Zakzewski *et al.*, 1998; Kanikkannan *et al*., 1999; Rastogi and Singh, 2003). Thioglycolate has also been found to enhance the rate of drug penetration through the human stratum corneum (Lee *et al*., 2008). As rats have a higher follicular density than humans, the insulin may be entering the skin through the transfollicular route. However, in human skin the route is more likely to be transepidermal. The enhanced skin permeability is thought to occur through the impairment of the barrier function of the epidermis via changes to the secondary structure of proteins, reducing the disulphide bonds, and disruption of lipid hydrocarbons from the stratum corneum with disordering of the lamellar packing (Wahlberg, 1972; Suhonen *et al*., 1999; Rastogi and Singh, 2003; Lee *et al*., 2008). Although this finding benefits insulin delivery and may have implications for other

percutaneous absorption studies, the use of depilatories in the general public could assist in greater penetration of toxic substances through the skin of the product consumers.

The use of thioglycolate as a depilatory has caused some cases of irritation of the skin at the area of application, which may not be surprising since it impairs the barrier function of the stratum corneum. In the case of thioglycolate being used as a treatment for hair tourniquet syndrome, it would be important not to cause more irritation to already swollen and inflamed tissue. Chemical burns have been caused when instructions have not been followed and the depilatory has been kept on the skin for too long, and when the depilatory has breached the epidermis, such as where hairs have been pulled out during thioglycolate application (Haque and Al-Ghazal, 2004). People with sensitive skin have reported irritation ranging from slight to moderate stinging, burning, and itching after the application of thioglycolate (Hahn, 1999; Moghimi *et al*., 2013). There are also some reported preferences to shaving than depilation due to irritation (Kindred *et al*., 2011). This shows that there is a need to reduce the irritation caused by thioglycolate depilatories.

Thioglycolate works as a depilatory by reducing the disulphide bonds in the KIFs and KAPs mainly in the hair cortex. Thioglycolate acts as a nucleophile and in an equilibrium reaction attacks the cystine in the KIFs and KAPs, converting it to cysteine (Wolfram and Underwood, 1966; Zabashta *et al*., 2012). A swelling of the hair up to 150% has been reported from this process, which is firstly due to the reduction of the disulphide bonds, and then the hair swells further from the penetration of water, completing the process within ten minutes (Reed *et al*., 1946; Powers and Barnett, 1952; Jachowicz and McMullen, 2011). Water alone would only account for a swelling of 10% in diameter and 1-2% longitudinally as the hydration breaks the hydrogen bonds and electrostatic bonds in the keratin (Corbett, 1976; Xiao and Hu, 2016). Along with keratin deformation, it was found that the CMC was partly solubilised during thioglycolate treatment (Chao *et al*., 1979; Strussman, 1983; Zahn *et al*., 1986). These studies show that thioglycolate is an effective depilatory yet it is evident that exposure to thioglycolate of living cell layers under the stratum corneum can cause cell death and tissue damage.

5.1.2. Skin structure and barrier function

The skin is an important organ, serving as a protective barrier against the external environment and is involved in homeostasis, mechanical integrity, water impermeability, metabolic processes, thermoregulation, and is the first line of defence against pathogens and chemical irritants (Candi *et al*., 2005; Segre, 2006; Pan *et al*., 2015). The skin is composed of the dermis and the epidermis; the epidermis taking the principal role in barrier function, and the innervated dermis supplying the epidermis with nutrients from the fibroblasts and its blood supply. In this study the epidermis is the focus as it is the protective barrier between the body and the depilatory treatment.

The epidermis consists of four main layers of cells (fig. 5.1B): the stratum basale, the stratum spinosum, the stratum granulosum and the stratum corneum. The living cell layers underneath the stratum corneum are 50-100µm thick, with the terminally differentiated stratum corneum at the skin surface forming the barrier. These cells are shed and continuously replaced by the cells in the basal layer which produce transit amplifying daughter cells. The progeny of the transit amplifying cells withdraw from the cell cycle and begin to differentiate and continue to do so as they migrate towards the skin surface, eventually becoming flattened and aneuclear cornified envelopes (Niemann and Watt, 2002; Blanpain and Fuchs, 2006; Watt *et al*., 2006). The stratum basale contains the epidermal stem cell niche (Jones, 1995; Jensen *et al*., 1999; Evans *et al*., 2013; Peng *et al*., 2015), and is usually only one cell thick (Brody, 1962; Fuchs, 2008). In the stratum spinosum, cells appear more cuboidal in shape (Elias and Friend, 1975). In the stratum granulosum, with differentiation the nuclei become more oval and less circular in shape, cells begin to flatten, and contain granules 0.2-0.3µm in diameter (Elias and Friend, 1975; Simpson *et al*., 2011). These are keratohyalin granules and are mainly composed of profilaggrin, which is insoluble, rich in histidine, and the precursor to filaggrin. Profilaggrin is proteolytically cleaved to filaggrin repeat units which bundle keratins during terminal differentiation of the keratinocytes (Rawlings and Harding, 2004; Cabanillas and Novak, 2016). The stratum corneum consists of 15-20 layers of corneocytes connected by corneodesmosomes, arranged more loosely closer to the surface (Skerrow *et al.,* 1989; Serre *et al*., 1991; Jarnik *et al*., 1998; Simpson *et al*., 2011). Corneocytes are without organelles and filled with keratin and water, surrounded by an insoluble cornified envelope of densely transglutaminase cross-linked proteins (Rice and Green, 1977; Nemes and Steinert, 1999; Simpson *et al*., 2011). The lipid-rich intercellular

matrix forms the hydrophobic barrier to the environment and is covalently linked to the cells, consisting mainly of long chain ceramides, free fatty acids and cholesterol which are organised into two crystalline lamellar phases (Ponec *et al*., 1988; Wertz and Downing, 1991; Hatta *et al*., 2006).

In this study the differentiation, proliferation, and acute stress response of HaCaT cells in 2D culture and HEKn cells forming a 3D epidermal model were tested after application of depilatory chemicals. This was tested through measuring levels of involucrin, keratin 14, Ki67, HSP27 and HSP70.

Involucrin has been found to be an early indicator of keratinocyte cornified envelope differentiation and part of the initial scaffold for cornified envelope assembly as it is the main substrate for the attachment of ceramides by ester linkages by transglutaminase to the cornified envelope (Steinert and Marekov, 1997; Marekov and Steinert, 1998; Steinert and Marekov, 1999; Sevilla *et al*., 2007; Simpson *et al*., 2011).

Keratin 14 is a type I keratin expressed in all basal cells, and transcription is gradually downregulated in favour of other keratins as the keratinocytes differentiate (Fuchs and Green, 1980; Moll *et al*., 1982; Fuchs, 2008). Ki67 is also expressed in the mitotically active basal cells, and was used to test the effect of the depilatories upon proliferation. Cells which were mitotic were stained brightly, and Ki67 could also indicate cells which were in S-phase from the speckled staining (Van Dierendonck *et al*., 1989; Manoir *et al*., 1991; Zambon, 2011).

Heat shock proteins (HSPs) are a highly conserved family of molecular chaperones with the role of assisting in the folding, assembly, maintenance and degradation of proteins, and become upregulated in response to stress, such as heat, oxidative stress, and inflammation (Bukau *et al*., 2006; Liberek *et al*., 2008; Yusuf *et al*., 2009). Stress to cells is believed to be moderated by HSPs through modulating JNK activation and other intracellular signal transduction pathways (Mosser *et al*., 2000). HSP27 and HSP70 are both investigated in this study in their response to depilatory treatment; HSP27 is found at high levels in the epidermis, and HSP70 is constitutively expressed in the epidermis and dermis (Huang *et al*., 2003; Yusuf *et al*., 2009). HSP27 has been shown to protect against protein aggregation caused by stress and is ATP-independent (Macario and Conway de Macario, 2007). In normal skin, HSP27 is upregulated and phosphorylated in the late phase of keratinocyte differentiation in the stratum spinosum and granulosum,

after which it becomes involved in barrier function as it interacts as a chaperone with involucrin in the cornified envelope (Gandour-Edwards, *et al*., 1994; Trautinger, *et al*., 1995; Jonak *et al*., 2002; Robitaille *et al*., 2010). HSP70 has been shown to assist in protein folding and is ATP-dependent (Macario and Conway de Macario, 2007).

Cellular stress leads to JNK activation and can precede apoptosis (fig. 5.1C). Pharmacological manipulation of a stress signalling pathway by inhibiting JNK, with the drug SP600125, leads to accelerated differentiation in epidermal keratinocytes (Gazel *et al*., 2006; Koehler *et al*., 2011). The JNK inhibitor II, SP600125, was designed to be a reversible, competitive inhibitor of cJun N-terminal kinase (JNK) with regard to ATP, and selectively inhibits all three forms of JNK (Bennett *et al*., 2001). In this investigation the hypothesis that chemical stress from depilatory treatments also leads to an increase in the rate of differentiation in order to rapidly clear away the damaged cells was tested. The effect of inhibiting JNK in 2D and 3D cultures treated with depilatory chemicals was also investigated with respect to differentiation, proliferation, apoptosis, and the heat shock protein response.

5.1.3. Aims of the study

The aims of this study were to find a depilatory chemical with equal or greater effectiveness at hair removal than the current best-on-market depilatories, and one that is less irritating to the skin. This was done by characterising the structural and morphological changes in the hairs from commercially available and experimental depilatory treatments. This has not previously been explored using label-free imaging with confocal microscopy, FLIM or time-lapse imaging. These techniques along with the novel methods developed in this study provided new approaches to elucidate the structural and morphological effects of the chemical depilatories on the hair.

With regards to the skin work, it has been found that manipulation of stress signalling accelerates differentiation (Maatta group, unpublished data); leading to the hypothesis that chemical stress from the depilatory chemicals also leads to an increase in the rate of differentiation in order to rapidly clear away the damaged cells and has consequent effects on cell proliferation and the acute stress response. The pathway through which cellular stress leads to increased differentiation is unknown; one possible pathway which may be involved is through JNK signalling. Cellular stress leads to JNK activation and can precede apoptosis (fig. 5.1C), and pharmacological manipulation of a stress

signalling pathway by inhibiting JNK has been shown to lead to accelerated differentiation in epidermal keratinocytes (Gazel *et al*., 2006; Koehler *et al*., 2011). The most efficacious depilatory chemicals were tested on HaCaT cells in 2D culture and on primary keratinocytes in a 3D epidermal model, and analysed using immunofluorescence, immunoblotting, and H&E staining. A JNK inhibitor was used to act as a positive control in order to accelerate differentiation, and in conjunction with the depilatory chemicals to see how this would change the keratinocyte responses. The effects of these hair depilatory chemicals on keratinocytes have not been previously studied, so the aim was to understand their effects on proliferation, differentiation and cell death in order to discover if these processes could play a part in the irritation caused by the hair depilatory chemicals.

5.2. Experimental approach

Hairs were treated with a variety of chemicals, either commercially available or experimentally developed. Many of those developed by P&G begin with “CHM” which stands for “chemical hair modification”. CHM1 and CHM2 are commercially available, the rest are experimental treatments. All the shown images are representative examples of the samples.

5.2.1. Hydration

Measurements were taken from four untreated Chinese scalp hairs at the widest point of the hair before hydration and after 10 minutes of hydration. The rate of swelling of three separate hairs was measured by P&G. In a separate study of the amount of swelling due to hydration above and below the skin interface, four plucked Caucasian scalp hairs were measured at the widest point of the hair before hydration and after 10 minutes of hydration. Measurements of the hair below the skin interface were taken where the hair is free of the bulb and curling back of the cuticle cells is present. The measurements above the skin interface were taken towards the distal tip of the hair.

5.2.2. Calcium thioglycolate (CHM1) and potassium thioglycolate (CHM2)

For CHM1, FLIM images were taken of six treated hairs transversely and three hairs longitudinally. For CHM2, FLIM images were taken of three treated hairs transversely and five hairs longitudinally. SEM and TEM images were taken of three treated Chinese scalp hairs. For hairs stained with AlexaFluor 633 C_5 maleimide, longitudinal imaging was not effective as the maleimide was unable to penetrate through the hair. However, imaging of hair transversely when the hair was stained after it had been cut was successful in showing the extent of the attack on the disulphide bridges in the keratin of treated hair. Six hairs were stained with the maleimide and imaged transversely. Six hairs were imaged dynamically with 0.45M potassium thioglycolate over 10 minutes. Percentage change of the hair width was taken by measuring the diameter of the hair before and after treatment.

5.2.3. Potassium thioglycolate and guanidine carbonate (CHM3)

FLIM images were taken of two hairs longitudinally and five hairs transversely. SEM and TEM images were taken of three treated Chinese scalp hairs. Four hairs were stained with AlexaFluor 633 C_5 maleimide and imaged transversely. Five hairs were imaged

dynamically with 0.45M potassium thioglycolate over 10 minutes. For the relative humidity experiment, nine potassium thioglycolate and guanidine treated Chinese scalp hairs were taken and placed in water (n=3), a controlled 70% relative humidity environment (n=3), or left at ambient humidity (n=3) for 18h at room temperature. Once removed from these conditions they were immediately placed in oil and imaged. Four hairs were imaged during 10 minutes of hydration with DI water, and images shown at 0, 1 and 10 minutes as the most expansion occurs between 0 and 2 minutes of hydration.

5.2.4. Guanidine carbonate pH12.5 (CHM4) and pH11.4 (CHM5)

FLIM images were taken of two hairs longitudinally and six hairs transversely. SEM and TEM images were taken of three treated Chinese scalp hairs. Six hairs were stained with AlexaFluor 633 C_5 maleimide and imaged transversely. Five hairs were imaged dynamically with 0.44M guanidine carbonate over 10 minutes. Four hairs were imaged during 10 minutes of hydration with DI water.

5.2.5. Lithium bromide (CHM22-25)

Spectral scans with nine laser lines were carried out on lithium bromide treated hairs in transverse section and averaged to produce emission spectra. Treatment was done under different temperatures for varying amounts of time. CHM22 = LiBr treatment at 25°C for 20 minutes. CHM23 = LiBr treatment at 85°C for 20 minutes. CHM24 = LiBr treatment at 25°C for 5 minutes. CHM25 = LiBr treatment at 25°C for 5 days. FLIM images were taken of six hairs transversely from each treatment.

5.2.6. CaI_2 + SLS

Confocal images were taken of three hairs treated with 28% SLS alone, and ten hairs treated with 25% calcium iodide and 2% SLS imaged longitudinally and six hairs imaged transversely. FLIM images were taken using 470nm of five hairs longitudinally and six hairs transversely.

5.2.7. CTAB + SLS

Confocal images were taken of six hairs longitudinally and five hairs transversely. FLIM images were taken of five hairs longitudinally and five hairs transversely.

5.2.8. HaCaT immunoblotting

Each experiment was repeated three times, actin and glyceraldehyde 3-phosphate dehydrogenase (GAPDH) were used as loading controls as β-tubulin amounts varied

across the samples. No extra bands were apparent on the blots except for the involucrin blot where the extra bands may have been due to secondary antibody polyclonal non-specificity. Only the bands at the correct molecular weight for involucrin (120kDa) were shown.

5.2.9. HEKn epidermal model

Previous research (unpublished) by Dr M. Roger on building the HEKn epidermal model according to a protocol provided by the vendor of the primary cells (LifeTech) showed that recently passaged P3 HEKn cells were optimal for use in the model. In this study, as recently passaged P3 cells were no longer an option, thawed P3 cells were compared to recently passaged P4 cells for building the epidermal model with triplicate repeats. Dr Roger also demonstrated that the cells should remain at the air-liquid interface for 10-20 days, and that 30 days was too long. This data informed the use of 10 days at the air-liquid interface in this study. Though both the P3 and P4 cells made good epidermal models, the P4 cells were chosen for use in this study because they gave thicker epidermal sections (fig. 5.2), possibly since the P3 cells had not recovered from being frozen. Additionally, more cells were available at passage 4 compared to passage 3.

Cryosections and paraffin sections at 48 and 96 hours post-treatment were made of each treatment of the HEKn epidermal models. The treatments were carried out in duplicate. These were done to explore whether the treatments had any effect upon the thickness, morphology, differentiation, proliferation, acute stress response, or apoptosis of the epidermis at the two time points. To measure the epidermal thickness, measurements were taken along cryosections of each sample and averaged. Cryosections were used as the inserts were embedded in the cryomedium flatly, whereas the inserts had a tendency to curl up during the paraffin embedding process.

5.3. Results

In this chapter the effects of commercial and novel chemical depilatory treatments on hair morphology and structure are explored. First, two widely available commercial depilatory formulations, Sally Hansen Facial Depilatory and Veet HydroRestor, were tested. Next, novel formulations developed by P&G were investigated, comprising potassium thioglycolate with guanidine carbonate, guanidine carbonate separately at pH12.5 and pH11.4, lithium bromide under different conditions, calcium iodide with sodium lauryl sulphate, and CTAB with sodium lauryl sulphate. The effect of hydration was also tested as a control for the effect upon the hair of the water component in all of the depilatories. Finally, the two most efficacious depilatories – potassium thioglycolate, and potassium thioglycolate with guanidine carbonate – were applied to HaCaT cells grown on a 2D surface and a 3D HEKn epidermal model to investigate the effects of the chemical stressors on keratinocyte differentiation, proliferation and acute stress.

5.3.1. Structural and morphological changes in hair caused by chemical modification

5.3.1.1. Hydration results in a small increase in hair diameter

First, the effect of hydration on the structure and morphology of hair was tested, as water is a component in all of the chemical depilatories. Snapshots of the hair at 1 minute and 2.5 minutes of hydration (fig. 5.3A) show there is a 2µm increase in diameter of the cuticle, and a 4µm increase in diameter of the cortex between these times, equivalent to a 6% increase in diameter. The increase in diameter appears similar in regions within the cortex, and it is difficult to locate which compartments are swelling more with hydration, though the hair swells more noticeably in width than length. No change in length was detected across the section of hair measured, but previous studies have found a 1-2% increase in hair length with hydration (Corbett, 1976; Xiao and Hu, 2016).

The change in diameter of hydrated hairs above and below the skin interface was measured after 10 minutes of hydration to compare any differences in the permeability of water (fig. 5.3B). Although three hairs showed a larger increase in diameter after hydration at the distal tip of the hair than the root, there is quite a large variation

between hairs, and one hair showed a larger increase in diameter at the root (p=0.471, Mann-Whitney U-test).

These results show that the hydration component of the chemical depilatories should only play a small role in the change in hair structure and morphology, though may play a larger role after the hair structure has been compromised by the chemicals in the depilatories.

5.3.1.2. Calcium thioglycolate (CHM1) is more efficacious at weakening the hair than other non-thioglycolate based chemical depilatories

Sally Hansen Facial Depilatory is specially developed for facial skin. P&G have determined its main constituents to be 3.3% calcium thioglycolate, calcium hydroxide and potassium hydroxide. The calcium thioglycolate breaks the disulphide bonds within cystine in keratin, thus making the hair weaker and easier to remove. Calcium thioglycolate is less efficacious at reducing disulphide bonds than potassium thioglycolate (P. Smith, P&G, unpublished data), because it is designed for use on a more sensitive skin area. Hereafter, the determined chemicals in the Sally Hansen Facial Depilatory, are referred to simply as calcium thioglycolate, or CHM1.

To see structural changes, 405nm autofluorescence images were taken, and to investigate changes in the chemical environments of fluorophores, FLIM at 470nm and 640nm was measured for the calcium thioglycolate treated hair. Figure 5.5 shows representative images of treated hair taken transversely (fig. 5.5A) and longitudinally at the cuticle (fig. 5.5B) and the cortex (fig. 5.5C) using 405nm autofluorescence, and FLIM with 470nm and 640nm. There is some loss of cuticle which is visible on the transverse optical sections, and disruption of the cuticle is apparent on the longitudinal optical sections of the cortex. As observed in the previous chapter, and reiterated by the FLIM images of the untreated control hair (fig. 5.4), when excited with 640nm the cuticle has a higher lifetime compared to the cortex, shown in figure 5.5 by the average cuticle lifetime of 2.60ns and the average cortex lifetime of 2.36ns.

These results show that calcium thioglycolate treatment affected the structure of the hair, particularly the cuticle, though appears less efficacious than treatments including potassium thioglycolate.

5.3.1.3. Potassium thioglycolate (CHM2) is the second most efficacious depilatory

Veet HydroRestor has been developed specially for body hair, though P&G have shown that it does not completely remove the thickest terminal hairs, such as beard hairs or pubic hairs and can cause irritation. P&G have determined its main constituents to be 0.45M potassium thioglycolate, 0.47M calcium hydroxide, and water. Potassium is on the Hofmeister series as well as calcium (Hofmeister, 1888). The Hofmeister series ranks ions on the strength of the salts against protein structure and solubility. Potassium combined with thioglycolate has a greater effect on denaturing keratin and reducing the disulphide bonds than calcium thioglycolate (Zhang and Cremer, 2006; Xie and Gao, 2013). The depilatory is at pH12.75 which is at the regulatory limit as advised by the European Union directorate general for health and food safety scientific committee on consumer safety. Hereafter, the determined chemicals in the Veet HydroRestor, are referred to simply as potassium thioglycolate, or CHM2.

FLIM and 405nm autofluorescence intensity images were taken of the potassium thioglycolate treated hair to explore whether there was an effect on the fluorescence lifetimes. Figure 5.6 shows representative images of hair treated for four minutes taken transversely and longitudinally at the cuticle and the cortex using 405nm autofluorescence, and FLIM with 470nm and 640nm. There appears to be a loss of cuticle cell layers in the transverse optical section of the hair, a thin layer remaining in the 470nm excitation image where the outside of the hair is coloured blue with a low lifetime of 3.30ns. The longitudinal optical sections of the hair show the cuticle is deformed with ridges and troughs. The cortex appears more normal.

Since potassium thioglycolate is a common depilatory, and the benchmark that any experimental formulations are compared to, its mode of action needed to be further characterised. Using the dynamic imaging method in conjunction with confocal microscopy, the potassium thioglycolate treatment was carried out on hair enabling structural and morphological changes to be observed throughout the hair over time for up to ten minutes, after which no further changes were observed. These images are different to those from the FLIM imaging (fig. 5.6) because in order to carry out FLIM the hairs had to be dried post-treatment so that they were stationary and had more structural integrity for the imaging. During treatment the cuticle is shown in figure 5.7 to increase dramatically in width; after one minute of application the shape of the cuticle

becomes deformed and uneven which is most pronounced at the cut end, after three minutes of application parts of the cuticle bulge out; by five minutes there are deep invaginations into the cuticle; after seven minutes the cuticle appears more uniform in morphology, as it does at ten minutes. At ten minutes post-treatment the diameter of the hair is vastly wider, there are gaps between the cuticle cells, and parts of the cuticle have broken away. The cortex is shown in figure 5.8, and by three minutes of treatment with potassium thioglycolate the morphology of the hair has become uneven with invaginations through the cuticle into the cortex. The hair continues to expand until ten minutes into treatment, and the final image clearly shows that the cortical cells and the organelle remnants within them have also expanded with the cortex. This may be occurring due to the keratin filaments becoming looser because of the broken disulphide bonds, and the water expanding the hair after the action of the potassium thioglycolate. To complement the confocal dynamic imaging data, FeSEM was carried out to observe the effects of potassium thioglycolate on the hair surface, and showed a varying amount of cuticle degradation after treatment (fig. 5.9). In some areas thioglycolate had caused a complete loss of cuticle and the cortex had become visible (fig. 5.9A). In other areas the intra-cuticle cell layers had peeled back (fig. 5.9B), and cuticle cell edges were jagged with cracked surfaces (fig. 5.9C). In other areas the cuticle cells had degraded and small holes had formed to the cuticle cell layer below (fig. 5.9D).

TEM confirmed the loss of cuticle cells showing fewer layers were present after treatment (fig. 5.10C). Interestingly, there was lighter staining around the circumference of the hair of approximately 10µm into the hair (fig. 5.10A). This may be showing the depth of thioglycolate penetration as the staining may be different for the areas where disulphide bonds have been broken. TEM also showed changes to the morphology of the hair, with deformations in the shape of the cuticle layer (fig. 5.10B). The electron microscopy data supports and confirms the observations made using confocal microscopy.

These results show that potassium thioglycolate is more efficacious as a depilatory than calcium thioglycolate, and treatment changes the chemical environment of the hair, as well as causes dramatic changes in the hair structure and morphology.

5.3.1.4. Potassium thioglycolate with guanidine carbonate (CHM3) is the most efficacious depilatory

P&G had developed experimental depilatories and they reasoned that addition of guanidine carbonate to thioglycolate would improve the efficacy of hair removal. Guanidine is a chaotropic agent and low on the order of cations in the Hofmeister series, which means it reduces the hydrophobic effect of proteins (Hofmeister, 1888; Zhang and Cremer, 2006; Xie and Gao, 2013). Keratin is hydrophobic which keeps its coiled-coil structure by lowering the surface energy (Hanukoglu and Ezra, 2014). Guanidine forms hydrogen bonds with the water which decreases the surface energy, and makes it easier for the keratin to unfold. Therefore, in addition to the previous 0.45M potassium thioglycolate commercial depilatory, 0.44M guanidine carbonate was added to increase the efficiency of the disulphide bridge reduction by making it more accessible for attack by thioglycolate.

FLIM was taken of the potassium thioglycolate and guanidine carbonate hair treated for four minutes to explore whether there was an effect on the fluorescence lifetimes. Figure 5.11 shows images of treated hair taken transversely and longitudinally at the cuticle and the cortex using 405nm autofluorescence, and FLIM with 470nm and 640nm. The transverse optical section shows there is still cuticle present on the hair, though some disruption is visible at the top of the image. The transverse FLIM images do not appear unusual and have distinctly lower cuticle lifetimes towards the hair surface, as shown by the blue colouring, with a lifetime of 3.15ns with 470nm excitation and of 1.99ns with 640nm excitation. The longitudinal images show ridges and troughs in the hair surface as was observed in hair treated with potassium thioglycolate alone. The cortex in the longitudinal images appears quite homogenous in lifetimes, particularly with 470nm excitation, with lifetimes only ranging from 3.46ns to 4.10ns.

The dynamic imaging method showed the changes occurring to the hair during treatment with potassium thioglycolate and guanidine carbonate. The cuticle increased in diameter from the first minute of treatment application and invaginations begin to appear (fig. 5.12). With time, the cuticle continued to increase in diameter, the invaginations became deeper, and holes were visible through the cuticle. After ten minutes of treatment the cuticle and circular organelle remnants were visible, suggesting some cell layers of cuticle had been lost. There was deformation of the cuticle

and the hair had expanded outside of the field of view. In the cortex (fig. 5.13) similar expansion took place with the cortical cells and organelle remnants which expanded by swelling. Invaginations into the hair through to the cortex were clear after five minutes of treatment, which possibly allowed further penetration of the depilatory into the hair. The expansion and deformation of the cuticle and cortex was greater with this treatment than with potassium thioglycolate alone.

FeSEM showed how the surface of the hair had been modified by the treatment. Some areas of the hair appeared more affected than other areas where only jagged cuticle cell edges were seen (fig. 5.14A). In other areas degradation of the cuticle led to the cortex becoming visible (fig. 5.14B). Large cracks were apparent in the cuticle (fig. 5.14C), and further degradation of the cuticle occurred through the creation of holes approximately 100nm in diameter (fig. 5.14D) which gradually became larger and exposed the cortex (fig. 5.14E). The structures from the degradation appeared to be made up of granules approximately 20nm in diameter (fig. 5.14F). The damage to the cuticle appeared more severe with potassium thioglycolate and guanidine carbonate than with potassium thioglycolate alone.

TEM confirmed the misshaping of the cuticle layer (fig. 5.15A) and a slight change to the approximate outer 10μm of the hair diameter, perhaps due to a change in hair structure caused by the disulphide reduction. TEM also showed that there were fewer cuticle cell layers after treatment (fig. 5.15B). The cuticle cells became detached after treatment as the CMC between them was weakened (fig. 5.15C), which was more pronounced in this treatment than just with potassium thioglycolate.

Hairs treated with potassium thioglycolate and guanidine carbonate resulted in the most swelling of the hair with treatment, and drastic deformation of the hair cuticle. This suggests more keratin has been reduced in this treatment than with calcium thioglycolate or potassium thioglycolate treatment alone.

5.3.1.5. Guanidine carbonate pH12.5 (CHM4) is not as effective alone

Guanidine carbonate was tested on the hair without potassium thioglycolate to see whether it alone, at a high pH, as a chaotropic agent could denature the keratin proteins to weaken the hair shaft.

FLIM was taken of the guanidine carbonate treated hair to explore whether there was an effect on the fluorescence lifetimes. Figure 5.16 shows images of treated hair taken transversely and longitudinally at the cuticle and the cortex using 405nm autofluorescence, and FLIM with 470nm and 640nm. The transverse optical sections of the autofluorescent hair and FLIM appeared relatively normal. The cuticle in the longitudinal section appeared more disrupted and has unusual areas of blue colouring on its surface with lifetimes of 2.83ns and 1.99ns with 470nm and 640nm excitation respectively. These could be areas of damage.

Dynamic imaging of the hair during guanidine carbonate treatment at pH12.5 showed the changes occurring in the hair with time (fig. 5.17). There was some expansion of the hair over the ten minutes of treatment time though it was not as dramatic as the treatments including potassium thioglycolate. There appeared to be little disruption to the hair structure.

FeSEM imaging allowed the cuticle to be observed at a higher resolution and magnification, which showed more damage to the cuticle than was apparent with confocal microscopy. The cuticle cell edges were jagged (fig. 5.18A) as with previous treatments. The upper compartments of some cuticle cell layers had been removed, only leaving remnants of the endocuticle (fig. 5.18B). At the edges of some cuticle cells degradation was visible (fig. 5.18C), and there were granules and cracks in the cuticle cell surface (fig. 5.18D).

TEM confirms the signs of degradation of the cuticle (fig. 5.19), though more cell layers remained than with thioglycolate treatments. As with the thioglycolate treatments there was separation between the cuticle cells, but this was limited to the outer cuticle cell layer. This suggests the guanidine carbonate was only able to compromise outer layers of cuticle cells.

These results show that even at pH12.5, guanidine carbonate did not act as an effective depilatory, despite some changes to the hair structure. Only in conjunction with potassium thioglycolate did guanidine make an effective depilatory.

5.3.1.6. Decreasing the alkalinity of guanidine carbonate to pH11.4 (CHM5) does not improve depilation

Guanidine carbonate at a lower pH11.4 was tested to evaluate the effect of decreasing the alkalinity. This was tested at a lower pH because it is better for safety and regulatory purposes in consumer products.

FLIM was taken of the guanidine carbonate treated hair to explore whether there was an effect on the fluorescence lifetimes. Figure 5.20 shows images of treated hair taken transversely and longitudinally at the cuticle and the cortex using 405nm autofluorescence, and FLIM with 470nm and 640nm. These images appeared relatively normal, except from the uneven lifetimes of the cuticle. In the previous chapter the cuticle lifetimes were shown to change with cuticle cell layer, but here the low blue lifetime of approximately 3ns in 470nm excited hair can be seen sporadically penetrating all cuticle cell layers. This is a slight but not significant reduction in lifetime compared to untreated hair and guanidine at pH12.5.

Dynamic imaging of the hair shows any changes as they happen. There appeared to be few changes over the ten minutes of treatment with guanidine carbonate at pH11.4. However, there did appear to be swelling at the cut end of the hair from three minutes of treatment which increased slightly until ten minutes of treatment time has passed (fig. 5.21). Swelling of the cortex was also observed and appeared to occur within the first five minutes of treatment (fig. 5.22).

FeSEM of the treated hair surface showed minor disruption to the cuticle cells. As seen in all treatments the cuticle cells had jagged edges (fig. 5.23A). In addition to this, the top cuticle cell layers were separated by approximately 50nm (fig. 5.23B). The cuticle cell surface was covered in deposits (fig. 5.23C) which appeared crystalline (fig. 5.23D). These may be salt crystal remnants from the treatment. As with the other treatments, the cuticle cell surface contained cracks (fig. 5.23E), and was covered in granules approximately 20nm in diameter (fig. 5.23F).

TEM showed that the cuticle was affected differently in different areas. Some parts of the cuticle showed signs of degradation and had fewer cuticle cell layers (fig. 5.24A). Other areas of the cuticle appeared unaffected by the treatment and had many cell layers (fig. 5.24B).

These results show that decreasing the alkalinity of guanidine carbonate to pH11.4 from pH12.5 caused little damage to the hair, and mainly affected the hair cuticle. Therefore, decreasing the pH did not improve depilation.

5.3.1.7. Changes in hair diameter with treatment

After treatment with the depilatory chemicals for ten minutes the average increase in hair diameter was measured to compare the extent of the swelling from the treatment. An average width increase of 136% (fig. 5.25) was found in the potassium thioglycolate treated hairs and was significantly different to hydrated hair as well as hair treated with other thioglycolate compositions and guanidine carbonate ($p=4.18x10^{-3}$, Kruskal-Wallis test). However, an even greater expansion in hair diameter was observed in hairs treated with potassium thioglycolate and guanidine carbonate, as after treatment there was an average diameter increase of 301% ($p=4.18x10^{-3}$, Kruskal-Wallis test) (fig. 5.25).

In hairs treated with guanidine carbonate alone at pH12.5 there was much less expansion of only 15%, which was not significantly different from control hair (fig. 5.25). Decreasing the alkalinity of the guanidine carbonate to pH11.4 gave an average increase of 13% in hair diameter after treatment, which was also not significantly different (fig. 5.25). This was the lowest increase in diameter among all the treatments with the exception of hydration.

These results show that potassium thioglycolate with guanidine carbonate had the greatest effect upon the morphology of the hair, resulting in dramatic swelling of the cuticle and the cortex.

5.3.1.8. Maleimide shows areas of disulphide bond reduction

Maleimide conjugated to 633nm AlexaFluor stained the thiol groups in hair (Taneda *et al*., 1980), and was used to stain the area which the potassium thioglycolate had attacked (fig. 5.26B). This transverse optical section of the hair showed an outer perimeter of the hair which was brightly stained with maleimide. The bright staining covered the cuticle along with the outer cortex, and formed a ring approximately 10µm thick around the outside of the hair. The hair morphology was also deformed, showing ridges and troughs on the surface, though the potassium thioglycolate appeared to have penetrated through the hair to an even depth. The maleimide staining supports the TEM data showing that the thioglycolate had penetrated approximately the outer 10µm of the hair and denatured it.

In potassium thioglycolate and guanidine carbonate treated hairs, maleimide stained the areas of the hair which were reduced to thiol groups by the thioglycolate. Much like the hairs treated with potassium thioglycolate alone, this treatment resulted in the outer approximate 10µm of the hair stained brightly to show the area of reduced disulphide bonds (fig. 5.26C).

The maleimide stain did not stain the perimeter of the hair when the hairs had been treated with guanidine carbonate alone for either pH12.5 or pH11.4 (fig. 5.26D and 5.27E respectively), as there had been no reduction to the disulphide bonds which create thiol groups. Both hairs treated with guanidine carbonate appeared similar to the untreated control hair stained with maleimide.

These results show that only the treatments containing potassium thioglycolate reduced the disulphide bonds in the hair, and appeared to penetrate the outer 10µm of the cuticle and cortex.

5.3.1.9. Post-treatment hydration change in hair diameter

The swelling of treated hairs after ten minutes of hydration in water was recorded to test the extent of structural damage to the hair by measuring the permeability of water into the hair through swelling.

After 10 minutes of hydration, which ensured the hair was fully hydrated (fig. 5.27), there was an 11.8% increase in hair diameter of hydrated control hairs ($p<0.001$, Wilcoxon paired test), though P&G measured an average swelling of 14.8% (fig. 5.27), combining the measurements gave an average of a 13.1% increase in hair diameter.

For hairs treated with calcium thioglycolate, P&G measured an average swelling of 15.0% after hydration (fig. 5.27), although this had a faster increase in diameter than non-thioglycolate treated hairs the difference was not significant after ten minutes.

There was a larger increase in swelling for hairs treated with potassium thioglycolate as measuring the swelling at the widest point gave an average increase of 33.5% after ten minutes hydration (fig. 5.27), and was significantly different to treatments not based upon potassium thioglycolate ($p=0.032$, Kruskal-Wallis test).

For hairs treated with potassium thioglycolate and guanidine carbonate P&G measured an average swelling of 39.7% after ten minutes of hydration (fig. 5.27) and this was

significantly higher than all the other treatments (p=0.032, Kruskal-Wallis test), suggesting potassium thioglycolate with guanidine carbonate causes the most structural damage to the hair.

Measuring the swelling at the widest point of guanidine carbonate at pH12.5 treated hairs alone gave an average increase of 13.1% after ten minutes hydration (fig. 5.27), and was not significantly different to the untreated control.

Decreasing the alkalinity of the guanidine carbonate to pH11.4 decreased the swelling slightly to 12.5% after ten minutes hydration, which was not significant, and was the lowest degree of swelling measured after that of untreated hair (fig. 5.27).

As hydration gave the greatest increase in hair diameter to hairs treated with potassium thioglycolate and guanidine carbonate (fig. 5.27), the effect of relative humidity on hairs treated with this depilatory was tested. This was done to evaluate whether the humidity of the air could affect the fluorescence lifetimes and therefore the chemical environment of the hair (fig. 5.28). There was no significant difference between ambient, 70% relative humidity, and hydrated hair when excited with 470nm (p=0.598, Kruskal-Wallis test). However, there was a significant difference when the hair was excited with 640nm between the cortex lifetimes in ambient and hydrated hair and in 70% relative humidity and hydrated hair ($p=6.74x10^{-3}$, Kruskal-Wallis test). This suggests that the treatment had an effect on the hair structure allowing the cortex to become more permeable to water.

These results showed that potassium thioglycolate with guanidine carbonate compromised the structural integrity of the hair more than any other treatment to allow for the greatest increase in swelling post-treatment with the addition of water.

5.3.1.10. Break ratio reduction shows the decrease in strength of the hair

The break ratio reduction of treated hairs was measured to compare the strength of the hairs after treatment. The break ratio reduction is a measure of depilatory efficiency and the amount the hair has been chemically weakened compared to untreated control hair, expressed as a percentage change. The breaking of the disulphide bonds by calcium thioglycolate led to a break ratio reduction of 15% (fig. 5.29). This reduction in strength was more than treatments without thioglycolate, but less than those with potassium thioglycolate.

The breaking of the disulphide bonds by potassium thioglycolate led to a break ratio reduction of 27% (fig. 5.29). This meant the strength of potassium thioglycolate treated hair was weaker than calcium thioglycolate treated hair, but stronger than hair treated with potassium thioglycolate with the addition of guanidine carbonate.

After treatment with potassium thioglycolate and guanidine carbonate, the hairs had a 56% reduction in strength, which was the largest reduction in strength of all hairs treated with thioglycolate or guanidine (fig. 5.29).

The disruption of the hair structure by guanidine carbonate at pH12.5 led to a break ratio reduction of 8% (fig. 5.29). This means the hair was weaker, but stronger than hair treated with thioglycolate. For hair treated with guanidine carbonate at pH11.4 the reduction in strength was by 2% (fig. 5.29), so there was little change, showing that the higher pH12.5 had a greater effect on the strength of the hair.

These results show that potassium thioglycolate with guanidine carbonate had the greatest effect upon the strength of the hair.

5.3.1.11. Lithium bromide (CHM22-25) changes hair morphology dependent upon treatment temperature and duration

Since the disulphide chemistry in thioglycolate depilatories has caused skin irritation in the past, other chemistries were investigated which alter the hair through different mechanisms. Lithium bromide has previously been shown to affect the structure and morphology of keratin fibres (Feughelman *et al*., 1958; Chapman, 1970), though it has not been investigated in the context of depilatory treatments. Lithium and bromine are both in the Hofmeister series and are capable of denaturing proteins (Zhang and Cremer, 2006; Xie and Goa, 2013). Lithium in water would normally be surrounded by a large hydration sphere. In this investigation, a saturated 8M lithium solution was used so there was not enough water for it to bond with. The lone pairs on the lithium make it very reactive and they form hydrogen bonds with nitrogen and oxygen atoms in the keratin. This pulls the hair together, making it shorter and wider (Feughelman *et al*., 1958; Chapman, 1970). The ability to make hairs shorter by contraction may be of interest to the hair care industry, as hairs could be treated to appear shorter in the skin for an extended period of time, perhaps reducing the need to remove them.

The effect of lithium bromide treatment temperature and duration was tested on the hair to evaluate the structural and morphological changes, and whether any of the conditions (table 5.1) would be suitable as a depilatory.

Treatment name	Temperature (°C)	Duration
CHM22	25	20 minutes
CHM23	85	20 minutes
CHM24	25	5 minutes
CHM25	25	5 days

Table 5.1. Hair treatment conditions with lithium bromide.

Label-free confocal microscopy using 405nm autofluorescence was used to examine the structure and morphology of the hair. Hairs treated at temperatures under 85°C or for under 20 minutes (CHM22 and CHM24) appeared more similar to each other than the hair treated at 85°C (CHM23) or for 5 days (CHM25) (fig. 5.30). The hair treated at 85°C or for 5 days appeared to have more compact cuticle cells, and the cortex of the hair treated at 85°C appeared swollen (fig. 5.30). These differences may be due to the rate of lithium bromide penetration, which is dependent upon concentration, hair diameter and temperature (Haly and Griffith, 1958; Feughelman *et al*., 1962). At room temperature a concentration of 8M lithium bromide could be expected to fully penetrate a thin hair of 50µm diameter in 5-7 hours, and no changes would be seen in the contraction of the hair until the fibre was almost completely saturated (Haly and Griffith, 1958; Feughelman *et al*., 1962). Since in two of the treatments, CHM22 and CHM24, hairs were only treated for 20 minutes and 5 minutes at 25°C, it is unlikely that the treated hairs had been fully penetrated with lithium bromide, and were therefore unlikely to show any morphological changes. The CHM25 hairs treated for 5 days may have had sufficient time for saturation of lithium bromide. The CHM23 treated hairs at 85°C appeared to have been at a high enough temperature to increase the rate of penetration so that the hair had undergone contraction after only 20 minutes. P&G found that these hairs had a 70% increase in diameter with a 20% decrease in length. The hair was observed to be very elastic, and P&G were only able to obtain break ratio reduction measurements for the hair treated at 25°C for 20 minutes, which was found to have an 8% reduction in strength compared to untreated hair. There may still have been a reduction in the strength of the hair despite the incomplete penetration of lithium bromide, as only some disruption of the keratin filaments may have been sufficient to weaken the hair.

Spectral scans were taken of the hair to test whether the emission spectra had been altered by the treatment. The emission spectra appeared normal, and the hair unlikely to contain much lithium bromide (fig. 5.31A and fig. 5.31C) appeared relatively similar to the hair constricted by the lithium bromide (fig. 5.31B and fig. 5.31D). This shows that the fluorophores are unlikely to have been affected by the lithium bromide.

To confirm that the fluorophores were unaffected by lithium bromide penetration, FLIM was carried out on the hairs. In transverse section the hairs appeared to have relatively similar fluorescence lifetimes no matter the conditions of lithium bromide treatment (fig. 5.32), and also appeared similar to the control hairs (fig. 5.4).

These results show that the penetration of lithium bromide into hair leading to contraction takes too long or is too hot for the treatment to be suitable as a depilatory. In addition to this, the high molarity required could become corrosive to the skin.

5.3.1.12. Calcium iodide and sodium lauryl sulphate cause breakage of cuticle cells

An additional mechanism of hair disruption was sought which did not utilise disulphide chemistry and would potentially cause less skin irritation. A solution of 25% calcium iodide and 2% sodium lauryl sulphate (SLS) was identified as a suitable alternative to test.

Previous studies have shown the uptake of metal ions from hard water into the hair. This includes calcium ions which are extracted from tap water into the cuticle, particularly into the sulphur-rich exocuticle and A-layer, and results in fibre stiffening (Smart *et al*., 2009; Evans *et al*., 2011). Anecdotal reports state that people experience hair loss when washing their hair in hard water areas, particularly when washing with the desalinated water in the Middle East.

In this investigation it was found that the calcium ions precipitated out of the hair cuticle when SLS was added, resulting in parts of the cuticle cell fracturing away. The cuticle is responsible for harnessing the torsional forces applied to hair (Wolfram and Albrecht, 1985), so if the cuticle is destroyed or weakened, the hair may be easier to remove.

Confocal microscopy was used to image the treated hair with 405nm autofluorescence to evaluate the effect of the treatment on the hair structure. First the hair was treated with a higher concentration of SLS alone to measure the effect of the detergent on untreated hair (fig. 5.33A). The 28% SLS treatment caused the cuticle cells of the hair to

become raised (fig. 5.33A). With the addition of 25% calcium iodide to 2% SLS the structure of the hair cuticle was affected to varying degrees. Some hairs only showed the cuticle cells on the surface of the hair becoming raised (fig. 5.33B). In other hairs many cell layers of the cuticle had been broken away by the precipitation of the calcium ions from the hair that the cortex became visible (fig. 5.33C). Using confocal microscopy, it was difficult to identify how many cell layers of the cuticle have been removed. To show that some cuticle cell layers can be removed and the hair still appears normal, beard hair was treated with the calcium iodide and SLS. The cuticle of the beard hair (fig. 5.33D) appeared similar to the apparently unaffected scalp hair (fig. 5.33E). However, as shown in chapter 3, the many cuticle cell layers of a beard hair block the penetration of light into the cortex, however, with calcium iodide and SLS treatment the cortex of a beard hair was visible (fig. 5.33D). This showed that the treatment had removed several layers of cuticle cells. The variability in the results also suggest that some areas of the cuticle are weaker or more susceptible to calcium ion uptake.

Following confocal microscopy, FLIM was taken of the treated hair in transverse and longitudinal optical section to see whether there was any effect upon the fluorophores and chemical environment of the hair. The FLIM images of the hair showed that the free edge of each cuticle cell has a lower lifetime of 2.94ns than the rest of the cuticle cell which has an average lifetime of 3.20ns (fig. 5.34). This could be caused by the raised cuticle cells exposing their internal constituents including the exocuticle and endocuticle, resulting in a different lifetime, or showing exposed areas of the cuticle which have been removed by the treatment. The cortex of the hair appears normal, as does the transverse section, the outer cuticle cell layer with a low lifetime of 3.04ns (fig. 5.34).

These results show that calcium iodide with SLS was effective at removing some of the cuticle cells. Repetition of the treatment over time may lead to hair loss, however it is unlikely to be suitable as a one-step hair removal treatment.

5.3.1.13. CTAB and SLS causes cuticle cell flaring with loss of 18-MEA

An alternative way to avoid skin irritation by thioglycolate was to test hair with 2% cetyltrimethylammonium bromide (CTAB) at pH 9.41 for 5 min, followed by 0.5% SLS for 5 min. CTAB has been shown to remove the covalently bound fatty acid 18-MEA from the outer β-layer of the cuticle cell CMC (Jones *et al*., 1996; Smith *et al*., 2010), and this

method was shown in the previous chapter to significantly change the fluorescence lifetimes of hairs after treatment.

Confocal microscopy was used to image the treated hair with 405nm autofluorescence to evaluate the effect of the treatment on the hair structure. The images show that the treatment caused varying degrees of cuticle cell flaring (fig. 5.35). Some hairs showed moderate cuticle cell flaring (fig. 5.35A), others had intense flaring where the cuticle cells were almost perpendicular to the hair shaft (fig. 5.35B), and still others showed little cuticle cell flaring (fig. 5.35C). This links to the lipid extraction using CTAB in the previous chapter, as the flared cuticle cells show the CMC of the cuticle has been disrupted, most likely by removal of 18-MEA.

Following confocal microscopy, FLIM was taken of the treated hair in transverse and longitudinal optical section to see whether there was any effect upon the fluorophores and chemical environment of the hair. As with the previous treatment which also caused cuticle cell flaring, the FLIM images of the hair show that the free edge of each cuticle cell had a lower lifetime of 3.25ns than the rest of the cuticle cell which had an average lifetime of 3.57ns (fig. 5.36). Again, this could be caused by the raised cuticle cells exposing the internal constituents, resulting in a different lifetime. The cortex of the hair appeared normal, as did the transverse section (fig. 5.36).

The treated hair was hydrated in water to test the extent of the structural damage done. P&G measured an average swelling of 10.8% after ten minutes hydration, which was not significant. This may be because CTAB does not disrupt the structure of the cortex which would allow for more hydration.

The strength of the hair was tested by measuring the break ratio reduction. For treated hair the reduction in fibre strength was by 5%.

These results indicate that while CTAB modified the hair cuticle by removing 18-MEA from its surface, resulting in cuticle cell flaring, it did not appear to cause sufficient structural damage to the hair to qualify it as a suitable candidate for chemical depilation.

5.3.1.14. Comparison of fluorescence lifetimes of treated hairs

Comparing the fluorescence lifetimes of calcium thioglycolate treated hairs with the other depilatory treatments as well as untreated and hydrated hairs (fig. 5.38), showed that there was a significant difference between the untreated hair cuticle and the lower

lifetime of the calcium thioglycolate treated hair cuticle when the hair was excited with 640nm ($p=5.49x10^{-3}$, Kruskal-Wallis test). There was also a significant difference between the lower lifetimes of the calcium thioglycolate treated hair cortices and those of potassium thioglycolate with guanidine treated hair and guanidine at pH11.4 treated hair ($p=2.98x10^{-4}$, Kruskal-Wallis test). There was no significant difference in hair excited with 470nm (fig. 5.37).

It was found that with 470nm excitation (fig. 5.37) and 640nm excitation (fig. 5.38), the potassium thioglycolate treated hairs lifetimes were significantly lower. This was true for the cuticle of hair excited with 470nm, giving significantly lower lifetimes than the cuticles of untreated, guanidine at pH12.5, lithium bromide at 25°C for 25 minutes, and CTAB with SLS treated hair ($p=9.00x10^{-6}$, Kruskal-Wallis test) (fig. 5.37A). The fluorophores of the cortices of the potassium thioglycolate treated hair at 470nm were also significantly affected compared to the cortices of untreated hair, and all of the treated hairs except calcium thioglycolate and lithium bromide at 25°C for five days ($p=3.00x10^{-5}$, Kruskal-Wallis test) (fig. 5.37B). Potassium thioglycolate treated hair that was excited with 640nm had significantly lower lifetimes in the cuticle compared to untreated hair, and hair treated with potassium thioglycolate with guanidine carbonate, and CTAB with SLS ($p=5.49x10^{-3}$, Kruskal-Wallis test) (fig. 5.38A). For the cortex excited with 640nm, potassium thioglycolate treated hair had significantly lower lifetimes than the cortices of hair treated with potassium thioglycolate with guanidine, and guanidine alone at either alkalinity ($p=2.98x10^{-4}$, Kruskal-Wallis test) (fig. 5.38B), suggesting the addition of guanidine may have a more significant impact upon the cortex.

The fluorescence lifetimes of potassium thioglycolate with guanidine carbonate treated hairs were compared to other treatments to evaluate the extent of the effect upon the chemical environment of the hair. There were fewer significant differences between this treatment and treatment with potassium thioglycolate alone. This may be because it is necessary to image the treated hairs using FLIM only after they have been dried, and some of the significant effects of the guanidine may have been reversed with the drying of the hair. The only significant differences found with this treatment in 470nm excited hair was that the cortex was significantly different to the cortex of hair treated with potassium thioglycolate alone ($p=3.00x10^{-5}$, Kruskal-Wallis test) (fig. 5.37B), and in 640nm excited hair the cortex was significantly different to the cortex of hair treated

with calcium thioglycolate and to hair treated with potassium thioglycolate ($p=2.98x10^{-4}$, Kruskal-Wallis test) (fig. 5.38B).

Comparison of the fluorescence lifetimes of the different treatments shows that hairs treated with guanidine carbonate at pH12.5 have significantly higher cuticle and cortex lifetimes when excited with 470nm than hair treated with potassium thioglycolate ($p=9.00x10^{-6}$ and $p=3.00x10^{-5}$ respectively, Kruskal-Wallis test), and of the 640nm excited cortex ($p=2.98x10^{-4}$, Kruskal-Wallis test), though this may simply be a reflection of the extent of damage caused by potassium thioglycolate. When compared to untreated hairs, guanidine carbonate treated hairs are not significantly different.

Guanidine carbonate at pH11.4 significantly changes the fluorescence lifetimes of the hair cortex when excited with 640nm ($p=2.98x10^{-4}$, Kruskal-Wallis test) (fig. 5.38B), but not with 470nm (fig. 5.37B).

Despite the chemical environment changing with the addition of lithium in the hair, the only significant difference in lifetime is that of the medullas of 470nm excited hair (fig. 5.37C) of the CHM25 hairs which were treated for 5 days ($p=8.52x10^{-3}$, Kruskal-Wallis test). Perhaps this is the only treatment in which the lithium bromide reached the medulla, however it was shown to have caused contraction also in the 85°C hair, so would have been present in the cortex, but there was no difference in lifetime. This suggests the possibility that FLIM cannot detect changes to the chemical environment with lithium bromide treatment, at least using the wavelengths available in our system.

There were no significant differences between the fluorescence lifetimes of calcium iodide and SLS treated hairs, and untreated hairs (fig. 5.37). This may be due to the fact that the calcium is removed from the hair by the SLS.

There were also no significant differences between the fluorescence lifetimes of CTAB and SLS treated hair, and untreated hair for 470nm (fig. 5.37) or 640nm (fig. 5.38) excitation.

These results show that significant differences in the fluorescence lifetimes compared to untreated or hydrated hairs were only observed in calcium thioglycolate, potassium thioglycolate, and pH11.4 guanidine carbonate treated hairs. Based upon the denaturant activity of these chemicals, these treatments have changed the chemical environment of molecules or functional groups in the hair by affecting the structure of

keratins. This data supports chapter 4, as disrupting the disulphide bonds within the hair changed the fluorescence lifetimes.

5.3.2. Investigation into the effects of the chemical stressors on keratinocytes

The two most efficacious depilatories – potassium thioglycolate, and potassium thioglycolate with guanidine carbonate – were applied to HaCaT cells grown on a 2D surface and a 3D HEKn epidermal model to investigate the effects of the chemical stressors on keratinocyte differentiation, survival and death, proliferation and acute stress. In addition, potassium thioglycolate and guanidine carbonate were tested on the keratinocytes separately to study the effects of each.

5.3.2.1. Cell survival assay shows few cells after treatment with 0.4M guanidine carbonate

A modified colony formation assay was adopted to test the ability of the HaCaT cells to grow and survive the effects of potassium thioglycolate and guanidine carbonate. Concentrations of 0.4M, 40mM, and 4mM each of potassium thioglycolate and guanidine carbonate were applied to the cells for four minutes (the application time of the depilatories), and the day following treatment the cells were stained with crystal violet and compared against untreated control cells and cells with only a PBS wash. The only treatment which appeared to affect the ability of the cells to form colonies and survive was the 0.4M guanidine carbonate solution (fig. 5.39). Cells were seeded at equal densities and had a similar confluence prior to treatment, however the 0.4M guanidine carbonate appeared to kill the cells, as a very low density of cells was observed (fig. 5.39). The potassium thioglycolate and lower concentrations of guanidine carbonate do not appear to have affected the cells as the staining appears similar to that of the controls (fig. 5.39).

5.3.2.2. Cell viability decreases with increasing depilatory concentration

The crystal violet staining in figure 5.39 is quite a crude measure of cell survival so a proper cell viability assay was carried out. The cell viability assay was carried out to assess whether HaCaT cells were metabolically active, and therefore viable, after treatment with varying concentrations of potassium thioglycolate and guanidine carbonate. The colorimetric change that results is recorded as an absorbance and is directly proportional to the number of living cells in the culture. The results showed that at the concentrations found in the depilatory treatments of 0.4M there were fewer viable cells (fig. 5.40). There was significantly low viability of HaCaT cells treated with

0.4M guanidine carbonate, the average metabolic activity at only 7% of that of the untreated cells (p=0.022, Kruskal-Wallis test). For 0.4M potassium thioglycolate, the average metabolic activity was at 76% of that of untreated cells. This supports the crystal violet data as both show few HaCaT cells remain after treatment with 0.4M guanidine carbonate. The crystal violet data showed that HaCaT cells remained after 0.4M potassium thioglycolate treatment, but this cell viability assay provides more accurate data and shows approximately a quarter of HaCaT cells were not viable after treatment.

The concentrations of the chemicals were lowered to reflect the decreased penetration of the chemicals through the skin to the basal cell layer in a real life usage situation (Lee *et al*., 2008). At 40mM the viability of the HaCaT cells was much higher than at 0.4M, the same for both potassium thioglycolate and guanidine carbonate with an average metabolic rate of 87% compared to untreated cells (fig. 5.40). The metabolic activity of the cells did not appear negatively affected by concentrations of 4mM potassium thioglycolate or 4mM guanidine carbonate. At these concentrations the metabolic activity was greater than or equal to the untreated control (fig. 5.40). JNK inhibitor II was used as a positive control as it drives the cells towards differentiation and cornification (Gazel *et al*., 2006), after which they would not be as metabolically active (fig. 5.40). The use of 50µM JNK inhibitor II significantly decreased the metabolic activity of the cells compared to untreated cells by 48% (p=0.022, Kruskal-Wallis test).

5.3.2.3. Western blotting shows no significant differences in protein expression levels after depilatory treatment

Western blotting was carried out to compare the levels of proteins in HaCaT cells after various treatments. The HSPs were tested for to find out if they were involved in the acute stress response of the HaCaT cells, and keratin 14 and involucrin were tested for to indicate levels of differentiation in the cells. Different proteins were tested for at different time points; at 1 hour post-treatment HSP27, HSP70 and keratin 14 were tested for, and at 48 hours post-treatment keratin 14 and involucrin were tested for. Actin and GAPDH did not vary with treatment and were used as loading controls. The treatments carried out on the cells were 0.45M, 45mM and 4.5mM potassium thioglycolate, each alone and with 50µM JNK inhibitor II, 44mM and 4.4mM guanidine carbonate, and untreated controls, 50µM JNK inhibitor II alone, and untreated cells with the corresponding amount of DMSO from the 50µM JNK inhibitor II samples added.

HaCaT cells were treated with both potassium thioglycolate and JNK inhibitor II simultaneously to test whether the JNK inhibitor would affect the differentiation, apoptosis, and the heat shock response of the HaCaT cells after chemical treatment, since JNK activation can precede apoptosis, inhibit differentiation and is modulated by HSPs (Mosser *et al*., 2000; Gazel *et al*., 2006; Lu *et al*., 2011). The depilatory treatments lasted for four minutes and were carried out in triplicate.

The amount of HSP27 did not vary significantly with any of the treatments ($p=0.376$, Kruskal-Wallis test). Nevertheless, in each experiment the quantity of HSP27 appeared to decrease with decreasing concentrations of potassium thioglycolate and guanidine carbonate, and was higher in untreated samples than in samples with DMSO, but the differences were not significant (fig. 5.41A).

The levels of HSP70 did not vary significantly with any of the treatments ($p=0.221$, Kruskal-Wallis test). However, again the amount of HSP70 in the untreated samples was always higher than in the untreated samples with DMSO, and the amount in 4.5mM potassium thioglycolate was always higher than in 0.45M potassium thioglycolate with JNK inhibitor II, but the differences were not significant (fig. 5.41B). Together, the results from HSP27 and HSP70 indicate that there were no significant changes in the expression of HSP with treatment.

The amount of keratin 14 found 1 hour post-treatment did not vary significantly with any of the treatments ($p=0.118$, Kruskal-Wallis test). Yet, in each experiment, less keratin 14 was always found in cells treated with 0.45M potassium thioglycolate and JNK inhibitor II than cells treated with 45mM or 4.5mM potassium thioglycolate and JNK inhibitor II, but the differences were not significant (fig. 5.42A).

The quantity of keratin 14 found 48 hours post-treatment did not vary significantly with any of the treatments ($p=0.122$, Kruskal-Wallis test). In each experiment higher than or equal levels of keratin 14 were found in 0.45M potassium thioglycolate compared to 45mM potassium thioglycolate, and more keratin 14 was found in 4.4mM than 44mM guanidine carbonate, but the differences were not significant (fig. 5.42B).

The amount of involucrin did vary significantly between samples with and without the JNK inhibitor II ($p=7.81\times10^{-7}$, Kruskal-Wallis test). In addition to this, in each experiment, though the differences were not significant, involucrin levels in cells treated with 4.5mM

potassium thioglycolate with JNK inhibitor II were always higher than in cells treated with 0.45M or 45mM potassium thioglycolate and JNK inhibitor II. Also, involucrin levels in 4.5mM potassium thioglycolate treated cells were always higher than in 4.4mM guanidine carbonate treated cells (fig. 5.43). Non-specific bands at lower molecular weights were excluded from analysis as they were likely to be from non-specific secondary polyclonal antibody binding. These results suggest only the JNK inhibitor is significantly affecting differentiation, and the depilatory treatments are not affecting the differentiation of the HaCaT cells.

5.3.2.4. Effect of depilatory chemicals on HaCaT expression of differentiation, proliferation and acute stress response proteins detected using immunofluorescence

HaCaT cells were grown in 2D cultures and treated with: 0.45M, 45mM and 4.5mM potassium thioglycolate with and without JNK inhibitor II; JNK inhibitor II alone; DMSO; and 44mM and 4.4mM guanidine carbonate. The higher concentration of 0.44M guanidine carbonate was not used as it was shown earlier to kill the HaCaT cells. Lower concentrations of potassium thioglycolate and guanidine carbonate were used upon HaCaT cells because they lack the defensive barrier function of the epidermal model reflecting upon the lower quantity which may reach the basal cell layer, and smaller concentrations can test for more acute responses from the HaCaT cells. Immunofluorescence was carried out on the HaCaT cells against HSP27, HSP70, keratin 14 and actin 1 hour post-treatment, and keratin 14, actin, involucrin and Ki67 48 hours post-treatment.

Staining of HaCaT cells 1 hour post-treatment against HSP27 showed slight changes with treatment, but they were not significantly different (fig. 5.46A). This supports the data obtained by Western blotting. HSP27 positive cells were found amongst the untreated cells as well as in all the treated cells, particularly at the edges of colonies (fig. 5.44). The average number of positive cells was lower in untreated cultures with added DMSO at 16% compared to 28% in the completely untreated culture (fig. 5.46A). Cells treated with the JNK inhibitor II also had lower HSP27 positive cells at 22% than untreated cells. With the addition of potassium thioglycolate the average number of HSP27 positive cells varied from 29% to 24% to 30% for 0.45M, 45mM and 4.5mM respectively, suggesting there is little true impact of the treatment upon HSP27 levels. When JNK inhibitor II was also added to the potassium thioglycolate treated cells, there were more HSP27 positive

cells, at 41%, 27% and 34% for 0.45M, 45mM and 4.5mM respectively. The average percentage of HSP27 positive cells found in guanidine carbonate treated cells was less than that found in the untreated cells, of 25% and 17% for 44mM and 4.4mM guanidine carbonate respectively.

As with HSP27, there was no significant difference between the levels of HSP70 positive cells with the treatments 1 hour post-treatment (fig. 5.46B), and HSP70 positive cells were found in untreated and treated samples (fig. 5.45). There were far fewer HSP70 positive cells in the untreated culture of only 10%, which increased to 36% with the addition of DMSO (fig. 5.46B). The average percentage of HSP70 positive cells decreased to 20% with the addition of JNK inhibitor II. With the addition of potassium thioglycolate the average number of HSP70 positive cells increased compared to untreated cells from 46% to 22% to 49% for 0.45M, 45mM and 4.5mM potassium thioglycolate respectively. The addition of the JNK inhibitor II to the potassium thioglycolate treated cells did little to change the percentage of HSP70 positive cells. The average percentage of HSP70 positive cells in guanidine carbonate treated cultures decreased with guanidine carbonate concentration, from 33% to 24% with 44mM and 4.4mM respectively.

Immunofluorescence showed that all the HaCaT cells express keratin 14 at 1 hour post-treatment particularly strongly at the edge of colonies, and there was little expression where the cells have differentiated at the centre of colonies (fig. 5.47). This was also seen in the cells 48 hours post-treatment, though the staining appeared weaker, perhaps due to higher levels of cell differentiation after an extra 47 hours (fig. 5.48).

Immunofluorescence showed that there were few involucrin positive cells 48 hours post-treatment in untreated, untreated with DMSO, and untreated with JNK inhibitor II cells (fig. 5.49). More cells appeared to be involucrin positive in potassium thioglycolate treated cultures, and then even slightly more in potassium thioglycolate treated cells with added JNK inhibitor II. Few cells were involucrin positive in 44mM guanidine carbonate treated cultures, and more were positive in 4.4mM guanidine carbonate treated cultures, which suggests there may not be a true difference between them.

All of the cells expressed filamentous actin, as detected by phalloidin binding, and stress fibres can be seen at the edges of colonies (fig. 5.44, 5.45, 5.47, 5.48). Interestingly, when the cells were treated with the JNK inhibitor II, the cells appeared much larger (fig. 5.48, 5.49), except for when there was not 100% confluency for which all cells appeared

the same size (fig. 5.44, 5.45, 5.47). This suggests that at complete confluency, inhibiting JNK allows cells to grow larger, perhaps because they are differentiating. Also, where the cells have been treated with depilatories, some cells may have been destroyed, creating more space for new cell growth. Counting the number of cells undergoing apoptosis gives a further indication whether the cells are negatively affected by the depilatories. Cells in which the nucleus was blebbing or with small, distorted and brightly DAPI stained nuclei were counted as apoptotic cells. Cells counted 1 hour post-treatment showed a higher average number of cells were apoptotic in the 0.45M potassium thioglycolate treatment with added JNK inhibitor than any other condition, followed by 45mM potassium thioglycolate, and finally the 44mM guanidine carbonate treatment (fig. 5.50A), though the differences were not significant. Apoptotic cells counted 48 hours post-treatment did show a significant increase in apoptosis after treatment with 0.45M potassium thioglycolate with added JNK inhibitor II ($p=5.30x10^{-5}$, Kruskal-Wallis test) (fig. 5.50B). The average percentage of untreated cells undergoing apoptosis was 0.7%, added DMSO increased that to 0.9%, and added JNK inhibitor II increased it further to 1.7% (fig. 5.50B). Potassium thioglycolate alone had a low rate of 1.2%, 0.6% and 1.0% for 0.45M, 45mM and 4.5mM respectively (fig. 5.50B). This is a different result to the cell viability assay which showed an average decrease in viability of 24%, 12% and 0% for 0.45M, 45mM and 4.5mM potassium thioglycolate respectively. This difference may be due to the cell viability assay measuring metabolically active cells, whereas counting the numbers of blebbing or fractured nuclei only gives the number of cells in a late stage of apoptosis and also does not account for cells which have previously apoptosed and have been washed away. Adding JNK inhibitor II to the potassium thioglycolate increased the number of apoptotic cells significantly to 3.9% for 0.45M potassium thioglycolate and non-significantly to 2.1% and 1.6% for 45mM and 4.5mM respectively, suggesting the JNK inhibitor II is not preventing apoptosis (fig. 5.50B). Guanidine carbonate treated cells also had slightly elevated levels of apoptotic cells of 1.7% and 1.0% for 44mM and 4.4mM guanidine carbonate respectively (fig. 5.50B). Again, this is different to the cell viability assay results which showed an average decrease in viability of 13% and 1% for 44mM and 4.4mM guanidine carbonate respectively. The reason for the difference in the percentages of viable cells for the 44mM treatment are similar to those described previously, but the decrease in only 1%

of the cells treated with 4.4mM shows the lowest concentration of guanidine carbonate is not affecting HaCaT cell viability.

The number of Ki67 positive cells were counted separately as mitotic (M-phase) cells and cells in S-phase. Immunofluorescence shows the bright cells as cells in M-phase and the speckled cells as cells in S-phase (fig. 5.49) (Van Dierendonck *et al*., 1989; Manoir *et al*., 1991; Zambon, 2011). In untreated cells, there was an average percentage of 1.6% of cells in M-phase, reducing slightly to 1.4% with the addition of DMSO, and to 0.4% with the addition of JNK inhibitor II (fig. 5.50B). Cells treated with potassium thioglycolate had fewer cells in M-phase than untreated cells at 0.9%, 1.2%, and 1.0% for 0.45M, 45mM and 4.5mM respectively (fig. 5.50B). The percentage of cells in M-phase significantly decreased in the potassium thioglycolate treated cells with added JNK inhibitor II to 0.2%, 0.03%, and 0.3% for 0.45M, 45mM and 4.5mM potassium thioglycolate respectively ($p=1.30x10^{-5}$, Kruskal-Wallis test) (fig. 5.50B). The percentage of cells in M-phase in guanidine carbonate treated cultures was closer to that of untreated cultures at 1.4% and 1.9% for 44mM and 4.4mM respectively (fig. 5.50B). There were many more cells in S-phase than in M-phase. There were significant differences between the numbers of cells in S-phase for each condition (p=0.053, Kruskal-Wallis test). In untreated cells 13% on average were in S-phase, and with addition of DMSO 12% were in S-phase, which increased to 30% with JNK inhibitor II (fig. 5.50B). Potassium thioglycolate also had higher levels of cells in S-phase than the untreated cells, averaging 20%, 16% and 21% for 0.45M, 45mM and 4.5mM respectively (fig. 5.50B). This remained similar for potassium thioglycolate treated cells with added JNK inhibitor II at 20%, 22% and 13% 0.45M, 45mM and 4.5mM respectively (fig. 5.50B). Guanidine carbonate treated cells varied from an average of 14% of cells in S-phase in 44mM solution to 29% in 4.4M solution (fig. 5.50B).

In conclusion, Western blot data supports the immunofluorescence data, as immunofluorescence of the HaCaT cells show that neither potassium thioglycolate nor guanidine carbonate significantly affected the levels of HSP in the cells. Involucrin was found to be stronger in potassium thioglycolate treated cells as well as when JNK inhibitor was added, unlike in the Western blot data. There was also a significant decrease in the number of cells in M-phase, an increase in the number of cells in S-phase, and increase in the number of apoptotic cells when potassium thioglycolate with added

JNK inhibitor II was used to treat the cells. Other findings included weaker staining of keratin 14 after an extra 47 hours growth post-treatment, and treatment with JNK inhibitor II was correlated with larger cell size. Therefore overall, the immunofluorescence results show that only when treated with potassium thioglycolate with added JNK inhibitor II, HaCaT cells were driven to differentiate and some were stressed into apoptosis.

5.3.2.5. Cornified envelopes are affected by potassium thioglycolate treatment

Cornified envelopes were extracted from rat ear tips (Maatta *et al*., 2001; Sevilla *et al*., 2007) so that the effects of potassium thioglycolate and guanidine carbonate could be tested upon the cells of the stratum corneum. The cornified envelopes were stained with Nile red to visualise the covalently bound lipids at the surface of the envelopes and imaged using confocal microscopy to look for changes in structure compared to the untreated control cornified envelopes (fig. 5.51A). The cornified envelopes tested with 0.1M guanidine carbonate showed that it had no effect upon them (fig. 5.51B), as they appeared similar to the controls (fig. 5.51A) in structure and Nile red staining. However, the cornified envelopes treated with 0.45M potassium thioglycolate showed a more irregular shape and brightly stained aggregates upon their surface (fig. 5.51C). The cornified envelopes treated with 0.2M potassium thioglycolate and 0.2M guanidine carbonate also showed signs of aggregates upon them (fig. 5.51D). Since stained with Nile red it is likely that these aggregates are lipid based. It appeared that lipid aggregates had formed on the cornified envelopes where the treatment included potassium thioglycolate. This may have occurred because thioglycolate has been shown to impair the stratum corneum barrier function of the skin through changes to the secondary structure of proteins, reducing the disulphide bonds, and disruption of lipid hydrocarbons from the stratum corneum (Wahlberg, 1972; Suhonen *et al*., 1999; Rastogi and Singh, 2003; Lee *et al*., 2008).

5.3.2.6. H&E of the 3D epidermal model shows treatment effects upon epidermal thickness and morphology

To provide a realistic model of the epidermis to test the chemical depilatories upon, a 3D model was made using HEKn cells. This model comprised all the epidermal cell layers, including the barrier function of the stratum corneum, so this model gave an added defence to the skin from the chaotropic depilatories.

Cryosections of the models were taken in order to obtain thickness measurements of the epidermis. The epidermal thickness may give an indication of the extent of proliferation or differentiation occurring, or whether cells had been destroyed by treatments. No significant differences were found between the thicknesses of untreated and treated epidermal models 48 hours post-treatment ($p=0.249$, Kruskal-Wallis test). This also supports the findings of the 2D cultures. However, many of the models did not grow very well and there was at times a distinct variation of thickness within an individual model which makes it difficult to have firm conclusions of thickness. Non-significant differences were noted between the samples. Untreated epidermis (fig. 5.52A) was thicker averaging at 42µm than with the addition of DMSO at 35µm (fig. 5.52B and 5.54A). JNK inhibitor II increased the average thickness of the epidermal model to 53µm (fig. 5.52C and 5.54A). Treatment with 0.45M potassium thioglycolate produced the thickest average epidermis of 60µm (fig. 5.52D and 5.54A), and addition of JNK inhibitor II decreased this thickness to 43µm (fig. 5.54E and 5.54A). The average thickness after treatment with 0.44M guanidine carbonate was 43µm and approximately equal to that of the untreated epidermal model (fig. 5.52F and 5.54A).

There was less of a difference between samples 96 hours post-treatment ($p=0.314$, Kruskal-Wallis test). Again there were small differences between the average thicknesses of the various epidermal treatments. Untreated epidermis alone (fig. 5.53A) was again thicker at 54µm than the untreated epidermis with the addition of DMSO at 42µm (fig. 5.53B and 5.54B). Unlike at 48 hours post-treatment, after 96 hours the epidermal models treated with JNK inhibitor II had the lowest average thicknesses of all the treatments of 31µm (fig. 5.53C and 5.54B). This may be due to the inhibition of JNK driving differentiation, and depleting the basal cells. Treatment with 0.45M potassium thioglycolate again gave the thickest average epidermal measurements of 58µm (fig. 5.53D and 5.54B), perhaps due to increased proliferation and differentiation, and again the average thickness decreased with inhibition of JNK to 46µm (fig. 5.53E and 5.54B). Finally, 96 hours post-treatment with 0.44M guanidine carbonate gave an average thickness of 45µm which is lower than that of the untreated epidermis (fig. 5.53F and 5.54B).

H&E stained paraffin sections show the morphology of the epidermal model after each treatment. The untreated epidermis after 12 days at the air-liquid interface (48 hours

post-treatment of other samples) shows the stratum basale, the stratum spinosum above, followed by the stratum granulosum, and finally the stratum corneum (fig. 5.55A). With the addition of DMSO as a control for JNK inhibitor II treated samples, there appeared to be little change to the morphology of the epidermis; the basal cells line the insert, and the stratum spinosum, granulosum and corneum are clearly present (fig. 5.55B). Some epidermal models treated with JNK inhibitor II for 48 hours showed few basal cells, though others had fewer differentiated cells and a thin stratum corneum (fig. 5.55C). Although unexpected, the accelerated differentiation caused by the JNK inhibition might have led to a model with a thin epidermis as it consequently drives a faster need to replace those cells and exhausts the proliferative potential of the basal cells. There appeared to be little effect of 0.45M potassium thioglycolate on the epidermis 48 hours post-treatment, as figure 5.55D shows, though the stratum corneum may be slightly thinner. There was not obvious damage to the stratum corneum as observed in the isolated cornified envelopes which had been treated with potassium thioglycolate, with the exception of the epidermal model in figure 5.55E where the uppermost layer of cells, possibly the stratum corneum, appeared deformed. The aggregates observed on the treated isolated cornified envelopes may have been washed away by the H&E process. With the addition of JNK inhibitor II the stratum corneum appeared thinner, and in figure 5.55E the stratum corneum appeared to be covered by a layer of denatured cellular matter. The epidermis 48 hours post-treatment with 0.44M guanidine carbonate appeared relatively normal (fig. 5.55F).

The epidermal models 96 hours post-treatment generally appeared to have depleted the stratum basale and appear thinner than the models at 48 hours post-treatment. The untreated epidermis 96 hours post-treatment shows the four strata (fig. 5.56A). The epidermis model treated with only DMSO appeared very thin with few basal cells (fig. 5.56B). The epidermis treated with JNK inhibitor II for 96 hours had few living cells as well as a relatively thin stratum corneum (fig. 5.56C). The morphology of the epidermis after 96 hours post-treatment with 0.45M potassium thioglycolate appeared quite organised, with many basal cells and cells of the stratum spinosum, though there were few cells of the stratum granulosum, and there was stratum corneum present (fig. 5.56D). With the addition of JNK inhibitor II to the previous treatment, few living cell layers result, with more differentiated cells present (fig. 5.56E). Finally, the epidermis 96 hours post-treatment with 0.44M guanidine carbonate appeared to have fewer basal

cells, but a thick stratum corneum (fig. 5.56F). These results show that the epidermal structure is relatively resistant to treatment with potassium thioglycolate and guanidine carbonate.

5.3.2.7. 3D epidermal model immunohistochemistry

Immunohistochemistry was performed upon paraffin sections of the 3D HEKn epidermal model against HSP27, HSP70, keratin 14, involucrin and phalloidin 48 hours and 96 hours post-treatment. Immunohistochemistry images showing Ki67 were not included because the antibody strongly binds to the insert the cells are grown on, causing difficulty in identifying Ki67 positive cells. The treatments were for four minutes with the depilatory strength 0.45M potassium thioglycolate and 0.44M guanidine carbonate separately. The full strength depilatories were used for a direct comparison to the effects upon the epidermis *in vivo*. As with the previous experiments, 50µM JNK inhibitor II was added to a potassium thioglycolate treatment to test its effects upon proliferation, differentiation, and the acute stress response. For controls, untreated cells were used alone, along with the separate addition of 50µM JNK inhibitor II and DMSO.

HSP27 was present in the stratum spinosum and granulosum of the untreated epidermis model after 12 days at the air-liquid interface (fig. 5.57A). This is where it has been shown to be expressed in normal epidermal tissue (Huang *et al*., 2003; Yusuf *et al*., 2009). It was also present in the stratum spinosum when DMSO had been added (fig. 5.57B). In JNK inhibitor II treated epidermis, HSP27 appeared to be present, though at lower levels and not continuously, in the stratum basale, spinosum and granulosum (fig. 5.57C). The cultures treated with 0.45M potassium thioglycolate showed the HPS27 present in the stratum spinosum and granulosum (fig. 5.57D). The addition of JNK inhibitor II to the potassium thioglycolate still showed HSP27 present in the stratum spinosum and granulosum, although there also appeared to be a layer of denatured cellular material on top of the stratum corneum which expressed HSP27 (fig. 5.57E). This may also be part of the stratum corneum as it is likely to bind antibodies non-specifically (Abreu-Velez *et al*., 2012). Finally, 0.44M guanidine carbonate treated hair showed HSP27 present in the stratum spinosum and granulosum (fig. 5.57). These results showed there is little change in HSP27 at 48 hours post-treatment. At 96 hours post-treatment there appeared to be little HSP27 expressed. It was still expressed, though faintly, in the untreated epidermis model stratum spinosum and granulosum at the

equivalent of 14 days at the air-liquid interface, and few basal cells are present (fig. 5.58A). With the addition of DMSO the signal was very faint and only just detectable in a couple of cells of the stratum spinosum or granulosum (fig. 5.58B). With the addition of JNK inhibitor II, HSP27 was barely detectable (fig. 5.58C). Treatment with 0.45M potassium thioglycolate seemed to cause the epidermis to express HSP27, as it appeared to be present in the stratum spinosum and granulosum layers (fig. 5.58D). The addition of JNK inhibitor II to the potassium thioglycolate treatment caused the HSP27 signal to appear diffuse and possibly present in the stratum corneum of the epidermis as well as the stratum spinosum and granulosum (fig. 5.58E). This may be due to the drive towards differentiation causing HSP27 to become involved in the cornified envelope. There was little and diffuse signal from the 0.44M guanidine carbonate treated cells of HSP27 (fig. 5.58F).

HSP70 is usually expressed constitutively throughout the epidermis (Huang *et al*., 2003; Yusuf *et al*., 2009). HSP70 expression was observed at low levels in the untreated epidermis model 48 hours post-treatment (fig. 5.59A). It was more clearly expressed throughout the living cell layers in the epidermal model treated with DMSO (fig. 5.59B). Expression of HSP70 was observed in the living cell layers and less strongly in the stratum corneum of the untreated epidermal model with added JNK inhibitor II (fig. 5.59C). The epidermal models treated with potassium thioglycolate show HSP70 was present mostly in the living cell layers, though the signal was weak (fig. 5.59D). With the addition of JNK inhibitor II to the potassium thioglycolate treated cells, there was stronger staining throughout the epidermis, including the cellular matter on top of the stratum corneum (fig. 5.59E). The epidermal model treated with guanidine carbonate showed the HSP70 expressed throughout the cell layers (fig. 5.59F). This shows there was expression of HSP70 48 hours post-treatment, however, there was no HSP70 expression in the epidermal model 96 hours post-treatment (fig. 5.60).

Keratin 14 is expressed in all active cells in the basal layer and downregulation occurs with differentiation (Fuchs and Green, 1980; Moll et al., 1982; Fuchs, 2008). The untreated epidermis showed the keratin 14 present in the stratum basale with expression tapering off with differentiation (fig. 5.59A). With the addition of DMSO to the untreated epidermis, keratin 14 expression was strong in the stratum basale and also in the stratum spinosum, it was less strong in the stratum granulosum and was not

detectable in the stratum corneum (fig. 5.59B). The presence of keratin 14 in the stratum spinosum was normal as it is a long-lived protein and does not necessarily disappear immediately when cells differentiate. This distribution of expression was also seen in the untreated epidermis with the addition of JNK inhibitor II (fig. 5.59C). In epidermal models treated with potassium thioglycolate there was strong expression in the stratum basale and spinosum layers, which reduces into the granulosum layer (fig. 5.59D). With the addition of JNK inhibitor II to the potassium thioglycolate treated epidermis, keratin 14 expression remained strong in the stratum basale, reducing with differentiation, however the cellular matter residing above the stratum corneum also expressed keratin 14 (5.58E). Expression of keratin 14 was also strong in epidermal models treated with guanidine carbonate, particularly in the basal cells and some cells of the stratum spinosum (fig. 5.59F). There was much less expression of keratin 14 in epidermal models 96 hours post-treatment (fig. 5.60). In the untreated epidermal model keratin 14 was expressed in the living cell layers (fig. 5.60A), but this expression decreased with the addition of DMSO (fig. 5.60B). The addition of JNK inhibitor II also saw a decrease in keratin 14 expression, though there was expression in the thin living cell layers (fig. 5.60C). Again, less expression of keratin 14 was observed in cells treated with potassium thioglycolate as more differentiation had occurred and there were fewer living cells present, especially basal cells. Though the bottom layer of cells appeared to be of the stratum spinosum and expressed keratin 14, with the layer above expressing less (fig. 5.60D). The epidermal models treated with potassium thioglycolate and JNK inhibitor II did not express any keratin 14 (fig. 5.60E). A small degree of keratin 14 expression was only observed in the least differentiated bottom layer of cells which appeared to be of the stratum spinosum in the guanidine carbonate treated epidermis (fig. 5.60F). The epidermal models with little keratin 14 expression suggest the mitotically active basal cell population have been depleted, and this occurred in 96 hour post-treatment models treated with potassium thioglycolate with JNK inhibitor and guanidine carbonate in particular.

Involucrin has been shown to be an early indicator of keratinocyte differentiation to the cornified envelope (Steinert and Marekov, 1997; Marekov and Steinert, 1998; Steinert and Marekov, 1999). In the untreated epidermal model 48 hours post-treatment involucrin expression began in the stratum spinosum and became stronger in the stratum granulosum, and a small amount appeared detectable in the stratum corneum

(fig. 5.61A). The expression pattern appeared similar with the addition of DMSO (fig. 5.61B). However, with the addition of JNK inhibitor II, involucrin appeared earlier in cell layers and expression in the cells beneath the stratum corneum appeared weaker than in untreated epidermis (fig. 5.61C). Epidermal models treated with potassium thioglycolate showed involucrin expression began in the stratum spinosum and increased in the stratum granulosum (fig. 5.61D). Again, the addition of JNK inhibitor II to the potassium thioglycolate treated cells caused the involucrin to appear earlier in the cell layers (fig. 5.61E). Here involucrin was also expressed in the cellular matter above the stratum corneum. Keratinocytes treated with guanidine carbonate also show involucrin expression in the stratum spinosum and granulosum (fig. 5.61F). Involucrin was expressed 96 hours post-treatment, though there may be fewer cell layers present to express it (fig. 5.62). In the untreated epidermal model 96 hours post-treatment, involucrin was expressed in the stratum spinosum and granulosum (fig. 5.62A). With the addition of DMSO there was less involucrin expression though it was still present in the outer living cell layers of the epidermis (fig. 5.62B). With the addition of JNK inhibitor II, involucrin expression was observed in stratum spinosum, increasing in the stratum granulosum and weakly in the stratum corneum (fig. 5.62C). Potassium thioglycolate treated epidermal models show involucrin expression started in the stratum spinosum and was stronger in the stratum granulosum, and weaker in the stratum corneum (fig. 5.62D). The addition of JNK inhibitor II to the potassium thioglycolate treated keratinocytes depleted the cell layers by 96 hours post-treatment, which resulted in weak involucrin expression in the remaining living cell layer of the stratum granulosum and in the stratum corneum (fig. 5.62E). Finally, treatment of keratinocytes with guanidine carbonate resulted in involucrin expression in the outer living cell layers of the epidermis (fig. 5.62F).

Phalloidin stained the filamentous actin in the epidermal models and showed the structure of the epidermis. In the untreated epidermis, 48 hours post-treatment, phalloidin stained all of the cell layers and increased in intensity in the stratum corneum (fig. 5.63A). With the addition of DMSO, phalloidin again stained the whole epidermis, particularly the stratum corneum (fig. 5.63B). Using phalloidin shows the stratum corneum is thicker in epidermal models treated with JNK inhibitor II for 48 hours (fig. 5.63C). Phalloidin also showed the intact stratum corneum of the potassium thioglycolate treated epidermal model (fig. 5.63D). With the addition of JNK inhibitor II

to the potassium thioglycolate treated cells, phalloidin stained all of the cell layers including the stratum corneum (fig. 5.63E). This was also true for guanidine carbonate treated cells (fig. 5.63F). For epidermal models 96 hours post-treatment, the phalloidin showed the extent of the stratum corneum along with the living cell layers. For the untreated epidermis, phalloidin showed there were still many living cell layers present with a thick epidermis (fig. 5.64A). With the addition of DMSO, the actin was stained brightly showing a thick stratum corneum, though there were fewer living cell layers (fig. 5.64B). There were even fewer living cell layers in the JNK inhibitor II treated epidermis, and the phalloidin staining showed the stratum corneum breaking away from the epidermis (fig. 5.64C). In the potassium thioglycolate treated keratinocytes there were more differentiated cell layers along with several layers of stratum corneum (fig. 5.64D). With the addition of JNK inhibitor II to potassium thioglycolate treated cells there were fewer living cell layers along with the stratum corneum layer (fig. 5.64E). The guanidine carbonate treated cells showed an equal number of living cell layers to the potassium thioglycolate treated cells and an intact stratum corneum for protection from the depilatory (fig. 5.64F).

In conclusion, the treatments did not appear to affect HSP expression in the epidermis. Increased differentiation caused by the JNK inhibitor II caused less keratin 14 expression, involucrin to appear earlier in the cell layers and a thicker stratum corneum. However, the depilatory treatments did not appear to have an effect on keratinocyte proliferation, differentiation or the acute stress response.

5.4. Discussion

5.4.1. Effects of depilatory treatments upon the hair

Each of the commercial and novel depilatory treatments are summarised and discussed with respect to their effect upon the hair.

5.4.1.1. The hydrophilic endocuticle and keratin filaments contribute to swelling during hair hydration

Hydration of the untreated hair caused a small increase in diameter of an average of 13.1%. A similar measure of swelling has been recorded previously as the hydration breaks the hydrogen bonds and electrostatic bonds in the keratin (Corbett, 1976; Xiao and Hu, 2016). The endocuticle is particularly susceptible to swelling with hydration due to its low cross-linking density and both the endocuticle and keratin contains hydrophilic polar groups contributing to swelling during hydration (Swift and Bews, 1976; Richena and Rezende, 2016). After treatment with depilatories containing potassium thioglycolate, water may contribute to the increase in the swelling of the hair after the structure has been compromised (Reed *et al*., 1946; Powers and Barnett, 1952).

It was found that there was no significant difference in the swelling of the sub-skin-surface root and distal tip of the hair. Since the root of the hair is in an aqueous environment in the skin (Mathes *et al*., 2016), once plucked it would have dried out. This would have allowed it to swell a similar amount to the distal tip of the hair once hydrated again.

5.4.1.2. Calcium thioglycolate is more efficacious than other non-thioglycolate based chemistries

Treatment of the hair with the Sally Hansen Facial Depilatory, the active depilatory component of which is calcium thioglycolate, showed that there was loss of cuticle and change to the fluorophores or chemical environment of the hair. This was shown by a significant difference between the lifetime of the untreated hair cuticle and that of the calcium thioglycolate treated hair cuticle when the hair was excited with 640nm. The chemical environment of the hair may have been changed by the reduction of the disulphide bonds in the hair. There are no published papers on the mechanism of calcium thioglycolate induced chemical hair changes, though the mechanism is likely to be similar to that of potassium thioglycolate. The experiments upon the 3D epidermal

model and the cornified envelopes also reflect some of the changes taking place in the hair. In some of the 3D models treated with potassium thioglycolate and JNK inhibitor II the top layers of the stratum corneum were denatured. Furthermore, in the potassium thioglycolate treated cornified envelopes stained with Nile red there were aggregates upon their surfaces. This suggests some structural and lipid damage to the corneocytes of the stratum corneum, which may also be occurring in the hair cuticle. This work is supported by previous studies of calcium thioglycolate application to the stratum corneum. These studies showed loosening and absence of the intracellular keratin matrix and weakening of the intercellular adhesion of cornified envelopes as well as the intercellular lipid lamellae (Wahlberg, 1972; Suhonen *et al*., 1999; Rastogi and Singh, 2003; Lee *et al*., 2008).

The breaking of the disulphide bonds by calcium thioglycolate led to a break ratio reduction of 15%. This reduction in strength was more than treatments without thioglycolate, but less than those with potassium thioglycolate, suggesting potassium thioglycolate is more efficacious than calcium thioglycolate.

An average swelling of 15.0% was reported after hydration of the treated hair, which although it had a faster increase in diameter than non-thioglycolate treated hairs, after ten minutes the difference was not significant. It may have had a faster increase in diameter than hairs treated with chemicals other than thioglycolate because the water molecules would be able to penetrate the hair faster since the structure had already been damaged by the reduction of disulphide bonds. However, the damage was not extensive enough to distinguish the swelling from that of untreated hair.

These results show that calcium thioglycolate treatment significantly affected the fluorescence lifetimes in the hair, therefore changing the chemical environment of the hair. This treatment also reduced the strength of the hair, though is less efficacious than treatments which include potassium thioglycolate as a component.

5.4.1.3. Potassium thioglycolate is the second most efficacious depilatory

Treatment of the hair with 0.45M potassium thioglycolate caused loss and deformation of the cuticle cell layers and dramatic swelling of the hair. This may be occurring due to the keratin filaments becoming looser due to the broken disulphide bonds (Jachowicz and McMullen, 2011), and the water expanding the hair after the action of the potassium thioglycolate (Reed *et al*., 1946; Powers and Barnett, 1952). An average width

increase was found of 136% and is significantly different to hydrated hair as well as hair treated with other thioglycolate compositions and guanidine carbonate. However, the TEM and maleimide showed the thioglycolate only attacked the outer 10µm of the hair. The large amount of swelling may be due to water accessing more of the keratin filaments in the cortex, which then evaporates back out when the hair dries. Measuring the swelling due to water at the widest point gave an average increase of 33.5%, and was significantly different to treatments not based upon potassium thioglycolate. The remaining swelling must be accounted for by the potassium thioglycolate solution.

FLIM measurements showed that potassium thioglycolate significantly changed the fluorophores or chemical environment in the hair, as the lifetimes were significantly lower than the untreated hair lifetimes. Potassium thioglycolate reduces disulphide bonds in the KIFs and KAPs within the hair, which is likely to change the protein-protein interactions between the amino acid residues, affecting fluorophores, particularly tryptophan and its kynurenine oxidative metabolites as the disulphide bond in cystine has a quenching effect upon their fluorescence (Jachowicz and McMullen, 2011). Previous studies show that thioglycolate preferentially reduces the disulphide bonds within KAPs in the matrix and between the KAPs and KIFs, than within KIFs (Zabashta *et al*., 2012). The bonds are reduced within the KAPs causing them to change from an ellipsoidal protein to multiple spherical proteins (Suzuta *et al*., 2012). Ridges and troughs were visible in the cuticle of hairs imaged for FLIM which required dried hairs, and was perhaps caused by the evaporation of water from the hair after it had permeated the compromised structure. Calcium and potassium thioglycolate have lower fluorescence lifetimes than control hair in this experiment, whereas in the last chapter they had higher lifetimes. This may be because in the previous chapter an aqueous solution diluted by an order of ten was used in order to preserve the hair cuticle structure and hairs were treated individually, whereas here the hair had been treated by P&G using cream and a bundle of hair. The difference between aqueous and cream solution is that aqueous thioglycolate is more available to attack the hair, whereas hair treated in bundles with cream is limited by the close packing of the fibre and the cream is less efficacious (Reed *et al*., 1946). The concentration of potassium thioglycolate and the type of treatment may have affected the fluorescence lifetimes, but with either treatment the differences to untreated hair are significant and likely due to the reduction of disulphide bonds.

The hair treated with potassium thioglycolate was also found to have a break ratio reduction of 27%. This means the strength of potassium thioglycolate treated hair is weaker than calcium thioglycolate treated hair, but stronger than hair treated with potassium thioglycolate with the addition of guanidine carbonate.

5.4.1.4. Potassium thioglycolate with guanidine carbonate is the most efficacious depilatory

Treatment of hair with 0.45M potassium thioglycolate and 0.44M guanidine carbonate resulted in the most damage to the hair. Treatment with potassium thioglycolate and guanidine carbonate caused invaginations into the hair and holes through the cuticle. Once the cuticle barrier was broken, this would have allowed more depilatory into the hair, contributing to the increased rate of swelling to a final increase in diameter of 301%. This is supported by a previous study which has shown that the high pH of thioglycolate raises the cuticle cells, facilitating increased depilatory penetration into the hair (Velasco *et al*., 2009). P&G measured an average swelling of 39.7% after hydration which was significantly higher than other treatments, showing that water accounts for some of the swelling during treatment.

The hair remains brightly autofluorescent after treatment which may be due to treatment of hair with thioglycolate. This increases tryptophan autofluorescence in the hair by decreasing the number of fluorescence quenching disulphide bonds, and increasing the space and mobility of the keratin chains (Jachowicz and McMullen, 2011).

Much like the hairs treated with potassium thioglycolate alone, this treatment resulted in the outer approximate 10µm of the hair stained brightly with maleimide to show the area of reduced disulphide bonds. Although both treatments appeared to have penetrated the hair by the same distance, since potassium thioglycolate and guanidine carbonate is the more efficacious treatment it is likely to have been more efficient due to the action of guanidine, reducing more disulphide bonds and loosening keratin filaments more than treatment with potassium thioglycolate alone to grant a greater expansion with treatment.

Cuticle cell layers became detached during treatment, which may have been because the CMC between the cuticle cell layers was dissolved (Chao *et al*., 1979; Strussman, 1983; Zahn *et al*., 1986). Alternatively, cuticle cell layers may have become detached due to the extraction of S100A3, a calcium-binding protein of high cysteine content

(Kizawa *et al*., 2002), from the endocuticle, which resulted in fracturing of the cuticle cell layers and loss of mechanical strength (Kizawa *et al*., 2005). This treatment degraded the cuticle cell layers, however some areas of the cuticle appeared less affected than others. The areas more affected may have already been thinner due to weathering, or there may have been an uneven distribution of chemicals in the treatment solution.

It was surprising that FLIM of the treated hair did not show significant differences in lifetime compared to untreated hair despite extreme changes to the hair structure and morphology. This may be due to the guanidine in the treatment affecting the lifetime, bringing it back closer to the lifetime of untreated hair. FLIM might be more effective in showing differences in chemical environment of hair surrounded by the treatment solution, because once the hair dries, the chemical environment changes, and fluorescence lifetimes will not reflect the total damage occurring in an applied setting.

Treatment with potassium thioglycolate and guanidine carbonate also gave a 56% reduction in the strength of the hair, which is the largest reduction in strength of all hair treated with thioglycolate or guanidine.

5.4.1.5. Guanidine carbonate is not as effective without thioglycolate

Treatment of the hair with guanidine carbonate at pH12.5 was shown only to disrupt the cuticle and showed little damage to the hair structure as a whole. Treatment of the hair with guanidine carbonate at pH11.4 would make a poor depilatory treatment as it appeared to have less effect on the structure and morphology of the hair than guanidine at the higher pH. Swelling was observed at the cut end of the hair, and there was an average increase in diameter of 13% after treatment, but it was not significantly different to control hair. This may be because although guanidine forms hydrogen bonds with the water which decreases the surface energy (Miyake and Oyama, 2009), and makes it easier for the keratin to unfold, the disulphide bonds within the hair are not cleaved. Guanidine carbonate and calcium hydroxide are used together as hair relaxers to chemically straighten curly hair. This occurs through the guanidine carbonate and calcium hydroxide reacting to produce calcium carbonate and the active chemical guanidine hydroxide. Guanidine hydroxide reacts with approximately 35% of the disulphide bonds in the cystine of the KIFs and KAPs to produce lanthionine ($C_6H_{12}N_2O_4S$) which is a monosulphide ester analogue of cystine (Khumalo *et al*., 2010; Miranda-Vilela *et al*., 2013). The treatment also results in minor hydrolysis of peptide bonds (Wong *et*

al., 1994). However, this process had little effect on the straight Chinese scalp hair fibres and does not sufficiently weaken the hair to be considered as a depilatory treatment.

The cuticle cell layers were shown to separate using TEM with guanidine at both pH12.5 and pH11.4. The guanidine may affect the CMC between the cells, perhaps caused by the loss of 18-MEA (Miranda-Vilela *et al*., 2013). FLIM did not show any difference in cuticle lifetimes between guanidine carbonate at pH12.5 treated hair cuticles and the cuticles of the control hair. This suggests FLIM may not show all changes in the cuticle chemical environment or changes occurred which involved fluorophores not excited by 470nm or 640nm. Although this may simply be due to the lower resolution of the FLIM images where the CMC may be undetectable.

Sporadic low fluorescence lifetimes were found on the cuticle of hair treated with guanidine at pH11.4, which could be damaged areas, and may be linked to the TEM images showing some cuticle cells are more affected by the treatment than others. Surprisingly, guanidine at pH11.4 had a significantly higher cortex lifetime when excited with 640nm than control hair. As guanidine at pH12.5 did not cause a significant change in lifetime, the decrease in alkalinity of the treatment may be responsible. Alternatively, it may simply be due to variation between hairs and a larger sample size is required.

Guanidine caused a break ratio reduction of 8% so the strength of the hair was decreased slightly. Previous studies have also shown a decrease in tensile strength of the hair (Miranda-Vilela *et al*., 2013). However, even at pH12.5, guanidine carbonate does not act as an effective depilatory, despite some changes to the hair structure. Only in conjunction with potassium thioglycolate does guanidine make an effective depilatory.

5.4.1.6. Lithium bromide changes hair morphology dependent upon treatment temperature and duration

Hair was treated with lithium bromide under four different conditions, only two of which appeared to affect the hair. Hair treated at 85°C or for 5 days appeared to have more compact cuticle cells, and the cortex of the hair treated at 85°C appeared swollen. The hair was observed to be very elastic which was likely due to the hydrogen bonds between the lithium bromide and keratin filaments stretching with the applied force. The break ratio reduction measurements for the hair treated at 25°C for 20 minutes found an 8% reduction in strength compared to untreated hair, so despite not affecting

the whole hair, a smaller degree of penetration by lithium bromide is still sufficient to reduce its strength and be of value to hair care companies. The emission spectra appear normal and the only significant difference in fluorescence lifetime was that of the medullas of 470nm excited hair of the hairs which were treated for 5 days, perhaps because the lithium bromide had infiltrated the medulla by this time.

As previously discussed, these differences may be due to the rate of lithium bromide penetration, which is dependent upon concentration, hair diameter and temperature (Haly and Griffith, 1958; Feughelman *et al*., 1962). The ability to make hairs shorter by contraction may be of interest to the hair care industry as hairs could be treated to appear shorter for longer, reducing the need to remove them. However, a catalyst may be required to speed up the process as these results show that penetration of lithium bromide into hair leading to contraction takes too long or is too hot for the treatment to be suitable as a depilatory. In addition to this, the high molarity required could become corrosive to the skin.

5.4.1.7. Calcium iodide and SLS cause breakage of cuticle cells

Hair was treated with calcium iodide which then precipitated out of the hair following the addition of SLS, resulting in parts of the cuticle cell fracturing away. A higher concentration of SLS at 28% caused the cuticle cells of the hair to become raised, as the strong surfactant would have removed some of the soluble lipids from the CMC and caused cuticle cell uplift (Gould and Sneath, 1985; Robbins, 2012). A study using 5% SLS showed that the cuticle cells became increasingly raised until they had been submerged in SLS for 15 hours, after which the cuticle cells became less raised (Singh and Umapathy, 2011). This study suggests that the raising of cuticle cells may also be due to swelling of the epicuticle and A-layer, which after 15 hours in SLS are eroded away (Singh and Umapathy, 2011).

With the addition of 25% calcium iodide to 2% SLS the structure of the hair cuticle is affected to varying degrees. Some hairs only showed the cuticle cells on the surface of the hair became raised, in other hairs many cell layers of the cuticle had been broken away by the precipitation of the calcium ions from the hair so that the cortex became visible. The visualisation of the beard hair cortex showed that the treatment removed several layers of cuticle cells. The variability in the results also suggest that some areas of the cuticle are weaker or more susceptible to calcium ion uptake. The calcium may

be binding to S100A3 in the endocuticle, which results in fracturing of the cuticle cell layers when it is precipitated with the SLS (Kizawa *et al*., 2005). The calcium which is precipitated out of the hair by the SLS may also be present in the exocuticle and A-layer (Smart *et al*., 2009; Evans *et al*., 2011).

There were no significant differences between the fluorescence lifetimes of calcium iodide and SLS treated hair, and untreated hair. This may be due to the fact that the calcium is removed from the hair by the SLS. Low lifetimes at the free edge of cuticle cells could be caused by the raised cuticle cells exposing the sublamellar structure of the cuticle, resulting in a different lifetime, or showing exposed areas of the cuticle which have been removed by the treatment.

These results show that calcium iodide with SLS is effective at removing some of the cuticle cells. Repetition of the treatment over time may lead to hair loss, however it is unlikely to be suitable as a one-step hair removal treatment.

5.4.1.8. CTAB and SLS causes cuticle cell flaring with loss of 18-MEA

Hair treated with CTAB and SLS caused varying degrees of cuticle cell flaring. This is likely due to the CTAB removing the 18-MEA from the outer β-layer of the CMC, as well as removal of some soluble lipids from the CMC by the SLS and swelling of the A-layer and epicuticle (Gould and Sneath, 1985; Singh and Umapathy, 2011; Robbins, 2012).

FLIM showed the free edge of each cuticle cell had a lower lifetime which could be caused by the raised cuticle cells exposing the cuticle sublamellar structure, resulting in a different lifetime. However, there were no significant differences between the fluorescence lifetimes of CTAB and SLS treated hair, and untreated hair. In the previous chapter, treatment of the hair with CTAB resulted in significantly different fluorescence lifetimes in the hair. The lifetime does not change significantly using the CTAB and SLS method because there may be residual CTAB on the hair and the released hair lipids may also be adhering to the hair surface as the hair was not rinsed under acidic conditions, as it was in the lipid extraction method (Smith *et al*., 2010).

CTAB and SLS treatment removes 18-MEA from the hair surface, making it more hydrophilic, and the treatment reduces the strength of the hair by 5%. The increased hydrophilicity and reduction in hair strength may make the treatment attractive to hair care research, perhaps as a primer to make the hair more pliable to further treatments.

5.4.2. Effects of depilatory treatments upon keratinocytes

Although the chemicals tested may prove of use to the hair care industry in ways other than hair-removal, potassium thioglycolate with guanidine carbonate was found to be the most efficacious depilatory, second only to the commercial depilatory, potassium thioglycolate. Both of which were chosen, as the best novel and commercial depilatories, to be tested upon HaCaT cells in 2D culture and HEKn cells in 3D culture.

The cell assays are discussed and then each of the proteins targeted with immunoblotting are summarised and discussed with respect to the effect upon them with potassium thioglycolate and guanidine carbonate.

5.4.2.1. Cell survival and cell viability assays show 0.4M guanidine carbonate kills the HaCaT cells

When the ability of the HaCaT cells to survive or remain viable was tested, it was revealed that 0.4M guanidine carbonate negatively affected these abilities. Very few HaCaT cells remain after 0.4M guanidine carbonate treatment, as shown by the cell viability assay measuring an average metabolic activity at only 7% of that of the untreated cells.

Guanidine carbonate is likely to affect the cells negatively because it is a chaotropic agent. The molecule guanidine hydroxide has been shown to cause irritation in the scalp when used as a hair relaxer (Syed, 1995; Syed and Naqvi, 2000). Hence the effects of guanidine carbonate on HaCaT cells were studied using lower concentrations in immunoblotting and immunofluorescence.

The fact that 0.4M guanidine carbonate lowers the viability of the HaCaT cells shows that it should not be used on wounds where the basal cells may be exposed.

5.4.2.2. Cornified envelopes are affected by potassium thioglycolate treatment

HaCaT cells treated with 0.45M and 0.2M potassium thioglycolate showed aggregates upon their surface. Thioglycolate has been shown to impair the barrier function of the skin through changes to the secondary structure of proteins, reducing the disulphide bonds, and disruption of lipid hydrocarbons from the stratum corneum (Wahlberg, 1972; Suhonen *et al*., 1999; Rastogi and Singh, 2003; Lee *et al*., 2008). Additionally, when beard hair was treated with potassium thioglycolate, aggregates appeared on the cuticle surface, similar in appearance to those upon the cornified envelopes. This suggests the

aggregates may have resulted from the disruption to the lipids and disulphide bonds in proteins of the cornified envelopes, however the isopeptide bonds induced by transglutaminase-3 are not affected and contribute most to cornified envelope rigidity (Thibaut *et al*., 2009).

5.4.2.3. Heat shock proteins 27 and 70 are not involved in the stress response to depilatory treatment

No significant differences were found in the levels of HSP27 or HSP70 between cell treatments. Only one non-significant finding was found which correlated between Western blotting, immunofluorescence of HaCaT cells and immunohistochemistry of the epidermal model. This finding was that HSP27 is higher in untreated samples than in samples with DMSO, so DMSO may inhibit HSP27 production slightly. In addition to this, less HSP is found 96 hours post-treatment. This is likely due to the expression of HSP attenuating with time, perhaps in response to handling of the cultures rather than due to the treatments as no significant differences were found between untreated cultures and treated cultures. There was no significant difference in HSP levels in cells treated with JNK inhibitor II, and JNK is modulated by HSPs (Mosser *et al*., 2000), again showing HSPs are unlikely to be involved in the response to depilatory treatment. These results suggest that stress to the cells from depilatory treatment is not affecting the HSP response.

HSP27 and HSP70 have been shown to be upregulated in dermal allergic contact hypersensitivity and are involved in the immune response as they activate the toll-like receptor-4 which stimulates production of cytokines by dendritic cells to increase antigen presentation by T-cells (Yusuf *et al*., 2009). A previous study shows HSP27 and HSP70 are induced by dermal exposure to the vesicant sulphur mustard, and their expression has been shown to be suppressed by JNK inhibitor, suggesting MAP kinases regulate HSP27 and HSP70 (Black *et al*., 2011).

Since stress to the skin has been observed from depilatory treatment in previous studies and cell viability has been lowered through depilatory treatment, it may be that proinflammatory cytokines are released after chemical depilatory treatment. There is evidence that that cytokines have a role in inflammation and expression of interleukin-1α, interleukin-1 receptor antagonist, interleukin-8, and interleukin-10 becomes raised in the epidermis (Hauser *et al*., 1986; Nickoloff and Naidu, 1994; Perkins *et al*., 2001).

One study has shown that guanidine carbonate treatment as a hair relaxer induces prostaglandin E_2, and the cytokines interleukin-1α and interleukin-1 receptor antagonist expression (Tackey *et al*., 2013). Future work should include assays such as ELISAs from conditioned media or RT-PCR to measure the cytokine response to chemical depilatory treatment to assess irritation in the skin.

5.4.2.4. Keratinocyte differentiation is not increased by depilatory treatment

No significant differences were found in levels of keratin 14 between cell treatments. There appeared to be less keratin 14 expression with time, as the more time spent at the air-liquid interface the lower the keratin 14 expression, which is likely due to differentiation depleting the numbers of basal cells where keratin 14 is primarily expressed.

Western blotting showed the amount of involucrin varied significantly only between cell cultures with and without the addition of JNK inhibitor II. This suggests only the JNK inhibitor is significantly affecting differentiation, not the depilatory treatments. Therefore, depilatory treatment does not increase levels of differentiation in keratinocytes.

Raised expression of involucrin was observed by immunofluorescence in potassium thioglycolate treated HaCaT cells with added JNK inhibitor. Raised expression was also observed by immunohistochemistry of the same treatment in the stratum corneum of the epidermal model. However, the levels of involucrin were significantly lower in JNK inhibitor treated cultures when analysed using Western blotting when they would be expected to be higher due to increased differentiation. Previous studies show that inhibiting JNK with the JNK inhibitor II, SP600125, increases differentiation of keratinocytes (Gazel *et al*., 2006; Kitagawa *et al*., 2014) with increased involucrin expression (Gazel *et al*., 2006). The reason for the low amounts of involucrin detected with JNK inhibition treatment in Western blots could be because the proteins of the cornified envelope are insoluble (Rice and Green, 1977; Nemes and Steinert, 1999). The protein extraction method for Western blotting may not have extracted the involucrin from the cornified envelope, leading to the small amounts of involucrin on the blots. Most of the involucrin may have been within an increased number of cornified envelopes in JNK inhibitor treated cultures, or there could be less involucrin in the living cell layers of the JNK inhibitor treated cultures due to increased differentiation.

In order to correctly measure the amount of involucrin present in JNK inhibitor II treated HaCaT cells, the involucrin cross-linked in the cornified envelopes needs to be liberated by trypsin digestion. However, analysis would be complicated by the cross-linked peptides containing parts of two different proteins. Alternatively, following a protocol from a successful blotting of involucrin should allow for correct quantification, such as in Gazel *et al*., 2006.

5.4.2.5. Proliferation does not increase with depilatory treatment

The proliferation marker, Ki67, showed there were significantly fewer cells in M-phase after potassium thioglycolate with JNK inhibitor II treatment. This significant difference was not observed in cells only treated with potassium thioglycolate or JNK inhibitor alone, so it is likely due to the combined effect of both treatments. The JNK inhibitor has been shown to reduce keratinocyte proliferation in previous studies (Gazel *et al*., 2006; Kitagawa *et al*., 2014), and this is supported by the significant increase in cells found in S-phase with JNK inhibitor treatment.

Epidermal thickness measurements showed no significant differences between the treatments, suggesting if differentiation or proliferation had increased, so too had the rate of cornified envelopes sloughing off the stratum corneum or being retained to keep the epidermal thickness relatively constant.

5.4.2.6. JNK inhibitor II treatment led to larger cells and increased apoptosis with potassium thioglycolate treatment

When confluent cells were treated with the JNK inhibitor II, the cells appeared much larger. This phenomenon is unreported in the literature. This suggests that inhibiting JNK increases the size of the cell morphology, perhaps because they are differentiating, which involves the flattening of keratinocytes. It would be interesting to study the effects of JNK inhibition on cytoskeletal organisation. In addition, where the cells have been treated with depilatories, some cells may have been destroyed, creating more space for new cell spreading, however JNK inhibition has also been shown to inhibit cell mobility (Gazel *et al*., 2006). The JNK inhibitor II affects a large fraction of the kinome (Fabian *et al*., 2005), so may also be affecting cell growth.

The numbers of cells undergoing apoptosis were counted using DAPI in immunofluorescence of HaCaT cells. The 1 hour post-treatment cultures showed a higher average number of cells were apoptotic in the 0.45M potassium thioglycolate

treatment with added JNK inhibitor than any other condition. This was followed by 45mM potassium thioglycolate, and finally the 44mM guanidine carbonate treatment, though these results were not significant. The 48 hours post-treatment differences are significant. There was a significant increase in apoptotic cells after treatment with 0.45M potassium thioglycolate with added JNK inhibitor II, suggesting the JNK inhibitor II is not preventing apoptosis and its inhibition may be promoting apoptosis. However, this finding is not supported by other studies, which have found that JNK inhibition provides protection against apoptosis of HaCaT cells when irradiated with UV light (Lee *et al*., 2009) or when cytotoxic chemicals have been applied to the cells (Lu *et al*., 2011; Black *et al*., 2013).

The cell viability assay showed that 0.4M guanidine carbonate significantly lowered cell viability to 7% that of untreated control cells and decreased viability of 0.4M potassium thioglycolate treated HaCaT cells to 76%. This shows that the depilatory chemicals do affect apoptosis of HaCaT cells, though keratinocytes in the epidermal model appear to have additional protection from the chemicals by the stratum corneum.

5.4.3. Conclusion

The most efficacious chemical hair depilatory is the novel combination of potassium thioglycolate with guanidine carbonate. The second most efficacious chemical hair depilatory is the commercial potassium thioglycolate as present in Veet HydroRestor. These two depilatories do not appear to affect keratinocyte differentiation, proliferation, or stress through the HSP pathway. Therefore, potassium thioglycolate with guanidine carbonate may be a viable product for market, though more research should be carried out upon any cytokine production in the skin. Additionally, these results show that potassium thioglycolate with guanidine carbonate should not be used upon damaged skin where basal cells may be exposed, as the HaCaT cells have been negatively affected by 0.4M guanidine carbonate. Nor should potassium thioglycolate with guanidine carbonate be used upon areas with a thinner stratum corneum, such as the face, as more layers of cornified envelopes should be present to protect the underlying living cell layers.

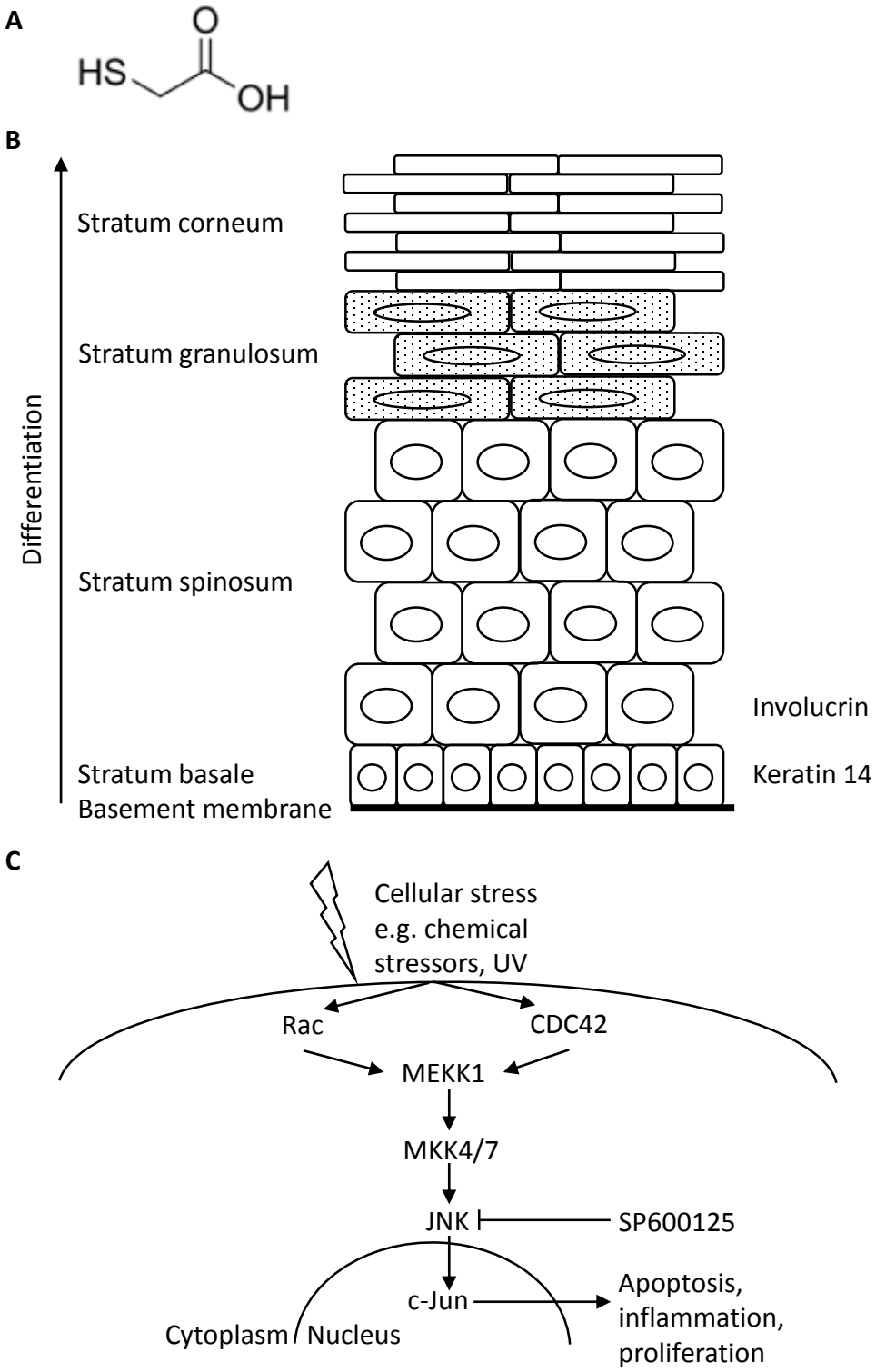

Fig. 5.1. A) Chemical structure of thioglycolic acid. B) Schematic of the epidermis. The four cell layers of the epidermis increasingly differentiate as they migrate to the skin surface. Keratin 14 is principally found in basal cells and involucrin expression starts at the stratum spinosum. **C) Simplified schematic of the JNK pathway.**

A

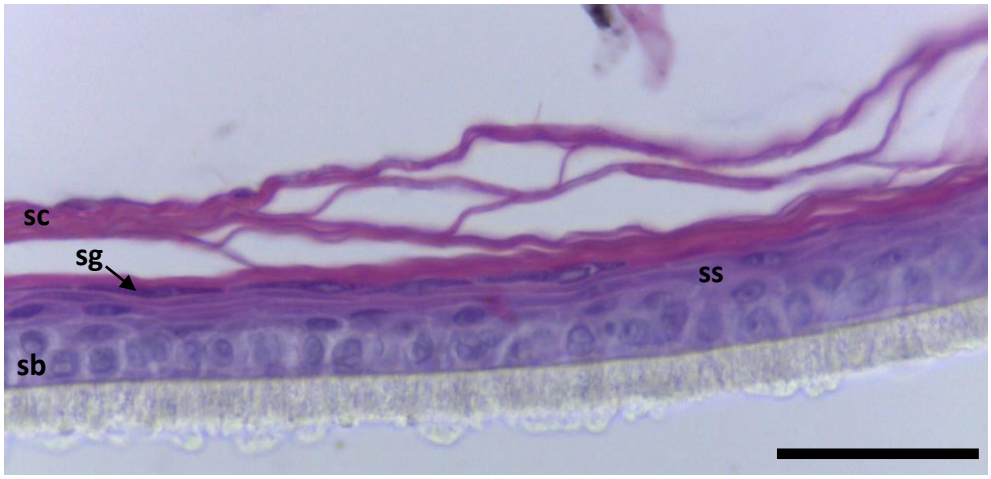

B

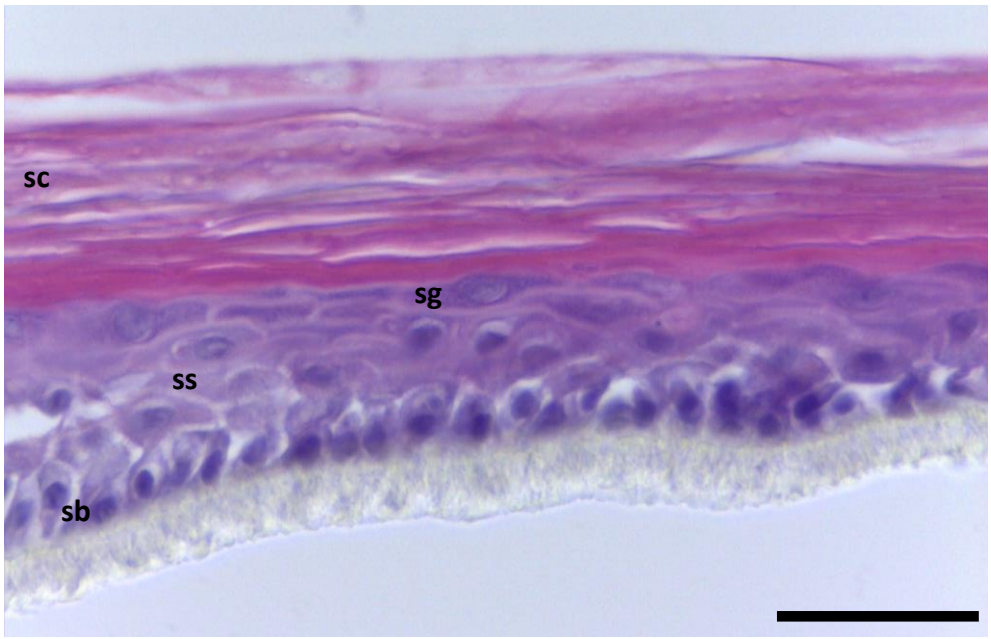

Fig. 5.2. H&E stained passage 3 and passage 4 HEKn epidermal models. A) Epidermal model using recently thawed P3 HEKn cells. A representative photomicrograph of 2 imaged models is shown. B) Epidermal model using recently passaged P4 HEKn cells. A representative photomicrograph of 3 imaged models is shown. Sc = stratum corneum, sg = stratum granulosum, ss = stratum spinosum, sb = stratum basale. Scale bars = 50µm.

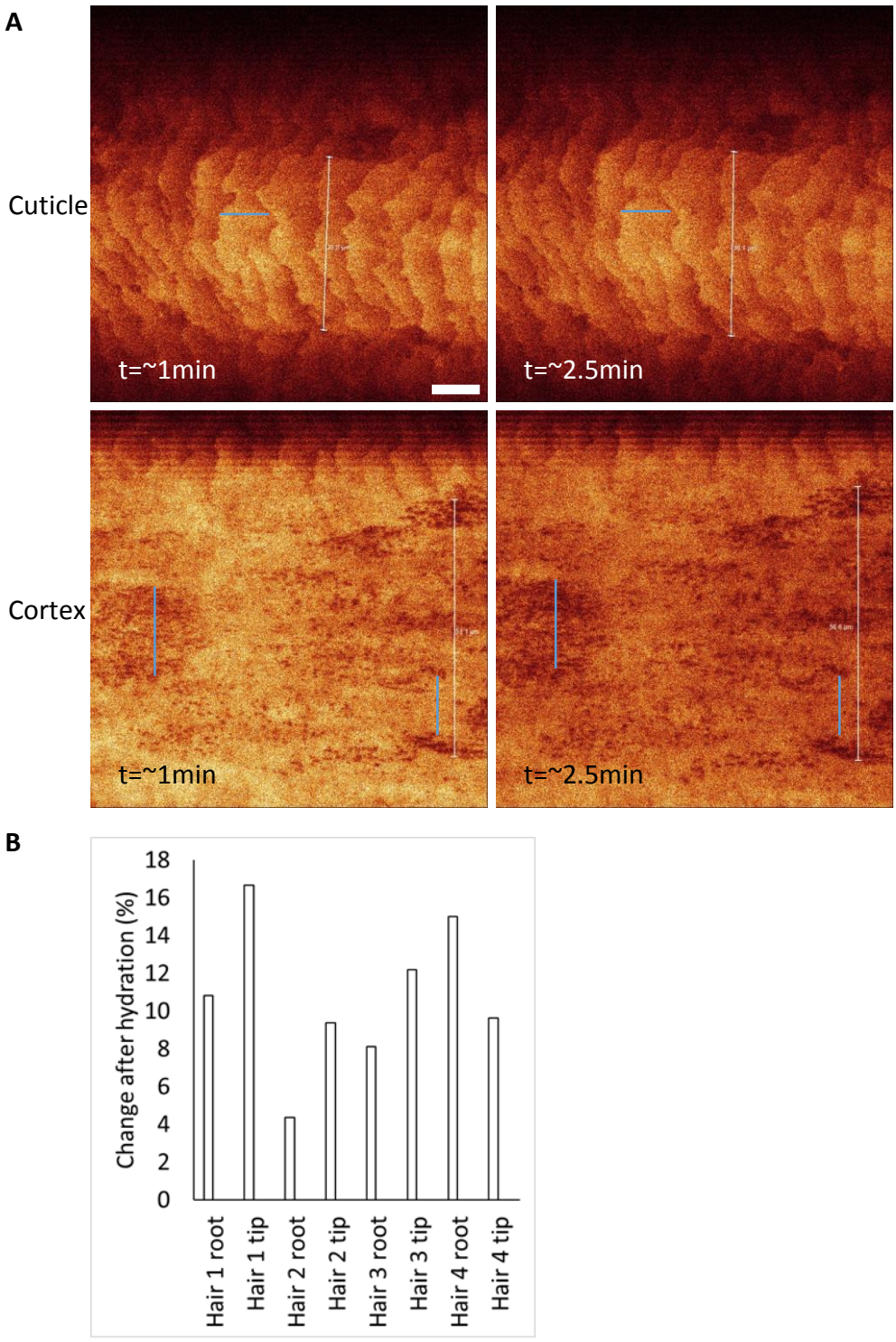

Fig. 5.3. Increase in untreated hair diameter with hydration in distilled water. A) The cuticle and cortex at approximately 1 minute and 2.5 minutes into hydration, with lines marking points of reference between the images. Representative photomicrographs of 4 imaged hairs are shown. B) Paired hairs above and below the skin interface (n=4). Scale bar = 10µm.

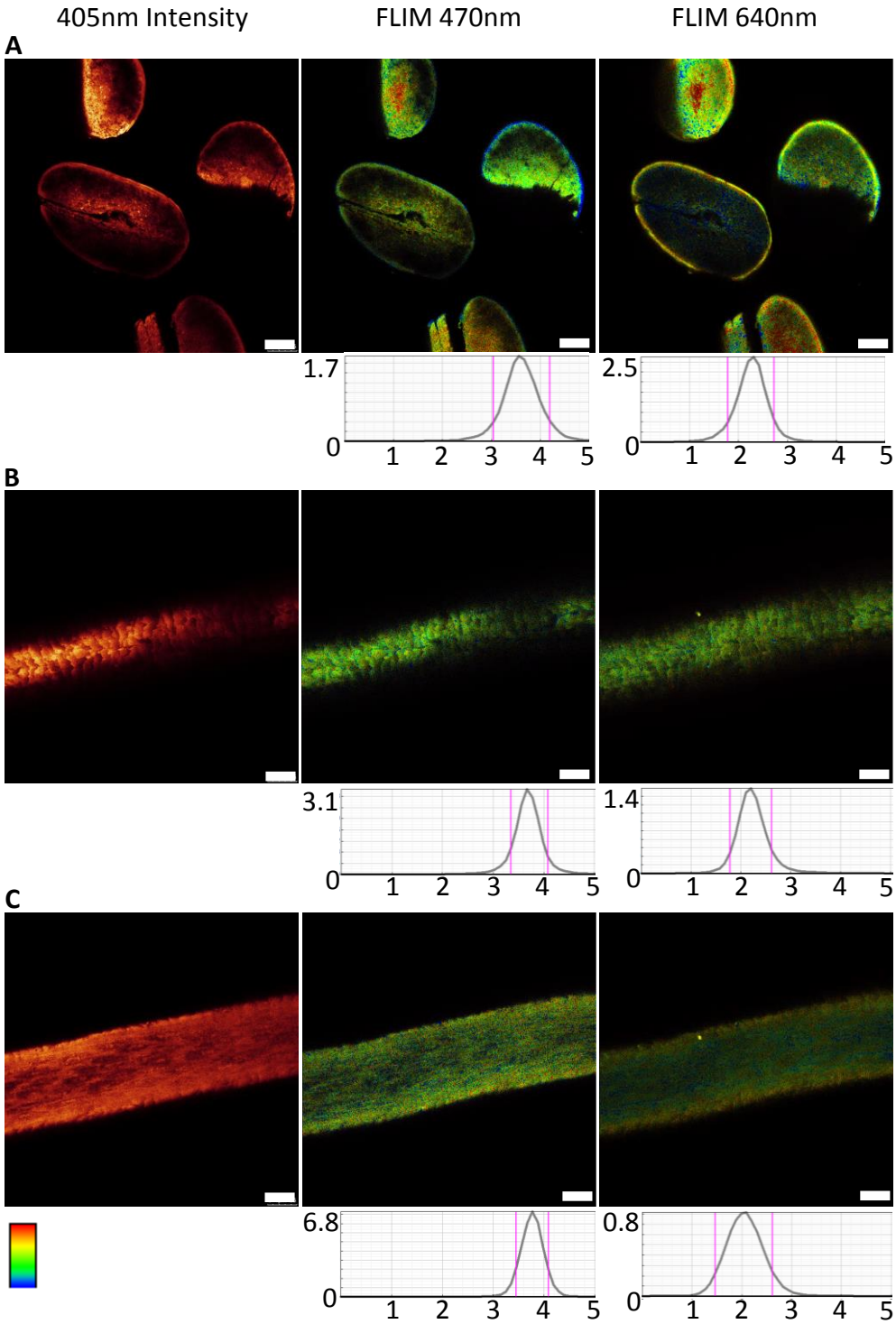

Fig. 5.4. Intensity and FLIM images of untreated control hairs. A) Transverse. B) Cuticle. C) Cortex. Intensity and FLIM images of transversely and longitudinally imaged hair showing the cuticle and cortex. Each FLIM image also shows a graph of the frequency of lifetimes, x-axis=time (ns), y-axis=frequency (M.counts). Representative photomicrographs of 36 imaged hairs are shown. N.B. The pink markers on the lifetime graphs indicate the upper (red) and lower (blue) lifetime limits. Scale bars = 25µm.

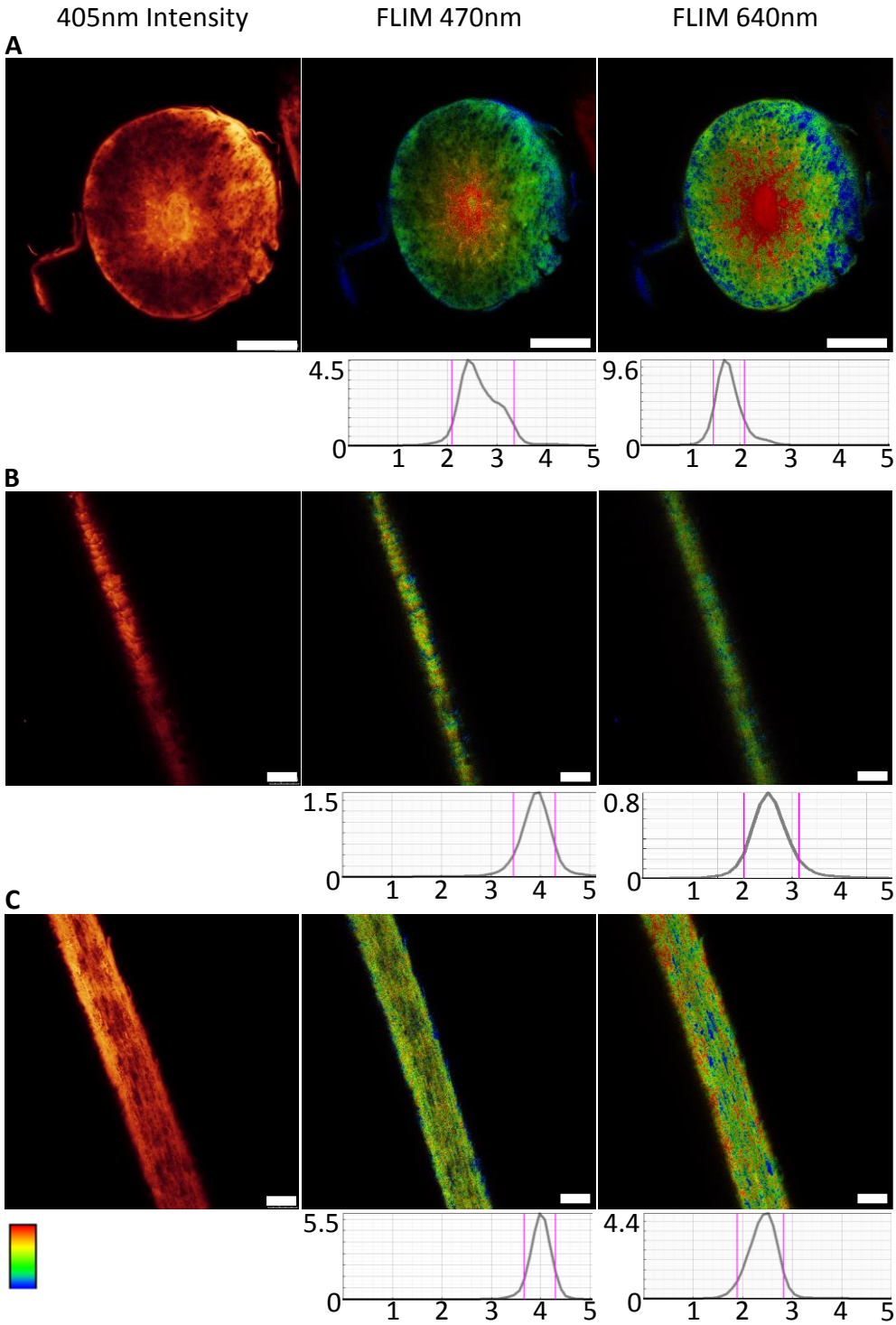

Fig. 5.5. Intensity and FLIM images of calcium thioglycolate treated hair. A) Transverse. B) Cuticle. C) Cortex. Intensity and FLIM images of transversely and longitudinally imaged hair showing the cuticle and cortex. Each FLIM image also shows a graph of the frequency of lifetimes, x-axis = time (ns), y-axis = frequency (M.counts). Representative photomicrographs of 9 imaged hairs are shown. N.B. The pink markers on the lifetime graphs indicate the upper (red) and lower (blue) lifetime limits. Scale bars = 25µm.

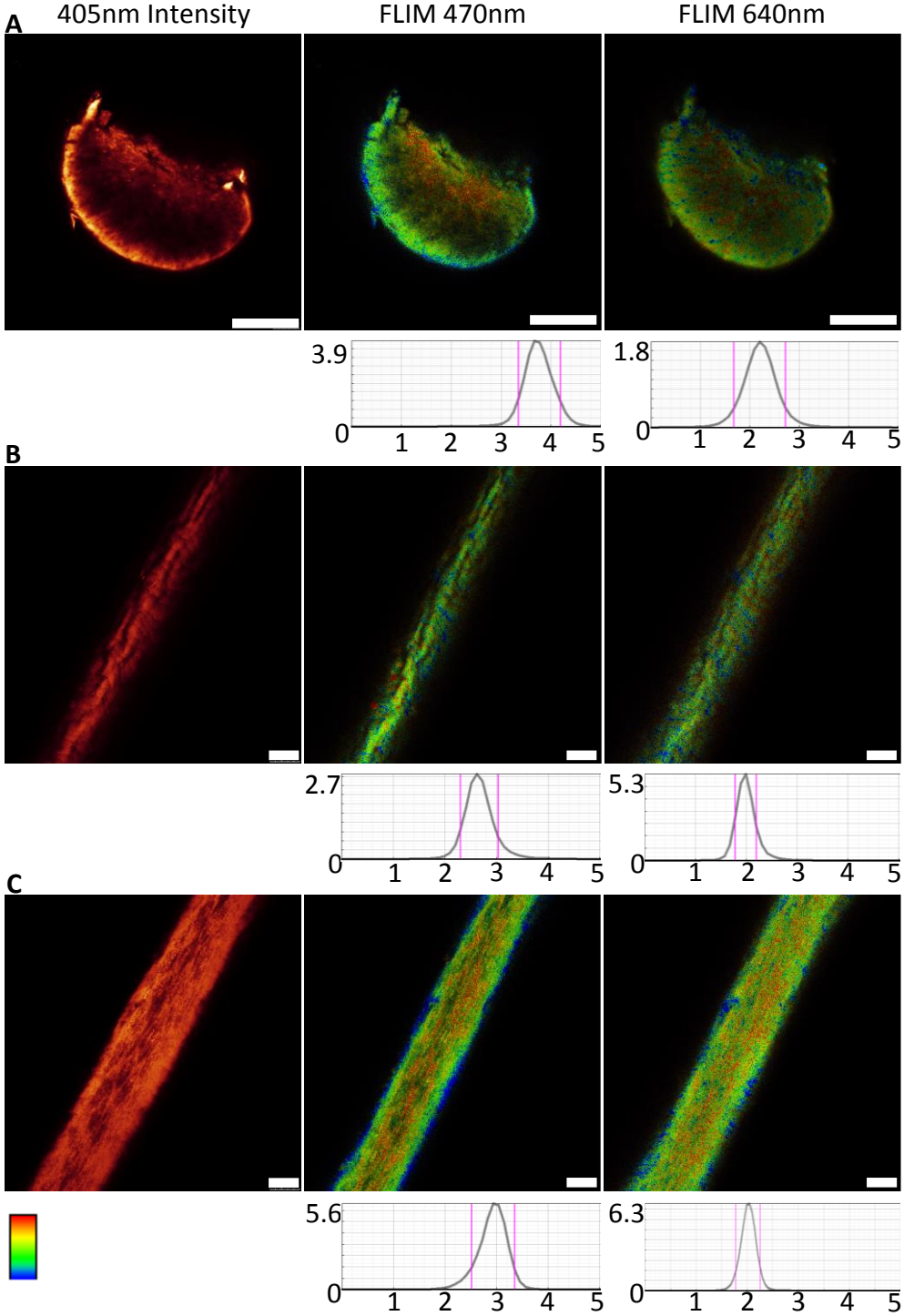

Fig. 5.6. Intensity and FLIM images of potassium thioglycolate treated hair. A) Transverse. B) Cuticle. C) Cortex. Intensity and FLIM images of transversely and longitudinally imaged hair showing the cuticle and cortex. Each FLIM image also shows a graph of the frequency of lifetimes, x-axis = time (ns), y-axis = frequency (M.counts). Representative photomicrographs of 8 imaged hairs are shown. N.B. The pink markers on the lifetime graphs indicate the upper (red) and lower (blue) lifetime limits. Scale bars = 25µm.

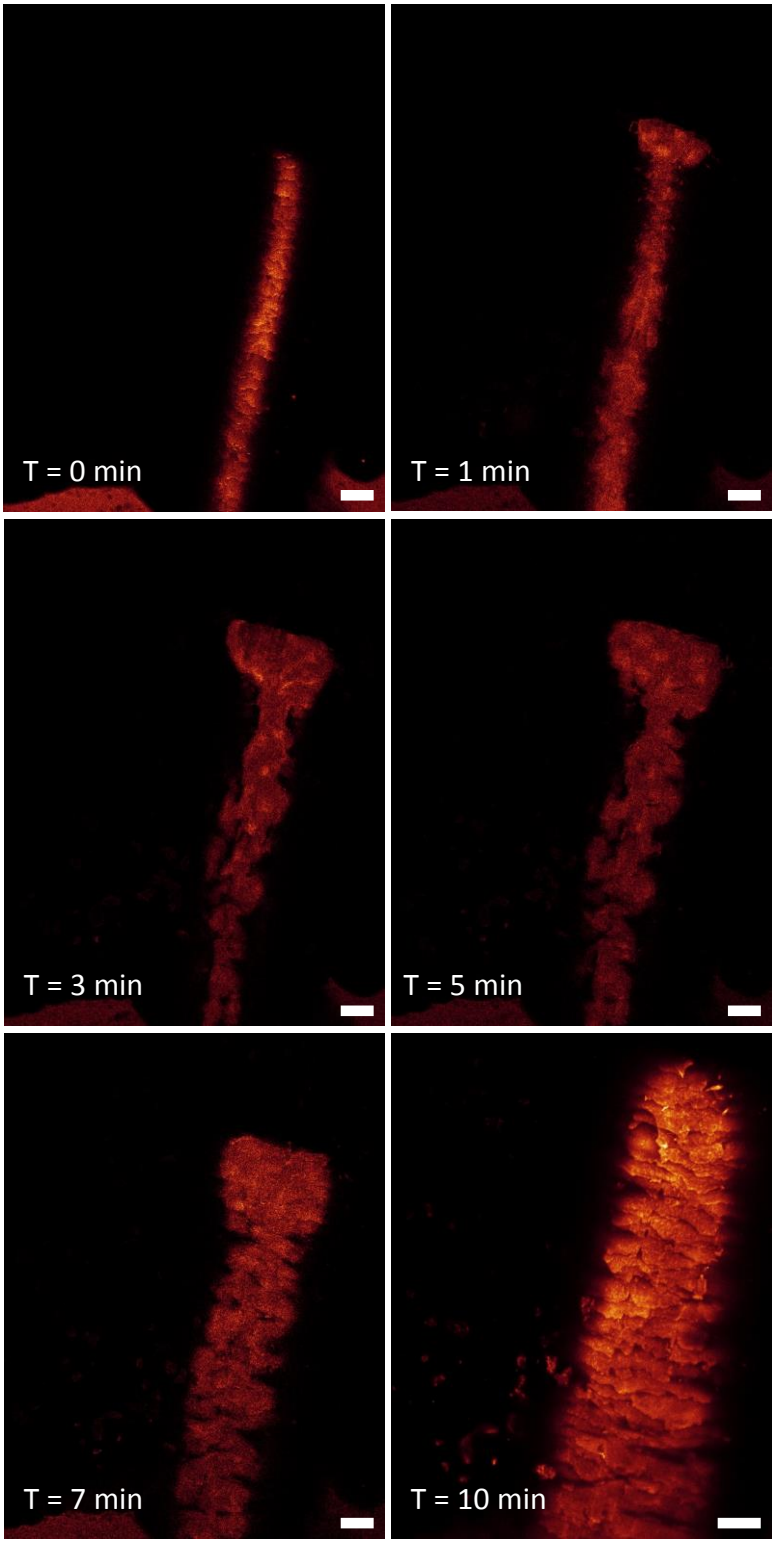

Fig. 5.7. Dynamic imaging confocal fluorescence intensity time lapse of potassium thioglycolate treated hair at the cuticle. 405nm excited autofluorescence. The final image is taken using higher resolution settings. T = time since start of treatment. Representative photomicrographs of 6 imaged hairs are shown. Scale bars = 25µm.

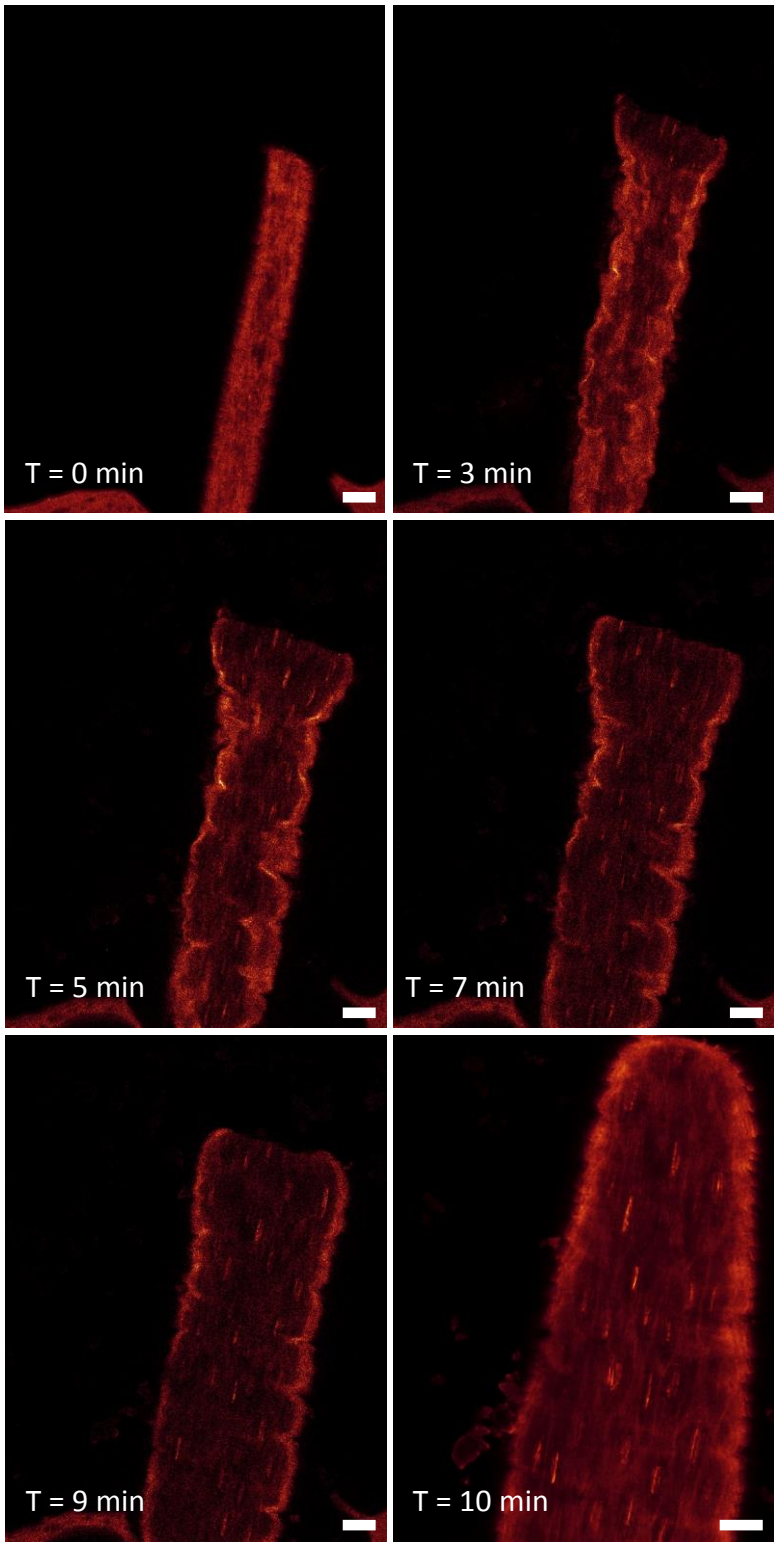

Fig. 5.8. Dynamic imaging confocal fluorescence intensity time lapse of potassium thioglycolate treated hair at the cortex. 405nm excited autofluorescence. The final image is taken using higher resolution settings. T = time since start of treatment. Representative photomicrographs of 6 imaged hairs are shown. Scale bars = 25µm.

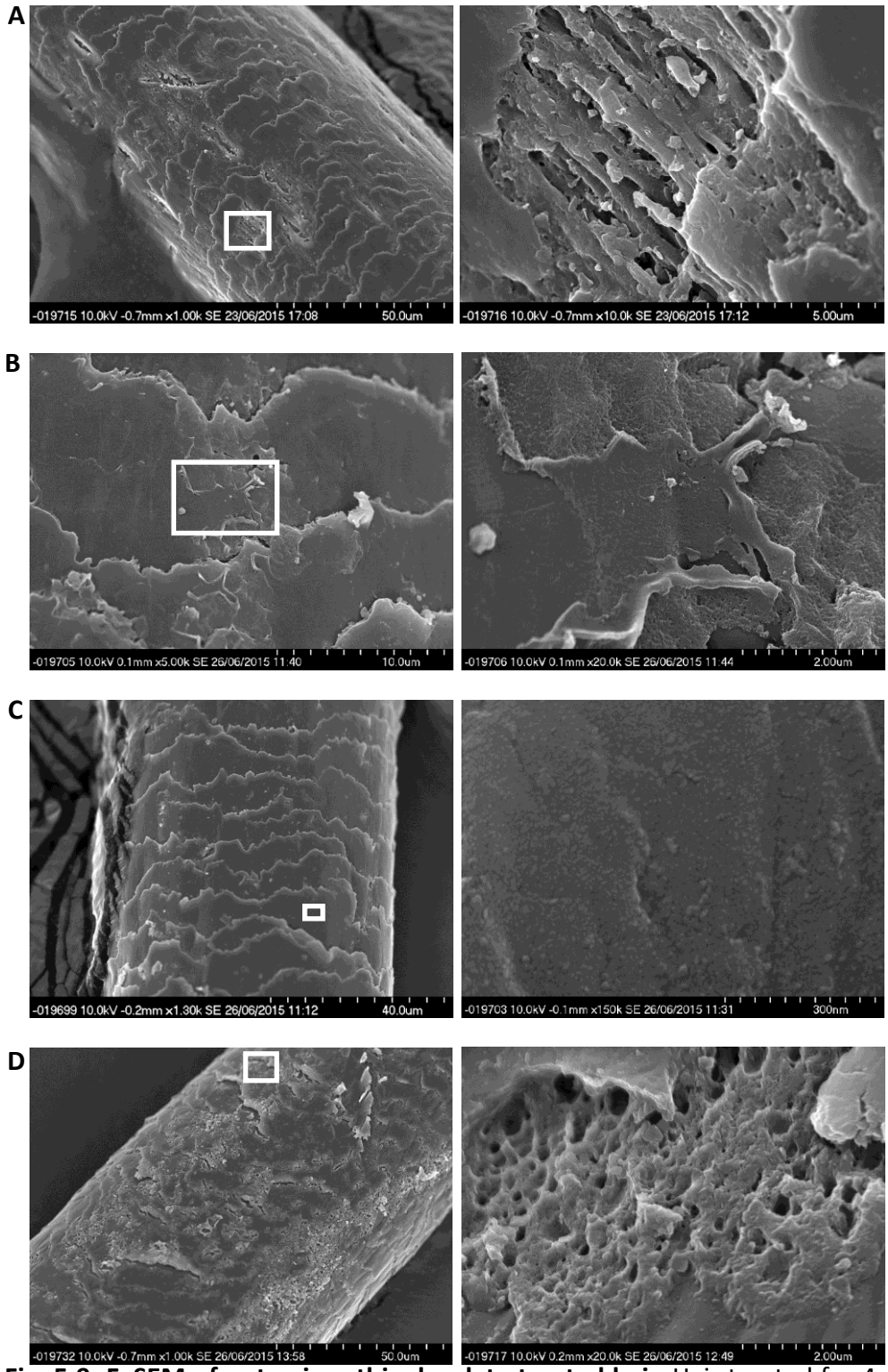

Fig. 5.9. FeSEM of potassium thioglycolate treated hair. Hair treated for 4 minutes with 0.45M thioglycolate, white boxes show corresponding magnified areas. A) Loss of cuticle showing through to the cortex. B) Intra-cuticle layers peeled back. C) Jagged cuticle edges which have cracks on the cuticle surface. D) Degradation of the cuticle. Representative photomicrographs of 3 imaged hairs are shown.

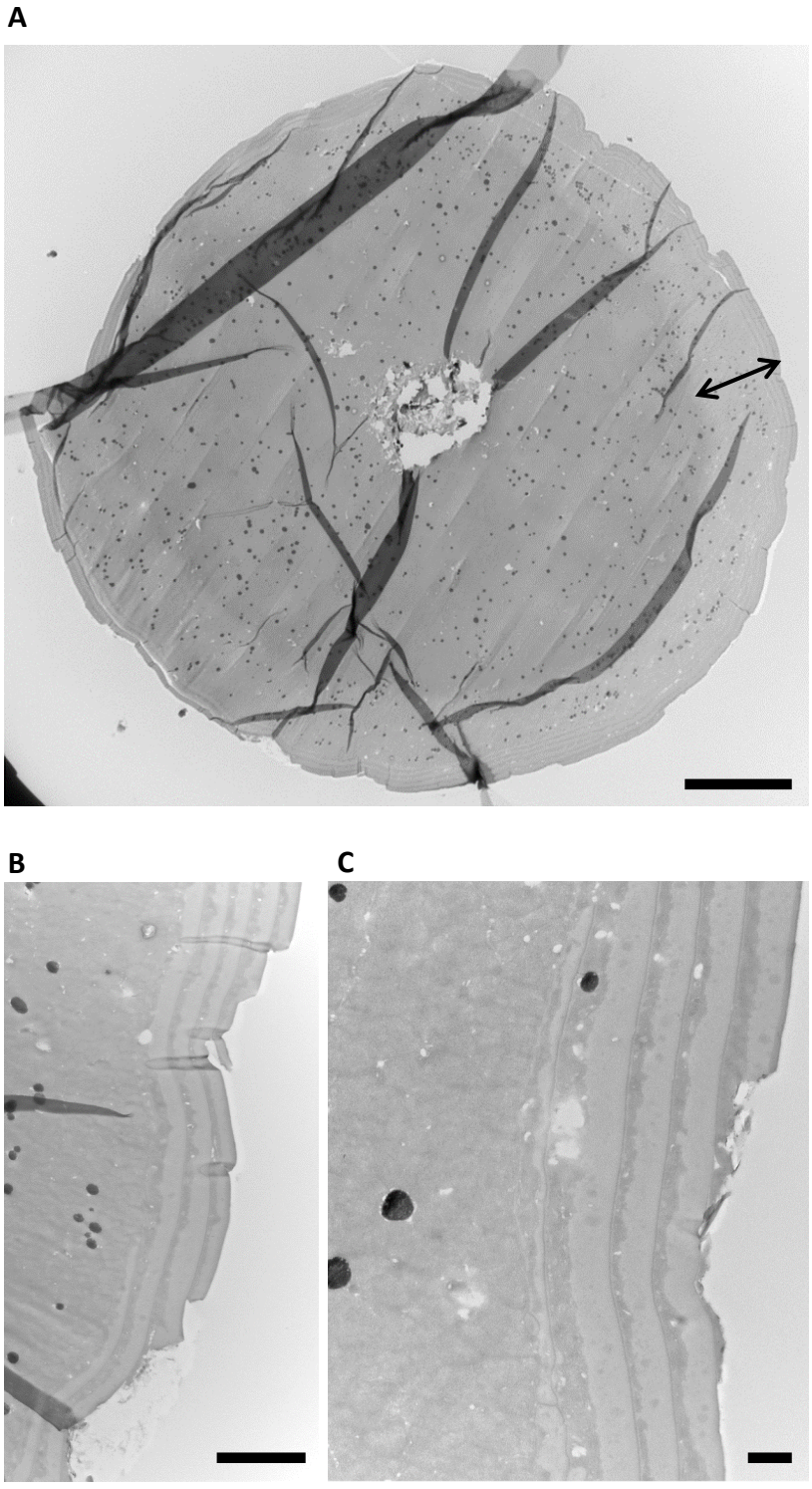

Fig. 5.10. TEM of potassium thioglycolate treated hair. Hair in transverse section treated for 4 minutes with 0.45M thioglycolate. A) Whole hair, a black arrow spans the lighter outer perimeter of the hair. B) Deformation in shape of cuticle. C) Fewer and degraded cuticle layers. Scale bars = (A) 10µm, (B) 500nm, (C) 2µm. Representative photomicrographs of 3 imaged hairs are shown.

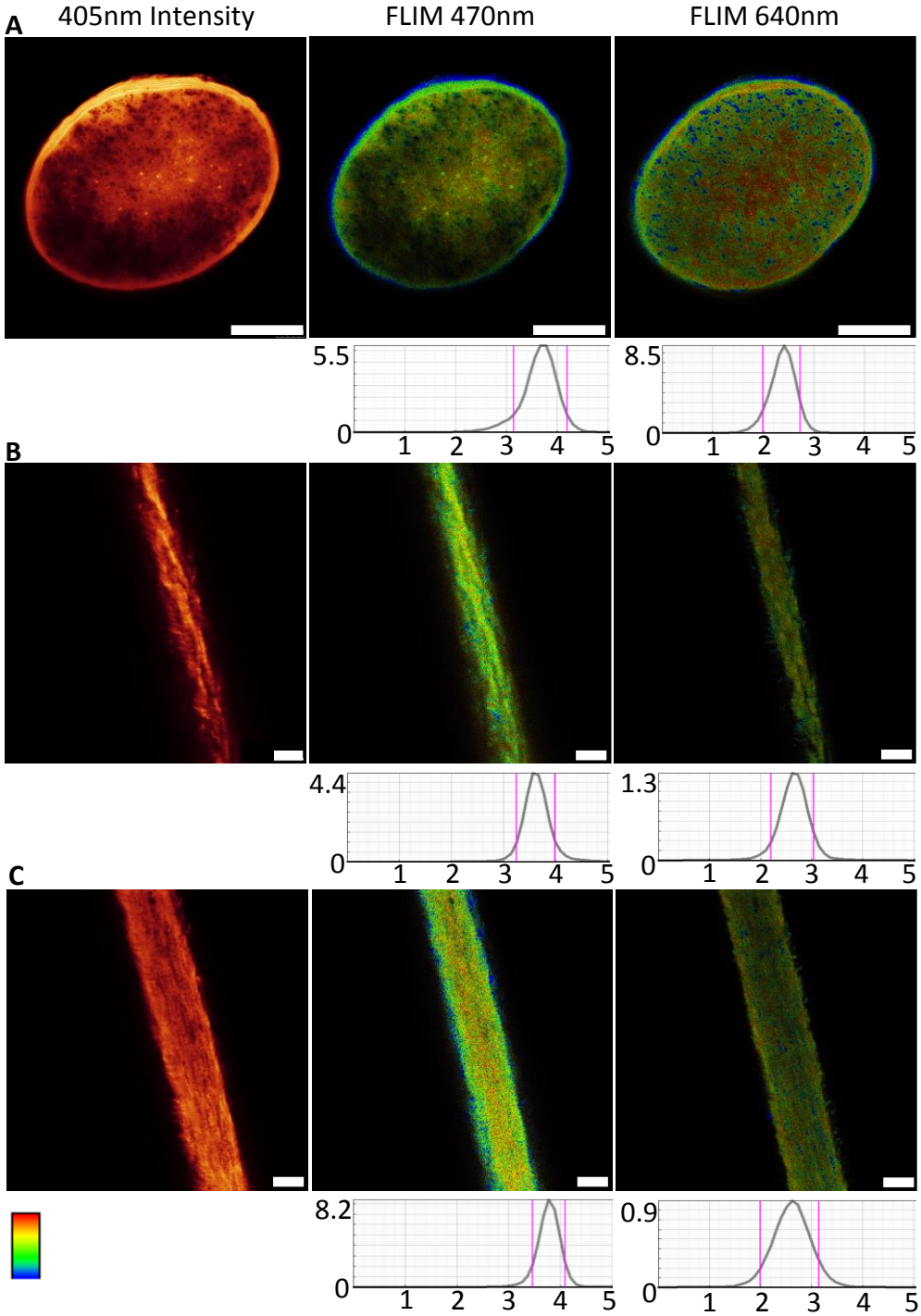

Fig. 5.11. Intensity and FLIM images of potassium thioglycolate and guanidine treated hair. A) Transverse. B) Cuticle. C) Cortex. Intensity and FLIM images of transversely and longitudinally imaged hair showing the cuticle and cortex. Each FLIM image also shows a graph of the frequency of lifetimes, x-axis = time (ns), y-axis = frequency (M.counts). Representative photomicrographs of 7 imaged hairs are shown. N.B. The pink markers on the lifetime graphs indicate the upper (red) and lower (blue) lifetime limits. Scale bars = 25µm.

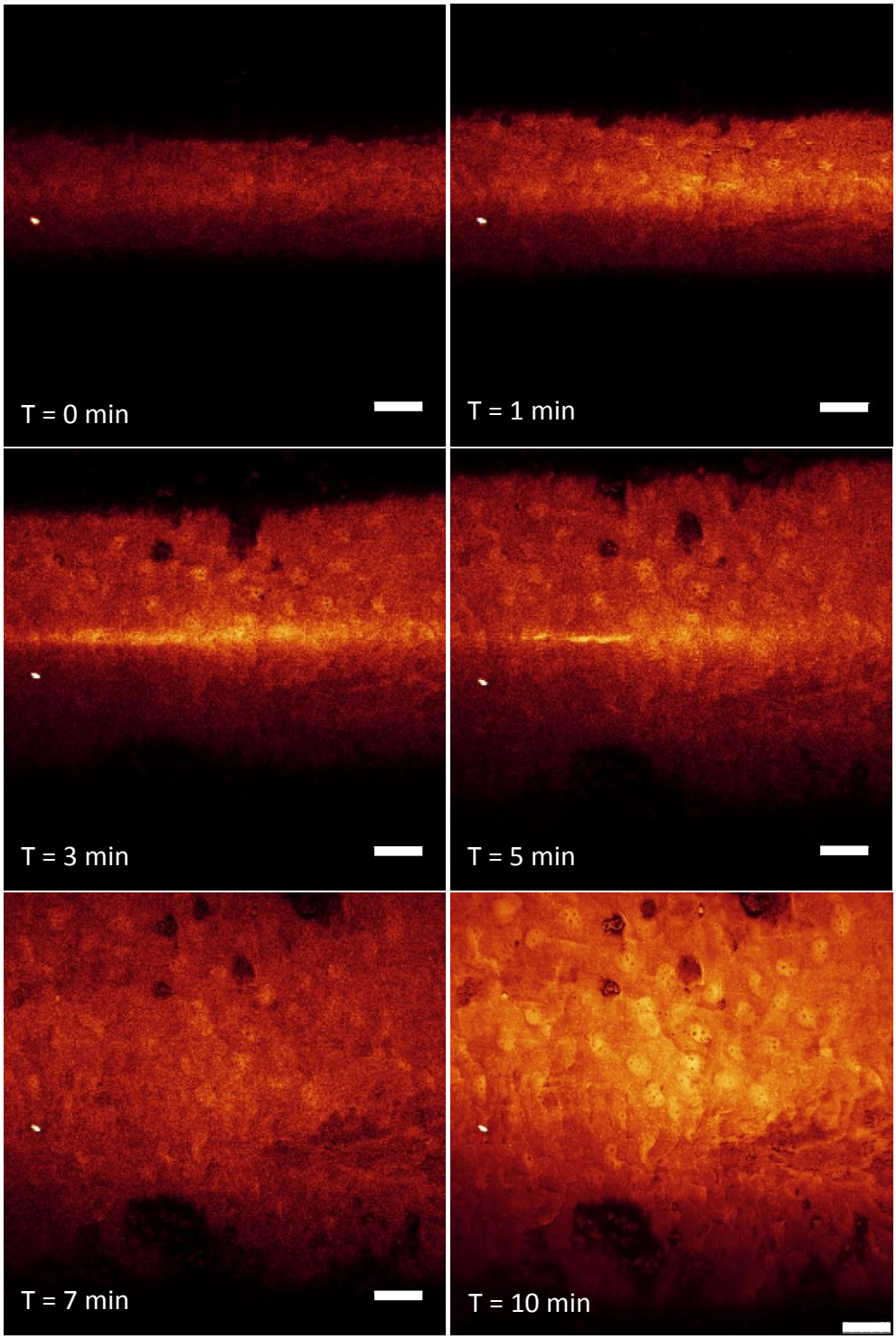

Fig. 5.12. Dynamic imaging confocal fluorescence intensity time lapse of potassium thioglycolate and guanidine carbonate treated hair at the cuticle. 405nm excited autofluorescence. The final image is taken using higher resolution settings. T = time since start of treatment. Representative photomicrographs of 5 imaged hairs are shown. Scale bars = 25µm.

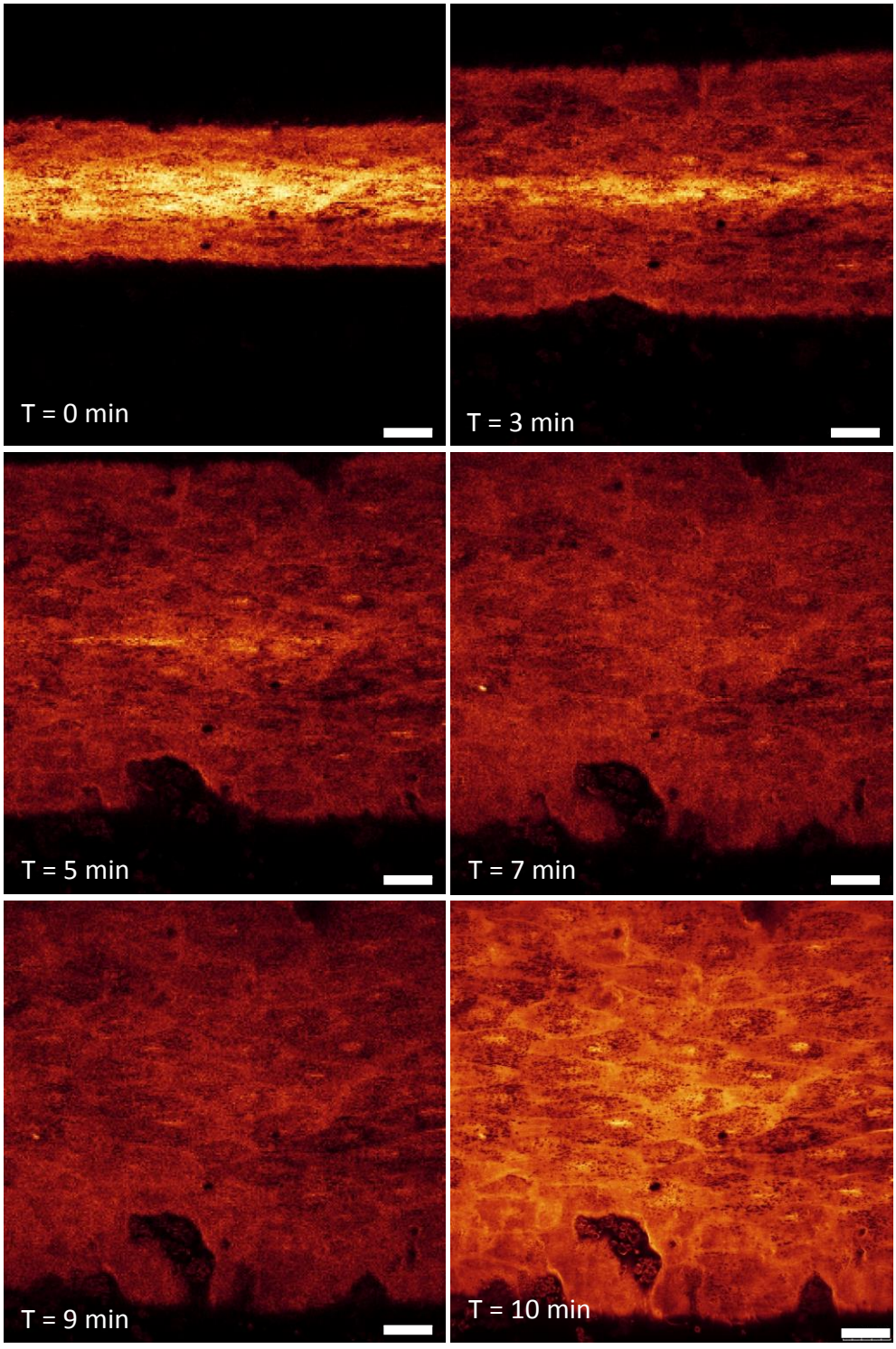

Fig. 5.13. Dynamic imaging confocal fluorescence intensity time lapse of potassium thioglycolate and guanidine carbonate treated hair at the cortex. 405nm excited autofluorescence. The final image is taken using higher resolution settings. T = time since start of treatment. Representative photomicrographs of 5 imaged hairs are shown. Scale bars = 25µm.

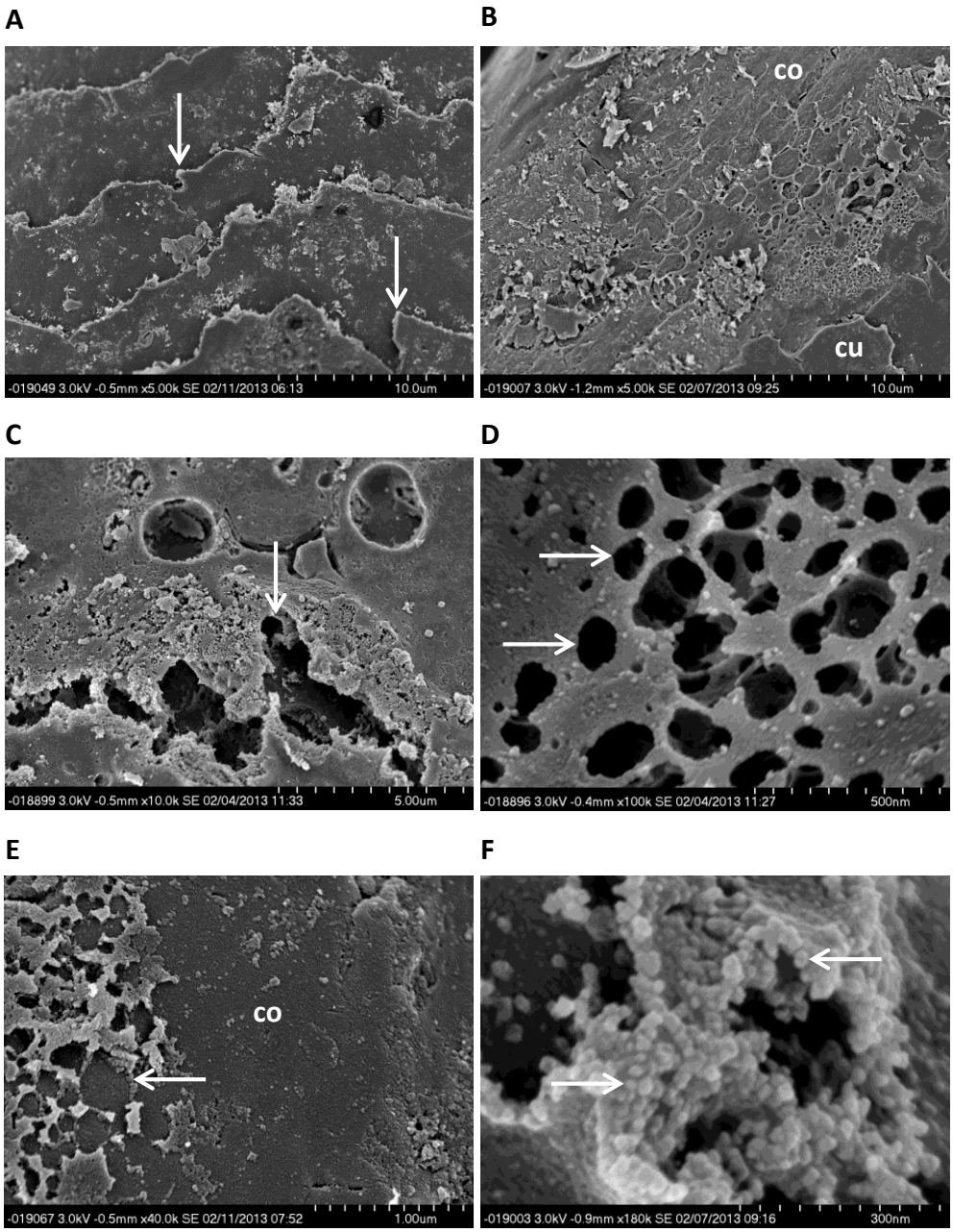

Fig. 5.14. FeSEM of potassium thioglycolate and guanidine carbonate treated hair. Hair treated for 4 minutes with 0.45M potassium thioglycolate and 0.44M guanidine carbonate. A) Jagged cuticle edges (arrows). B) Degradation of the cuticle (cu) through to the cortex (co). C) Large cracks in the cuticle. D) Holes in the cuticle of approximately 100nm in diameter (arrows). E) Holes in the cuticle get larger (arrow) exposing the cortex (co). F) Structures from degradation made up of granules approximately 20nm in diameter. Representative photomicrographs of 3 imaged hairs are shown.

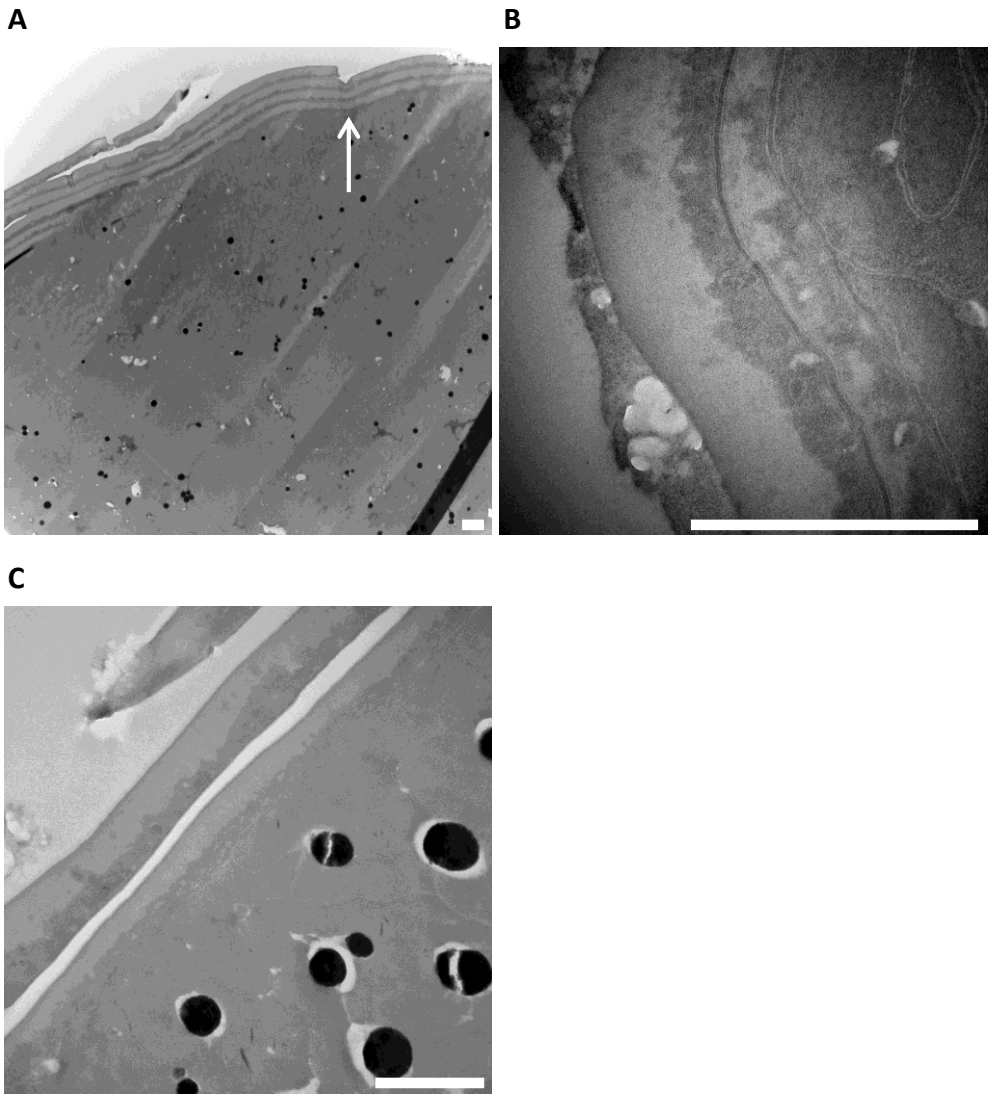

Fig. 5.15. TEM of potassium thioglycolate and guanidine carbonate treated hair. Hair in transverse section treated for 4 minutes with 0.45M potassium thioglycolate and 0.44M guanidine carbonate. A) Misshaping of the cuticle layer (arrow). B) Fewer cuticle layers. C) Cuticle cells become detached. Representative photomicrographs of 3 imaged hairs are shown. Scale bars = 1µm.

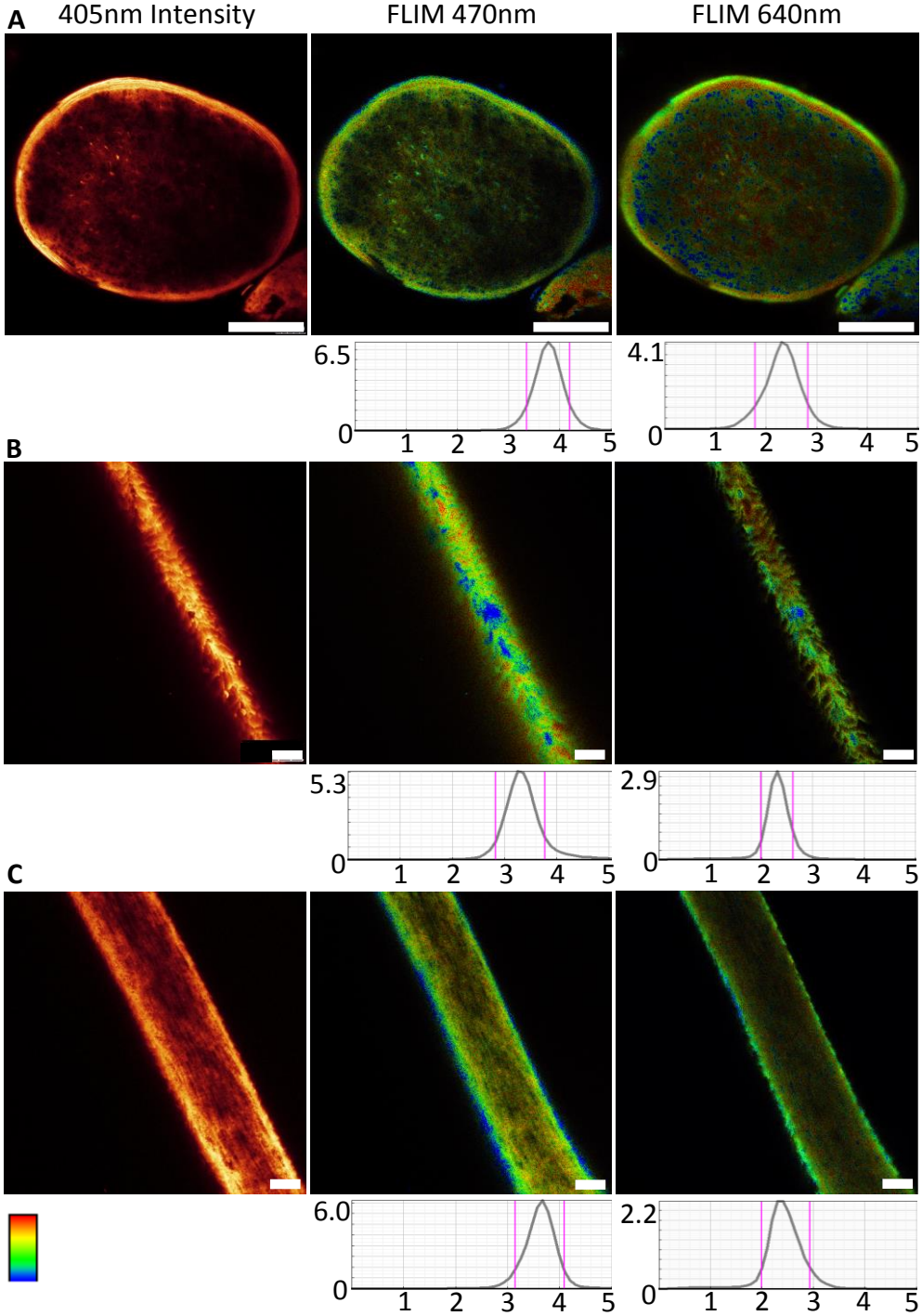

Fig. 5.16. Intensity and FLIM images of guanidine carbonate pH12.5 treated hair. A) Transverse. B) Cuticle. C) Cortex. Intensity and FLIM images of transversely and longitudinally imaged hair showing the cuticle and cortex. Each FLIM image also shows a graph of the frequency of lifetimes, x-axis = time (ns), y-axis = frequency (M.counts). Representative photomicrographs of 8 imaged hairs are shown. N.B. The pink markers on the lifetime graphs indicate the upper (red) and lower (blue) lifetime limits. Scale bars = 25µm.

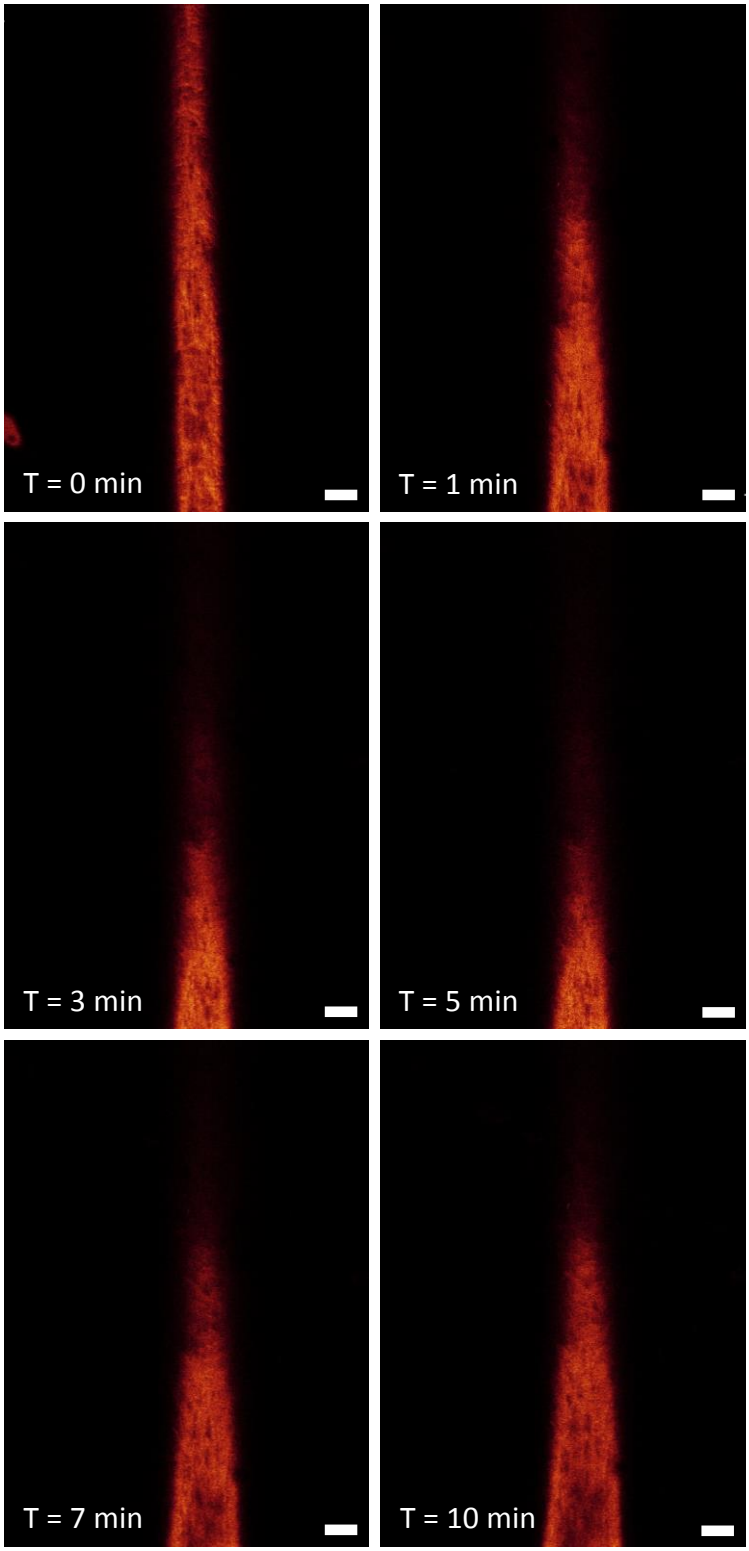

Fig. 5.17. Dynamic imaging confocal fluorescence intensity time lapse of guanidine carbonate pH12.5 treated hair. 405nm excited autofluorescence of the hair during treatment. T = time since start of treatment. Representative photomicrographs of 5 imaged hairs are shown. Scale bars = 25µm.

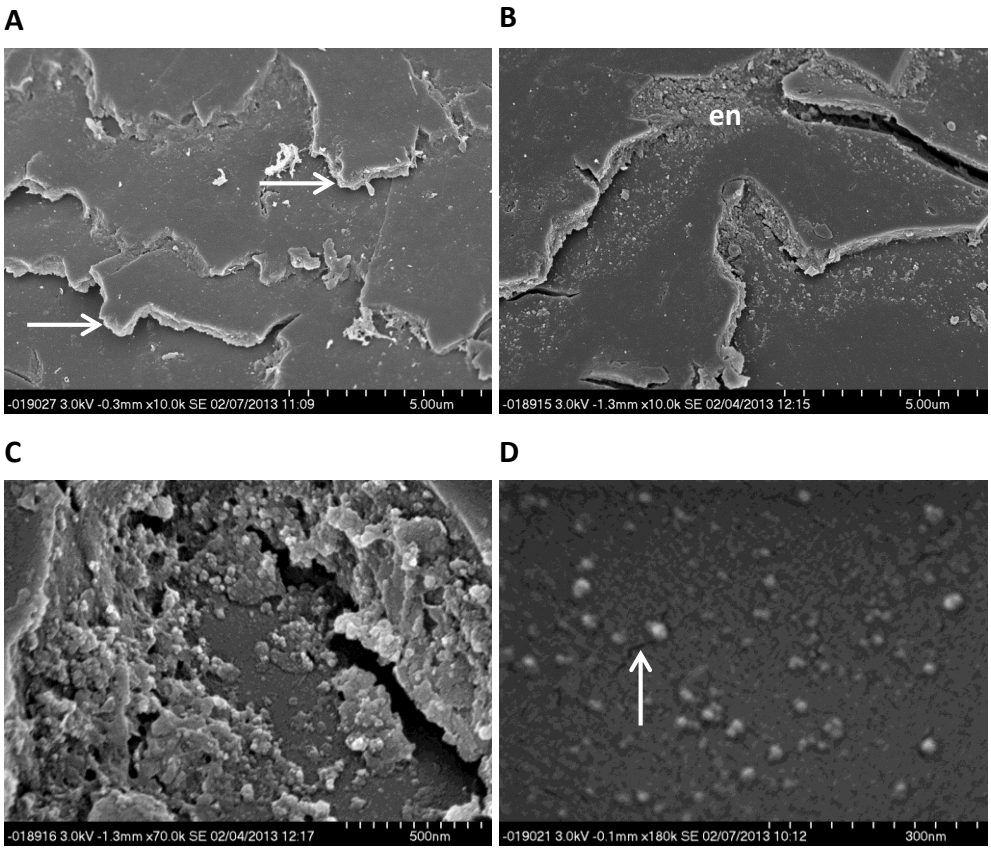

Fig. 5.18. FeSEM of guanidine carbonate pH12.5 treated hair. Hair treated for 4 minutes with 0.44M guanidine carbonate at pH12.5. A) Jagged cuticle edges. B) Endocuticle (en) residue. C) Degradation of cuticle cell. D) Cracks (arrow) and granules on cuticle surface. Representative photomicrographs of 3 imaged hairs are shown.

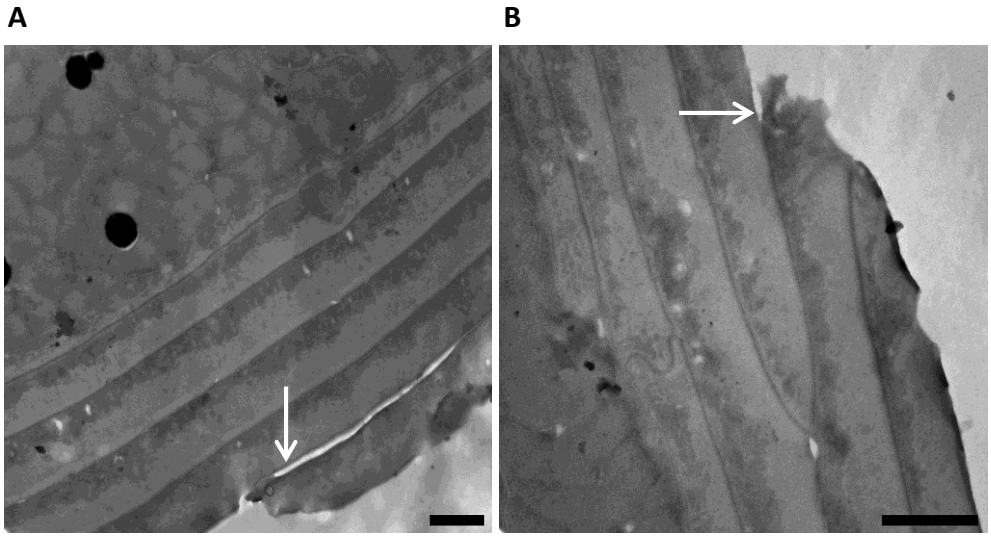

Fig. 5.19. TEM of guanidine carbonate pH12.5 treated hair. Hair in transverse section treated for 4 minutes with 0.44M guanidine carbonate pH12.5. Cuticles show signs of degradation (arrows) with separation occurring between the outer cells. Scale bars = 500nm. Representative photomicrographs of 3 imaged hairs are shown.

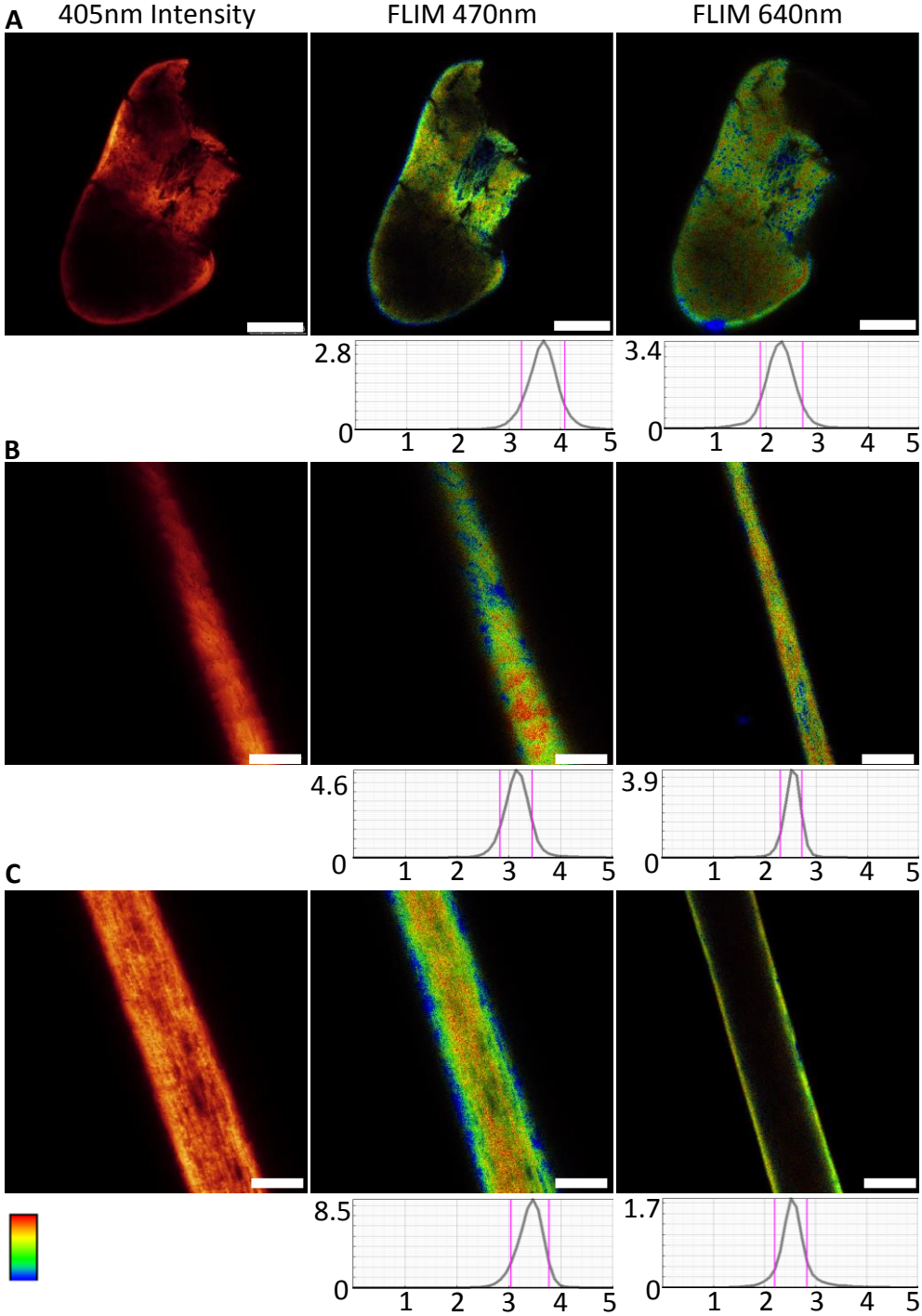

Fig. 5.20. Intensity and FLIM images of guanidine carbonate pH11.4 treated hair. A) Transverse. B) Cuticle. C) Cortex. Intensity and FLIM images of transversely and longitudinally imaged hair showing the cuticle and cortex. Each FLIM image also shows a graph of the frequency of lifetimes, x-axis = time (ns), y-axis = frequency (M.counts). Representative photomicrographs of 8 imaged hairs are shown. N.B. The pink markers on the lifetime graphs indicate the upper (red) and lower (blue) lifetime limits. Scale bars = 25µm.

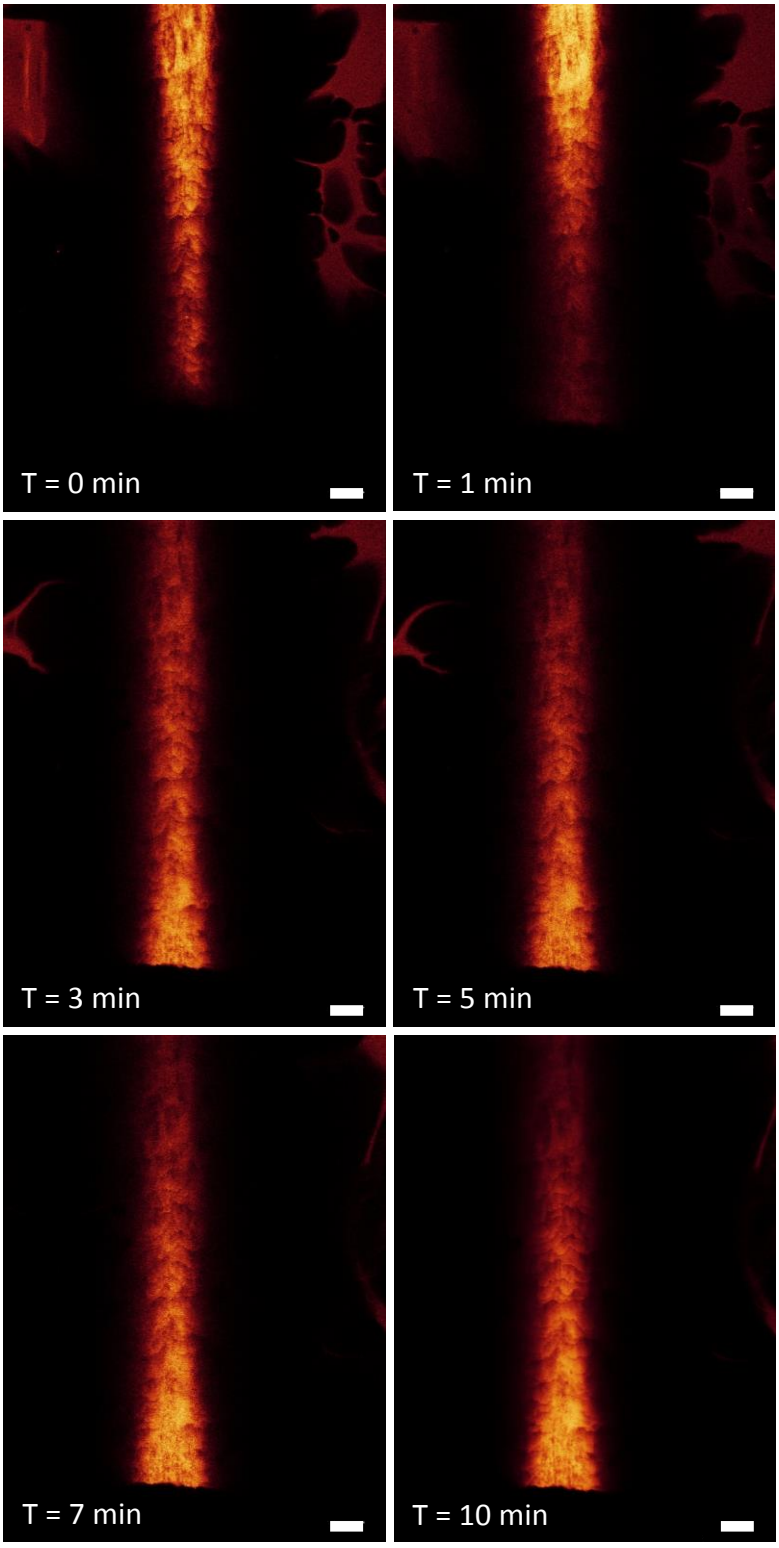

Fig. 5.21. Dynamic imaging confocal fluorescence intensity time lapse of guanidine carbonate pH11.4 treated hair at the cuticle. 405nm excited autofluorescence. The final image is taken using higher resolution settings. T = time since start of treatment. Representative photomicrographs of 5 imaged hairs are shown. Scale bars = 25µm.

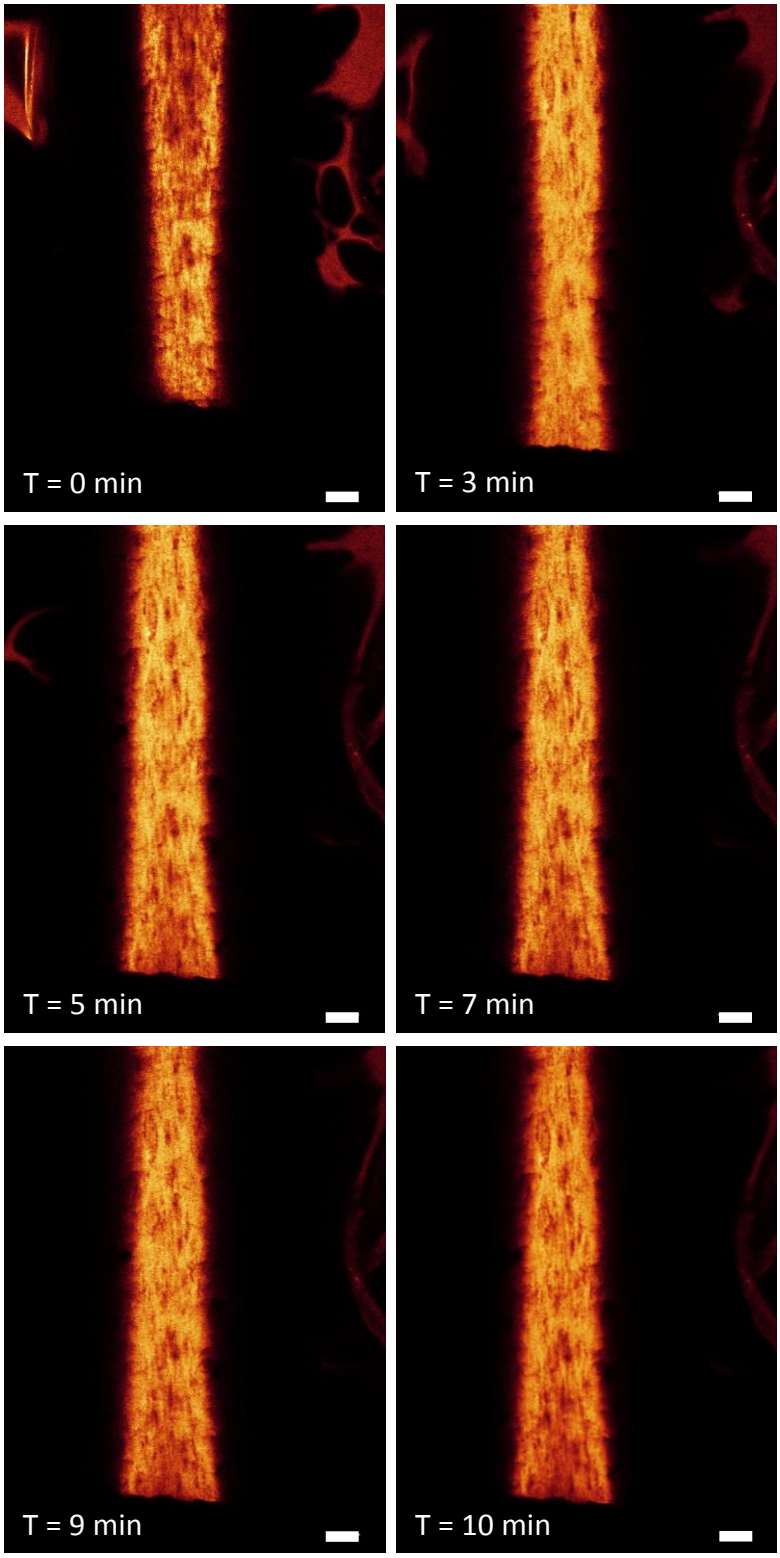

Fig. 5.22. Dynamic imaging confocal fluorescence intensity time lapse of guanidine carbonate pH11.4 treated hair at the cortex. 405nm excited autofluorescence. The final image is taken using higher resolution settings. T = time since start of treatment. Representative photomicrographs of 5 imaged hairs are shown. Scale bars = 25µm.

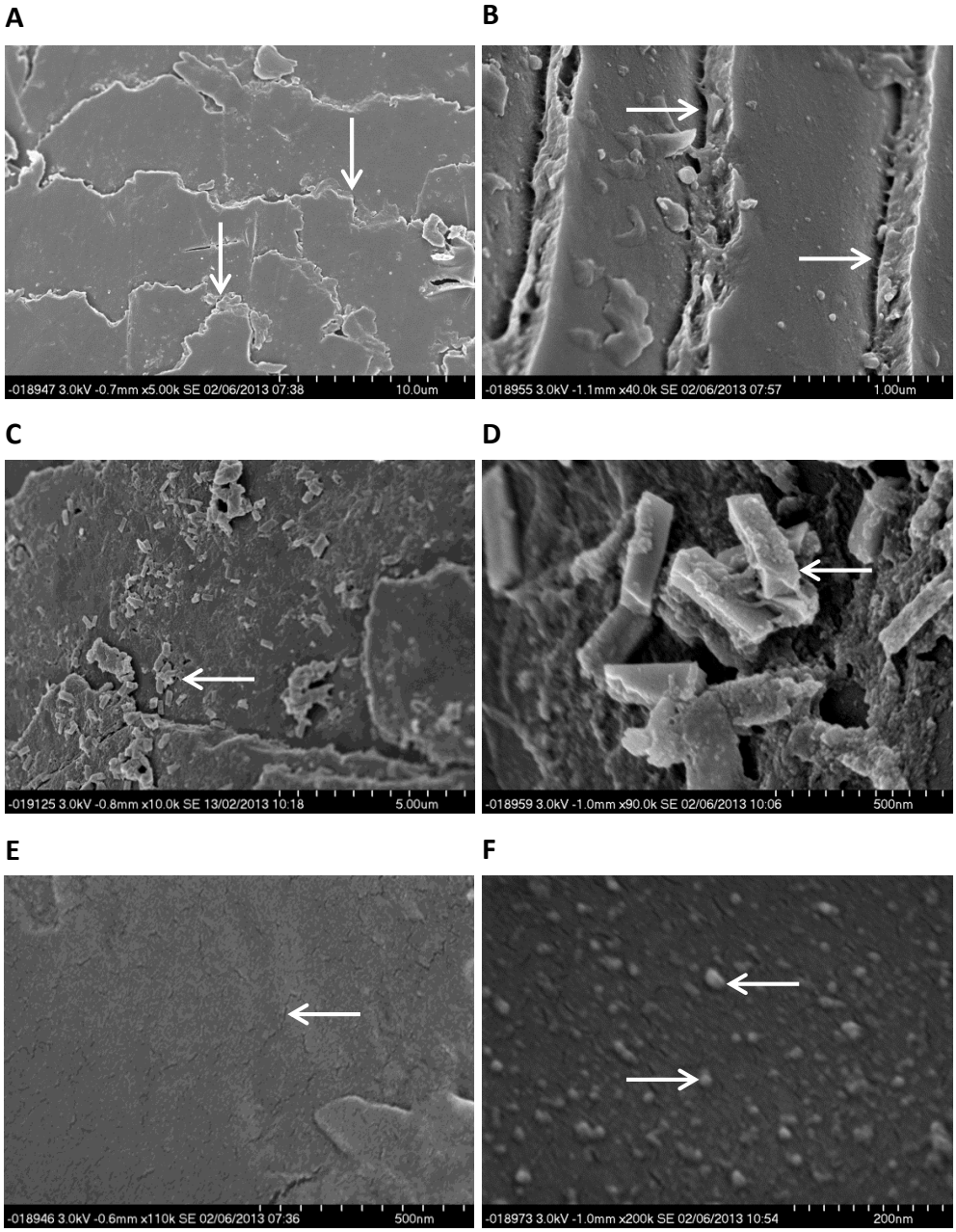

Fig. 5.23. FeSEM of guanidine carbonate pH11.4 treated hair. Hair treated for 4 minutes with 0.44M guanidine carbonate at pH11.4. A) Jagged cuticle edges (arrows). B) Cuticle cells separating by approximately 50nm (arrows). C) Cuticle surface covered in deposits (arrow). D) Deposits (arrow) appear crystalline. E) Cracks in cuticle surface (arrow). F) Cuticle surface covered in granules (arrows) approximately 20nm in diameter. Representative photomicrographs of 3 imaged hairs are shown.

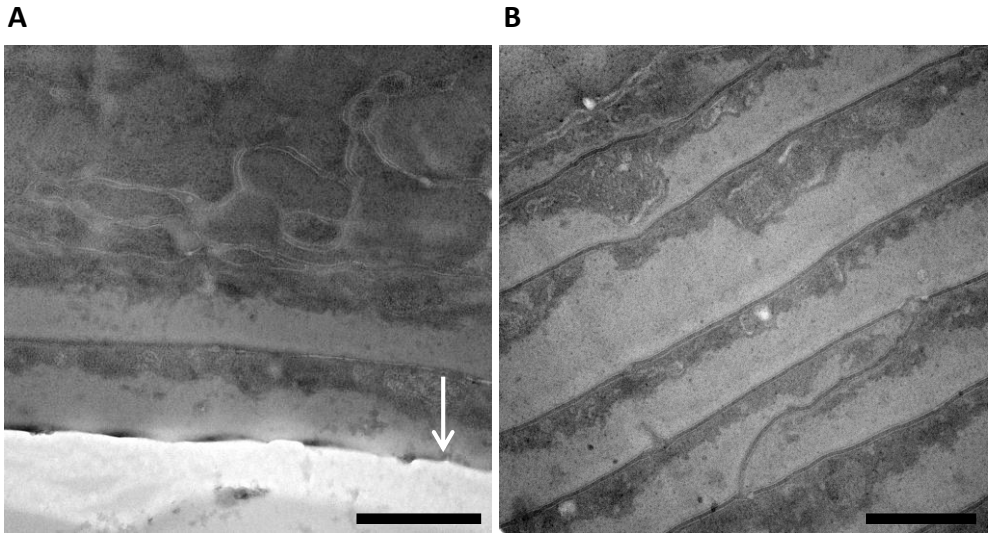

Fig. 5.24. TEM of guanidine carbonate pH11.4 treated hair. Hair in transverse section treated for 4 minutes 0.44M guanidine carbonate pH11.4. A) Cuticle shows signs of degradation (arrows) with fewer cuticle cell layers. B) Some hair cuticles appear unaffected by the treatment with many cell layers. Representative photomicrographs of 3 imaged hairs are shown. Scale bars = 500nm.

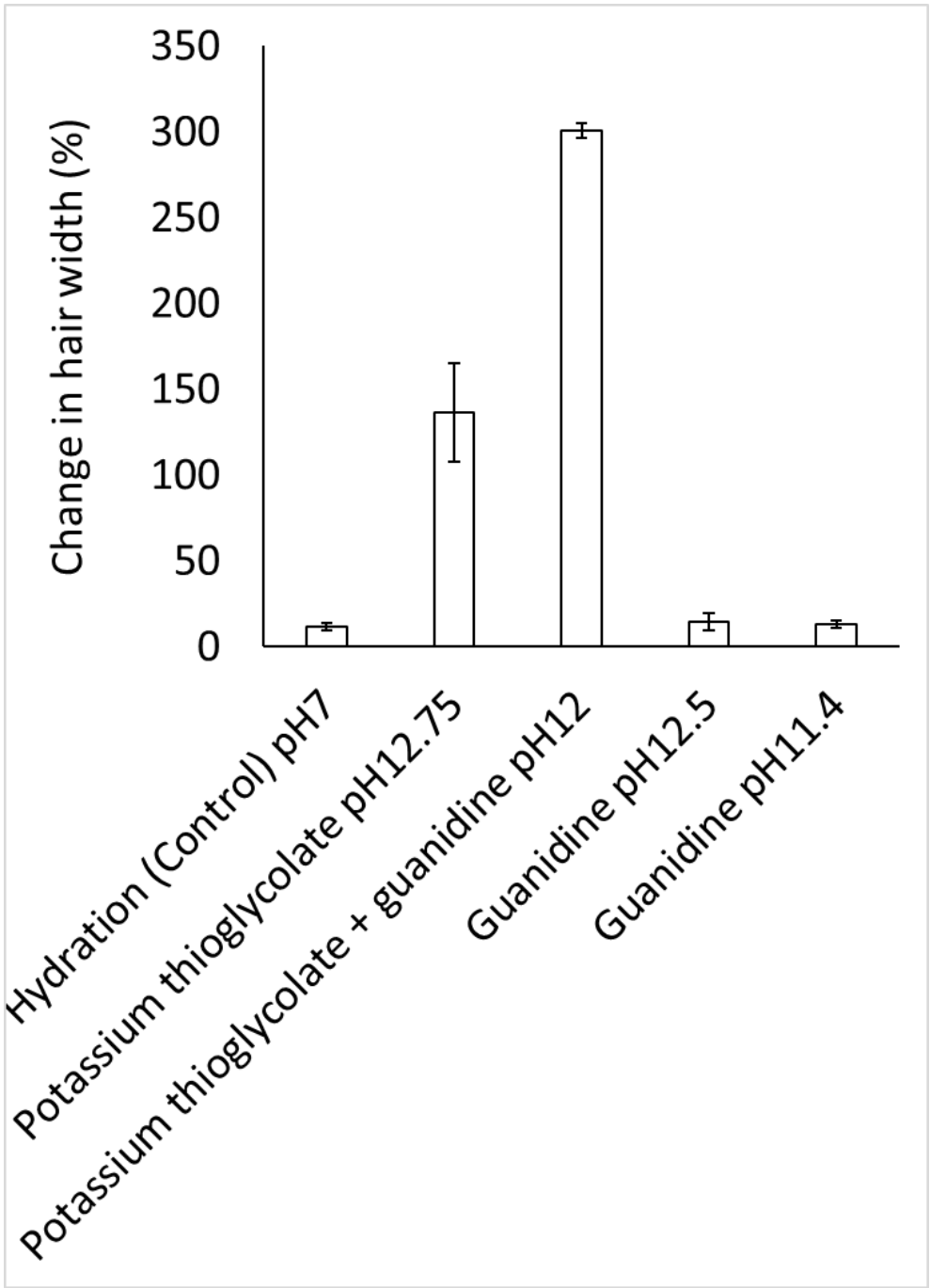

Fig. 5.25. Percentage change in hair diameter after treatment for 10 minutes. Thioglycolate and guanidine based chemistries. Fully hydrated hair used as control. Hydration (n=8), potassium thioglycolate (n=5), potassium thioglycolate + guanidine (n=3), guanidine pH12.5 (n=5), guanidine pH11.4 (n=3). Error bars = +/- 2*SEM.

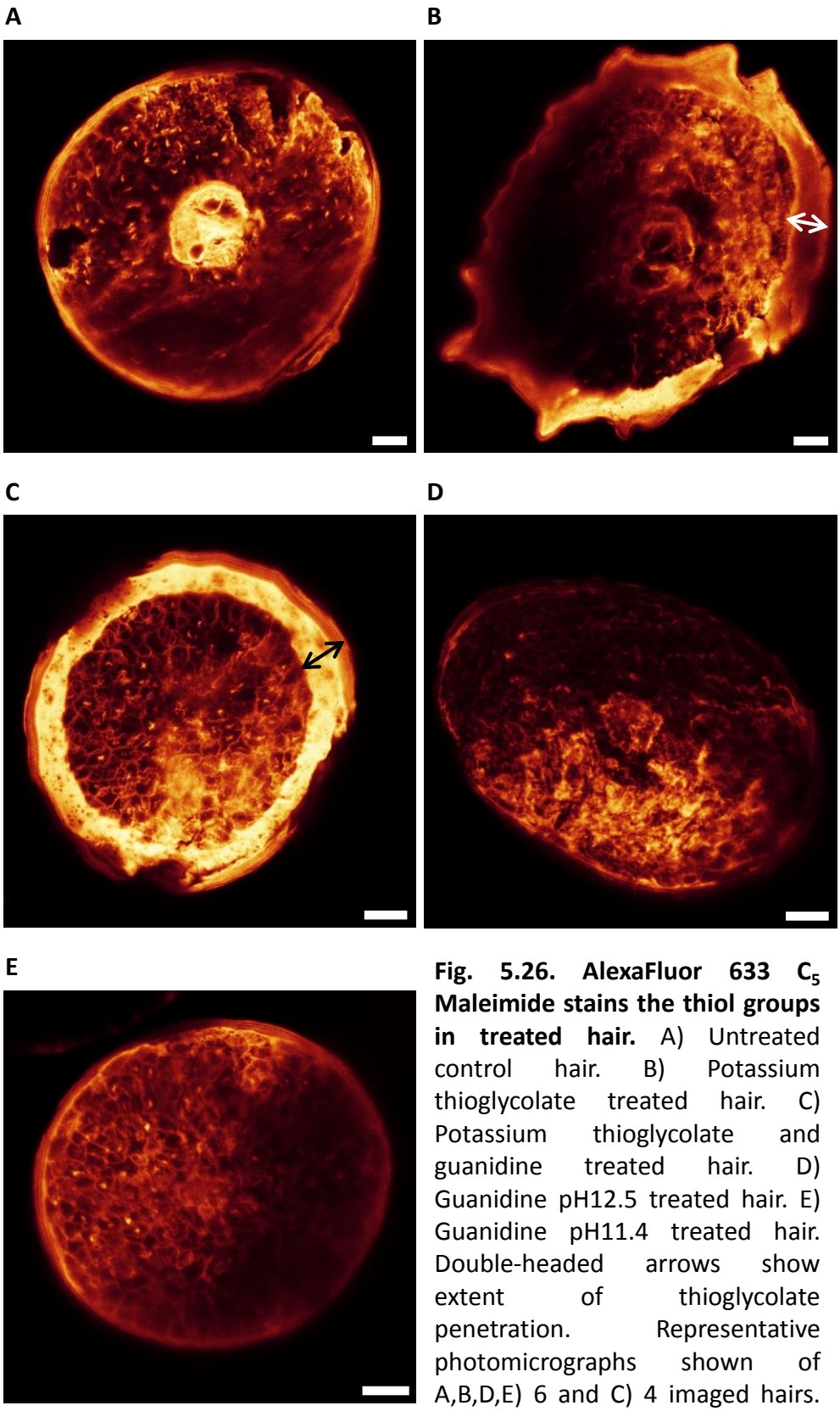

Fig. 5.26. AlexaFluor 633 C_5 Maleimide stains the thiol groups in treated hair. A) Untreated control hair. B) Potassium thioglycolate treated hair. C) Potassium thioglycolate and guanidine treated hair. D) Guanidine pH12.5 treated hair. E) Guanidine pH11.4 treated hair. Double-headed arrows show extent of thioglycolate penetration. Representative photomicrographs shown of A,B,D,E) 6 and C) 4 imaged hairs. Scale bars = 10µm.

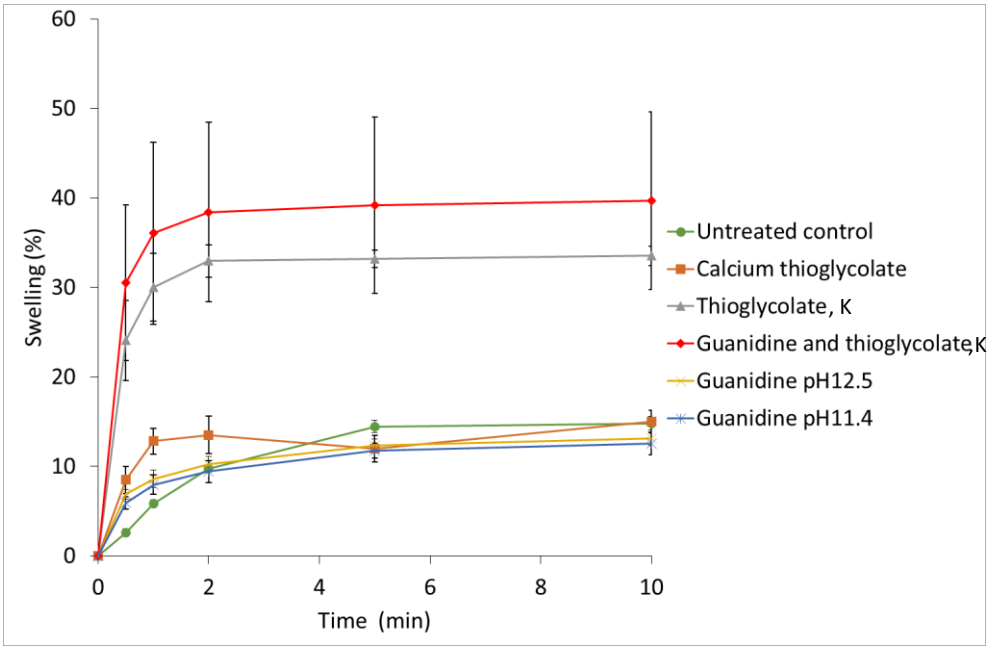

Fig. 5.27. Percentage increase in hair diameter over 10 minutes hydration in DI water. For untreated and treated hair with thioglycolate and guanidine chemistries (n=3 per treatment). Error bars = +/-SEM. Work carried out by P&G.

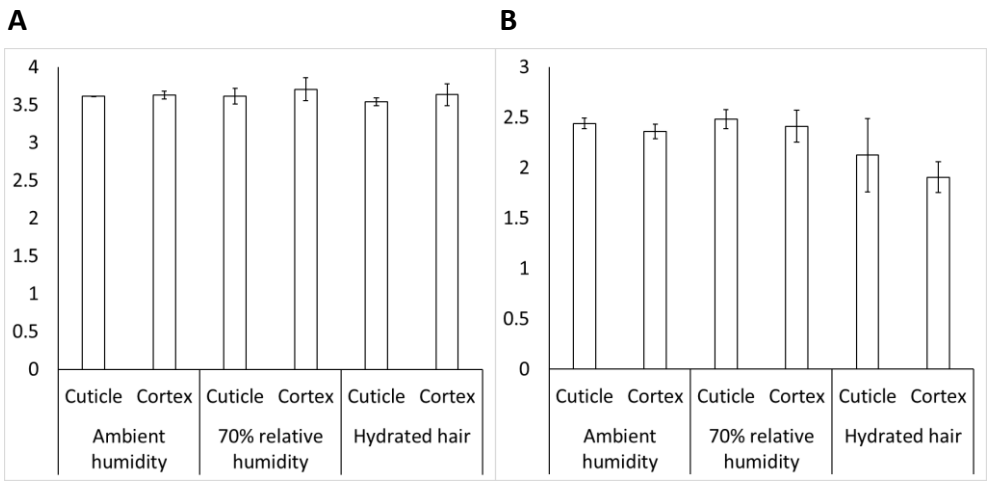

Fig. 5.28. Average fluorescence lifetimes of potassium thioglycolate and guanidine carbonate treated hair at ambient humidity, 70% humidity and hydrated hair. A) Hairs excited with 470nm (n=3 per treatment). B) Hairs excited with 640nm (n=3 per treatment). Error bars = +/- 2*SEM.

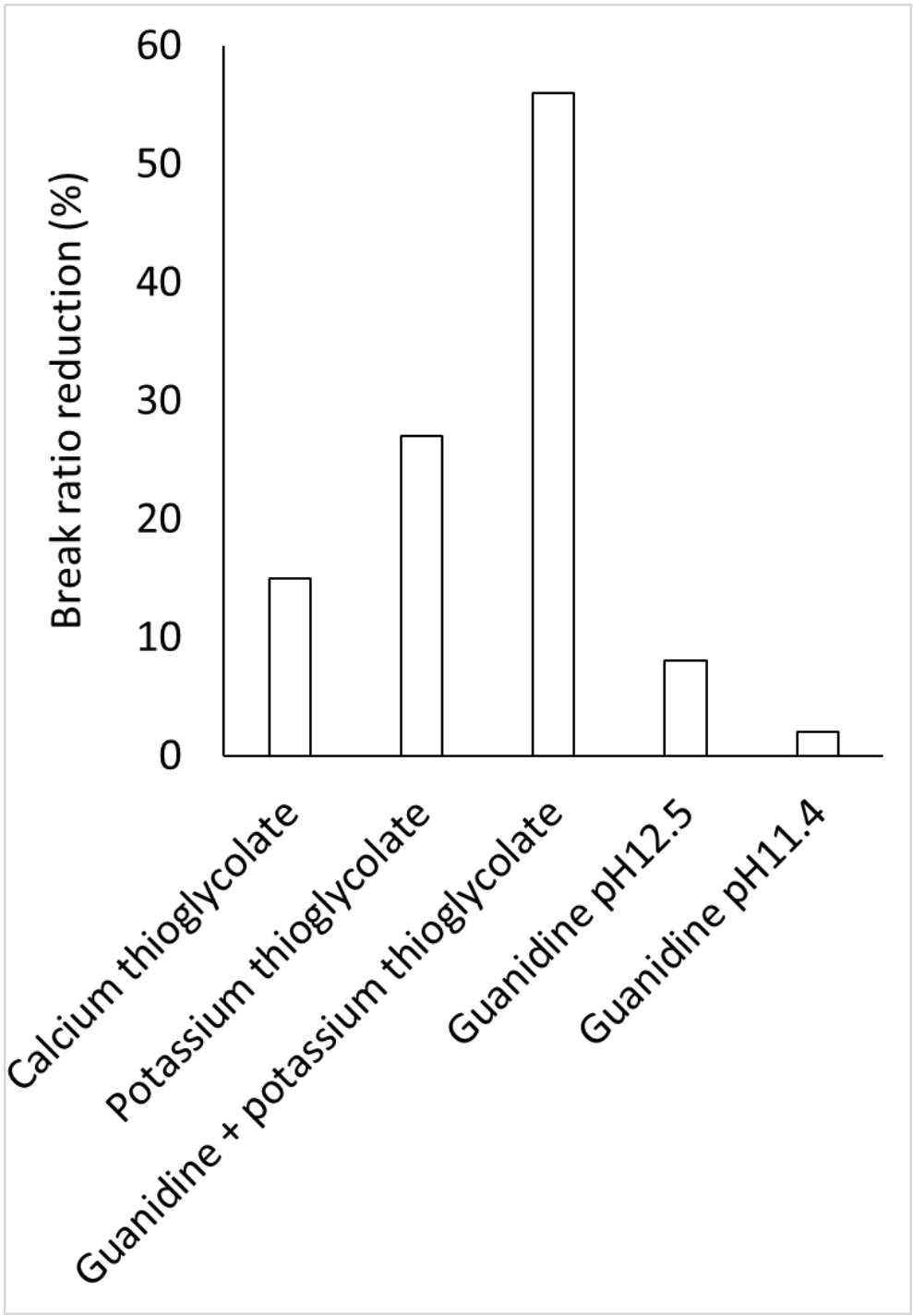

Fig. 5.29. Break ratio reduction of treated hairs with thioglycolate and guanidine chemistries. The higher the break ratio reduction, the more the hair has been weakened by the treatment (n=25). Work carried out by P&G.

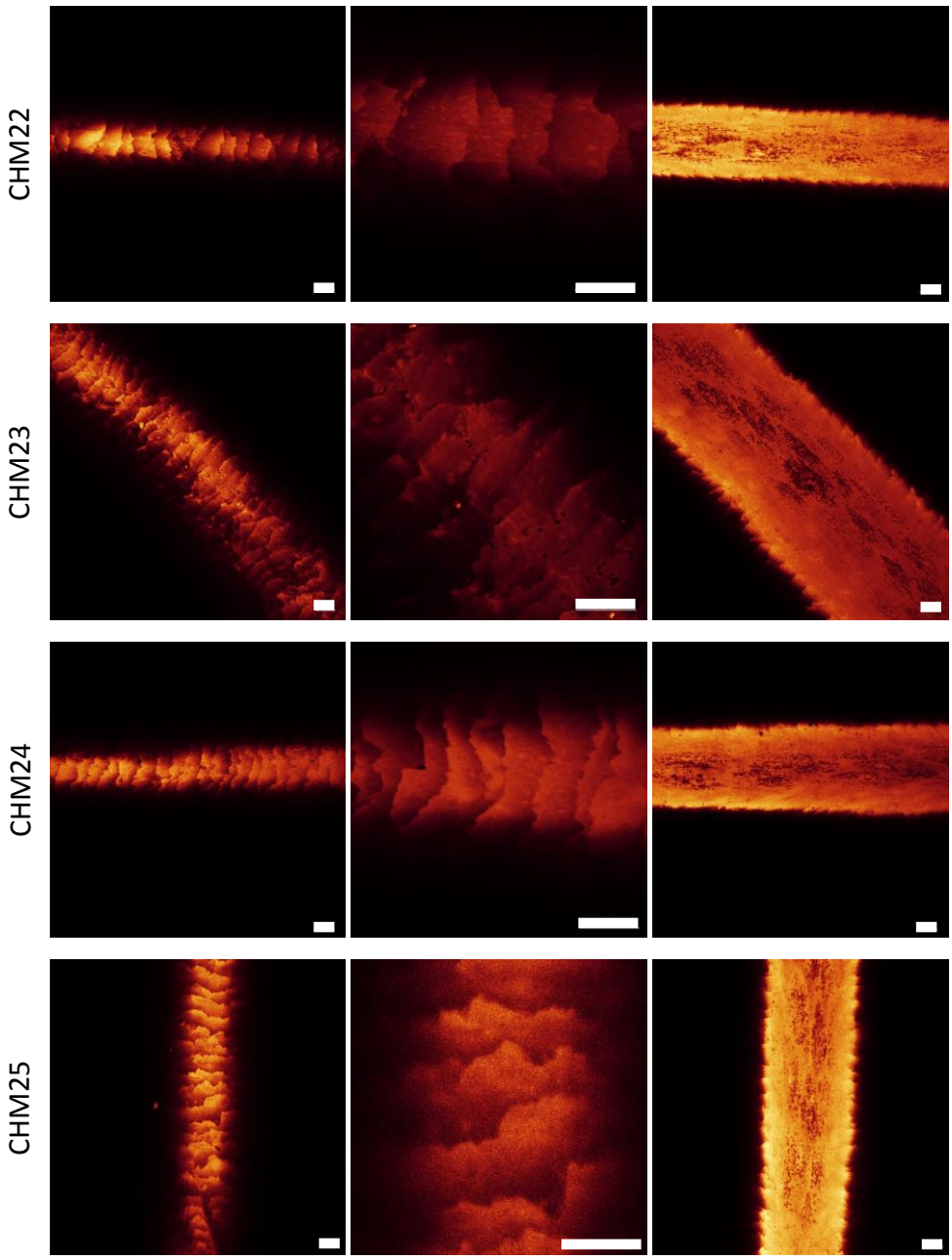

Fig. 5.30. Confocal fluorescence intensity images of hair treated with lithium bromide. Hair treated with 8M lithium bromide at the cuticle, the cuticle magnified, and the cortex. CHM22 = LiBr treatment at 25°C for 20 minutes. CHM23 = LiBr treatment at 85°C for 20 minutes. CHM24 = LiBr treatment at 25°C for 5 minutes. CHM25 = LiBr treatment at 25°C for 5 days. Representative photomicrographs shown of 9 imaged hairs of each treatment. Scale bars = 10µm.

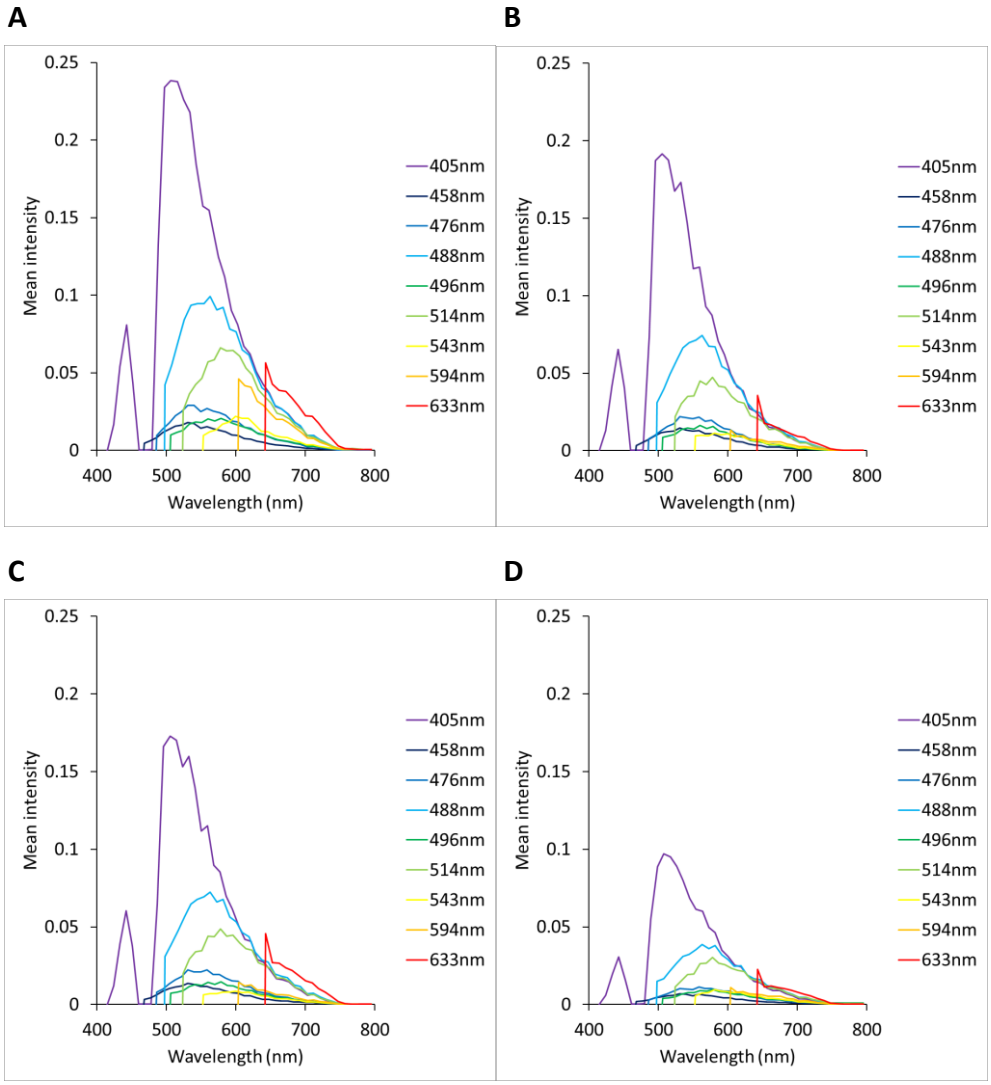

Fig. 5.31. Emission spectra of hair treated with lithium bromide. Hair treated with lithium bromide under four conditions excited with nine laser lines. A) CHM22 = LiBr treatment at 25°C for 20 minutes. B) CHM23 = LiBr treatment at 85°C for 20 minutes. C) CHM24 = LiBr treatment at 25°C for 5 minutes. D) CHM25 = LiBr treatment at 25°C for 5 days. These emission spectra for one hair are representative of the five hairs analysed.

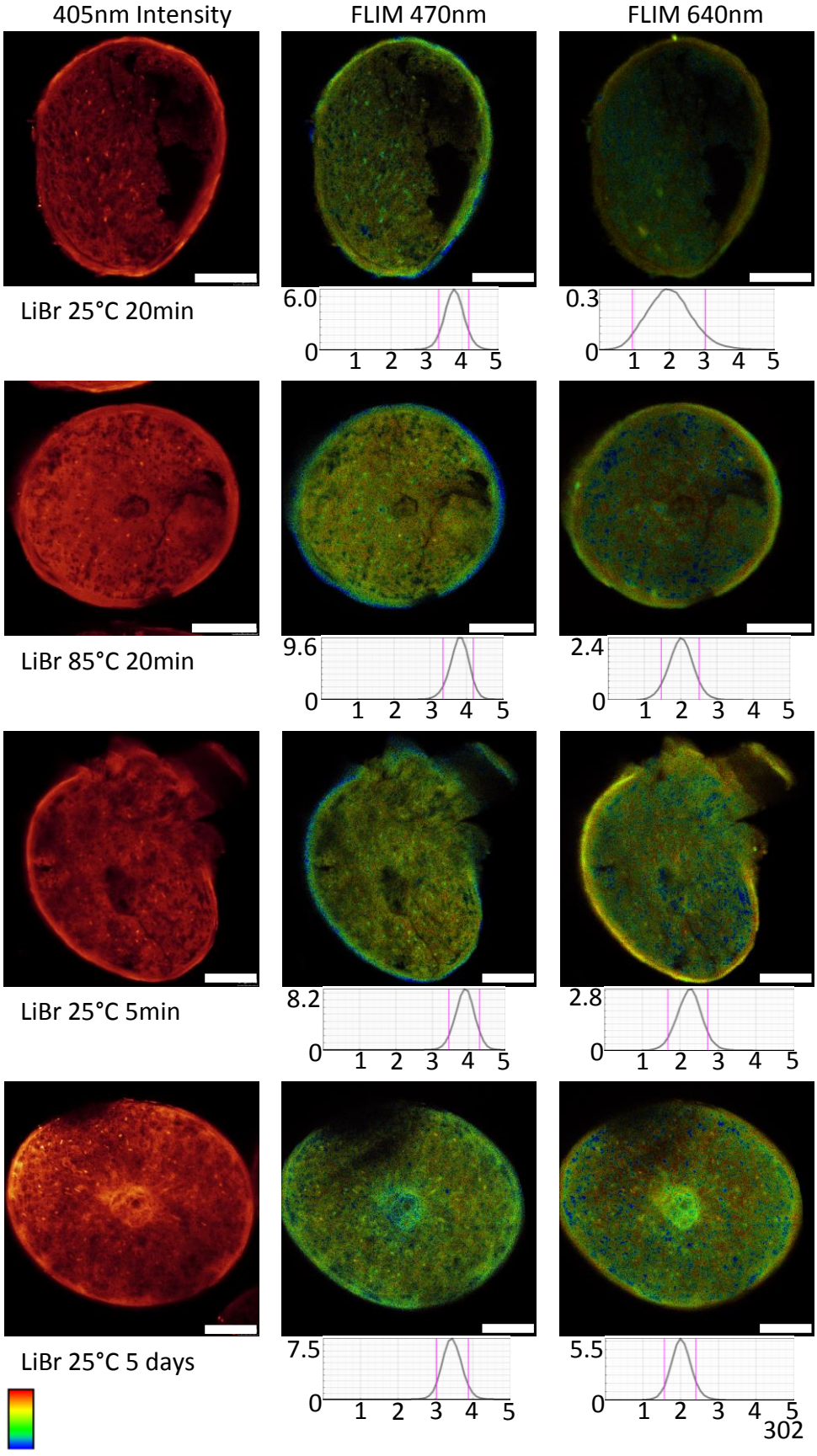
405nm Intensity
FLIM 470nm
FLIM 640nm
LiBr 25°C 20min
6.0
0
1 2 3 4 5
0.3
0
1 2 3 4 5
LiBr 85°C 20min
9.6
0
1 2 3 4 5
2.4
0
1 2 3 4 5
LiBr 25°C 5min
8.2
0
1 2 3 4 5
2.8
0
1 2 3 4 5
LiBr 25°C 5 days
7.5
0
1 2 3 4 5
5.5
0
1 2 3 4 5

Fig. 5.32. Intensity and FLIM images of hair treated with 8M lithium bromide. Images of transversely imaged hair treated with four lithium bromide solutions in which the time and temperature are varied. Each FLIM image also shows a graph of the frequency of lifetimes, x-axis = time (ns), y-axis = frequency (M.counts). Representative photomicrographs of 6 imaged hairs for each treatment are shown. N.B. The pink markers on the lifetime graphs indicate the upper (red) and lower (blue) lifetime limits. Scale bars = 25µm.

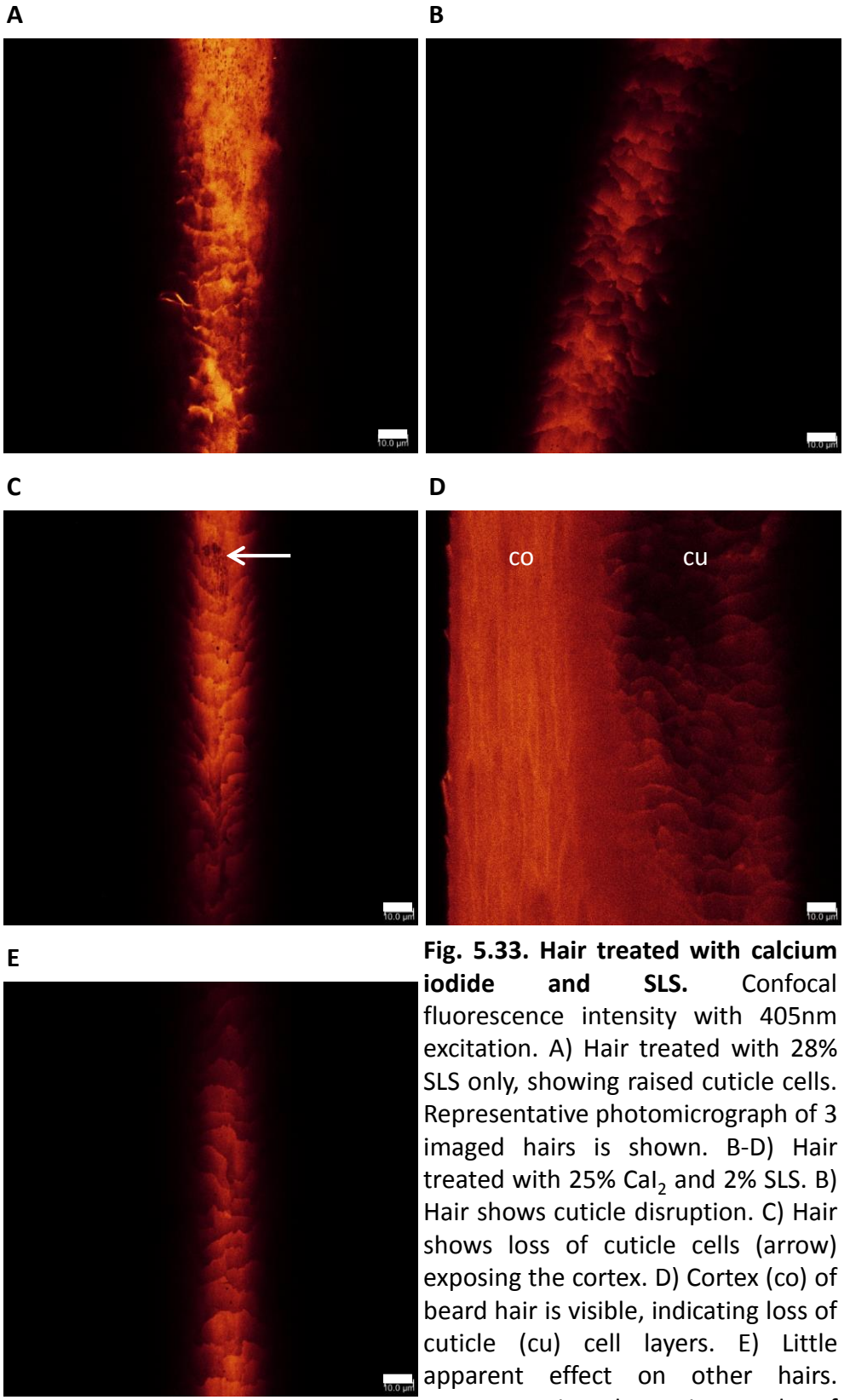

Fig. 5.33. Hair treated with calcium iodide and SLS. Confocal fluorescence intensity with 405nm excitation. A) Hair treated with 28% SLS only, showing raised cuticle cells. Representative photomicrograph of 3 imaged hairs is shown. B-D) Hair treated with 25% CaI_2 and 2% SLS. B) Hair shows cuticle disruption. C) Hair shows loss of cuticle cells (arrow) exposing the cortex. D) Cortex (co) of beard hair is visible, indicating loss of cuticle (cu) cell layers. E) Little apparent effect on other hairs. Representative photomicrographs of 10 imaged hairs are shown. Scale bars = 10µm.

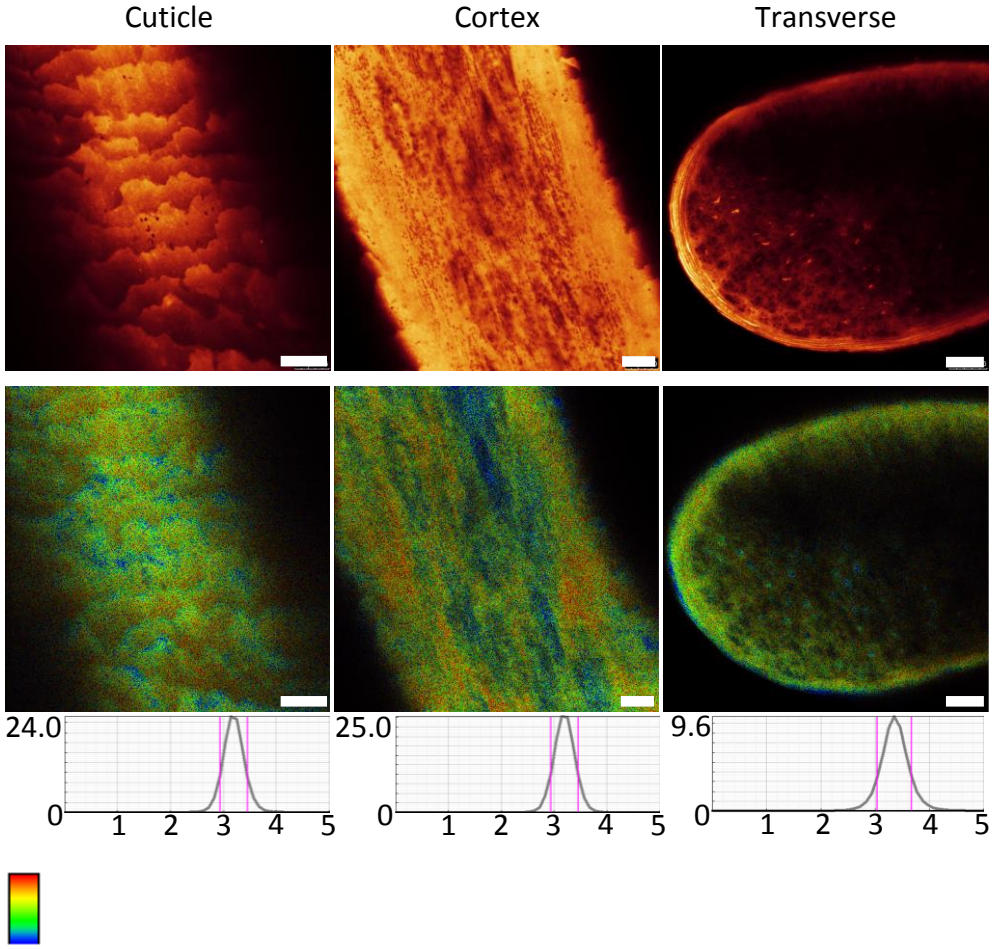

Fig. 5.34. Intensity and FLIM images of CaI_2 + SLS treated hair. 405nm intensity and 470nm FLIM images of transversely imaged hair and longitudinally imaged hair showing the cuticle and cortex. Each FLIM image also shows a graph of the frequency of lifetimes, x-axis = time (ns), y-axis = frequency (M.counts). Representative photomicrographs of 5 longitudinally and 6 transversely imaged hairs are shown. N.B. The pink markers on the lifetime graphs indicate the upper (red) and lower (blue) lifetime limits. Scale bars = 10µm.

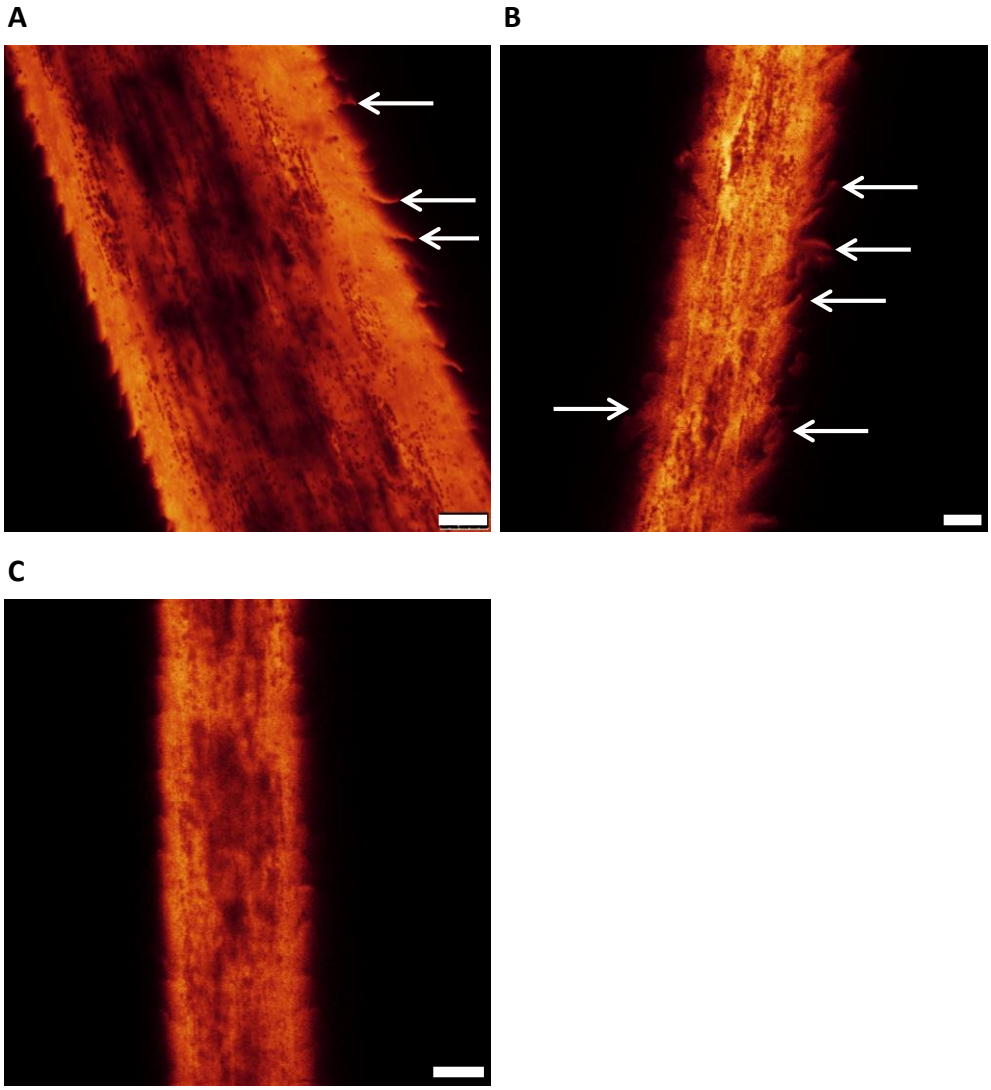

Fig. 5.35. Fluorescence intensity images of hair treated with CTAB and SLS. Confocal microscopy with 405nm excitation of Chinese head hairs treated with 2% CTAB pH9.41 for 5 minutes and 0.5% SLS for 5 minutes, showing varying degrees of cuticle flaring. A) Moderate cuticle flaring. B) Intense cuticle flaring. C) Little cuticle flaring. Representative photomicrographs of 6 imaged hairs are shown. Scale bars = 10µm.

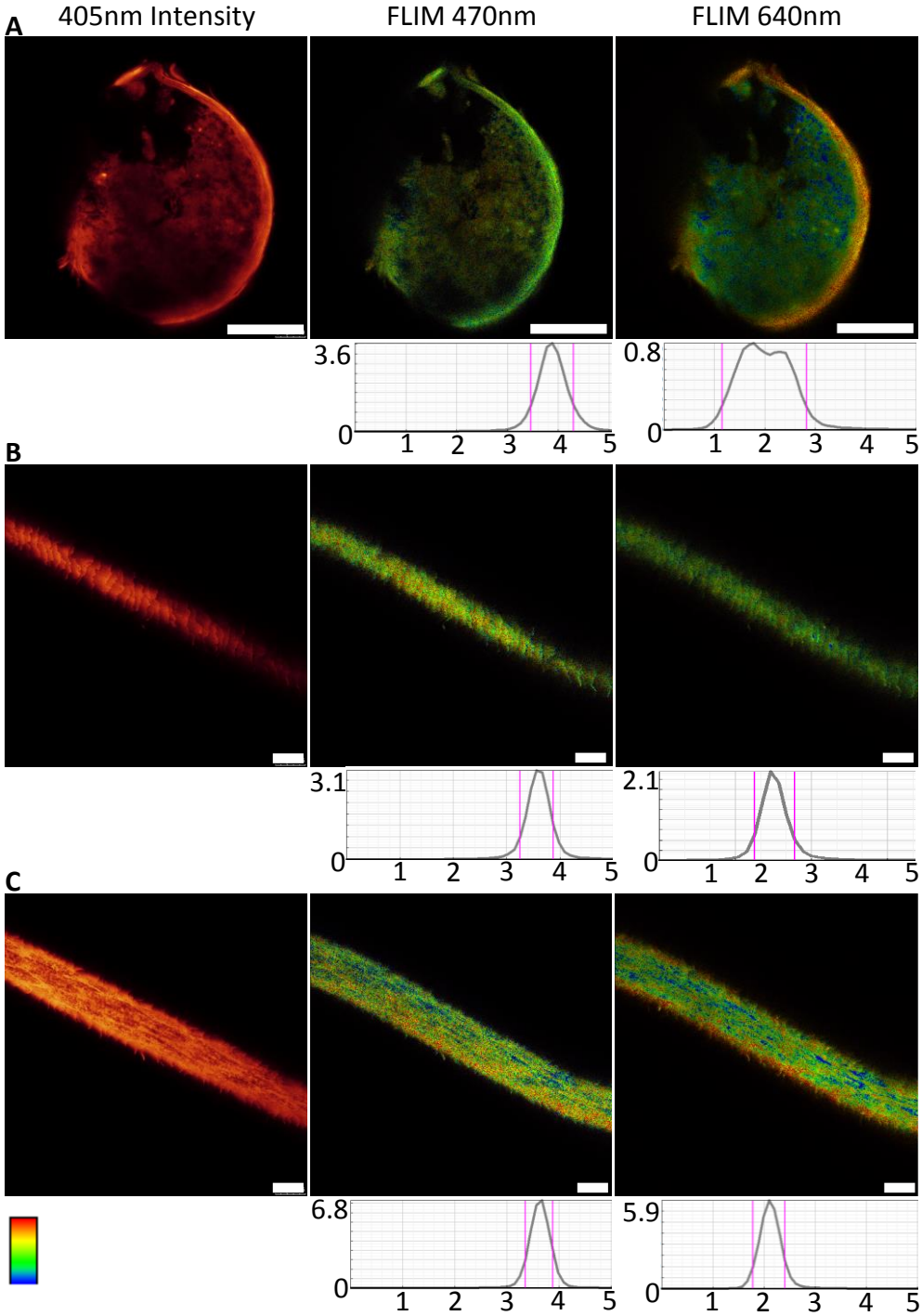

Fig. 5.36. Intensity and FLIM images of CTAB and SLS treated hair. A) Transverse. B) Cuticle. C) Cortex. Intensity and FLIM images of transversely and longitudinally imaged hair showing the cuticle and cortex. Each FLIM image also shows a graph of the frequency of lifetimes, x-axis = time (ns), y-axis = frequency (M.counts). Representative photomicrographs of 10 imaged hairs are shown. N.B. The pink markers on the lifetime graphs indicate the upper (red) and lower (blue) lifetime limits. Scale bars = 25µm.

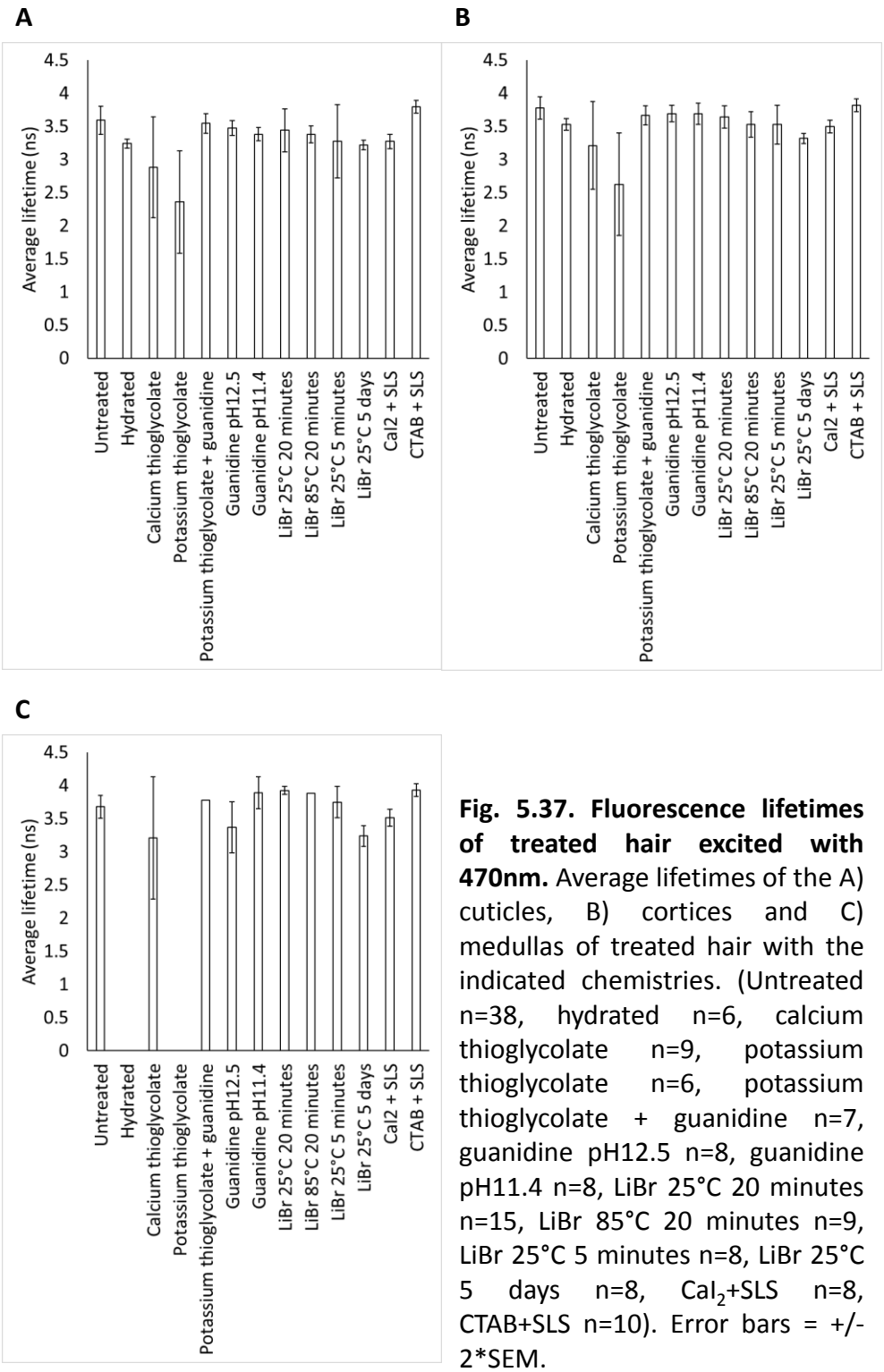

Fig. 5.37. Fluorescence lifetimes of treated hair excited with 470nm. Average lifetimes of the A) cuticles, B) cortices and C) medullas of treated hair with the indicated chemistries. (Untreated n=38, hydrated n=6, calcium thioglycolate n=9, potassium thioglycolate n=6, potassium thioglycolate + guanidine n=7, guanidine pH12.5 n=8, guanidine pH11.4 n=8, LiBr 25°C 20 minutes n=15, LiBr 85°C 20 minutes n=9, LiBr 25°C 5 minutes n=8, LiBr 25°C 5 days n=8, CaI_2+SLS n=8, CTAB+SLS n=10). Error bars = +/- 2*SEM.

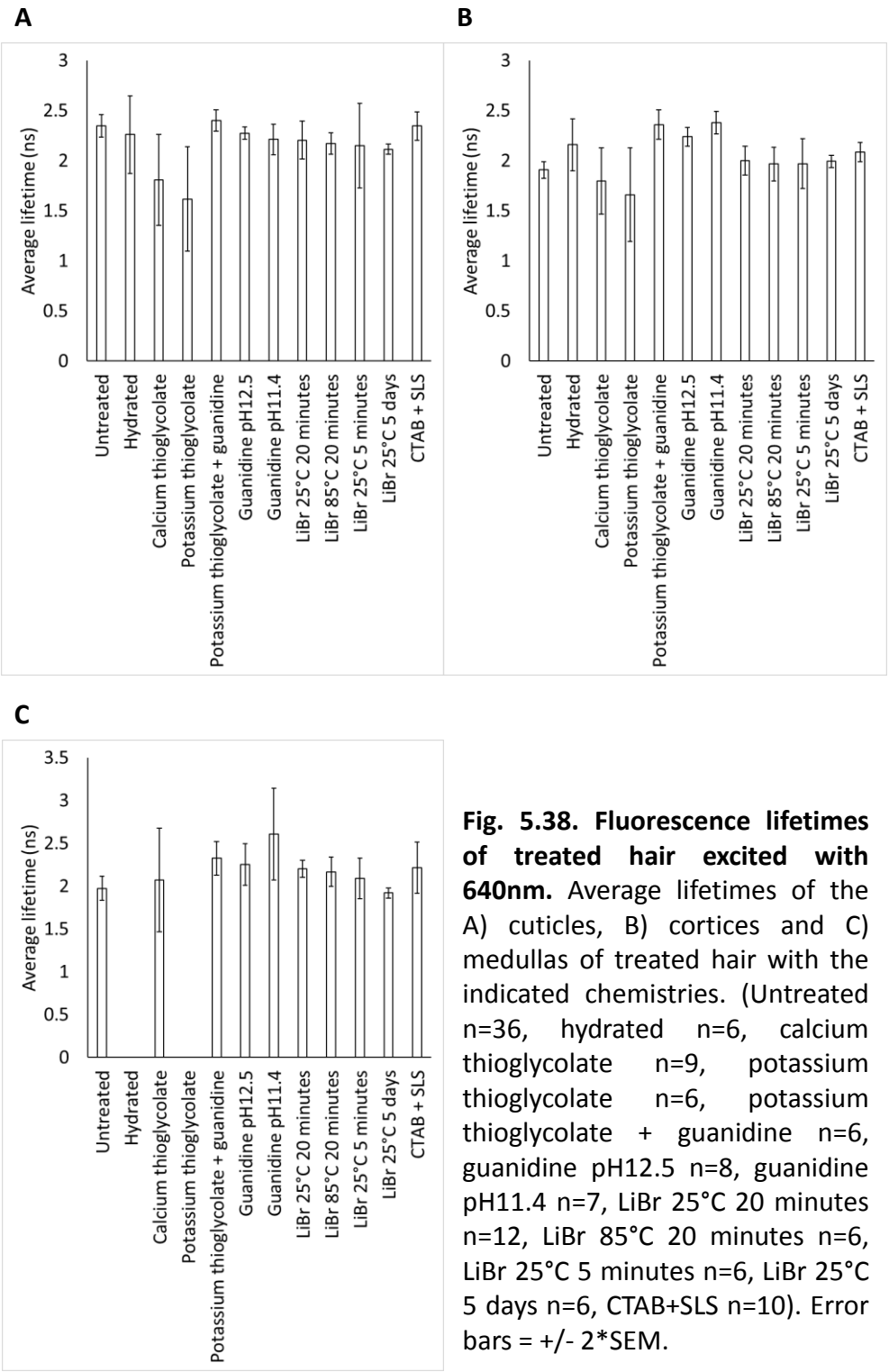

Fig. 5.38. Fluorescence lifetimes of treated hair excited with 640nm. Average lifetimes of the A) cuticles, B) cortices and C) medullas of treated hair with the indicated chemistries. (Untreated n=36, hydrated n=6, calcium thioglycolate n=9, potassium thioglycolate n=6, potassium thioglycolate + guanidine n=6, guanidine pH12.5 n=8, guanidine pH11.4 n=7, LiBr 25°C 20 minutes n=12, LiBr 85°C 20 minutes n=6, LiBr 25°C 5 minutes n=6, LiBr 25°C 5 days n=6, CTAB+SLS n=10). Error bars = +/- 2*SEM.

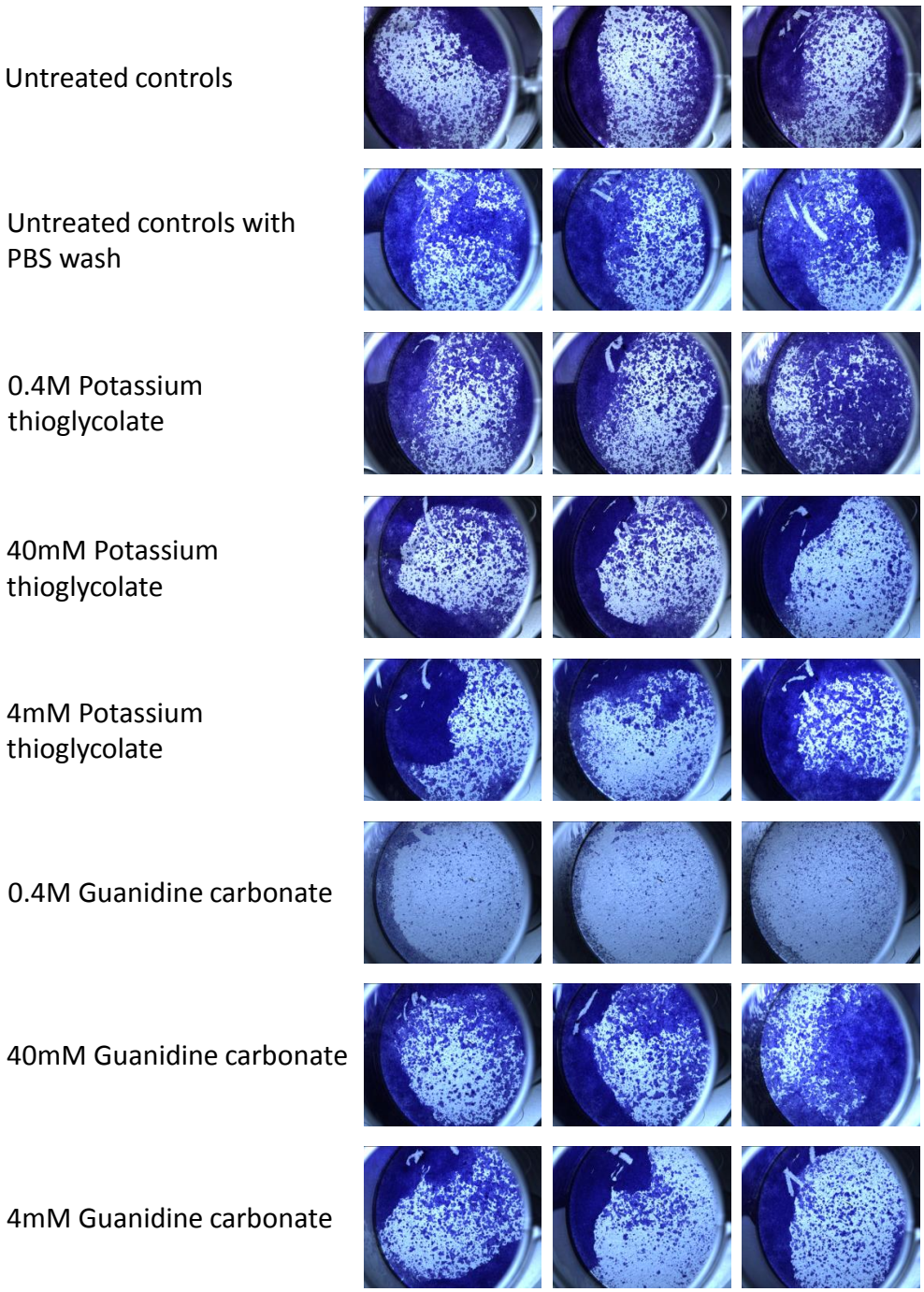

Fig. 5.39. Modified colony formation assay of treated HaCaT cells. HaCaT cells treated for 4 minutes with indicated chemicals in triplicate.

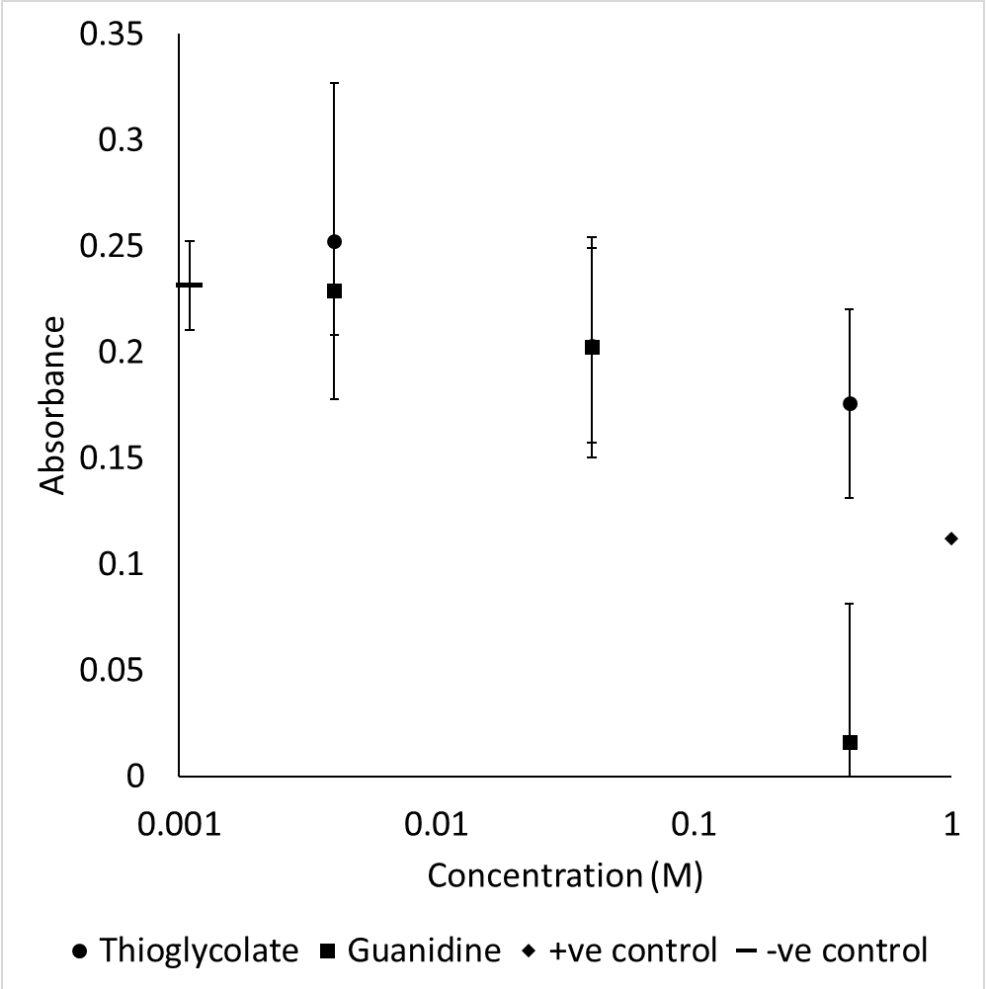

Fig. 5.40. Cell viability assay of treated HaCaT cells. HaCaT cells treated with 0.4M, 40mM, and 4mM each of potassium thioglycolate and guanidine carbonate for 4 minutes. Negative control was untreated HaCaT cells, positive control was HaCaT cells treated with 50µM JNK inhibitor II. (For each treatment n=3). Log scale bar for concentration. Error bars = +/- 2*SEM.

A

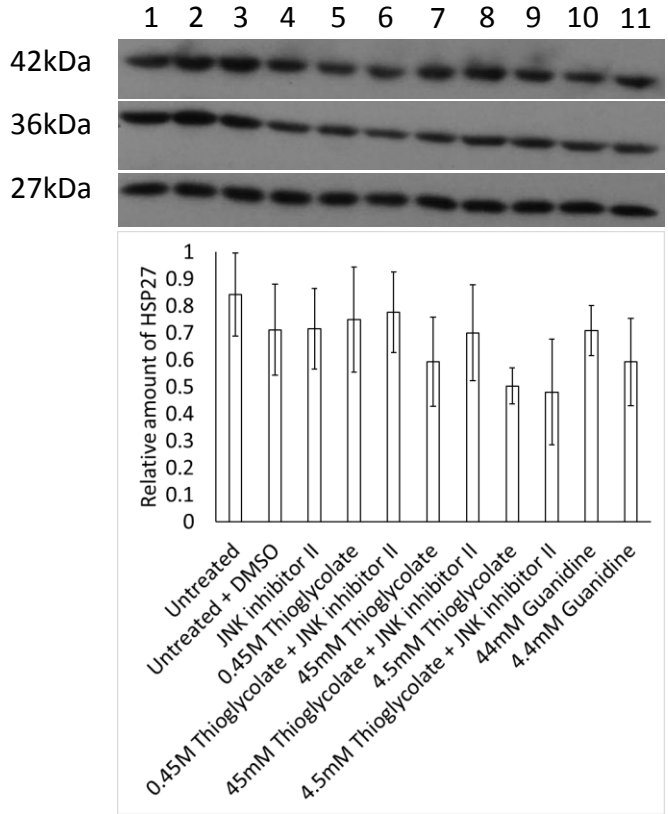
1 2 3 4 5 6 7 8 9 10 11
42kDa
Actin
36kDa
GAPDH
27kDa
HSP27
Relative amount of HSP27
1
0.9
0.8
0.7
0.6
0.5
0.4
0.3
0.2
0.1
0
Untreated
Untreated + DMSO
JNK inhibitor II
0.45M Thioglycolate
0.45M Thioglycolate + JNK inhibitor II
45mM Thioglycolate
45mM Thioglycolate + JNK inhibitor II
4.5mM Thioglycolate
4.5mM Thioglycolate + JNK inhibitor II
44mM Guanidine
4.4mM Guanidine

B

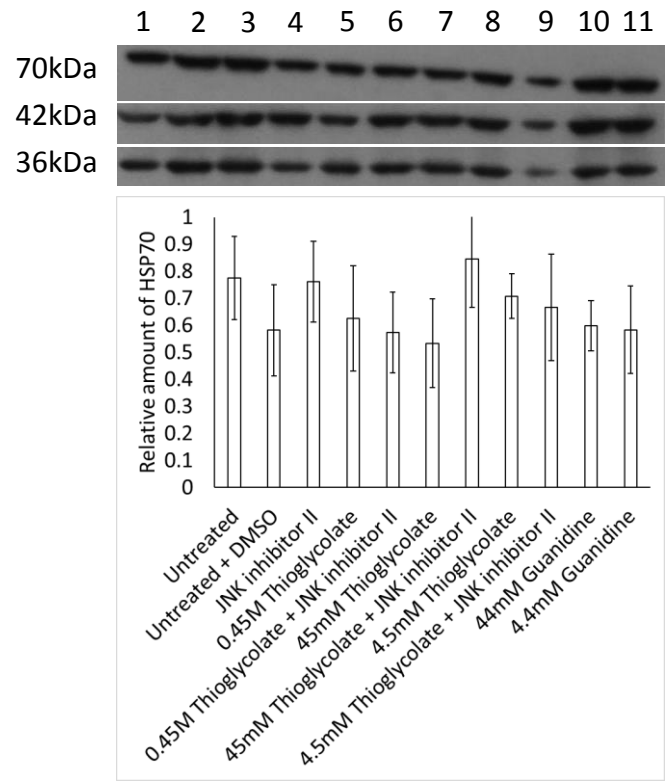
1 2 3 4 5 6 7 8 9 10 11
70kDa
HSP70
42kDa
Actin
36kDa
GAPDH
Relative amount of HSP70
1
0.9
0.8
0.7
0.6
0.5
0.4
0.3
0.2
0.1
0
Untreated
Untreated + DMSO
JNK inhibitor II
0.45M Thioglycolate
0.45M Thioglycolate + JNK inhibitor II
45mM Thioglycolate
45mM Thioglycolate + JNK inhibitor II
4.5mM Thioglycolate
4.5mM Thioglycolate + JNK inhibitor II
44mM Guanidine
4.4mM Guanidine

Fig. 5.41. Western blots of HSPs in HaCaT cells 1 hour post-treatment. HaCaT cells treated for 4 minutes with depilatory chemicals and harvested 1 hour post-treatment, and immunoblotted for the following proteins: A) HSP27, 1:1000 mouse monoclonal anti-HSP27 and 1:1000 polyclonal goat anti-mouse conjugated HRP; B) HSP70, 1:500 mouse monoclonal anti-HSP70 and 1:1000 polyclonal goat anti-mouse conjugated HRP. In both used loading controls: 1:2000 rabbit polyclonal anti-GAPDH and 1:3000 donkey anti-rabbit conjugated HRP, and 1:500 mouse monoclonal anti-actin and 1:1000 polyclonal goat anti-mouse conjugated HRP. Lane 1 = untreated. Lane 2 = untreated + DMSO. Lane 3 = 50µM JNK inhibitor II. Lane 4 = 0.45M potassium thioglycolate. Lane 5 = 0.45M potassium thioglycolate + 50µM JNK inhibitor II. Lane 6 = 45mM potassium thioglycolate. Lane 7 = 45mM potassium thioglycolate + 50µM JNK inhibitor II. Lane 8 = 4.5mM potassium thioglycolate. Lane 9 = 4.5mM potassium thioglycolate + 50µM JNK inhibitor II. Lane 10 = 44mM guanidine carbonate. Lane 11 = 4.4mM guanidine carbonate. Corresponding graphs show relative amounts of protein. Representative blots of experiments repeated in triplicate. Error bars = +/- 2*SEM.

A

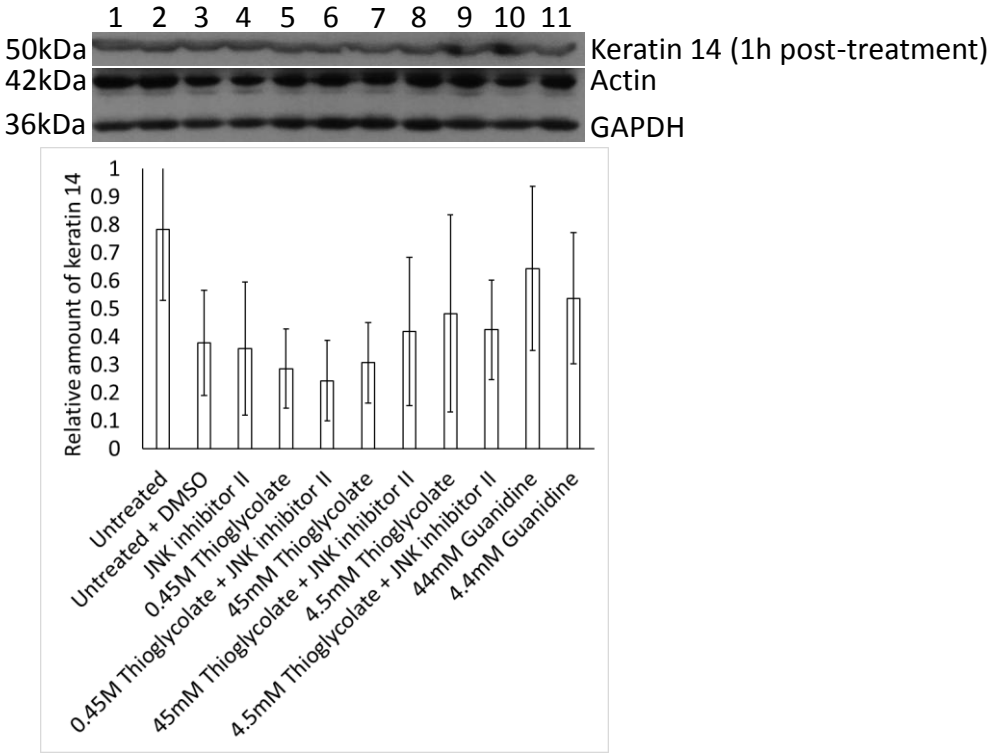
1 2 3 4 5 6 7 8 9 10 11
50kDa
42kDa
36kDa
Keratin 14 (1h post-treatment)
Actin
GAPDH
Relative amount of keratin 14
1
0.9
0.8
0.7
0.6
0.5
0.4
0.3
0.2
0.1
0
Untreated
Untreated + DMSO
JNK inhibitor II
0.45M Thioglycolate
0.45M Thioglycolate + JNK inhibitor II
45mM Thioglycolate
45mM Thioglycolate + JNK inhibitor II
4.5mM Thioglycolate
4.5mM Thioglycolate + JNK inhibitor II
44mM Guanidine
4.4mM Guanidine

B

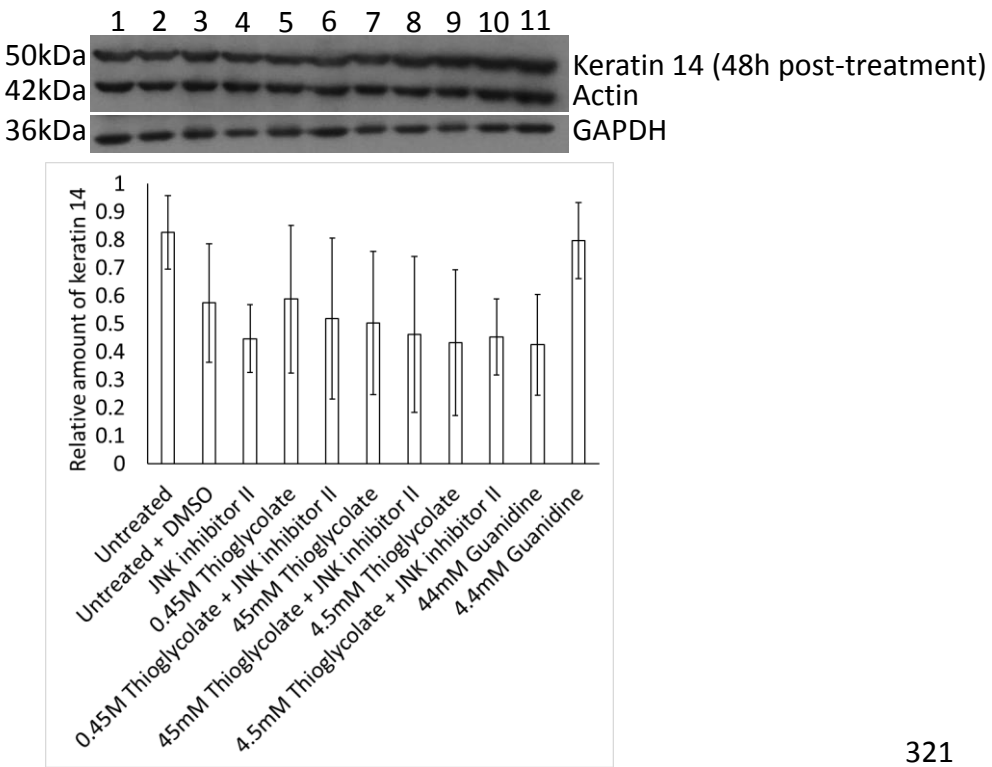
1 2 3 4 5 6 7 8 9 10 11
50kDa
42kDa
36kDa
Keratin 14 (48h post-treatment)
Actin
GAPDH
Relative amount of keratin 14
1
0.9
0.8
0.7
0.6
0.5
0.4
0.3
0.2
0.1
0
Untreated
Untreated + DMSO
JNK inhibitor II
0.45M Thioglycolate
0.45M Thioglycolate + JNK inhibitor II
45mM Thioglycolate
45mM Thioglycolate + JNK inhibitor II
4.5mM Thioglycolate
4.5mM Thioglycolate + JNK inhibitor II
44mM Guanidine
4.4mM Guanidine

Fig. 5.42. Western blots of keratin 14 in HaCaT cells 1 hour and 48 hours post-treatment. HaCaT cells treated for 4 minutes with depilatory chemicals and harvested: A) 1 hour post-treatment, 1:800 mouse monoclonal anti-keratin 14 and 1:1000 polyclonal goat anti-mouse conjugated HRP; B) 48 hours post-treatment, 1:800 mouse monoclonal anti-keratin 14 and 1:1000 polyclonal goat anti-mouse conjugated HRP. In both used loading controls: 1:2000 rabbit polyclonal anti-GAPDH and 1:3000 donkey anti-rabbit conjugated HRP, and 1:500 mouse monoclonal anti-actin and 1:1000 polyclonal goat anti-mouse conjugated HRP. Lane 1 = untreated. Lane 2 = untreated + DMSO. Lane 3 = 50µM JNK inhibitor II. Lane 4 = 0.45M potassium thioglycolate. Lane 5 = 0.45M potassium thioglycolate + 50µM JNK inhibitor II. Lane 6 = 45mM potassium thioglycolate. Lane 7 = 45mM potassium thioglycolate + 50µM JNK inhibitor II. Lane 8 = 4.5mM potassium thioglycolate. Lane 9 = 4.5mM potassium thioglycolate + 50µM JNK inhibitor II. Lane 10 = 44mM guanidine carbonate. Lane 11 = 4.4mM guanidine carbonate. Corresponding graphs show relative amounts of keratin 14. Representative blots of experiments repeated in triplicate. Error bars = +/- 2*SEM.

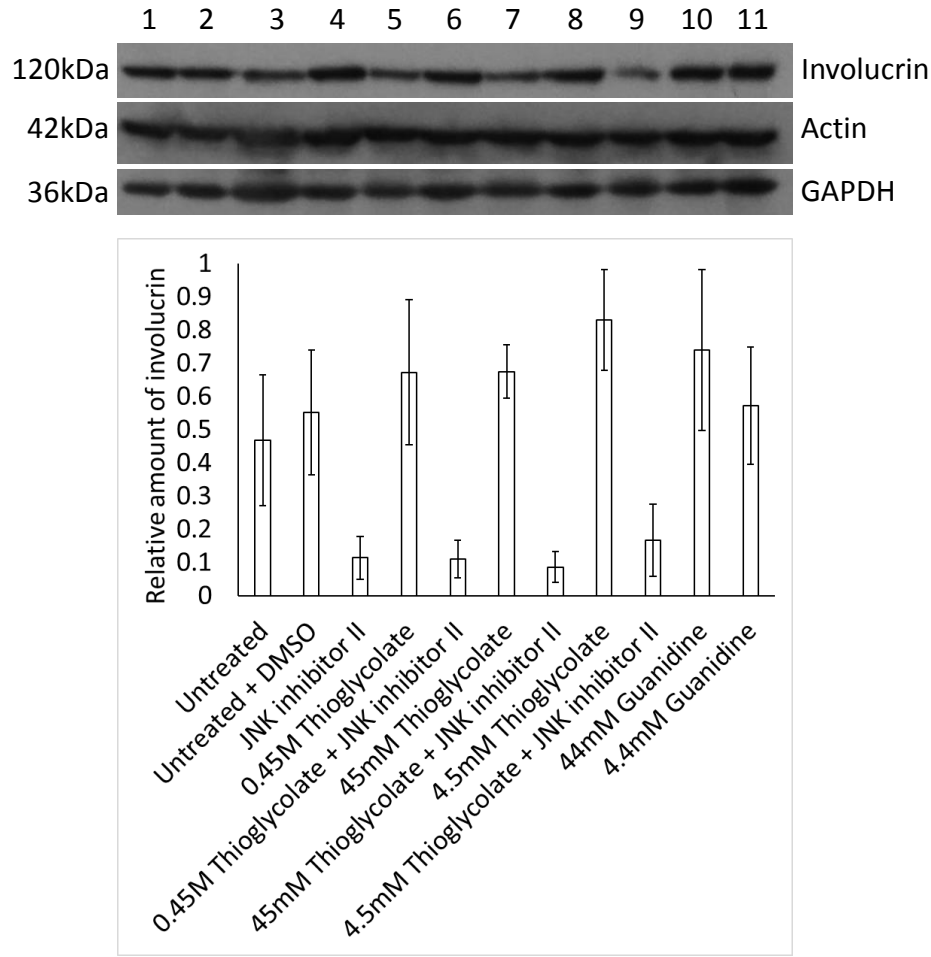

Fig. 5.43. Western blots of involucrin in HaCaT cells 48 hours post-treatment. HaCaT cells treated for 4 minutes with depilatory chemicals and harvested 48 hours post-treatment, and immunoblotted for involucrin. Used 1:1000 mouse monoclonal anti-involucrin, 1:500 mouse monoclonal anti-actin and 1:1000 polyclonal goat anti-mouse conjugated HRP, 1:2000 rabbit polyclonal anti-GAPDH and 1:3000 donkey anti-rabbit conjugated HRP. Lane 1 = untreated. Lane 2 = untreated + DMSO. Lane 3 = 50µM JNK inhibitor II. Lane 4 = 0.45M potassium thioglycolate. Lane 5 = 0.45M potassium thioglycolate + 50µM JNK inhibitor II. Lane 6 = 45mM potassium thioglycolate. Lane 7 = 45mM potassium thioglycolate + 50µM JNK inhibitor II. Lane 8 = 4.5mM potassium thioglycolate. Lane 9 = 4.5mM potassium thioglycolate + 50µM JNK inhibitor II. Lane 10 = 44mM guanidine carbonate. Lane 11 = 4.4mM guanidine carbonate. Corresponding graph shows relative amounts of involucrin. Representative blot of experiment repeated in triplicate. Error bars = +/- 2*SEM.

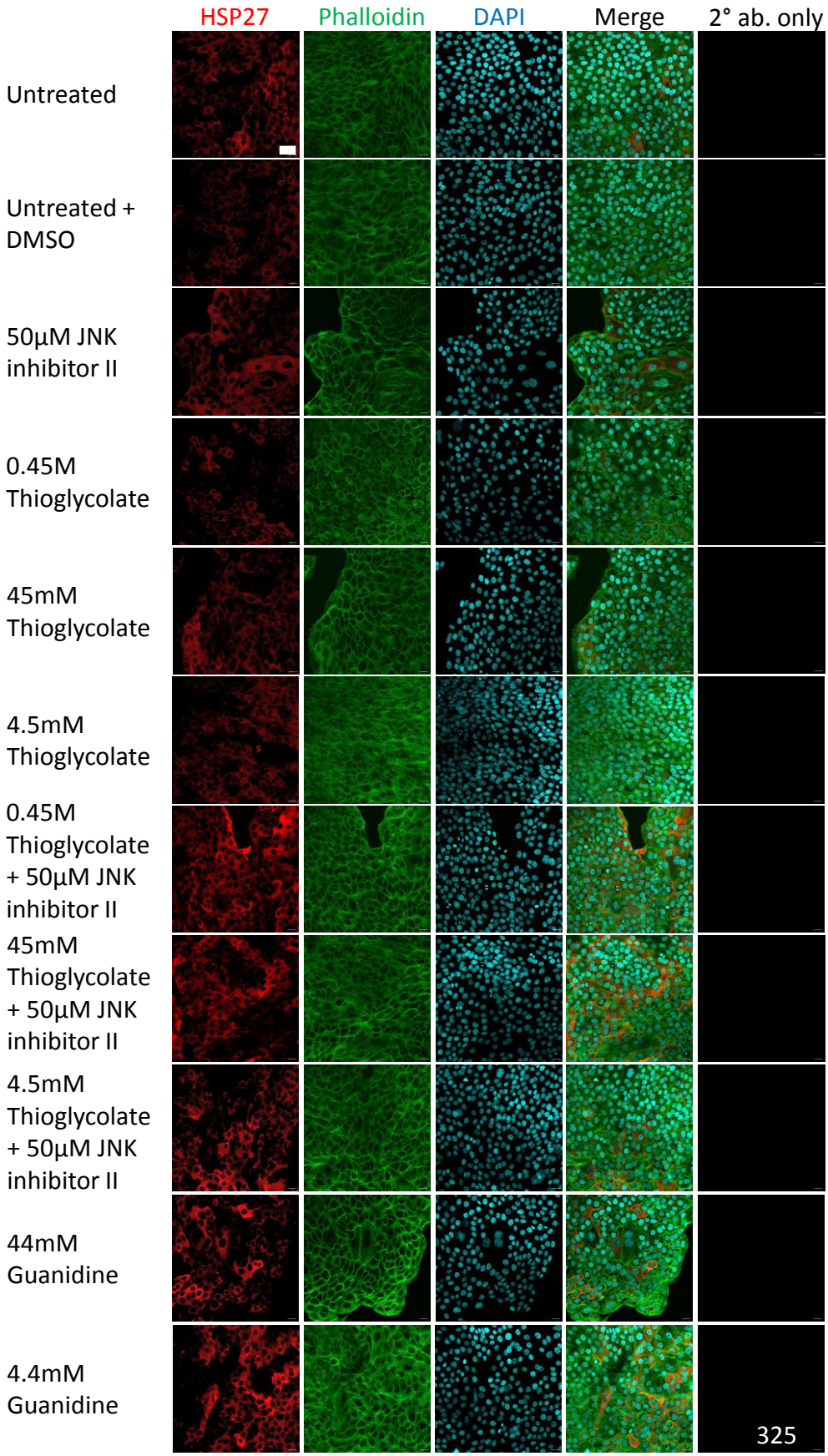
HSP27
Phalloidin
DAPI
Merge
2° ab. only
Untreated
Untreated + DMSO
50µM JNK inhibitor II
0.45M Thioglycolate
45mM Thioglycolate
4.5mM Thioglycolate
0.45M Thioglycolate + 50µM JNK inhibitor II
45mM Thioglycolate + 50µM JNK inhibitor II
4.5mM Thioglycolate + 50µM JNK inhibitor II
44mM Guanidine
4.4mM Guanidine
325

Fig. 5.44. Immunofluorescence of HSP27, actin and DAPI in HaCaT cells 1 hour post-treatment. Immunofluorescence with 1:500 mouse monoclonal anti-HSP27 and 1:800 goat anti-mouse AlexaFluor 594, and 1:500 phalloidin AlexaFluor 488, and 1:1000 DAPI. Representative photomicrographs of experiments repeated in triplicate. Scale bar = 50µm.

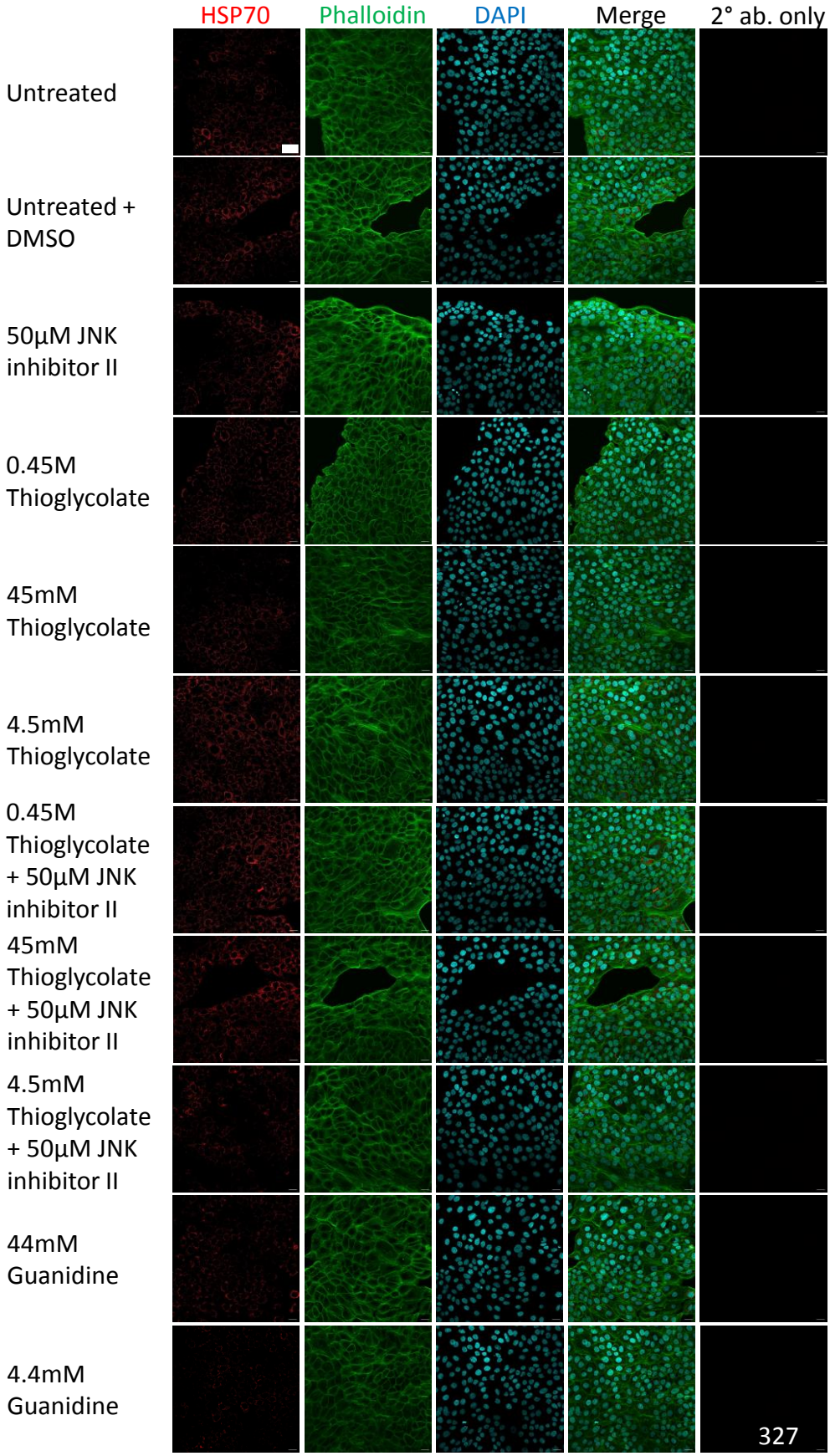
HSP70
Phalloidin
DAPI
Merge
2° ab. only
Untreated
Untreated + DMSO
50µM JNK inhibitor II
0.45M Thioglycolate
45mM Thioglycolate
4.5mM Thioglycolate
0.45M Thioglycolate + 50µM JNK inhibitor II
45mM Thioglycolate + 50µM JNK inhibitor II
4.5mM Thioglycolate + 50µM JNK inhibitor II
44mM Guanidine
4.4mM Guanidine

Fig. 5.45. Immunofluorescence of HSP70, actin and DAPI in HaCaT cells 1 hour post-treatment. Immunofluorescence with 1:200 mouse monoclonal anti-HSP70 and 1:800 goat anti-mouse AlexaFluor 594, and 1:500 phalloidin AlexaFluor 488, and 1:1000 DAPI. Representative photomicrographs of experiments repeated in triplicate. Scale bar = 50µm.

A

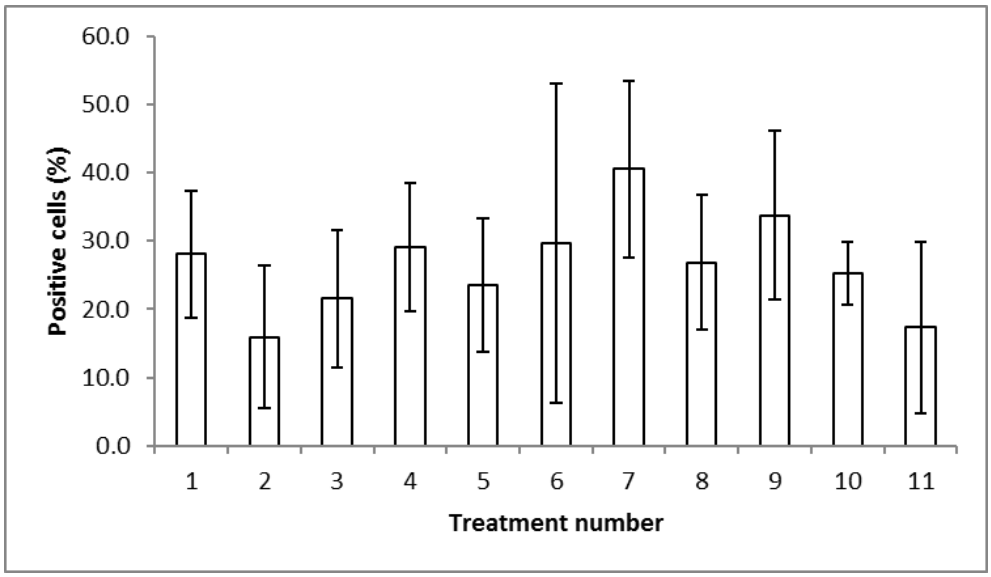

B

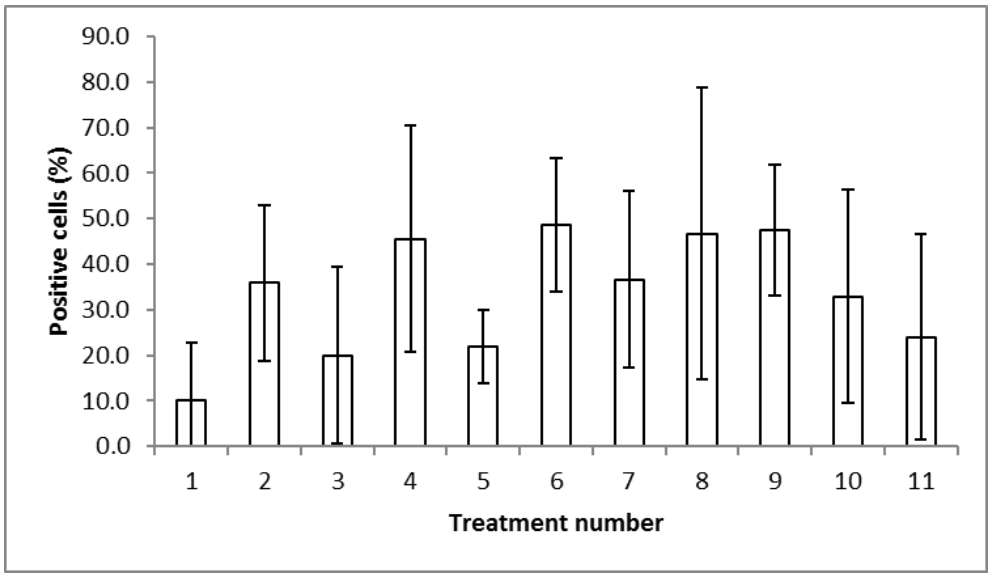

Fig. 5.46. Percentage of positive HaCaT cells for HSPs 1 hour post-treatment. A) HSP27. B) HSP70. Treatment numbers: 1) untreated; 2) untreated + DMSO; 3) untreated + 50µM JNK inhibitor II; 4) 0.45M potassium thioglycolate; 5) 45mM potassium thioglycolate; 6) 4.5mM potassium thioglycolate; 7) 0.45M potassium thioglycolate + 50µM JNK inhibitor II; 8) 45mM potassium thioglycolate + 50µM JNK inhibitor II; 9) 4.5mM potassium thioglycolate + 50µM JNK inhibitor II; 10) 44mM guanidine carbonate; 11) 4.4mM guanidine carbonate. Experiments were repeated in triplicate. Error bars = +/- SD.

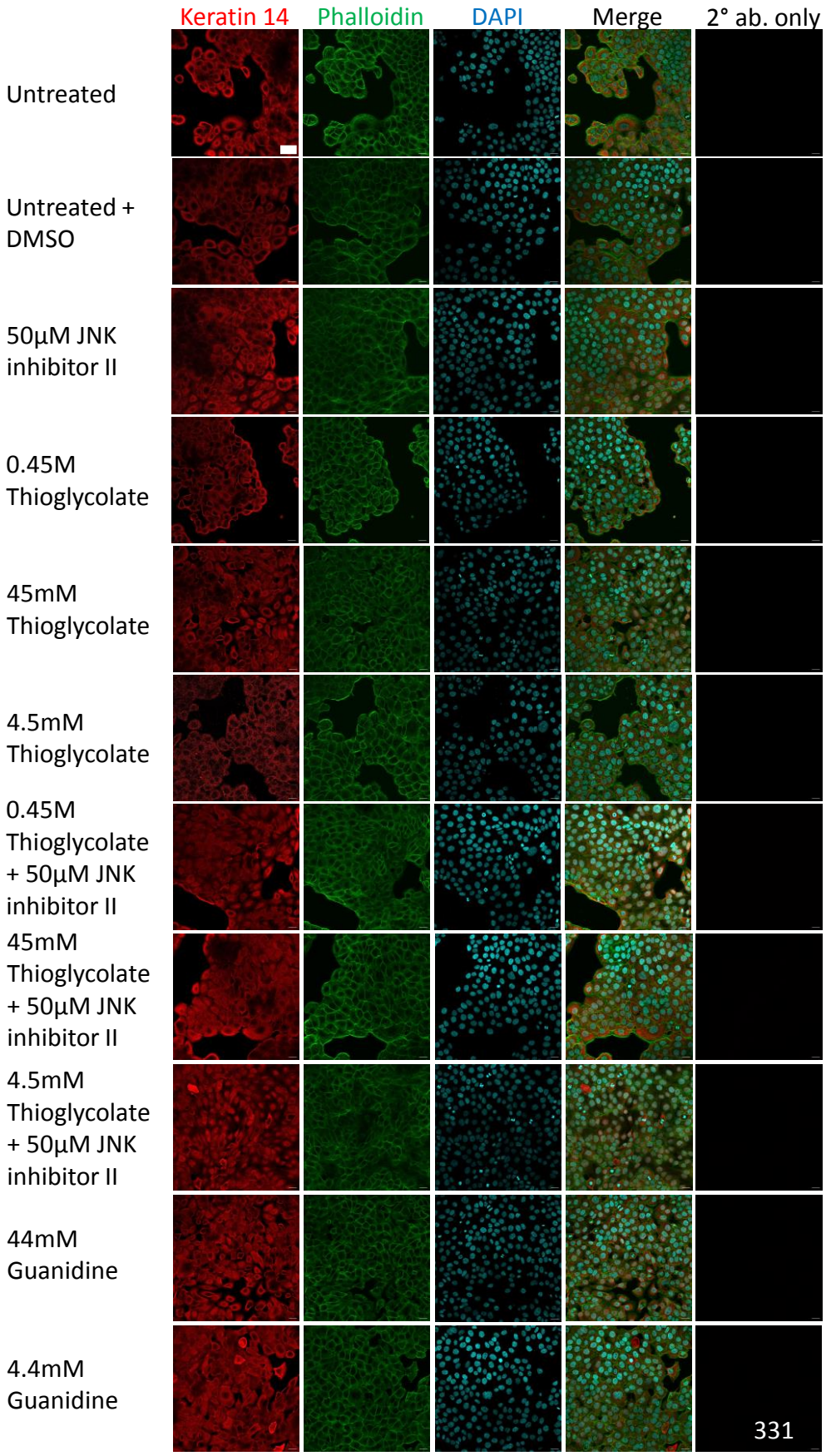
Keratin 14
Phalloidin
DAPI
Merge
2° ab. only
Untreated
Untreated + DMSO
50µM JNK inhibitor II
0.45M Thioglycolate
45mM Thioglycolate
4.5mM Thioglycolate
0.45M Thioglycolate + 50µM JNK inhibitor II
45mM Thioglycolate + 50µM JNK inhibitor II
4.5mM Thioglycolate + 50µM JNK inhibitor II
44mM Guanidine
4.4mM Guanidine

Fig. 5.47. Immunofluorescence of keratin 14, actin and DAPI in HaCaT cells 1 hour post-treatment. Immunofluorescence with 1:200 mouse monoclonal anti-keratin 14 and 1:800 goat anti-mouse AlexaFluor 594, and 1:500 phalloidin AlexaFluor 488, and 1:1000 DAPI. Representative photomicrographs of experiments repeated in triplicate. Scale bar = 50µm.

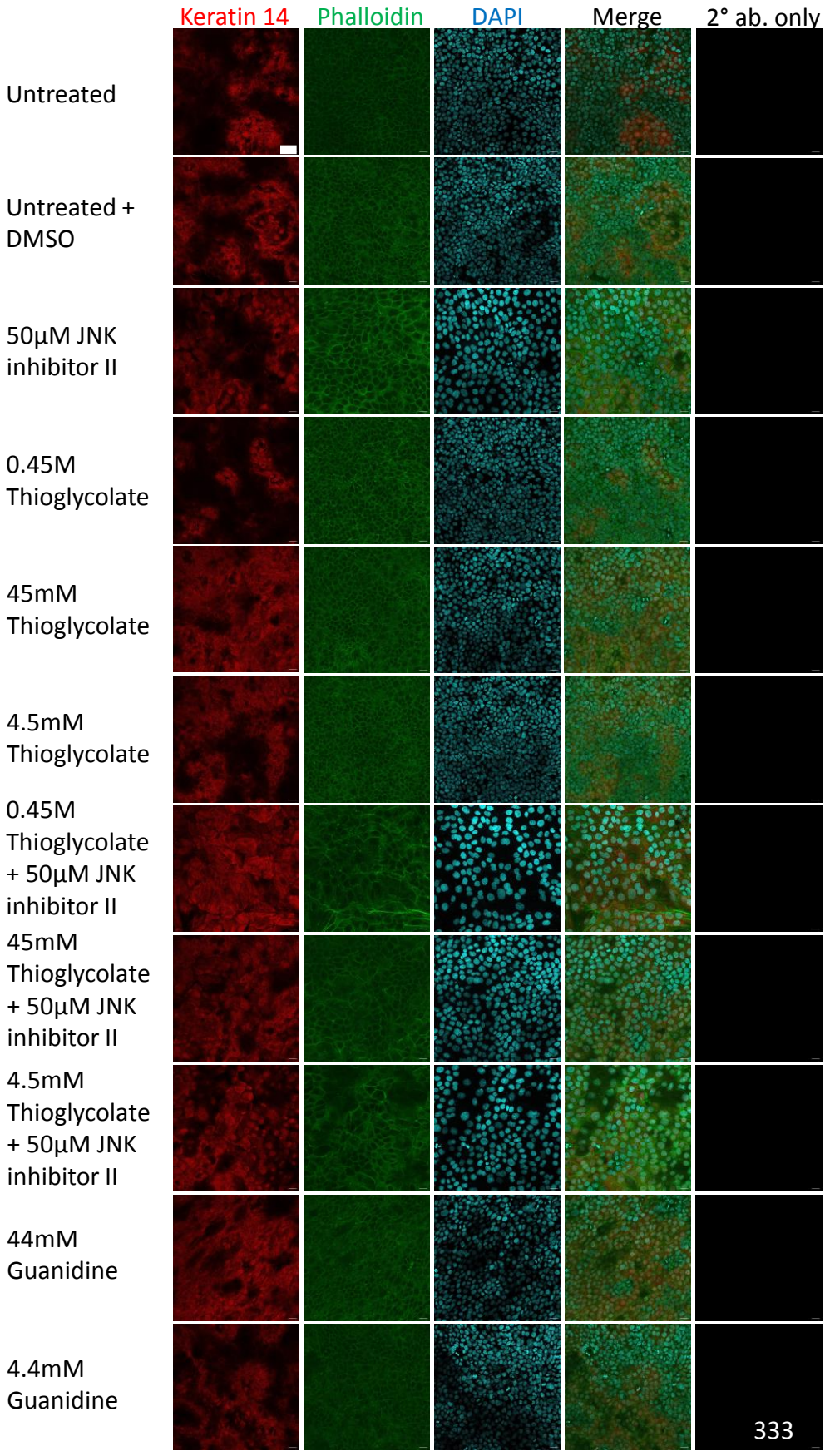
Keratin 14
Phalloidin
DAPI
Merge
2° ab. only
Untreated
Untreated + DMSO
50µM JNK inhibitor II
0.45M Thioglycolate
45mM Thioglycolate
4.5mM Thioglycolate
0.45M Thioglycolate + 50µM JNK inhibitor II
45mM Thioglycolate + 50µM JNK inhibitor II
4.5mM Thioglycolate + 50µM JNK inhibitor II
44mM Guanidine
4.4mM Guanidine

Fig. 5.48. Immunofluorescence of keratin 14, actin and DAPI in HaCaT cells 48 hours post-treatment. Immunofluorescence with 1:200 mouse monoclonal anti-keratin 14 and 1:800 goat anti-mouse AlexaFluor 594, and 1:500 phalloidin AlexaFluor 488, and 1:1000 DAPI. Representative photomicrographs of experiments repeated in triplicate. Scale bar = 50µm.

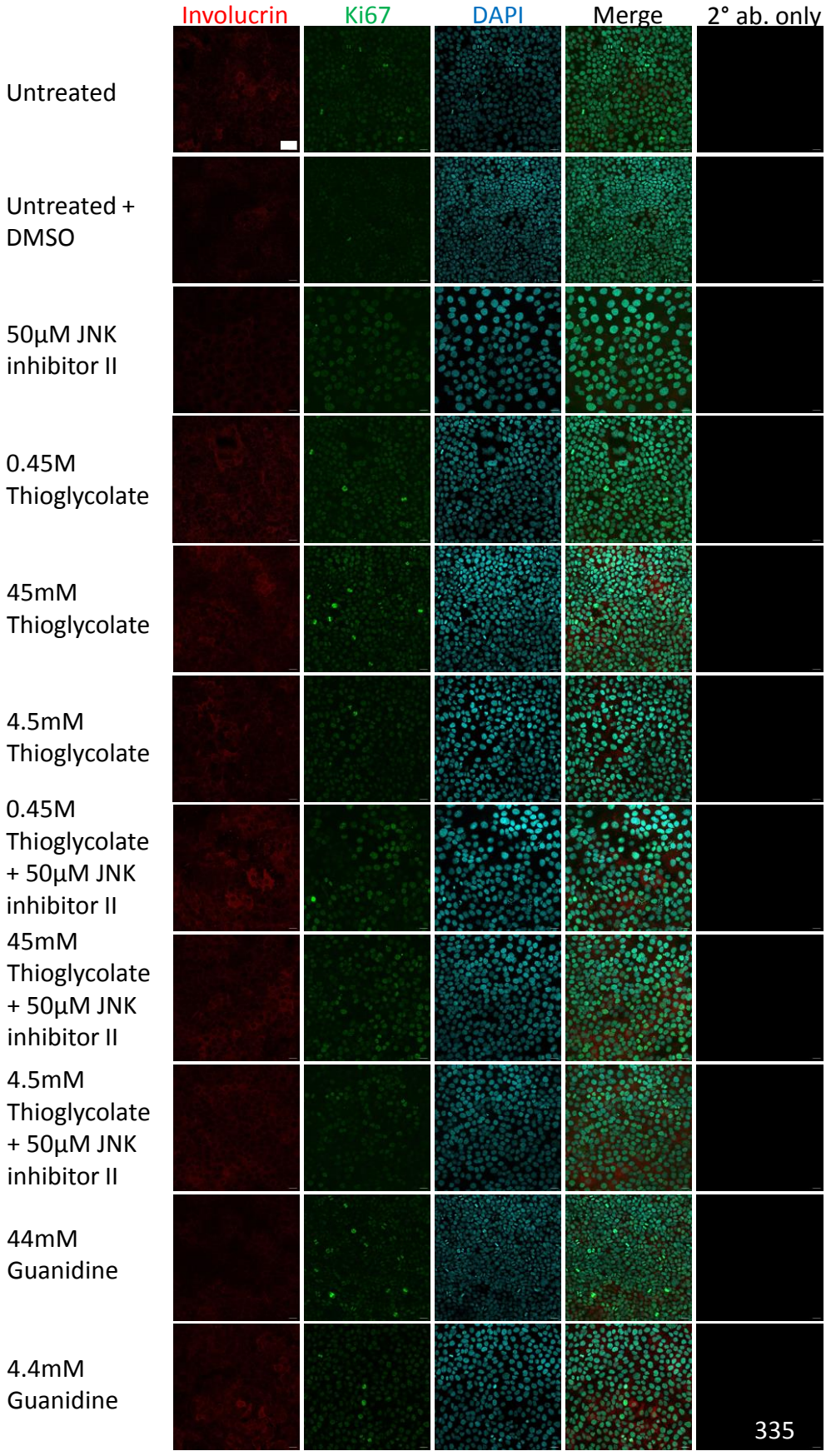
Involucrin
Ki67
DAPI
Merge
2° ab. only
Untreated
Untreated + DMSO
50µM JNK inhibitor II
0.45M Thioglycolate
45mM Thioglycolate
4.5mM Thioglycolate
0.45M Thioglycolate + 50µM JNK inhibitor II
45mM Thioglycolate + 50µM JNK inhibitor II
4.5mM Thioglycolate + 50µM JNK inhibitor II
44mM Guanidine
4.4mM Guanidine

Fig. 5.49. Immunofluorescence of involucrin, Ki67, and DAPI in HaCaT cells 48 hours post-treatment. Immunofluorescence with 1:200 mouse monoclonal anti-involucrin and 1:800 goat anti-mouse AlexaFluor 594, and 1:250 rabbit monoclonal anti-Ki67 and 1:800 goat anti-rabbit AlexaFluor 488, and 1:1000 DAPI. Representative photomicrographs of experiments repeated in triplicate. Scale bar = 50µm.

A

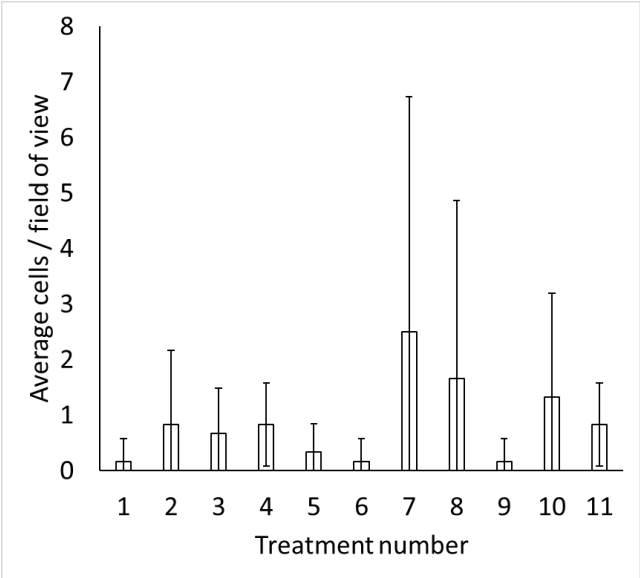
Average cells / field of view
0
1
2
3
4
5
6
7
8
1 2 3 4 5 6 7 8 9 10 11
Treatment number

B

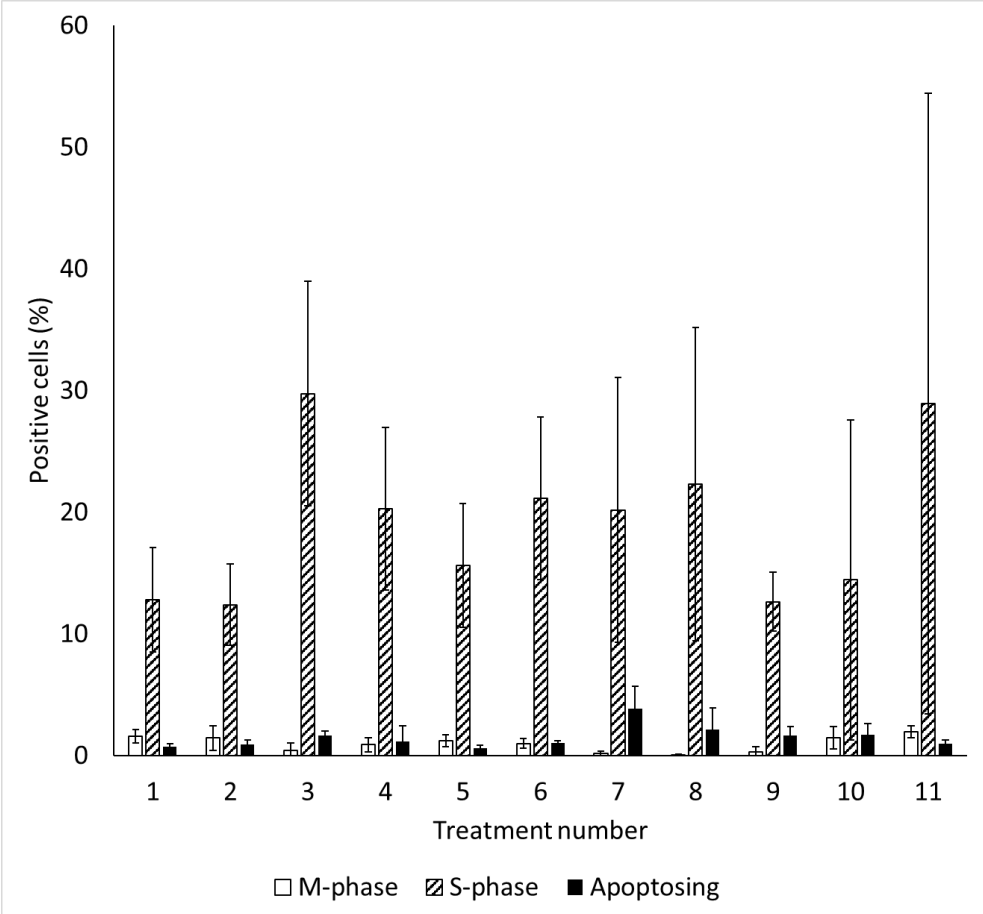
Positive cells (%)
0
10
20
30
40
50
60
1 2 3 4 5 6 7 8 9 10 11
Treatment number
M-phase
S-phase
Apoptosing

Fig. 5.50. Average number of HaCaT cells for each treatment showing number of apoptotic cells and cell cycle phase. Counted using Ki67 as the indicator for cell cycle and DAPI as the indicator for apoptosis. A) 1 hour post treatment showing number of apoptotic cells. The field of view is 387.5µm x 387.5µm. B) 48 hours post-treatment showing number of apoptotic cells and numbers of cells in M-phase and S-phase of the cell cycle. Treatment numbers: 1) untreated; 2) untreated+DMSO; 3) untreated + 50µM JNK inhibitor II; 4) 0.45M potassium thioglycolate; 5) 45mM potassium thioglycolate; 6) 4.5mM potassium thioglycolate; 7) 0.45M potassium thioglycolate + 50µM JNK inhibitor II; 8) 45mM potassium thioglycolate + 50µM JNK inhibitor II; 9) 4.5mM potassium thioglycolate + 50µM JNK inhibitor II; 10) 44mM guanidine carbonate; 11) 4.4mM guanidine carbonate. Experiments were repeated in triplicate. Error bars = +/- SD.

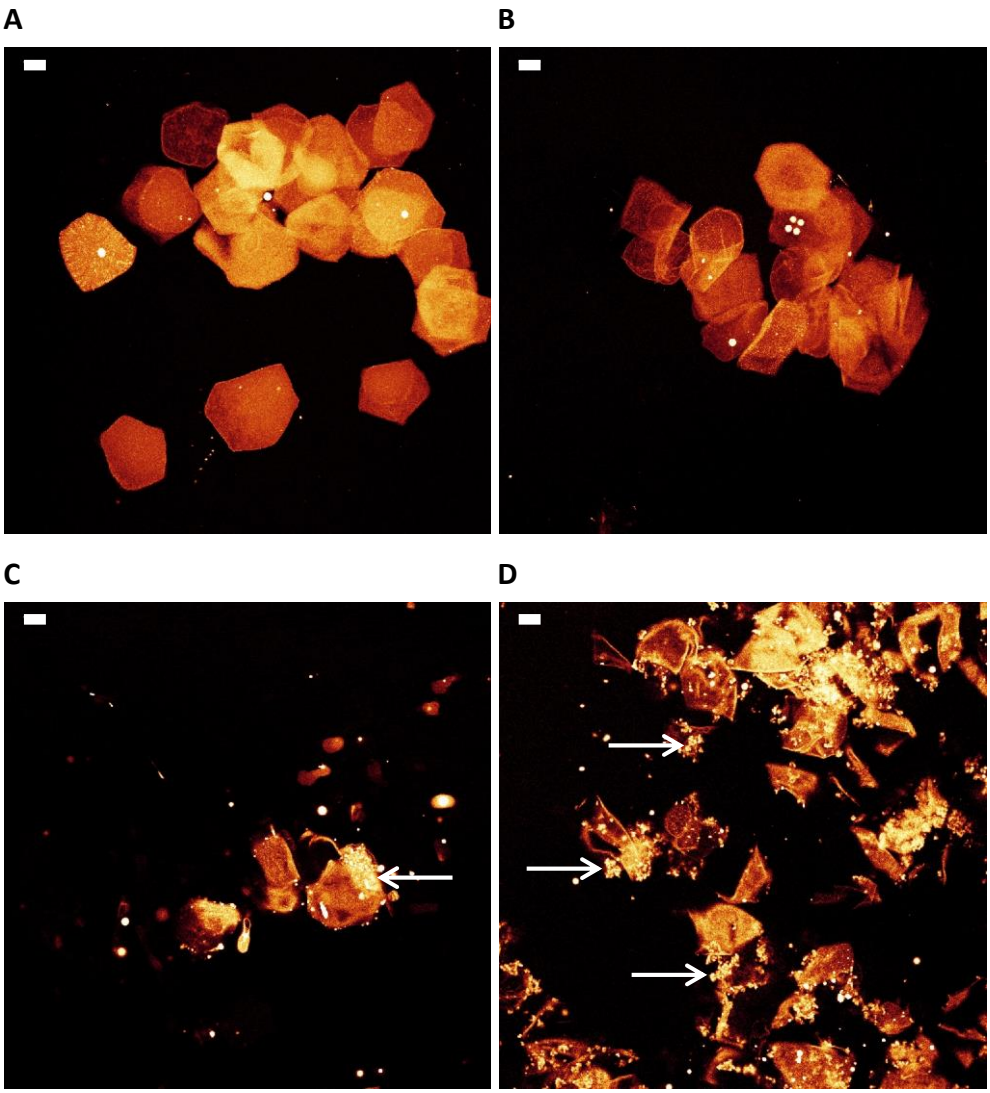

Fig. 5.51. Thioglycolate and guanidine treated cornified envelopes. Cornified envelopes from 24 month old rat ear stained with 0.6mg/ml Nile red. A) Untreated control cells. B) 0.1M Guanidine carbonate treated cells. C) 0.45M Potassium thioglycolate treated cells. D) 0.2M Potassium thioglycolate and 0.2M guanidine carbonate treated cells. Arrows indicate brightly stained aggregates. Representative photomicrographs of the experiment repeated in triplicate. Scale bars = 10µm.

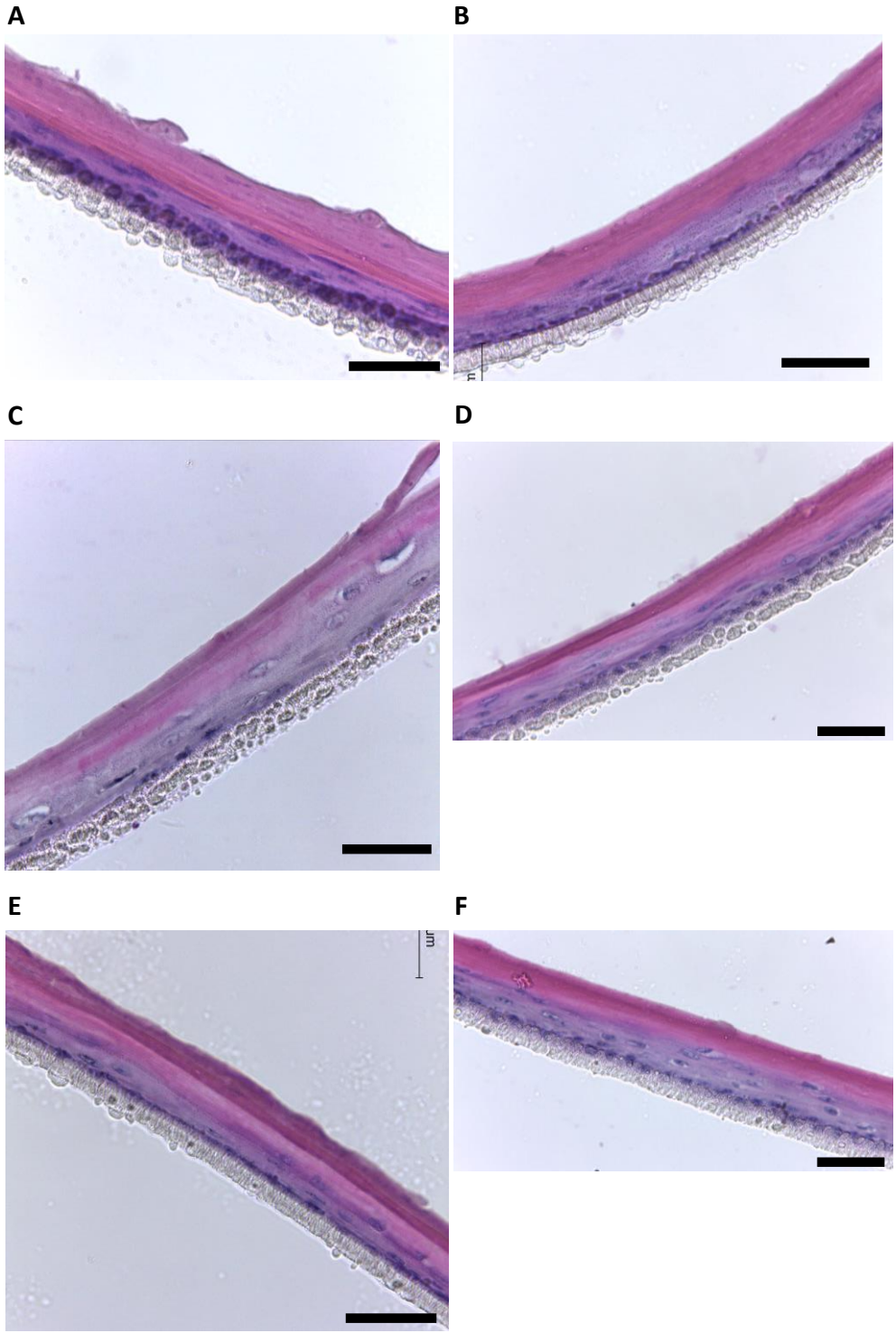

Fig. 5.52. Cryosections of the HEKn epidermal model stained with H&E 48 hours post-treatment. A) Untreated. B) Untreated + DMSO. C) 50µM JNK inhibitor II. D) 0.45M Potassium thioglycolate. E) 0.45M Potassium thioglycolate + 50µM JNK inhibitor II. F) 0.44M Guanidine carbonate. Representative photomicrographs of the treatments which were carried out in duplicate. Scale bars = 50µm.

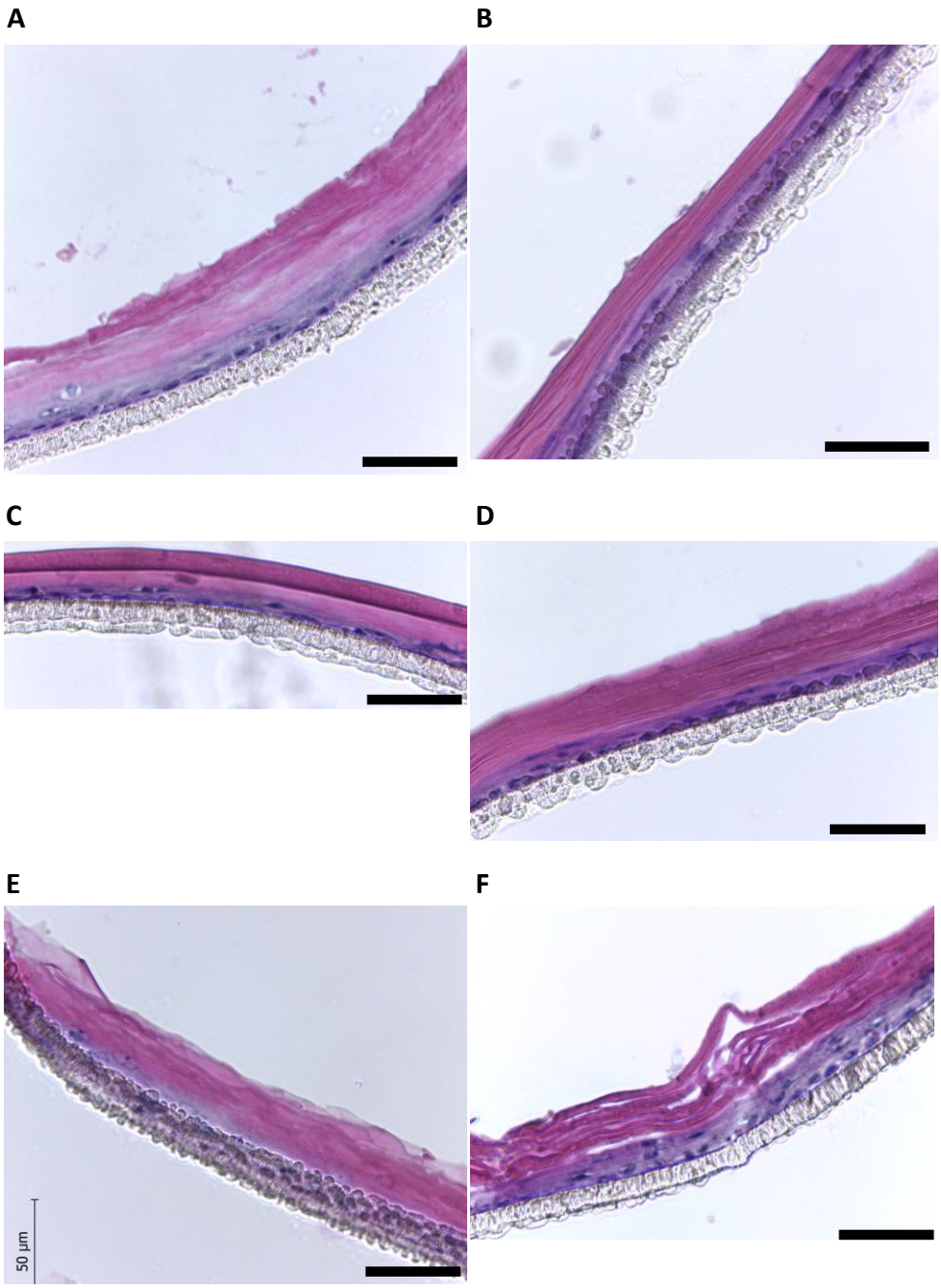

Fig. 5.53. Cryosections of the HEKn epidermal model stained with H&E 96 hours post-treatment. A) Untreated. B) Untreated + DMSO. C) 50µM JNK inhibitor II. D) 0.45M Potassium thioglycolate. E) 0.45M Potassium thioglycolate + 50µM JNK inhibitor II. F) 0.44M Guanidine carbonate. Representative photomicrographs of the treatments which were carried out in duplicate. Scale bars = 50µm.

A

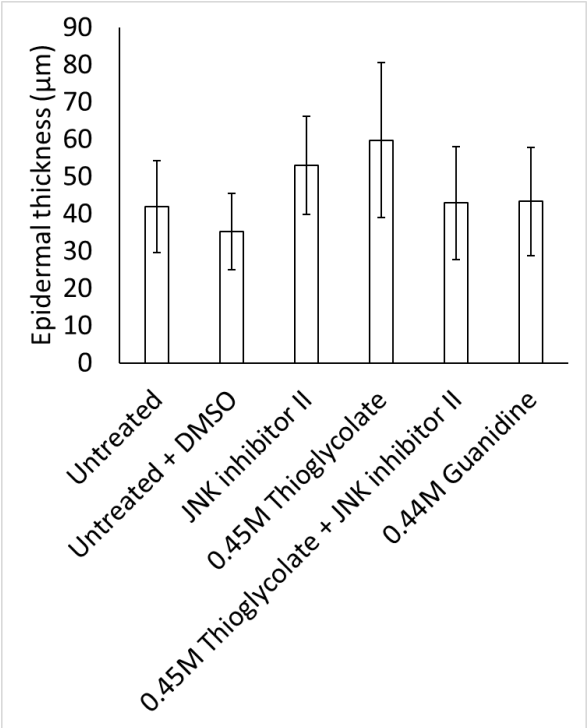

B

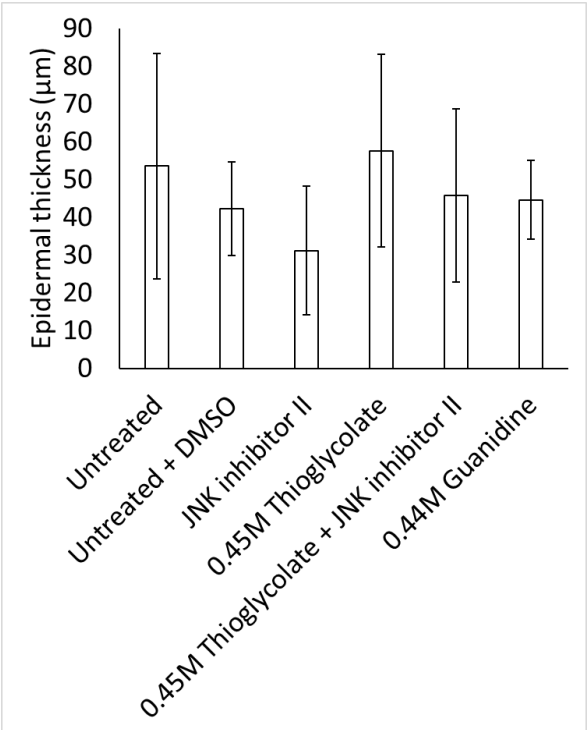

Fig. 5.54. HEKn epidermal thickness measurements after indicated treatments. A) 48 hours post-treatment. B) 96 hours post-treatment. Experiments repeated in duplicate. Error bars = +/- 2*SEM.

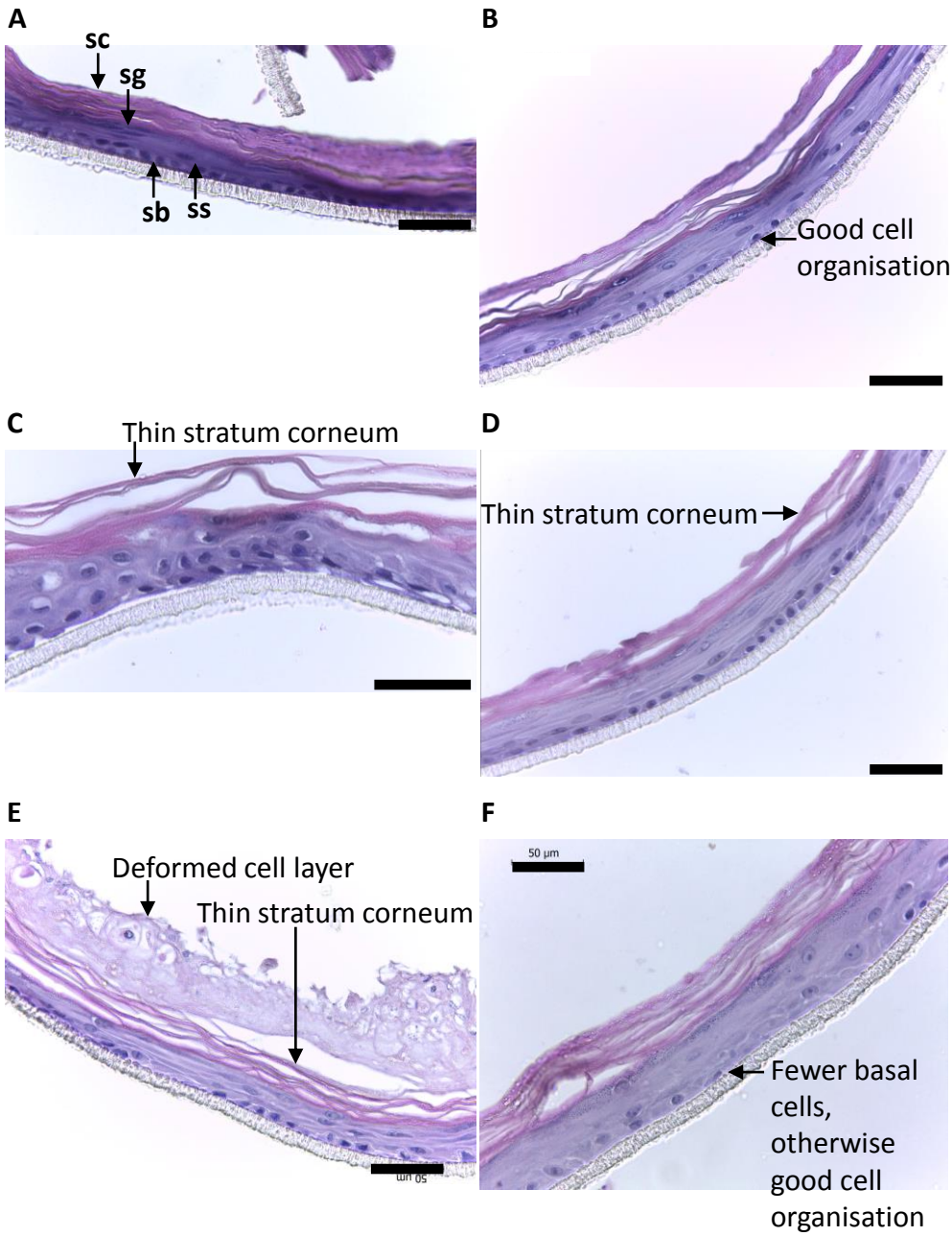

Fig. 5.55. Paraffin sections of the HEKn epidermal model stained with H&E 48 hours post-treatment. A) Untreated. B) Untreated + DMSO. C) 50µM JNK inhibitor II. D) 0.45M Potassium thioglycolate. E) 0.45M Potassium thioglycolate + 50µM JNK inhibitor II. F) 0.44M Guanidine carbonate. Sc = stratum corneum, sg = stratum granulosum, ss = stratum spinosum, sb = stratum basale. Representative photomicrographs of the treatments which were carried out in duplicate. Scale bars = 50µm.

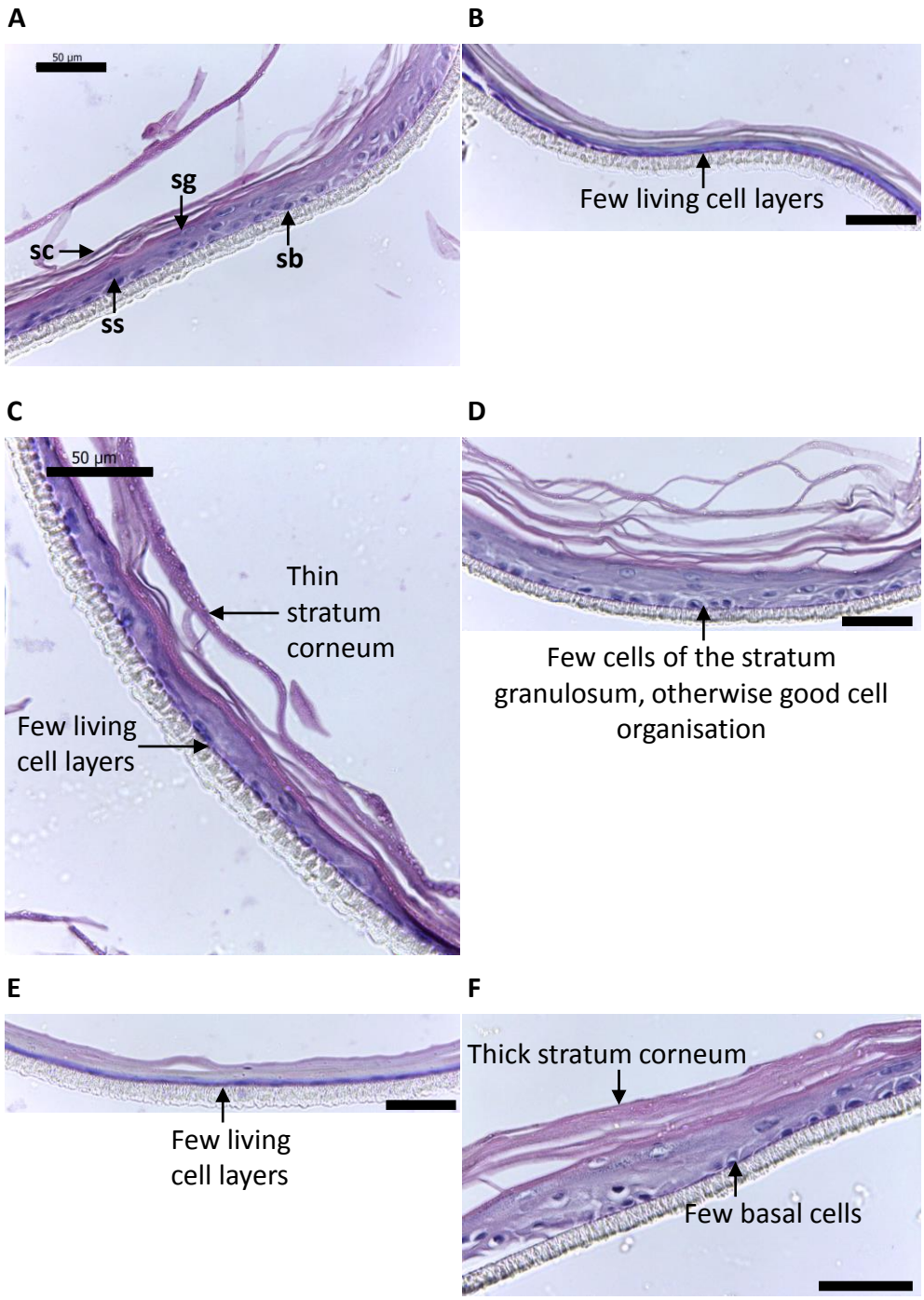

Fig. 5.56. Paraffin sections of the HEKn epidermal model stained with H&E 96 hours post-treatment. A) Untreated. B) Untreated + DMSO. C) 50µM JNK inhibitor II. D) 0.45M Potassium thioglycolate. E) 0.45M Potassium thioglycolate + 50µM JNK inhibitor II. F) 0.44M Guanidine carbonate. Sc = stratum corneum, sg = stratum granulosum, ss = stratum spinosum, sb = stratum basale. Representative photomicrographs of the treatments which were carried out in duplicate. Scale bars = 50µm.

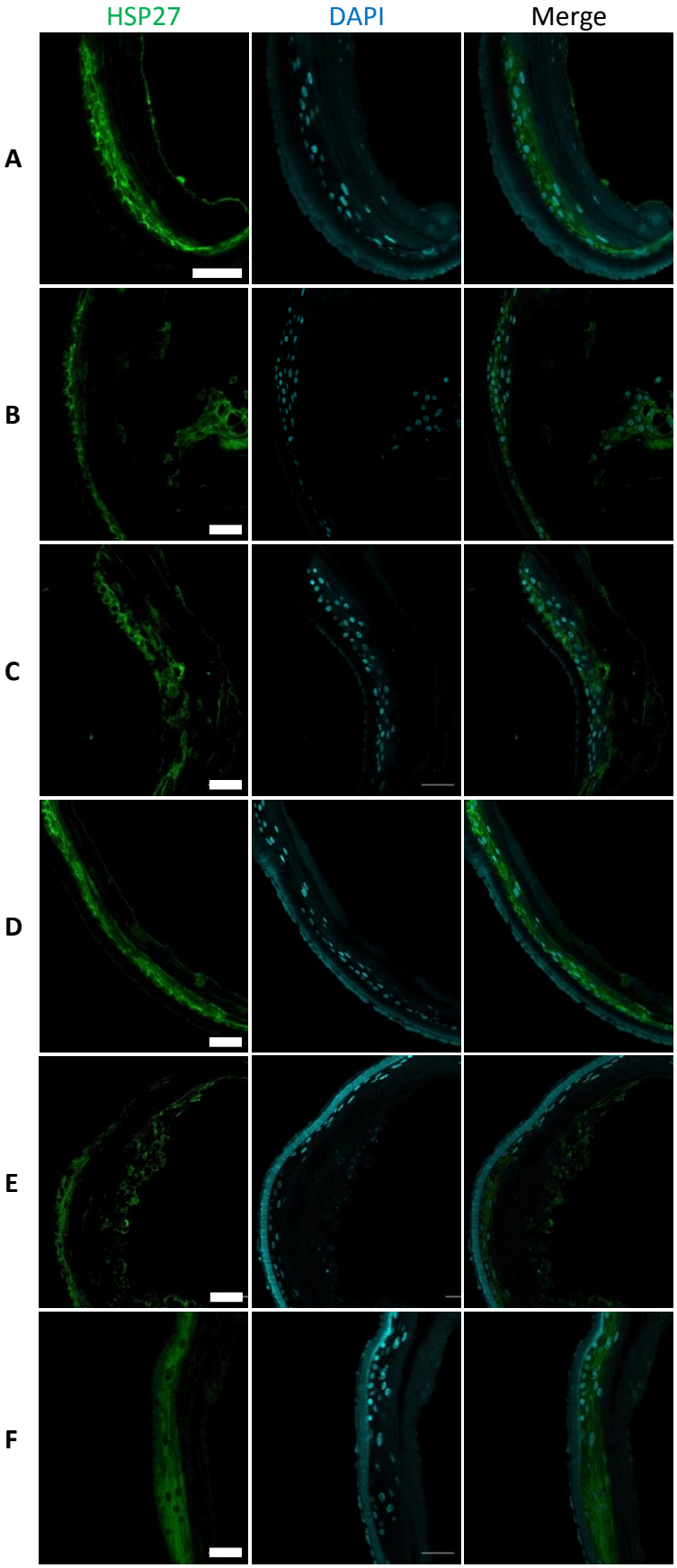
HSP27
DAPI
Merge
A
B
C
D
E
F

Fig. 5.57. Immunohistochemistry of HSP27 and DAPI in the epidermal model with HEKn cells 48 hours post-treatment. A) Untreated. B) Untreated + DMSO. C) 50μM JNK inhibitor II. D) 0.45M Potassium thioglycolate. E) 0.45M Potassium thioglycolate + 50μM JNK inhibitor II. F) 0.44M Guanidine carbonate. Immunohistochemistry with 1:500 mouse monoclonal anti-HSP27 and 1:1000 goat anti-mouse AlexaFluor 488, and 1:1000 DAPI. Secondary antibody only controls gave no signal. Scale bars = 50μm.

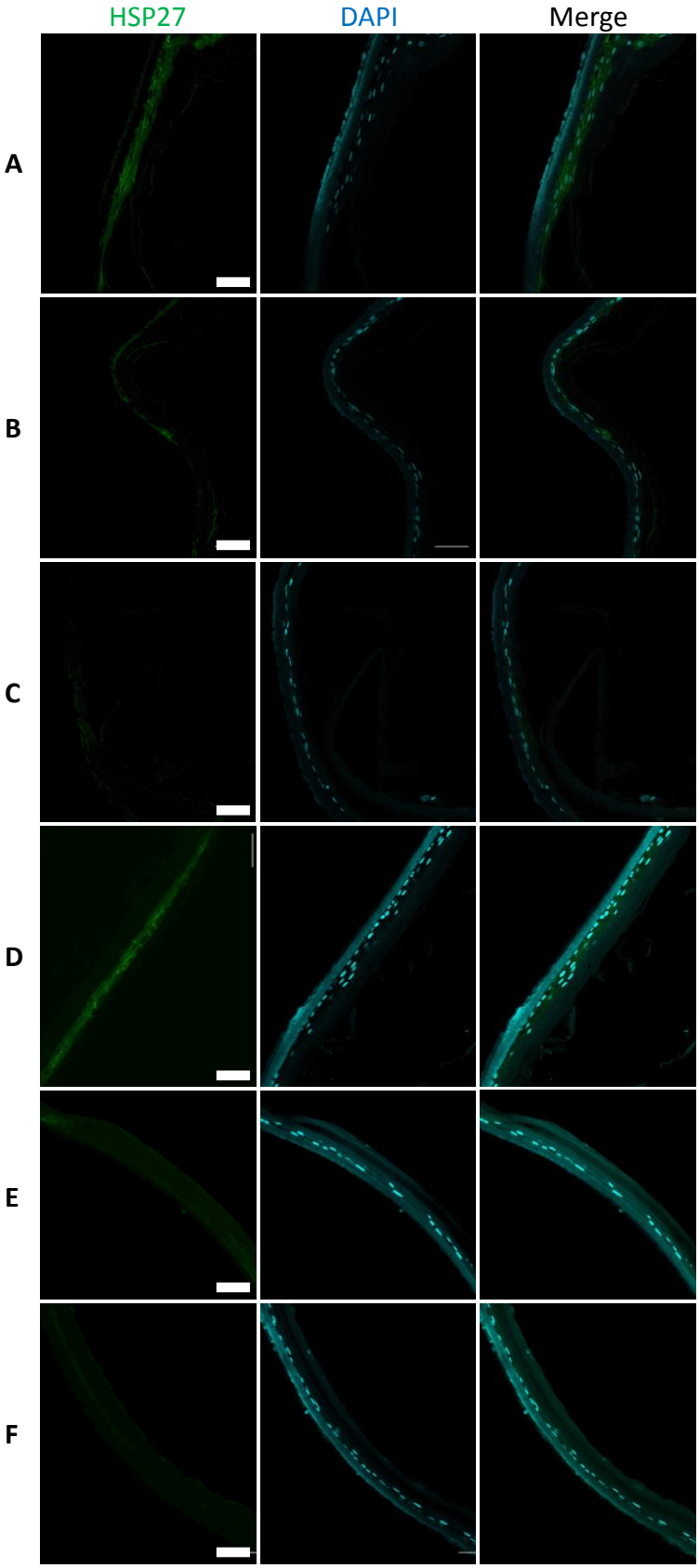
HSP27
DAPI
Merge
A
B
C
D
E
F

Fig. 5.58. Immunohistochemistry of HSP27 and DAPI in the epidermal model with HEKn cells 96 hours post-treatment. A) Untreated. B) Untreated + DMSO. C) 50μM JNK inhibitor II. D) 0.45M Potassium thioglycolate. E) 0.45M Potassium thioglycolate + 50μM JNK inhibitor II. F) 0.44M Guanidine carbonate. Immunohistochemistry with 1:500 mouse monoclonal anti-HSP27 and 1:1000 goat anti-mouse AlexaFluor 488, and 1:1000 DAPI. Secondary antibody only controls gave no signal. Scale bars = 50μm.

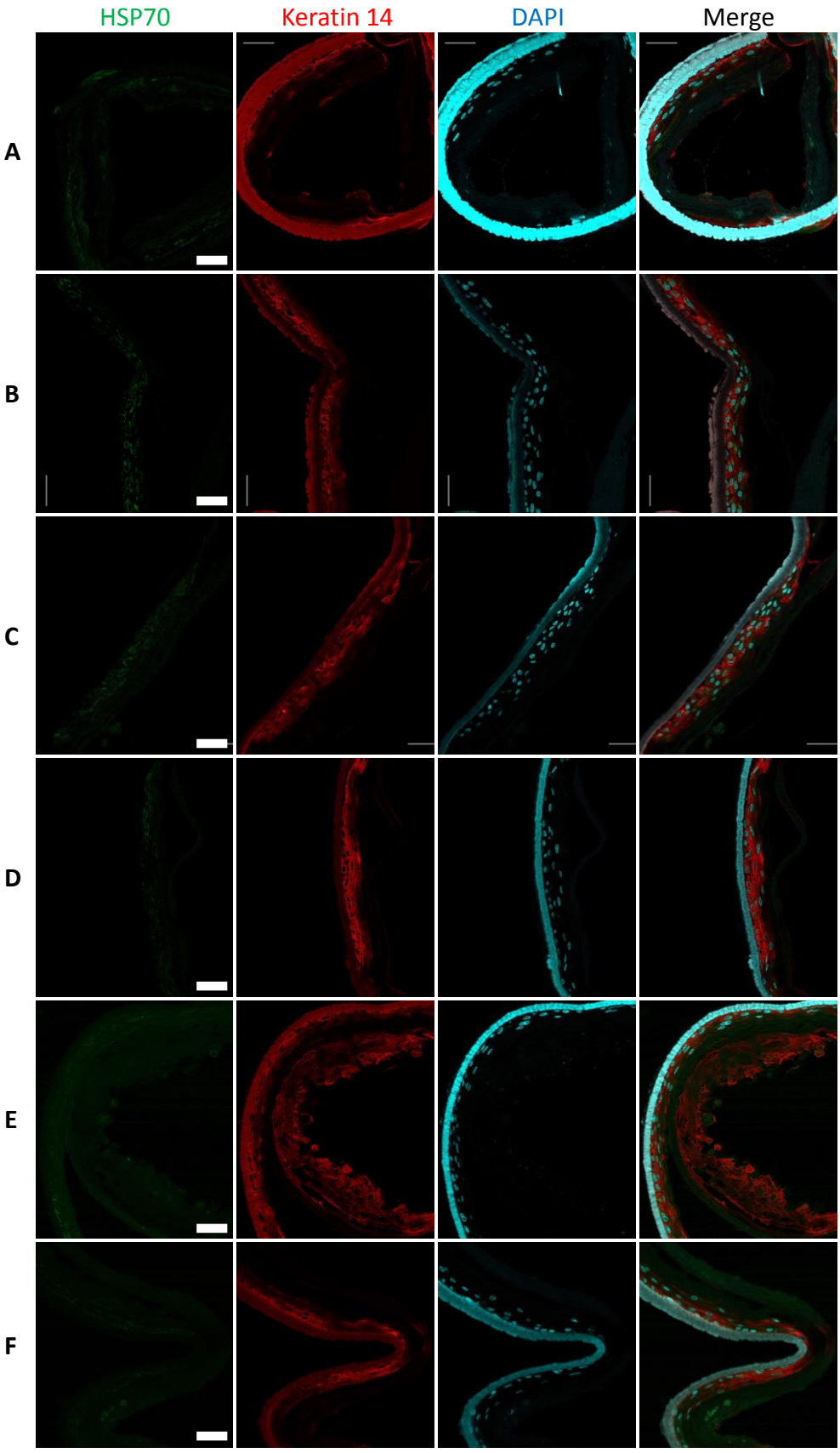
HSP70
Keratin 14
DAPI
Merge
A
B
C
D
E
F

Fig. 5.59. Immunohistochemistry of HSP70, keratin 14, and DAPI in the epidermal model with HEKn cells 48 hours post-treatment. A) Untreated. B) Untreated + DMSO. C) 50µM JNK inhibitor II. D) 0.45M Potassium thioglycolate. E) 0.45M Potassium thioglycolate + 50µM JNK inhibitor II. F) 0.44M Guanidine carbonate. Immunohistochemistry with 1:1000 mouse monoclonal anti-HSP70 and 1:1000 goat anti-mouse AlexaFluor 488, 1:1000 rabbit polyclonal anti-keratin 14 and 1:1000 chicken anti-rabbit AlexaFluor 594, and 1:1000 DAPI. Secondary antibody only controls gave no signal. Scale bars = 50µm.

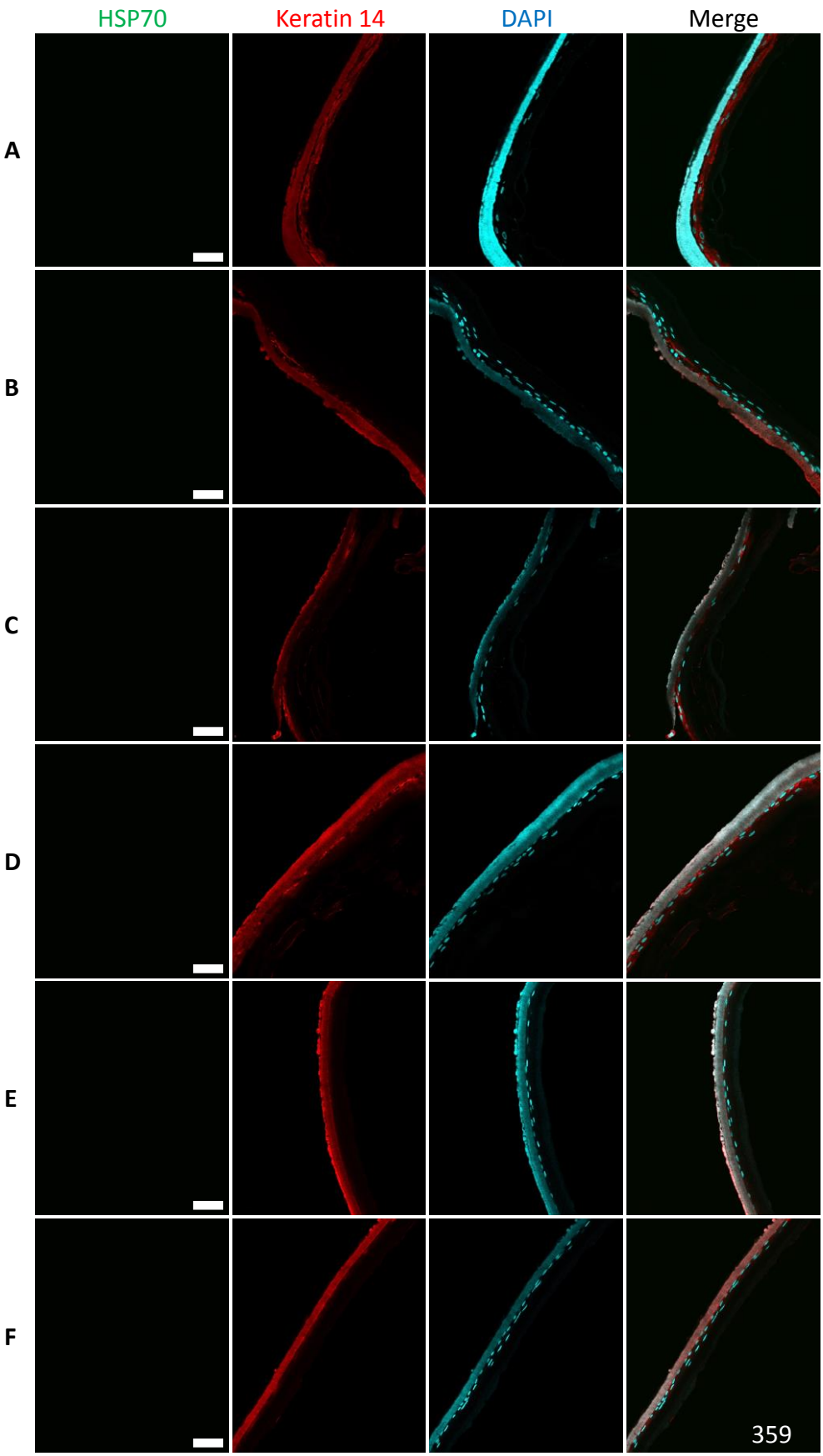
HSP70
Keratin 14
DAPI
Merge
A
B
C
D
E
F
359

Fig. 5.60. Immunohistochemistry of HSP70, keratin 14, and DAPI in the epidermal model with HEKn cells 96 hours post-treatment. A) Untreated. B) Untreated + DMSO. C) 50µM JNK inhibitor II. D) 0.45M Potassium thioglycolate. E) 0.45M Potassium thioglycolate + 50µM JNK inhibitor II. F) 0.44M Guanidine carbonate. Immunohistochemistry with 1:1000 mouse monoclonal anti-HSP70 and 1:1000 goat anti-mouse AlexaFluor 488, 1:1000 rabbit polyclonal anti-keratin 14 and 1:1000 chicken anti-rabbit AlexaFluor 594, and 1:1000 DAPI. Secondary antibody only controls gave no signal. Scale bars = 50µm.

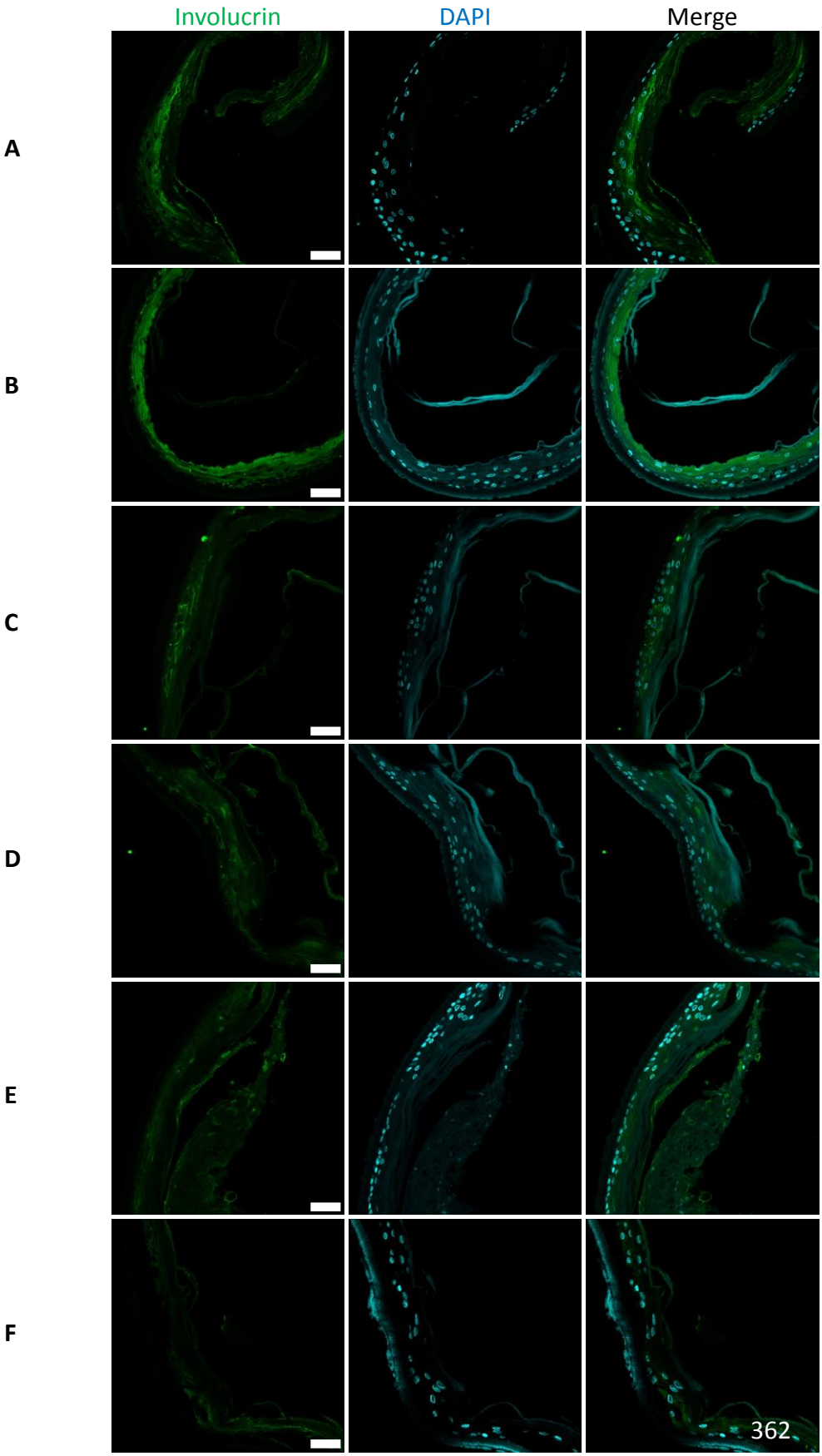
Involucrin
DAPI
Merge
A
B
C
D
E
F
362

Fig. 5.61. Immunohistochemistry of involucrin and DAPI in the epidermal model with HEKn cells 48 hours post-treatment. A) Untreated. B) Untreated + DMSO. C) 50μM JNK inhibitor II. D) 0.45M Potassium thioglycolate. E) 0.45M Potassium thioglycolate + 50μM JNK inhibitor II. F) 0.44M Guanidine carbonate. Immunohistochemistry with 1:750 mouse monoclonal anti-involucrin and 1:1000 goat anti-mouse AlexaFluor 488, and 1:1000 DAPI. Secondary antibody only controls gave no signal. Scale bars = 50μm.

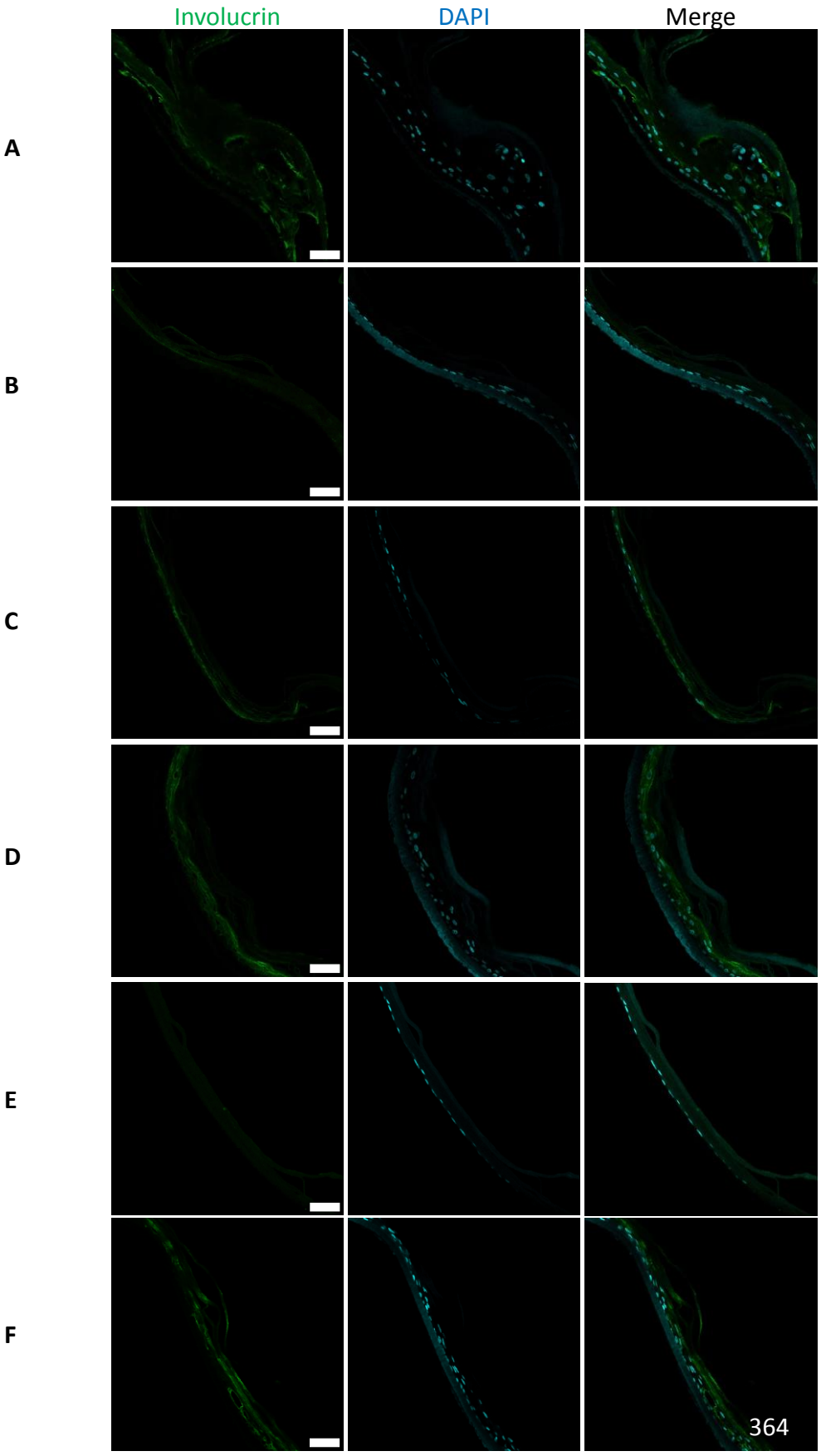
Involucrin
DAPI
Merge
A
B
C
D
E
F
364

Fig. 5.62. Immunohistochemistry of involucrin and DAPI in the epidermal model with HEKn cells 96 hours post-treatment. A) Untreated. B) Untreated + DMSO. C) 50μM JNK inhibitor II. D) 0.45M Potassium thioglycolate. E) 0.45M Potassium thioglycolate + 50μM JNK inhibitor II. F) 0.44M Guanidine carbonate. Immunohistochemistry with 1:750 mouse monoclonal anti-involucrin and 1:1000 goat anti-mouse AlexaFluor 488, and 1:1000 DAPI. Secondary antibody only controls gave no signal. Scale bars = 50μm.

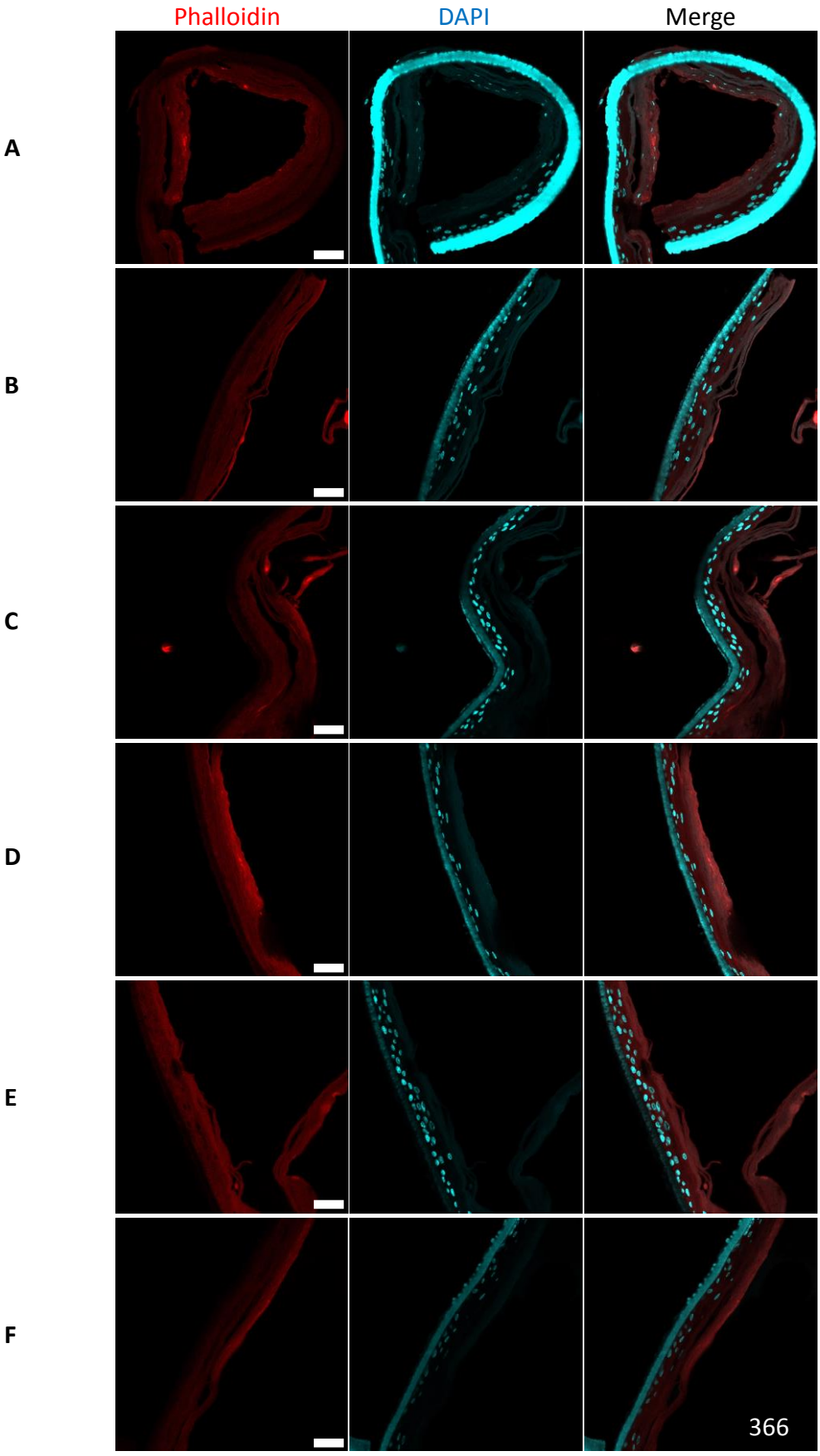
Phalloidin
DAPI
Merge
A
B
C
D
E
F
366

Fig. 5.63. Immunohistochemistry of actin and DAPI in the epidermal model with HEKn cells 48 hours post-treatment. A) Untreated. B) Untreated + DMSO. C) 50µM JNK inhibitor II. D) 0.45M Potassium thioglycolate. E) 0.45M Potassium thioglycolate + 50µM JNK inhibitor II. F) 0.44M Guanidine carbonate. Immunohistochemistry with 1:500 phalloidin AlexaFluor 488, and 1:1000 DAPI. Scale bars = 50µm.

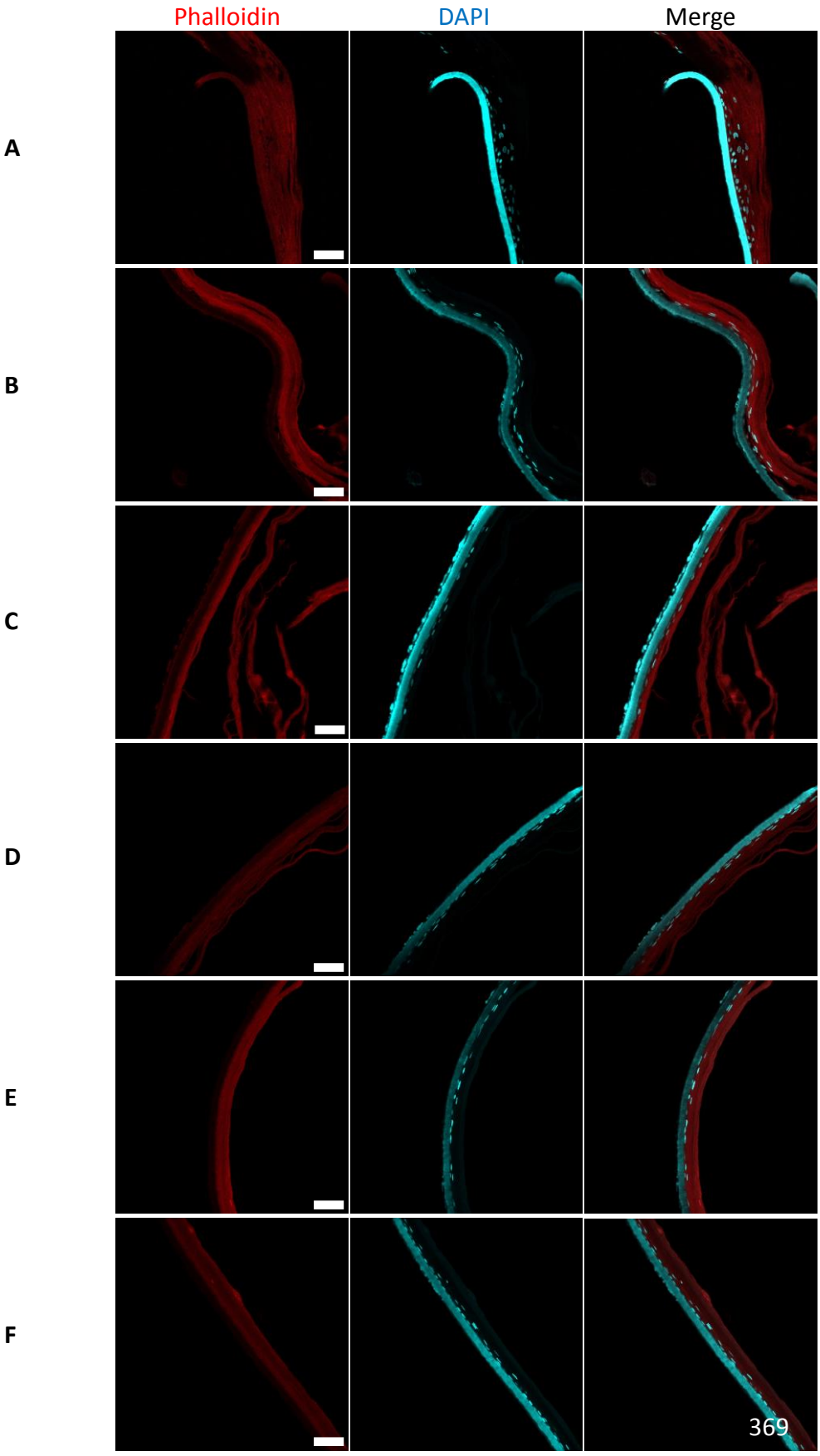
Phalloidin
DAPI
Merge
A
B
C
D
E
F

Fig. 5.64. Immunohistochemistry of actin and DAPI in the epidermal model with HEKn cells 96 hours post-treatment. A) Untreated. B) Untreated + DMSO. C) 50µM JNK inhibitor II. D) 0.45M Potassium thioglycolate. E) 0.45M Potassium thioglycolate + 50µM JNK inhibitor II. F) 0.44M Guanidine carbonate. Immunohistochemistry with 1:500 phalloidin AlexaFluor 488, and 1:1000 DAPI. Scale bars = 50µm.

Chapter 6

General Discussion

6.1. Conclusion

Hair has long been an object of interest, for people interested in a wide range of fields from hair care to medicine to forensics to textiles (Bost, 1993; Shimomura and Christiano, 2010; Plowman *et al*., 2012; Crawford and Hernandez, 2014; Kim *et al*., 2016). In this study human head hair was investigated both for pure scientific research into its structure which may later inform other research, and for the hair care industry into the effects of chemical depilatory treatments upon the hair and skin.

6.1.1. Summary of findings

Key accomplishments in this study were the development of an optical transverse imaging method as well as a dynamic imaging method. These methods contributed to many of the significant discoveries in this study. The optical transverse imaging method supports traditional methods of imaging the hair transversely such as by embedding the hair in resin (Swift *et al*., 2000; Kelch *et al*., 2000; Cruz *et al.*, 2013), but has the advantage of being a faster and label-free method which does not require embedding or physical sectioning. Novel key findings regarding the native structure of hair were found for each of the hair compartments: the cuticle, the cortex and the medulla. Overall structures can be resolved using label-free autofluorescence. Each wavelength studied excited the hair, some more specifically than others, as 405nm excited the whole hair especially the exocuticle, CMC, cortical cells and organelle remnants, whereas 594nm and 633nm excitation mainly excited the free edge of the cuticle cells.

Novel findings regarding the cuticle included multiple fluorescent lifetimes across the cuticle cell layers, indicating that they are potentially composed of multiple chemical environments. Four observable classes of cuticle population were found with possible differing components of covalently bound lipids, including 18-MEA, and KIFs and KAPs across the cuticle cell layers. The existing literature treats the cuticle as a homogenous structure and does not recognise differences between the layers. The use of FLIM provides a relatively new way of observing the hair, and experiments to alter the native state of the hair with exploration of the changes in lifetime give new insights into the chemical composition of structures. The cuticle cell length as well as cuticle circular organelle remnant number were found to possibly be an indicator of wear, and with sufficient cell layers, the cuticle could halt the penetration of light into the cortex. The

cuticle of the hair from a patient with an uncharacterised hair and skin disorder was shown to be poorly differentiated and distinguishable from healthy hair by the use of the transverse optical section method in confocal microscopy and FLIM. However, the use of this technique in the medical arena could be limited by the cost of the microscope. Additionally, cross-sectioning the hair for transverse imaging can result in a jagged cut, and it is difficult to consistently obtain cleanly cut sections of hair. Although, depending upon the depth of the hair breakage, optically sectioning the hair past the point where it was broken can limit the damage observed.

Advances were made with respect to the cortex and cortical cells as they were found to have differing lifetimes when excited with 640nm and 470nm. The fluorescence lifetimes tended to increase with depth into the cortex, which could be accounted for by more glycine/tyrosine KAPs towards the centre of the hair (Shimomura and Ito, 2005), whereas the outer cortex has steryl glycoside-like lipids containing N-acetylglucosamine (Takahashi and Yoshida, 2014). The remnants in cortical cells may be both nucleic and from other organelles. FLIM may provide a method to help distinguish nuclear remnants from melanosome remnants and other organelle remnants such as mitochondria. In a study on one hair, a positive correlation was found between cortical organelle remnant area and the corresponding cortical cell area. The larger cortical cells in the earlier months of hair growth had smaller organelle remnants compared to those of the latter months, perhaps due to seasonal changes in hair growth, or nutritional or health factors (Randall and Botchkareva, 2009; Trueb, 2015). However, the validity of this data is limited as the data is only representative of one hair. Finally, by probing autofluorescence and reflection, a new method was developed to distinguish between eumelanin and pheomelanin through label-free optical sectioning of the hair.

Some progress was made regarding the structure of the medulla. The globular air spaces of the medulla were reflective, whereas the filamentous components of the medulla were autofluorescent. In addition to this, it was found that the more autofluorescent the medulla, the longer its fluorescence lifetime.

With regards to the effect of depilatories on the hair, thioglycolate-containing depilatories were the most effective. The experimental combination of potassium thioglycolate with guanidine carbonate caused the most damage to the hair. Dynamic imaging showed the mechanism of action of the depilatories upon the hair, which

demonstrated the drastic deformation of the cuticle and swelling of the cortex over time with the treatments involving potassium thioglycolate. The use of FLIM allowed chemical changes such as the reduction of disulphide bonds to be examined. These techniques complement the use of electron microscopy which is the preferred microscopy technique in previous works, though the mechanism of depilatory chemicals upon human hair has not been investigated for decades using microscopy (Reed *et al*., 1946; Powers and Barnett, 1952; Wolfram and Underwood, 1966; Chao *et al*., 1979; Strussman, 1983; Zahn *et al*., 1986). The advantage of using dynamic imaging is that temporal and spatial information is generated on the effect of the depilatory upon the hair. Dynamic imaging as well as FLIM offers a rejuvenated platform for the imaging of hair treatments. Guanidine carbonate alone disrupted the cuticle cell CMC but showed little other damage to the hair structure as a whole. Hair was treated with lithium bromide under four different conditions, only two of which appeared to affect the hair. Hair treated at 85°C or for 5 days appeared to have more compact cuticle cells, and the cortex of the hair treated at 85°C appeared swollen. Calcium iodide and SLS treatment to the hair resulted in parts of the cuticle cell fracturing away. Hair treated with CTAB and SLS caused varying degrees of cuticle cell flaring. This is likely due to the CTAB and SLS removing the 18-MEA and some soluble lipids from the outer β-layer of the CMC (Gould and Sneath, 1985; Smith *et al*., 2010; Singh and Umapathy, 2011; Robbins, 2012). The investigation into the effect of depilatory chemicals upon the hair also gives new and supporting information on the structure of hair. The use of maleimide showed the depth of penetration of potassium thioglycolate into the hair and demonstrates the resistance and impermeability of the hair cortex, whilst showing that the cuticle is less resistant to the changes in morphology from reducing KIFs and KAPs. This suggests the disulphide bonds may have a greater role in sustaining the morphology of the cuticle than the cortex. The fact that CTAB, SLS and guanidine all raise the cuticle cells by extracting some soluble lipids from the CMC and 18-MEA shows that the lipids are important for the adhesion of cuticle cells.

The main findings of the potassium thioglycolate and guanidine carbonate treatments on keratinocytes were that very few HaCaT cells remain viable after 0.4M guanidine carbonate treatment, as shown by the cell survival assay and the cell viability assay measuring an average metabolic activity at only 7% of that of the untreated cells.

Cornified envelopes treated with potassium thioglycolate showed aggregates upon their surface. Regarding the effects on certain proteins, no significant differences were found in the levels of HSP27 or HSP70 between cell treatments which means any stress response created by the depilatories is occurring through another pathway. Additionally, no significant differences were found in levels of keratin 14 between cell treatments, although there appeared to be less keratin 14 expression with time. Western blotting showed the amount of involucrin varied significantly only between cell cultures with and without the addition of JNK inhibitor II. Finally, the proliferation marker, Ki67, showed there were significantly fewer cells in M-phase and significantly more cells in S-phase after potassium thioglycolate with JNK inhibitor II treatment. These results showed that the two most efficacious depilatory treatments did not affect keratinocyte differentiation, proliferation or the stress response through the HSP pathway, and the structural integrity of the living cells of the epidermal model was maintained through the protection provided by the stratum corneum. Therefore, the experimental depilatory treatment remains as a potentially viable product for market.

The stratum corneum and the cuticle are analogous structures. Both provide a barrier to the rest of the skin or hair (Tate *et* al., 1993; Gamez-Garcia, 1999; Ruetsch *et al*., 2000; Harper and Kamath, 2007; Robbins, 2012; Serita *et al*., 2014), both comprise layers of dead keratinised cells surrounded by lipids (Rice and Green, 1977; Nemes and Steinert, 1999; Ponec *et al*., 1988; Wertz and Downing, 1991; Langbein *et al*., 2001; Hatta *et al*., 2006; Thibaut *et al*., 2009; Robbins, 2012), both contain desmosomes (Swift and Smith, 2002; Alibardi *et al*., 2013; Olivry and Dunston, 2015), and both contain isopeptide cross-linking produced by transglutaminase-3 which make them more resistant to chemical damage (Rice *et al*., 1994; Rice and Green, 1977; Nemes and Steinert, 1999; Thibaut *et al*., 2009; Laatsch *et al*., 2014). The treatment of potassium thioglycolate on the stratum corneum and the cuticle revealed that aggregates form on the surface of both types of cell. These aggregates may be formed from the extraction of lipids from the cornified envelope and the cuticle, such as fatty acids, ceramides and cholesterol (Chao *et al*., 1979; Strussman, 1983; Zahn *et al*., 1986; Eckhart *et al*., 2013). The aggregates may also be the result of reduced disulphide bonds breaking down the structure of some proteins, such as cystine in KIFs and KAPs in the cuticle and S100A3 in cornified envelopes (Bradbury and Ley, 1972; Swift and Bews, 1976; Swift, 1999; Shimomura and Ito, 2005;

Kizawa *et al*., 2011; Stanic *et al*., 2015). The isopeptide cross-links in both cell types give resistance to chemical assault, however the cuticle was more susceptible to thioglycolate than the stratum corneum. Although once the hair was dried the cuticle resumed a more native shape, suggesting the isopeptide cross-links are maintaining some of the cuticle morphology.

These findings show how this study has contributed to the field, through experimentation creating novel findings on the structure and morphology of hair and depilatory action upon the hair and skin.

6.1.2. Limitations

The main limitation encountered with the data was the relatively small sample number, both of hair and cells, which limits the confidence of statistical data (McDonald, 2014). Additional repetition of cell experiments was limited due to time and other resources, and more repetition of some hair experiments was not carried out also due to time restraints both with the use of experimental facilities and lack of time nearing the project end. Some sample availability of hair was also limited, such as ginger hair, and in the uncharacterised hair disorder study the hair of additional healthy age and gender-matched subjects of the same ethnicity would have been useful. In general, more hairs are needed for increased reliability of data, as there is much hair to hair variation even within individuals as reported in the literature (Robbins, 2012) and evident from FLIM imaging of cuticle structures in this study.

With regards to the work on the keratinocytes, a limitation common to all researchers is the subjectivity of the counting of fluorescently positive cells in immunofluorescence (Russell *et al*., 2009; Bogdanov *et al*., 2014). This limitation is somewhat mitigated by also performing Western blotting which is a more objective technique. Western blotting also aids in judging the specificity of the antibody to the protein by the molecular weight, whereas immuno-staining alone carries the risk of being less specific (Jarius and Wildemann, 2013). Further controls to test the specificity of the antibodies would be useful in addition to the secondary-only antibody controls, such as by using primary antibodies specific to plants when testing on human skin samples.

Dynamic imaging of the hair during treatment could only be done with the hair on a longitudinal axis. This was because if the hair was transversely orientated there was too

much movement of the hair from the action of the depilatories and contact of the hair with the glass cover slip was lost.

The lipid extractions and protein changes for the investigation into the multiple fluorescence lifetimes of the cuticle had known affects upon the cuticle in each of the methods, such as the loss of soluble lipids, 18-MEA, or reduction of disulphide bonds (Wolfram and Underwood, 1966; Wertz and Downing, 1988; Masukawa *et al*., 2005b; Pappinen *et al.*, 2008; *Smith et al*., 2010). However, many variables and unintentional chemical changes remain which could also affect the fluorescence lifetimes of hair, although pH change is not one of these (unpublished data from Hawkins and Maatta groups). In future experiments, it would be useful to have used standards, such as 18-MEA, in the experiments as positive controls.

6.2. Future research

This study has opened new avenues of enquiry into the structure of hair and its interaction with chemicals. Given more time and funding, the following are areas which could be further explored.

More repeats could be carried out for the hair studies, as there is much variation within and between individuals, and additional repeats would lead to a higher level of confidence in the results. The “melanin-like particles” study analysed three to six hairs from each colour and would benefit from a larger sample size to provide greater confidence in the statistical validity of the data. Likewise, the statistical analysis of the FLIM data would benefit from studying more samples of different colours. Another experiment which would greatly benefit from an increased sample number is the study which examined the structures along a year of hair growth. The number of beard hairs analysed using FLIM should also be increased. More club hairs and the attached matrix could be analysed using FLIM for hairs in telogen and anagen, as only three of each were analysed in this study. Finally, calcium iodide with SLS was not tested using the 640nm laser so it would be useful to gather this data in the future.

The effort to identify the organelle remnants could be continued further than the examination of hairs in this study which used TEM, maleimide and FLIM, by the sectioning of hair with a microtome and application of nucleic stains. This may prove more fruitful than the previous use of DAPI and anti-lamin A/C because physical

sectioning could expose the interior of the nucleus, whereas previously the nucleic side may have been made inaccessible by the nuclear envelope.

A larger study would be needed on more hairs along longer sections of hair of at least 24cm to statistically validate the patterns observed in the measurements along a year of hair growth. This would ascertain whether the trends observed along 12cm of hair of the structure sizes are random, seasonal, or have any other annual pattern. However, detailed imaging of such long hair samples would be very labour intensive. To mitigate this, fewer measurements could be made across more hairs.

The CTAB lipid extraction method should be carried out using the GC/MS analysis method by Smith *et al*., 2010 to show that 18-MEA is being removed from the hair cuticle. Through the use of other GC/MS methods further lipids could be identified from the lipid extractions of hair. Internal standards could also be used to quantify the amounts of lipid present.

If not constrained by the policy restricting research involving animals, animal models with known mutations or ablations for KIFs, KAPs or hair lipids could be investigated to probe if the presence or absence of specific molecules can be linked to changes in hair structure and fluorescence lifetime. These results could also be used potentially for diagnostic purposes in human disease. Genetic mutations or ablations could be made to the enzymes generating hair cuticle lipids, such as the enzyme branched chain 2-oxo acid dehydrogenase for generating 18-MEA (Jones and Rivett, 1997). Genetics studies on mice by using a keratin gene cluster resource such as that by Hesse *et al*. would provide information on keratins to mutate or ablate (Hesse *et al*., 2004). Mouse mutants used in previous studies and the effects on the hair shaft are reviewed in Nakamura *et al*. and this provides a useful resource for choosing mouse mutants (Nakamura *et al*., 2013). Of particular interest is the epidermal targeted mutation Notch1 mouse model, which results in hair containing bulbous perturbations in the hair shafts as well as disorganised and fewer trichohyalin granules in the medulla (Pan *et al*., 2004). The DLX3 epidermal targeted mutant mouse model has undifferentiated hair shafts, which would be interesting to examine using the techniques developed in this study (Hwang *et al*., 2008). The forkhead box Q1 satin mouse model would be useful for investigating changes to the fluorescence lifetimes due to the abnormal keratinisation of the hair shafts (Major, 1955). Finally, the SRY-box containing gene 21 mouse model would

further studies into the cuticle fluorescence lifetimes as it possesses abnormal cuticle formation, and is also missing the interlocking structure between the cuticle and the inner root sheath (Kiso *et al*., 2009).

Human diseases where the keratin mutations are known could also be useful to further explore changes in hair structure and the effects upon fluorescence lifetime. This would be faster and cheaper than using animal models, though less controlled. One such disease which could be investigated is monilethrix, which has been shown to have mutations in several keratin genes including hHb1, hHb3, hHb6, subfamilies of K81, K83, and K86 respectively (Winter *et al*., 1998; van Steensel *et al*., 2005; Winter *et al*., 1997). These keratins are expressed in the cortex and medulla (Langbein *et al*., 2010), so it would be interesting to see how this would affect the lifetime. Pachyonychia congenita and autosomal recessive hypotrichosis with woolly hair are diseases where there are mutations in K17 and K25 respectively which are also expressed in the medulla (Smith *et al*., 2001; Zernov *et al*., 2016). There may also be changes to the fluorescence lifetime of the medulla in these diseases. A disease which affects keratin in the cuticle is ectodermal dysplasia of hair and nail type, which has a mutation in KRTHB5, a subfamily of K85 (Naeem *et al*., 2006). As well as informing how changing a keratin in the cuticle may affect its structure and fluorescence lifetime, KRTHB5 is also expressed in the matrix in the cortex so changes may also be observed there (Langbein *et al.*, 2010). Finally, maple syrup urine disease would also be interesting to use in FLIM as hairs do not have 18-MEA (Smith and Swift, 2005). It would be interesting to compare the fluorescence lifetimes of these hairs against those of CTAB treated Chinese scalp hairs. FLIM could then also be used as a useful diagnostic tool to provide further insight into diseases and enhance diagnostic methods, as it has been used in this study for the uncharacterised hair and skin disorder.

To further compare the differences between the hair of the patient affected with the uncharacterised hair and skin disorder with healthy hair, lipid extractions could be performed to identify any differences in lipid composition. The hair could also be sectioned and immuno-stained against the various keratins to test for differences in types of KIF and KAP.

Successfully combining the transverse imaging method and the dynamic imaging method would allow for transverse dynamic imaging. This would provide a new

perspective on the hair during treatments and would allow for greater insight into the actions of chemicals upon the cuticle cell layers which are visible only through transverse imaging.

The methods developed in this study could be used to further investigate structural and chemical changes in hair as a response to external damage (such as UV radiation, chemical bleaching and heat). The methods could also be used to potentially visualise the penetration dynamics of hair dye chemicals into the hair and whether the penetration routes are transcellular or intercellular, offering greater resolution and temporal and spatial freedom than previous studies (Wortmann *et al*., 1997; Kelch *et al*., 2000; Formanek *et al*., 2006).

To gather more information on the action of the depilatory chemicals upon the hair and skin, the concentrations of the chemicals could be varied beyond those found in commercial products. Cell survival and death assays could be carried out to determine the percentage of cells surviving each treatment and concentration.

Stress to the skin has been observed from depilatory treatment in previous studies (Syed, 1995; Hahn, 1999; Syed and Naqvi, 2000; Haque and Al-Ghazal, 2004; Kindred *et al*., 2011; Tackey *et al*., 2013) and cell viability has been lowered through depilatory treatment, yet heat shock proteins do not appear to be involved. It may be that proinflammatory cytokines are released after chemical depilatory treatment, as they are after a hair relaxer treatment (Tackey *et al*., 2013). Such cytokines could be tested for including interleukin-1α, interleukin-1 receptor antagonist, interleukin-8, and interleukin-10. Future work should include assays such as ELISAs from conditioned media or RT-PCR to measure the cytokine response to chemical depilatory treatment to assess irritation in the skin. It would be particularly useful to use a multi-plexing method to perform the cytokine analysis as this would allow a wide panel of cytokines to be targeted simultaneously, which would greatly save on time while remaining a highly sensitive technique. Multiplex Bead Array assays would be suitable, as found on the Luminex system, or alternatively the electrochemiluminescent Meso Scale Discovery Sector Imager would be appropriate for this function (Khan *et al*., 2004; Dabitao *et al*., 2011).

The thickness of the stratum corneum of the epidermis varies according to the body site (Bohling *et al*., 2014). The thickness of the stratum corneum necessary to protect the living keratinocytes beneath from the negative effects of the chemical depilatories could be determined. The effect of the depilatories on epidermal models with differing stratum corneum thicknesses could be measured using the cytokine assays. Varied thicknesses of the stratum corneum may be achieved, possibly through the use of JNK inhibitor II to increase differentiation, which should be used earlier than day 10 of the air-liquid interface so as not to deplete the numbers of basal cells.

These suggested experiments will add further insight into the contribution this study has made to the field. The expanding field of hair and skin research continues to yield exciting results. The work carried out in this study has advanced the knowledge of the structure and morphology of hair and the action of chemical stressors upon the hair and skin. This research, and the results of suggested future research, have the potential to have an impact in both the consumer good and healthcare industries, as well as scientific blue-sky research.

Bibliography

Abreu-Velez, A.M., Googe, P.B., Howard, M.S., (2012). Immune reactivity in psoriatic munro-saboureau microabscesses, stratum corneum and blood vessels. *N. Am. J. Med. Sci.*; 4: 257-265

Ahluwalia, G., Styczynski, P., Shander, D., (2000). Inhibition of hair growth. *USA*; US6093748

Al-Nuaimi, Y., Hardman, J.A., Haslam, I.S., Biro, T., Toth, B.I., Farjo, N., Farjo, B., Philpott, M., Watson, R., Grimaldi, B., Kloepper, J.E., Paus, R., (2014). A meeting of two chronobiological systems: period1 and BMAL1 modulate the human hair cycle. *J. Invest. Dermatol*.; 134: 610-619

Alibardi, L., (2012). Ultrastructure immunolocalisation of involucrin in the medulla and inner root sheath of the human hair. *Annals Anatomy*; 194: 345-350

Alibardi, L., (2016). Ultrastructural localisation of hair keratins, high sulphur keratin-associated proteins and sulfhydryl oxidase in the human hair. *Anat. Sci. Int.*; 1-14

Alibardi, L., Tsuchiya, M., Watanabe, S., Nocker, B., (2013). Ultrastructural localisation of desmoglein and plakophilin in the human hair suggests that the cell membrane complex is a long desmosomal remnant. *Acta Histochemcia*; 115: 879-886

Allworden, K.Z., (1916). The properties of wool and a new method for detecting damaged wool. An*gew Chem.*; 29: 77-78

Alruwaili, N., Alshehri, H.A., Halimeh, B., (2015). Hair tourniquet syndrome: successful management with a painless technique. *Int. J. Pediat. Adoles. Med.*; 2: 34-37

Amiel, J., Bougeard, G., Francannet, C., Raclin, V., Munnich, A., Lyonnet, S., Frebourg, T., (2001). TP63 gene mutation in ADULT syndrome. *Eur. J. Hum. Genet*.; 9: 642-645

Andl, T., Ahn, K., Kairo, A., Chu, E.Y., Wine-Lee, L., Reddy, S.T., Croft, N.J., Cebra-Thomas, J.A., Metzger, G., Chambon, P., Lyons, K.M., Mishina, Y., Seykora, J.T., Crenshaw, E.B., Millar, S.E., (2004). Epithelial Bmpra1a regulates differentiation and proliferation in postnatal hair follicles and is essential for tooth development. *Development*; 131: 2257-2268

Auber, L., (1952). The anatomy of follicle producing wool-fibres, with special reference to keratinisation. *Transactions of the Royal Society of Edinburgh;* 62: 191-254

Baldassarre, G., Mussa, A., Banaudi, E., Rossi, C., Tartaglia, M., Silengo, M., Ferrero, G.B., (2014). Phenotypic variability associated with the invariant SHOC2 c.4A>G (p.Ser2Gly) missense mutation. *Am. J. Med. Genet. A*.; 164A: 3120-3125

Banerjee, A.R., (1962). Variations in the medullary structure of human head hair. *Proc. Nat. Inst. Sci. India*; 29: 306-316

Basel-Vanagaite, L., Attia, R., Ishida-Yamamoto, A., Rainshtein, L., Ben Amitai, D., Lurie, R., Pasmanik-Chor, M., Indelman, M., Zvulunov, A., Saban, S., Magal, N., Sprecher, E., Shohat, M., (2007). Autosomal recessive ichthyosis with hypotrichosis caused by a

mutation in ST14, encoding type II transmembrane serine protease matriptase. *Am. J. Hum. Genet*.; 80: 467-477

Baque, C.S.O., Zhou, J., Gu, W., Collaudin, C., Kravtchenko, S., Kempf, J.Y., Saint-Leger, D., (2012). Relationships between hair growth rate and morphological parameters of human straight hair: a same law above ethnical origins? *Int. J. Cosmet. Sci.*; 34: 111-116

Bazzi, H., and Christiano, A.M., (2007). Broken hearts, woolly hair, and tattered skin: when desmosomal adhesion goes awry. *Curr. Opin. Cell Biol.*; 19: 515-520

Becker, W., (2012). Fluorescence lifetime imaging – techniques and applications. *J. Microscopy*; 247: 119-136

Bennett, B.L., Sasaki, D.T., Murray, B.W., O'Leary, E.C., Sakata, S.T., Xu, W., Leisten, J.C., Motiwala, A., Pierce, S., Satoh, Y., Bhagwat, S.S., Manning, A.M., Anderson, D.W., (2001). SP600125, an anthrapyrazolone inhibitor of Jun N-terminal kinase. *Proc. Natl. Acad. Sci. USA*; 98: 13681-13683

Berezin, M.Y., and Achilefu, S., (2010). Fluorescence lifetime measurements and biological imaging. *Chem. Rev.*; 110: 2641-2684

Bhogal, R.K., Mouser, P.E., Higgins, C.A., Turner, G.A., (2014). Protease activity, localisation and inhibition in the human hair follicle. *Int. J. Cosmet. Sci.*; 36: 46-53

Bhushan, B., (2010). *Biophysics of human hair*. Biological and medical physics, Biomedical engineering. Springer-Verlag Berlin Heidelberg

Bichsel, K.J., Hammiller, B., Trempus, C.S., Li, Y.H., Hansen, L.A., (2016). The epidermal growth factor receptor decreases Strathmin 1 and triggers catagen entry in the mouse. *Exp. Dermatol*.; 25: 275-281

Birbeck, M.S.C., and Mercer, E.H., (1957). The electron microscopy of the human hair follicle. II. The hair cuticle. *J. Biophys. Biochem. Cytol.*; 3: 215-222

Black, A.T., Hayden, P.J., Casillas, R.P., Heck, D.E., Gerecke, D.R., Sinko, P.J., Laskin, D.L., Laskin, J.D., (2011). Regulation of Hsp27 and Hsp70 expression in human and mouse skin construct models by caveolae following exposure to the model sulphur mustard vesicant, 2-chloroethyl ethyl sulphide. *Toxicol. Appl. Pharmacol.*; 253: 112-120

Blanpain, C., and Fuchs, E., (2006). Epidermal stem cells of the skin. *Annu. Rev. Cell dev. Biol.*; 22: 339-373

Blaydon, D.C., Biancheri, P., Di, W.L., Plagnol, V., Cabral, R.M., Brooke, M.A., van Heel, D.A., Ruschendorf, F., Toynbee, M., Walne, A., O'Toole, E.A., Martin, J.E., Lindley, K., Vulliamy, T., Abrams, D.J., MacDonald, T.T., Harper, J.I., Kelsell, D.P., (2011). Inflammatory skin and bowel disease linked to ADAM17 deletion. *N. Engl. J. Med*.; 365: 1502-1508

Bogdanov, A., Endresz, V., Urban, S., Lantos, I., Deak, J., Burian, K., Onder, K., Ayaydin, F., Balazs, P., Virok, D.P., (2014). Application of DNA chip scanning technology for automatic detection of Chlamydia trachomatis and Chlamydia pneumoniae inclusions. *Antimicrob. Agents Chemo.*; 58: 405-413

Bohling, A., Bielfeldt, S., Himmelmann, A., Keskin, M., Wilhelm, K.P., (2014). Comparison of the stratum corneum thickness measured in vivo with confocal Raman spectroscopy and confocal reflectance microscopy. *Skin Res. Technol.*; 20: 50-57

Bost, R.O., (1993). Hair analysis - perspectives and limits of a proposed forensic method of proof: a review. *Forensic Sci. Int.*; 63: 31-42

Botchkarev, V.A., Botchkareva, N.V., Peters, E.M., Paus, R., (2004). Epithelial growth control by neurotrophins: leads and lessons from the hair follicle. *Prog. Brain. Res.*; 146: 493-513

Botchkarev, V.A., and Kishimoto, J., (2003). Molecular control of epithelial-mesenchymal interactions during hair follicle cycling. *J. Invest. Dermatol. Symp. Proc.*; 8: 46-55

Botchkareva, N.V., Ahluwalia, G., Shander, D., (2006). Apoptosis in the hair follicle. *J. Invest. Dermatol.*; 126: 258-264

Botchkareva, N.V., Kahn, M., Ahluwalia, G., Shander, D., (2007). Survivin in the human hair follicle. *J. Invest. Dermatol*.; 127: 479-482

Botchkareva, N.V., Khlgatian, M., Longley, B.J., Botchkarev, V.A., Gilchrest, B.A., (2001). SCF/c-kit signalling is required for cyclic regeneration of the hair pigmentation unit. *FASEB. J.*; 15: 645-658

Bradbury, J.H. Chapman, G.V., Hambly., King, N.L.R*.,* (1966). Separation of chemically unmodified histological components of keratin fibers and analyses of cuticle. *Nature;* 210: 1333–1334

Bradbury, J.H., and Ley, K.F., (1972). The chemical composition of wool. XI: separation and analysis of exocuticle and endocuticle. *Aust. J. Biol. Sci.*; 25: 1235-1247

Bradbury, J.H., and O'Shea, J.M., (1969). Keratin fibres II. Separation and analysis of medullary cells. *Aust. J. Biol. Sci.*; 22: 1205-1215

Bradford, M.M., (1976). Rapid and sensitive method for the quantitation of microgram quantities of protein utilizing the principle of protein-dye binding. *Anal. Biochem*.; 72:248-254

Brenner, M., and Hearing, V.J., (2008). The protective role of melanin against UV damage in human skin. Photochem Photobiol.; 84: 539-549

Bridgeman-Shah, S., (2004). The medical and surgical therapy of pseudofolliculitis barbae. *Dermatologic Therapy*; 17: 158-163

Briki, F., Busson, B., Doucet, J., (1998). Organisation of microfibrils in keratin fibres studied by X-ray scattering: modelling using the paracrystal concept. *Biochim. Biophys. Acta.*; 1429: 57-68

Bringans, S.D., Plowman, J.E., Dyer, J.M., Clerens, S., Vernon, J.A., Bryson, W.G., (2007). Characterisation of the exocuticle a-layer proteins of wool. *Exp. Dermatol.*; 16: 951-960

Brody, I., (1962). The ultrastructure of the epidermis in psoriasis vulgaris as revealed by electron microscopy: 1. The dermo-epidermal junction and the stratum basal in parakeratosis without keratohyalin. *J. Ultrastruc. Res.*; 6: 304-323

Buffoli, B., Rinaldi, F., Labanca, M., Sorbellini, E., Trink, A., Guanziroli, E., Rezzani, R., Rodella, L.F., (2014). The human hair: from anatomy to physiology. *Int. J. Dermatol.*; 53: 331-341

Bukau, B., Weissman, J., Horwich, A., (2006). Molecular chaperones and protein quality control. *Cell*; 125: 443-451

Cabanillas, B., and Novak, N., (2016). Atopic dermatitis and filaggrin. *Curr. Opin. Immunol.*; 42: 1-8

Calderon, P., Otberg, N., Shapiro, J., (2009). Uncombable hair syndrome. *J. Am. Acad. Dermatol*.; 61: 512-515

Candi, E., Schmidt, R., Melino, G., (2005). The cornified envelope: a model of cell death in the skin. *Nat. Rev. Mol. Cell Biol.*; 6: 328-340

Cavalier-Smith, T., (2005). Economy, speed and size matter: evolutionary forces driving nuclear genome miniaturization and expansion. *Ann. Bot*.; 95: 147–175

Celli, A., Crumrine, D., Meyer, J.M., Mauro, T.M., (2016). Endoplasmic reticulum calcium regulates epidermal barrier response and desmosomal structure. *J. Invest. Dermatol*.; 136: 1840-1847

Chao, J., Newsom, E., Wainwright, I., (1979). Comparison of the effects of some reactive chemicals on the proteins of the whole hair, cuticle and cortex. *J. Soc. Cosmet. Chem*.; 30: 401-413

Chapalain, V., Winter, H., Langbein, L., Le Roy, J.M., Labreze, C., Nikolic, M., Schweizer, J., Taieb, A., (2002). Is the loose anagen hair syndrome a keratin disorder? A clinical and molecular study. *Arch. Dermatol*.; 138: 501-506

Chapman, B.M., (1970). Observations on the mechanical behaviour of Lincoln-wool fibres supercontracted in lithium bromide solution. *J. Textile inst.*; 61: 448-457

Chapman, D.M., (1997). The nature of cuticular “ruffles” on slowly plucked anagen hair roots. *J. Cutan. Pathol.*; 24: 434-439

Chavanas, S., Bodemer, C., Rochat, A., Hamel-Teillac, D., Ali, M., Irvine, A.D., Bonafé, J.L., Wilkinson, J., Taïeb, A., Barrandon, Y., Harper, J.I., de Prost, Y., Hovnanian, A., (2000). Mutations in SPINK5, encoding a serine protease inhibitor, cause Netherton syndrome. *Nat. Genet*.; 25: 141-142

Chelly, J., Tümer, Z., Tønnesen, T., Petterson, A., Ishikawa-Brush, Y., Tommerup, N., Horn, N., Monaco, A.P., (1993). Isolation of a candidate gene for Menkes disease that encodes a potential heavy metal binding protein. *Nat. Genet*.; 3: 14-19

Choi, W.J., Pi, L.Q., Min, G., Lee, W.S., Lee, B.H., (2012). Qualitative investigation of fresh human scalp hair with full-field optical coherence tomography. *J. Biomed. Optics*; 17: 0360101-0360106

Clement, J-L., Hagege, R., Le Pareux, A., Connet, J., Gastaldi, G., (1981). New concepts about hair identification revealed by electron microscope studies. *J. Forensic Studies*; 26: 447-458

Clifton-Bligh, R.J., Wentworth, J.M., Heinz, P., Crisp, M.S., John, R., Lazarus, J.H., Ludgate, M., Chatterjee, V.K., (1998). Mutation of the gene encoding human TTF-2 associated with thyroid agenesis, cleft palate and choanal atresia. *Nat. Genet*.; 19: 399-401

Contreras-Jurado, C., Lorz, C., García-Serranoa, L., Paramiob, J.M., Arandaa, A., (2015). Thyroid hormone signalling controls hair follicle stem cell function. *Mol. Biol. Cell*; 26: 1263-1272

Corbett, J.F., (1976). The chemistry of hair-care products. *JSDC*; 92: 285-303

Corcuff, P., Gremillet, P., Jourlin, M., Duvault, Y., Leroy, F., Leveque, J.L., (1993). 3D reconstruction of human hair by confocal microscopy. *J. Soc. Cosmet. Chem.*; 44: 1-12

Crawford, K., and Hernandez, C., (2014). A review of hair care products for black individuals. *Cutis*.; 93: 289-293

Crewther, W.G., Dowling, L.M., Steinert, P.M., Parry, D.A.D., (1983). Structure of intermediate filaments. *Int. J. Biol. Macromol*.; 5: 267-274

Cruz, C.F., Fernandes, M.M., Gomes, A.C., Coderch, L., Marti, M., Mendez, S., Gales, L., Azoia, N.G., Shimanovich, U., Cavaco-Paulo, A., (2013). Keratins and lipids in ethnic hair. *Int. J. Cosmet. Sci.*; 35: 244-249

Dabitao, D., Margolick, J.B., Lopez, J., Bream, J.H., (2011). Multiplex measurement of proinflammatory cytokines in human serum: comparison of the meso scale discovery electrochemiluminescence assay and the cytometric bead array. *J. Immunol. Meth.*; 372: 71-77

Das-Chaudhuri, A.B., Chopra, V.P., (1984). Variation in hair histological variables: medulla and diameter. *Hum. Hered.*; 34: 217-221

DasGupta, R., and Fuchs, E., (1999). Multiple roles for activated LEF/TCF transcription complexes during hair follicle development and differentiation. *Development;* 126: 4557-4568

De la Mettrie, R., Saint-Leger, D., Loussouarn, G., Garcel, A., Porter, C., Langaney, A., (2007). Shape variability and classification of human hair: a worldwide approach. *Hum. Biol.*; 79: 265-281

De Melo, S., Takato, S., Sousa, M., Melo, M.J., Parola, A.J., (2007). Revisiting Perkin's dye(s): the spectroscopy and photophysics of two new mauveine compounds (B2 and C). *Chem. Commun. (Camb.)*; 25: 2624-2626

Denizot, F. and Lang, R., (1986). Rapid colorimetric assay for cell growth and survival: modifications to the tetrazolium dye procedure giving improved sensitivity and reliability. *J. Immuno. Methods*; 89: 271-277

Demehri, S., and Kopan, R., (2009). Notch signalling in bulge stem cells is not required for selection of hair follicle fate. *Development*; 136: 891-896

Dimitrow, E., Riemann, I., Ehlers, A., Koehler, M.J., Norgauer, J., Elsner, P., Konig, K., Kaatz, M., (2009). Spectral fluorescence lifetime detection and selective melanin imaging by multiphoton laser tomography for melanoma diagnosis. *Exp. Dermatol*.; 18: 509-515

Donati, G., Proserpio, V., Lichtenberger, B.M., Natsuga, K., Sinclair, R., Fujiwara, H., Watt, F.M., (2014). Epidermal Wnt/β-catenin signalling regulates adipocyte differentiation via secretion of adipogenic factors. *Proc. Nat. Acad. Sci. U.S.A.*; 111: 1501-1509

Driskell, R., Jahoda, C.A.B., Chuong, C.M., Watt, F., Horsley, V., (2014). Defining dermal adipose tissue. *Exp. Dermatol.*; 23: 629-631

Eckhart, L., Lippens, S., Tschachler, E., Declercq, W., (2013). Cell death by cornfication. *BBA. Mol. Cell Res.*; 1833: 3471-3480

Edgar, B.A., Zielke, N., Gutierrez, C., (2014). Endocycles: a recurrent evolutionary innovation for post-mitotic cell growth. *Nat. Rev. Mol. Cell Biol.*; 15: 197-210

Ehlers, A., Riemann, I., Stark, M., Konig, K., (2007). Multiphoton fluorescence lifetime imaging of human hair. *Micros. Res. Techni.*; 70: 154-161

Elias, P.M., and Friend, D.S., (1975). The permeability barrier in mammalian epidermis. *J. Cell biol.*; 65: 180-191

Elleder, M., and Borovansky, J., (2001). Autofluorescence of melanins induced by ultraviolet radiation and near-ultraviolet light. A histochemical and biochemical study. *The Histochemical J.*; 33: 273-281

Enshell-Seijffers, D., Lindon, C., Kashiwagi, M., Morgan, B.A., (2010). Beta-catenin activity in the dermal papilla regulates morphogenesis and regeneration of hair. *Devel. Cell*; 18: 633-642

Evans, A.O., Marsh, J.M., Wickett, R.R., (2011). The structural implications of water hardness metal uptake by human hair. *Int. J. Cosmet. Sci.*; 33: 477-482

Evans, N.D., Oreffo, R.O.C., Healy, E., Thurner, P.J., Man, Y.H., (2013). Epithelial mechanobiology, skin wound healing, and the stem cell niche. *J. Mech. Behav. Biomed. Mat.*; 28: 397-409

Fabian, M.A., Biggs, W.H., Treiber, D.K., Atteridge, C.E., Azimioara, M.D., Benedetti, M.G., Carter, T.A., Ciceri, P., Edeen, P.T., Floyd, M., Ford, J.M., Galvin, M., Gerlach, J.L., Grotzfeld, R.M., Herrgard, S., Insko, D.E., Insko, M.A., Lai, A.G., Lélias, J.M., Mehta, S.A., Milanov, Z.V., Velasco, A.M., Wodicka, L.M., Patel, H.K., Zarrinkar, P.P., Lockhart, D.J., (2005). A small molecule-kinase interaction map for clinical kinase inhibitors. *Nat. Biotechnol*.; 23: 329-336

Farag, M.R., Ghoniem, M.H., Abou-Hadeed, A.H., Dhama, K., (2015). Forensic investigation of some wild animal hair using light and scanning electron microscopy. *Adv. Anim. Vet. Sci.*; 3: 559-568

Feoktistova, M., Geserick, P., Leverkus, M., (2016). Crystal violet assay for determining viability of cultured cells. *Cold Spring Harb. Protoc.*; doi:10.1101/pdb.prot087379

Fernandez, E., Barba, C., Alonso, C., Marti, M., Parra, J.L., Coderch, L., (2011). Photodamage determination of human hair. *J. Photochemistry and photobiology B: biology.*; 106: 101-106

Festa, E., Fretz, J., Berry, R., Schmidt, B., Rodeheffer, M., Horowitz, M., Horsley, V., (2011). Adipocyte lineage cells contribute to the skin stem cell niche to drive hair cycling. *Cell*; 146: 761-771

Feughelman, M., Haly, A.R., and Mason, P., (1962). Contraction of keratin fibres in aqueous lithium bromide. *Nature*.; 96: 957-958

Feughelman, M., Haly, A.R., and Mitchell, T.W., (1958). The nature of permanent set in keratin fibres. *Text. Res. J.*; 28: 655-659

Fichtel, J.C., Richards, J.A., Davis, L.S., (2007). Trichorrexis nodosa secondary to argininosuccinicaciduria. *Pediatr. Dermatol*.; 24: 25-27

Filshie, B.K., and Rogers, G.E., (1964). The fine structure of alpha keratins. *J. Mol. Biol.*; 3: 784-786

Fischer, T.W., Slominski, A., Tobin, D.J., Paus, R., (2008). Melatonin and the hair follicle. *J. Pineal Res.*; 44: 1-15

Fischer, H., Szabo, S., Scherz, J., Jaeger, K., Rossiter, H., Buchberger, M., Ghannadan, M., Hermann, M., Theussl, HC., Tobin, D.J., Wagner, E.F., Tschachler, E., Eckhart, L., (2011). Essential role of the keratinocyte-specific endonuclease DNase1L2 in the removal of nuclear DNA from hair and nails. *J. Invest. Dermatol.*; 131: 1208-1215

Fisher, E.J., Berk, D.R., Greene, R.E., Shaner, P., Sweet, S.C., Mallory, S.B., (2006). Preferred methods of excess hair removal in pediatric patients with lung transplantation. *J. Am. Acad. Dermatol.*; 55: 320-323

Fleger-Weckmann, A., Ustun, Y., Kloepper, J., Paus, R., Bloch, W., Chen, Z.L., Wegner, J., Sorokin, L., Langbein, L., Eckes, B., Zigrino, P., Krieg, T., Nischt, R., (2016). Deletion of the epidermis derived laminin γ1 chain leads to defects in the regulation of late hair morphogenesis. *Matrix Biol.*; http://dx.doi.org/10.1016/j.matbio.2016.05.002

Foitzik, K., Krause, K., Conrad, F., Nakamura, M., Funk, W., Paus, R., (2006). Human scalp hair follicles are both a target and a source of prolactin, which serves as an autocrine and/or paracrine promotor of apoptosis-driven hair follicle regression. *Am. J. Pathol.*; 168: 748-756

Foitzik, K., Lindner, G., Muller-Rover, S., Maurer, M., Botchkareva, N., Botchkarev, V., Handjiski, B., Metz, M., Hibino, T., Soma, T., Dotto, G.P., Paus, R., (2000). Control of murine hair follicle regression (catagen) by TGF-β1 in vivo. *FASEB*; 14: 752-760

Formanek, F., De Wilde, Y., Luengo, G.S., Querleux, B., (2006). Investigation of dyed human hair fibres using apertureless near-field scanning optical microscopy. *J. Micros.*; 224: 197-202

Fowler, S.D., Brown, W.J., Warfel, J., Greenspan, P., (1987). Use of Nile red for the rapid in situ quantitation of lipids on thin-layer chromatograms. *J. Lipid Res.*; 28: 1225-1232

Fraser, R.D., MacRae, T.P., Suzuki, E., (1976). Structure of the alpha-keratin microfibril. *J. Mol. Biol.*; 108: 435-452

Fuchs, E., (2008). Skin stem cells: rising to the surface. *J. Cell Biol.*; 180: 273

Fuchs, E., and Green, H., (1980). Changes in keratin gene expression during terminal differentiation of the keratinocyte. *Cell*; 19: 1033-1042

Fujikawa, H., Fujimoto, A., Farooq, M., Ito, M., Shimomura, Y., (2012). Characterisation of the human hair keratin-associated protein 2 (KRTAP2) gene family. *J. Invest. Dermatol.*; 132: 1806-1813

Fujikawa, H., Fujimoto, A., Farooq, M., Ito, M., Shimomura, Y., (2013). Characterisation of the human hair shaft cuticle-specific keratin-associated protein 10 family. *J. Invest. Dermatol.*; 133: 2780-2782

Fujimoto, A., Farooq, M., Fujikawa, H., Inoue, A., Ohyama, M., Ehama, R., Nakanishi, J., Hagihara, M., Iwabuchi, T., Aoki, J., Ito, M., Shimomura, Y., (2012). A missense mutation within the helix initiation motif of the keratin K71 gene underlies autosomal dominant woolly hair/hypotrichosis*. J. Invest. Dermatol*.; 132: 2342-2349

Fujimoto, S., Takase, T., Kadono, N., Maekubo, K., Hirai, Y., (2014). Krtap11-1, a hair keratin-associated protein, as a possible crucial element for the physical properties of hair shafts. *J. Dermatol. Sci.*; 74: 39-47

Furio, L., Pampalakis, G., Michael, I.P., Nagy, A., Sotiropoulou, G., Hovnanian, A., (2015). KLK5 inactivation reverses cutaneous hallmarks of Netherton syndrome. *PLoS Genet.*; 11: e1005389

Fusenig, N.E., Amer, S.M., Boukamp, P. and Worst, P.K., (1978). Characteristics of chemically transformed mouse epidermal cells in vitro and in vivo. *Bulletin du Cancer*; 65: 271-279

Galletly, N.P., McGinty, J., Dunsby, C., Teixeira, F., Requejo-Isidro, J., Munro, I., Elson, D.S., Neil, M.A.A., Chu, A.C., French, P.M.W., Stamp, G.W., (2008). Fluorescence lifetime imaging distinguishes basal cell carcinoma from surrounding uninvolved skin. *Brit. J. Dermatol*.; 159: 152-161

Gamez-Garcia, M., (1999). Plastic yielding and fracture of human hair cuticles by cyclical torsional stresses. *J. Cosmet. Sci.*; 50: 69-77

Gandarillas, A., and Freije, A., (2014). Cycling up the epidermis: reconciling 100 years of debate. *Exp. Dermatol.*; 23: 87-91

Gandour-Edwards, R., McClaren, M., Isseroff, R.R., (1994). Immunolocalisation of low-molecular-weight stress protein HSP27 in normal skin and common cutaneous lesions. *Am. J. Dermatopathol.*; 16: 504-509

Gazel, A., Banno, T., Walsh, R., Blumenburg, M., (2006). Inhibition of JNK promotes differentiation of epidermal keratinocytes. *J. Biol. Chem.*; 281: 20530-20541

Genander, M., Cook, P.J., Ramskold, D., Keyes, B.E., Mertz, A.F., Sandberg, R., Fuchs, E., (2014). BMP signalling and its pSMAD1/5 target genes differentially regulate hair follicle stem cell lineages. *Cell stem cell*; 15: 619-633

Geyfman, M., Gordon, W., Paus, R., Andersen, B., (2011). Identification of telogen markers underscores that telogen is far from a quiescent hair cycle stage. *J. Invest. Dermatol.*; 132: 721-724

Geyfman, M., Kumar, V., Liu, Q., Ruiz, R., Gordon, W., Espitia, F., Cam, E., Millar, S.E., Smyth, P., Ihler, A., Takahashi, J.S., Andersen, B., (2012). Brain and muscle Arnt-like protein-1 (BMAL1) controls circadian cell proliferation and susceptibility to UVB-induced DNA damage in the epidermis. *Proc. Natl. Acad. Sci. USA.*; 109: 11758-11763

Geyfman, M., Plikus, M., Treffeisen, E., Andersen, B., Paus, R., (2015). Resting no more: re-defining telogen, the maintenance stage of the hair growth cycle. *Biol. Rev.*; 90: 1179-1196

Gharzi, A., Reynolds, A.J., Jahoda, C.A., (2003). Plasticity of hair follicle dermal cells in wound healing and induction. *Exp. Dermatol.*; 12: 126-136

Giehl, K.A., Ferguson, D.J., Dawber, R.P.R., Pittelkow, M.R., Foehles, J., de Berker, D.A., (2004). Update on detection, morphology and fragility in pili annulati in three kindreds. *J. Eur. Acad. Dermatol. Venereol*.; 18: 654-658

Giehl, K.A., Rogers, M.A., Radivojkov, M., Tosti, A., De Berker, D.A.R., Weinlich, G., Schmuth, M., Ruzicka, T., Eckstein, G.N., (2009). Pili annulati: refinement of the locus on chromosome 12q24.33 to a 2.9-Mb interval and candidate gene analysis. *Br. J. Dermatol*.; 160: 527-533

Giglia-Mari, G., Coin, F., Ranish, J.A., Hoogstraten, D., Theil, A., Wijgers, N., Jaspers, N.G.J., Raams, A., Argentini, M., van der Spek, P.J., Botta, E., Stefanini, M., Egly, J., Aebersold, R., Hoeijmakers, J.H.J., Vermeulen, W., (2004). A new, tenth subunit of TFIIH is responsible for the DNA repair syndrome trichothiodystrophy group A. *Nat. Genet*.; 36: 714-719

Gillespie, J.M., (1991). The structural proteins of hair: isolation, characterisation and regulation of biosynthesis. *Physiology, biochemistry and molecular biology of the skin. Ed. L.A.Goldsmith.* Oxford University Press, Oxford, p. 625-659

Girman, C.J., Rhodes, T., Lilly, F.R.W., Guo, S.S., Siervogal, R.M., Patrick, D.L., Chumlea, W.C., (1998). Effects of self-perceived hair loss in a community sample of men. *Dermatol.*; 197: 223-229

Gould, J.G., and Sneath, R.L., (1985). Electron microscopy-image analysis: quantitation of ultrastructural changes in hair fibre cross sections as a result of cosmetic treatment. *J. Soc. Cosmet. Chem.*; 36: 53-59

Greco, V., Chen, T., Rendl, M., Schober, M., Pasolli, H.A., Stokes, N., Dela Cruz-Racelis, J., Fuchs, E., (2009). A two-step mechanism for stem cell activation during hair regeneration. *Cell Stem Cell*; 4: 155-169

Greenwell, M.D., Willner, A., Kirk, P.L., (1941). Human hair studies: III. Refractive index of crown hair. *J. Criminal law and criminol.*; 31: 746-752

Gruber, J.V., and Kerschman, R., (2004). Microscopic high-resolution digital volumetric imaging of human hair fibres. *J. Cosmet. Sci.*; 55: S29-S35

Hadjur, C., Daty, G., Madry, G., Corcuff, P., (2002). Cosmetic assessment of the human hair by confocal microscopy. *Scanning*; 24: 59-64

Hahn, G.S., (1999). Strontium is a potent and selective inhibitor of sensory irritation. *Dermatologic surgery*; 25: 689-694

Haly, A.R., and Griffith, J., (1958). Penetration and supercontraction of keratin fibres by lithium bromide solutions. *Text. Res. J.*; 28: 32-40

Hallegot, P., Peteranderl, R., Lechene, C., (2004). In-situ imaging mass spectrometry analysis of melanin granules in the human hair shaft. *J. Invest. Dermatol*.; 122: 381-386

Hameka, H.F., Jensen, J.O., Ong, K.K., Samuels, A.C., Vlahacos, C.P., (1998). Fluorescence of cysteine and cystine. *J. Phys. Chem.*; 102: 361-367

Hanukoglu, I., and Ezra, L., (2014). Proteopedia entry: coiled-coil structure of keratins. *Biochem. Mol. Biol. Educ.*; 42: 93-94

Haque, F.A.K.M., and Al-Ghazal, S., (2004). Burn from hair removal cream – a case report. *Burns*; 30: 866-867

Hardy, D., (1973). Quantitative hair form variation in seven populations. *Am. J. Phys. Anthrop.*; 39: 7-18

Harland, D.P., Vernon, J.A., Walls, R.J., Woods, J.L., (2011). Transmission electron microscopy staining methods for the cortex of human hair: a modified osmium method and comparison with other stains. *J. Microscopy*; 243: 184-196

Harland, D.P., Walls, R.J., Vernon, J.A., Dyer, J.M., Woods, J.L., Bell, F., (2014). Three-dimensional architecture of macrofibrils in the human scalp hair cortex. *J. Struct. Biol.*; 185: 397-404

Harper, P., (1989). Maple syrup urine disease in calves: a clinical, pathological and biochemical study. *Aust. Vet. J.*; 66: 46-49

Harper, D.L., and Kamath, Y.K., (2007). The effect of treatments on the sheer modulus of human hair measured by the single fibre torsion pendulum. *J. Cosmet. Sci.*; 58: 329-337

Harries, M.J., Meyer, K., Chaudhry, I., Kloepper, E.J., Poblet, E., Griffiths, C.E., Paus, R., (2013). Lichen planopilaris is characterised by immune privilege collapse of the hair follicle's epidermal stem cell niche. *J. Pathol.*; 231: 236-247

Harrison, J.L. and Davis, K.D., (1999). Cold-evoked pain varies with skin type and cooling rate: a psychophysical study in humans. *Pain*; 83: 123-135

Hatta, I., Ohta, N., Inoue, K., Yagi, N., (2006). Coexistence of two domains in intercellular lipid matrix of stratum corneum. *Biochim. Biophys. Acta*; 1758: 1830-1836

Hauser, C., Saurat, J.H., Schmitt, A., Jaunin, F., Dayer, J.M., (1986). Interleukin 1 is present in normal human epidermis. *J. Immunol.*; 136: 3317-3323

Hebert, J.M., Rosenquist, T., Gotz, J., Martin, G.R., (1994). FGF5 as a regulator of the hair growth cycle: evidence from targeted and spontaneous mutations. *Cell*; 78: 1017-1025

Hesse, M., Zimek, A., Weber, K., Magin, T.M., (2004). Comprehensive analysis of keratin gene clusters in humans and rodents. *Euro. J. Cell Biol.*; 83: 19-26

Hibino, T., and Nishiyama, T., (2004). Role of TGF-β2 in the human hair cycle. *J. Dermatol. Sci.*; 35: 9-18

Higgins, C.A., Westgate, G.E., Jahoda, C.A.B., (2009). From telogen to exogen: mechanisms underlying formation and subsequent loss of the hair club fibre. *J. Invest. Dermatol.*; 129: 2100-2108

Higgins, C.A., Westgate, G.E., Jahoda, C.A.B., (2011). Modulation in proteolytic activity is identified as a hallmark of exogen by transcriptional profiling of hair follicles. *J. Invest. Dermatol.*; 131: 2349-2357

Hinson, J.T., Fantin, V.R., Schönberger, J., Breivik, N., Siem, G., McDonough, B., Sharma, P., Keogh, I., Godinho, R., Santos, F., Esparza, A., Nicolau, Y., Selvaag, E., Cohen, B.H.,

Hoppel, C.L., Tranebjaerg, L., Eavey, R.D., Seidman, J.G., Seidman, C.E., (2007). Missense mutations in the BCS1L gene as a cause of the Bjornstad syndrome. *N. Engl. J. Med*.; 356: 809-819

Hirao, T., Denda, M., Takahashi, M., (2001). Identification of immature cornified envelopes in the barrier-impaired epidermis by characterisation of their hydrophobicity and antigenicities of the components. *Experimental dermatology*; 10: 35-44

Hofmeister, F., (1888). *Arch. Exp. Pathol. Pharmacol*. 24: 247-260

Holmes, A.W., (1961). A fatty acid/protein complex in human hair. *Nature*; 189: 923

Hoting, E., and Zimmermann, M., (1996). Photochemical alterations in human hair. Part III: investigations of internal lipids. *J. Soc. Cosmet. Chem.*; 47: 201-211

Hoting, E., and Zimmerman, M., (1997). Sunlight induced modification in bleached, permed or dyed human hair. *J. Cosmet. Sci.*; 48: 79-91

Hou, C., Miao, Y., Wang, X., Chen, C., Lin, B., Hu, Z., (2016). Expression of matrix metalloproteinases and tissue inhibitor of matrix metalloproteinases in the hair cycle. *Exp. Therap. Med.*; 12: 231-237

Hsu, Y.C., Pasolli, H.A., Fuchs, E., (2011). Dynamics between stem cells, niche, and progeny in the hair follicle. *Cell*; 144: 92-105

Huang, C.M., Foster, K.W., DeSilva, T., Zhang, J., Shi, Z., Yusuf, N., Van Kampen, K.R., Elmets, C.A., Tang, D.C., (2003). Comparative proteomic profiling of murine skin. *J. Invest. Dermatol.*; 121: 51-64

Hwang, J., Mehrani, T., Millar, S.E., Morasso, M.I., (2008). Dlx3 is a crucial regulator of hair follicle differentiation and cycling. Development; 135: 3149-3159

Imran, T., Zafar, L., Rehan, M., Nasir, A., Tariq, P.A., Batool, I., (2012). Chediak-Higashi syndrome presenting in accelerated phase. *J. Coll. Physicians Surg. Pak*.; 22: 539-541

Inoue, T., Sasaki, I., Yamaguchi, M., Kizawa, K., (2000). Elution of S100A3 from hair fibre: New model for hair damage emphasising the loss of S100A3 from cuticle. *J. Cosmet. Sci.*; 51: 15-25

Ito, A., Inoue, T., Kawai, T., Taki, Y., Inoue, S., Shimizu, T., Shinohara, K., (2016). Difference in the distributions between Ca content and the degree of oxidative damage in human hair determined by X-ray imaging. *AIP. Conf. Proc.*; 1696: 020021

Ito, S., and Wakamatsu, K., (2003). Quantitative analysis of eumelanin and pheomelanin in humans, mice, and other animals: a comparative review. *Pigment cell res.*; 16: 523-531

Ito, S., and Wakamatsu, K., (2011). Diversity of human hair pigmentation as studied by chemical analysis of eumelanin and pheomelanin. *J. Euro. Acad. Dermatol. Venereol.*; 25: 1369-1380

Ito, S., Wakamutsu, K., Ozeki, H., (2000). Chemical analysis of melanins and its application to the study of the regulation of melanogenesis. *Pigment cell res.*; 13: 103-109

Jachowicz, J., and McMullen, R.L., (2011). Tryptophan fluorescence in hair-examination of contributing factors. *J. Cosmet. Sci.*; 62: 291-304

Janich, P., Pascual, G., Merlos-Suarez, A., Battle, E., Ripperger, J., Albrecht, U., Cheng, H.Y., Obrietan, K., Di Croce, L., Benitah, S.A., (2011). The circadian molecular clock creates epidermal stem cell heterogeneity. *Nature*; 480: 209-214

Jarius, S., Wildemann, B., (2013). Aquaporin-4 antibodies (NMO-IgG) as a serological marker of neuromyelitis optica: a critical review of the literature. *Brain Pathol.*; 23: 661-683

Jarnik, M., Simon, M.N., Steven, A.C., (1998). Cornified cell envelope assembly model based on electron microscopic determination of thickness and projected density. *J. Cell Sci.*; 111: 1051-1060

Jenkins, B.J., and Powell, B.C., (1994). Differential expression of genes encoding a cysteine rich keratin family in the hair cuticle. *J. Invest. Dermatol*.; 103: 310-317

Jensen, K.B., Collins, C.A., Nascimento, E., Tan, D.W., Frye, M., Itami, S., Watt, F.M., (2009). Lrig1 expression defines a distinct multipotent stem cell population in mammalian epidermis. *Cell Stem Cell*; 4: 427-439

Jensen, U.B., Lowell, S., Watt, F.M., (1999). The spatial relationship between stem cells and their progeny in the basal layer of human epidermis: a new view based on whole0mount labelling and lineage analysis. *Development*; 126: 2409-2418

John, S., Thiebach, L., Frie, C., Mokkapati, S., Bechtel, M., Nischt, R., Rosser-Davies, S., Paulsson, M., Smyth, N., (2012). Epidermal transglutaminase (TGase 3) is required for proper hair development, but not the formation of the epidermal barrier. *PLoS One*; 7: e34252

Jonak, C., Klosner, G., Kokesch, C., Fodinger, D., Honigsmann, H., Trautinger, F., (2002). Subcorneal colocalisation of the small heat shock protein, hsp27, with keratins and proteins of the cornified cell envelope. *Br. J. Dermatol.*; 147: 13-19

Jones, P.H., (1995). *The isolation and characterisation of human epidermal stem cells.* University College London, London

Jones, L.N., (2001). Hair structure anatomy and comparative anatomy. *Clinics Dermatol.*; 19: 95-103

Jones, L.N., Peet, D.J., Danks, D.M., Negri, A.P., Rivett, D.E., (1996). Hairs from patients with maple syrup urine disease show a structural defect in the fibre cuticle. *J. Invest. Dermatol*.; 106: 461-464

Jones, L.N., and Rivett, D.E., (1997). The role of 18-MEA in the structure and formation of mammalian hair fibres. *Micron*.; 28: 469-485

Jones, L.N., Rogers, G.E., Rufaut, N., Sinclair, R.D., (2010). Location of keratin-associated proteins in developing fibre cuticle cells using immunoelectron microscopy. *Int. J. Trichol.*; 2: 89-95

Kalkbrenner, U., Korner, A., Hocker, H., Rivett, D.E., (1990). Studies on the lipid composition of wool. *In: Proceedings of 8th international wool textile research conference*, vol I. Christchurch, p. 398–407

Kamath, Y., Bradford, I., Hornby, S., Ramaprasad, K., Ruetsch, S., Weigmann, H.D., (1995). Analysis and quantification of hair damage. *Prog. Rep. TRI Princeton*; 9: 20-31

Kanikkannan, N., Singh, J., Ramarao, P., (1999). Transdermal iontophoretic delivery of bovine insulin and monomeric human insulin analogue. *J. Control Release*; 59: 99-105

Kantaputra, P.N., Hamada, T., Kumchai, T., McGrath, J.A., (2003). Heterozygous mutation in the SAM domain of p63 underlies Rapp-Hodgkin ectodermal dysplasia. *J. Dent. Res*.; 82: 433-437

Kassenbeck, P., (1981). *Hair research. Ch.3: Morphology and fine structure of hair.* Springer Berlin Heidelberg, p.52-64

Kato, M., Shimizu, A., Yokoyama, Y., Kaira, K., Shimomura, Y., Ishida-Yamamoto, A., Kamei, K., Tokunaga, F., Ishikawa, O., (2015). An autosomal recessive mutation of DSG4 causes monilethrix through the ER stress response. *J. Invest. Dermatol*.; 135: 1253-1260

Kazantseva, A., Goltsov, A., Zinchenko, R., Grigorenko, A.P., Abrukova, A.V., Moliaka, Y.K., Kirillov, A.G., Guo, Z., Lyle, S., Ginter, E.K., Rogaev, E.I., (2006). Human hair growth deficiency is linked to a genetic defect in the phospholipase gene LIPH. *Science*; 314: 982-985

Kelch, A., Wessel, S., Will, T., Hintze, U., Wepf, R., Wiesendanger, R., (2000). Penetration pathways of fluorescent dyes in human hair fibres investigated by scanning near-field optical microscopy. *J. Microscopy*; 200: 179-186

Khan, S.S., Smith, M.S., Reda, D., Suffredini, A.F., McCoy, J.P., (2004). Multiplex bead array assays for detection of soluble cytokines: comparisons of sensitivity and quantitative values among kits from multiple manufacturers. *Cytometry B;* 61B: 35-39

Khumalo, N.P., Stone, J., Gumedze, F., McGrath, E., Ngwanya, M., de Berker, D., (2010). “Relaxers” damage hair: Evidence from amino acid analysis. *J. Am. Acad. Dermatol.*; 62: 402-408

Kiawa, K., Troxler, H., Kleinert, P., Inoue, T., Toyoda, M., Morohashi, M., Heizmann, C.W., (2002). Characterisation of the cysteine-rich calcium-binding S100A3 protein from human hair cuticles. *Biochem. Biophys. Res. Commun.*; 299: 857-862

Kim, J.C., Duverger, O., Hwang, J., Morasso, M.I., (2015). Epidermal stem cells in the isthmus/infundibulum influence hair shaft differentiation: evidence from targeted DLX3 deletion. *J. Invest. Dermatol*.; 135: 299-301

Kim, K.H., Kabir, E., Jahan, S.A., (2016). The use of personal hair dye and its implications for human health. *Environ. Int.*; 89-90: 222-227

Kimura, H., Mukaida, M., Mori, A., (1999). Detection of stimulants in hair by laser microscopy. *J. Anal. Toxicology*; 23: 577-580

Kindred, C., Oresajo, C.O., Yatskayer, M., Halder, R.M., (2011). Comparative evaluation of men’s depilatory composition versus razor in black men. *Cutis*; 88: 98-103

Kinebuchi, S., Kobori, T., Hori, Y., (1971). Behavior of melanosomes in melanocytes and keratinocytes of Japanese skin and black hair. *In*: Kawamura, T., Fitzpatrick, T.B., Seiji, J., *Abnormal melanocytes*. University Park, Baltimore, p.195

Kirkbride, P.K., and Tridico, S.R., (2010). The application of laser scanning confocal microscopy to the examination of hairs and textile fibres: an initial investigation. *Forensic Sci. Int.*; 195: 28-35

Kiso, M., Tanaka, S., Saba, R., Matsuda, S., Shimizu, A., Ohyama, M., Okano, H.J., Shiroishi, T., Okano, H., Saga, Y., (2009). The disruption of Sox21-mediated hair shaft cuticle differentiation causes cyclic alopecia in mice. *Proc. Natl. Acad. Sci. U.S.A.*; 106: 9292-9297

Kitagawa, N., Inai, Y., Higuchi, Y., Iida, H., Inai, T., (2014). Inhibition of JNK in HaCaT cells induced tight junction formation with decreased expression of cytokeratin 5, cytokeratin 17 and desmoglein 3. *Histochem. Cell biol.*; 142: 389-399

Kizawa, K., Inoue, T., Yamaguchi, M., Kleinert, P., Troxler, H., Heizmann, C.W., Iwamoto, Y., (2005). Dissimilar effect of perming and bleaching treatment on cuticles: advanced hair damage model based on elution and oxidation of S100A3 protein. *J. Cosmet. Sci.*; 56: 219-226

Kizawa, K., Takahara, H., Unno, M., Heizmann, C.W., (2011). S100 and S100 fused-type protein families in epidermal maturation with special focus on S100A3 in mammalian hair cuticles. *Biochimie*; 93: 2038-2047

Kizawa, K., Troxler, H., Kleinert, P., Inoue, T., Toyoda, M., Morohashi, M., Heizmann, C.W., (2002). Characterisation of the cysteine-rich calcium-binding S100A3 protein from human hair cuticles. *Biochem. Biophys. Res. Commun.*; 299: 857-862

Koehler, K., Mielke, K., Schunck, M., Neumann, C., Herdegen, T., Proksch, E., (2011). Distinct roles of JNK-1 and ERK-2 isoforms in permeability barrier repair and wound healing. *Euro. J. Cell biol*.; 90: 565-571

Kobielak, K., Stokes, N., de la Cruz, J., Polak, L., Fuchs, E., (2007). Loss of a quiescent niche but not follicle stem cells in the absence of bone morphogenetic protein signalling. *Proc. Nat. Acad. Sci. U.S.A.; 104: 10063-10068*

Koch, J., Aitzetmiiller, K., Bittorf, G., Waibel, J., (1982) Hair lipids and their contribution to the perception of hair oiliness. *J. Soc. Cosmet*. *Chem.*; 33: 317-326

Koehn, H., Clerens, S., Deb-Choudhury, S., Morton, J.D., Dyer, J.M., Plowman, J.E., (2009). Higher sequence coverage and improved confidence in the identification of cysteine-rich proteins from the wool cuticle using combined chemical and enzymatic digestion. *J. Proteomics*; 73: 323-330

König, K., (2008). Clinical multiphoton tomography. *J. Biophoton*.; 1: 13-23

König, K., and Riemann, I., (2003). High-resolution multiphoton tomography of human skin with subcellular spatial resolution and picosecond time resolution. *J. Biom. Opt.*; 8: 432-439

Krasieva, T.B., Stringari, C., Liu, F., Sun, C-H., Kong, Y., Balu, M., Meyskens, F.L., Gratton, E., Tromberg, B.J., (2012). Two-photon excited fluorescence lifetime imaging and spectroscopy of melanins *in vitro* and *in vivo. J. Biomed. Opt*.; 18: 031107

Kreplak, L., Briki, F., Duvault, Y., Doucer, J., Merigoux, C., Leroy, F., Leveque, L., Miller, L., Carr, G.L., Williams, G.P., Dumas, P., (2001a). Profiling lipids across Caucasian and Afro-

American hair transverse cuts, using synchroton infrared microspectrometry. *Int. J. Cosmet. Sci.*; 23: 369-374

Kreplak, L., Merigoux, C., Briki, F., Flot, D., Doucet, J., (2001b). Investigation of human hair cuticle structure by microdiffraction: direct observation of cell membrane complex swelling. *Biochim. Biophys. Acta.*; 1547: 268-274

Kwan, K.M., Li, A.G., Wang, X.J., Wurst, W., Behringer, R.R., (2004). Essential roles of BMPR-1A signalling in differentiation and growth of hair follicles and in skin tumorigenesis. *Genesis;* 39: 10-25

Laatsch, C.N., Durbin-Johnson, B.P., Rocke, D.M., Mukwana, S., Newland, A.B., Flagler, M.J., Davis, M.G., Eigenheer, R.A., Phinney, B.S., Rice, R.H., (2014). Human hair shaft proteomic profiling: individual differences, site specificity and cuticle analysis. *PeerJ*; 2: e506

Laemmli, U.K., (1970). Cleavage of structural proteins during the assembly of the head of bacteriophage T4. *Nature*; 227: 680 – 685

Lagarde, J.M., Peyre, P., Redoules, D., Black, D., Briot, M., Gall, Y., (1994). Confocal microscopy of hair. *Cell biology and toxicology*; 10:301-304

Lakowicz, J.R., (2006). *Principles of fluorescence spectroscopy*. 3rd ed. Springer, p.66, 98

Lakowicz, J.R., Szmacinski, H., Nowaczyk, K., Berndt, K.W., Johnson, M., (1992). Fluorescence lifetime imaging. *Anal. Biochem.*; 202: 316-330

Langbein, L., Rogers, M.A., Praetzel, S., Bockler, D., Schirmacher, P., (2007). Novel type I hair keratins K39 and K40 are the last to be expressed in differentiation of the hair: completion of the human hair catalog. *J. Invest. Dermatol*.; 127: 1532-1535

Langbein, L., Rogers, M.A., Winter, H., Praetzel, S., Beckhaus, U., Rackwitz, H.R., Schweizer, J., (1999). The catalog of human hair keratins. I. Expression of the nine type I members in the hair follicle. *J. Biol. Chem.*; 274: 19874-19884

Langbein, L., Rogers, M.A., Winter, H., Praetzel, S., Schweizer, J., (2001). The catalog of human hair keratins. II. Expression of the six type II members in the hair follicle and the combined catalog of human type I and II keratins. *J. Biol. Chem.*; 276: 35123-35132

Langbein, L., and Schweizer, J., (2005). Keratins of the human hair follicle. *Int. Rev. Cytol*.; 243: 1-78

Langbein, L., Yoshida, H., Praetzel-Wunder, S., Parry, D.A., Schweizer, J., (2010). The keratins of the human beard hair medulla: the riddle in the middle. *J. Invest. Dermatol*.; 130: 55-73

Larson, B., Banks, P., Sherman, H., Rothenburg, M., (2012). Automation of cell-based drug absorption assays in 96-well format using permeable support systems. *J. Lab. Autom.*; 17: 222-232

Lau, K., Paus, R., Tiede, S., Day, P., Bayat, A., (2009). Exploring the role of stem cells in cutaneous wound healing. *Exp. Dermatol.*; 18: 921-933

Lay, K., Kume, T., Fuchs, E., (2016). FOXC1 maintains the hair follicle stem cell niche and governs stem cell quiescence to preserve long-term tissue-regenerating potential. *PNAS;* 113: e1506-e1525

LeBeau, M.A., Montgomery, M.A., Brewer, J.D., (2011). The role of variations in growth rate and sample collection on interpreting results of segmental analyses of hair. *Forensic Sci. Int*.; 210: 110-116

Lee, J.N., Jee, S.H., Chan, C.C., Lo, W., Dong, C.Y., Lin, S.J., (2008). The effects of depilatory agents as penetration enhancers on human stratum corneum structures. *J. Invest. Dermatol*.; 128: 2240-2247

Lee, J., Kang, S., Lilja, K.C., Colletier, K.J., Scheitz, C.J.F., Zhang, Y.V., Tumbar, T., (2016). Signalling couples hair follicle stem cell quiescence with reduced histone H3 K4/K9/K27me3 for proper tissue homeostasis. *Nature Comm.*; 7: 11278

Lee, J., and Tumbar, T., (2012). Hairy tale of signalling in hair follicle development and cycling. *Semin. Cell Dev. Biol.*; 23: 906-916

Lee, Y.S., Sohn, K.C., Kim, K.H., Cho, M.J., Hur, G.M., Yoon, T.J., Kim, S.K., Lee, K., Lee, J.H., Kim, C.D., (2009). Role of protein kinase C delta in X-ray-induced apoptosis of keratinocyte. *Exp. Dermatol.*; 18: 50-56

Leeder, J.D., and Bradbury, J.H., (1968). Confirmation of epicuticle on keratin fibres. *Nature*; 218: 694-695

Leeder, J.D., Bishop, D.G., Jones, L.N., (1983). Internal lipids of wool fibres. *Text. Res. J.*; 53: 402-407

Leeder, J.D., and Rippon, J.A., (1982). Histological differentiation of wool fibres in formic acid. *J. Text. Inst*.; 73: 149-151

Leeder, J.D., and Rippon, J.A., (1985). Changes induced in the properties of wool by specific epicuticle modification. *J. Soc. Dyes colourists*; 101: 11-16

Leita-Silva, V.R., Le Lamer, M., Sanchez, W.Y., Liu, D.C., Sanchez, W.H., Morrow, I., Martin, D., Silva, H.D.T., Prow, T.W., Grice, J.E., Roberts, M.S., (2013). The effect of formulation on the penetration of coated and uncoated zinc oxide nanoparticles into the viable epidermis of human skin *in vivo*. *Euro. J. Pharma. Biopharma.*; 84: 297-308

Li, N., Liu, S., Zhang, H.S., Deng, Z.L., Zhao, H.S., Zhao, Q., Lei, X.H., Ning, L.N., Cao, Y.J., Wang, H.B., Liu, S., Duan, E.K., (2016). Exogenous R-spondin1 induces precocious telogen-to-anagen transition in mouse hair follicles. *Int. J. Mol. Sci.*; 17: 582

Liang, C., Morris, A., Schlucker, S., Imoto, K., Price, V.H., Menefee, E., Wincovitch, S.M., Levin, I.W., Tamura, D., Strehle, K.R., Kraemer, K.H., DiGiovanna, J.J., (2006). Structural and molecular hair abnormalities in trichothiodystrophy. *J. Invest. Dermatol.*; 126: 2210-2216

Liberek, K., Lewandowska, A., Zietkiewicz, S., (2008). Chaperones in control of protein disaggregation. *EMBO J*.; 27: 328-335

Lien, W.H., Guo, X.Y., Polak, L., Lawton, L.N., Young, R.A., Zheng, D.Y., Fuchs, E., (2011). Genome-wide maps of histone modifications unwind in vivo chromatin states of the hair follicle lineage. *Cell Stem Cell*; 9: 219-232

Lin, K.K., Kumar, V., Geyfman, M., Chudova, D., Ihler, A.T., Smyth, P., Paus, R., Takahashi, J.S., Andersen, B., (2009). Circadian clock genes contribute to the regulation of hair follicle cycling. *PLoS Genetics;* 5: e1000573

Lindberg, J., Philip, B., Gralen, N., (1948). Occurrence of thin membranes in the structure of wool. *Nature*; 162: 458-459

Lindner, G., Botchkarev, V.A., Botchkareva, N.V., Ling, G., van der Veen, C., Paus, R., (1997). Analysis of apoptosis during hair follicle regression (catagen). *Am. J. Pathol.*; 151: 1601-1617

Liu, K.M., Chen, Y.J., Shen, L.F., Haddad, A.N.S., Song, I.W., Chen, L.Y., Chen, Y.J., Wu, J.Y., Yen, J.J.Y., Chen, Y.T., (2015). Cyclic alopecia and abnormal epidermal cornification in *Zdhhc13*-deficient mice reveal the importance of palmitoylation in hair and skin differentiation. *J. Invest. Dermatol.*; 135: 2603-2610

Lu, P.H., Kuo, T.C., Chang, K.C., Chang, C.H., Chu, C.Y., (2011). Gefitinib-induced epidermal growth factor receptor-independent keratinocyte apoptosis is mediated by the JNK activation pathway. *Brit. J. Dermatol.*; 164: 38-46

Lu, Z., Yuan, Z., Miyoshi, T., Wang, Q., Su, Z., Chang, C.C., Shi, W., (2011). Identification of *Soat1* as a quantitative trait locus gene on mouse chromosome 1 contributing to hyperlipidemia. *PLoS One*; 6: e25344

Lurie, R., Danziger, Y., Kaplan, Y., Sulkes, J., Abramson, E., Mimouni, M., (1996). Acquired pili torti - a structural hair shaft defect in anorexia nervosa. *Cutis*.; 57: 151-156

Määttä, A., DiColandrea, T., Groot, K., Watt, F.M., (2001). Gene targeting of envoplakin, a cytoskeletal linker protein and precursor of the epidermal cornified envelope. *Mol. Cell. Biol*.; 21: 7047-7053

Macario, A.J., and Conway de Macario, E., (2007). Molecular chaperones: multiple functions, pathologies, and potential applications. *Front. Biosci.*; 12: 2588-2600

Major, M.H., (1955). New mutants, satin, sa. *Mouse News Lett.*; 12: 47

Manoir, S., Guillaud, P., Camus, E., Seigneurin, D., Brugal, G., (1991). Ki-67 labelling in postmitotic cells defines different Ki-67 pathways within the 2c compartment. *Cytometry*; 12: 455-463

Marekov, L.N., and Steinert, P.M., (1998). Ceramides are bound to structural proteins of the human foreskin epidermal cornified cell envelope. *J. Biol. Chem.*; 273: 17763-17770

Marsh, J.M., Davis, M.G., Lucas, R.L., Reilman, R., Styczynski, P.B., Li, C., Mamak, M., McComb, D.W., Williams, R.E., Godfrey, S., Navqi, K.R., Chechik, V., (2015). Preserving fibre health: reducing oxidative stress throughout the life of the hair fibre. *Int. J. Cosmet. Sci.*; 37: 16-24

Masukawa, Y., Narita, H., Imokawa, G., (2005a). Characterisation of the lipid composition at the proximal root regions of human hair. *J. Cosmet. Sci.*; 56: 1-16

Masukawa, Y., Tsujimura, H., Imokawa, G., (2005b). A systematic method for the sensitive and specific determination of hair lipids in combination with chromatography. *J. Chromatogaphy B*; 823: 131-142

Mathes, C., Brandner, J.M., Laue, M., Raesch, S.S., Hansen, S., Failla, A.V., Vidal, S., Moll, I., Schaefer, U.F., Lehr, C.M., (2016). Tight junctions form a barrier in porcine hair follicles. *Euro. J. Cell Biol.*; 95: 89-99

Matsunaga, R., Abe, R., Ishii, D., Watanabe, S., Kiyoshi, M., Nocker, B., Tsuchiya, M., Tsumoto, K., (2013). Bidirectional binding property of high glycine-tyrosine keratin-associated protein contributes to the mechanical strength and shape of hair. *J. Struct. Biol.*; 183: 484-494

McKoy, G., Protonotarios, N., Crosby, A., Tsatsopoulou, A., Anastasakis, A., Coonar, A., Norman, M., Baboonian, C., Jeffery, S., McKenna, W.J., (2000). Identification of a deletion in plakoglobin in arrhythmogenic right ventricular cardiomyopathy with palmoplantar keratoderma and woolly hair (Naxos disease). *Lancet*; 355: 2119-2124

McDonald, J.H., (2014). *Handbook of biological statistics.* 3rd ed. Sparky House Publishing, Baltimore, Maryland, p.111-114

McGrath, J.A., Duijf, P.H., Doetsch, V., Irvine, A.D., de Waal, R., Vanmolkot, K.R., Wessagowit, V., Kelly, A., Atherton, D.J., Griffiths, W.A., Orlow, S.J., van Haeringen, A., Ausems, M.G., Yang, A., McKeon, F., Bamshad, M.A., Brunner, H.G., Hamel, B.C., van Bokhoven, H., (2001). Hay-Wells syndrome is caused by heterozygous missense mutations in the SAM domain of p63. *Hum. Mol. Genet*.; 10: 221-229

McGrath, J.A., McMillan, J.R., Shemanko, C.S., Runswick, S.K., Leigh, I.M., Lane, E.B., Garrod, D.R., Eady, R.A., (1997). Mutations in the plakophilin 1 gene result in ectodermal dysplasia/skin fragility syndrome. *Nat. Genet*.; 17: 240-244

Mecklenburg, L., Tobin, D.J., Muller-Rover, S., Handjiski, B., Wendt, G., Peters, E.M., Pohl, S., Moll, I., Paus, R., (2000). Active hair growth (anagen) is associated with angiogenesis. *J. Invest. Dermatol.*; 114: 909-916

Mehlem, A., Hagberg, C.E., Muhl, L., Eriksson, U., Falkevall, A., (2013). Imaging of neutral lipids by oil red O for analysing the metabolic status in health and disease. *Nature Protocols*; 8: 1149-1154

Menkart, J., Wolfram, L.J., Mao, I., (1966). Caucasian hair, Negro hair and wool: similarities and differences. *J. Soc. Cosmet. Chem.*; 17: 769-788

Mercer, J.F., Livingston, J., Hall, B., Paynter, J.A., Begy, C., Chandrasekharappa, S., Lockhart, P., Grimes, A., Bhave, M., Siemieniak, D., (1993). Isolation of a partial candidate gene for Menkes disease by positional cloning. *Nat. Genet*.; 3: 20-25

Millington, K.R., (2006). Photoyellowing of wool. Part 2: photoyellowing mechanisms and methods of prevention. *Color Technol.*; 122: 301-316

Miranda-Vilela, A.L., Botelho, A.J., Muehlmann, L.A., (2013). An overview of chemical straightening of human hair: technical aspects, potential risks to hair fibre health and legal issues. *Int. J. Cosmet. Sci.*; 36: 2-11

Miyake, M., and Oyama, N., (2009). Effect of amidoalkyl group as a spacer on aggregation properties of guanidine-type surfactants. *J. Colloid Interf. Sci.*; 330: 180-185

Moghimi, H.R., Jamali, B., Farahmand, S., Shafaghi, B., (2013). Effect of essential oils, hydrating agents, and ethanol on hair removal efficiency of thioglycolates. *J. Cosmet. Dermatol*.; 12: 41-48

Molho-Pessach, V., Lerer, I., Abeliovich, D., Agha, Z., Abu Libdeh, A., Broshtilova, V., Elpeleg, O., Zlotogorski, A., (2008). The H syndrome is caused by mutations in the nucleoside transporter hENT3. *Am. J. Hum. Genet*.; 83: 529-534.

Moll, R., Franke, W.W., Schiller, D.L., Geiger, B., Krepler, R., (1982). The catalogue of human cytokeratins: patterns of expression in normal epithelia, tumours and cultured cells. *Cell*; 31: 11-24

Moncrieff, R.W., (1954). *Wool shrinkage and its prevention*. 1st ed. London, Chemical publishing company

Mosmann, T., (1983). Rapid colorimetric assay for cellular growth and survivals: application to proliferation and cytotoxic assays. *J. Immuno. Methods*; 65: 55-63

Mosser, D.D., Caron, A.W., Bourget, L., Meriin, A.B., Sherman, M.Y., Morimoto, R.I., Massie, B., (2000). The chaperone function of hsp70 is required for protection against stress-induced apoptosis. *Mol. Cell biol.*; 20: 7146-7159

Muller-Rover, S., Handjiski, B., van der Veen, C., Eichmuller, S., Foitzik, K., McKay, I.A., Stenn, K.S., Paus, R., (2001). A comprehensive guide for the accurate classification of murine hair follicles in distinct hair cycle stages. *J. Invest. Dermatol.*; 117: 3-15

Naeem, M., Wajid, M., Lee, K., Leal, S.M., Ahmed, W., (2006). A mutation in the hair matrix and cuticle keratin KRTHB5 gene causes ectodermal dysplasia of hair and nail type. *J. Med. Genet*.; 43: 274-279

Nakabayashi, K., Amann, D., Ren, Y., Saarialho-Kere, U., Avidan, N., Gentles, S., MacDonald, J.R., Puffenberger, E.G., Christiano, A.M., Martinez-Mir, A., Salas-Alanis, J.C., Rizzo, R., Vamos, E., Raams, A., Les, C., Seboun, E., Jaspers, N.G.J., Beckmann, J.S., Jackson, C.E., Scherer, S.W., (2005). Identification of C7orf11 (TTDN1) gene mutations and genetic heterogeneity in nonphotosensitive trichothiodystrophy. *Am. J. Hum. Genet*.; 76: 510-516

Nakamura, M., Schneider, M.R., Schmidt-Ullrich, R., Paus, R., (2013). Mutant laboratory mice with abnormalities in hair follicle morphogenesis, cycling, and/or structure: an update. *J. Dermatol. Sci.*; 69: 6-29

Nakamura, Y., Tanaka, P., Watanade, A., (1975). Electrokinetic studies on the surface structure of wool fibres. 5th International Wool Textile Conference, Aachen, II, 34-43

Nataraja, M.T., and Roy, J.M., (2015). Study on hair morphology to distinguish the dominant races in Malaysia for forensic investigation. *J. Forensic Sci. Criminol.*; 3: 1-6

Negri, A.P., Cornell, H.J., Rivett, D.E., (1993). A model for the surface of keratin fibres. *Text. Res. J.*; 63: 109-115

Negri, A.P., Rankin, D.A., Nelson, W.G., Rivett, D.E., (1996). A transmission electron microscope study of covalently bound fatty acids in the cell membranes of wool fibers. *Text. Res. J.*; 66: 491-495

Nehme, N., El Malti, R., Roux-Buisson, N., Caignault, J.R., Bouvagnet, P., (2012). Evidence for genetic heterogeneity in Carvajal syndrome. *Cell Tissue Res*.; 348: 261-264

Nemes, Z., and Steinert, P.M., (1999). Bricks and mortar of the epidermal barrier. *Exp. Mol. Med.*; 31: 5-19

Nezirevic, D., Arstrand, K., Kagedal, B., (2007). Hydrophilic interaction liquid chromatographic analysis of aminohydroxyphenlyalanines from melanin pigments. *J. Chromatog. A*; 1163: 70-79

Nicolaides, N., Fu, H.C., Rice, G.R., (1968). The skin surface lipids of man compared with those of eighteen species of animal. *J. Invest.Dermatol*.; 51: 83-89

Nickoloff, B.J., and Naidu, Y., (1994). Perturbation of epidermal barrier function correlates with initiation of cytokine cascade in human skin. *J. Am. Acad. Dermatol.*; 30: 534-546

Niemann, C., and Watt, F.M., (2002). Designer skin: lineage commitment in postnatal epidermis. *Trends cell biol.*; 12: 185-192

Nishimura, E.K., Jordan, S.A., Oshima, H., Yoshida, H., Osawa, M., Moriyama, M., Jackson, I.J., Barrandon, Y., Miyachi, Y., Nishikawa, S., (2002). Dominant role of the niche in melanocyte stem-cell fate determination. *Nature*; 416: 854-860

Norgett, E.E., Hatsell, S.J., Carvajal-Huerta, L., Cabezas, J.C., Common, J., Purkis, P.E., Whittock, N., Leigh, I.M., Stevens, H.P., Kelsell, D.P., (2000). Recessive mutation in desmoplakin disrupts desmoplakin-intermediate filament interactions and causes dilated Cardiomyopathy, woolly hair and keratoderma. *Hum. Mol. Genet*.; 9: 2761-2766

Nutbrown, M. and Randall, V.A., (1995). Differences between connective tissue-epithelial junctions in human skin and the anagen hair follicle. *J. Invest. Dermatol.*; 104: 90-94

Ogikubo, S., Nakabayashi, T., Adachi, T., Islam, M.S., Yoshizawa, T., Kinjo, M., Ohta, N., (2011). Intracellular pH sensing using autofluorescence lifetime microscopy. *J. Phys. Chem. B*; 115: 10385-10390

Oh, J.W., Kloepper, J., Langan, E.A., Kim, Y., Yeo, J., Kim, M.J., Hsi, T.C., Rose, C., Yoon, G.S., Lee, S.J., Seykora, J., Kim, J.C., Sung, Y.K., Kim, M., Paus, R., Plikus, M.V., (2016). A guide to studying human hair follicle cycling in vivo. *J. Invest. Dermatol.*; 136: 34-44

Ohta, N., Oka, T., Inoue, K., Yagi, N., Kato, S., Hatta, I., (2005). Structural analysis of human hair in aqueous solutions using microbeam X-ray diffraction. *J. Appl. Cryst.*; 38: 274-279

Olivry, T., and Dunston, S.M., (2015). Expression patterns of superficial epidermal adhesion molecules in an experimental dog model of acute atopic dermatitis skin lesions. *Vet. Dermatol*.; 26: 53-e18

Orentreich, N., (1969). Scalp hair replacement in men. *Advances in biology of the skin. Vol. 9: Hair growth.* Oxford: Pergamon Press, p.99-108

Osawa, M., Egawa, G., Mak, S.S., Moriyama, M., Freter, R., Yonetani, S., Beermann, F., Nishikawa, S., (2006). Molecular characterisation of melanocyte stem cells in their niche. *Develop.*; 132: 5589-5599

Ozturk, O.A., Pakula, H., Chmielowiec, J., Qi, J., Stein, S., Lan, L., Sasaki, Y., Rajewsky, K., Birchmeier, W., (2016). Gab1 and Mapk signalling are essential in the hair cycle and hair follicle stem cell quiescence. *Cell Rep.*; 13: 561-572

Page, M.E., Lombard, P., Ng, F., Gottgens, B., Jensen, K.B., (2013). The epidermis comprises autonomous compartments maintained by distinct stem cell populations. *Cell Stem Cell*; 13: 471-482

Pan, T.L., Wang, P.W., Aljuffali, I.A., Huang, C.T., Lee, C.W., Fang, J.Y., (2015). The impact of urban particulate pollution on skin barrier function and the subsequent drug absorption. *J. Dermatol. Sci.*; 78: 51-60

Pan, Y., Lin, M.H., Tian, X., Cheng, H.T., Gridley, T., Shen, J., Kopan, R., (2004). Gamma-secretase functions through Notch signalling to maintain skin appendages but is not required for their patterning or initial morphogenesis. *Dev. Cell*; 7: 731-743

Panteleyev, A.A., Jahoda, C.A., Christiano, A.M., (2001). Hair follicle predetermination. *J. Cell Sci.*; 114: 3419-3431

Pappinen, S., Hermansson, M., Kuntsche, J., Somerharju, P., Wertz, P., Urtti, A., Suhonen, M., (2008). Comparison of rat epidermal keratinocyte organotypic culture (ROC) with intact human skin: Lipid composition and thermal phase behaviour of the stratum corneum. *Biochim. Biophys. Acta*.; 1778: 824-834

Pasternack, S.M., von Kügelgen, I., Al Aboud, K., Lee, Y.A., Rüschendorf, F., Voss, K., Hillmer, A.M., Molderings, G.J., Franz, T., Ramirez, A., Nürnberg, P., Nothen, M.M., Betz, R.C., (2008). G-protein coupled receptor P2Y5 and its ligand LPA are involved in maintenance of human hair growth. *Nat. Genet*.; 40: 329-334

Patel, A., Poterlowicz, G., Westgate, N., Botchkareva, V., Farjo, N., (2015). Age-associated changes in gene expression programs in human hair follicle. *J. Anat.*; 226: 200

Paus, R., Arck, P., Tiede, S., (2008). (Neuro-)endocrinology of epithelial hair follicle stem cells. *Mol. Cell. Endocrin.*; 288: 38-51

Paus, R., and Cotsarelis, G., (1999). The biology of hair follicles. *N. Engl. J. Med.*; 341: 491-497

Peng, Y., Xuan, M., Leung, V.Y.L., Cheng, B., (2015). Stem cells and aberrant signalling of molecular systems in skin aging. *Age. Res. Rev.*; 19: 8-21

Perkins, M.A., Osterhues, M.A., Farage, M.A., Robinson, M.K., (2001). A noninvasive method to assess skin irritation and compromised skin conditions using simple tape adsorption of molecular markers of inflammation. *Skin res. Technol*.; 7: 227-237

Peters, D.E., and Bradbury, J.H., (1972). The chemical composition of wool X. Material digested by trypsin from fibres and cortical cells. *Aust. J. Biol. Sci.*; 25: 1225-1234

Piper, L.P.S., (1966). A mechanism of attachment between the cuticle and cortex of mammalian hair. *J. Text. Inst.*; 57: 185-190

Plowman, J.E., Deb-Choudhury, S., Clerens, S., Thomas, A., Cornellison, C.D., Dyer, J.M., (2012). Unravelling the proteome of wool: towards markers of wool quality traits. *J. Proteomics*; 75: 4315-4324

Plowman, J.E., Paton, L.N., Bryson, W.G., (2007). The differential expression of proteins in the cortical cells of wool and hair fibres. *Exp. Dermatol*.; 16: 707-714

Poblet, E., Jimenez, F., De Cabo, C., Prieto-Martin, A., Sanchez-Prieto, R., (2005). The calcium-binding protein calretinin is a marker of the companion cell layer of the human hair follicle. *B. J. Dermatol.*; 125: 1316-1320

Ponec, M., Weerheim, A., Kempenaar, J., Mommaas, A.M., Nugteren, D.H., (1988). Lipid composition of cultured human keratinocytes in relation to their differentiation. *J. Lipid. Res.*; 29: 949-961

Potter, C.S., Kern, M.J., Bayboo, M.A., Pruett, N.D., Godwin, A.R., Sundberg, J.P., Awgulewitsch, A., (2015). Dysregulated expression of sterol O-acyltransferase 1 (*Soat1*) in the hair shaft of *Hoxc13* null mice. *Exp. Mol. Pathol*.; 99: 441-444

Powers, D.H., and Barnett, G., (1952). A study of the swelling of hair in thioglycolate solutions and its reswelling. *J. Soc. Cosmet. Chem*.; 4: 92-100

Provenzano, P.P., Inman, D.R., Eliceiri, K.W., Knittel, J.G., Yan, L., Rueden, C.T., White, J.G., Keely, P.J., (2008b). Collagen density promotes mammary tumour initiation and progression. *BMC Med.*; 6: 11

Provenzano, P.P., Rueden, C.T., Trier, S.M., Yan, L., Ponik, S.M., Inman, D.R., Keely, P.J., Eliceiri, K.W., (2008a). Nonlinear optical imaging and spectral-lifetime computational analysis of endogenous and exogenous fluorophores in breast cancer. *J. Biomed. Opt*.; 13: 031220-1–11

Quinn, Jr.N.J., (1971). Toe tourniquet syndrome. *Pediatrics*; 48: 145-146

Rafik, M.E., Doucet, J., Briki, F., (2004). The intermediate filament architecture as determined by X-ray diffraction modelling of hard α-keratin. *Biophys. J.*; 86: 3893-3904

Ramirez Prada, D., Delgado, G. Hidalgo Patiño, C. A., Pérez-Navero, J., Gil Campos, M., (2011). Using of WHO guidelines for the management of severe malnutrition to cases of marasmus and kwashiorkor in a Colombia children's hospital. *Nutr. Hosp*.; 26: 977-983.

Ramirez-Zacarias, J.L., Castro-Munozledo, F., Kuri-Harcuch, W., (1992). Quantitation of adipose conversion and triglycerides by staining intracytoplasmic lipids with oil red O. *Histochemistry*; 97: 493-497

Randall, V.A., and Botchkareva, N.V., (2009). *The biology of hair growth*. Cosmetic applications of laser and light-based systems. William Andrew Inc. p.3-35

Randall, V.A., and Ebling, E.J.G., (1991). Seasonal changes in human hair growth. *Br. J. Dermatol.*; 124: 146-151

Randebrock, R., (1964). Neue erkenntnesse uber den morphologischen aufbau des menschlichen hares*. J. Soc. Cosmet. Chem*.; 15: 691-700

Rastogi, S.K., and Singh, J., (2003). Passive and iontrophoretic transport enhancement of insulin through porcine epidermis by depilatories: permeability and fourier transformation infrared spectroscopy studies. *AAPS PharmSciTech*.; 4: 1-9

Rawlings, A.V., and Harding, C.R., (2004). Moisturisation and skin barrier function. *Dermatol. Therapy*; 17: 43-48

Reddy, S., Andl, T., Bagasra, A., Lu, M.M., Epstein, D.J., Morrisey, E.E., Millar, S.E., (2001). Characterisation of Wnt gene expression in developing and postnatal hair follicles and identification of Wnt5a as a target of Sonic hedgehog in hair follicle morphogenesis. *Mech. Dev.*; 107: 69-82

Reed, R.E., Humoller, F.L., DenBeste, M., (1946). Permanent waving of human hair: the cold process. *American association for the advancement of science*; 1: 109

Rendl, M., Lewis, L., Fuchs, E., (2005). Molecular dissection of mesenchymal-epithelial interactions in the hair follicle. *PLoS Biol.*; 3: e331

Rezza, A., Wang, Z., Sennett, R., Qiao, W., Wang, D., Heitman, N., Mok, K.W., Clavel, C., Yi, R., Zandstra, P., Ma'ayan, A., Rendl, M., (2016). Signalling networks among stem cell precursors, transit-amplifying progenitors, and their niche in developing hair follicles. *Cell Rep.*; 14: 3001-3018

Ribeiro, A., Matama, T., Cruz, C.F., Gomes, A.C., Cavaco-Paulo, A.M., (2013). Potential of human γD-crystallin for hair damage repair: insights into the mechanical properties and biocompatibility. *Int. J. Cosmet. Sci.*; 35: 458-466

Ribera, M., Fernandez-Chico, N., Casals, M., (2010). Pseudofolliculitis barbae. *Actas Dermo-Sifiliográficas (English Edition)*; 101: 749-757

Rice, R.H., and Green, H., (1977). The cornified envelope of terminally differentiated human epidermal keratinocytes consists of cross-linked protein. *Cell*; 11: 417-422

Rice, R.H., Wong, V.J., Pinkerton, K.E., (1994). Ultrastructural visualisation of cross-linked protein features in epidermal appendages. *J. Cell sci.*; 107: 1985-1992

Richards, R.N., Uy, M., Meharg, G., (1990). Temporary hair removal in patients with hirsutism: a clinical study. *Cutis*; 45: 199-202

Richards-Kortum, R., Drezek, R., Sokolov, K., Pavlova, I., Follen, M., (2003). Survey of endogenous biological fluorophores. *Handbook of Biomedical Fluorescence*. Marcel Dekker Inc. New York, Basel, p.237-264

Richena, M., and Rezende, C.A., (2015). Effect of photodamage on the outermost cuticle layer of human hair. *J. Photochem. Photobiol. B*; 153: 296-304

Richena, M., and Rezende, C.A., (2016). Morphological degradation of human hair cuticle due to simulated sunlight irradiation and washing. *J. Photochem. Photobiol. B. Biol.*; 161: 430-440

Robbins, C., (2009). The cell membrane complex: three related but different cellular cohesion components of mammalian hair fibres. *J. Cosmet. Sci.*; 60: 437-465

Robbins, C.R., (2012). *Chemical and physical behaviour of human hair*. 5th ed. Springer Science and Business Media

Robbins, C.R., and Kelly, C.H., (1970). Amino acid composition of human hair. *Text Res. J.;* 40: 891–896

Robitaille, H., Simard-Bisson, C., Larouche, D., Tanguay, R.M., Blouin, R., Germain, L., (2010). The small heat-shock protein Hsp27 undergoes ERK-dependent phosphorylation and redistribution to the cytoskeleton in response to dual leucine zipper-bearing kinase expression. *J. Invest. Dermatol.*; 130: 74-85

Rogers, G.E., and Koike, K., (2009). Laser capture microscopy in a study of expression of structural proteins in the cuticle cells of human hair. *Exp. Dermatol.*; 18: 541-547

Rogers, M.A., Langbein, L., Praetzel, S., Giehl, K., (2008). Characterisation and expression analysis of the hair keratin associated protein KAP26.1. *Brit. J. Dermatol*.; 159: 725-729

Rogers, M.A., Langbein, L., Praetzel, S., Winter, H., Schweizer, J., (2006). Human hair keratin-associated proteins (KAPs). *Int. Rev. Cytol.*; 251: 209-263

Rogers, M.A., Langbein, L., Winter, H., Beckmann, I., Praetzel, S., Schweizer, J., (2004). Hair keratin associated proteins: characterisation of a second high sulphur KAP group domain on human chromosome 21. *J. Invest. Dermatol.*; 122: 147-158

Rogers, M.A., Langbein, L., Winter, H., Ehmann, C., Praetzel, S., Korn, B., Schweizer, J., (2001). Characterisation of a cluster of human high/ultrahigh sulphur keratin-associated protein genes embedded in the type I keratin gene domain on chromosome 17q12-21. *J. Biol. Chem.*; 276: 19440-19451

Rogers, M.A., Winter, H., Langbein, L., Wollschlager, A., Praetzel, S., Jave, L.F., Schweizer, J., (2007). Characterisation of human KAP24.1, a cuticular hair keratin-associated protein with unusual amino-acid composition and repeat structure. *J. Invest. Dermatol.*; 127: 1197-1204

Rompolas, P., Mesa, K.R., Greco, V., (2013). Spatial organisation within a niche as a determinant of stem-cell fate. *Nature*; 502: 513-518

Rudnicka, L., Olszewska, M., Rakowska, A., (2008). In vivo reflectance confocal microscopy: usefulness for diagnosing hair diseases. *J. Dermatol. Case Rep.*; 2: 55-59

Ruetsch, S.B., Kamath, Y., Weigmann, H.D., (2000). Photodegradation of human hair: an SEM study. *J. Cosmet. Sci.*; 51: 103-125

Russell, R.A., Adams, N.M., Stephens, D.A., Batty, E., Jensen, K., Freemont, P.S., (2014). Segmentation of fluorescence microscopy images for quantitative analysis of cell nuclear architecture. *Biophys. J.*; 96: 3379-3389

Sato, N., Leopold, P.L., Crystal., R.G., (1999). Induction of the hair growth phase in postnatal mice by localised transient expression of Sonic hedgehog. *J. Clin. Invest.*; 104: 855-864

Sato-Miyaoka, M., Hisatsune, C., Ebisui, E., Ogawa, N., Takahashi-Iwanaga, H., Mikoshiba, K., (2012). Regulation of hair shedding by the type 3 IP3 receptor. *J. Invest. Dermatol*.; 132: 2137-2147

Schweitzer, D., Schenke, S., Hammer, M., Schweitzer, F., Jentsch, S., Birckner, E., Becker, W., (2007). Towards metabolic mapping of the human retina. *Microsc. Res. Tech*.; 70: 403-409

Scott, G.V., and Robbins, C., (1980). Effects of surfactant solutions on hair fibre friction. *J. Soc.Cosmet. Chem*.; 31: 179-200

Seiberg, M., Marthinuss, J., Stenn, K.S., (1995). Changes in expression of apoptosis-associated genes in skin mark early catagen. *J. Invest. Dermatol*.; 104: 78-82

Segre, J.A., (2006). Epidermal barrier formation and recovery in skin disorders. *J. Clin. Invest*.; 116: 1150-1158

Serita, K., Murakami, H., Kawayama, I., Takahashi, Y., Yoshimura, M., Mori, Y., Tonouchi, M., (2014). Evaluation of human hairs with terahertz wave. *Optic. Engin.*; 53: 031205

Serre, G., Mils, V., Haftek, M., Vincent, C., Croute, F., Reano, A., Ouhayoun, J.P., Bettinger, S., Soleilhavoup, J.P., (1991). Identification of late differentiation antigens of

human cornified epithelia, expressed in re-organized desmosomes and bound to cross-linked envelope. *J. Invest. Dermatol*. 97: 1061-1072

Sevilla, L.M., Nachat, R., Groot, K.R., Klement, J.F., Uitto, J., Djian, P., Määttä, A., Watt, F.M., (2007). Mice deficient in involucrin, envoplakin, and periplakin have a defective epidermal barrier. *JCB*; 179: 1599-1612

Sheela, S.R., Manoj, L., Injody, S.J., (2004). Griscelli syndrome: Rab 27a mutation. *Indian Pediatr*.; 41: 944-947

Shimomura, Y., Aoki, N., Ito, M., Rogers, M.A., Langbein, L., Schweizer, J., (2003). Characterisation of human keratin-associated protein 1 family members. *J. Invest. Dermatol. Symp. Proc.*; 8: 96-99

Shimomura, Y., and Christiano, A.M., (2010). Biology and genetics of hair. *Annu. Rev. Genomics Hum. Genet.*; 11: 109-132

Shimomura, Y., and Ito, M., (2005). Human hair keratin-associated proteins. *J. Invest. Dermatol. Symp. Proc.*; 10: 230-233

Shimomura, Y., Wajid, M., Ishii, Y., Shapiro, L., Petukhova, L., Gordon, D., Christiano, A.M., (2008). Disruption of P2RY5, an orphan G protein-coupled receptor, underlies autosomal recessive woolly hair. *Nat. Genet*.; 40: 335-339

Shimomura, Y., Wajid, M., Petukhova, L., Kurban, M., Christiano, A.M., (2010). Autosomal-dominant woolly hair resulting from disruption of keratin 74 (KRT74), a potential determinant of human hair texture. *Am. J. Hum. Genet*.; 86: 632-638

Shirokova, V., Biggs, L.C., Jussila, M., Ohyama, T., Groves, A.K., Mikkola, M.L., (2016). Foxi3 deficiency compromises hair follicle stem cell specification and activation. *Stem Cells*; 34: 1896-1908

Silengo, M., Valenzise, M., Spada, M., Ferrero, G.B., Ferraris, S., Dassi, P., Jarre, L., (2003). Hair anomalies as a sign of mitochondrial disease. *Eur. J. Pediatr*.; 162: 459-461

Simpson, C.L., Patel, D.M., Green, K.J., (2011). Deconstructing the skin: cytoarchitectural determinants of epidermal morphogenesis. *Nat. Rev. Mol. Cell Biol.*; 12: 565-580

Singh, B., and Umapathy, S., (2011). Effect of SDS on human hair: study on the molecular structure and morphology. *J. Biophotonics*; 4: 315-323

Skala, M.C., Riching, K.M., Gendron-Fitzpatrick, A., Eickhoff, J., Eliceiri, K.W., White, J.G., Ramanujam, N., (2007). In vivo multiphoton microscopy of NADH and FAD redox states, fluorescence lifetimes, and cellular morphology in precancerous epithelia. *PNAS USA*; 104: 19494-19499

Skerrow, C.J., Clelland, D.G., Skerrow, D., (1989). Changes to desmosomal antigens and lectin-binding sites during differentiation in normal human epidermis: a quantitative ultrastructural study. *J. Cell Sci*.; 92: 667-677

Smart, K.E., Kilburn, M., Schroeder, M., Martin, B.G., Hawes, C., Marsh, J.M., Grovenor, C.R., (2009). Copper and calcium uptake in coloured hair. *J. Cosmet. Sci.*; 60: 337-345

Smith, A.A., Li, J., Liu, B., Hunter, D., Pyles, M., Gillette, M., Dhamdhere, G.R., Abo, A., Oro, A., Helms, J.A., (2016). Activating hair follicle stem cells via R-spondin2 to stimulate hair growth. *J. Invest. Dermatol*.; 136: 1549-1558

Smith, E., Farrand, B., Shen, J., (2010). The removal of lipid from the surface of wool to promote the subsequent enzymatic process with modified protease for wool shrink resistance. *Biocatalysis and Biotansformation*; 28: 329-338

Smith, F.J., Coleman, C.M., Bayoumy, N.M., Tenconi, R., Nelson, J., David, A., McLean, W.H., (2001). Novel keratin 17 mutations in pachyonychia congenital type 2. *J. Invest. Dermatol*.; 116: 806-808

Smith, J.R., and Swift, J.A., (2005). Maple syrup urine disease hair reveals the importance of 18-methyleicosanoic acid in cuticular delamination. *Micron.*; 36: 261-266

Son, H.H., Lee, D.Y., Seo, H.S., Jeong, J., Moon, J.Y., Lee, J.E., Chung, B.C., Kim, E., Choi, M.H., (2016). Hair sterol signatures coupled to multivariate data analysis reveal an increased 7β-hydroxycholesterol production in cognitive impairment. *J. Steroid Biochem. Mol. Biol.*; 155: 9-17

Stanic, V., Bettini, J., Montoro, F.E., Stein, A., Evans-Lutterodt, K., (2015). Local structure of human hair spatially resolved by sub-micron X-ray beam. *Nature*; 5: 17347

Steinert, P.M., and Marekov, L.N., (1997). Direct evidence that involucrin is a major early isopeptide cross-linked component of the keratinocyte cornified cell envelope. *J. Biol. Chem.*; 272: 2021-2030

Steinert, P.M., and Marekov, L.N., (1999). Initiation and assembly of the cell envelope barrier structure of stratified squamous epithelia. *Mol. Biol. Cell*; 10: 4247-4261

Stenn, K., (2005). Exogen is an active, separately controlled phase of the hair growth cycle. *J. Am. Acad. Dermatol.*; 52: 374-375

Stewart, M.E., Downing, D.T., Strauss, J.S., (1983). Sebum secretion and sebaceous lipids. *Dermatol. Clin*.; 1: 335-344

Stoner, C.J., Bininda-Emonds, O.R.P., Caro, T., (2003). The adaptive significance of colouration in lagomorphs. *Biol. J. Linnean Soc.*; 79: 309-328

Strumia, R., Borghi, A., Colombo, E., Manzato, E., Gualandi, M., (2005). Low prevalence of twisted hair in anorexia nervosa. *Clin. Exp. Dermatol*.; 30: 349-350

Strussman, A., (1983). Deutsches Wollforschungsinstitut, internal project report.

Sugata, K., Sakai, S., Noriaki, N., Osanai, O., Kitahara, T., Takema, Y., (2009). Imaging of melanin distribution using multiphoton autofluorescence decay curves. *Skin research and technology*; 16: 55-59

Suhonen, M.T., Bouwstra, J.A., Urtti, A., (1999). Chemical enhancement of percutaneous absorption in relation to stratum corneum structural alterations. *J. Control Release*; 59: 149-161

Suzuta, K and Arai, K., (2015). Disulphide cross-linked network structure of intermediate filament and matrix in hair and wool cortices. *Soc. Fiber sci. Tech.*; 71: 237-249

Suzuta, K., Ogawa, S., Takeda, Y., Kaneyama, K., Arai, K., (2012). Intermolecular disulphide cross-linked structural change induced by permanent wave treatment of human hair with thioglycolic acid. *J. Cosmet. Sci.*; 63: 117-196

Swift, J.A., (1979). Minimum depth electron probe X-ray microanalysis as a means for determining the sulphur content of the human hair surface. *Scanning*; 2: 83-88

Swift, J.A., (1999). Human hair cuticle: biologically conspired to the owner's advantage. *J. Cosmet. Sci.*; 50: 23-47

Swift, J., and Bews, B., (1974). The chemistry of human hair cuticle. I: a new method for physical isolation of cuticle. *J. Soc. Cosmet. Chem*.; 25: 13-21

Swift, J., and Bews, B., (1976). The chemistry of human hair cuticle - III: the isolation and amino acid analysis of various subfractions of the cuticle obtained by pronase and trypsin digestion. *J. Soc. Cosmet. Chem.*; 27: 289-300

Swift, J.A., Chahal, S.P., Challoner, N.I., Parfrey, J.E., (2000). Investigations on the penetration of hydrolysed wheat proteins into human hair by confocal laser-scanning fluorescence microscopy. *J. Cosmet. Sci.*; 51: 193-203

Swift, J.A. and Smith, J.R., (2000). Atomic force microscopy of human hair. *Scanning*; 22: 310-318

Swift, J.A., and Smith, J.R., (2001). Microscopical investigations on the epicuticle of mammalian keratin fibres. *J. Microscopy*; 204: 203-211

Swift, J.A., and Smith, J.R., (2002). Lamellar subcomponents of the cuticular cell membrane complex of mammalian keratin fibres show friction and hardness contrast by AFM. *J. Microscopy*; 206: 182-193

Syed, A.N., (1995). Ethnic hair care products. *J. Soc. Cosmet. Chem.*; 12: 235-259

Syed, A.N., and Naqvi, A.R., (2000). Comparing the irritation potential of lye and no-lye relaxers. *Cosmet. Toiletries*; 115: 47-52

Szabo, S., Jaeger, K., Fischer, H., Tchachler, E., Parson, W., Eckhart, L., (2012). In situ labelling of DNA reveals interindividual variation in nuclear DNA breakdown in hair and may be useful to predict success of forensic genotyping of hair. *Int. J. Legal Med.*; 126: 63-70

Tackey, R.N., Bryant, H., Parks, F.M., (2012). Cytokine expression correlates with differential sensory perception between lye and no-lye relaxers. *J. Cosmet. Sci.*; 64: 111-117

Takahashi, T., Hayashi, R., Okamoto, M., Inoue, S., (2006). Morphology and properties of Asian and Caucasian hair. *J. Cosmet. Sci.*; 57: 327-338

Takahashi, T., and Yoshida, S., (2014). Distribution of glycolipid and unsaturated fatty acids in human hair. *Lipids*; 49: 905-917

Takayama, K., Salazar, E.P., Broughton, B.C., Lehmann, A.R., Sarasin, A., Thompson, L.H., Weber, C.A., (1996). Defects in the DNA repair and transcription gene ERCC2(XPD) in trichothiodystrophy. *Am. I. Hum. Genet*.; 58: 263-270

Taneda, A., Ogawa, H., Hashimoto, K., (1980). The histochemical demonstration of protein-bound sulfhydryl groups and disulphide bonds in human hair by a new staining method (DACM staining). *J. Invest. Dermatol.*; 75: 365-369

Tate, M.L., Kamath, Y.K., Ruetsch, S.B., Weigmann, H.D., (1993). Quantification and prevention of hair damage. *J. Soc. Cosmet. Chem.*; 44: 347-371

Thibaut, S., Cavusoglu, N., de Becker, E., Zerbib, F., Bednarczyk, A., Schaeffer, C., van Dorsselaer, A., Bernard, B.A., (2009). Transglutaminase-3 enzyme: a putative actor in human hair shaft scaffolding? *J. Invest. Dermatol.*; 129: 449-459

Thody, A.J., Higgins, E.M., Wakamatsu, K., Ito, S., Burchill, S.A., Marks, J.M., (1991). Pheomelanin as well as eumelanin is present in human epidermis. *J. Invest. Dermatol*.; 97: 340-344

Tiede, S., Kloepper, J.E., Bodo, E., Tiwari, S., Kruse, C., Paus, R., (2007). Hair follicle stem cells: walking the maze. *Eur. J. Cell Biol.*; 86: 355-376

Tiselius, A., (1937). A new apparatus for electrophoretic analysis of colloidal mixtures. *Transactions of the Faraday Society*; 33: 524–531

Tobin, D.J., (2009). Aging of the hair follicle pigmentation system. *Int. J.Trichology*; 1: 83-93

Tobin, D.J., Hagen, E., Botchkarev, V.A., Paus, R., (1998). Do hair bulb melanocytes undergo apoptosis during hair follicle regression (catagen)? *J. Invest. Dermatol*.; 111: 941-947

Tobin, D.J., Slominski, A., Botchkarev, V., Paus, R., (1999). The fate of hair follicle melanocytes during the hair growth cycle. *J. Invest. Dermatol.*; 4: 323-332

Trautinger, F., Kindas-Mugge, I., Dekrout, B., Knobler, R.M., Metze, D., (1995). Expression of the 27-kDa heat shock protein in human epidermis and in epidermal neoplasms: an immunohistological study. *Br. J. Dermatol*.; 133: 194-202

Trueb, R.M., (2015). Effect of ultraviolet radiation, smoking and nutrition on hair. *Curr. Probl. Dermatol.*; 47: 107-120

Tsuji, Y., Denda, S., Soma, T., Raftery, L., Momoi, T., Hibino, T., (2003). A potential suppressor of TGF-β delays catagen progression in hair follicles. *J. Invest. Dermatol. Smp. Proc.*; 8: 65-68

Tumbar, T., Guasch, G., Greco, V., Blanpain, C., Lowry, W.E., Rendl, M., Fuchs, E., (2004). Defining the epithelial stem cell niche in skin. *Sci.*; 303: 359-363

Ulrich, V., Fischer, P., Riemann, I., Konig, K., (2004). Compact multiphoton/single photon laser scanning microscope for spectral imaging and fluorescence lifetime imaging. *Scanning*; 26: 217-225

Van Dierendonck, J.H., Keyzer, R., Cornelisse, J.C., Van de Velde, C.J., (1989). Nuclear distribution of the Ki-67 antigen during the cell cycle: comparison with growth fraction in human breast cancer cells. *Cancer res.*; 49: 2999-3006

Van Neste, D., Leroy, T., Conil, S., (2007). Exogen hair characterisation in human scalp. *Skin Res. Technol.*; 13: 436-443

Van Steensel, M.A., Steijlen, P.M., Bladergroen, R.S., Vermeer, M., van Geel, M., (2005). A mis-sense mutation in the type II hair keratin hHb3 is associated with monilethrix. *J. Med. Genet.*; 42: 19

Varkonyi, A., Boda, M., Endreffy, E., Németh, I., Timár, E., (1998). Coeliac disease: always something to discover. *Scand. J. Gastroenterol Suppl*.; 228: 122-129

Velasco, M.R.V., Baby, A.R., Sarruf, F.D., Kaneko, T.M., Samad, R.E., Vieira Junior, N.D., De Freitas, A.Z., (2009). Prospective ultramorphological characterisation of human hair by optical coherence tomography. *Skin Res Technol.*; 15: 440-443

Vulpe, C., Levinson, B., Whitney, S., Packman, S., Gitschier, J., (1993). Isolation if a candidate gene for Menkes disease and evidence that it encodes a copper-transporting ATPase. *Nat. Genet*.; 3: 7-13

Wagner, R.D.C.C., Kiyohara, P.K., Silveira, M., Joekes, I., (2007). Electron microscopic observations of human hair medulla*. J. Microscopy*; 226: 54-63

Wahlberg, J.E., (1972). Impairment of skin barrier function by depilatories. *J. Invest. Dermatol*.; 59: 160-162

Wang, L., Siegenthaler, J.A., Dowell, R.D., Yi, R., (2016). Foxc1 reinforces quiescence in self-renewing hair follicle stem cells. *Science*; 351: 613-617

Wasif, N., Naqvi, S.K., Basit, S., Ali, N., Ansar, M., Ahmad W., (2011). Novel mutations in the keratin-74 (KRT74) gene underlie autosomal dominant woolly hair/hypotrichosis in Pakistani families. *Hum. Genet*.; 129: 419-424

Watt, F.M., Lo Celso, C., Silva-Vargas, V., (2006). Epidermal stem cells: an update. *Curr. Opin. Genet. Dev.*; 16: 518-524

Weeda, G., Eveno, E., Donker, I., Vermeulen, W., Chevallier-Lagente, O., Taïeb, A., Stary, A., Hoeijmakers, J.H., Mezzina, M., Sarasin, A., (1997). A mutation in the XPB/ERCC3 DNA repair transcription gene, associated with trichothiodystrophy. *Am. J. Hum. Genet*.; 60: 320-329

Wei, G., Bhushan, B., Torgerson, P.M., (2005). Nanomechanical characterisation of human hair using nanoindentation and SEM. *Ultramicroscopy*; 105: 248-266

Wen, Y., Liu, Y., Xu, Y., Zhao, Y., Hua, R., Wang, K., Sun, M., Li, Y., Yang, S., Zhang, X.J., Kruse, R., Cichon, S., Betz, R.C., Nothen, M.M., van Steensel, M.A., van Geel, M., Steijlen, P.M., Hohl, D., Huber, M., Dunnill, G.S., Kennedy, C., Messenger, A., Munro, C.S., Terrinoni, A., Hovnanian, A., Bodemer, C., de Prost, Y., Paller, A.S., Irvine, A.D., Sinclair, R., Green, J., Shang, D., Liu, Q., Luo, Y., Jiang, L., Chen, H.D., Lo, W.H., McLean, W.H., He, C.D., Zhang, X., (2009). Loss-of-function mutations of an inhibitory upstream ORF in the human hairless transcript cause Marie Unna hereditary hypotrichosis. *Nat. Genet*.; 41: 228-233

Wennig, R., (2000). Potential problems with the interpretation of hair analysis results. *Forensic Sci. Int.*; 107: 5-12

Wertz, P.W., and Downing, D.T., (1988). Integral lipids of human hair. *Lipids*; 23: 878-881

Wertz, P.W., and Downing, D.T., (1989). Integral lipids of mammalian hair. *Comp. Biochem. Phys. B: Comp. Biochem.*; 92b: 759-761

Wertz, P.W., and Dowing, D.T., (1991). *Epidermal lipids*. Physiology, Biochemistry, and Molecular Biology of the Skin (2nd ed.), Oxford Univ. Press, p. 205–236

Whittock, N.V., Wan, H., Morley, S.M., Garzon, M.C., Kristal, L., Hyde, P., McLean, W.H., Pulkkinen, L., Uitto, J., Christiano, A.M., Eady, R.A., McGrath, J.A., (2002). Compound heterozygosity for non-sense and mis-sense mutations in desmoplakin underlies skin fragility/woolly hair syndrome. *J. Invest. Dermatol*.; 118: 232-238

Wilson, E.B., (1925). The karyoplasmic ratio. *In* The Cell in Development and Heredity. 3rd ed. The Macmillan Company, New York, p. 727–733

Wilson, T., (2011). Resolution and optical sectioning in the confocal microscope. *J. Micros.*; 244: 113-121

Winter, H., Labreze, C., Chapalain, V., Surleve-Bazeille, J.E., Mercier, M., Rogers, M.A., Taieb, A., Schweizer, J., (1998). A variable monilethrix phenotype associated with a novel mutation, Glu402Lys, in the helix termination motif of the type II hair keratin hHb1. *J. Invest. Dermatol*.; 111: 169-172

Winter, H., Rogers, M.A., Langbein, L., Stevens, H.P., Leigh, I.M., Labrèze, C., Roul, S., Taieb, A., Krieg, T., Schweizer, J., (1997). Mutations in the hair cortex keratin hHb6 cause the inherited hair disease monilethrix. *Nat. Genet*.; 16: 372-374

Winter, H., Schissel, D., Parry, D.A., Smith, T.A., Liovic, M., Birgitte Lane, E., Edler, L., Langbein, L., Jave-Suarez, L.F., Rogers, M.A., Wilde, J., Peters, G., Schweizer, J., (2004). An unusual Ala12Thr polymorphism in the 1A alpha-helical segment of the companion layer-specific keratin K6hf: evidence for a risk factor in the etiology of the common hair disorder pseudofolliculitis barbae. *J. Invest. Dermatol*.; 122: 652-657.

Wolfram, L.J., and Albrecht, L., (1985). Torsional behaviour of human hair. *J. Soc. Cosmet. Chem.*; 36: 87-99

Wolfram, L.J., and Lindemann, M., (1971). Some observations on the hair cuticle. *J. Soc. Cosmet. Chem.;* 22: 839–850

Wolfram, L.J., and Underwood, D.L., (1966). The equilibrium between the disulphide linkage in hair keratin and sulphite or mercaptan. *Text. Res. J*.; 36: 947-953

Wong, M., Wis-Surel, G., Epps, J., (1994). Mechanism of hair straightening. *J. Soc. Cosmet. Chem.*; 45: 347-352

Woo, W.M., and Oro, A.E., (2011). Snapshot: hair follicle stem cells. *Cell*; 146: 334

Wortmann, F.J., Wortmann, G., Zahn, H., (1997). Pathways for dye diffusion in wool fibres. *Text. Res. J.*; 64: 720-724

Xiao, X., and Hu, J., (2016). Animal hairs as water-stimulated shape memory materials: mechanism and structural networks in molecular assemblies. *Sci. Rep.*; 6: 26393

Xie, W.J., and Gao, Y.Q., (2013). A simple theory for the Hofmeister series. *J. Phys. Chem. Lett.*; 4: 4247-4252

Yang, L.L., Liu, B., Li, Y., Wang, S.X., Xu, Y., Wang, D.P., Ye, H.H., Shang, S.C., Zhang, G.Z., Peng, R.Y., Zeng, L., Li, W.L., (2014). iRhom2 mutation leads to aberrant hair follicle differentiation in mice. *PLoS One*; 9: e115114

Yano, K., Brown, L.F., Detmar, M., (2001). Control of hair growth and follicle size by VEGF-mediated angiogenesis. *J. Clin. Invest.*; 107: 409-417

Ye, M., Wang, Y., Qian, M., Chen, X., Hu, X., (2011). Preparation and properties of the melanin from *Lachnum singerianum*. *Int. J. of Basic and Applied Sci*.; 11: 51-58

Yoshida, H., Taguchi, H., Kitahara, T., Takema, Y., Visscher, M.O., Schweizer, J., Langbein, L., (2013). Keratins of the human occipital hair medulla: androgenic regulation of *in vitro* hair keratin K37 expression. *Brit. J. Dermatol.*; 169: 218-221

Yuan, S., Li, F., Meng, Q., Zhao, Y., Chen, L., Zhang, H., Xue, L., Zhang, X., Lengner, C., Yu, Z., (2015). Post-transcriptional regulation of keratinocyte progenitor cell expansion, differentiation, and hair follicle regression by *miR-22*. *PLoS Genet.*; 11: e1005253

Yuhki, M., Yamada, M., Kawano, M., Iwasato, T., Itohara, S., Yoshida, H., Ogawa, M., Mishina, Y., (2004). BMPR1A signalling is necessary for hair follicle cycling and hair shaft differentiation in mice. *Development*; 131: 1825-1833

Yusuf, N., Nasti, T.H., Huang, C.M., Huber, B.S., Jaleel, T., Lin, H.Y., Xu, H., Elmets, C.A., (2009). Heat shock proteins HSP27 and HSP70 are present in the skin and are important mediators of allergic contact hypersensitivity. *J. Immunol.*; 182: 675-683

Zabashta, Y.F., Kasprova, A.V., Senchurov, S.P., Grabovskii, Y.E., (2012). The location of the thioglycolic acid molecules in intrafibrillar unordered areas of the human hair keratin structure. *Int. J. Cosmet. Sci.*; 34: 223-225

Zahn, H., Hilterhaus, S., Strussman, A., (1986). Bleaching and permanent waving aspects of hair research. *J. Soc. Cosmet. Chem*.; 37: 159-175

Zakzewski, C.A., Wasilewski, J., Cawley, P., Ford, W., (1998). Transdermal delivery of regular insulin to chronic diabetic rats: effect of skin preparation and electrical enhancement. *J. Control Release*; 50: 267-272

Zambon, A.C., (2011). Use of the Ki67 promoter to label cell cycle entry in living cells. *Cytometry A*; 77: 564-570

Zanet, J., Freije, A., Ruiz, M., Coulon, V., Sanz, J.R., Chiesa, J., Gandarillas, A., (2010). A mitosis block links active cell cycle with human epidermal differentiation and results in endoreplication. *PLoS One*; 5: e15701

Zernov, N.V., Skoblov, M.Y., Marakhonov, A.V., Shimomura, Y., Vasilyeva, T.A., Konovalov, F.A., Abrukova, A.V., Zinchenko, R.A., (2016). Autosomal recessive hypotrichosis with woolly hair caused by a mutation in the keratin 25 gene expressed in hair follicles. *J. Invest. Dermatol.*; 136: 1097-1105

Zhang, H., Nan, W., Wang, S., Zhang, T., Si, H., Wang, D., Yang, F., Li, G., (2016). Epidermal growth factor promotes proliferation of dermal papilla cells via Notch signalling pathway. *Biochim.*; 127: 10-18

Zhang, Y.V., Cheong, J., Ciapurin, N., McDermitt, D.J., Tumbar, T., (2009). Distinct self-renewal and differentiation phases in the niche of infrequently dividing hair follicle stem cells. *Cell Stem Cell*; 5: 267-278

Zhang, Y., and Cremer, P.S., (2006). Interactions between macromolecules and ions: The Hofmeister series. *Curr. Opin. Chem. Biol.*; 10: 658-663

Zlotogorski, A., Marek, D., Horev, L., Abu, A., Ben-Amitai, D., Gerad, L., Ingber, A., Frydman, M., Reznik-Wolf, H., Vardy, D.A., Pras, E., (2006). An autosomal recessive form

of monilethrix is caused by mutations in DSG4: clinical overlap with localised autosomal recessive hypotrichosis. *J. Invest. Dermatol*.; 126: 1292-1296